

Methods in  
**ENZYMOLOGY**

**Volume 600**

**Mechanisms of DNA Recombination  
and Genome Rearrangements:  
Methods to  
Study Homologous Recombination**

*Edited by*

**Maria Spies and Anna Malkova**





VOLUME SIX HUNDRED

# **METHODS IN ENZYMولوجY**

Mechanisms of DNA Recombination  
and Genome Rearrangements:  
Methods to Study Homologous  
Recombination

# METHODS IN ENZYMOLOGY

*Editors-in-Chief*

**ANNA MARIE PYLE**

*Departments of Molecular, Cellular and Developmental  
Biology and Department of Chemistry  
Investigator, Howard Hughes Medical Institute  
Yale University*

**DAVID W. CHRISTIANSON**

*Roy and Diana Vagelos Laboratories  
Department of Chemistry  
University of Pennsylvania  
Philadelphia, PA*

*Founding Editors*

**SIDNEY P. COLOWICK and NATHAN O. KAPLAN**



VOLUME SIX HUNDRED

# METHODS IN ENZYMولوجY

Mechanisms of DNA Recombination  
and Genome Rearrangements:  
Methods to Study Homologous  
Recombination

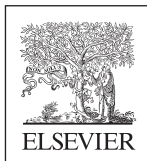
Edited by

**MARIA SPIES**

*University of Iowa Carver College of Medicine,  
Iowa City, IA, United States*

**ANNA MALKOVA**

*University of Iowa, Iowa City, IA, United states*



**ACADEMIC PRESS**

An imprint of Elsevier

Academic Press is an imprint of Elsevier  
50 Hampshire Street, 5th Floor, Cambridge, MA 02139, United States  
525 B Street, Suite 1800, San Diego, CA 92101–4495, United States  
The Boulevard, Langford Lane, Kidlington, Oxford OX5 1GB, United Kingdom  
125 London Wall, London, EC2Y 5AS, United Kingdom

First edition 2018

Copyright © 2018 Elsevier Inc. All rights reserved.

No part of this publication may be reproduced or transmitted in any form or by any means, electronic or mechanical, including photocopying, recording, or any information storage and retrieval system, without permission in writing from the publisher. Details on how to seek permission, further information about the Publisher's permissions policies and our arrangements with organizations such as the Copyright Clearance Center and the Copyright Licensing Agency, can be found at our website: [www.elsevier.com/permissions](http://www.elsevier.com/permissions).

This book and the individual contributions contained in it are protected under copyright by the Publisher (other than as may be noted herein).

### Notices

Knowledge and best practice in this field are constantly changing. As new research and experience broaden our understanding, changes in research methods, professional practices, or medical treatment may become necessary.

Practitioners and researchers must always rely on their own experience and knowledge in evaluating and using any information, methods, compounds, or experiments described herein. In using such information or methods they should be mindful of their own safety and the safety of others, including parties for whom they have a professional responsibility.

To the fullest extent of the law, neither the Publisher nor the authors, contributors, or editors, assume any liability for any injury and/or damage to persons or property as a matter of products liability, negligence or otherwise, or from any use or operation of any methods, products, instructions, or ideas contained in the material herein.

ISBN: 978-0-12-814429-9

ISSN: 0076-6879

For information on all Academic Press publications  
visit our website at <https://www.elsevier.com/books-and-journals>



Working together  
to grow libraries in  
developing countries

[www.elsevier.com](http://www.elsevier.com) • [www.bookaid.org](http://www.bookaid.org)

*Publisher:* Zoe Kruze

*Acquisition Editor:* Zoe Kruze

*Editorial Project Manager:* Alina Cleju

*Production Project Manager:* Divya KrishnaKumar

*Cover Designer:* Mark Roberts

Typeset by SPi Global, India

# CONTENTS

|  |             |
|--|-------------|
| <i>Contributors</i>  | <i>xiii</i> |
| <i>Preface</i>   | <i>xvii</i> |
| <b>1. Processing of DNA Double-Strand Breaks in Yeast</b>                          | <b>1</b>    |
| Robert Gnügge, Julyun Oh, and Lorraine S. Symington                                |             |
| 1. Introduction  | 2           |
| 2. Cell Cultivation and DSB Generation   | 4           |
| 3. Genomic DNA Extraction  | 6           |
| 4. DNA Quantification  | 7           |
| 5. Resection Quantification  | 8           |
| Acknowledgments  | 23          |
| References   | 23          |
| <b>2. Methods to Study DNA End Resection I: Recombinant Protein Purification</b>   | <b>25</b>   |
| Roopesh Anand, Cosimo Pinto, and Petr Cejka  |             |
| 1. Introduction to DNA End Resection   | 26          |
| 2. Expression of Recombinant Proteins in Insect Cells                              | 27          |
| 3. Large-Scale Protein Purification of DNA End Resection Proteins                  | 34          |
| Acknowledgments  | 59          |
| References   | 59          |
| <b>3. Methods to Study DNA End Resection II: Biochemical Reconstitution Assays</b> | <b>67</b>   |
| Cosimo Pinto, Roopesh Anand, and Petr Cejka  |             |
| 1. Introduction  | 68          |
| 2. Short-Range DNA End Resection by MRN and CtIP                                   | 69          |
| 3. Long-Range DNA End Resection by DNA2–BLM and DNA2–WRN                           | 87          |
| Acknowledgments  | 103         |
| References   | 103         |

---

|   |            |
|---|------------|
| <b>4. Direct Quantitative Monitoring of Homology-Directed DNA Repair of Damaged Telomeres</b>                 | <b>107</b> |
| Priyanka Verma, Robert L. Dilley, Melina T. Gyparakis, and Roger A. Greenberg                                 |            |
| 1. Introduction   | 108        |
| 2. Direct Detection of Break-Induced Telomere Synthesis   | 109        |
| 3. In Vivo Imaging of DNA Double-Strand Break-Induced Telomere Mobility                                       | 127        |
| References  | 131        |
| <b>5. Kinetic Analysis of the Exonuclease Activity of the Bacteriophage T4 Mre11–Rad50 Complex</b>            | <b>135</b> |
| Tibebe A. Teklemariam, Osvaldo D. Rivera, and Scott W. Nelson   |            |
| 1. Introduction   | 136        |
| 2. Assays Using Plasmids and PCR Products   | 138        |
| 3. End-Labeled Oligonucleotide Substrates   | 142        |
| 4. Determining Exonuclease Polarity   | 146        |
| 5. 2-Aminopurine-Based Oligonucleotide Substrates   | 148        |
| 6. Conclusions  | 153        |
| References  | 153        |
| <b>6. Expression, Purification, and Biochemical Evaluation of Human RAD51 Protein</b>                         | <b>157</b> |
| Shyamal Subramanyam and Maria Spies   |            |
| 1. Introduction   | 158        |
| 2. System for the Bacterial Expression of Human RAD51 Protein   | 159        |
| 3. Equipment, Materials, and Reagents   | 160        |
| 4. Bacterial Expression of the RAD51 Protein From the pCH1/RAD51o Plasmid                                     | 163        |
| 5. Purification of RAD51  | 164        |
| 6. FRET-Based DNA-Binding Assay to Measure ssDNA-Binding Activity of the RAD51 Recombinase                    | 167        |
| 7. Three-Strand DNA Strand Exchange Assay   | 170        |
| 8. Conclusions  | 175        |
| Acknowledgments   | 176        |
| References  | 176        |
| <b>7. Determining the RAD51-DNA Nucleoprotein Filament Structure and Function by Cryo-Electron Microscopy</b> | <b>179</b> |
| Lingyun Zhao, Jingfei Xu, Weixing Zhao, Patrick Sung, and Hong-Wei Wang                                       |            |
| 1. Introduction   | 180        |
| 2. Purification of hRAD51   | 183        |
| 3. Assembly of Presynaptic, Postsynaptic, and Arrested Synaptic Complexes                                     | 184        |

|   |            |
|---|------------|
| 4. Negative Staining EM   | 185        |
| 5. Cryo-EM Sample Preparation   | 187        |
| 6. Cryo-EM Data Collection  | 188        |
| 7. Image Processing and Reconstruction  | 189        |
| 8. Conclusion and Perspectives  | 195        |
| Acknowledgments   | 195        |
| References  | 196        |
| <b>8. Observation and Analysis of RAD51 Nucleation Dynamics at Single-Monomer Resolution</b>                  | <b>201</b> |
| Shyamal Subramanyam, Colin D. Kinz-Thompson, Ruben L. Gonzalez Jr., and Maria Spies                           |            |
| 1. Introduction   | 202        |
| 2. Observing RAD51 Nucleation on ssDNA Using Total Internal Reflection Fluorescence Microscopy                | 206        |
| 3. Ensemble Analysis of Single-Molecule Data  | 217        |
| 4. Real-Time Observation and Analysis of RAD51 Nucleation Using ebFRET  | 219        |
| 5. Conclusions  | 227        |
| Acknowledgments   | 229        |
| References  | 229        |
| <b>9. TIRF-Based Single-Molecule Detection of the RecA Presynaptic Filament Dynamics</b>                      | <b>233</b> |
| Sung H. Kim   |            |
| 1. Introduction   | 234        |
| 2. Total Internal Reflection Fluorescence-Based SM-FRET Measurement   | 236        |
| 3. Nucleation   | 241        |
| 4. End-Dependent Presynaptic Filament Dynamics  | 243        |
| 5. Protein Scaffold Shift Within Presynaptic Filament   | 246        |
| 6. ATP-Dependent Conformational Change  | 248        |
| 7. Conclusions  | 251        |
| Acknowledgment  | 251        |
| References  | 251        |
| <b>10. The RadA Recombinase and Paralogs of the Hyperthermophilic Archaeon <i>Sulfolobus solfataricus</i></b> | <b>255</b> |
| Michael L. Rolfmeier and Cynthia A. Haseltine   |            |
| 1. Introduction   | 256        |
| 2. Biochemical Approaches to Study of the <i>S. solfataricus</i> SsoRadA Protein and Its Paralogs             | 258        |

|   |            |
|---|------------|
| 3. Methods Shared Across Protocols  | 259        |
| 4. Heterologous Protein Purification  | 261        |
| 5. ATPase Activity Assays   | 272        |
| 6. DNA and ATP Binding Assays   | 276        |
| 7. Mechanistic Recombination Assays   | 279        |
| 8. Summary and Conclusion   | 282        |
| References  | 283        |
| <br>  |            |
| <b>11. Reconstituting the 4-Strand DNA Strand Exchange</b>  | <b>285</b> |
| Olga M. Mazina and Alexander V. Mazin   |            |
| 1. Introduction   | 286        |
| 2. Preparation of DNA Substrates for 4-Strand DNA Exchange  | 288        |
| 3. Preparation of Joint Molecules   | 297        |
| 4. Branch Migration of Joint Molecules  | 300        |
| 5. Summary and Conclusion   | 303        |
| Acknowledgments   | 304        |
| References  | 304        |
| Further Reading   | 305        |
| <br>  |            |
| <b>12. Purification of <i>Saccharomyces cerevisiae</i> Homologous Recombination Proteins Dmc1 and Rdh54/Tid1 and a Fluorescent D-Loop Assay</b> | <b>307</b> |
| Yuen-Ling Chan and Douglas K. Bishop  |            |
| 1. Introduction   | 308        |
| 2. Overexpression of Dmc1   | 310        |
| 3. Purification of Dmc1   | 312        |
| 4. D-Loop Assay Using Fluorescent Dye-Tagged ssDNA  | 317        |
| Acknowledgment  | 319        |
| References  | 319        |
| <br>  |            |
| <b>13. Probing Dynamic Assembly and Disassembly of Rad51 Tuned by Srs2 Using smFRET</b>   | <b>321</b> |
| Yupeng Qiu, Hye Ran Koh, and Sua Myong  |            |
| 1. Filament Formation by Rad51  | 322        |
| 2. ATP-Dependent Activity of Srs2 on DNA  | 328        |
| 3. The Srs2 Activity on the Rad51 Filament  | 339        |
| 4. Conclusions  | 343        |
| References  | 343        |

---

|   |            |
|---|------------|
| <b>14. The Recombination Mediator BRCA2: Architectural Plasticity of Recombination Intermediates Revealed by Single-Molecule Imaging (SFM/TIRF)</b> | <b>347</b> |
| Arshdeep Sidhu, Dejan Ristic, Humberto Sánchez, and Claire Wyman  |            |
| 1. Introduction   | 348        |
| 2. Organization and Architectural Plasticity of Protein and DNA–Protein Assemblies: Single-Molecule SFM Imaging                                     | 350        |
| 3. SFM Imaging to Reveal and Quantify Protein Architectural Plasticity  | 354        |
| 4. SFM Analysis of RAD51 Filament and Joint Molecules   | 358        |
| 5. Identifying Specific Proteins in Complex Structures by Fluorescence: BRCA2–RAD51 Complexes Analyzed by TIRF–SFM                                  | 364        |
| 6. Conclusions  | 371        |
| References  | 371        |
| <b>15. Single-Molecule Dynamics and Localization of DNA Repair Proteins in Cells</b>  | <b>375</b> |
| Maarten W. Paul, Alex N. Zelensky, Claire Wyman, and Roland Kanaar  |            |
| 1. Introduction   | 376        |
| 2. Generating Cells With Endogenously Expressed Fusion Proteins for Live-Cell Imaging   | 378        |
| 3. Mobility Assays  | 389        |
| 4. Relative Position of Proteins in DSB Foci  | 396        |
| 5. Conclusion/Perspective   | 403        |
| References  | 404        |
| <b>16. Single-Stranded DNA Curtains for Studying the Srs2 Helicase Using Total Internal Reflection Fluorescence Microscopy</b>                      | <b>407</b> |
| Luisina De Tullio, Kyle Kaniecki, and Eric C. Greene  |            |
| 1. Introduction   | 408        |
| 2. Methods  | 412        |
| 3. Conclusions and Future Directions  | 433        |
| Acknowledgments   | 433        |
| References  | 434        |
| <b>17. Single-Molecule Analysis of Replication Protein A–DNA Interactions</b>   | <b>439</b> |
| Fletcher E. Bain, Laura A. Fischer, Ran Chen, and Marc S. Wold  |            |
| 1. Expression and Purification of RPA   | 440        |
| 2. Labeling of RPA  | 444        |

---

|  |            |
|--|------------|
| 3. Single-Molecule Analysis of RPA–DNA Interactions: How to Do It                              | 446        |
| Acknowledgments  | 460        |
| References   | 460        |
| <b>18. Single-Molecule Studies of ssDNA-Binding Proteins Exchange</b>                          | <b>463</b> |
| Olivia Yang and Taekjip Ha   |            |
| 1. Introduction  | 464        |
| 2. Single-Molecule FRET Experimental Strategies  | 465        |
| 3. Notes   | 474        |
| 4. Summary   | 476        |
| Acknowledgments  | 477        |
| References   | 477        |
| <b>19. Dissecting the Recombination Mediator Activity of BRCA2 Using Biochemical Methods</b>   | <b>479</b> |
| Catharina von Nicolai, Åsa Ehlén, Juan S. Martinez, and Aura Carreira                          |            |
| 1. Introduction  | 480        |
| 2. Biochemical Assays to Study the Mediator Function of BRCA2                                  | 481        |
| 3. Conclusions and Future Directions   | 509        |
| References   | 510        |
| <b>20. Approaches to Understanding the Mediator Function of Brh2 in <i>Ustilago maydis</i></b> | <b>513</b> |
| Qingwen Zhou, William K. Holloman, and Milorad Kojic   |            |
| 1. Introduction  | 514        |
| 2. Biochemical Methods   | 516        |
| 3. Genetic Methods   | 519        |
| Acknowledgments  | 523        |
| References   | 523        |
| <b>21. GEN1 Endonuclease: Purification and Nuclease Assays</b>                                 | <b>527</b> |
| Ying Wai Chan and Stephen C. West  |            |
| 1. Introduction  | 528        |
| 2. Purification of GEN1  | 529        |
| 3. Cleavage of Synthetic DNA Substrates  | 533        |
| 4. Cleavage of Cruciform-Containing Plasmids by GEN1   | 538        |
| 5. Summary   | 540        |
| Acknowledgments  | 540        |
| References   | 541        |

---

|  |            |
|--|------------|
| <b>22. Biochemical and Structural Properties of Fungal Holliday Junction-Resolving Enzymes</b> | <b>543</b> |
| Yijin Liu, Alasdair Freeman, Anne-Cécile Déclais, Anton Gartner, and David M.J. Lilley         |            |
| 1. Holliday Junctions and Their Resolution   | 544        |
| 2. The Resolution Process  | 544        |
| 3. A Mechanism Ensuring Productive Junction Resolution   | 546        |
| 4. Processing of Holliday Junctions in Eukaryotes  | 550        |
| 5. Genes for the FEN1/XPG1 Superfamily in Thermophilic Fungi                                   | 551        |
| 6. Expression and Purification of GEN1 From <i>C. thermophilum</i>                             | 552        |
| 7. The Biochemical Properties of CtGEN1  | 553        |
| 8. The Crystal Structure of a CtGEN1-Product Complex   | 560        |
| 9. The Interaction of CtGEN1 With Four-Way DNA Junctions Deduced From the Crystal Lattice      | 562        |
| 10. Comparison With Other Junction-Resolving Enzymes   | 563        |
| Acknowledgments  | 564        |
| References   | 564        |
| <br>   |            |
| <b>23. Preparation and Resolution of Holliday Junction DNA Recombination Intermediates</b>     | <b>569</b> |
| Rajvee Shah Punatar and Stephen C. West  |            |
| 1. Introduction  | 569        |
| 2. Preparation of DNA Substrates   | 571        |
| 3. Generation and Purification of $\alpha$ -Structures   | 583        |
| 4. In Vitro Resolution Assays  | 585        |
| 5. Notes   | 587        |
| Acknowledgments  | 588        |
| References   | 589        |

This page intentionally left blank

# CONTRIBUTORS

**Roopesh Anand**

Institute for Research in Biomedicine, Università della Svizzera italiana, Bellinzona, Switzerland

**Fletcher E. Bain**

University of Iowa Carver College of Medicine, Iowa City, IA, United States

**Douglas K. Bishop**

University of Chicago, Chicago, IL, United States

**Aura Carreira**

Institut Curie, PSL Research University; Paris Sud University, Paris-Saclay University, CNRS, UMR3348, Orsay, France

**Petr Cejka**

Institute for Research in Biomedicine, Università della Svizzera italiana, Bellinzona; Institute of Biochemistry, Swiss Federal Institute of Technology, Zurich, Switzerland

**Ying Wai Chan**

The Francis Crick Institute, London, United Kingdom

**Yuen-Ling Chan**

University of Chicago, Chicago, IL, United States

**Ran Chen**

Washington University, St. Louis, MO, United States

**Anne-Cécile Déclais**

Cancer Research UK Nucleic Acid Structure Research Group, The University of Dundee, Dundee, United Kingdom

**Luisina De Tullio**

Columbia University, New York, NY, United States

**Robert L. Dilley**

Basser Research Center for BRCA, Perelman School of Medicine, University of Pennsylvania, Philadelphia, PA, United States

**Åsa Ehlén**

Institut Curie, PSL Research University; Paris Sud University, Paris-Saclay University, CNRS, UMR3348, Orsay, France

**Laura A. Fischer**

University of Iowa Carver College of Medicine, Iowa City, IA, United States

**Alasdair Freeman**

Cancer Research UK Nucleic Acid Structure Research Group, The University of Dundee, Dundee, United Kingdom

**Anton Gartner**

Cancer Research UK Nucleic Acid Structure Research Group, The University of Dundee, Dundee, United Kingdom

**Robert Gnügge**

Columbia University Medical Center, New York, NY, United States

**Ruben L. Gonzalez Jr.**

Columbia University, New York, NY, United States

**Roger A. Greenberg**

Basser Research Center for BRCA, Perelman School of Medicine, University of Pennsylvania, Philadelphia, PA, United States

**Eric C. Greene**

Columbia University, New York, NY, United States

**Melina T. Gyparaki**

Basser Research Center for BRCA, Perelman School of Medicine, University of Pennsylvania, Philadelphia, PA, United States

**Taekjip Ha**

Johns Hopkins School of Medicine; Howard Hughes Medical Institute; Johns Hopkins University, Baltimore, MD, United States

**Cynthia A. Haseltine**

School of Molecular Biosciences, Washington State University, Pullman, WA, United States

**William K. Holloman**

Weill Cornell Medical College, New York, NY, United States

**Roland Kanaar**

Department of Molecular Genetics, Cancer Genomics Center Netherlands, Erasmus University Medical Center, Rotterdam, The Netherlands

**Kyle Kaniecki**

Columbia University, New York, NY, United States

**Sung H. Kim**

School of Biological Science, Institute of Molecular Biology and Genetics, Seoul National University, Seoul, Republic of Korea

**Colin D. Kinz-Thompson**

Columbia University, New York, NY, United States

**Hye Ran Koh**

Johns Hopkins University, Baltimore, MD, United States; Chung-Ang University, Seoul, South Korea

**Milorad Kojic**

Weill Cornell Medical College, New York, NY, United States

**David M.J. Lilley**

Cancer Research UK Nucleic Acid Structure Research Group, The University of Dundee, Dundee, United Kingdom

**Yijin Liu**

Cancer Research UK Nucleic Acid Structure Research Group, The University of Dundee, Dundee, United Kingdom

**Juan S. Martinez**

Institut Curie, PSL Research University; Paris Sud University, Paris-Saclay University, CNRS, UMR3348, Orsay, France

**Alexander V. Mazin**

Drexel University College of Medicine, Philadelphia, PA, United States

**Olga M. Mazina**

Drexel University College of Medicine, Philadelphia, PA, United States

**Sua Myong**

Johns Hopkins University, Baltimore, MD, United States

**Scott W. Nelson**

Iowa State University, Ames, IA, United States

**Julyun Oh**

Columbia University Medical Center, New York, NY, United States

**Maarten W. Paul**

Department of Molecular Genetics, Cancer Genomics Center Netherlands, Erasmus University Medical Center, Rotterdam, The Netherlands

**Cosimo Pinto**

Institute of Molecular Cancer Research, University of Zurich, Zurich, Switzerland

**Yupeng Qiu**

Johns Hopkins University, Baltimore, MD, United States

**Dejan Ristic**

Erasmus University Medical Center, Rotterdam, The Netherlands

**Oswaldo D. Rivera**

Iowa State University, Ames, IA, United States

**Michael L. Rolfsmeier**

School of Molecular Biosciences, Washington State University, Pullman, WA, United States

**Humberto Sánchez**

Kavli Institute of Nanoscience, Faculty of Applied Sciences, Delft University of Technology, Delft, The Netherlands

**Rajvee Shah Punatar**

The Francis Crick Institute, London, United Kingdom

**Arshdeep Sidhu**

Erasmus University Medical Center, Rotterdam, The Netherlands

**Maria Spies**

University of Iowa Carver College of Medicine, Iowa City, IA, United States

**Shyamal Subramanyam**

University of Iowa Carver College of Medicine, Iowa City, IA, United States

**Patrick Sung**

Yale University, New Haven, CT, United States

**Lorraine S. Symington**

Columbia University Medical Center, New York, NY, United States

**Tibebe A. Teklemariam**

Iowa State University, Ames, IA, United States

**Priyanka Verma**

Basser Research Center for BRCA, Perelman School of Medicine, University of Pennsylvania, Philadelphia, PA, United States

**Catharina von Nicolai**

Institut Curie, PSL Research University; Paris Sud University, Paris-Saclay University, CNRS, UMR3348, Orsay, France

**Hong-Wei Wang**

Ministry of Education Key Laboratory of Protein Sciences, Tsinghua-Peking Joint Center for Life Sciences, Beijing Advanced Innovation Center for Structural Biology, School of Life Sciences, Tsinghua University, Beijing, China

**Stephen C. West**

The Francis Crick Institute, London, United Kingdom

**Marc S. Wold**

University of Iowa Carver College of Medicine, Iowa City, IA, United States

**Claire Wyman**

Department of Molecular Genetics, Cancer Genomics Center Netherlands; Department of Radiation Oncology, Erasmus University Medical Center, Rotterdam, The Netherlands

**Jingfei Xu**

Ministry of Education Key Laboratory of Protein Sciences, Tsinghua-Peking Joint Center for Life Sciences, Beijing Advanced Innovation Center for Structural Biology, School of Life Sciences, Tsinghua University, Beijing, China

**Olivia Yang**

Johns Hopkins School of Medicine, Baltimore, MD, United States

**Alex N. Zelensky**

Department of Molecular Genetics, Cancer Genomics Center Netherlands, Erasmus University Medical Center, Rotterdam, The Netherlands

**Lingyun Zhao**

Ministry of Education Key Laboratory of Protein Sciences, Tsinghua-Peking Joint Center for Life Sciences, Beijing Advanced Innovation Center for Structural Biology, School of Life Sciences, Tsinghua University, Beijing, China

**Weixing Zhao**

Yale University, New Haven, CT, United States

**Qingwen Zhou**

Weill Cornell Medical College, New York, NY, United States

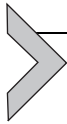
## PREFACE

Homologous genetic recombination remains the most enigmatic process in DNA metabolism. The molecular machines of recombination preserve the integrity of the genetic material in all organisms and generate genetic diversity in evolution. The same molecular machines that support genetic integrity by orchestrating accurate repair of the most deleterious DNA lesions, however, also promote survival of cancerous cells and emergence of radiation and chemotherapy resistance. The machinery and the cellular process of recombination are intrinsically interconnected with those of DNA replication and repair. Recent work from many labs has revealed new and deeper connections between these 3Rs of genome maintenance.

These two volumes in this “Mechanisms of DNA Recombination and Genome Rearrangements” set offer a comprehensive set of cutting-edge methods to study various aspects of homologous recombination and cellular processes that utilize the enzymatic machinery of recombination. The two volumes feature contributions by the leading experts in the field of DNA repair, recombination, replication, and genome stability. The chapters within document methods are presently cutting edge, but will become a standard laboratory practice in the years to come. The first volume in the set (Volume 600, “Mechanisms of DNA Recombination and Genome Rearrangements: Methods to Study Homologous Recombination”) concerns with the methods to study the initiation of homologous recombination, the central step in recombination, which involves formation of the recombinase nucleoprotein filament, homology search and DNA strand exchange, and the methods to study the processing of the recombination intermediates through resolution or dissolution. The second volume in the series (Volume 601, “Mechanisms of DNA Recombination and Genome Rearrangements: Intersection Between Homologous Recombination, DNA Replication, and DNA Repair”) focuses on the methods to study the interface between recombination and replication, selection of recombination as homology-directed DNA repair pathway, homologous recombination machinery as a target for anticancer drug discovery, and meiotic recombination. In addition, the second volume covers a number of topics that recently emerged in the field of recombination, including mutagenesis associated with recombination, recombination between RNA and DNA, recombination initiated by DNA nicks, and recombination in a context of heterochromatin.

We selected the topics and contributors with a goal that these volumes to become a useful reference for the researchers engaged in the field of DNA repair, DNA recombination, DNA replication, and genome stability. The techniques described in the chapters range from cellular imaging to biochemical, structural, and single-molecule approaches, to drug discovery and next-generation sequencing. We hope to see this two-volume set as a well-used reference in the labs actively studying these processes and those contemplating entering the field. The chapters are written in a way to make the methodology accessible not only to the established experts but to a broader group of researchers, from undergraduates and rotation students to postdoctoral fellows and faculty who wish to expand their research programs.

MARIA SPIES AND ANNA MALKOVA  
University of Iowa



# Processing of DNA Double-Strand Breaks in Yeast

Robert Gnügge<sup>2</sup>, Julyun Oh<sup>2</sup>, Lorraine S. Symington<sup>1</sup>

Columbia University Medical Center, New York, NY, United States

<sup>1</sup>Corresponding author: e-mail address: lss5@cumc.columbia.edu

## Contents

|  |    |
|--|----|
| 1. Introduction  | 2  |
| 2. Cell Cultivation and DSB Generation                         | 4  |
| 2.1 Equipment  | 4  |
| 2.2 Solutions and Reagents                                     | 4  |
| 2.3 Procedure  | 5  |
| 2.4 Notes  | 6  |
| 3. Genomic DNA Extraction                                      | 6  |
| 3.1 Equipment  | 6  |
| 3.2 Solutions and Reagents                                     | 7  |
| 3.3 Procedure  | 7  |
| 3.4 Note   | 7  |
| 4. DNA Quantification  | 7  |
| 4.1 Equipment  | 8  |
| 4.2 Solutions and Reagents                                     | 8  |
| 4.3 Procedure  | 8  |
| 4.4 Note   | 8  |
| 5. Resection Quantification                                    | 8  |
| 5.1 Band Disappearance Assay                                   | 8  |
| 5.2 Alkaline Gel Electrophoresis to Detect ssDNA Intermediates | 15 |
| 5.3 Quantitative PCR   | 18 |
| Acknowledgments  | 23 |
| References   | 23 |

## Abstract

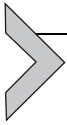
Single-stranded DNA (ssDNA) intermediates are essential for homology-dependent repair of DNA double-strand breaks (DSBs) and for the DNA damage response. Here we describe methods routinely used to identify ssDNA intermediates formed by end

<sup>2</sup> Equally contributed.

processing of site-specific DSBs in *Saccharomyces cerevisiae*. These methods have been applied in other model systems and human cell lines, and are useful tools to gain insight into the enzymes that process DSBs and how they are regulated.

## ABBREVIATIONS

|              |                            |
|--------------|----------------------------|
| <b>DSB</b>   | double-strand break        |
| <b>dsDNA</b> | double-stranded DNA        |
| <b>HR</b>    | homologous recombination   |
| <b>NHEJ</b>  | nonhomologous end joining  |
| <b>qPCR</b>  | quantitative real-time PCR |
| <b>RPA</b>   | replication protein A      |
| <b>ssDNA</b> | single-stranded DNA        |



## 1. INTRODUCTION

DNA double-strand breaks (DSBs) are hazardous lesions that must be accurately repaired to maintain genome integrity. Eukaryotic cells have two main mechanisms to repair DSBs: nonhomologous end joining (NHEJ) and homologous recombination (HR) (Ceccaldi, Rondinelli, & D'Andrea, 2016). NHEJ involves the direct ligation of the DSB ends, while HR uses an undamaged homologous duplex as a template for repair. The choice between these pathways is governed by an early step of HR, namely, degradation of the 5' terminated strands to generate long stretches of single-stranded DNA (ssDNA), a process termed end resection (Symington, Rothstein, & Lisby, 2014). The ssDNA overhangs produced by end resection are essential for Rad51-catalyzed strand invasion as well as for DNA damage checkpoint signaling (Finn, Lowndes, & Grenon, 2012; Symington et al., 2014). While the initiation of end resection is crucial for HR, extensive tracts of ssDNA are detrimental to cells because they are prone to degradation or modification of exposed bases (Roberts et al., 2012; Zierhut & Diffley, 2008). Consequently, how cells regulate the initiation and extent of end resection is a major focus of scientific inquiry.

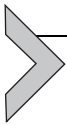
Studies in the budding yeast *Saccharomyces cerevisiae* have led the way in identification of the nucleases that catalyze end resection in eukaryotes, and in elucidating how they are regulated (Symington, 2016). Molecular analysis of end resection has been facilitated by use of the rare-cutting endonucleases, HO or I-SceI, expressed from a galactose-inducible promoter

(Mimitou & Symington, 2008; Plessis, Perrin, Haber, & Dujon, 1992; White & Haber, 1990). In the case of HO, >95% of cells in a population of growing cells endure a single DSB at the mating-type (*MAT*) locus 60 min after expression of the endonuclease. Normally, the HO-induced DSB is repaired using one of two transcriptionally silent donor cassettes, *HML* or *HMR*, as templates (Haber, 2012). To study end resection without the complication of competing repair intermediates, the donor cassettes are deleted or strand invasion is prevented by a *rad51Δ* mutation. I-SceI endonuclease has no natural site in the nuclear genome of yeast, but synthetic sites have been introduced at various loci to provide targets for I-SceI cleavage (Plessis et al., 1992). The disadvantage of using I-SceI is the lower cutting efficiency as compared with HO. Resection can also be studied during meiosis where the Spo11 topoisomerase-like protein creates DSBs at around 160 sites in the yeast genome. In yeast strains with highly synchronous meiosis, resection at Spo11 hotspots is readily detected by physical and sequencing-based approaches (Cao, Alani, & Kleckner, 1990; Mimitou, Yamada, & Keeney, 2017; Sun, Treco, & Szostak, 1991).

Here, we describe the methods used by our laboratory to measure resection tract lengths in mitotically dividing *S. cerevisiae*. Similar techniques have been applied to fission yeast and human cells (Langerak, Mejia-Ramirez, Limbo, & Russell, 2011; Zhou, Caron, Legube, & Paull, 2014). These methods capitalize on the finding that most restriction endonucleases cleave their recognition sites in double stranded (ds), but not ssDNA. Prior to the onset of end resection, restriction endonuclease sites in sequences flanking the DSB are sensitive to cleavage. As resection proceeds from the DSB 5' ends, the flanking DNA becomes progressively single stranded, rendering it resistant to cleavage by restriction endonucleases. Therefore, resistance to digestion can be used to detect resection intermediates by Southern blot hybridization of genomic DNA with appropriate probes or by quantitative PCR (qPCR) methods, as described in detail below (White & Haber, 1990; Zierhut & Diffley, 2008). Since end resection results in loss of one of the template strands, qPCR can be used to detect the corresponding 50% reduction in signal as an alternative to the method described here (Eapen, Sugawara, Tsabar, Wu, & Haber, 2012). In addition, Lydall and colleagues developed a PCR-based method to detect ssDNA at telomeres that has also been used to measure resection at DSBs (Zubko, Maringele, Foster, & Lydall, 2006).

Several other molecular and cytological methods are currently in use to measure end resection in yeast and mammalian cells. For example, since the ssDNA formed by end resection is initially bound by replication protein

A (RPA), focus formation of fluorescently tagged RPA or RPA enrichment at a DSB as measured by chromatin immunoprecipitation can be used to detect resection intermediates (Bantele, Ferreira, Gritenaite, Boos, & Pfander, 2017; Barlow, Lisby, & Rothstein, 2008; Yamane et al., 2013). Another method takes advantage of an antibody that recognizes bromodeoxyuridine (BrdU) incorporated into DNA only when the DNA is single stranded. Cells grown in the presence of BrdU incorporate the modified nucleotide during DNA replication. After treating cells with a DSB-inducing agent, such as ionizing radiation, the resected ends can be detected cytologically using the BrdU antibody, by FACS, or by analysis of stretched chromatin fibers gently isolated from cells (Cruz-García, Lopez-Saavedra, & Huertas, 2014; Sartori et al., 2007; Tkac et al., 2016). The advantage of the RPA focus formation and BrdU methods is that they can be applied to DSB-inducing agents that cleave genomic DNA randomly.



## 2. CELL CULTIVATION AND DSB GENERATION

We use yeast strains with an integrated *GAL10-HO* cassette to control DSB formation at the *MAT* locus (Herskowitz & Jensen, 1991). The cells are precultured in YPL (Note 1) to repress *HO* expression and then arrested in the G2/M phase such that the cells are in a resection-proficient cell cycle stage (Note 2) (Symington, 2016). We induce *HO* expression by addition of galactose to the medium and then collect samples in a time course experiment.

### 2.1 Equipment

- Temperature-controlled orbital shaker with tube and flask holders
- Sterile 50-mL glass culture tubes with lids
- Sterile 500-mL baffled culture flasks with lids
- Spectrophotometer and cuvettes (or alternative equipment) for cell titer determination
- Cooled centrifuge for 50-mL centrifugation tubes
- Cooled centrifuge for 1.5-mL centrifugation tubes
- 50-mL disposable centrifugation tubes
- 1.5-mL disposable centrifugation tubes

### 2.2 Solutions and Reagents

- YPD agar plates (1% yeast extract; 2% peptone; 2% glucose; 1.5% agar)
- YPL liquid media (1% yeast extract; 2% peptone; 3.15% lactic acid; adjusted to pH 5.5 with sodium hydroxide)

- Yeast strains (*MATa* or *MATα leu2::GAL10-HO::LEU2 hmlΔ hmrΔ*, and further mutations whose influence on resection is to be analyzed)
- DMSO
- Nocodazole, 2 mg/mL in DMSO (store at  $-20^{\circ}\text{C}$ )
- Sodium azide, 10% in water (store at  $4^{\circ}\text{C}$ )
- TE (10 mM Tris-HCl, pH 8.0; 1 mM EDTA) with 0.1% sodium azide (prepare freshly, store on ice)
- 20% galactose in water (dissolve at room temperature, filter sterilize, store at room temperature)

### 2.3 Procedure

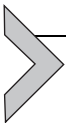
1. Restreak yeast strains on YPD agar plates and grow overnight at  $30^{\circ}\text{C}$ .
2. Inoculate a small amount of cells into 5 mL of YPL in a 50-mL glass tube and grow overnight at  $30^{\circ}\text{C}$  with vigorous shaking (e.g., 200 rpm with a 2.5-cm circular shaking orbit).
3. In the morning of the following day, dilute the cultures into 5 mL YPL medium in a 50-mL glass tube, adjusting the cell density, such that the culture is in mid-log growth phase in the evening ( $\sim 2 \times 10^7$  cells/mL). Grow at  $30^{\circ}\text{C}$  with vigorous shaking.
4. In the evening, dilute the culture into 100 mL YPL medium in a 500-mL baffled culture flask (Note 3), adjusting the cell density, such that a titer of  $\sim 5 \times 10^6$  cells/mL is expected the next morning. Grow overnight at  $30^{\circ}\text{C}$  with vigorous shaking.
5. In the morning of the following day, adjust the cell titer to  $5 \times 10^6$  cells/mL.
6. Add DMSO to a final concentration of 1%.
7. Add Nocodazole to a final concentration of 13.33  $\mu\text{g}/\text{mL}$ .
8. Grow for 2 h at  $30^{\circ}\text{C}$  with vigorous shaking.
9. Add Nocodazole to an accumulative final concentration of 20  $\mu\text{g}/\text{mL}$ .
10. Grow for 1 h at  $30^{\circ}\text{C}$  with vigorous shaking.
11. Check G2/M arrest microscopically. The vast majority of cells should have large buds and show the characteristic “dumbbell” shape (Rosebrock, 2017). Grow longer and recheck microscopically if necessary.
12. Collect the first cell culture sample (around  $1.5 \times 10^8$  cells per time point). Add sodium azide to a final concentration of 0.1% and handle the samples on ice subsequently. Pellet cells by centrifugation at  $4^{\circ}\text{C}$  and  $2000 \times g$  for 5 min. Decant supernatant. Resuspend pellets in 1 mL TE with 0.1% sodium azide. Transfer into 1.5-mL centrifugation tubes.

Pellet cells by centrifugation at 4°C at top speed for 2 min. Remove supernatant by pipetting. Store pellets at −20°C.

13. Add galactose to the remaining culture to a final concentration of 2% and continue growth at 30°C with vigorous shaking.
14. Collect further samples as described in step 12. We usually collect samples 0, 0.5, 1, 2, 4, and 6 h after galactose addition.

## 2.4 Notes

1. Other nonrepressing carbon sources, such as raffinose, can be used instead of lactate in the growth medium.
2. End resection is repressed in the G1 phase of the cell cycle and highest during S phase (Ira et al., 2004; Zierhut & Diffley, 2008). To ensure homogeneity of cell cycle phase when comparing different strains, we prefer to use G2–M arrested cells, even though resection levels are lower compared with exponentially grown cultures (Ira et al., 2004).
3. For correct cell titer adjustments in steps 3 and 4, record growth curves of the strains in YPL. As a rough estimate, our yeast strains usually have a 0.5-fold longer generation time in YPL than in YPD.



## 3. GENOMIC DNA EXTRACTION

We routinely extract genomic DNA from the collected cell pellets using a glass bead/phenol method (Hoffman & Winston, 1987) or using a commercial kit (Epicentre MasterPure™ Yeast DNA Purification Kit). A more gentle method to extract DNA involving enzymatic removal of the yeast cell walls can be used and is recommended for the alkali gel method (Section 5.2), but this requires more time and handling steps (Borner & Cha, 2015). The quick prep glass bead/phenol method is fast and inexpensive, but the DNA is more fragmented. We usually recover 3–15 µg of genomic DNA from each of the collected samples ( $1.5 \times 10^8$  cells).

### 3.1 Equipment

- Cooled centrifuge for 1.5-mL centrifuge tubes
- 1.5-mL disposable centrifuge tubes
- Vortexer with foam platform attachment for 1.5-mL centrifuge tubes
- Water bath (37°C)

### 3.2 Solutions and Reagents

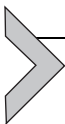
- Break buffer: 2% Triton X-100, 1% SDS, 0.1 M sodium chloride, 10 mM Tris-HCl (pH 8.0), 1 mM EDTA
- Acid-washed glass beads, 0.4–0.6 mm in diameter (Sigma)
- Phenol:chloroform:isoamylalcohol (25:24:1)
- RNase A: 5 mg/mL in 0.01 M sodium acetate, pH 7.4 (boil for 15 min to destroy DNase, aliquot, and store at  $-20^{\circ}\text{C}$ )
- 4 M ammonium acetate ( $\text{NH}_4\text{OAc}$ )
- Ethanol
- TE (10 mM Tris-HCl, pH 8.0; 1 mM EDTA)

### 3.3 Procedure

1. Add 200  $\mu\text{L}$  of Break buffer to cell pellet.
2. Add about 0.3 g acid-washed glass beads.
3. Add 200  $\mu\text{L}$  of phenol:chloroform:isoamylalcohol (25:24:1).
4. Vortex for 3 min (Note 1).
5. Add 200  $\mu\text{L}$  of TE.
6. Centrifuge for 5 min at top speed.
7. Transfer aqueous layer to new 1.5-mL centrifuge tube.
8. Add 1 mL of 100% Ethanol and invert to mix.
9. Centrifuge for 1 min at top speed.
10. Decant Ethanol and dry the pellet for 5 min.
11. Resuspend the pellet in 0.4 mL TE and add 5  $\mu\text{L}$  of 5 mg/mL RNase A.
12. Incubate the samples at  $37^{\circ}\text{C}$  for 10 min.
13. Add 10  $\mu\text{L}$  of 4 M  $\text{NH}_4\text{OAc}$  and 1 mL of Ethanol. Invert to mix.
14. Centrifuge for 1 min at top speed.
15. Decant and wash the pellet with 1 mL of 70% Ethanol.
16. Centrifuge for 1 min at top speed, decant, and dry the pellet.
17. Resuspend the pellet in 50–100  $\mu\text{L}$  of TE.

### 3.4 Note

1. Longer vortexing gives higher DNA yields, but the DNA is more fragmented.



---

## 4. DNA QUANTIFICATION

For DNA quantification, we use the QuantiFluor<sup>®</sup> dsDNA Kit from Promega with some adjustments of the manufacturer's instructions. We found that this fluorescence-based method results in more reliable

quantification compared to absorption-based methods, which usually overestimate DNA concentrations (data not shown).

## 4.1 Equipment

- 96-well plates
- 96-well plate reader with 504 nm excitation and 531 nm emission filter (e.g., TECAN infinite M200)

## 4.2 Solutions and Reagents

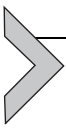
- QuantiFluor<sup>®</sup> dsDNA Kit from Promega

## 4.3 Procedure

1. Prepare a dilution series of the kit's DNA standard (Note 1). Prepare 40  $\mu\text{L}$  of DNA solutions with 0, 0.3125, 0.625, 1.25, 2.5, 5, and 10 ng/ $\mu\text{L}$  in TE.
2. Dilute the genomic DNA solutions 1:100 in TE (40  $\mu\text{L}$  final volume).
3. Prepare DNA dye working solution by diluting the DNA dye 1:400 in TE.
4. Pipette 200  $\mu\text{L}$  of DNA dye working solution and 10  $\mu\text{L}$  of DNA standard or genomic DNA solution into a 96-well plate in technical triplicates. Mix by pipetting. Avoid air bubbles.
5. Incubate for 5 min in the dark.
6. Read fluorescence.
7. Analyze the data. Identify linear range of the DNA standard curve. Perform a linear regression. Calculate the concentration of the genomic DNA samples, taking the dilution factor into account.

## 4.4 Note

1. The DNA standard dilution series and the diluted genomic DNA sample can be conveniently prepared in a 96-well plate. Use a multichannel pipette for mixing and transfer into another 96-well plate preloaded with the DNA dye working solution.



---

## 5. RESECTION QUANTIFICATION

### 5.1 Band Disappearance Assay

In this assay, the disappearance of the HO-cut *StyI* (or *StyI* and *XhoI*) restriction fragment over time is used to obtain the fraction of resected

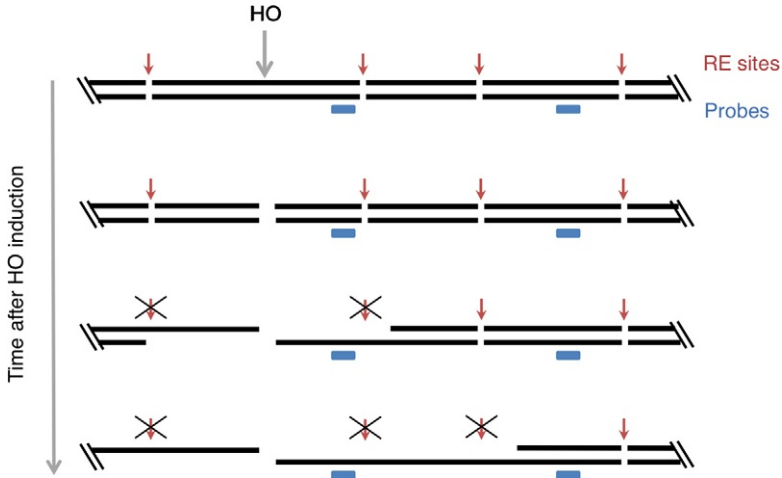


**Fig. 1** Schematic of the band disappearance assay. The cartoon shows the location of the HO-cut site and restriction endonuclease (RE) sites (not to scale). After DSB formation, the 5' ends are resected. As each RE site becomes single stranded, it becomes resistant to cleavage by the enzyme, resulting in disappearance of restriction fragments over time. Different probes are used to monitor disappearance of specific restriction fragments.

DNA (Fig. 1) (Ira et al., 2004; Zhu, Chung, Shim, Lee, & Ira, 2008). Genomic DNA is digested with *StyI* (or *StyI* and *XhoI*) restriction endonuclease and analyzed by Southern blot hybridization using a probe that recognizes a sequence on one side of the HO-induced DSB at the *MAT* locus. The 400bp *MAT* probe described here hybridizes to 1.8- or 0.9-kb fragments for *MAT $\alpha$*  or *MAT $\beta$*  cells, respectively, when digested with *StyI*. After HO cutting, the *MAT* probe hybridizes to a 0.7-kb fragment in both mating types. The intensity of the 0.7-kb HO-cut band diminishes over time as the *StyI* restriction site located 0.7kb from the HO cut becomes single stranded due to resection. An example is shown in Fig. 2. Resection intermediates can sometimes be seen as higher molecular weight species, but due to heterogeneity in length of the ssDNA overhangs they do not form discrete bands, unless alkali gels are used (see Section 5.2). DNA probes that hybridize to genomic regions flanked by *StyI* (or *StyI* and *XhoI*) restriction sites at various distances from the DSB site can be used to monitor extensive resection by their disappearance at later times (Fig. 1) (Zhu et al., 2008).

### 5.1.1 Equipment

- Glass baking dishes and glass plates (18 × 20 cm<sup>2</sup>)
- Orbital shaker

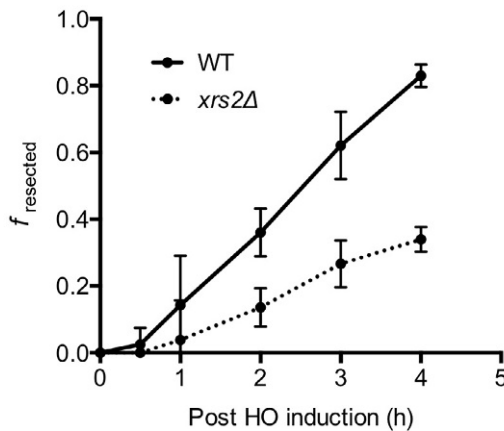
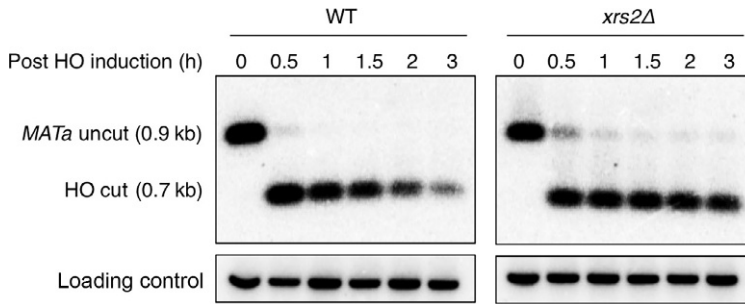


**Fig. 2** Band disappearance assay. Southern blot analysis of genomic DNA from wild-type (WT) and *xrs2Δ* cells digested with *StyI*. MAT 0.7 kb probe is used to detect MAT locus fragments and SAE2 ORF probe is used for loading control. The graph below shows quantification of three independent trials. The error bars indicate standard deviation (SD).

- UV cross-linker
- Hybridization oven
- Typhoon scanner (GE Healthcare)

### 5.1.2 Solutions and Reagents

- Primers (primer sequences are listed in Table 1)
- TBE: 0.1 M Tris, 0.1 M boric acid, 0.02 M EDTA
- Agarose

**Table 1** Sequences of Primers Used for Probes for the Band Disappearance Assay

| Primers <sup>a</sup>              | Sequence (5'-3')              | Restriction Enzyme(s)       | Probe Size (bp) | Targeted Fragment Size (kb) |
|-----------------------------------|-------------------------------|-----------------------------|-----------------|-----------------------------|
| MAT 0.7kb probe fw                | CTTAGCATCATTCTTTGTTCTTATC     | <i>StyI</i>                 | 405             | 0.7                         |
| MAT 0.7kb probe rev               | CCAAGGGAGAGAAGACTTG           |                             |                 |                             |
| MAT 2.7kb probe fw                | TCGTCCTCGGCATCAACAC           | <i>StyI</i> and <i>XhoI</i> | 710             | 2.4                         |
| MAT 2.7kb probe rev               | GGGTTTCAAGAATCTGTTTTCACT      |                             |                 |                             |
| MAT 6.8kb probe fw                | CGCCTCTTCAATCGAATCTCACC       | <i>StyI</i> and <i>XhoI</i> | 600             | 2.3                         |
| MAT 6.8kb probe rev               | GGCCATTGAAGAAGGTATTGTATTTGTTG |                             |                 |                             |
| MAT 11.5kb probe fw               | CGGTGAAGACTACGGTGAAG          | <i>StyI</i> and <i>XhoI</i> | 458             | 0.5                         |
| MAT 11.5kb probe rev              | GGCAAACGAGTGGCTCTTC           |                             |                 |                             |
| MAT 16kb probe fw                 | GGGTTTGCCTATTGAAAACTG         | <i>StyI</i> and <i>XhoI</i> | 617             | 2.8                         |
| MAT 16kb probe rev                | CAGCTCTTTCGATGAATTTTAATTTC    |                             |                 |                             |
| ADE2 5' ORF fw (loading control)  | TTCCAATCCTCTTGATATCG          | <i>StyI</i> and <i>XhoI</i> | 648             | 7                           |
| ADE2 5' ORF rev (loading control) | TCGTTAATAAGCAATTCCCC          |                             |                 |                             |
| ADE2 3' ORF fw (loading control)  | CACAACTCTGGACATTATACC         | <i>StyI</i> and <i>XhoI</i> | 879             | 1.4                         |
| ADE2 3' ORF rev (loading control) | ATAAGCTTCGTAACCGACAG          |                             |                 |                             |
| SAE2 ORF fw (loading control)     | GCTCTGATACTGTAATCCACGA        | <i>StyI</i>                 | 416             | 3.8                         |
| SAE2 ORF rev (loading control)    | TTTGTCCCTCGTTCCCTTCC          |                             |                 |                             |

<sup>a</sup>The primers and probes are designed to detect loss of the restriction enzyme site located at the indicated distance in kb from the HO-cut site.

- *StyI*, *XhoI* and  $10 \times$  CutSmart<sup>®</sup> Buffer (New England Biolabs)
- Depurination solution: 0.25 M HCl
- Denaturing solution: 0.5 M sodium hydroxide, 1.5 M sodium chloride
- Neutralization solution: 1 M Tris-HCl, pH 7.4; 1.5 M sodium chloride
- $20 \times$  SSC: 3 M sodium chloride, 0.3 M sodium citrate
- Wash solution 1:  $2 \times$  SSC + 0.1% SDS
- Wash solution 2:  $1 \times$  SSC + 0.1% SDS
- Amersham Hybond-N+ (GE Healthcare)
- Amersham Rapid-hyb buffer (GE Healthcare)
- [ $\alpha$ -<sup>32</sup>P]dCTP (PerkinElmer)
- RadPrime DNA Labeling System (Invitrogen)
- Illustra MicroSpin G-50 Columns (GE Healthcare)
- Whatman 3MM chromatography paper (GE Healthcare)
- Plastic wrap
- Parafilm

### 5.1.3 Procedure

1. Restriction enzyme digestion and DNA blotting
  1. Digest  $\sim 5 \mu\text{g}$  of genomic DNA with 20 U of restriction enzyme(s) in 35  $\mu\text{L}$  total reaction volume for 2 h at 37°C. Refer to [Table 1](#) for restriction enzyme(s).
  2. Separate DNA fragments by agarose gel electrophoresis (0.8%). Stain the gel with 0.5  $\mu\text{g}/\text{mL}$  ethidium bromide in TBE for 1 h to visualize the DNA ladder.
  3. Use a razor blade to remove unused areas of the gel and transfer it to a glass baking dish (Note 1).
  4. Rinse the gel with ddH<sub>2</sub>O two times and soak it with Depurination solution for 10 min with gentle shaking.
  5. Rinse the gel with ddH<sub>2</sub>O two times and soak it with Denaturing solution for 30 min with gentle shaking.
  6. Rinse the gel with ddH<sub>2</sub>O two times and soak it with Neutralization solution for 30 min with gentle shaking.
  7. Set up a transfer apparatus: Half fill a tray or glass baking dish with  $2 \times$  SSC. Place a glass plate on top to make a platform and cover with a wick made of two layers of Whatman soaked in  $2 \times$  SSC. Role away any bubbles with a pipette (Note 2).
  8. Cut Nylon hybridization transfer membrane (Amersham, Hybond-N+) and 5 pieces of Whatman paper to the size of the gel.

9. Gently place the gel on the wick platform, faced down. Role away any bubbles trapped. Surround the gel with strips of parafilm to prevent transfer buffer from being absorbed directly into the paper towels.
10. Place some  $2 \times$  SSC on the gel so that it makes a thin layer and gently lay the transfer membrane on top. Role away any bubbles.
11. Place two  $2 \times$  SSC-soaked pieces of Whatmans cut to the size of the gel and three additional dry Whatmans of the same size on top of the gel, making sure no bubbles are trapped.
12. Stack at least 5 cm of paper towels or absorbent towels on top, followed by a glass plate and a weight.
13. Allow the transfer to proceed 8–24 h (Note 3).
14. Place the membrane on a dry piece of Whatman and UV cross-link the membrane. We use  $0.12\text{J}/\text{cm}^2$  of UV (Note 4).

**Notes:**

1. The gel can be cut between expected sizes of loading control and *MAT* fragments to transfer them separately. Alternatively, the membrane can be cut after the transfer, but it may be difficult to identify where to cut since the DNA ladder will not be visible on the membrane.
  2. The standard Southern blot protocol uses  $20 \times$  or  $10 \times$  SSC for transfer, but we have found that  $2 \times$  SSC is sufficient.
  3. After the transfer, the gel can be visualized on a UV transilluminator to check if the transfer was successful; no fluorescence indicates successful transfer.
  4. After cross-linking, the blot may be used immediately or dried for storage at room temperature.
2. Prehybridization
    1. Prewarm hybridization buffer to  $65^\circ\text{C}$  (Note 1).
    2. Roll the blot along its length with the DNA side up and place it in a hybridization tube (Note 2).
    3. Add prewarmed hybridization buffer until it covers the length of the tube when the tube is horizontal. Rotate the tube and allow the membrane to stick to the inner surface of the tube.
    4. Rotate the tube in  $65^\circ\text{C}$  hybridization oven for at least 15 min.

**Notes:**

1. We use Amersham Rapid-hyb buffer from GE Healthcare, which allows for shorter prehybridization and hybridization time. Other hybridization buffers can be used, such as Denhardt's and Church buffers.
2. Minimize overlapping the membrane inside the hybridization tube. Use nylon mesh to separate blot layers if necessary.

### 3. Probe Preparation and Hybridization

1. PCR amplify and gel purify desired probes from purified genomic DNA using primers listed in [Table 1](#) (Note 1).
2. Pipette 25–50 ng of purified probe into 1.5-mL centrifuge tube and bring the volume to 10  $\mu\text{L}$  with ddH<sub>2</sub>O (Note 2).
3. Denature the DNA by boiling for 3–5 min and then cool it on ice for 3–5 min.
4. Follow the RadPrime DNA Labeling System's standard labeling protocol on ice (Note 3):

|  |  |
|--|--|
| Denatured DNA probe                    | 10 $\mu\text{L}$                                     |
| 0.5 mM dATP                            | 1 $\mu\text{L}$                                      |
| 0.5 mM dGTP                            | 1 $\mu\text{L}$                                      |
| 0.5 mM dTTP                            | 1 $\mu\text{L}$                                      |
| 2.5 $\times$ Random Primers Solution   | 10 $\mu\text{L}$                                     |
| Kelnow Fragment (40 U/ $\mu\text{L}$ ) | 0.5 $\mu\text{L}$                                    |
| [ $\alpha$ - <sup>32</sup> P]dCTP      | 2.5 $\mu\text{L}$ (approximately 25 $\mu\text{Ci}$ ) |

5. Vortex the reaction briefly, centrifuge 15–30 s, and then incubate at 37°C for 10 min.
6. Add 2.5  $\mu\text{L}$  Stop buffer and 50  $\mu\text{L}$  of ddH<sub>2</sub>O.
7. Column purify with MicroSpin G-50 Column.
8. Denature the probe by heating on 98°C heat block for 3–5 min and chill on ice for 3–5 min.
9. Add the denatured probe to the hybridization tube. Aim to drop the probe in the middle of the tube directly into the hybridization buffer without touching the membrane.
10. Hybridize at 65°C hybridization oven with rotation for at least 1 h.
11. Decant the hybridization buffer and rinse the membrane and the tube with wash solution 1.
12. Decant and add wash solution 1 until the volume occupies about 30% of the tube. Rotate in 65°C for 20 min and repeat the wash once more.
13. For the third wash, use wash solution 2 and wash for 30 min.
14. Remove the membrane from the tube and drain it on Whatman.
15. Wrap the membrane in plastic wrap and expose to X-ray film or Phosphor screen.

**Notes:**

1. Probes must be gel purified to minimize nonspecific background signal. The MAT 0.7 kb probe is the only probe listed in [Table 1](#) that will distinguish between HO-cut and uncut fragments.
2. Use of excessive probe DNA could result in high background.
3. We use the RadPrime DNA Labeling System from Invitrogen, but many other labeling kits are available. We found that half of the manufacturer's recommended reaction size (25  $\mu$ L) is sufficient for hybridization.
4. Analysis and Quantification
  1. Use ImageJ to quantify the intensity of each band—loading control, uncut, HO cut.
  2. Normalize uncut and HO-cut bands with the loading control band.
  3. To calculate the fraction of resected DNA, use the following equation:

$$f = 1 - \frac{\text{cut}(t_i)}{\text{uncut}(t_0) - \text{uncut}(t_i)}$$

## 5.2 Alkaline Gel Electrophoresis to Detect ssDNA Intermediates

While the band disappearance method can be used to monitor the extent of end resection, it does not identify the strand removed or the integrity of the ssDNA overhang. Denaturing alkaline electrophoresis followed by Southern hybridization with strand-specific riboprobes close to the DSB site is a useful method to identify the polarity of end resection and approximate lengths of resection tracts ([White & Haber, 1990](#)). A 3'-specific single-stranded probe detects higher molecular weight bands, each of which corresponds to the intact 3' end at the HO-cut site and the next restriction site that was within dsDNA ([Fig. 3](#)). A 5'-specific single-stranded probe hybridizes to partially processed 5' ends and disappears over time as the strand to which it hybridizes is degraded. While we routinely generate riboprobes, a single primer PCR with [ $\alpha$ - $^{32}$ P]dCTP in the reaction can be used to generate ssDNA probes using the MAT 400 bp PCR product ([Table 1](#)).

### 5.2.1 Solutions and Reagents

- Glycogen (20 mg/mL)
- 3 M sodium acetate
- Ethanol (100%, 70%)

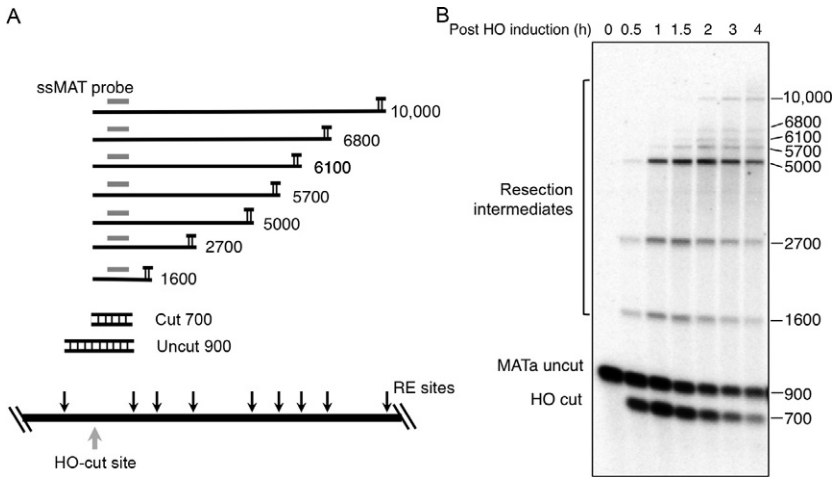


**Fig. 3** Alkaline gel electrophoresis to detect ssDNA intermediates. (A) Schematic of *MAT* locus showing location of HO-cut site, probe, and RE sites (not to scale). Processing of the HO-induced DSB renders the DNA single stranded and resistant to digestion with REs, giving rise to distinct sets of fragments. (B) Alkaline electrophoresis of *StyI*- and *BstXI*-digested genomic DNA probed with a 3'-specific riboprobe. Note that in this analysis, HO was expressed from a plasmid resulting in lower HO-cutting efficiency.

- 10× Alkaline agarose gel electrophoresis buffer: 500mM sodium hydroxide, 10mM EDTA
- 6× Alkaline gel loading buffer: 300mM sodium hydroxide, 18% Ficoll (Type 400, Pharmacia), 0.15% bromocresol green, 0.25% xylene blue
- Alkaline transfer buffer: 0.4 M sodium hydroxide, 1 M sodium chloride
- Neutralization buffer II: 0.5 M Tris-HCl (pH 7.2), 1 M sodium chloride
- pGEM-MAT Forward, pGEM-MAT Reverse plasmids (Mimitou & Symington, 2008)
- Ambion® MAXIscript® T7 in vitro Transcription Kit
- [ $\alpha$ -<sup>32</sup>P]UTP

### 5.2.2 Procedure

1. Restriction enzyme digestion and alkaline gel electrophoresis
  1. Digest 5–10µg of genomic DNA with 20 U of *StyI* and *BstXI* restriction enzymes in 50µL total reaction volume for 2 h at 37°C.

2. Add 1  $\mu\text{L}$  of 20 mg/mL glycogen, 5  $\mu\text{L}$  of 3 M sodium acetate, and 200  $\mu\text{L}$  of Ethanol.
3. Incubate at  $-20^{\circ}\text{C}$  for 1 h.
4. Centrifuge at top speed for 10 min.
5. Decant and wash the pellet with 70% Ethanol.
6. Decant and dry the pellet.
7. Resuspend the pellet in 20  $\mu\text{L}$  of 1  $\times$  alkaline agarose gel electrophoresis buffer and add alkaline gel loading buffer to 1  $\times$ .
8. Prepare 1% gel by dissolving agarose in  $\text{dH}_2\text{O}$  with 9/10 volume and allow it to cool at  $50^{\circ}\text{C}$ .
9. Add alkaline agarose gel electrophoresis buffer to 1  $\times$  and pour immediately into an electrophoresis casting tray.
10. Load samples once the gel is solidified.
11. Start electrophoresis at 35 V. When samples have entered the gel, turn the power supply off and place a glass plate on top of the gel (Note 1).
12. Continue electrophoresis in the cold room at 35 V overnight (Note 2).
13. (Optional) To visualize DNA ladder, cut the lane with DNA ladder, incubate with Neutralization solution II for 1 h, and then stain it with 0.5  $\mu\text{g}/\text{mL}$  ethidium bromide in TBE for at least 1 h before checking under the UV transilluminator.

**Notes:**

1. Glass plate is put on top of the gel to prevent the diffusion of bromocresol green dye out of the gel and to prevent the gel from floating.
2. Alkaline gels heat up faster than neutral gels during electrophoresis. Therefore, low voltage should be used and the apparatus set up in a cold room.
2. Alkaline transfer
  1. Soak the gel in 1  $\times$  alkaline transfer buffer for 20 min.
  2. Set up the transfer apparatus and allow the gel to transfer onto the Nylon transfer membrane in alkaline transfer buffer overnight (see [Section 5.1.3](#)).
  3. Neutralize the membrane by soaking it in Neutralization buffer II for at least 15 min.
3. Probe preparation and Southern blot
  1. Follow the Ambion<sup>®</sup> MAXIscript<sup>®</sup> T7 in vitro Transcription Kit protocol for labeling reaction:

*DNA template*

For 3' ssRNA probe: 1 µg pGEM-MAT Forward

For 5' ssRNA probe: 1 µg pGEM-MAT Reverse

|                                  |                             |
|----------------------------------|-----------------------------|
| 10 µM dATP                       | 1 µL                        |
| 10 µM dCTP                       | 1 µL                        |
| 10 µM dGTP                       | 1 µL                        |
| T7 enzyme mix                    | 2 µL                        |
| 10 × transcription buffer        | 2 µL                        |
| [α- <sup>32</sup> P]UTP          | 5 µL (approximately 50 µCi) |
| Nuclease-free ddH <sub>2</sub> O | Total volume to 20 µL       |

2. Vortex the reaction briefly, centrifuge 15–30 s, and then incubate at 37°C for 10–20 min.
3. Add 1 µL of DNaseI and incubate at 37°C for 15 min.
4. (Optional) Add 50 µL of ddH<sub>2</sub>O and column purify with MicroSpin G-50 Column.
5. Denature the probe by boiling on 98°C heat block for 3–5 min and chill on ice for 3–5 min.
6. Proceed with Southern blot hybridization as in [Section 5.1](#).

### 5.3 Quantitative PCR

To measure resection by qPCR we use an approach first described by [Zierhut and Diffley \(2008\)](#). The qPCR amplicon is a genomic DNA sequence in the vicinity of the HO-cut site. The sequence is chosen such that it contains a restriction endonuclease site. Digestion of the genomic DNA with the respective restriction enzyme prior to PCR will prevent amplification. However, once resection has passed the restriction site and renders it single stranded, digestion is no longer possible and the template is amplified ([Fig. 4](#)). Amplicons at various distances from the HO-induced DSB can be used to monitor how far resection extends. To normalize for the fraction of cells that received the DSB, an amplicon containing the HO-cut site is used. An amplicon in the *ADH1* gene is used to correct for differences in template concentrations. In the following, we describe the qPCR assay in a 384-well format using the Biorad SsoAdvanced™ Universal SYBR® Green Mix on a Biorad CFX384™ Real-Time System. If other qPCR mixes or systems are used, the protocol might need some adjustment.

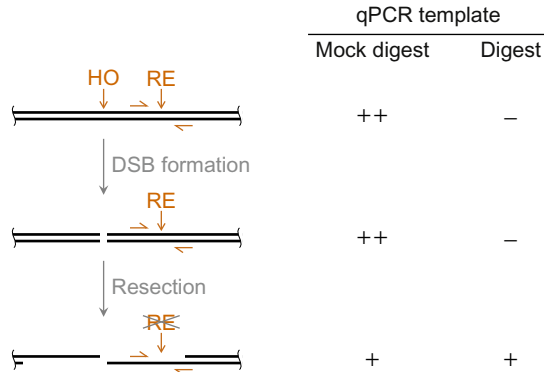


**Fig. 4** Principle of the qPCR assay. Schematic showing HO and RE sites. When the RE site is double stranded, it is susceptible to cleavage destroying the template for PCR using primers flanking the RE site. The ssDNA formed by resection is resistant to cleavage by the RE and can be PCR amplified. Note that for both mock and digested DNA only one template strand is amplified when resection has passed the site corresponding to a 50% decrease in signal relative to dsDNA.

### 5.3.1 Equipment

- Water bath (37°C)
- Repeater pipette
- qPCR plates and seals
- Centrifuge with swing-out microplate carrier
- qPCR machine

### 5.3.2 Solutions and Reagents

- SYBR Green real-time PCR mix
- Primers (primer sequences are listed in [Table 2](#))
- *StyI* or *RsaI* and 10 × CutSmart<sup>®</sup> Buffer (New England Biolabs)

### 5.3.3 Procedure

1. Restriction enzyme digestion and qPCR
  1. Prepare mock digestion and digestion reactions sufficient for a volume of 4.4 μL per well of the qPCR plate, containing 2.5 ng/μL genomic DNA in 1 × CutSmart<sup>®</sup> Buffer. Add 5 U restriction enzyme per μg DNA for the digestion reactions.
  2. Incubate at 37°C for 2 h.
  3. Prepare qPCR master mixes. A reaction volume of 5.6 μL qPCR master mix is needed per well of the qPCR plate. Add 0.06 μL

**Table 2** Primers for the qPCR Assay

| <b>Oligo Target and Direction</b> | <b>Restriction Enzyme</b> | <b>Sequence</b>               |
|-----------------------------------|---------------------------|-------------------------------|
| MATa HO-cut site (HOcs) fw        | —                         | TCAATGATTA AAAATAGCATAGTCGGGT |
| MATa HOcs rev                     | —                         | CGTCAACCACTCTACAAAACCA        |
| MATalpha HOcs fw                  | —                         | CTGAAGAATGGCACGCGGAC          |
| MATalpha HOcs rev                 | —                         | CTTCCCAATATCCGTCACCACGT       |
| ADH1 fw                           | —                         | GTAAAGGGCTGGAAGATCGG          |
| ADH1 rev                          | —                         | TTGTTGGAAAGAACCGTCGT          |
| 98bp downstream of HOcs fw        | <i>RsaI</i>               | TGGTGACGGATATTGGGAAGA         |
| 98bp downstream of HOcs rev       | <i>RsaI</i>               | CGCCACGACCACACTCTATA          |
| 640bp downstream of HOcs fw       | <i>RsaI</i>               | ACTTATCTTTATCTTATTCGCCTTCTTG  |
| 640bp downstream of HOcs rev      | <i>RsaI</i>               | GAGAAGACTTGTGGCGAAGA          |
| 726bp downstream of HOcs fw       | <i>StyI</i>               | TCATCTTCGCCACAAGTCTTCTCTC     |
| 726bp downstream of HOcs rev      | <i>StyI</i>               | CCTGTTCTTAGCTTGTACCAGAGGA     |
| 5.7kb downstream of HOcs fw       | <i>StyI</i>               | CCACCTTCATCGGTAAACGTAC        |
| 5.7kb downstream of HOcs rev      | <i>StyI</i>               | CAGCTCCACTTGATGCTTCC          |
| 10kb downstream of HOcs fw        | <i>StyI</i>               | CTTGCCTCCCTTCAAGCGC           |
| 10kb downstream of HOcs rev       | <i>StyI</i>               | GGGAGGAGCAGGTGAATTTGG         |

of both forward and reverse primers (10  $\mu\text{M}$  stock concentration) per  $\mu\text{L}$  SYBR Green real-time PCR mix. Store protected from light on ice.

4. Pipette 5.6  $\mu\text{L}$  of qPCR master mix and 4.4  $\mu\text{L}$  of (mock-) digested genomic DNA in the wells of the qPCR plate. Make technical triplicates. Include nontemplate controls (Note 1).
  5. Seal the plate with an adhesive transparent qPCR plate seal.
  6. Mix by vortexing.
  7. Spin for 2 min at  $1000 \times g$  at room temperature.
  8. Place the qPCR plate in the qPCR machine and run the following program: 95°C for 10 min,  $40 \times$  (95°C for 1 min, 58°C for 1 min). Record a melting curve.
2. Data analysis

We derived a formula to quantify resection by combining the ssDNA quantification equation from Zierhut and Diffley (2008) and the equation from Pfaffl (2001) for the relative quantification in real-time PCR. The fraction of cells in which resection passed the restriction site ( $RS$ ) is

$$x = \frac{2}{\left( \frac{(E_{RS})^{\Delta C_q(\text{digest}-\text{mock})}}{(E_{ADH1})^{\Delta C_q(\text{digest}-\text{mock})}} + 1 \right)} \cdot f$$

where  $E_{RS}$  and  $E_{ADH1}$  are the primer efficiencies for the  $RS$  and  $ADH1$  amplicons,  $\Delta C_q(\text{digest} - \text{mock})$  is the difference between quantification cycles for the digested minus the mock-digested sample, and  $f$  is the fraction of genomes where HO cleaved the  $MAT$  locus (Note 2).  $f$  can be calculated as

$$f = 1 - \frac{(E_{HOcs})^{\Delta C_q(t_0-t)}}{(E_{ADH1})^{\Delta C_q(t_0-t)}}$$

where  $E_{HOcs}$  and  $E_{ADH1}$  are the primer efficiencies for the HO-cut site and  $ADH1$  amplicons (Note 3) and  $\Delta C_q(t_0 - t)$  is the difference between the quantification cycles at the first time point (before galactose induction of  $HO$ ) and the evaluated time point. The derivation of the formula for  $x$  as well as an Excel spreadsheet and an R script for the qPCR data analysis are available on request. Fig. 5 shows a typical plot of resection data from wild-type and resection-deficient (*exo1 $\Delta$  sgs1 $\Delta$* ) cells.

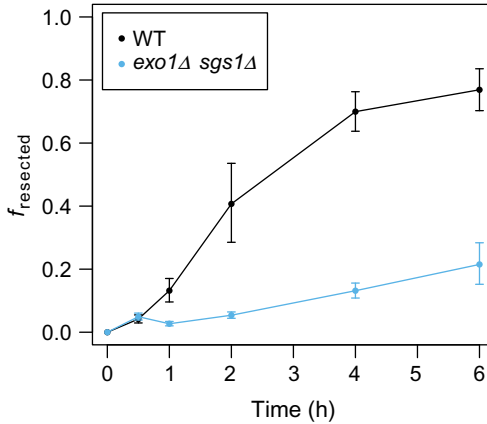


**Fig. 5** Example of a qPCR data plot. The fraction of resected DNA is plotted against time for wild-type (WT) and  $exo1\Delta sgs1\Delta$  cells. Primers flanking the *RsaI* site located 640 bp downstream from the HO-cute site were used for qPCR. The *error bars* indicate SD from three independent trials.

### 5.3.4 Notes

1. We generally confirm that the nontemplate controls give rise to high  $C_q$  values (usually greater than 35) and that the melting curves indicate a single PCR product and the absence of primer dimers.
2. HO-cutting kinetics and efficiency can be analyzed by plotting  $f$  vs time. Note that the genotype of the strains can impact on HO cutting. Under optimal conditions, HO cleaves very efficiently and rapidly; usually 0.5 h after HO induction, about 95% of the cell genomes have received a cut at the *MAT* locus and for later time points nearly 100% of the genomes are cut. However, in strains with a genotype resulting in poor growth, HO cutting can be delayed and incomplete. These differences underpin the importance of including  $f$  in the formula of  $x$ .
3. Primer efficiencies can be determined by analyzing a 1:10 dilution series of undigested genomic DNA in a qPCR assay. Plotting  $C_q$  values vs  $\log(\text{DNA concentration})$  should show a linear relationship. The efficiency  $E$  can be calculated as

$$E = 10^{-\left(\frac{1}{b}\right)}$$

where  $b$  is the slope of the line. On our qPCR system, efficiencies for the primers in [Table 2](#) are between 1.96 and 2.03.

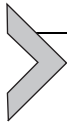
## ACKNOWLEDGMENTS

We thank C. Zierhut and J. Diffley for sharing W303 derivatives with *HML* and *HMR* loci deleted. End resection studies in our laboratory are supported by grants from the National Institutes of Health (R01GM041784 and P01CA174653).

## REFERENCES

- Bantele, S. C., Ferreira, P., Gritenaite, D., Boos, D., & Pfander, B. (2017). Targeting of the Fun30 nucleosome remodeller by the Dpb11 scaffold facilitates cell cycle-regulated DNA end resection. *eLife*, 6. <https://doi.org/10.7554/eLife.21687>.
- Barlow, J. H., Lisby, M., & Rothstein, R. (2008). Differential regulation of the cellular response to DNA double-strand breaks in G1. *Molecular Cell*, 30(1), 73–85. <https://doi.org/10.1016/j.molcel.2008.01.016>.
- Borner, G. V., & Cha, R. S. (2015). Analysis of meiotic recombination and homolog interaction during yeast meiosis. *Cold Spring Harbor Protocols*, 2015(10), 914–924. <https://doi.org/10.1101/pdb.prot085050>.
- Cao, L., Alani, E., & Kleckner, N. (1990). A pathway for generation and processing of double-strand breaks during meiotic recombination in *S. cerevisiae*. *Cell*, 61(6), 1089–1101.
- Ceccaldi, R., Rondinelli, B., & D'Andrea, A. D. (2016). Repair pathway choices and consequences at the double-strand break. *Trends in Cell Biology*, 26(1), 52–64. <https://doi.org/10.1016/j.tcb.2015.07.009>.
- Cruz-Garcia, A., Lopez-Saavedra, A., & Huertas, P. (2014). BRCA1 accelerates CtIP-mediated DNA-end resection. *Cell Reports*, 9(2), 451–459. <https://doi.org/10.1016/j.celrep.2014.08.076>.
- Eapen, V. V., Sugawara, N., Tsabar, M., Wu, W. H., & Haber, J. E. (2012). The *Saccharomyces cerevisiae* chromatin remodeler Fun30 regulates DNA end resection and checkpoint deactivation. *Molecular and Cellular Biology*, 32(22), 4727–4740. <https://doi.org/10.1128/MCB.00566-12>.
- Finn, K., Lowndes, N. F., & Grenon, M. (2012). Eukaryotic DNA damage checkpoint activation in response to double-strand breaks. *Cellular and Molecular Life Sciences*, 69(9), 1447–1473. <https://doi.org/10.1007/s00018-011-0875-3>.
- Haber, J. E. (2012). Mating-type genes and MAT switching in *Saccharomyces cerevisiae*. *Genetics*, 191(1), 33–64. <https://doi.org/10.1534/genetics.111.134577>.
- Herskowitz, I., & Jensen, R. E. (1991). Putting the HO gene to work: Practical uses for mating-type switching. *Methods in Enzymology*, 194, 132–146.
- Hoffman, C. S., & Winston, F. (1987). A ten-minute DNA preparation from yeast efficiently releases autonomous plasmids for transformation of *Escherichia coli*. *Gene*, 57(2–3), 267–272.
- Ira, G., Pelliccioli, A., Balijja, A., Wang, X., Fiorani, S., Carotenuto, W., et al. (2004). DNA end resection, homologous recombination and DNA damage checkpoint activation require CDK1. *Nature*, 431(7011), 1011–1017. <https://doi.org/10.1038/nature02964>.
- Langerak, P., Mejia-Ramirez, E., Limbo, O., & Russell, P. (2011). Release of Ku and MRN from DNA ends by Mre11 nuclease activity and Ctp1 is required for homologous recombination repair of double-strand breaks. *PLoS Genetics*, 7(9), e1002271. <https://doi.org/10.1371/journal.pgen.1002271>.
- Mimitou, E. P., & Symington, L. S. (2008). Sae2, Exo1 and Sgs1 collaborate in DNA double-strand break processing. *Nature*, 455(7214), 770–774. <https://doi.org/10.1038/nature07312>.
- Mimitou, E. P., Yamada, S., & Keeney, S. (2017). A global view of meiotic double-strand break end resection. *Science*, 355(6320), 40–45. <https://doi.org/10.1126/science.aak9704>.

- Pfaffl, M. W. (2001). A new mathematical model for relative quantification in real-time RT-PCR. *Nucleic Acids Res*, 29, e45.
- Plessis, A., Perrin, A., Haber, J. E., & Dujon, B. (1992). Site-specific recombination determined by I-SceI, a mitochondrial group I intron-encoded endonuclease expressed in the yeast nucleus. *Genetics*, 130(3), 451–460.
- Roberts, S. A., Sterling, J., Thompson, C., Harris, S., Mav, D., Shah, R., et al. (2012). Clustered mutations in yeast and in human cancers can arise from damaged long single-strand DNA regions. *Molecular Cell*, 46(4), 424–435. <https://doi.org/10.1016/j.molcel.2012.03.030>.
- Rosebrock, A. P. (2017). Synchronization and arrest of the budding yeast cell cycle using chemical and genetic methods. *Cold Spring Harbor Protocols*, 2017(1). <https://doi.org/10.1101/pdb.prot088724>.
- Sartori, A. A., Lukas, C., Coates, J., Mistrik, M., Fu, S., Bartek, J., et al. (2007). Human CtIP promotes DNA end resection. *Nature*, 450(7169), 509–514. <https://doi.org/10.1038/nature06337>.
- Sun, H., Treco, D., & Szostak, J. W. (1991). Extensive 3'-overhanging, single-stranded DNA associated with the meiosis-specific double-strand breaks at the ARG4 recombination initiation site. *Cell*, 64(6), 1155–1161.
- Symington, L. S. (2016). Mechanism and regulation of DNA end resection in eukaryotes. *Critical Reviews in Biochemistry and Molecular Biology*, 51(3), 195–212. <https://doi.org/10.3109/10409238.2016.1172552>.
- Symington, L. S., Rothstein, R., & Lisby, M. (2014). Mechanisms and regulation of mitotic recombination in *Saccharomyces cerevisiae*. *Genetics*, 198(3), 795–835. <https://doi.org/10.1534/genetics.114.166140>.
- Tkac, J., Xu, G., Adhikary, H., Young, J. T., Gallo, D., Escribano-Diaz, C., et al. (2016). HELB is a feedback inhibitor of DNA end resection. *Molecular Cell*, 61(3), 405–418. <https://doi.org/10.1016/j.molcel.2015.12.013>.
- White, C. I., & Haber, J. E. (1990). Intermediates of recombination during mating type switching in *Saccharomyces cerevisiae*. *The EMBO Journal*, 9(3), 663–673.
- Yamane, A., Robbiani, D. F., Resch, W., Bothmer, A., Nakahashi, H., Oliveira, T., et al. (2013). RPA accumulation during class switch recombination represents 5'-3' DNA-end resection during the S-G2/M phase of the cell cycle. *Cell Reports*, 3(1), 138–147. <https://doi.org/10.1016/j.celrep.2012.12.006>.
- Zhou, Y., Caron, P., Legube, G., & Paull, T. T. (2014). Quantitation of DNA double-strand break resection intermediates in human cells. *Nucleic Acids Research*, 42(3), e19. <https://doi.org/10.1093/nar/gkt1309>.
- Zhu, Z., Chung, W. H., Shim, E. Y., Lee, S. E., & Ira, G. (2008). Sgs1 helicase and two nucleases Dna2 and Exo1 resect DNA double-strand break ends. *Cell*, 134(6), 981–994. <https://doi.org/10.1016/j.cell.2008.08.037>.
- Zierhut, C., & Diffley, J. F. (2008). Break dosage, cell cycle stage and DNA replication influence DNA double strand break response. *The EMBO Journal*, 27(13), 1875–1885. <https://doi.org/10.1038/emboj.2008.111>.
- Zubko, M. K., Maringele, L., Foster, S. S., & Lydall, D. (2006). Detecting repair intermediates in vivo: Effects of DNA damage response genes on single-stranded DNA accumulation at uncapped telomeres in budding yeast. *Methods in Enzymology*, 409, 285–300. [https://doi.org/10.1016/S0076-6879\(05\)09016-6](https://doi.org/10.1016/S0076-6879(05)09016-6).



# Methods to Study DNA End Resection I: Recombinant Protein Purification

Roopesh Anand\*, Cosimo Pinto<sup>†</sup>, Petr Cejka\*<sup>‡,1</sup>

\*Institute for Research in Biomedicine, Università della Svizzera italiana, Bellinzona, Switzerland

<sup>†</sup>Institute of Molecular Cancer Research, University of Zurich, Zurich, Switzerland

<sup>‡</sup>Institute of Biochemistry, Swiss Federal Institute of Technology, Zurich, Switzerland

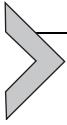
<sup>1</sup>Corresponding author: e-mail address: petr.cejka@irb.usi.ch

## Contents

|   |    |
|---|----|
| 1. Introduction to DNA End Resection                              | 26 |
| 2. Expression of Recombinant Proteins in Insect Cells             | 27 |
| 2.1 Baculovirus Production (Low- and High-Titer Virus)            | 28 |
| 2.2 Protein Expression in Sf9 Cells                               | 32 |
| 3. Large-Scale Protein Purification of DNA End Resection Proteins | 34 |
| 3.1 Purification of the MRN Complex                               | 34 |
| 3.2 Purification of Phosphorylated CtIP                           | 39 |
| 3.3 Purification of DNA2  | 45 |
| 3.4 Purification of Human WRN and BLM Helicase                    | 49 |
| 3.5 Expression and Purification of RPA                            | 55 |
| Acknowledgments   | 59 |
| References  | 59 |

## Abstract

Accurate repair of DNA double-strand breaks (DSBs) is carried out by homologous recombination. In order to repair DNA breaks by the recombination pathway, the 5'-terminated DNA strand at DSB sites must be first nucleolytically processed to produce 3'-overhang. The process is termed DNA end resection and involves the interplay of several nuclease complexes. DNA end resection commits DSB repair to the recombination pathway including a process termed single-strand annealing, as resected DNA ends are generally nonligatable by the competing nonhomologous end-joining machinery. Biochemical reconstitution experiments provided invaluable mechanistic insights into the DNA end resection pathways. In this chapter, we describe preparation procedures of key proteins involved in DNA end resection in human cells, including the MRE11–RAD50–NBS1 complex, phosphorylated variant of CtIP, the DNA2 nuclease–helicase with its helicase partners Bloom (BLM) or Werner (WRN), as well as the single-stranded DNA-binding protein replication protein A. The availability of recombinant DNA end resection factors will help to further elucidate resection mechanisms and regulatory processes that may involve novel protein partners and posttranslational modifications.



## 1. INTRODUCTION TO DNA END RESECTION

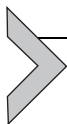
DNA double-strand breaks (DSBs) can be repaired by either non-homologous end-joining (NHEJ), microhomology-mediated end-joining, homologous recombination (HR), and single-strand annealing (SSA) pathways. Whereas end joining and SSA-based repair is often mutagenic, HR is template directed and therefore largely accurate. In most cases in vegetative cells, the sister chromatid is used as a repair template to restore the integrity of genetic information during DSB repair by the recombination pathway (Kowalczykowski, 2015).

DNA end resection initiates the repair of DSBs via HR and SSA and prevents their ligation by error-prone NHEJ (Cejka, 2015; Huertas, 2010; Paull, 2010; Symington, 2016). Therefore, the decision whether or not to resect DNA breaks directly affects the pathway choice in DSB repair. In resection, the 5'-terminated DNA strand is specifically degraded. The 5' → 3' nucleolytic DNA degradation generates 3'-terminated strands of single-stranded DNA (ssDNA) at DSB sites. ssDNA is a substrate for the replication protein A (RPA), which binds ssDNA with high affinity. Subsequently, RPA is replaced by the recombinase RAD51 forming a nucleoprotein filament, which invades homologous DNA and primes DNA synthesis (Kowalczykowski, 2015). The missing DNA sequence at the break sites is then copied from the template DNA, which ultimately leads to the restoration of the broken DNA molecule. For detailed information about recombination mechanisms, we refer readers to several excellent recent reviews (Kowalczykowski, 2015; Prakash, Zhang, Feng, & Jasin, 2015).

DNA end resection proceeds in two main steps: short-range and long-range resection. Briefly, the short-range process is catalyzed by the MRE11–RAD50–NBS1 (MRN) complex in human cells. MRN is recruited to DNA ends, where CtIP stimulates MRE11's endonuclease activity to incise the 5'-terminated DNA-strand internal to the DSB site (Anand, Ranjha, Cannavo, & Cejka, 2016; Cannavo & Cejka, 2014; Deshpande, Lee, Arora, & Paull, 2016; Neale, Pan, & Keeney, 2005). The 3' → 5' exonuclease of MRE11 is believed to function downstream of this initial cleavage, resecting the 5'-terminated DNA-strand back toward the DNA break (Garcia, Phelps, Gray, & Neale, 2011; Neale et al., 2005; Shibata et al., 2014). Either of two separate pathways subsequently catalyzes 5' → 3' long-range DNA end resection: the exonuclease EXO1 or the WRN/BLM–DNA2 complex in

vegetative cells (Gravel, Chapman, Magill, & Jackson, 2008; Mimitou & Symington, 2008; Sturzenegger et al., 2014; Zhu, Chung, Shim, Lee, & Ira, 2008). This leads to extended 3'-terminated ssDNA of hundreds to thousands nucleotides in length that is suitable for the downstream steps in the recombination pathway (Chung, Zhu, Papusha, Malkova, & Ira, 2010; Mimitou, Yamada, & Keeney, 2017; Zakharyevich et al., 2010). DNA end resection has been extensively reviewed in the past years (Cejka, 2015; Daley, Niu, Miller, & Sung, 2015; Huertas, 2010; Paull, 2010; Symington, 2016).

Here we describe the expression and purification of human proteins that belong to the core DNA end resection machinery, including the MRN complex, CtIP, the DNA2 nuclease–helicase as well as Werner (WRN) and Bloom (BLM) helicases and RPA. As we express all proteins except for RPA in *Spodoptera frugiperda* 9 (*Sf9*) insect cells, we include a brief section that summarizes our experience with the handling of *Sf9* cells, preparation of recombinant baculoviruses and protein production. We then present detailed procedures for purification of selected DNA end resection proteins. The availability of recombinant proteins allows us to study the detailed mechanisms of DNA end resection and to evaluate the effect of potential cofactors and regulators. These methods may help identify small molecule inhibitors of the resection pathways, which are candidates for future anticancer treatments.



## 2. EXPRESSION OF RECOMBINANT PROTEINS IN INSECT CELLS

Biochemical analysis is an invaluable tool that helps us to understand the function of proteins or protein complexes at the molecular level. This approach requires the expression and purification of the desired recombinant proteins in sufficient quantities. Among several available expression systems, *S. frugiperda* 9 (*Sf9*) or *Sf21* insect cells are routinely used for protein expression with various modifications (Hitchman, Possee, & King, 2009, 2012; King, Hitchman, & Possee, 2016). The main advantages of the insect expression system compared to bacteria (in most cases *Escherichia coli*) include improved solubility and yields of particularly high molecular weight proteins and the capacity to posttranslationally modify the expressed polypeptides. For example, phosphorylation of the resection factor CtIP at numerous residues is essential for its capacity to promote the nuclease of MRE11 (Anand et al., 2016; Deshpande et al., 2016; Huertas, Cortes-Ledesma, Sartori,

Aguilera, & Jackson, 2008; Huertas & Jackson, 2009), as will be introduced below. Such modifications are generally not possible to achieve in bacterial expression systems.

Below, we summarize the key steps required for recombinant protein production in insect cells with a system used by us and our colleagues to produce DNA end resection proteins (Anand et al., 2016; Deshpande et al., 2016; Paull & Gellert, 1998; Pinto, Kasaciunaite, Seidel, & Cejka, 2016; Sturzenegger et al., 2014). The preparation of recombinant proteins in insect cells involves the generation of a recombinant baculovirus, which is amplified to produce a high-titer virus suitable for protein production. We recommend the handbook “Guide to Baculovirus Expression Vector Systems (BEVS) and Insect Cell Culture Techniques” (Invitrogen) for general recommendations regarding the baculovirus-based protein expression in *Sf9* cells. The key steps with numerous modifications will be briefly described below.

## 2.1 Baculovirus Production (Low- and High-Titer Virus)

### 2.1.1 Equipment

- Flat-top platform shaker (Heidolph unimax 2010 or equivalent), with 2 cm rotation radius. Place inside an incubator set at 27°C. Alternatively, use a dedicated shaker/incubator for *Sf9* cultures.
- Electroporator (Biorad Gene Pulser II or equivalent).
- 125 mL (Corning, 431143) and 500 mL (Corning, 431145) Erlenmeyer flasks (or equivalent) for suspension cell culture.

### 2.1.2 Buffers and Reagents

- *Sf9* cells (Gibco, 11496 015)
- LB agar (AppliChem, A0927)
- LB medium (AppliChem, A0954)
- SOC medium (2% tryptone, 0.5% yeast extract, 10 mM NaCl, 2.5 mM KCl, 10 mM MgCl<sub>2</sub>, 10 mM MgSO<sub>4</sub>, 20 mM glucose in water). Filter-sterilize
- MAX Efficiency DH10Bac Competent Cells (Invitrogen, 10361012). We initially purchased these chemocompetent cells, but later prepared as electrocompetent
- Kanamycin sulfate (Gibco, 15160047)
- Gentamicin (50 mg/mL, Sigma-Aldrich, G1397)
- 5-Bromo-4-chloro-3-indolyl- $\beta$ -D-galactopyranoside (X-gal, Sigma-Aldrich, B4252)

- Isopropyl  $\beta$ -D-1-thiogalactopyranoside (IPTG, Sigma-Aldrich, I6758)
- Plasmid mini kit (Qiagen, 12125)
- X-gal-Kan-Gen plate: LB agar plate supplemented with gentamicin (7  $\mu$ g/mL), kanamycin (50  $\mu$ g/mL), X-gal (40  $\mu$ g/mL), and IPTG (40  $\mu$ g/mL)
- TransIT-insect transfection reagent (Mirus Bio, MIR 6104)
- Hyclone SFX-insect cell culture media (Gibco, SH30278.02)
- Fetal bovine serum (Gibco, 10270106)

### 2.1.3 Procedure for Production of Low-Titer Virus (Primary Virus)

1. Transform 10 ng of the respective pFastBac1 transfer vector into competent DH10Bac *E. coli* cells using the standard procedure.
2. Add 1 mL SOC medium to the *E. coli* cells immediately after transformation and incubate the cells for 5 h at 37°C with constant agitation.
3. Dilute 10  $\mu$ L of the *E. coli* culture in 100  $\mu$ L of sterile water, and plate on X-gal-Kan-Gen plates. Depending on the competence of the DH10Bac cells, the volume of the plated cell suspension may need to be varied.
4. Incubate the plates for 24 h at 37°C and 24 h at 4°C to optimally differentiate blue and white colonies.
5. While many colonies will be blue, identify several large white colonies and restreak the cells on new X-gal-Kan-Gen plates. Incubate the plates for 16 h at 37°C.
6. Verify that the restreaked cells are indeed white and inoculate the cells into 8 mL LB medium (2 times 4 mL cultures) containing kanamycin (50  $\mu$ g/mL) and gentamicin (7  $\mu$ g/mL). Incubate the cultures in agitation for 16 h at 37°C.
7. Extract bacmid DNA using Qiagen plasmid mini kit according to manufacturer's instructions with the following modifications: (a) grow 2 times 4 mL of the *E. coli* culture for each sample and resuspend, lyse, and neutralize pellet from each 4 mL culture with 0.3 mL buffers P1, P2, and P3, respectively (see Qiagen Quick start protocol). Upon centrifugation, apply sequentially the two supernatants on a single Qiagen-tip column and (b) elute bacmid DNA with buffer QF (Qiagen) preheated to 65°C.
8. Dissolve bacmid DNA in 50  $\mu$ L TE buffer pH 8.0 overnight at 4°C. Mix gently by tapping the tube. The average DNA concentration determined spectrophotometrically is  $\sim$ 200 ng/ $\mu$ L.

9. Transfect *Sf9* cells in a 6-well plate with the bacmid DNA using TransIT-insect cells transfection reagent according to manufacturer's instructions.
10. Collect the low-titer primary virus 72 h after transfection and perform a dot-blot assay (see [Section 2.1.4](#)) to estimate virus titer.
11. Add 5% fetal bovine serum to each virus. Viruses can be stored at 4°C for 2–3 months or at –80°C for several years (snap freeze with liquid nitrogen).

### Notes

- The bacmid DNA is prone to breakage due to its large size. Handle as gently as possible. Pipet very slowly.
- We find the Qiagen plasmid mini (12125) kit more reliable in terms of bacmid DNA yield than other methods involving phenol–chloroform extraction.
- We maintain *Sf9* cells in a suspension culture in shaker flasks, and split every 2–3 days. For optimal results, it is essential to work with exponentially growing cells with >95% viability, as determined by staining with trypan blue (Sigma-Aldrich, T6146). Only initial transfection (step 9 above) is performed with cells that were allowed to settle, all other infections (see below) are carried out in shaker flasks.
- The rotation speed of the suspension culture is a critical parameter for proper cell growth. Using a shaker with 2 cm rotation radius, we find 120 rpm/min optimal for 125 mL flasks (for 25–50 mL culture volumes) as well as 500 mL flasks (100–200 mL culture volumes). There is no need to fix the flasks on top of the orbital shaker.
- It is generally possible to reuse the cell culture flasks upon washing and autoclaving.

### 2.1.4 Dot-Blot Assay to Estimate Virus Titer

The “Guide to Baculovirus Expression Vector Systems (BEVS) and Insect Cell Culture Techniques” (Invitrogen) details virus plaque assay that can be used to determine virus titer. This is important to know in order to verify that the transfection of *Sf9* cells with baculovirus DNA was successful, and to determine the amount of virus to be used in a subsequent amplification step. Below we describe a simple dot-blot assay that can be used to estimate virus titer based on detection of the viral gp64 envelope protein. We recommend using a virus with a known titer as a standard in each dot-blot assay, which can be compared to the test samples.

#### 2.1.4.1 Equipment

- Biomolecular imager LAS-4000 mini (GE healthcare) or equivalent

#### 2.1.4.2 Buffers and Reagents

- Nitrocellulose membrane, such as Amersham Protran Supported 0.2  $\mu\text{m}$  NC (Amersham, GE healthcare, 10600128)
- Primary antibody: Baculovirus envelope gp64 monoclonal antibody (AcV5) (ebioscience, 14-6995-82)
- Secondary antibody: Amersham ECL Mouse IgG, HRP-linked whole Ab (from sheep) (GE healthcare, NA931)
- ECL solution (WesternBright, Advansta, K-12045-D50 or equivalent)
- 1X phosphate-buffered saline (PBS) pH 7.4 (1.37 mM NaCl, 2.7 mM KCl, 10 mM  $\text{Na}_2\text{HPO}_4$ , 1.8 mM  $\text{KH}_2\text{PO}_4$ )
- Tween 20 (Sigma-Aldrich, P9416)
- PBS-T, PBS with 0.1% Tween 20

#### 2.1.4.3 Procedure

1. Spot 2  $\mu\text{L}$  of standard and test samples of primary or secondary virus on appropriately sized nitrocellulose membrane. Allow 5–10 min for drying.
2. Block the membrane in PBS-T with 5% nonfat dry milk powder or equivalent (w/v) for 15 min at room temperature.
3. Add primary antibody (diluted 1:1000 in 5% milk in PBS-T) and incubate the membrane for 1 h with constant agitation at room temperature.
4. Wash the membrane two times with PBS-T for 5 min.
5. Add secondary antibody (diluted 1:5000 in 5% milk in PBS-T) and incubate for 1 h with constant agitation at room temperature.
6. Wash the membrane three times for 5 min with PBS-T.
7. Develop the membrane with ECL reagents according to manufacturers' instructions.

#### Notes

- Primary antibody in 5% milk/PBS-T can be reused multiple times when stored at  $-20^\circ\text{C}$ .
- We recommend performing the dot-blot assay with freshly prepared viral stocks only (or with viral stock/standard that has been stored at  $-80^\circ\text{C}$  in small aliquots). Virus that has been stored for extended period of time at  $4^\circ\text{C}$  may give rise to signal in the dot-blot assay, but may not have the corresponding infectious potency.

### 2.1.5 Procedure for Production of High-Titer Virus

The low-titer “primary” virus resulting from the transfection of *Sf9* cells in a 6-well plate must be subsequently amplified to obtain larger volume of high-titer secondary and tertiary virus that is usable for protein production.

1. Seed 50 mL *Sf9* cells at  $0.5 \times 10^6$ /mL in insect culture media in 125 mL flask (see Section 2.1.1) and incubate at 27°C at 120 rpm for 1 day.
2. Infect the cells with appropriate volume of primary virus (generally 50–1000  $\mu$ L, as determined by dot-blot or plaque assay) and incubate at 27°C at 120 rpm for 48 h.
3. Centrifuge the cells at  $500 \times g$  for 10 min at room temperature in a 50 mL conical tube and collect the supernatant containing secondary virus.
4. Perform the dot-blot assay to verify that virus amplification was successful and to estimate the titer of the amplified secondary virus.
5. Add fetal bovine serum (5% final concentration, v/v) to the secondary virus and store at 4°C for several months or at  $-80^\circ\text{C}$  for several years.

#### Notes

- The secondary virus can be further amplified to produce tertiary virus using a similar procedure. Generally, we use 25–75  $\mu$ L of the secondary virus for amplification in 50 mL cell culture, as determined by dot-blot assay.
- The volumes of *Sf9* cell culture for virus amplification can be scaled up or down as needed.

## 2.2 Protein Expression in *Sf9* Cells

It is important to test the quality of each prepared secondary or tertiary baculovirus stock by performing small-scale protein expression assays before proceeding to large-scale experiments. In this chapter, we describe general recommendations for the infection of *Sf9* cells for protein production.

### 2.2.1 Equipment

- See Section 2.1.1
- Centrifuges with compatible rotors for both large (1 L) and small (50 mL) volumes capable of cooling to 4°C

### 2.2.2 Buffers and Reagents

- See Section 2.1.2
- For the phospho-protein CtIP (see below): Okadaic acid, potassium salt (Merck, 459618), and (S)-(+)-camptothecin (CPT, Sigma-Aldrich, C9911)

### 2.2.3 Infection of Cells With High-Titer Baculovirus for Protein Production

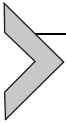
1. Seed appropriate volume of *Sf9* cells at  $0.5 \times 10^6$ /mL in 125 or 500 mL Erlenmeyer flasks and incubate at 27°C at 120 rpm for 1 day. We typically use 50 mL culture volumes for initial small-scale experiments to test for protein expression levels.
2. Infect *Sf9* cells with determined amount of secondary or tertiary virus (see dot-blot assay, [Section 2.1.4](#) and Notes below) or a combination of viruses and incubate at 27°C for 52 h.
3. Optional: For phosphoproteins such as CtlP, add okadaic acid (25 nM) after 48 h and CPT (1  $\mu$ M) after 51 h of incubation. See note below for more details.
4. Harvest the cells 52 h after infection at  $500 \times g$  for 10 min at 4°C.
5. Discard the supernatant and resuspend the cell pellet with ice-cold PBS buffer. Centrifuge again at  $500 \times g$  for 10 min at 4°C.
6. Discard the supernatant and store the pellet at  $-80^\circ\text{C}$  after snap freezing with liquid nitrogen.

#### Notes

- The amount of secondary virus to be used for cell infection depends on the virus titer. See “Guide to Baculovirus Expression Vector Systems (BEVS) and Insect Cell Culture Techniques” (Invitrogen). As a general rule, we start with  $\sim 750 \mu\text{L}$  of secondary or tertiary virus per 50 mL *Sf9* cells, which can be scaled according to the volume of the cell culture. The optimal amount may need to be determined empirically.
- To express protein complexes, infect cells with a combination of recombinant baculoviruses. As a general rule, we start with  $\sim 750 \mu\text{L}$  of each virus per 50 mL cell culture. Optimal ratio may need to be determined empirically.
- We typically harvest cells 52 h after infection, however this may also need to be varied to achieve optimal protein expression. Longer infection times may increase yield, but often result in partial degradation (truncation) of the expressed protein.
- Upon determining the expression level from small-scale experiments, the cultures should be scaled up for each respective recombinant protein or multiprotein complex. It is possible to grow 800 mL cells in 3.6 L Erlenmeyer flasks (Fernbach design) at 80 rpm, or use multiple 200 mL cultures in 500 mL Erlenmeyer flasks at 120 rpm. The optimal cell culture volumes and flask sizes may need to be determined empirically. We often achieve better yields in the 500 mL flasks. The recommended *Sf9*

cell culture volumes for the respective resection proteins are given in the sections below.

- For CtIP, we use okadaic acid (25 nM) for the last 4 h of cell culture prior to harvesting. Okadaic acid is a potent inhibitor of P1/P2 protein phosphatases. The treatment with okadaic acid thus helps to preserve CtIP in its phosphorylated state. To further activate protein phosphorylation cascades, we treat the cells with camptothecin (1  $\mu$ M) 1 h before harvesting. Camptothecin is a specific topoisomerase I inhibitor that results in DNA breaks, activating ATM/ATR-dependent DNA damage response. Treatment of cells with camptothecin does not damage cellular proteins.



### 3. LARGE-SCALE PROTEIN PURIFICATION OF DNA END RESECTION PROTEINS

#### 3.1 Purification of the MRN Complex

The human MRN complex consists of MRE11, RAD50, and NBS1 subunits (Lamarche, Orazio, & Weitzman, 2010). MRN is a multifunctional protein complex that plays various roles in DNA repair including in HR (Gobbini, Cassani, Villa, Bonetti, & Longhese, 2016; Nimonkar et al., 2011), but also in DNA damage signaling to activate ATM (Lee & Paull, 2004, 2005). Deletion of any subunit of the MRN complex is incompatible with life in human and mouse cells (Buis et al., 2008; Luo et al., 1999). In humans, hypomorphic mutations in MRE11 cause ataxia-telangiectasia-like disorder, whereas mutations in the NBS1 gene give rise to Nijmegen breakage syndrome (NBS) (Carney et al., 1998; Komatsu, 2016; Stewart et al., 1999; Tauchi et al., 2002; Taylor, Groom, & Byrd, 2004). Both disorders predispose affected individuals to various malignant cancers. No such mutations have been reported for RAD50 yet, which may indicate the requirement for the functional integrity of the RAD50 factor.

In terms of enzymatic activity *in vitro*, MRE11 alone or within the MRN complex is a manganese-dependent 3'  $\rightarrow$  5' ssDNA exonuclease, as well as an endonuclease on various secondary DNA structures including hairpins, loops, and junctions of single- and double-stranded DNA (dsDNA). Additionally, the MRN complex can also partially unwind dsDNA by its DNA melting activity (Furuse et al., 1998; Paull & Gellert, 1998, 1999; Trujillo & Sung, 2001). Many structural studies from various organisms have revealed that MRE11 with RAD50 exists as a dimer in a M<sub>2</sub>R<sub>2</sub> arrangement (Hopfner et al., 2001; Lammens et al., 2011; Williams et al., 2008). Both subunits of the MRE11–RAD50 heterodimer

bind DNA and together bridge DNA ends (de Jager et al., 2001; Williams et al., 2008). The RAD50 subunit is an ATPase that regulates the conformation of the MRN complex that is essential for its activity, in particular for endonucleolytic cleavage (Deshpande et al., 2014; Mockel, Lammens, Schele, & Hopfner, 2012; Williams et al., 2011). NBS1 is the least conserved component of the MRN complex that has no enzymatic activity on its own. NBS1 (Xrs2 in *Saccharomyces cerevisiae*) mediates MRN entry into the nucleus as it contains a nuclear localization signal and promotes checkpoint signaling through binding to the ATM kinase. Interestingly in yeast, Xrs2 is largely dispensable for DNA end resection, as long as Mre11 is fused with a nuclear localization signal (Oh, Al-Zain, Cannavo, Cejka, & Symington, 2016). In contrast NBS1 in high eukaryotes is essential for DNA end resection (Anand et al., 2016; Deshpande et al., 2016; Kim et al., 2017), revealing a difference between low and high eukaryotes.

As mentioned above, MRN along with CtIP initiates short-range DNA end resection (Sartori et al., 2007). This function requires the integrity of the MRE11 nuclease active site in high eukaryotes, whereas the Mre11 nuclease may be dispensable for the resection of “clean” DSBs in yeast (Buis et al., 2008; Llorente & Symington, 2004; Mimitou & Symington, 2010; Zhu et al., 2008). The 3' → 5' polarity of the MRE11 exonuclease is the opposite than that required for HR, as all DSB models posit that 5'-terminated DNA must be specifically degraded (Paull & Gellert, 1998; Trujillo, Yuan, Lee, & Sung, 1998; White & Haber, 1990). To this point, a bidirectional resection model has been proposed, wherein MRE11 initially cleaves 5'-terminated DNA internal to a DSB site endonucleolytically, and subsequently degrades DNA back toward the 5' DNA end using its 3' → 5' exonuclease activity (Cannavo & Cejka, 2014; Garcia et al., 2011; Hopkins & Paull, 2008; Neale et al., 2005; Shibata et al., 2014). While many aspects of this reaction remain to be understood, there is now strong evidence in support of this model from multiple organisms. All subunits of the MRN complex and phosphorylated CtIP are required for the initial endonucleolytic cleavage.

Here we describe large-scale purification of the recombinant MRN complex from *Sf9* cells. The procedure exploits the 6X histidine and FLAG tags at the C-termini of MRE11 and RAD50, respectively. The pFastBac1-derived plasmid constructs used for the preparation of baculoviruses are pFB-MRE11-6X his (pTP17) and pFB-NBS1 (pTP36), which were prepared by Paull and Gellert (1998, 1999) and pFB-RAD50-FLAG (Anand et al., 2016). The typical yield of the recombinant MRN heterotrimer from 3.2L *Sf9* cell culture is ~66 µg (Fig. 1).

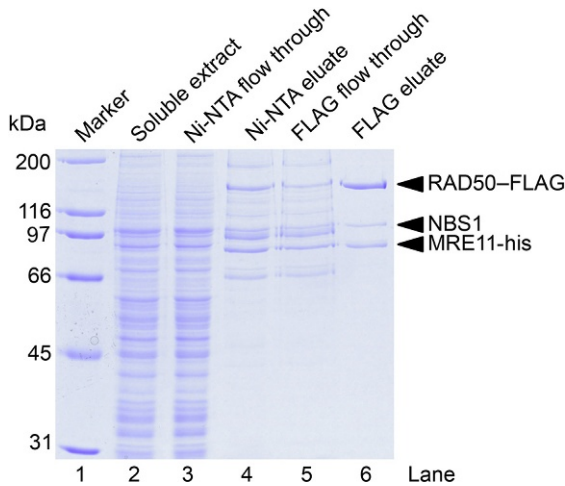


**Fig. 1** Representative MRN purification. Samples were analyzed on polyacrylamide gel and stained with Coomassie Brilliant Blue. Marker, molecular weight standard, broad range (Biorad), 1  $\mu$ g per band; Ni-NTA flow through and eluate, flow through and eluate from Ni-NTA resin; FLAG flow through and eluate, flow through and eluate from Anti-FLAG affinity resin.

### 3.1.1 Equipment

- High speed centrifuge with compatible rotors capable of handling both low and high volumes at 4°C

### 3.1.2 Buffers and Reagents

- Disposable 5 mL (Thermofisher Scientific, 29922) and 10 mL (Thermofisher Scientific, 29924) polypropylene columns
- Nickel–nitrilotriacetic acid (Ni-NTA) agarose resin (Qiagen, 30230)
- Glycerol anhydrous (AppliChem, A2926 or equivalent), prepare 50% solution (v/v) with water
- Lysis buffer: 50 mM Tris–HCl pH 7.5, 2 mM  $\beta$ -mercaptoethanol ( $\beta$ -ME, Sigma–Aldrich, M6250), 1 mM phenylmethane sulfonyl fluoride (PMSF, AppliChem, A0999), 1 mM ethylenediaminetetraacetic acid (EDTA, Sigma–Aldrich, EDS), 20 mM imidazole (Sigma–Aldrich, I202), protease inhibitor cocktail (Sigma–Aldrich, P8340) diluted 1:400, 30  $\mu$ g/mL leupeptin (Merck Millipore, EI8)
- Ni-NTA wash buffer: 50 mM Tris–HCl pH 7.5, 2 mM  $\beta$ -ME, 1 mM PMSF, 1 mM EDTA, 20 mM imidazole, 10  $\mu$ g/mL leupeptin, 10% glycerol, 300 mM NaCl

- Ni-NTA elution buffer: 50 mM Tris-HCl pH 7.5, 1 mM  $\beta$ -ME, 1 mM PMSF, 1 mM EDTA, 120 mM imidazole, 10% glycerol, 300 mM NaCl
- Dilution buffer: 50 mM Tris-HCl pH 7.5, 1 mM PMSF, 1 mM EDTA, 10% glycerol, 300 mM NaCl
- FLAG wash buffer: 50 mM Tris-HCl pH 7.5, 0.5 mM  $\beta$ -ME, 1 mM PMSF, 10% glycerol, 150 mM NaCl
- FLAG elution buffer: FLAG wash buffer supplemented with 150  $\mu$ g/mL 3X FLAG peptide (Sigma-Aldrich, F4799)
- Anti-FLAG M2 Affinity Gel (Sigma-Aldrich, A2220)

### 3.1.3 Procedure

1. Determine the frozen *Sf9* cell pellet volume. Here we describe purification of the MRN complex from 3.2L of cell culture resulting in a total pellet size of  $\sim$ 32mL. The steps described below can be scaled according to the cell pellet volume.
2. All purification steps are carried out on ice or at 4°C. Precool all buffers before use.
3. Thaw frozen cells together with  $\sim$ 3 cell pellet volumes of lysis buffer. In our example, we add 96 mL of lysis buffer to 32 mL cell pellet resulting in total 128 mL solution.
4. Transfer the suspension into a cold beaker of appropriate size.
5. Incubate the mixture at 4°C for 20 min using a magnetic stirrer to assure gentle mixing.
6. Add ice-cold glycerol to a final concentration of 16.7% (v/v). We add 64 mL of 50% glycerol.
7. Add 6.5% volume of ice-cold 5 M NaCl (final concentration 305 mM). We add 12.48 mL of 5 M NaCl.
8. Incubate for 30 min with gentle mixing, using a magnetic stir bar.
9. Centrifuge the mixture at  $48,000 \times g$  for 30 min to obtain soluble extract. Keep a small aliquot of the soluble extract for later analysis.
10. During centrifugation, preequilibrate Ni-NTA resin by gravity flow. In our example, we recommend a total of 16 mL (32 mL of 50% slurry) of Ni-NTA resin, to be equally divided into four 10 mL plastic disposable columns (4 mL of packed resin per each column). Wash Ni-NTA resin with water and equilibrate with Ni-NTA wash buffer.
11. Transfer the equilibrated Ni-NTA resin from the four columns into four 50 mL conical tubes. Distribute soluble extract into the tubes.
12. Incubate the suspension for 1 h with gentle agitation.

13. Centrifuge the sample at  $2000 \times g$  for 2 min. Keep a small aliquot of the supernatant (Ni-NTA flow through) for later analysis.
14. Pool the Ni-NTA resin and wash batch wise with Ni-NTA wash buffer four times, centrifuge as described above.
15. Transfer and distribute the Ni-NTA resin back into the four plastic columns.
16. Wash the resin in each column with  $\sim 40$  mL Ni-NTA wash buffer by gravity flow.
17. Elute the bound proteins from resin in five 2 mL fractions of Ni-NTA elution buffer. Avoid mixing the resin during the elution step.
18. Determine protein concentration in the eluate fractions using a Bradford assay or equivalent.
19. Optional: Analyze the Ni-NTA eluate by polyacrylamide gel electrophoresis. We typically perform this step in initial small-scale experiments, but skip it when performing large-scale preparations to minimize purification time.
20. Pool best eluate fractions from all columns in one 50 mL conical tube. Keep an aliquot (Ni-NTA eluate) for later analysis.
21. Add 1 volume of dilution buffer to the sample. Use multiple 50 mL conical tubes if total volume exceeds 50 mL.
22. Preequilibrate 0.8 mL FLAG resin (1.6 mL 50% slurry) in one 5 mL plastic disposable column by gravity flow. Wash with 3 mL 0.1 M glycine-HCl pH 3.5 and then immediately with 15 mL FLAG wash buffer.
23. Add the equilibrated FLAG resin to the MRN-containing solution in the conical tube and incubate for 1 h with gentle agitation.
24. Transfer the solution back into the 5 mL column. Collect and keep an aliquot of the FLAG flow through for later analysis.
25. Wash the resin with 40 mL FLAG wash buffer by gravity flow.
26. Elute the bound proteins with six 0.4 mL fractions of FLAG elution buffer. From the second to the fifth elution step, stop the flow in the column for 3 min and gently resuspend the resin in the elution buffer. Subsequently, unplug the column and collect the eluate aliquot.
27. Determine protein concentration in the eluate fractions using a Bradford assay or equivalent.
28. Pool fractions with the highest protein concentration, aliquot, snap freeze with liquid nitrogen and store at  $-80^{\circ}\text{C}$ .
29. Analyze soluble extract, Ni-NTA flow through, Ni-NTA eluate, FLAG flow through and final FLAG eluate by polyacrylamide gel electrophoresis (Fig. 1). Determine protein concentration in the final sample.

## Notes

- For initial small-scale experiments, perform steps 1–19 with cell pellets obtained from 50 mL of *Sf9* cell culture. Perform all steps in a 1.5 or 2 mL reaction tubes batch wise. Scale down all volumes accordingly. We also recommend performing small-scale experiments with FLAG-resin only: modify all buffers accordingly and use only 0.5 mM  $\beta$ -ME in the lysis buffer. It may be necessary to repeat the small-scale expression/purification experiments several times to determine the optimal ratio of the MRE11, RAD50, and NBS1 baculoviruses. We often observed that a stoichiometric ratio of the subunits within the MRN complex is obtained when using RAD50 > MRE11 virus.
- Prepare all buffers just prior to use: in particular  $\beta$ -ME and PMSF are unstable in aqueous solutions.
- We prefer salt extraction of proteins as compared to cell lysis, as the procedure described in steps 7 and 8 preserves the integrity of the nuclear membrane. This in turn limits the release of DNA into the extract and limits the possibility of nuclease contamination in the protein preparation. We observed no difference in yield of recombinant MRN when cell lysis was performed.
- The large-scale purification of the MRN complex takes approximately 7 h.
- Both Ni-NTA and anti-FLAG resins may be recycled and used several times according to manufacturer's recommendations.

## 3.2 Purification of Phosphorylated CtIP

CtIP is a critically important factor for DNA end resection (Sartori et al., 2007). Mechanistically, at least one of the key functions of CtIP is to promote the endonuclease activity of MRE11, which is essential to cleave 5'-terminated DNA strands in the vicinity of protein-blocked DSBs (Anand et al., 2016; Deshpande et al., 2016). This endonuclease clipping initiates DSB processing and commits its repair to the recombination machinery. However, the phenotypes associated with defects in CtIP and its homologs such as yeast Sae2 are generally more severe than those caused by MRE11 nuclease-deficient mutations, suggesting that CtIP/Sae2 have additional functions on top of being cofactors of the MRE11 nuclease. To this point, it has been suggested that CtIP/Sae2 removes MRX from DNA ends or counteracts the effect of checkpoint proteins such as Rad9 in yeast (Bonetti et al., 2015; Chen et al., 2015; Gobbini et al., 2015; Puddu

et al., 2015). Additionally, CtIP/Sae2 was proposed to possess an intrinsic nuclease activity, which however remains undefined (Lengsfeld, Rattray, Bhaskara, Ghirlando, & Paull, 2007; Makharashvili et al., 2014; Wang et al., 2014).

It is well established that the function of CtIP and its homologs in DNA end resection is dependent on its phosphorylation (Fu et al., 2014; Huertas et al., 2008; Huertas & Jackson, 2009; Manfrini, Guerini, Citterio, Lucchini, & Longhese, 2010). Although CtIP is well expressed during the G1 phase of the cell cycle, its phosphorylation in S-phase and G2-phase is essential for resection and thus HR. According to the current models, CtIP is phosphorylated by cyclin-dependent kinase (CDK) upon entering S-phase, which activates its capacity to promote MRN. Particularly, the phosphorylation of CtIP at the T847 CDK-site is necessary for these reactions (Huertas & Jackson, 2009). This mode of regulation is remarkably conserved in evolution, as yeast Sae2 must be phosphorylated at the corresponding S267 site to promote resection by yeast Mre11 (Huertas et al., 2008). In humans, CtIP is also targeted at S327 by CDK, which mediates CtIP's interaction with the proresection factor BRCA1 (Yu & Chen, 2004). Additionally, CtIP/Sae2 is also modified upon DNA damage by the ATM and ATR kinases (Baroni, Viscardi, Cartagena-Lirola, Lucchini, & Longhese, 2004; Fu et al., 2014; Liang, Suhandynata, & Zhou, 2015; Peterson et al., 2013). The function of these sites in the regulation of CtIP activity remains to be defined.

Here, we describe large-scale purification of recombinant CtIP from *Sf9* cells. The *Sf9* cell culture was treated with okadaic acid and camptothecin as described in Section 2.2.3. This procedure exploits maltose-binding protein (MBP) tag at the N-terminus and 10X his-tag at the C-terminus of CtIP. The MBP tag is cleaved off during purification. The pFastBac1-derived plasmid construct used for the preparation of the CtIP baculovirus is pFB-MBP-CtIP-his. The typical yield of recombinant CtIP from 2.4 L *Sf9* cell culture is ~110 µg (Fig. 2).

### 3.2.1 Equipment

- Sonicator (Sonopuls GM70, Bandelin or equivalent)
- High speed centrifuge with compatible rotors capable of handling both low and high volumes at 4°C

### 3.2.2 Buffers and Reagents

- Disposable 5 mL (Thermofisher Scientific, 29922) and 10 mL (Thermofisher Scientific, 29924) polypropylene columns

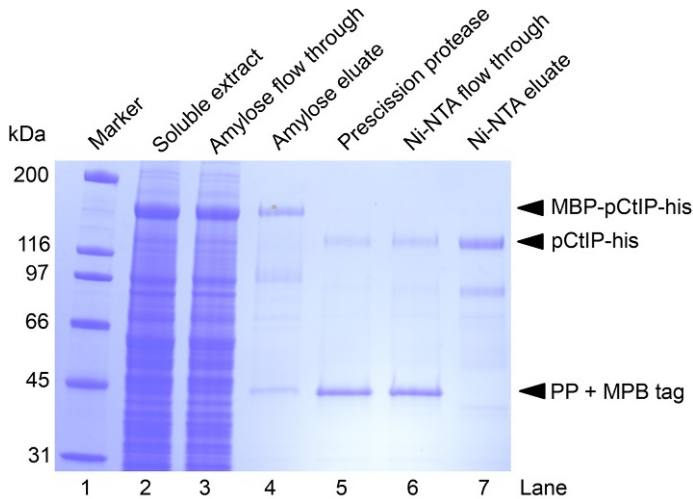


**Fig. 2** Representative phosphorylated CtIP purification. Samples were analyzed on polyacrylamide gel and stained with Coomassie Brilliant Blue. Marker, molecular weight standard, broad range (Biorad), 1  $\mu$ g per band; amylose flow through and eluate, flow through and eluate from amylose resin; precission protease, amylose eluate with precission protease; Ni-NTA flow through and eluate, flow through and eluate from Ni-NTA resin, PP; precission protease, MBP; maltose-binding protein.

- Spectra/Por 4 dialysis membrane molecular weight cut-off RC (MWCO) 12–14 kDa (Spectrum Labs, 132700)
- Glycerol anhydrous (AppliChem, A2926 or equivalent), prepare 50% solution (v/v) with water
- Lysis buffer: 50 mM Tris–HCl pH 8.5, 1 mM DL–dithiothreitol (DTT) (Sigma–Aldrich, D9779), 1 mM PMSF (AppliChem, A0999), 1 mM EDTA (Sigma–Aldrich, EDS), protease inhibitor cocktail (P8340, Sigma–Aldrich) diluted 1:400, 30  $\mu$ g/mL leupeptin (Merck Millipore, EI8), 300 mM NaCl, 10% glycerol, 0.5% Nonidet P 40 substitute (Sigma–Aldrich, 74385), 25 nM okadaic acid, Potassium salt (Merck, 459618), 1 mM sodium orthovanadate (Sigma–Aldrich, 72060), 20 mM sodium fluoride (Sigma–Aldrich, S7920), 15 mM sodium pyrophosphate (Sigma–Aldrich, P8135)
- Amylose wash buffer I: 50 mM Tris–HCl pH 7.5, 2 mM  $\beta$ -ME (Sigma–Aldrich, M6250), 1 mM PMSF, 10% glycerol, 250 mM NaCl, 0.5% Nonidet P 40 substitute
- Amylose wash buffer II: same as amylose wash buffer I but with no NP 40 substitute

- Amylose elution buffer: same as amylose wash buffer II but supplemented with 10 mM D (+) maltose monohydrate (Sigma-Aldrich, M9171)
- Ni-NTA wash buffer: 50 mM Tris-HCl pH 7.5, 2 mM  $\beta$ -ME, 1 mM PMSF, 1 mM EDTA, 20 mM imidazole (Sigma-Aldrich, I202), 10% glycerol, 150 mM NaCl
- Ni-NTA elution buffer: same as Ni-NTA wash buffer but supplemented with 300 mM imidazole
- Dialysis buffer: same as Ni-NTA wash buffer but with no imidazole
- Ni-NTA agarose resin (Qiagen, 30230)
- Amylose resin (NEB, E8021)
- Precission protease, recombinant (see note below)

### 3.2.3 Procedure

1. Determine the *Sf9* cell pellet volume. Here we describe the purification of CtIP from 2.4 L of cell culture resulting in a total pellet size of  $\sim$ 24 mL. The steps described below can be scaled according to the cell pellet volume.
2. Carry out all subsequent steps either on ice or at 4°C. Precool all buffers before use.
3. Thaw frozen cells together with  $\sim$ 3 cell pellet volumes of lysis buffer. In our example, we add 72 mL of lysis buffer to 24 mL pellet resulting in total 96 mL solution.
4. Divide the cell suspension equally into three 50 mL conical tubes. Do not exceed 35 mL in each tube.
5. Sonicate each suspension 6X for 45 s at 70% power. These settings apply to the sonicator listed under “equipment” above: use equivalent settings with other machines if possible. To avoid overheating of the sample, cool the cell lysate and the sonicator probe with ice at regular intervals (after  $\sim$ every two cycles). Clean the probe with deionized water after cooling with ice.
6. Centrifuge the lysate at  $48,000 \times g$  for 45 min to obtain soluble extract. Keep an aliquot of the soluble extract for later analysis.
7. During centrifugation, preequilibrate the amylose resin. We recommend using a total of 12 mL resin, corresponding to 24 mL of 50% slurry. Divide the resin equally into three disposable 10 mL chromatography columns (4 mL of packed resin in each column). Wash the resin with water, followed by lysis buffer.
8. Transfer the equilibrated resin from the three columns into three 50 mL conical tubes and distribute the cleared extract into the tubes. Incubate the samples batch wise for 1 h with gentle agitation.

9. Centrifuge the samples at  $2000 \times g$  for 2 min. Keep an aliquot of the supernatant (amylose flow through) for later analysis. Discard the rest of the supernatant.
10. Resuspend each resin with 40 mL amylose wash buffer I. Repeat the above procedure 3X to wash the resin.
11. Transfer the partially washed amylose resin back to the three 10 mL columns (4 mL of packed resin per each column). Wash the resin in each column with 30 mL amylose wash buffer I first, followed by 10 mL amylose wash buffer II.
12. Add 2 mL of amylose elution buffer to each column and discard the flow through.
13. Add 12 mL of amylose elution buffer to each column and collect the amylose eluate. Pool eluates from the three columns into one 50 mL conical tube. Keep an aliquot of the amylose eluate for later analysis.
14. Optional: Analyze the amylose eluate by polyacrylamide gel electrophoresis. We typically perform this step in initial small-scale experiments, but skip it when performing large-scale preparations to minimize purification time.
15. Estimate the total protein concentration in the pooled eluate with Bradford or similar assay.
16. Add 1/5 of recombinant prescission protease (w/w) compared to the total protein in the pooled amylose eluate to cleave the MBP tag. Incubate the sample for 2 h at 4°C (not on ice) and gently mix the sample at regular intervals. At the end of the incubation, keep an aliquot of the cleaved amylose eluate for later analysis.
17. During the prescission protease digest, equilibrate 0.8 mL Ni-NTA resin (1.6 mL slurry) in one 5 mL plastic disposable column by gravity flow. Wash with 5 mL water and 10 mL Ni-NTA wash buffer.
18. Add imidazole (20 mM final concentration) to the cleaved amylose eluate.
19. Add the equilibrated Ni-NTA resin to the cleaved amylose eluate and incubate for 1 h with gentle agitation to allow CtIP binding to the Ni-NTA resin.
20. Transfer the suspension back to the 5 mL column by gravity flow. Collect an aliquot of the Ni-NTA flow through for later analysis.
21. Wash the packed Ni-NTA resin with 40 mL Ni-NTA wash buffer.
22. Elute CtIP with eight fractions of 0.4 mL Ni-NTA elution buffer.
23. Determine the protein concentration in the eluate fractions using Bradford assay or similar. Pool fractions containing the highest concentration of protein.

24. Dialyze the pooled eluate for 2 h against 1 L dialysis buffer to remove excess imidazole. Gently stir the dialysis buffer with a magnetic stir bar.
25. Distribute the dialyzed CtIP preparation into small aliquots, snap freeze with liquid nitrogen, and store the protein at  $-80^{\circ}\text{C}$ .
26. Analyze aliquots from soluble extract, amylose flow through, amylose eluate, cleaved amylose eluate, Ni-NTA flow through and final sample by polyacrylamide gel electrophoresis (Fig. 2). Determine protein concentration in the final sample.

### Notes

- For initial small-scale experiments, carry out steps 1–14 with cell pellets obtained from 50 mL of S $\beta$ 9 cell culture. Perform all steps in a 1.5 or 2 mL reaction tubes batch wise. Scale down all volumes accordingly.
- The phosphorylation status of CtIP can be determined by treatment with lambda phosphatase (NEB, P0753; use  $\sim 200$  U per  $1\ \mu\text{g}$  of CtIP) for 15 min at  $30^{\circ}\text{C}$ , which should result in electrophoretic mobility shift upon separation by polyacrylamide gel electrophoresis.
- Nonphosphorylated CtIP protein prepared without phosphatase inhibitors is not capable to promote the MRE11 nuclease.
- Prepare all buffers immediately prior to use: in particular  $\beta$ -ME and DTT are unstable in aqueous solutions.
- Recombinant precession protease can be obtained commercially from several suppliers. We express our own, using pGEX-GST-PP construct (Kowalczykowski laboratory, UC Davis). The expression vector was obtained by cloning human rhinovirus 14 LP protease (GenBank [M12168.1](#)) into BamHI and EcoRI sites of pGEX-1 $\lambda$ T (GE Healthcare), creating a fusion of GST tag with the rhinovirus protease. The recombinant polypeptide is then expressed in *E. coli* and purified by single step affinity chromatography with glutathione sepharose resin (Clontech, 635607) using standard procedures.
- The average purification time of CtIP is  $\sim 12$  h. Do not interrupt the procedure to avoid loss of activity.
- We obtain higher CtIP yields upon sonication of the cell suspension, in contrast to salt extraction or other lysis methods. We observed no loss of CtIP activity (in terms of capacity to promote the MRN endonuclease) when sonication was employed.
- Amylose and Ni-NTA resin can be recycled and used several times according to manufacturer's recommendations.

### 3.3 Purification of DNA2

Dna2 was initially described in yeast as an Okazaki fragment processing factor, which is necessary to remove DNA flaps forming during lagging strand DNA synthesis (Bae, Bae, Kim, & Seo, 2001; Bae & Seo, 2000). Much later, the function of Dna2 in long-range DNA end resection in conjunction with Sgs1 was discovered (Zhu et al., 2008). However, DNA replication and DNA end resection are not the only processes that rely on Dna2's activity: Dna2 was shown to act in other pathways including telomere maintenance (Choe, Budd, Imamura, Hoopes, & Campbell, 2002), long-patch base excision repair (Zheng et al., 2008), and checkpoint signaling (Kumar & Burgers, 2013). In contrast to the yeast homolog, the function of human DNA2 is much less defined. While its role together with WRN or BLM helicase in long-range DNA end resection is conserved in evolution (Nimonkar et al., 2011; Sturzenegger et al., 2014), its function in Okazaki fragment processing remains undefined. Instead, human DNA2 was shown to be required for successful completion of DNA replication, possibly in response to endogenous DNA damage (Duxin et al., 2012). Human DNA2, in concert with the WRN helicase, is also involved in the degradation of reversed forks helping to restart replication (Thangavel et al., 2015). Another report described the pathological degradation of nascent DNA by DNA2 and WRN during interstrand crosslink repair (Wang et al., 2015).

In terms of enzymatic activity, DNA2 is a 5' → 3' and 3' → 5' ssDNA nuclease that requires a free DNA end (Bae et al., 1998; Masuda-Sasa, Imamura, & Campbell, 2006). However, under physiological conditions when RPA is present, DNA2 degrades ssDNA only with 5' → 3' polarity, suggesting that only this directionality of the nuclease is likely to be relevant in vivo (Cejka et al., 2010; Nimonkar et al., 2011; Niu et al., 2010). In addition to its nuclease, DNA2 and its homologs contain a well-conserved helicase domain (Budd & Campbell, 1995). While DNA2 can unwind dsDNA in the 5' → 3' direction when its nuclease activity is attenuated, the motor activity of DNA2 likely primarily functions as a ssDNA translocase to facilitate degradation of ssDNA rather than as a DNA helicase to unwind dsDNA (Levikova, Klaue, Seidel, & Cejka, 2013; Levikova, Pinto, & Cejka, 2017; Miller et al., 2017; Pinto et al., 2016).

Here we describe large-scale purification of the recombinant human DNA2 from *Sf9* cells. The procedure exploits the N-terminal 6X his-tag and the C-terminal FLAG-tag, and the corresponding transfer vector is pFB-His-hDNA2-FLAG (Pinto et al., 2016). To improve yield, the human

*DNA2* gene sequence was codon optimized for the expression in *Sf9* insect cells. The typical yield of wild-type human DNA2 from 3L *Sf9* cell culture is  $\sim 370 \mu\text{g}$  (Fig. 3).

### 3.3.1 Equipment

- High speed centrifuge with compatible rotors capable of handling both low and high volumes at  $4^\circ\text{C}$

### 3.3.2 Buffers and Reagents

Important: degas and chill all buffers on ice before use. Prepare all buffers just before use.

- Disposable 5 mL (Thermofisher Scientific, 29922) and 10 mL (Thermofisher Scientific, 29924) polypropylene columns
- Glycerol anhydrous (AppliChem, A2926 or equivalent), prepare 50% solution (v/v) with water
- Lysis buffer: 50 mM Tris-HCl pH 7.5, 2 mM  $\beta$ -ME (Sigma-Aldrich, M6250), 1 mM PMSF (AppliChem, A0999), 1 mM EDTA (Sigma-Aldrich, EDS), 10 mM imidazole (Sigma-Aldrich, I202), protease inhibitor cocktail (Sigma-Aldrich, P8340) diluted 1:250, 30  $\mu\text{g}/\text{mL}$  leupeptin (Merck Millipore, E18)

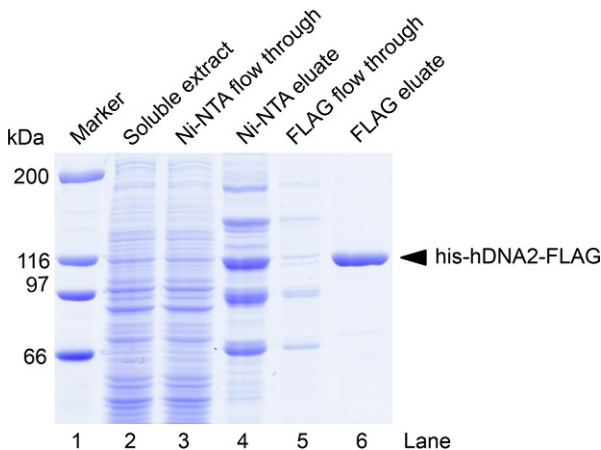


**Fig. 3** Representative human DNA2 purification. Samples were analyzed on polyacrylamide gel and stained with Coomassie Brilliant Blue. Marker, molecular weight standard, broad range (Biorad), 1  $\mu\text{g}$  per band; Ni-NTA flow through and eluate, flow through and eluate from Ni-NTA resin; FLAG flow through and eluate, flow through and eluate from anti-FLAG affinity resin.

- Ni-NTA wash buffer 1M: 50 mM Tris-HCl pH 7.5, 2 mM  $\beta$ -ME, 1 mM PMSF, 1 mM EDTA, 10 mM imidazole, 1:1000 protease inhibitor cocktail, 30  $\mu$ g/mL leupeptin, 10% glycerol, 1 M NaCl
- Ni-NTA wash buffer 300 mM: Same as Ni-NTA wash buffer 1 M but with 300 mM NaCl instead of 1 M NaCl
- Ni-NTA wash buffer 150 mM: Same as Ni-NTA wash buffer 1 M but with 150 mM NaCl instead of 1 M NaCl
- Ni-NTA elution buffer: Ni-NTA wash buffer 150 mM supplemented with 300 mM imidazole
- FLAG wash buffer 150 mM: 50 mM Tris-HCl pH 7.5, 0.5 mM  $\beta$ -ME, 1 mM PMSF, 10% glycerol, 150 mM NaCl
- FLAG elution buffer: FLAG wash buffer 150 mM supplemented with 150  $\mu$ g/mL 3X FLAG peptide (Sigma-Aldrich, F4799)
- Ni-NTA agarose resin (Qiagen, 30230)
- Anti-FLAG M2 Affinity Gel (Sigma-Aldrich, A2220)

### 3.3.3 Procedure

1. Determine the *Sf9* cell pellet volume. Here we describe the purification of DNA2 from 3 L of *Sf9* cell culture resulting in a total pellet size of  $\sim$ 30 mL. The steps described below can be scaled up or down according to the cell pellet volume.
2. Carry out all subsequent steps either on ice or at 4°C.
3. Thaw frozen *Sf9* cells together with  $\sim$ 3 volumes of lysis buffer. In our example, we add 90 mL lysis buffer to the 30 mL pellet resulting in a total suspension volume of 120 mL.
4. Transfer the suspension into a cold beaker and incubate for 20 min with gentle agitation using a magnetic stir bar.
5. Add glycerol to a final concentration of 16.7%. We add 60 mL of 50% glycerol.
6. Add 6.5% volume of ice-cold 5 M NaCl (final concentration 305 mM). We add 11.7 mL of 5 M NaCl.
7. Incubate the suspension for 30 min with gentle mixing using a magnetic stir bar.
8. Centrifuge the mixture at  $48,000 \times g$  for 30 min to obtain soluble extract. Keep a small aliquot for later analysis.
9. During centrifugation, equilibrate the Ni-NTA resin. We recommend using a total of 8 mL Ni-NTA resin (16 mL of 50% slurry). Distribute the resin into two 10 mL disposable chromatography columns (4 mL

- packed resin per column). Wash the resin in each column with 10 mL water and 20 mL Ni-NTA wash buffer 300 mM by gravity flow.
10. Transfer the cleared soluble extract into 50 mL conical tubes. Distribute the equilibrated Ni-NTA resin equally to the soluble extract.
  11. Incubate the suspension batch wise for 1 h with gentle agitation to allow DNA2 binding to the Ni-NTA resin.
  12. Centrifuge the sample at  $2000 \times g$  for 2 min. Keep an aliquot of the Ni-NTA flow through for later analysis, discard the rest of the supernatant.
  13. Resuspend the resin with Ni-NTA wash buffer 1 M and pool the resin into one conical tube. Wash the pooled resin batch wise 5X with 40 mL Ni-NTA wash buffer 1 M, repeating the centrifugation step described above. Discard supernatant.
  14. Transfer and distribute the resin back to the two 10 mL disposable columns. Wash each column with 40 mL Ni-NTA wash buffer 1 M by gravity flow.
  15. Wash each column with 10 mL Ni-NTA wash buffer 150 mM by gravity flow.
  16. Elute bound proteins from the Ni-NTA resin in each column with ten 1 mL fractions using Ni-NTA elution buffer. Determine protein concentration in the eluate fractions using a Bradford or an equivalent assay.
  17. Pool 1 mL fractions with the highest concentration of proteins from both columns. We recommend selecting five fractions from each column. Keep an aliquot of the pooled Ni-NTA eluate for later analysis.
  18. Optional: Analyze the Ni-NTA eluate by polyacrylamide gel electrophoresis. We typically perform this in initial small-scale experiments, but skip this step when performing large-scale preparations to minimize purification time.
  19. Add four volumes of FLAG wash buffer 150 mM to the Ni-NTA eluate, i.e., 40 mL FLAG wash buffer 150 mM to 10 mL Ni-NTA eluate. This step is necessary to lower  $\beta$ -ME concentration to avoid chemical reduction of the FLAG antibody.
  20. Equilibrate 0.5 mL FLAG resin (1 mL of 50% slurry) in a 5 mL disposable chromatography column by gravity flow. Wash the resin with 3 mL 0.1 M glycine HCl pH 3.5 and then immediately with 15 mL FLAG wash buffer 150 mM.
  21. Add the equilibrated FLAG resin to the diluted Ni-NTA eluate and incubate for 1 h with gentle mixing.

22. Transfer the suspension back to the 5 mL column by gravity flow. Keep an aliquot of FLAG flow through for later analysis.
23. Wash the resin with 30 mL FLAG wash buffer 150 mM by gravity flow.
24. Elute bound DNA2 from the FLAG resin with five 0.5 mL fractions of FLAG elution buffer. For fractions 2–4, stop the flow of the column, gently mix the resin with the elution buffer and incubate for 3 min. Unplug the column and collect the eluate.
25. Determine protein concentration in the eluate fractions using a Bradford or an equivalent assay. Pool fractions containing the highest concentrations of protein.
26. Aliquot the DNA2 preparation, snap freeze with liquid nitrogen and store at  $-80^{\circ}\text{C}$ .
27. Analyze soluble extract, Ni-NTA flow through, Ni-NTA eluate, FLAG flow through and final FLAG eluate by polyacrylamide gel electrophoresis (Fig. 3). Determine protein concentration in the final sample.

### Notes

- For initial small-scale experiments, carry out steps 1–18 with cell pellets obtained from 50 mL of *Sf9* cell culture. Perform all steps in a 1.5 or 2 mL reaction tubes batch wise. Scale down all volumes accordingly. We also recommend performing small-scale experiments with FLAG resin: adjust all buffers accordingly and use only 0.5 mM  $\beta$ -ME in the lysis buffer.
- Ni-NTA and FLAG resins can be recycled and reused several times according to resin manufacturer's instructions.
- We often achieved similar yields with wild-type and nuclease-deficient DNA2, while the yields of helicase-deficient and nuclease- and helicase-deficient (double-dead) DNA2 variants were  $\sim 10$ -fold lower.
- As DNA2 contains an iron-sulfur cluster (Pokharel & Campbell, 2012; Yeeles, Cammack, & Dillingham, 2009) that is prone to oxidation, it is necessary to work under reducing conditions. As FLAG resin is not compatible with high concentration of reducing agents, we recommend degassing all buffers.
- The average purification time is  $\sim 9$  h. Do not interrupt the procedure to avoid loss of DNA2's activity.

### 3.4 Purification of Human WRN and BLM Helicase

BLM and WRN are two out of five human members of the RECQ helicase family (Larsen & Hickson, 2013). Mutations in BLM associate with Bloom

syndrome, a rare disorder that predisposes affected individuals to most cancer types. The characteristic cellular hallmark of BLM-deficient cells is an elevated frequency of sister chromatid exchanges, resulting from processing of recombination intermediates into crossovers in the absence of BLM. The BLM helicase, together with topoisomerase III $\alpha$  and cofactors RMI1/RMI2, catalyze the processing of double Holliday junctions into noncrossover products, preventing thus alternative pathways leading to crossovers (Wu & Hickson, 2003). The resulting genome instability in BLM-deficient cells may be the underlying cause of BLM-associated cancers. The BLM helicase also possesses an antirecombinational activity through its capacity to disrupt RAD51 nucleoprotein filaments and D-loops (Bugreev, Yu, Egelman, & Mazin, 2007), which may prevent illegitimate recombination. The function of BLM in DNA end resection was discovered in 2008, when it was shown to physically and functionally interact with DNA2 (Gravel et al., 2008; Zhu et al., 2008).

Mutations in WRN associate with Werner syndrome characterized by premature aging and cancer predisposition (Larsen & Hickson, 2013). Unlike BLM, the cellular functions of WRN are much less defined. Initially, WRN was linked with base excision repair due to its functional interaction with NEIL1 glycosylase (Das et al., 2007) and DNA polymerase  $\beta$  (Harrigan et al., 2003) as well as in DNA replication and telomere metabolism (Brosh et al., 2001; Opresko et al., 2004). The function of WRN in DNA end resection was first demonstrated in *Xenopus laevis* egg extracts, and only later in human cells (Liao, Toczylowski, & Yan, 2008; Sturzenegger et al., 2014). These and subsequent studies demonstrated that WRN physically and functionally interacts with DNA2, and that the WRN–DNA2 pair may play a more important role than BLM–DNA2 complex in some cases (Pinto et al., 2016). The choice of WRN or BLM as a partner of DNA2, as well as DNA2- or EXO1-catalyzed branches of DNA end resection remains to be defined. RPA is an integral component of the BLM/WRN–DNA2 resection machinery.

In terms of enzymatic activity, both BLM and WRN are helicases that unwind dsDNA with a 3'  $\rightarrow$  5' polarity, i.e., translocate on one of the DNA strands in a 3'  $\rightarrow$  5' direction. ATP hydrolysis is essential for the helicase activity of both proteins, and the respective helicase-deficient variants can be prepared by mutating the ATP-binding/hydrolysis domains, resulting in inactive variants BLM K695A and WRN K577M, respectively. DNA unwinding by both BLM and WRN is stimulated by RPA, which prevents annealing of the unwound single strands of DNA, as well as provides

additional species-specific stimulatory function that likely depends on physical interactions between RPA and BLM/WRN (Bohr et al., 2000; Brosh et al., 2000; Larsen & Hickson, 2013). Additionally, WRN contains an N-terminal exonuclease domain exhibiting a weak 3' → 5' exonuclease activity on 3' recessed DNA ends (Bohr et al., 2000). Although the function of WRN nuclease remains to be defined, evidence available to date suggests that it is dispensable for DNA end resection (Sturzenegger et al., 2014).

Here we describe large-scale purification of the recombinant human WRN helicase from *Sf9* cells. The purification procedure exploits an N-terminal MBP and a C-terminal 10X his affinity tags. The MBP tag is cleaved off during purification. As our BLM construct bears identical affinity tags, the same purification procedure can be applied for preparing recombinant BLM as well. The corresponding transfer vectors are pFB-MBP-WRN-his and pFB-MBP-BLM-his (Pinto et al., 2016). The typical yield of wild-type or mutant WRN from 2.4 L *Sf9* insect cell culture is ~200 µg (Fig. 4). The average yield of recombinant BLM from 2 L *Sf9* cells is ~110 µg.

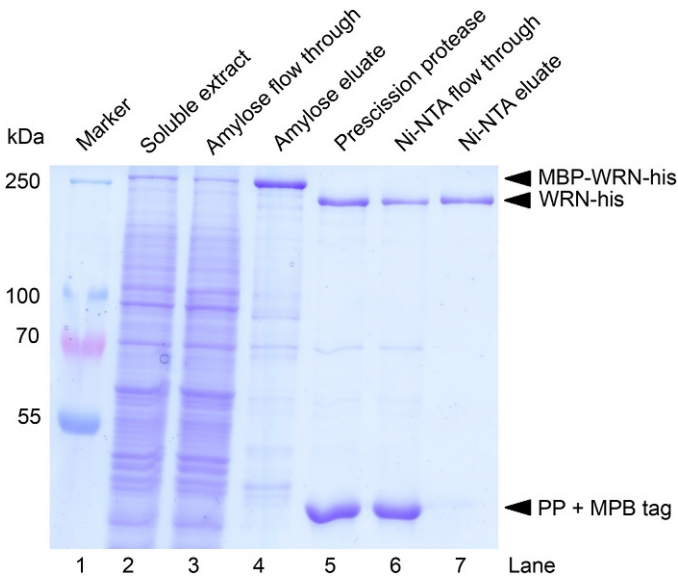


**Fig. 4** Representative WRN purification. Samples were analyzed on polyacrylamide gel and stained with Coomassie Brilliant Blue. Purification of WRN variant K577M is shown. Marker, Pageruler Plus prestained protein ladder 10–250 kDa (ThermoFisher Scientific, 26619); amylose flow through and eluate, flow through and eluate from amylose resin; prescission protease, amylose eluate with prescission protease; Ni-NTA flow through and eluate, flow through and eluate from Ni-NTA resin, PP; prescission protease, MBP; maltose-binding protein.

### 3.4.1 Equipment

- High speed centrifuge with compatible rotors capable of handling both low and high volumes at 4°C

### 3.4.2 Buffers and Reagents

- Disposable 5 mL (ThermoFisher Scientific, 29922) and 10 mL (ThermoFisher Scientific, 29924) polypropylene columns
- Spectra/Por 3 dialysis membrane MWCO 3.5 kDa (Spectrum Labs, 132720)
- Glycerol anhydrous (AppliChem, A2926 or equivalent), prepare 50% solution (v/v) with water
- Lysis buffer: 50 mM Tris-HCl pH 7.5, 2 mM  $\beta$ -ME (Sigma-Aldrich, M6250), 1 mM PMSF (AppliChem, A0999), 1 mM EDTA (Sigma-Aldrich, EDS), protease inhibitor cocktail (Sigma-Aldrich, P8340) diluted 1:250, 30  $\mu$ g/mL leupeptin (Merck Millipore, E18)
- Amylose wash buffer 1 M: 50 mM Tris-HCl pH 7.5, 5 mM  $\beta$ -ME, 1 mM PMSF, 10% glycerol, 1 M NaCl
- Amylose wash buffer 300 mM: Same as amylose wash buffer 1 M but with 300 mM NaCl instead of 1 M NaCl
- Amylose elution buffer: 50 mM Tris-HCl pH 7.5, 5 mM  $\beta$ -ME, 1 mM PMSF, 10% glycerol, 300 mM NaCl, 10 mM D (+) maltose monohydrate (Sigma-Aldrich, M9171)
- Ni-NTA buffer A1: 50 mM Tris-HCl pH 7.5, 5 mM  $\beta$ -ME, 1 mM PMSF, 10% glycerol, 1 M NaCl, 58 mM imidazole
- Ni-NTA buffer A2: Same as Ni-NTA buffer A1 but with 150 mM NaCl instead of 1 M NaCl
- Ni-NTA buffer B: 50 mM Tris-HCl pH 7.5, 5 mM  $\beta$ -ME, 1 mM PMSF, 10% glycerol, 100 mM NaCl, 300 mM imidazole
- Dialysis buffer: 50 mM Tris-HCl pH 7.5, 5 mM  $\beta$ -ME, 0.5 mM PMSF, 10% glycerol, 100 mM NaCl
- Amylose resin (NEB, E8021)
- Ni-NTA agarose resin (Qiagen, 30230)
- Precission protease, recombinant (see Notes in [Section 3.2.3](#))

### 3.4.3 Procedure

1. Determine the *Sf9* cell pellet volume. Here we describe the purification of WRN from 2.4 L *Sf9* cell culture resulting in a total pellet size of  $\sim$ 24 mL. The procedure can be scaled up or down accordingly.
2. Perform all subsequent steps on ice or at 4°C.

3. Thaw the frozen cell pellet with three pellet volumes of lysis buffer. In our example, we add 72 mL lysis buffer to the 24 mL pellet resulting in a total suspension volume of 96 mL.
4. Transfer the suspension into a cold beaker and incubate for 20 min with gentle agitation using a magnetic stir bar.
5. Add ice-cold glycerol to a final concentration of 16.7%. We add 48 mL of 50% glycerol.
6. Add 6.5% volume of ice-cold 5 M NaCl to a final concentration of 305 mM. We add 9.36 mL 5 M NaCl. Incubate for 30 min with gentle agitation using a magnetic stir bar.
7. Centrifuge the mixture at  $48,000 \times g$  for 30 min to obtain soluble extract. Keep a small aliquot of soluble extract for later analysis.
8. During centrifugation, equilibrate 8 mL of amylose resin (16 mL of 50% slurry). Distribute the resin into two 10 mL disposable chromatography columns by gravity flow (4 mL packed resin in each column). Wash the resin in each column with 10 mL water and 15 mL amylose wash buffer 300 mM by gravity flow.
9. Transfer the cleared soluble extract into 50 mL conical tubes and distribute the equilibrated amylose resin into the samples.
10. Incubate the suspension for 1 h with gentle agitation to allow WRN binding to the resin.
11. Centrifuge the sample at  $2000 \times g$  for 2 min. Collect an aliquot of the amylose flow through for later analysis and discard the rest of the supernatant.
12. Resuspend the amylose resin with amylose wash buffer 1 M and pool all resin into one conical tube. Wash the resin 4X with 40 mL amylose wash buffer 1 M, repeating the centrifugation step described above.
13. Transfer the resin back to the two chromatography columns and wash each column with 70 mL amylose wash buffer 1 M.
14. Elute bound proteins with ten 1 mL fractions of amylose elution buffer.
15. Optional: Analyze the amylose eluate by polyacrylamide gel electrophoresis. We typically perform this in initial small-scale experiments, but skip this step when performing large-scale preparations to minimize purification time.
16. Determine protein concentration in the eluate fractions using Bradford or a similar assay. Pool fractions containing the highest concentration of protein. Keep an aliquot of the amylose eluate for later analysis.

17. Determine the total protein concentration in the amylose eluate and add prescission protease to cleave the MBP tag. We add 20  $\mu\text{g}$  prescission protease to 100  $\mu\text{g}$  MBP–WRN. Incubate the solution at 4°C (not on ice) for 1 h and stir the solution occasionally. Collect an aliquot of the cleaved amylose eluate for later analysis.
18. During protein cleavage by prescission protease, equilibrate 0.5 mL (1 mL 50% slurry) of Ni-NTA resin in a 5 mL chromatography column by gravity flow. Wash the resin with 5 mL water and 10 mL amylose elution buffer supplemented with 10 mM imidazole.
19. Add imidazole to the cleaved sample to a final concentration of 10 mM.
20. Add the equilibrated Ni-NTA resin to the cleaved amylose eluate. Incubate the suspension for 1 h with gentle agitation.
21. Transfer the resin back to the 5 mL chromatography column by gravity flow. Wash the resin with 30 mL Ni-NTA buffer A1. Keep an aliquot of the Ni-NTA flow through for later analysis.
22. Wash the resin with 5 mL Ni-NTA buffer A2 by gravity flow.
23. Elute bound WRN from the Ni-NTA resin with five 0.5 mL fractions using Ni-NTA buffer B.
24. Determine protein concentration in the Ni-NTA eluate fractions using Bradford or a similar assay. Pool fractions containing the highest protein concentration.
25. Dialyze the pooled Ni-NTA eluate against 1 L dialysis buffer for 1.5 h to reduce imidazole concentration in the sample.
26. Aliquot the final WRN preparation, snap freeze with liquid nitrogen and store at  $-80^{\circ}\text{C}$ .
27. Analyze soluble extract, amylose flow through, amylose eluate, cleaved amylose eluate, Ni-NTA flow through and final Ni-NTA eluate by polyacrylamide gel electrophoresis (Fig. 4). Determine protein concentration in the final sample.

### Notes

- For initial small-scale experiments, carry out steps 1–15 with cell pellets obtained from 50 mL of *S9* cell culture. Perform all steps in a 1.5 or 2 mL reaction tubes batch wise. Scale down all volumes accordingly.
- Amylose and Ni-NTA resins can be recycled and reused several times according to manufacturer's instructions.
- The average purification time is  $\sim 12$  h. We strongly recommend performing the purification in 1 day without interruptions to avoid loss of activity.

### 3.5 Expression and Purification of RPA

Human RPA is one of the central proteins in DNA metabolism. It was initially found as a component of the minimal system required for the replication of the simian virus 40 (Wobbe et al., 1987). Since then, key roles of RPA have been discovered in almost all DNA metabolic pathways, including replication, transcription, and repair (Wold, 1997). Human RPA is a heterotrimeric complex consisting of 70, 32, and 14kDa subunits. RPA shows a strong affinity for ssDNA and a much lower affinity for dsDNA. The strong ssDNA-binding capacity of RPA represents the key biochemical function of RPA. By forming a tight nucleoprotein complex, RPA stabilizes and protects ssDNA, as well as helps to remove secondary DNA structures (Wold, 1997). At the same time, the function of RPA goes clearly beyond ssDNA binding. RPA physically and functionally interacts with components of the replication and repair machineries, which adds a species-specific component to its function. RPA mutations that specifically affect its role in DNA repair or recombination but not in DNA replication have been identified, suggesting that RPA functions in distinct DNA metabolic processes may be separable (Umezu, Sugawara, Chen, Haber, & Kolodner, 1998). The mechanistic details however still remain largely undefined.

RPA promotes several steps of the DNA recombination pathway; including DNA end resection, DNA strand exchange, DNA synthesis, and processing of Holliday junctions. Although RPA promotes the recruitment of MRX to DSBs in yeast (Seeber et al., 2016), a function of RPA in short-range DNA end resection has not been reported (Chen, Lisby, & Symington, 2013). RPA clearly promotes long-range DNA end resection by WRN-DNA2 or BLM-DNA2, where it stimulates both DNA unwinding by the RecQ family helicase, as well as directs polarity of DNA degradation by hDNA2 to the unwound 5'-terminated DNA strand, and thus ensures the correct polarity of resection (Nimonkar et al., 2011; Pinto et al., 2016). RPA may also promote DNA end resection by EXO1 (Cannavo, Cejka, & Kowalczykowski, 2013; Chen et al., 2013), although the interplay of EXO1 and RPA is somewhat more complex and RPA can also inhibit EXO1 under other experimental conditions (Gong, Handa, Kowalczykowski, & de Lange, 2017; Nicolette et al., 2010).

The RPA purification protocol described below represents a minor modification of the procedure established by Wold and colleagues (Binz, Dickson, Haring, & Wold, 2006). Unlike other components of the resection machinery, we use the *E. coli* expression system for the production of the RPA heterotrimer.

### 3.5.1 Equipment

- Liquid chromatography system, such as ÄKTA pure (GE Healthcare)
- Sonicator (Sonopuls GM70, Bandelin) or equivalent such as French press
- High speed centrifuge with compatible rotors capable of handling both low and high volumes at 4°C
- 5 mL HiTrap Blue HP (17-0412-01), 5 mL HiTrap desalting (17-1408-01), 1 mL HiTrap Q HP (17-1153-01) chromatography columns (all GE Healthcare) or equivalents

### 3.5.2 Buffers and Reagents

- *E. coli* BL21(DE3) pLysS cells (Promega, L1195) or equivalent
- pET11d-tRPA expression vector (Binz et al., 2006)
- SOC medium: 2% tryptone, 0.5% yeast extract, 10 mM NaCl, 2.5 mM KCl, 10 mM MgCl<sub>2</sub>, 10 mM MgSO<sub>4</sub>, 20 mM glucose. Filter-sterilize
- LB medium (AppliChem, A0954). Autoclave
- IPTG (Sigma-Aldrich, I6758), 0.1 M solution. Filter-sterilize
- Glycerol anhydrous (AppliChem, A2926 or equivalent), prepare 50% solution (v/v) with water
- Sodium thiocyanate (Sigma-Aldrich, 251410)
- Lysis buffer (no salt): 25 mM Tris pH 8.0, 0.25 mM EDTA, 0.01% NP 40 substitute (Sigma-Aldrich, 74385), 1 mM DTT (Sigma-Aldrich, D9779), 10% glycerol, 1 mM PMSF (AppliChem, A0999), as well as variants of this buffer with various salts (see below). Filter to remove debris. Prepare just prior to purification. Precool to 4°C
- Ampicillin sodium salt (AppliChem, A0839)
- Protease inhibitor cocktail (Sigma-Aldrich, P8465)

### 3.5.3 RPA Expression in *E. coli*

1. Transform *E. coli* BL21(DE3) pLysS cells with 50 ng of pET11d-tRPA plasmid (Binz et al., 2006), coding for all three subunits of human RPA, using standard procedures. Resuspend the transformation mixture in 1 mL SOC medium and incubate at 37°C for 1 h.
2. Inoculate 100 µL of the transformation mixture into 1 L of LB of media with ampicillin (100 µg/mL) in a 5 L Erlenmeyer flask. Inoculate a total of five flasks (total media volume 5 L), and incubate at 27°C without shaking overnight.
3. The next morning, increase the temperature to 37°C and start shaking the culture vigorously. Monitor optical density of the culture.

4. Induce the expression of RPA when optical density of the culture reaches  $\sim 0.6$  with  $0.4 \text{ mM}$  IPTG, cool the culture and incubate overnight at  $18^\circ\text{C}$  while shaking.
5. Spin the cells at  $5000 \text{ g}$  for  $30 \text{ min}$  and decant the supernatant. Freeze the cell pellets in liquid nitrogen and store the frozen pellets at  $-80^\circ\text{C}$ .

#### Notes

1. We observed significant variability in RPA expression when we plated the electroporation mixture and tested individual colonies. This may be due to toxicity of leaky RPA expression, which may lead to selection against high expressing clones. The step described in point (2) eliminates this variability.
2. Frozen cell pellets can be stored for extended time at  $-80^\circ\text{C}$ .

#### 3.5.4 Purification of RPA

1. Cell pellets were pooled and resuspended in  $60 \text{ mL}$  lysis buffer without salt. Add protease inhibitor cocktail as recommended by the manufacturer. Perform this and all subsequent steps at  $4^\circ\text{C}$  or on ice.
2. Lyse the cells by sonication or French press according to instrument manufacturer's recommendation.
3. Spin the cell lysate at  $48,000 \times g$  for  $30 \text{ min}$  to obtain soluble extract. Preserve a small aliquot for analysis by polyacrylamide gel.
4. Using liquid chromatography system, equilibrate  $5 \text{ mL}$  HiTrap Blue HP column with lysis buffer at flow rate of  $1 \text{ mL/min}$ .
5. Apply the sample on column at  $0.4 \text{ mL/min}$ . Collect a small aliquot of flow through for later analysis.
6. Perform the following washing steps at  $1 \text{ mL/min}$ ,  $20 \text{ mL}$  for each buffer:
  - lysis buffer with  $50 \text{ mM}$  KCl;
  - lysis buffer with  $800 \text{ mM}$  KCl; and
  - lysis buffer with  $500 \text{ mM}$  NaSCN.
7. Elute RPA with lysis buffer containing  $1.5 \text{ M}$  NaSCN. Collect  $1.5 \text{ mL}$  fractions.
8. Analyze fractions containing protein by running the samples on a polyacrylamide gel and stain with Coomassie Brilliant Blue. Pool fractions containing RPA (Fig. 5A). Retain a small aliquot of the sample for later analysis.
9. Exchange the sample buffer (containing  $1.5 \text{ M}$  NaSCN) with lysis buffer containing  $50 \text{ mM}$  KCl. To do that, repeat the following procedure. Equilibrate  $5 \text{ mL}$  HiTrap desalting column with lysis buffer

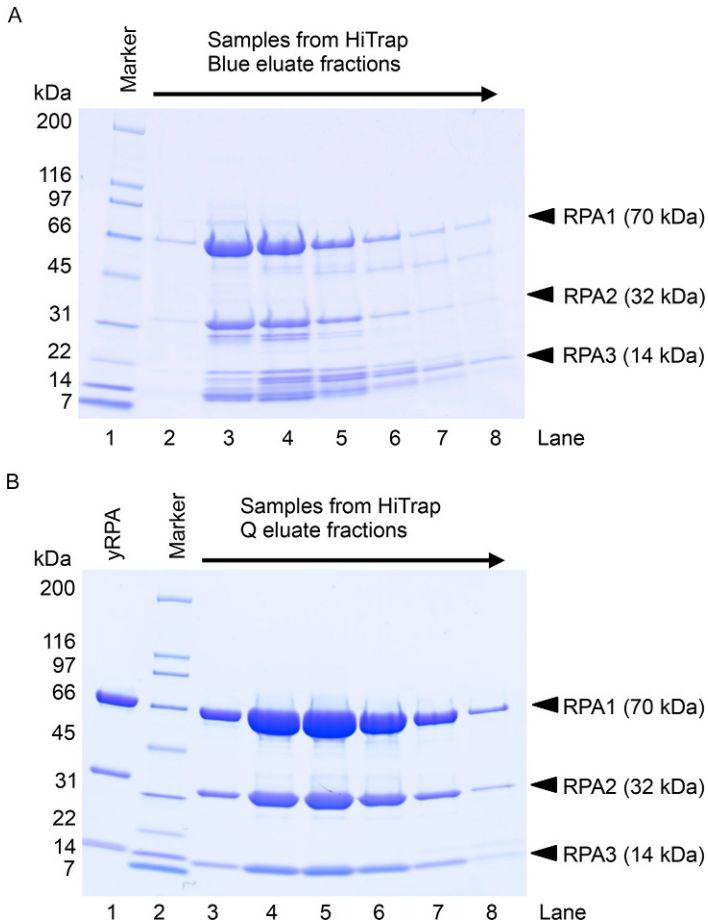


**Fig. 5** Representative human RPA purification. Samples were analyzed on polyacrylamide gel and stained with Coomassie Brilliant Blue. (A) Lane 1, marker, molecular weight standard, broad range (Biorad), 1  $\mu$ g per band. Lanes 2–8, selected fractions from HiTrap Blue eluate. (B) Lane 1, yRPA, yeast RPA was loaded as a control; Lane 2, marker, molecular weight standard, broad range (Biorad), 1  $\mu$ g per band. Lanes 3–8, selected fractions from HiTrap Q eluate.

containing 50 mM KCl. Each time, apply 1.5 mL of the sample onto the column using a syringe by hand. Connect the column to the liquid chromatography system equilibrated with lysis buffer containing 50 mM KCl. Using flow rate of 1 mL/min, collect five 1 mL fractions. Throughout elution, monitor UV absorbance and conductivity. In our setup, the first two fractions contain most of the protein, while the thiocyanate salt only appears at later fractions. Pool protein-containing

fractions with conductivity corresponding to 50 mM KCl-containing lysis buffer. Repeat the above procedure until you process the entire pooled HiTrap Blue eluate.

10. Using liquid chromatography system, equilibrate 1 mL HiTrap Q column with lysis buffer containing 50 mM KCl. Apply the desalted RPA preparation using a flow rate of 0.3 mL/min. Keep an aliquot of the flow through sample for later analysis.
11. Wash the column with 20 mL lysis buffer containing 50 mM KCl. Elute the sample with 10 mL gradient of lysis buffer ranging from 50 mM to 800 mM KCl. Collect 0.3 mL fractions.
12. Analyze fractions containing protein by SDS-PAGE and stain the protein with Coomassie Brilliant Blue. Pool fractions containing RPA (Fig. 5B). The RPA should be >95% pure at this point. The typical yield from 5 L culture is ~10 mg of RPA at concentration of ~50  $\mu$ M.
13. Distribute RPA in small aliquots and snap freeze in liquid nitrogen. Keep at  $-80^{\circ}\text{C}$  for long-term storage and up to ~1 month at  $4^{\circ}\text{C}$ .

### Notes

1. We use the HiTrap desalting column instead of dialysis in step 9, which prevents protein precipitation. In case precipitation still occurs, centrifuge the sample prior to applying on HiTrap Q column (30 min at  $48,000 \times g$  at  $4^{\circ}\text{C}$ ) and only apply the supernatant on the column. Alternatively, hydroxyapatite column may also be used in this step, as described previously (Binz et al., 2006).
2. The procedure can be interrupted overnight upon application of RPA on either HiTrap Blue or HiTrap Q column, or upon elution from HiTrap Q column before testing the individual fractions.

### ACKNOWLEDGMENTS

We thank members of the Cejka laboratory (Elda Cannavo, Lepakshi Ranjha, and Sean Howard) for comments on the manuscript. Funding by the Swiss National Science Foundation, European Research Council and Swiss Cancer League (all to P.C.) is gratefully acknowledged.

### REFERENCES

- Anand, R., Ranjha, L., Cannavo, E., & Cejka, P. (2016). Phosphorylated CtIP functions as a co-factor of the MRE11-RAD50-NBS1 endonuclease in DNA end resection. *Molecular Cell*, 64(5), 940–950. <https://doi.org/10.1016/j.molcel.2016.10.017>.
- Bae, S. H., Bae, K. H., Kim, J. A., & Seo, Y. S. (2001). RPA governs endonuclease switching during processing of Okazaki fragments in eukaryotes. *Nature*, 412(6845), 456–461. <https://doi.org/10.1038/35086609>.

- Bae, S. H., Choi, E., Lee, K. H., Park, J. S., Lee, S. H., & Seo, Y. S. (1998). Dna2 of *Saccharomyces cerevisiae* possesses a single-stranded DNA-specific endonuclease activity that is able to act on double-stranded DNA in the presence of ATP. *The Journal of Biological Chemistry*, 273(41), 26880–26890.
- Bae, S. H., & Seo, Y. S. (2000). Characterization of the enzymatic properties of the yeast dna2 Helicase/endonuclease suggests a new model for Okazaki fragment processing. *The Journal of Biological Chemistry*, 275(48), 38022–38031. <https://doi.org/10.1074/jbc.M006513200>.
- Baroni, E., Viscardi, V., Cartagena-Lirola, H., Lucchini, G., & Longhese, M. P. (2004). The functions of budding yeast Sae2 in the DNA damage response require Mec1- and Tel1-dependent phosphorylation. *Molecular and Cellular Biology*, 24(10), 4151–4165.
- Binz, S. K., Dickson, A. M., Haring, S. J., & Wold, M. S. (2006). Functional assays for replication protein A (RPA). *Methods in Enzymology*, 409, 11–38. [https://doi.org/10.1016/S0076-6879\(05\)09002-6](https://doi.org/10.1016/S0076-6879(05)09002-6).
- Bohr, V. A., Cooper, M., Orren, D., Machwe, A., Piotrowski, J., Sommers, J., et al. (2000). Werner syndrome protein: Biochemical properties and functional interactions. *Experimental Gerontology*, 35(6–7), 695–702.
- Bonetti, D., Villa, M., Gobbini, E., Cassani, C., Tedeschi, G., & Longhese, M. P. (2015). Escape of Sgs1 from Rad9 inhibition reduces the requirement for Sae2 and functional MRX in DNA end resection. *EMBO Reports*, 16(3), 351–361. <https://doi.org/10.15252/embr.201439764>.
- Brosh, R. M., Jr., Li, J. L., Kenny, M. K., Karow, J. K., Cooper, M. P., Kureekattil, R. P., et al. (2000). Replication protein A physically interacts with the Bloom's syndrome protein and stimulates its helicase activity. *The Journal of Biological Chemistry*, 275(31), 23500–23508. <https://doi.org/10.1074/jbc.M001557200>.
- Brosh, R. M., Jr., von Kobbe, C., Sommers, J. A., Karmakar, P., Opresko, P. L., Piotrowski, J., et al. (2001). Werner syndrome protein interacts with human flap endonuclease 1 and stimulates its cleavage activity. *The EMBO Journal*, 20(20), 5791–5801. <https://doi.org/10.1093/emboj/20.20.5791>.
- Budd, M. E., & Campbell, J. L. (1995). A yeast gene required for DNA replication encodes a protein with homology to DNA helicases. *Proceedings of the National Academy of Sciences of the United States of America*, 92(17), 7642–7646.
- Bugreev, D. V., Yu, X., Egelman, E. H., & Mazin, A. V. (2007). Novel pro- and anti-recombination activities of the Bloom's syndrome helicase. *Genes & Development*, 21(23), 3085–3094. <https://doi.org/10.1101/gad.1609007>.
- Buis, J., Wu, Y., Deng, Y., Leddon, J., Westfield, G., Eckersdorff, M., et al. (2008). Mre11 nuclease activity has essential roles in DNA repair and genomic stability distinct from ATM activation. *Cell*, 135(1), 85–96. <https://doi.org/10.1016/j.cell.2008.08.015>.
- Cannavo, E., & Cejka, P. (2014). Sae2 promotes dsDNA endonuclease activity within Mre11-Rad50-Xrs2 to resect DNA breaks. *Nature*, 514(7520), 122–125. <https://doi.org/10.1038/nature13771>.
- Cannavo, E., Cejka, P., & Kowalczykowski, S. C. (2013). Relationship of DNA degradation by *Saccharomyces cerevisiae* exonuclease 1 and its stimulation by RPA and Mre11-Rad50-Xrs2 to DNA end resection. *Proceedings of the National Academy of Sciences of the United States of America*, 110(18), E1661–1668. <https://doi.org/10.1073/pnas.1305166110>.
- Carney, J. P., Maser, R. S., Olivares, H., Davis, E. M., Le Beau, M., Yates, J. R., 3rd, et al. (1998). The hMre11/hRad50 protein complex and Nijmegen breakage syndrome: Linkage of double-strand break repair to the cellular DNA damage response. *Cell*, 93(3), 477–486.

- Cejka, P. (2015). DNA end resection: Nucleases team up with the right partners to initiate homologous recombination. *The Journal of Biological Chemistry*, 290, 22931–22938. <https://doi.org/10.1074/jbc.R115.675942>.
- Cejka, P., Cannavo, E., Polaczek, P., Masuda-Sasa, T., Pokharel, S., Campbell, J. L., et al. (2010). DNA end resection by Dna2-Sgs1-RPA and its stimulation by Top3-Rmi1 and Mre11-Rad50-Xrs2. *Nature*, 467(7311), 112–116. <https://doi.org/10.1038/nature09355>.
- Chen, H., Donnianni, R. A., Handa, N., Deng, S. K., Oh, J., Timashev, L. A., et al. (2015). Sae2 promotes DNA damage resistance by removing the Mre11-Rad50-Xrs2 complex from DNA and attenuating Rad53 signaling. *Proceedings of the National Academy of Sciences of the United States of America*, 112(15), E1880–E1887. <https://doi.org/10.1073/pnas.1503331112>.
- Chen, H., Lisby, M., & Symington, L. S. (2013). RPA coordinates DNA end resection and prevents formation of DNA hairpins. *Molecular Cell*, 50(4), 589–600. <https://doi.org/10.1016/j.molcel.2013.04.032>.
- Choe, W., Budd, M., Imamura, O., Hoopes, L., & Campbell, J. L. (2002). Dynamic localization of an Okazaki fragment processing protein suggests a novel role in telomere replication. *Molecular and Cellular Biology*, 22(12), 4202–4217.
- Chung, W. H., Zhu, Z., Papusha, A., Malkova, A., & Ira, G. (2010). Defective resection at DNA double-strand breaks leads to de novo telomere formation and enhances gene targeting. *PLoS Genetics*, 6(5), e1000948. <https://doi.org/10.1371/journal.pgen.1000948>.
- Daley, J. M., Niu, H., Miller, A. S., & Sung, P. (2015). Biochemical mechanism of DSB end resection and its regulation. *DNA Repair (Amst)*, 32, 66–74. <https://doi.org/10.1016/j.dnarep.2015.04.015>.
- Das, A., Boldogh, I., Lee, J. W., Harrigan, J. A., Hegde, M. L., Piotrowski, J., et al. (2007). The human Werner syndrome protein stimulates repair of oxidative DNA base damage by the DNA glycosylase NEIL1. *The Journal of Biological Chemistry*, 282(36), 26591–26602. <https://doi.org/10.1074/jbc.M703343200>.
- de Jager, M., van Noort, J., van Gent, D. C., Dekker, C., Kanaar, R., & Wyman, C. (2001). Human Rad50/Mre11 is a flexible complex that can tether DNA ends. *Molecular Cell*, 8(5), 1129–1135.
- Deshpande, R. A., Lee, J. H., Arora, S., & Paull, T. T. (2016). Nbs1 converts the human Mre11/Rad50 nuclease complex into an endo/exonuclease machine specific for protein-DNA adducts. *Molecular Cell*, 64(3), 593–606. <https://doi.org/10.1016/j.molcel.2016.10.010>.
- Deshpande, R. A., Williams, G. J., Limbo, O., Williams, R. S., Kuhnlein, J., Lee, J. H., et al. (2014). ATP-driven Rad50 conformations regulate DNA tethering, end resection, and ATM checkpoint signaling. *The EMBO Journal*, 33(5), 482–500. <https://doi.org/10.1002/embj.201386100>.
- Duxin, J. P., Moore, H. R., Sidorova, J., Karanja, K., Honaker, Y., Dao, B., et al. (2012). Okazaki fragment processing-independent role for human Dna2 enzyme during DNA replication. *The Journal of Biological Chemistry*, 287(26), 21980–21991. <https://doi.org/10.1074/jbc.M112.359018>.
- Fu, Q., Chow, J., Bernstein, K. A., Makhharashvili, N., Arora, S., Lee, C. F., et al. (2014). Phosphorylation-regulated transitions in an oligomeric state control the activity of the Sae2 DNA repair enzyme. *Molecular and Cellular Biology*, 34(5), 778–793. <https://doi.org/10.1128/MCB.00963-13>.
- Furuse, M., Nagase, Y., Tsubouchi, H., Murakami-Murofushi, K., Shibata, T., & Ohta, K. (1998). Distinct roles of two separable in vitro activities of yeast Mre11 in mitotic and meiotic recombination. *The EMBO Journal*, 17(21), 6412–6425. <https://doi.org/10.1093/emboj/17.21.6412>.

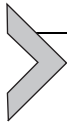
- Garcia, V., Phelps, S. E., Gray, S., & Neale, M. J. (2011). Bidirectional resection of DNA double-strand breaks by Mre11 and Exo1. *Nature*, *479*(7372), 241–244. <https://doi.org/10.1038/nature10515>.
- Gobbini, E., Cassani, C., Villa, M., Bonetti, D., & Longhese, M. P. (2016). Functions and regulation of the MRX complex at DNA double-strand breaks. *Microbial Cell (Graz, Austria)*, *3*(8), 329–337. <https://doi.org/10.15698/mic2016.08.517>.
- Gobbini, E., Villa, M., Gnugnoli, M., Menin, L., Clerici, M., & Longhese, M. P. (2015). Sae2 function at DNA double-strand breaks is bypassed by dampening Tel1 or Rad53 activity. *PLoS Genetics*, *11*(11), e1005685. <https://doi.org/10.1371/journal.pgen.1005685>.
- Gong, Y., Handa, N., Kowalczykowski, S. C., & de Lange, T. (2017). PHF11 promotes DSB resection, ATR signaling, and HR. *Genes & Development*, *31*(1), 46–58. <https://doi.org/10.1101/gad.291807.116>.
- Gravel, S., Chapman, J. R., Magill, C., & Jackson, S. P. (2008). DNA helicases Sgs1 and BLM promote DNA double-strand break resection. *Genes & Development*, *22*(20), 2767–2772. <https://doi.org/10.1101/gad.503108>.
- Harrigan, J. A., Opresko, P. L., von Kobbe, C., Kedar, P. S., Prasad, R., Wilson, S. H., et al. (2003). The Werner syndrome protein stimulates DNA polymerase beta strand displacement synthesis via its helicase activity. *The Journal of Biological Chemistry*, *278*(25), 22686–22695. <https://doi.org/10.1074/jbc.M213103200>.
- Hitchman, R. B., Possee, R. D., & King, L. A. (2009). Baculovirus expression systems for recombinant protein production in insect cells. *Recent Patents on Biotechnology*, *3*(1), 46–54.
- Hitchman, R. B., Possee, R. D., & King, L. A. (2012). High-throughput baculovirus expression in insect cells. *Methods in Molecular Biology*, *824*, 609–627. [https://doi.org/10.1007/978-1-61779-433-9\\_33](https://doi.org/10.1007/978-1-61779-433-9_33).
- Hopfner, K. P., Karcher, A., Craig, L., Woo, T. T., Carney, J. P., & Tainer, J. A. (2001). Structural biochemistry and interaction architecture of the DNA double-strand break repair Mre11 nuclease and Rad50-ATPase. *Cell*, *105*(4), 473–485.
- Hopkins, B. B., & Paull, T. T. (2008). The P. furiosus mre11/rad50 complex promotes 5' strand resection at a DNA double-strand break. *Cell*, *135*(2), 250–260. <https://doi.org/10.1016/j.cell.2008.09.054>.
- Huertas, P. (2010). DNA resection in eukaryotes: Deciding how to fix the break. *Nature Structural & Molecular Biology*, *17*(1), 11–16. <https://doi.org/10.1038/nsmb.1710>.
- Huertas, P., Cortes-Ledesma, F., Sartori, A. A., Aguilera, A., & Jackson, S. P. (2008). CDK targets Sae2 to control DNA-end resection and homologous recombination. *Nature*, *455*(7213), 689–692. <https://doi.org/10.1038/nature07215>.
- Huertas, P., & Jackson, S. P. (2009). Human CtIP mediates cell cycle control of DNA end resection and double strand break repair. *The Journal of Biological Chemistry*, *284*(14), 9558–9565. <https://doi.org/10.1074/jbc.M808906200>.
- Kim, J. H., Grosbart, M., Anand, R., Wyman, C., Cejka, P., & Petrini, J. H. (2017). The Mre11–Nbs1 interface is essential for viability and tumor suppression. *Cell Reports*, *18*(2), 496–507. <https://doi.org/10.1016/j.celrep.2016.12.035>.
- King, L. A., Hitchman, R., & Possee, R. D. (2016). Recombinant baculovirus isolation. *Methods in Molecular Biology*, *1350*, 73–94. [https://doi.org/10.1007/978-1-4939-3043-2\\_4](https://doi.org/10.1007/978-1-4939-3043-2_4).
- Komatsu, K. (2016). NBS1 and multiple regulations of DNA damage response. *Journal of Radiation Research*, *57*(Suppl. 1), i11–i17. <https://doi.org/10.1093/jrr/rww031>.
- Kowalczykowski, S. C. (2015). An overview of the molecular mechanisms of recombinational DNA repair. *Cold Spring Harbor Perspectives in Biology*, *7*(11). <https://doi.org/10.1101/cshperspect.a016410>.
- Kumar, S., & Burgers, P. M. (2013). Lagging strand maturation factor Dna2 is a component of the replication checkpoint initiation machinery. *Genes & Development*, *27*(3), 313–321. <https://doi.org/10.1101/gad.204750.112>.

- Lamarche, B. J., Orazio, N. I., & Weitzman, M. D. (2010). The MRN complex in double-strand break repair and telomere maintenance. *FEBS Letters*, 584(17), 3682–3695. <https://doi.org/10.1016/j.febslet.2010.07.029>.
- Lammens, K., Bemeleit, D. J., Mockel, C., Clausing, E., Schele, A., Hartung, S., et al. (2011). The Mre11:Rad50 structure shows an ATP-dependent molecular clamp in DNA double-strand break repair. *Cell*, 145(1), 54–66. <https://doi.org/10.1016/j.cell.2011.02.038>.
- Larsen, N. B., & Hickson, I. D. (2013). RecQ helicases: Conserved guardians of genomic integrity. *Advances in Experimental Medicine and Biology*, 767, 161–184. [https://doi.org/10.1007/978-1-4614-5037-5\\_8](https://doi.org/10.1007/978-1-4614-5037-5_8).
- Lee, J. H., & Paull, T. T. (2004). Direct activation of the ATM protein kinase by the Mre11/Rad50/Nbs1 complex. *Science*, 304(5667), 93–96. <https://doi.org/10.1126/science.1091496>.
- Lee, J. H., & Paull, T. T. (2005). ATM activation by DNA double-strand breaks through the Mre11-Rad50-Nbs1 complex. *Science*, 308(5721), 551–554. <https://doi.org/10.1126/science.1108297>.
- Lengsfeld, B. M., Rattray, A. J., Bhaskara, V., Ghirlando, R., & Paull, T. T. (2007). Sae2 is an endonuclease that processes hairpin DNA cooperatively with the Mre11/Rad50/Xrs2 complex. *Molecular Cell*, 28(4), 638–651. <https://doi.org/10.1016/j.molcel.2007.11.001>.
- Levikova, M., Klaue, D., Seidel, R., & Cejka, P. (2013). Nuclease activity of *Saccharomyces cerevisiae* Dna2 inhibits its potent DNA helicase activity. *Proceedings of the National Academy of Sciences of the United States of America*, 110(22), E1992–2001. <https://doi.org/10.1073/pnas.1300390110>.
- Levikova, M., Pinto, C., & Cejka, P. (2017). The motor activity of DNA2 functions as an ssDNA translocase to promote DNA end resection. *Genes & Development*, 31(5), 493–502. <https://doi.org/10.1101/gad.295196.116>.
- Liang, J., Suhandynata, R. T., & Zhou, H. (2015). Phosphorylation of Sae2 mediates Forkhead-associated (FHA) domain-specific interaction and regulates its DNA repair function. *The Journal of Biological Chemistry*, 290(17), 10751–10763. <https://doi.org/10.1074/jbc.M114.625293>.
- Liao, S., Toczylowski, T., & Yan, H. (2008). Identification of the *Xenopus* DNA2 protein as a major nuclease for the 5'→3' strand-specific processing of DNA ends. *Nucleic Acids Research*, 36(19), 6091–6100. <https://doi.org/10.1093/nar/gkn616>.
- Llorente, B., & Symington, L. S. (2004). The Mre11 nuclease is not required for 5' to 3' resection at multiple HO-induced double-strand breaks. *Molecular and Cellular Biology*, 24(21), 9682–9694. <https://doi.org/10.1128/MCB.24.21.9682-9694.2004>.
- Luo, G., Yao, M. S., Bender, C. F., Mills, M., Bladl, A. R., Bradley, A., et al. (1999). Disruption of mRad50 causes embryonic stem cell lethality, abnormal embryonic development, and sensitivity to ionizing radiation. *Proceedings of the National Academy of Sciences of the United States of America*, 96(13), 7376–7381.
- Makharashvili, N., Tubbs, A. T., Yang, S. H., Wang, H., Barton, O., Zhou, Y., et al. (2014). Catalytic and noncatalytic roles of the CtIP endonuclease in double-strand break end resection. *Molecular Cell*, 54(6), 1022–1033. <https://doi.org/10.1016/j.molcel.2014.04.011>.
- Manfrini, N., Guerini, I., Citterio, A., Lucchini, G., & Longhese, M. P. (2010). Processing of meiotic DNA double strand breaks requires cyclin-dependent kinase and multiple nucleases. *The Journal of Biological Chemistry*, 285(15), 11628–11637. <https://doi.org/10.1074/jbc.M110.104083>.
- Masuda-Sasa, T., Imamura, O., & Campbell, J. L. (2006). Biochemical analysis of human Dna2. *Nucleic Acids Research*, 34(6), 1865–1875. <https://doi.org/10.1093/nar/gkl070>.
- Miller, A. S., Daley, J. M., Pham, N. T., Niu, H., Xue, X., Ira, G., et al. (2017). A novel role of the Dna2 translocase function in DNA break resection. *Genes & Development*, 31(5), 503–510. <https://doi.org/10.1101/gad.295659.116>.

- Mimitou, E. P., & Symington, L. S. (2008). Sae2, Exo1 and Sgs1 collaborate in DNA double-strand break processing. *Nature*, 455(7214), 770–774. <https://doi.org/10.1038/nature07312>.
- Mimitou, E. P., & Symington, L. S. (2010). Ku prevents Exo1 and Sgs1-dependent resection of DNA ends in the absence of a functional MRX complex or Sae2. *The EMBO Journal*, 29(19), 3358–3369. <https://doi.org/10.1038/emboj.2010.193>.
- Mimitou, E. P., Yamada, S., & Keeney, S. (2017). A global view of meiotic double-strand break end resection. *Science*, 355(6320), 40–45. <https://doi.org/10.1126/science.aak9704>.
- Mockel, C., Lammens, K., Schele, A., & Hopfner, K. P. (2012). ATP driven structural changes of the bacterial Mre11:Rad50 catalytic head complex. *Nucleic Acids Research*, 40(2), 914–927. <https://doi.org/10.1093/nar/gkr749>.
- Neale, M. J., Pan, J., & Keeney, S. (2005). Endonucleolytic processing of covalent protein-linked DNA double-strand breaks. *Nature*, 436(7053), 1053–1057. <https://doi.org/10.1038/nature03872>.
- Nicolette, M. L., Lee, K., Guo, Z., Rani, M., Chow, J. M., Lee, S. E., et al. (2010). Mre11-Rad50-Xrs2 and Sae2 promote 5' strand resection of DNA double-strand breaks. *Nature Structural & Molecular Biology*, 17(12), 1478–1485. <https://doi.org/10.1038/nsmb.1957>.
- Nimonkar, A. V., Genschel, J., Kinoshita, E., Polaczek, P., Campbell, J. L., Wyman, C., et al. (2011). BLM-DNA2-RPA-MRN and EXO1-BLM-RPA-MRN constitute two DNA end resection machineries for human DNA break repair. *Genes & Development*, 25(4), 350–362. <https://doi.org/10.1101/gad.2003811>.
- Niu, H., Chung, W. H., Zhu, Z., Kwon, Y., Zhao, W., Chi, P., et al. (2010). Mechanism of the ATP-dependent DNA end-resection machinery from *Saccharomyces cerevisiae*. *Nature*, 467(7311), 108–111. <https://doi.org/10.1038/nature09318>.
- Oh, J., Al-Zain, A., Cannavo, E., Cejka, P., & Symington, L. S. (2016). Xrs2 dependent and independent functions of the Mre11–Rad50 complex. *Molecular Cell*, 64(2), 405–415. <https://doi.org/10.1016/j.molcel.2016.09.011>.
- Opresko, P. L., Otterlei, M., Graakjaer, J., Bruheim, P., Dawut, L., Kolvraa, S., et al. (2004). The Werner syndrome helicase and exonuclease cooperate to resolve telomeric D loops in a manner regulated by TRF1 and TRF2. *Molecular Cell*, 14(6), 763–774. <https://doi.org/10.1016/j.molcel.2004.05.023>.
- Paull, T. T. (2010). Making the best of the loose ends: Mre11/Rad50 complexes and Sae2 promote DNA double-strand break resection. *DNA Repair (Amst)*, 9(12), 1283–1291. <https://doi.org/10.1016/j.dnarep.2010.09.015>.
- Paull, T. T., & Gellert, M. (1998). The 3' to 5' exonuclease activity of Mre 11 facilitates repair of DNA double-strand breaks. *Molecular Cell*, 1(7), 969–979.
- Paull, T. T., & Gellert, M. (1999). Nbs1 potentiates ATP-driven DNA unwinding and endonuclease cleavage by the Mre11/Rad50 complex. *Genes & Development*, 13(10), 1276–1288.
- Peterson, S. E., Li, Y., Wu-Baer, F., Chait, B. T., Baer, R., Yan, H., et al. (2013). Activation of DSB processing requires phosphorylation of CtIP by ATR. *Molecular Cell*, 49(4), 657–667. <https://doi.org/10.1016/j.molcel.2012.11.020>.
- Pinto, C., Kasaciunaite, K., Seidel, R., & Cejka, P. (2016). Human DNA2 possesses a cryptic DNA unwinding activity that functionally integrates with BLM or WRN helicases. *eLife*, 5. <https://doi.org/10.7554/eLife.18574>.
- Pokharel, S., & Campbell, J. L. (2012). Cross talk between the nuclease and helicase activities of Dna2: Role of an essential iron-sulfur cluster domain. *Nucleic Acids Research*, 40(16), 7821–7830. <https://doi.org/10.1093/nar/gks534>.
- Prakash, R., Zhang, Y., Feng, W., & Jasin, M. (2015). Homologous recombination and human health: The roles of BRCA1, BRCA2, and associated proteins. *Cold Spring Harbor Perspectives in Biology*, 7(4), a016600. <https://doi.org/10.1101/cshperspect.a016600>.

- Puddu, F., Oelschlaegel, T., Guerini, I., Geisler, N. J., Niu, H., Herzog, M., et al. (2015). Synthetic viability genomic screening defines Sae2 function in DNA repair. *The EMBO Journal*, *34*, 1509–1522. <https://doi.org/10.15252/embj.201590973>.
- Sartori, A. A., Lukas, C., Coates, J., Mistrik, M., Fu, S., Bartek, J., et al. (2007). Human CtIP promotes DNA end resection. *Nature*, *450*(7169), 509–514. <https://doi.org/10.1038/nature06337>.
- Seeber, A., Hegnauer, A. M., Hustedt, N., Deshpande, I., Poli, J., Eglinger, J., et al. (2016). RPA mediates recruitment of MRX to forks and double-strand breaks to hold sister chromatids together. *Molecular Cell*, *64*(5), 951–966. <https://doi.org/10.1016/j.molcel.2016.10.032>.
- Shibata, A., Moiani, D., Arvai, A. S., Perry, J., Harding, S. M., Genois, M. M., et al. (2014). DNA double-strand break repair pathway choice is directed by distinct MRE11 nuclease activities. *Molecular Cell*, *53*(1), 7–18. <https://doi.org/10.1016/j.molcel.2013.11.003>.
- Stewart, G. S., Maser, R. S., Stankovic, T., Bressan, D. A., Kaplan, M. I., Jaspers, N. G., et al. (1999). The DNA double-strand break repair gene hMRE11 is mutated in individuals with an ataxia-telangiectasia-like disorder. *Cell*, *99*(6), 577–587.
- Sturzenegger, A., Burdova, K., Kanagaraj, R., Levikova, M., Pinto, C., Cejka, P., et al. (2014). DNA2 cooperates with the WRN and BLM RecQ helicases to mediate long-range DNA end resection in human cells. *The Journal of Biological Chemistry*, *289*(39), 27314–27326. <https://doi.org/10.1074/jbc.M114.578823>.
- Symington, L. S. (2016). Mechanism and regulation of DNA end resection in eukaryotes. *Critical Reviews in Biochemistry and Molecular Biology*, *51*, 195–212. <https://doi.org/10.3109/10409238.2016.1172552>.
- Tauchi, H., Kobayashi, J., Morishima, K., van Gent, D. C., Shiraishi, T., Verkaik, N. S., et al. (2002). Nbs1 is essential for DNA repair by homologous recombination in higher vertebrate cells. *Nature*, *420*(6911), 93–98. <https://doi.org/10.1038/nature01125>.
- Taylor, A. M., Groom, A., & Byrd, P. J. (2004). Ataxia-telangiectasia-like disorder (ATLD)–its clinical presentation and molecular basis. *DNA Repair (Amst)*, *3*(8–9), 1219–1225. <https://doi.org/10.1016/j.dnarep.2004.04.009>.
- Thangavel, S., Berti, M., Levikova, M., Pinto, C., Gomathinayagam, S., Vujanovic, M., et al. (2015). DNA2 drives processing and restart of reversed replication forks in human cells. *The Journal of Cell Biology*, *208*(5), 545–562. <https://doi.org/10.1083/jcb.201406100>.
- Trujillo, K. M., & Sung, P. (2001). DNA structure-specific nuclease activities in the *Saccharomyces cerevisiae* Rad50\*Mre11 complex. *The Journal of Biological Chemistry*, *276*(38), 35458–35464. <https://doi.org/10.1074/jbc.M105482200>.
- Trujillo, K. M., Yuan, S. S., Lee, E. Y., & Sung, P. (1998). Nuclease activities in a complex of human recombination and DNA repair factors Rad50, Mre11, and p95. *The Journal of Biological Chemistry*, *273*(34), 21447–21450.
- Umez, K., Sugawara, N., Chen, C., Haber, J. E., & Kolodner, R. D. (1998). Genetic analysis of yeast RPA1 reveals its multiple functions in DNA metabolism. *Genetics*, *148*(3), 989–1005.
- Wang, A. T., Kim, T., Wagner, J. E., Conti, B. A., Lach, F. P., Huang, A. L., et al. (2015). A dominant mutation in human RAD51 reveals its function in DNA interstrand crosslink repair independent of homologous recombination. *Molecular Cell*, *59*(3), 478–490. <https://doi.org/10.1016/j.molcel.2015.07.009>.
- Wang, H., Li, Y., Truong, L. N., Shi, L. Z., Hwang, P. Y., He, J., et al. (2014). CtIP maintains stability at common fragile sites and inverted repeats by end resection-independent endonuclease activity. *Molecular Cell*, *54*(6), 1012–1021. <https://doi.org/10.1016/j.molcel.2014.04.012>.
- White, C. I., & Haber, J. E. (1990). Intermediates of recombination during mating type switching in *Saccharomyces cerevisiae*. *The EMBO Journal*, *9*(3), 663–673.

- Williams, R. S., Moncalian, G., Williams, J. S., Yamada, Y., Limbo, O., Shin, D. S., et al. (2008). Mre11 dimers coordinate DNA end bridging and nuclease processing in double-strand-break repair. *Cell*, *135*(1), 97–109. <https://doi.org/10.1016/j.cell.2008.08.017>.
- Williams, G. J., Williams, R. S., Williams, J. S., Moncalian, G., Arvai, A. S., Limbo, O., et al. (2011). ABC ATPase signature helices in Rad50 link nucleotide state to Mre11 interface for DNA repair. *Nature Structural & Molecular Biology*, *18*(4), 423–431. <https://doi.org/10.1038/nsmb.2038>.
- Wobbe, C. R., Weissbach, L., Borowiec, J. A., Dean, F. B., Murakami, Y., Bullock, P., et al. (1987). Replication of simian virus 40 origin-containing DNA in vitro with purified proteins. *Proceedings of the National Academy of Sciences of the United States of America*, *84*(7), 1834–1838.
- Wold, M. S. (1997). Replication protein A: A heterotrimeric, single-stranded DNA-binding protein required for eukaryotic DNA metabolism. *Annual Review of Biochemistry*, *66*, 61–92. <https://doi.org/10.1146/annurev.biochem.66.1.61>.
- Wu, L., & Hickson, I. D. (2003). The Bloom's syndrome helicase suppresses crossing over during homologous recombination. *Nature*, *426*(6968), 870–874. <https://doi.org/10.1038/nature02253>.
- Yeeles, J. T., Cammack, R., & Dillingham, M. S. (2009). An iron-sulfur cluster is essential for the binding of broken DNA by AddAB-type helicase–nucleases. *The Journal of Biological Chemistry*, *284*(12), 7746–7755. <https://doi.org/10.1074/jbc.M808526200>.
- Yu, X., & Chen, J. (2004). DNA damage-induced cell cycle checkpoint control requires CtpP, a phosphorylation-dependent binding partner of BRCA1 C-terminal domains. *Molecular and Cellular Biology*, *24*(21), 9478–9486. <https://doi.org/10.1128/MCB.24.21.9478-9486.2004>.
- Zakharyevich, K., Ma, Y., Tang, S., Hwang, P. Y., Boiteux, S., & Hunter, N. (2010). Temporally and biochemically distinct activities of Exo1 during meiosis: Double-strand break resection and resolution of double Holliday junctions. *Molecular Cell*, *40*(6), 1001–1015. <https://doi.org/10.1016/j.molcel.2010.11.032>.
- Zheng, L., Zhou, M., Guo, Z., Lu, H., Qian, L., Dai, H., et al. (2008). Human DNA2 is a mitochondrial nuclease/helicase for efficient processing of DNA replication and repair intermediates. *Molecular Cell*, *32*(3), 325–336. <https://doi.org/10.1016/j.molcel.2008.09.024>.
- Zhu, Z., Chung, W. H., Shim, E. Y., Lee, S. E., & Ira, G. (2008). Sgs1 helicase and two nucleases Dna2 and Exo1 resect DNA double-strand break ends. *Cell*, *134*(6), 981–994. <https://doi.org/10.1016/j.cell.2008.08.037>.



# Methods to Study DNA End Resection II: Biochemical Reconstitution Assays

Cosimo Pinto\*, Roopesh Anand<sup>†</sup>, Petr Cejka<sup>†,‡,1</sup>

\*Institute of Molecular Cancer Research, University of Zurich, Zurich, Switzerland

<sup>†</sup>Institute for Research in Biomedicine, Università della Svizzera italiana, Bellinzona, Switzerland

<sup>‡</sup>Institute of Biochemistry, Swiss Federal Institute of Technology, Zurich, Switzerland

<sup>1</sup>Corresponding author: e-mail address: petr.cejka@irb.usi.ch

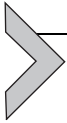
## Contents

|   |     |
|---|-----|
| 1. Introduction   | 68  |
| 2. Short-Range DNA End Resection by MRN and CtIP  | 69  |
| 2.1 Basic Protocols: Preparation of Oligonucleotide-Based DNA Substrates and Polyacrylamide Gel Electrophoresis | 71  |
| 2.2 Protein Quality Control Testing: Nuclease Contamination Assay   | 77  |
| 2.3 Assays to Monitor the Exonuclease Activity of the MRN Complex   | 80  |
| 2.4 Assays to Monitor the Endonuclease Activity of the MRN Complex and CtIP Near Protein-Blocked DNA Ends       | 83  |
| 3. Long-Range DNA End Resection by DNA2–BLM and DNA2–WRN  | 87  |
| 3.1 Preparation of Plasmid-Length DNA Substrates  | 88  |
| 3.2 Protein Quality Control: DNA Unwinding Assay  | 98  |
| 3.3 DNA End Resection Assays With DNA2–BLM or DNA2–WRN  | 100 |
| Acknowledgments   | 103 |
| References  | 103 |

## Abstract

DNA end resection initiates the largely accurate repair of DNA double-strand breaks (DSBs) by homologous recombination. Specifically, recombination requires the formation of 3' overhangs at DSB sites, which is carried out by nucleases that specifically degrade 5'-terminated DNA. In most cases, DNA end resection is a two-step process, comprising of initial short-range followed by more processive long-range resection. In this chapter, we describe selected assays that reconstitute both the short- and long-range pathways. First, we define methods to study the exonuclease and endonuclease activities of the MRE11-RAD50-NBS1 (MRN) complex in conjunction with phosphorylated cofactor CtIP. This reaction is particularly important to initiate processing of DNA breaks and to recruit components belonging to the subsequent long-range pathway. Next, we describe assays that reconstitute the concerted reactions of Bloom (BLM) or Werner (WRN) helicases that function together with the DNA2 nuclease–helicase, and

which are as a complex capable to resect DNA of kilobases in length. The reconstituted reactions allow us to understand how the resection pathways function at the molecular level. The assays will be invaluable to define regulatory mechanisms and to identify inhibitory compounds, which may be valuable in cancer therapy.



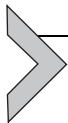
## 1. INTRODUCTION

DNA double-strand breaks (DSBs) represent one of the most deleterious forms of DNA damage. A failure to repair DSBs may be fatal in non-dividing cells in case the break interrupts an essential gene, whereas broken DNA in dividing cells may lead to chromosome missegregation in mitosis. Incorrect or misregulated DSB repair gives rise to genome instability including substitutions and frameshift mutations, translocations, chromosome fusions, and other types of genome rearrangements (Jackson & Bartek, 2009). DSB repair is dependent on either of two main pathways, non-homologous end joining (NHEJ) and homologous recombination (HR). Whereas NHEJ can occur in any phase of the cell cycle, it is template independent and therefore often mutagenic. HR, which is restricted to the S and G2 phases of the cell cycle, is a more accurate pathway as it uses a template, which is usually the sister chromatid in vegetative cells (Kowalczykowski, 2015). DNA end resection, a process where the 5'-terminated DNA strand is specifically degraded at DSB sites leading to 3' ssDNA overhangs, initiates and commits DSB repair to the HR pathway (Cejka, 2015; Daley, Niu, Miller, & Sung, 2015; Symington, 2016).

DNA end resection occurs in two distinct steps known as short- and long-range DNA end resection (Mimitou & Symington, 2008; Zhu, Chung, Shim, Lee, & Ira, 2008). During the initial short-range resection, limited 5' DNA end degradation takes place, which is primarily carried out by the MRE11-RAD50-NBS1 (MRN) complex in conjunction with CtIP in human cells (Paull & Gellert, 1998; Sartori et al., 2007). MRE11 appears to be the critical nuclease responsible for this process. MRE11's involvement in 5' → 3' DNA end resection had been puzzling, as recombinant MRE11 possesses nuclease activity with the opposite, 3' → 5' polarity (Paull & Gellert, 1998). To this point, a bidirectional model was proposed, wherein MRN first cleaves the 5'-terminated DNA strand endonucleolytically internal to the DSB site. Subsequently, the MRN complex proceeds back toward the DNA end using its 3' → 5' exonuclease activity (Garcia, Phelps, Gray, & Neale, 2011; Neale, Pan, & Keeney, 2005;

Shibata et al., 2014). The endonucleolytic cleavage gives rise to a suitable entry site for the long-range DNA end resection, which is catalyzed by either EXO1 or DNA2–BLM/DNA2–WRN nuclease complexes (Gravel, Chapman, Magill, & Jackson, 2008; Nimonkar et al., 2011; Sturzenegger et al., 2014). The bidirectional resection model has been supported by evidence from multiple experimental systems ranging from yeast to humans. The first support came from yeast meiotic cells, which require the initial endonucleolytic clipping to resect Spo11-bound DNA breaks (Garcia et al., 2011; Keeney & Kleckner, 1995; Neale et al., 2005). Later, experiments with specific *endo*- or exonuclease inhibitors of the MRE11 nuclease demonstrated that its endonuclease precedes the exonuclease in human cells (Shibata et al., 2014), and biochemical reconstitution experiments with yeast and human proteins revealed that CtIP and homologues promote the endonucleolytic cleavage of the 5'-terminated DNA strand by MRN (MRX in yeast) near protein-blocked DSBs (Anand, Ranjha, Cannavo, & Cejka, 2016; Deshpande, Lee, Arora, & Paull, 2016). The separation of DNA end resection into two separate steps helps to remove diverse lesions from DNA ends including covalently bound proteins by MRN–CtIP, and the subsequent long-range resection processes generates sufficient lengths of DNA that facilitate successful homology search and repair (Symington, 2016).

In this chapter, we describe biochemical methods that allow reconstituting elements of the DNA end resection pathways. These assays help us understand the process of DNA end resection but may also be used to search for inhibitory compounds, which are of interest in cancer therapy. Additionally, reconstituted resection reactions will be invaluable in defining the role of regulatory mechanisms. This includes posttranslational modifications of the core components of the resection machinery, or the interplay of these factors with regulatory factors or additional nucleases.



---

## 2. SHORT-RANGE DNA END RESECTION BY MRN AND CtIP

The initial short-range DNA end resection of DSBs by MRE11 and its partners is restricted to ~300 nt in length. This value was obtained from experiments in yeast cells, in which the long-range DNA end resection pathways had been eliminated by mutagenesis (Mimitou & Symington, 2008; Zhu et al., 2008). These studies demonstrated that yeast Mre11–Rad50–Xrs2 (MRX, homologue of the human MRN complex) and Sae2

(homologue of human CtIP) are capable to resect DNA of this length; however, it is not clear whether this corresponds to the DNA length resected by Mre11 in wild-type background when the long-range resection pathways are present (Paull, 2010). The DNA length that can be processed by human MRN and CtIP proteins is not yet well defined (Zhou, Caron, Legube, & Paull, 2014). In addition to the nucleolytic function of MRN–CtIP, the complex also has a structural role in the recruitment of components that belong to the long-range resection pathways (Nimonkar et al., 2011). Furthermore, MRN promotes DNA damage signaling via the ATM kinase (Lee & Paull, 2004, 2005). While the requirement for MRX and Sae2 in resection can be bypassed in yeast in some cases (in particular when processing chemically “clean” DNA ends), MRN and CtIP appear to be essential for resection in human cells (Llorente & Symington, 2004; Mimitou & Symington, 2010; Sartori et al., 2007).

The short-range DNA end resection is likely initiated by MRN cleaving 5'-terminated DNA endonucleolytically internal to the DSB site, with MRE11 providing the critical nuclease activity (Anand et al., 2016; Cannavo & Cejka, 2014; Deshpande et al., 2016; Hopkins & Paull, 2008). The endonucleolytic DNA clipping by MRE11 requires RAD50 and its ATPase activity, and is promoted by NBS1. The endonucleolytic cleavage by the MRN complex is further strongly stimulated by phosphorylated CtIP. Phosphorylation of the T847 cyclin-dependent kinase site is among the residues that need to be phosphorylated to support CtIP's capacity to promote the MRN endonuclease (Anand et al., 2016; Deshpande et al., 2016). Whereas MRE11 on its own or within the MRN complex is a 3' → 5' exonuclease on unprotected ends, the MRN endonuclease cleaves primarily the 5'-terminated DNA strand in the vicinity of protein blocks (Anand et al., 2016; Deshpande et al., 2016). These blocks thus inhibit the 3' → 5' exonuclease and direct the endonucleolytic cleavage to the 5'-terminated strand. There are many aspects of this reaction that remain to be clarified, including the identity of the physiological protein blocks. Additionally, while MRE11 is likely the primary nuclease involved in short-range DNA end resection, other nucleases such as EXD2 may play a role in this process, but its involvement on a mechanistic level remains undefined (Broderick et al., 2016). CtIP/Sae2 was also proposed to harbor intrinsic nuclease activity, but its involvement in DNA end resection is not clear (Lengsfeld, Rattray, Bhaskara, Ghirlando, & Paull, 2007; Makharashvili et al., 2014; Wang et al., 2014).

In this chapter, we describe assays that can be used to monitor the exonuclease as well the endonuclease activity of the MRN complex in

conjunction with CtIP by using oligonucleotide-based DNA substrates. The nuclease of the recombinant MRN complex shows limited processivity, and oligonucleotide-based DNA substrates are thus optimal to monitor this activity. To study the  $3' \rightarrow 5'$  MRN exonuclease, either  $5'$ - or  $3'$ -labeled dsDNA substrates can be used. When using a  $3'$ -labeled substrate, the activity of MRN gives rise to a single detectable product of low molecular weight, migrating at the lower part of the gel. Instead, when using a  $5'$ -labeled substrate, the MRN exonuclease leads to visible products of various lengths, which correspond to the progression of the MRN exonuclease in the  $3' \rightarrow 5'$  direction. When monitoring the endonuclease activity of MRN, similar  $5'$ - or  $3'$ -labeled oligonucleotide-based DNA substrates can be used, but the DNA ends should be blocked to inhibit the exonucleolytic and promote the endonucleolytic cleavage. To monitor the endonucleolytic cleavage, the reactions also need to be supplemented with phosphorylated CtIP. In the accompanying chapter “Methods to study DNA end resection I: Recombinant protein purification” by Anand et al., we describe methods to express and purify recombinant DNA end resection proteins. Here, we describe in detail reconstitution of DNA end resection assays.

## 2.1 Basic Protocols: Preparation of Oligonucleotide-Based DNA Substrates and Polyacrylamide Gel Electrophoresis

This chapter summarizes very basic methods that we use to prepare various oligonucleotide-based DNA substrates, as well as our hands-on protocol how to run denaturing polyacrylamide gels using simple laboratory equipment.

### 2.1.1 Procedure: Preparation of $^{32}\text{P}$ -Labeled Oligonucleotide-Based DNA Substrates

Important: Always use protective clothing and shield when handling radioactive material. Follow your institution's guidelines on how to use and discard radioactive material.

#### 2.1.1.1 Buffers and Reagents

- Oligonucleotides (see [Table 1](#))
- Disposable illustra-MicroSpin G-25 columns (GE Healthcare, 27-5325-01) or equivalent
- [ $\alpha$ - $^{32}\text{P}$ ] cordycepin 5'-triphosphate 10  $\mu\text{Ci}/\mu\text{L}$  (PerkinElmer, NEG026250UC or equivalent)
- [ $\gamma$ - $^{32}\text{P}$ ] adenosine 5'-triphosphate 10  $\mu\text{Ci}/\mu\text{L}$  (Hartmann Analytics, SRP-301 or equivalent)

**Table 1** Sequence of Oligonucleotides Described in This Chapter

| Oligonucleotide Name | Sequence (5'-3')  |
|----------------------|---|
| X12-3                | GACGTCATAGACGATTACATTGCTAGGACATGCTG<br>TCTAGAGACTATCGC                                      |
| X12-4NC              | GCGATAGTCTCTAGACAGCATGTCCTAGCAAGCCA<br>GAATTCGGCAGGCTA                                      |
| X12-4C               | GCGATAGTCTCTAGACAGCATGTCCTAGCAATGTA<br>ATCGTCTATGACGTC                                      |
| PC210                | <b>G</b> TAAAGTGCCGCGGTGCGGGTGCCAGGGCGTGCCCT<br>TGGGCTCCCCGGGCGCGTACTCCACCTCATGCAT <b>C</b> |
| PC211                | GATGCATGAGGTGGAGTACGCGCCCGGGGAGCCCA<br>AGGGCACGCCCTGGCACCCGCACCGCGGCACT <b>TAC</b>          |

Bold "T" represents the position of biotin modification.

- T4 Polynucleotide Kinase 10,000 units/mL (New England Biolabs, M0201L or equivalent) with supplied buffer
- Terminal transferase 20,000 units/mL (New England Biolabs, M0315 or equivalent) with supplied buffers
- Annealing buffer 10 × (0.5 M Tris-HCl, pH 7.5, 100 mM MgCl<sub>2</sub>)

### 2.1.1.2 Procedure I: Preparation of 5'-Labeled Duplex DNA Substrates

1. Mix 11.25 μL oligonucleotide 1 (1 μM stock concentration, in molecules; final concentration 300 nM, in molecules) with 3.75 μL T4 polynucleotide kinase reaction buffer 10 × (New England Biolabs, final concentrations: 70 mM Tris-HCl, pH 7.6, 10 mM MgCl<sub>2</sub>, 5 mM dithiothreitol [DTT]), 2 μL T4 polynucleotide kinase (20 units) and 3 μL [ $\gamma$ -<sup>32</sup>P] adenosine 5'-triphosphate (30 μCi) on ice and bring the reaction volume to 37.5 μL with deionized water.
2. Incubate the reaction at 37°C for 1 h to radioactively label oligonucleotide 1 at the 5' end. Heat-inactivate the reaction at 65°C for 5 min.
3. Purify the radiolabeled oligonucleotide from the rest of the reaction mixture using one illustra-MicroSpin G-25 column according to manufacturer's recommendations.
4. Due to ~10% loss of the oligonucleotide on column and ~10% increase of the sample volume upon purification, we consider the final concentration of the radiolabeled oligonucleotide 250 nM.

5. Mix 10  $\mu\text{L}$  radiolabeled oligonucleotide 1 (final 50 nM), 5  $\mu\text{L}$  10  $\times$  annealing buffer (final concentrations: 50 mM Tris-HCl pH 7.5, 10 mM  $\text{MgCl}_2$ ), and 5  $\mu\text{L}$  unlabeled oligonucleotide 2 (1  $\mu\text{M}$  stock concentration, in molecules; final concentration 100 nM, in molecules, corresponding to twofold excess over labeled DNA). Bring the reaction volume up to 50  $\mu\text{L}$  with deionized water.
6. Incubate the mixture at 95°C for 3 min. Turn off the heat block (or oven) to allow for slow cooling of the sample until it reaches room temperature (several hours to overnight).
7. The final concentration of the labeled duplex DNA substrate is  $\sim$ 50 nM (in molecules).

#### 2.1.1.3 Procedure II: Preparation of 3'-Labeled Duplex DNA Substrates

1. Mix 7.5  $\mu\text{L}$  oligonucleotide 1 (1  $\mu\text{M}$  stock concentration, in molecules; final concentration 300 nM, in molecules) with 2.5  $\mu\text{L}$  terminal transferase reaction buffer 10  $\times$  (final concentrations: 50 mM potassium acetate pH 7.9, 20 mM Tris-acetate, 10 mM magnesium acetate), 2.5  $\mu\text{L}$   $\text{CoCl}_2$  (final 0.25 mM), 1  $\mu\text{L}$  terminal transferase (20 units), and 5  $\mu\text{L}$  [ $\alpha$ - $^{32}\text{P}$ ] cordycepin 5'-triphosphate (50  $\mu\text{Ci}$ ) on ice and bring the reaction volume to 25  $\mu\text{L}$  with deionized water.
2. Incubate the reaction at 37°C for 1 h to radioactively label oligonucleotide 1 at the 3' end.
3. Heat-inactivate the reaction for 20 min at 75°C.
4. Purify the radiolabeled oligonucleotide from the rest of the reaction mixture using one illustra-MicroSpin G-25 column according to manufacturer's recommendations.
5. Due to  $\sim$ 10% loss of the oligonucleotide on column and  $\sim$ 10% increase of the sample volume during purification, we consider the final concentration of the radiolabeled oligonucleotide 250 nM.
6. Mix 8  $\mu\text{L}$  radiolabeled oligonucleotide 1 (final 100 nM, in molecules), 2  $\mu\text{L}$  10  $\times$  annealing buffer (final concentrations: 50 mM Tris-HCl pH 7.5, 10 mM  $\text{MgCl}_2$ ) and 4  $\mu\text{L}$  unlabeled oligonucleotide 2 (1  $\mu\text{M}$  stock concentration, in molecules; final concentration 200 nM, in molecules, corresponding to twofold excess over labeled DNA). Bring the reaction volume up to 20  $\mu\text{L}$  with deionized water.
7. Incubate the mixture at 95°C for 2 min. Turn off the heat block (or oven) to allow for slow cooling of the sample until it reaches room temperature (several hours to overnight).
8. The final concentration of the labeled duplex DNA substrate is  $\sim$ 100 nM.

## Notes

- We recommend using oligonucleotides purified by polyacrylamide gel-based electrophoresis.
- The concentration of the complementary unlabeled oligonucleotide used in the annealing reactions described above is twofold higher compared to the  $^{32}\text{P}$ -labeled oligonucleotide. This generally allows for good efficiency of DNA annealing. The optimal ratio may need to be determined empirically by annealing the respective DNA oligonucleotides at various ratios. In reactions where the excess of the unlabeled oligonucleotide may be a problem, the annealed substrate should be purified upon separation by polyacrylamide gel electrophoresis.
- In case free label, either  $[\alpha\text{-}^{32}\text{P}]$  cordycepin 5'-triphosphate or  $[\gamma\text{-}^{32}\text{P}]$  adenosine 5'-triphosphate is still detectable in the substrate preparation after one purification step on the illustra-MicroSpin G-25 column, repeat the purification step using another G-25 column.
- Store the labeled substrate in an appropriate container at  $-20^{\circ}\text{C}$ .

### **2.1.2 Resolution of Short DNA Fragments by Native or Denaturing Polyacrylamide Gel Electrophoresis**

Short DNA molecules (from 1 to  $\sim 200$  nt in length) may be analyzed by native or denaturing polyacrylamide gel electrophoresis. Native gel electrophoresis does not separate the two strands of dsDNA nor unfold secondary DNA structures. It is thus the method of choice when analyzing, e.g., products of a helicase reaction. While native gels are simple to run, they do not allow precise separation of the DNA molecules. Denaturing polyacrylamide gel electrophoresis instead separates the two strands of a DNA duplex, and thus only the  $^{32}\text{P}$ -labeled DNA strand will be detected. Compared to native gels, denaturing gels achieve much better separation of the DNA fragments and are therefore ideally suitable to analyze products of nuclease reactions.

Dedicated electrophoretic systems for separating DNA fragments (especially denaturing or “sequencing” polyacrylamide systems) are available commercially, which result in single-nucleotide resolution. Below, we describe a method that makes use of the Mini-PROTEAN Tetra Cell apparatus that is typically used to separate proteins (Bio-Rad; equivalent systems from other manufacturer’s can be used), which is available in almost any laboratory. This procedure is simple to perform allowing higher throughput than most “sequencing” systems, although it has a lower resolution ( $\sim 2\text{--}3$  nt). This is however sufficient for most DNA end resection experiments (Anand et al., 2016; Cannavo & Cejka, 2014).

### 2.1.2.1 Equipment

- Mini-PROTEAN Tetra Cell vertical gel electrophoresis system (Bio-Rad, 165800 EDU) or equivalent
- PowerPac HC High-Current Power Supply (Bio-Rad, 1645052) or equivalent
- Storage Phosphor Screens (GE Healthcare)
- Typhoon FLA 9500 (GE Healthcare)
- Whatman 3MM CHR Chromatography Paper (GE Healthcare, 3030-917) or Whatman ion exchange chromatography paper DE81 (GE Healthcare, 3658-915), see note below.

### 2.1.2.2 Buffers and Reagents

- Urea (AppliChem, A1049)
- Ammonium persulfate (APS) (AppliChem, A2941 or equivalent), prepare 10% solution in water.
- 5 × TBE (450 mM Tris, 450 mM borate, 10 mM ethylenediaminetetraacetic acid [EDTA]) buffer
- Tetramethylethylenediamine (TEMED, Bio-Rad, 1610801 or equivalent)
- Acrylamide/Bis solution, 19:1 (40%, Bio-Rad, 1610144 or equivalent)
- Fixing solution (40% methanol, 10% acetic acid, 5% glycerol)
- 2 × Loading dye (95% formamide, 20 mM EDTA, 1 mg/mL bromophenol blue)
- Proteinase K, recombinant, PCR grade, 14–22 mg/mL (Roche, 03115828001 or equivalent)
- Stop solution (150 mM EDTA, 2% sodium dodecyl sulfate, 30% glycerol, 1 mg/mL bromophenol blue)

### Notes

- We list manufacturers and respective product catalogue numbers for reagents that we use in our laboratory; equivalent products from other suppliers may also be used.
- The DE81 chromatography paper is used as a support for drying both polyacrylamide and agarose gels containing DNA. Due to its positive charge, the paper binds negatively charged DNA, which makes sure DNA gets retained during drying. This prevents contamination of the gel drier, as well as allows reliable quantitation of the radioactive signal. Unfortunately, the product has been discontinued by Whatman (GE Healthcare). We tested a number of alternatives, but the only product that fully retains DNA was a nylon membrane (e.g., Amersham Hybond-N+, GE Healthcare, RPN119B), which is however very

expensive. In our experiments, DE81 paper (or replacement) is not necessary when drying denaturing polyacrylamide gels, and therefore regular filter paper (such as Whatman 3MM CHR Chromatography Paper) can be used instead. When drying native polyacrylamide gels, three layers of the 3MM paper may be used in some cases, but this may lead to errors during data analysis/quantitation. Generally, DNA fragments of smaller molecular weight are retained less efficiently than larger DNA fragments or protein-bound DNA complexes. DE81 or an equivalent must be used when drying agarose gels (see [Section 3.2.3](#)).

### 2.1.2.3 Procedure for the Preparation and Running of Denaturing Polyacrylamide Gels

1. In one 50-mL conical tube, add 6.3 g urea, 3 mL  $5 \times$  TBE buffer, and 5.6 mL acrylamide/bis-acrylamide solution (40%), which is sufficient for two 15% denaturing gels. Vary the amount of acrylamide/bis-acrylamide to achieve desired concentration. Bring the volume up to 15 mL with deionized water and dissolve the urea by vigorous agitation of the tube ( $\sim 10$  min). Filter ( $0.45 \mu\text{M}$ ) the solution to remove debris.
2. Add  $9 \mu\text{L}$  TEMED and  $70 \mu\text{L}$  10% APS to the mixture and cast the gels using manufacturer's instructions. Allow at least 1 h for polymerization. Assemble the gels in the electrophoresis chamber according to manufacturer's instructions. Fill the chamber with  $1 \times$  TBE buffer.
3. Flush the wells of each gel with  $1 \times$  TBE buffer and prerun the gels for 30 min at room temperature. Using the Mini-PROTEAN Tetra Cell system (gel dimensions  $7.2 \times 8.6$  cm, thickness 1 mm), we use 18 W constant power for one gel, or 36 W when running two gels in a single tank. Do not run four gels in one tank.
4. Denature the reaction samples upon adding an equal volume of  $2 \times$  loading dye at  $95^\circ\text{C}$  for 4 min, briefly cool on ice, and spin at  $10,000 \times g$  for 15 s at  $4^\circ\text{C}$  to collect any condensed solution. Keep samples on ice.
5. Flush wells with  $1 \times$  TBE buffer and load no more than  $15 \mu\text{L}$  sample as soon as possible (corresponding to  $\sim 1/2$  of the total reaction volume, see below). Run the gels using the power setting as above until the bromophenol blue reaches the bottom part of the gel just before running out ( $\sim 15$ – $20$  min).
6. Fix each gel in 25 mL fixing solution for 30 min at room temperature with gentle agitation.
7. Wash the gels twice with deionized water and place them on Whatman 3MM CHR chromatography paper. Dry the gels for 1 h using a gel dryer according to manufacturer's instructions.

8. Expose the dried gels to a storage phosphor screen and read the signal with a typhoon imager.

#### 2.1.2.4 Procedure for the Preparation and Running of Native Polyacrylamide Gels

1. To prepare two 10% native gels, mix 3 mL 5 × TBE, 3.75 mL 40% acrylamide/bis-acrylamide solution, and 8.1 mL water in a 50-mL conical tube. Add 15 μL TEMED and 150 μL 10% APS, mix and immediately cast the gels. Allow 30 min for gel polymerization. Assemble the gels in the electrophoresis chamber according to manufacturer's instructions. Fill the chamber with 1 × TBE buffer and rinse the wells with 1 × TBE buffer.
2. Terminate the respective biochemical reactions (15 μL volume) with 5 μL stop solution and 1 μL proteinase K for 15 min at 37°C. Load 21 μL sample per well and run the gel at 80 V (using Mini-PROTEAN Tetra Cell system, Bio-Rad, corresponding to ~ 6–7 V/cm) for ~1 h until bromophenol blue reaches the lower part of the gel.
3. Place the resolved gel on DE81 or 3MM paper, dry and analyze the gels as described earlier.

#### Notes

- We recommend including a molecular weight marker in denaturing gels, such as low-molecular weight marker, 10–100 nt (Affimatrix/USB, Alfa Aesar, J76410). This should be labeled at the 5' end: use 1 μL marker (50 ng each fragment), 2.5 μL 10 × T4 polynucleotide kinase buffer, 1.5 μL T4 polynucleotide kinase (15 units), 3 μL [ $\gamma$ -<sup>32</sup>P] adenosine 5'-triphosphate (30 μCi), 17 μL water (total volume 25 μL). Incubate and process as described in [Section 2.1.1.2](#). Use appropriate dilution that gives rise to a radioactive signal of similar intensity to the reaction substrate.
- Gels may disintegrate during the drying process in case the vacuum is not strong enough, or if there are fluctuations in vacuum power.
- Do not load more than ~15 μL sample per well on denaturing gels; this leads to better resolution and better image quality.

## 2.2 Protein Quality Control Testing: Nuclease Contamination Assay

Purified recombinant proteins should be devoid of nuclease contamination, which may degrade reaction substrates and interfere with the interpretation of DNA end resection experiments. Although insect cells have various advantages over *Escherichia coli* host systems for protein expression, such as the capacity to express large proteins and the presence of posttranslational

modification machineries, they are more likely to be a source of contaminating nucleases. As DNA nucleases function catalytically, even trace amounts of contamination that are not detectable by polyacrylamide gel electrophoresis may render recombinant protein preparation unsuitable for experimentation. To this point, when preparing soluble extracts from *Spodoptera frugiperda* 9 (*Sf9*) cells, we recommend using a salt extraction method (see chapter "Methods to study DNA end resection I: Preparation of recombinant proteins" by Anand et al. in the same issue of *Methods in Enzymology*) as opposed to mechanical or chemical lysis to preserve the integrity of the nuclear membrane. This prevents the release of large amounts of DNA to the soluble extract, which often carries nucleases that may nonspecifically bind chromatography resins. In most cases, extended washing of chromatography resins (up to  $\sim 100$  resin volumes) eliminates nuclease contaminations: when possible, this can be carried out with buffers containing higher salt concentrations or include low amounts (such as 0.1%) of nonionic detergents such as NP-40 or equivalents. In other cases, it may be necessary to add additional separation steps to the purification procedure.

Contaminating nucleases are particularly problematic when working with proteins that are nucleases themselves such as many DNA end resection proteins. Due to the overlapping substrate specificity, it may be difficult to determine whether the nuclease activity of a recombinant nuclease is intrinsic to the protein of interest, or whether it stems from an unrelated contaminant. To this point, it is necessary to prepare a nuclease-dead variant of each resection nuclease, using an identical expression and purification procedure to the wild-type protein. The nuclease-dead variant should then be used as a negative control in DNA end resection assays.

Below, we describe a very sensitive nuclease assay, which can be used to test for the presence of potential nuclease contaminations in recombinant protein preparations. DNA end resection assays in most cases contain linear single or double-stranded DNA, either as substrate, intermediate, or reaction product. The assay below scores for nuclease contamination using a Y-structure oligonucleotide-based DNA substrate. This substrate contains both dsDNA and 3'- and 5'-terminated ssDNA arms, and can be thus used to detect nucleases with various substrate preferences.

### 2.2.1 Equipment

- See [Section 2.1](#) for equipment required for substrate preparation and polyacrylamide gel electrophoresis

### 2.2.2 Buffers and Reagents

- Recombinant protein preparation
- 1 M Tris-acetate pH 7.5
- Bovine serum albumin (BSA, 20 mg/mL, New England Biolabs, B9000 or equivalent)
- 1 M DTT
- 1 M magnesium acetate
- Stop solution (150 mM EDTA, 2% sodium dodecyl sulfate, 30% glycerol, 1 mg/mL bromophenol blue)
- Proteinase K, recombinant, PCR grade (14–22 mg/mL, Roche, 03115828001 or equivalent)
- DNA substrate: Prepare Y-structure DNA substrate by annealing 5'-end <sup>32</sup>P-labeled X12-3 (50 nt) with unlabeled X12-4NC (50 nt) oligonucleotide as described in [Section 2.1.1.2](#). The Y-structure contains 31 bp of dsDNA, and 3' as well as 5'-terminated ssDNA arms of 19 nt in length. The radioactive label will be positioned at the end of the 5'-terminated ssDNA arm. See [Table 1](#) for the list of oligonucleotides.

### 2.2.3 Procedure: Nuclease Contamination Assay

1. Determine the number of protein samples to prepare appropriate volume of the reaction master mix. The volume of a single reaction is 15  $\mu$ L.
2. Prepare master mix containing 25 mM Tris-acetate pH 7.5, 1 mM DTT, 0.1 mg/mL BSA, 2 mM magnesium acetate, and 1 nM (in molecules) DNA substrate.
3. Distribute 14  $\mu$ L master mix into each tube.
4. Add protein samples (up to  $\sim$ 1  $\mu$ L, as required).
5. Mix gently and incubate the reaction at 37°C for 30 min.
6. Stop the reaction by adding 5  $\mu$ L stop solution and 1  $\mu$ L proteinase K. Mix well and incubate the sample at 37°C for 15 min.
7. Separate the reaction products by electrophoresis in 10% native polyacrylamide gel in 1  $\times$  TBE buffer as described in [Section 2.1.2.4](#). Using Mini-PROTEAN Tetra Cell system, we recommend running the gels at 80 V (corresponding to  $\sim$  6–7 V/cm) for  $\sim$ 45 min until bromophenol blue dye reaches the middle part of the gel.
8. Transfer the gel on Whatman 3MM CHR Chromatography Paper (or equivalent, see notes in [Section 2.1.2.2](#)) and dry for 1 h using a gel dryer.
9. Expose the dried gel to a storage phosphor screen and read the signal with an imager (see [Fig. 1](#)).

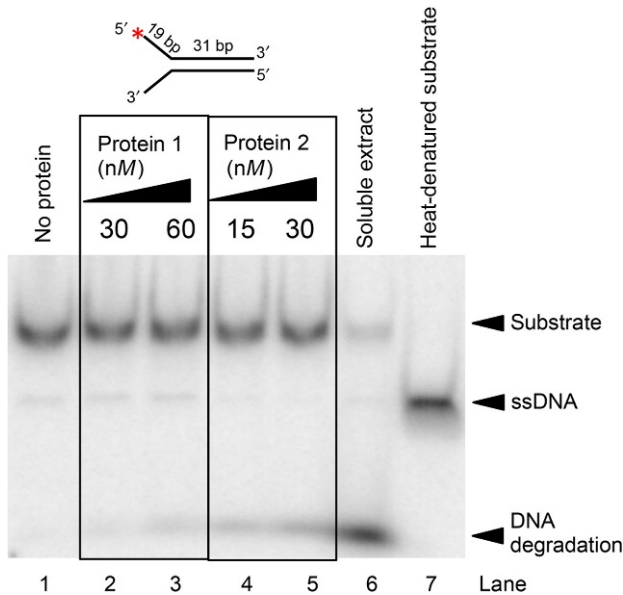


**Fig. 1** Native polyacrylamide gel (10%) showing representative nuclease contamination assay (Section 2.2) using 5'-end  $^{32}\text{P}$ -labeled Y-structure DNA substrate (50-mer, oligonucleotides X12-3 and X12-4NC). The red asterisk indicates the position of the  $^{32}\text{P}$ -label.

## Notes

- In case the volume of the sample to be tested is significantly larger than 1  $\mu\text{L}$ , the master mix composition and volume per tube may need to be adjusted accordingly.
- Always include one substrate-only reaction with 1  $\mu\text{L}$  protein storage buffer as a negative control. Use 0.5–1  $\mu\text{L}$  soluble extract from *S9* cells as a positive control.
- We recommend separating the reaction products using native gel electrophoresis. This detects degradation of either of the two oligonucleotides that make up the Y structure substrate.

## 2.3 Assays to Monitor the Exonuclease Activity of the MRN Complex

Recombinant MRE11 as well as the MRN complex possesses manganese-dependent  $3' \rightarrow 5'$  exonuclease activity on dsDNA (Paul & Gellert, 1998). Human RAD50 enhances the exonuclease activity of MRE11, while NBS1 has an inhibitory effect. ATP has no major effect on the MRE11

exonuclease in isolation or in complex with other components of the MRN complex (Deshpande et al., 2016; Paull & Gellert, 1998; Trujillo et al., 2003; Trujillo & Sung, 2001).

### 2.3.1 Equipment

- See [Section 2.1](#) for equipment required for substrate preparation and polyacrylamide gel electrophoresis.

### 2.3.2 Buffers and Reagents

- Recombinant protein(s)
- 1 M Tris-HCl pH 7.5
- BSA (20 mg/mL, New England Biolabs, B9000 or equivalent)
- 1 M DTT
- 1 M manganese acetate
- 1 M magnesium acetate (optional)
- 0.1 M phosphoenolpyruvate (Sigma-Aldrich, P0564 or equivalent)
- Pyruvate kinase from rabbit muscle (25 units/ $\mu$ L, Sigma-Aldrich, P1506 or equivalent)
- Adenosine 5'-Triphosphate (ATP) disodium, crystalline (Amersham Biosciences, 27-1006-01 or equivalent)
- Proteinase K, recombinant, PCR grade (14–22 mg/mL, Roche, 03115828001 or equivalent)
- Fixing solution (40% methanol, 10% acetic acid, 5% glycerol)
- 2 $\times$  Loading dye (95% formamide, 20 mM EDTA, 1 mg/mL bromophenol blue)
- DNA substrate: Prepare dsDNA substrate by annealing 5'-end  $^{32}$ P-labeled X12-3 (50 nt) with unlabeled X12-4C (50 nt) oligonucleotide as described in [Section 2.1.1.2](#). See [Table 1](#) for the list of oligonucleotides.

### 2.3.3 Procedure

1. Determine the number of reactions to be performed. The volume of a single reaction is 15  $\mu$ L.
2. Assemble desired volume of reaction master mix in nuclease-free water containing 25 mM Tris-HCl pH 7.5, 1 mM DTT, 0.25 mg/mL BSA, 1 mM ATP, 1 mM phosphoenolpyruvate, 80 units/mL pyruvate kinase, 5 mM manganese acetate and 1 nM (in molecules, 5' or 3'-end labeled) DNA substrate on ice.
3. Distribute 14  $\mu$ L master mix into each tube on ice.

4. Add appropriate dilution of the recombinant protein (up to 2  $\mu\text{L}$ ) to the reactions on ice. Mix gently by pipetting (do not vortex).
5. Incubate the reactions at 37°C for desired time.
6. Stop the reactions by adding 0.5  $\mu\text{L}$  10% SDS, 0.5  $\mu\text{L}$  0.5 M EDTA, 0.5  $\mu\text{L}$  proteinase K and incubate at 50°C for 30 min.
7. Add  $\sim 16.5 \mu\text{L}$  (equal to the sample volume) of  $2 \times$  loading dye into the reactions.
8. Incubate the samples for 4 min at 95°C, briefly chill on ice, and spin at  $10,000 \times g$  for 15 s. Separate the products by denaturing polyacrylamide gel electrophoresis as described in [Section 2.1.2.3](#).
9. Place the fixed gels on Whatman 3MM CHR Chromatography Paper and dry them for 1 h using a gel dryer.
10. Expose the dried gel to a storage phosphor screen for appropriate time (1 h to overnight in most cases) and read the signal with a typhoon imager (see [Fig. 2](#)).

### Notes

- The reactions can be performed in multiple ways, including by testing several concentrations of the MRN preparation (we recommend

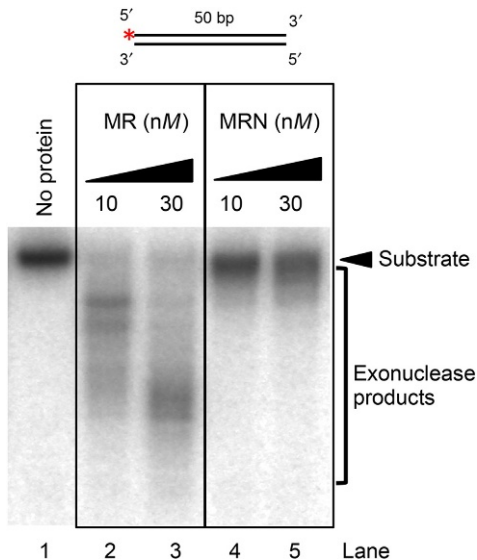


**Fig. 2** Denaturing polyacrylamide gel (15%) showing representative exonuclease assay ([Section 2.3](#)) with wild-type MR (lanes 2 and 3) and MRN (lanes 4 and 5) complexes using 5'-end  $^{32}\text{P}$ -labeled dsDNA (50-mer, oligonucleotides X12-3 and X12-4C, 5 nM). The assay was carried out in a buffer containing 1 mM manganese acetate and 5 mM magnesium acetate at 37°C for 2 h. The *red asterisk* indicates the position of the  $^{32}\text{P}$ -label.

10–50 nM range) or by performing a kinetic assay. To perform a kinetic assay, assemble the reaction of a correspondingly larger volume and remove 15  $\mu\text{L}$  samples at determined time points. The reactions can then be snap-frozen in liquid nitrogen and processed together upon collecting the last time point sample as described in step 6 and beyond.

- The composition of the master mix can be varied as required. The described reaction buffer optimally promotes the MRN exonuclease. The exonuclease activity of MRN can be further accelerated by using higher DNA concentration (such as 5 nM, in molecules) or lower pH (such as 7.0, R. Anand and P. Cejka, unpublished observations). The presence of ATP and the ATP regeneration system (pyruvate kinase and phosphoenolpyruvate) does not significantly affect the MRE11 exonuclease. However, as ATP affects the conformation of the MRN complex and mediates the formation of the MR dimer (Deshpande et al., 2014; Lammens et al., 2011; Williams et al., 2008), we prefer to include this cofactor in the reaction buffer. This makes the conformation of MRN consistent with endonuclease assays, where ATP is required (see Section 2.4) (Anand et al., 2016).
- Always include a substrate-only sample on each polyacrylamide gel.
- The proteinase K treatment prevents the sample from getting “stuck” in the wells and generally leads to better DNA separation.
- In case the volume of the proteins added into a single reaction mixture exceeds 2  $\mu\text{L}$ , the composition of the reaction buffer may need to be adjusted. Additionally, the reactions may be inhibited by sodium chloride (NaCl), which is present in the recombinant proteins’ storage buffer. In cases when different concentrations of salt (or other reagents) are introduced into the reactions with the recombinant proteins’ storage buffer, it is necessary to make the reaction conditions equivalent. To this point, supplement the reaction buffer accordingly.
- In case recombinant proteins need to be diluted prior to the biochemical assay, use protein dilution buffer (25 mM Tris–HCl pH 7.5, 50 mM NaCl, 0.1 mg/mL BSA, 1 mM DTT) immediately before adding to the reaction mixture.

## 2.4 Assays to Monitor the Endonuclease Activity of the MRN Complex and CtIP Near Protein-Blocked DNA Ends

To prevent the 3'  $\rightarrow$  5' exonuclease and promote the endonuclease of MRE11, we block both ends of oligonucleotide-based dsDNA with biotin–streptavidin (Anand et al., 2016). We observed that the presence

of protein blocks directs the endonuclease activity of the MRN–CtIP proteins and their yeast homologues to the 5′-terminated DNA strand (Anand et al., 2016; Cannavo & Cejka, 2014). This is in agreement with the DSB repair model and direct observations that posit that specifically the 5′-terminated DNA strand is degraded. In contrast to the manganese-dependent 3′ → 5′ exonuclease reactions, where the MRE11 polypeptide is sufficient, the endonuclease clipping assay also requires the following components: RAD50 and its ATPase activity, NBS1, phosphorylated CtIP, ATP, magnesium (manganese only is not sufficient), and protein blocks that bind to the substrate’s ends (Anand et al., 2016; Deshpande et al., 2016).

The MRN complex shows endonuclease activity on various DNA secondary structures such as loops, hairpins, and junctions of single- and double-stranded DNA (Paull & Gellert, 1998). Previously, endonucleolytic cleavage of circular ssDNA such as M13mp18 or  $\Phi$ X174 bacteriophage had been used as a very sensitive assay to monitor the endonuclease of MRN and its homologues (Sartori et al., 2007; Williams et al., 2008). However, this activity is not strictly dependent on CtIP/Sae2 and is partially independent of the ATP hydrolytic activity of RAD50 (Anand et al., 2016; Cannavo & Cejka, 2014; Williams et al., 2008). As ATP hydrolysis by RAD50 is required for DSB repair and meiosis in yeast (Chen et al., 2005), and Sae2 appears to be strictly required for the processing of protein-blocked meiotic DNA ends that are known to require endonucleolytic clipping (Keeney & Kleckner, 1995), the M13-based assays may not adequately mimic the physiological reaction. The oligonucleotide-based endonuclease assay described here, which requires CtIP and ATP hydrolysis by RAD50, may thus be a better model to study the physiologically relevant process that initiates DSB repair.

### 2.4.1 Equipment

- See Section 2.1 for equipment required for substrate preparation and polyacrylamide gel electrophoresis

### 2.4.2 Buffers and Reagents

To monitor the endonucleolytic cleavage by MRN–CtIP, the DNA ends of the dsDNA substrate need to be blocked. In the protocol below, we recommend using an oligonucleotide-based dsDNA with four biotin labels (see Table 1, resulting from annealing of oligonucleotides PC210 and PC211). Each oligonucleotide contains internal biotin labels near both 5′ and 3′ ends, resulting in “quadruple” blocked dsDNA substrate upon incubation with streptavidin. Although even a single streptavidin block at the 5′ end is sufficient to observe endonucleolytic cleavage by MRN–CtIP, we

observed higher efficiency of cleavage with the “quadruple” blocked substrate (Anand et al., 2016). Likely, the unblocked DNA ends sequester active MRN complex, which limits the availability of other MRN molecules to cleave the substrate endonucleolytically. As the biotin labels at both PC210 and PC211 oligonucleotides are internal to the ends, both oligonucleotides can be labeled either at the 5' or 3' end with T4 polynucleotide kinase or terminal transferase, respectively (see Section 2.1.1). The procedure below recommends labeling the PC210 oligonucleotide at the 3' end, which gives us the highest labeling efficiency.

- Recombinant proteins
- 1 M Tris–HCl pH 7.5
- BSA (20 mg/mL, New England Biolabs, B9000 or equivalent)
- 1 M DTT
- 1 M manganese acetate
- 1 M magnesium acetate
- 0.1 M phosphoenolpyruvate (Sigma–Aldrich, P0564 or equivalent)
- Pyruvate kinase from rabbit muscle (25 units/μL, Sigma–Aldrich, P1506 or equivalent)
- ATP disodium, crystalline (Amersham Biosciences, 27-1006-01 or equivalent)
- Proteinase K, recombinant, PCR grade (14–22 mg/mL, Roche, 03115828001 or equivalent)
- Fixing solution (40% methanol, 10% acetic acid, 5% glycerol)
- 2× Loading dye (95% formamide, 20 mM EDTA, 1 mg/mL bromophenol blue)
- Streptavidin (Sigma, 85878)
- DNA substrate: Prepare dsDNA substrate by annealing 3'-end <sup>32</sup>P-labeled PC210 (70 nt) with unlabeled PC211 (70 nt) oligonucleotide (see Section 2.1.1.3). See Table 1 for the list of oligonucleotides.

### 2.4.3 Procedure

1. Determine the number of reactions to be performed. The volume of a single reaction is 15 μL.
2. Prepare appropriate volume of master mix in nuclease-free water containing 25 mM Tris–HCl pH 7.5, 1 mM DTT, 0.25 mg/mL BSA, 1 mM ATP, 1 mM manganese acetate, 5 mM magnesium acetate, and 1 nM (in molecules) DNA substrate.
3. Add streptavidin (15 nM final concentration, per tetramer) into the master mix and incubate the reaction for 5 min at room temperature to block DNA ends.

4. Add 13  $\mu\text{L}$  master mix into each reaction tube on ice.
5. Add MRN (we recommend 25 nM,  $\sim 1 \mu\text{L}$ ) and/or pCtIP (we recommend 60 nM,  $\sim 1 \mu\text{L}$ ) into the reactions on ice and mix gently (do not vortex).
6. Incubate the reactions at 37°C for 30 min.
7. Stop the reactions by adding 0.5  $\mu\text{L}$  0.5 M EDTA and 0.5  $\mu\text{L}$  proteinase K and incubate the mixture at 50°C for 30 min.
8. Add  $\sim 16.5 \mu\text{L}$  (equal to the sample volume) of 2  $\times$  loading dye into the reactions.
9. Incubate the samples for 4 min at 95°C. Briefly chill on ice and spin at  $10,000 \times g$  for 15 s. Separate the reaction products by denaturing polyacrylamide gel electrophoresis as described in Section 2.1.2.3. We recommend loading no more than  $\sim 16 \mu\text{L}$  sample per well.
10. Place the fixed gels on Whatman 3MM CHR Chromatography Paper and dry them for 1 h (or until dry) using a gel dryer.
11. Expose the dried gel to a storage phosphor screen for appropriate time (1 h to overnight in most cases) and read the signal with a typhoon imager (see Fig. 3).

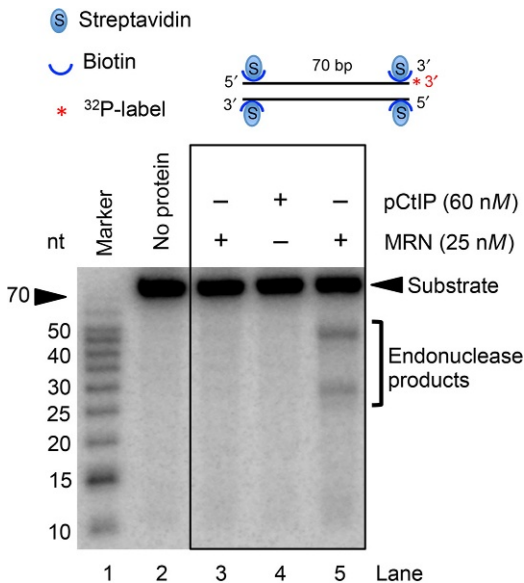
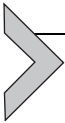


**Fig. 3** Denaturing polyacrylamide gel (15%) showing representative endonuclease assay (Section 2.4) with wild-type MRN complex and hyperphosphorylated CtIP (pCtIP), as indicated, using 3'-end  $^{32}\text{P}$ -labeled dsDNA (70-mer, oligonucleotides PC210 and PC211) blocked with streptavidin. The red asterisk indicates the position of the  $^{32}\text{P}$ -label. Experiment is similar to that published previously (Anand et al., 2016).

## Notes

- The reactions and composition of the master mix can be varied in multiple ways, see our notes in [Section 2.3.3](#).
- In case the volume of proteins to be added into a single reaction exceeds 2  $\mu\text{L}$ , the composition of the reaction buffer may need to be adjusted. Specifically, the reactions may be inhibited by NaCl, which is present in the recombinant proteins' storage buffer. We observed that up to  $\sim 50\text{mM}$  NaCl has no effect on the endonucleolytic cleavage ([Anand et al., 2016](#)), and we generally consider NaCl concentrations up to  $\sim 25\text{mM}$  as negligible. In cases when higher concentrations of salt are introduced into some reactions with recombinant proteins, it is necessary to supplement the other reactions in the respective experiment with salt to make its concentration identical in all samples. This may however lower the efficacy of DNA cleavage.



## 3. LONG-RANGE DNA END RESECTION BY DNA2–BLM AND DNA2–WRN

Upon initiation of DNA end resection by the short-range DNA end resection complex comprised of MRN and CtIP, DNA end resection tracks are extended by the long-range resection nucleases. Two separate pathways have been described for long-range resection in human cells leading to the formation of extensive 3' ssDNA overhangs. The first pathway is catalyzed by the 5'  $\rightarrow$  3' exonuclease EXO1, and the second pathway is executed by DNA2 ([Liao, Toczylowski, & Yan, 2011](#); [Nimonkar et al., 2011](#); [Nimonkar, Ozsoy, Genschel, Modrich, & Kowalczykowski, 2008](#)). Unlike EXO1 that degrades 5'-terminated ssDNA within dsDNA, the nuclease of DNA2 can only act on ssDNA. This requires DNA2 to pair with a helicase partner: it has been demonstrated that DNA2 forms a complex with BLM or WRN ([Gravel et al., 2008](#); [Pinto, Kasaciunaite, Seidel, & Cejka, 2016](#); [Sturzenegger et al., 2014](#)). Both BLM and WRN belong to the SF2 helicase family that unwind DNA in a 3'  $\rightarrow$  5' direction, i.e., translocate on the 3'-terminated DNA strand ([Larsen & Hickson, 2013](#)). Although BLM was initially identified as the sole partner of DNA2 in DNA end resection ([Gravel et al., 2008](#); [Nimonkar et al., 2011](#)), several laboratories reported later that WRN also functions together with DNA2 and that WRN might be even more important than BLM in some cases ([Liao, Guay, Toczylowski, & Yan, 2012](#); [Liao, Toczylowski, & Yan, 2008](#); [Pinto et al., 2016](#); [Sturzenegger et al., 2014](#); [Thangavel et al., 2015](#); [Wang et al., 2015](#)). Either of these

DNA helicases then provides the prerequisite ssDNA for the DNA2 nuclease. The individual subunits of the DNA2–BLM and DNA2–WRN complex stimulate each other activities, giving rise to a model where both enzymes form an integrated molecular machine that is more than a sum of its parts (Daley, Chiba, Xue, Niu, & Sung, 2014; Levikova, Pinto, & Cejka, 2017; Pinto et al., 2016).

Interestingly, DNA2 alone possesses a ssDNA-specific nuclease activity that cleaves both 3'- and 5'-terminated ssDNA (Bae & Seo, 2000; Masuda-Sasa, Imamura, & Campbell, 2006), and its involvement in DNA end resection had thus been puzzling. The polarity paradox was resolved when biochemical studies demonstrated that the single-strand DNA-binding protein RPA only allows 5' → 3' DNA degradation by blocking the 3' → 5' exonuclease of human and yeast DNA2/Dna2 (Cejka et al., 2010; Nimonkar et al., 2011; Niu et al., 2010; Yan, Toczylowski, McCane, Chen, & Liao, 2011). RPA is thus a crucial factor that confers the correct polarity to the DNA2 nuclease, which is required to establish the long 3'-terminated ssDNA overhangs needed for homology search in the recombination pathways. DNA2 also possesses a well-conserved DNA helicase domain. Most likely, the motor of DNA2 does not function as a helicase in DNA end resection, but rather as a single-strand DNA translocase to facilitate degradation of ssDNA unwound by BLM or WRN (Levikova et al., 2017; Miller et al., 2017). Finally, WRN has a weak 3' → 5' nuclease activity, which is, however, not believed to function in DNA end resection (Sturzenegger et al., 2014).

Here we describe DNA end resection assays that can be used to monitor the long-range DNA end processing by DNA2 in complex with RPA and either BLM or WRN. As the nuclease of DNA2 is highly processive, we describe assays that utilize plasmid length DNA substrates.

### 3.1 Preparation of Plasmid-Length DNA Substrates

In this chapter, we describe procedures for the preparation of plasmid-length DNA substrates with various overhangs and/or secondary structures at the ends, which can be used in DNA end resection assays:

- (a) pUC19/*Hind*III substrate: Digestion of the pUC19 vector with *Hind*III restriction endonuclease results in 2686 bp-long (~2.7 kbp) linear DNA with 5' overhangs of 4 nt in length.
- (b) pOH-S-based substrates: The pOH-S vector is a pUC19-derived vector containing a tandem array of Nt/Nb.BbvCI sites separated by *Stu*I

site in the middle of the array (Sturzenegger et al., 2014). Digestion of the pOH-S vector with *StuI* followed by either *Nt.BbvCI* or *Nb.BbvCI* gives rise to 2748bp-long (~2.7 kbp) linear DNA with 3' or 5' ssDNA overhangs of ~26–29 nt in length at both DNA ends, respectively (Fig. 4A and B). The ssDNA overhangs are of sufficient length to bind RPA with high affinity.

- (c) pAttP-S-based substrates: Linear DNA resulting from annealing of two oligonucleotides forming an *AttB* recognition site is recombined with pAttP-S vector containing an *AttP* recognition site in a reaction catalyzed by  $\Phi$ C31 integrase (Fig. 5A and B) (Cannavo & Cejka, 2014; Groth, Olivares, Thyagarajan, & Calos, 2000; Smith, Brown, McEwan, & Rowley, 2010). This reaction linearizes the pAttP-S vector and places any sequence/structure/modification that had been originally present in the annealed duplex flanking the *AttB* recognition site to the ends of the plasmid-length DNA molecule.

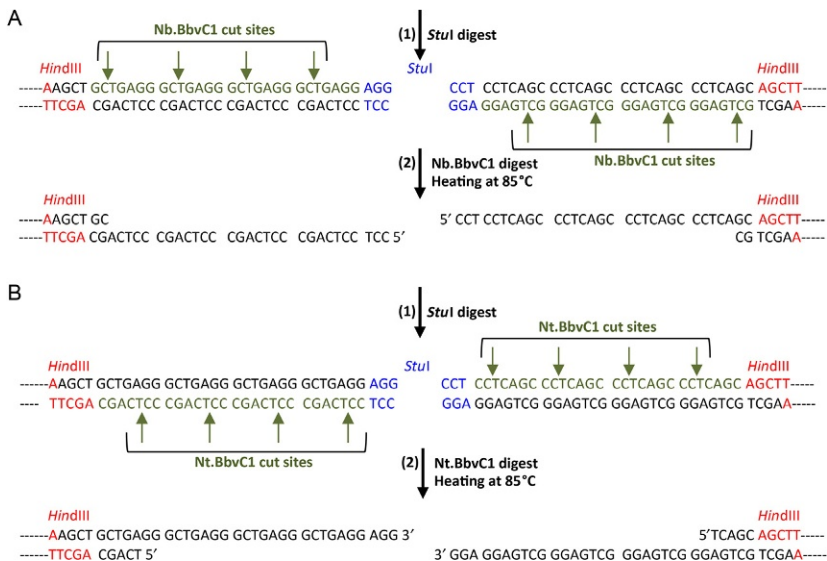


**Fig. 4** A schematic representation of the preparation of overhanged plasmid-length DNA substrates using pOH-S vector (Section 3.1.2). (A) Digestion of pOH-S vector with *StuI* (recognition sites in blue) and *Nb.BbvCI* (in green), followed by partial DNA denaturation leads to overhanged DNA with 5'-terminated ssDNA tails of 29 nt in length. Green arrows indicate *Nb.BbvCI* cut sites. The *HindIII* site (in red) was used to insert the cassette into pUC19. (B) Digestion of pOH-S vector with *StuI* (in blue) and *Nt.BbvCI* (in green), followed by partial DNA denaturation leads to overhanged DNA with 3'-terminated ssDNA tails of 26 nt in length. Green arrows indicate *Nt.BbvCI* cut sites.

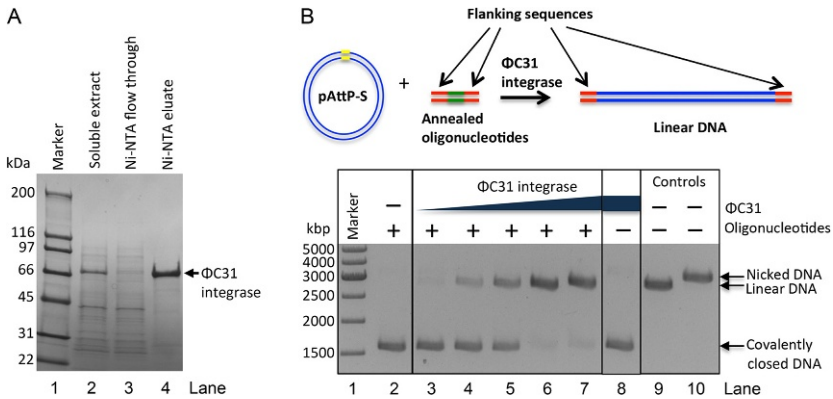


**Fig. 5** Preparation of pAttP-S-based DNA substrates. (A) Representative purification of  $\Phi$ C31 integrase (Section 3.1.3). The indicated samples show soluble extract, flow through from Ni-NTA sepharose, eluate from Ni-NTA sepharose (final sample). (B) Representative site-specific recombination assay with oligonucleotide-based DNA containing attB site (in green) and flanking sequences (in red) and pAttP-S vector (in blue) with attP site (in yellow), as described in Section 3.1.4.  $\Phi$ C31 integrase reaction yields linear DNA (in blue), with DNA sequences originally flanking the attB site in oligonucleotide-based DNA duplex placed at DNA ends of the plasmid-length DNA (in red). Various concentrations of  $\Phi$ C31 integrase were used. The reactions were separated on 1% agarose gel stained with ethidium bromide. Lane 9, linear DNA control; Lane 10, nicked DNA control.

### 3.1.1 Preparation of pUC19/HindIII DNA Substrates (a)

#### 3.1.1.1 Buffers and Reagents

- pUC19 vector (e.g., New England Biolabs, N3041)
- HindIII-HF restriction endonuclease (New England Biolabs, R3104 or equivalent)
- Phenol:Chloroform:Isoamyl Alcohol 25:24:1, saturated with 10 mM Tris pH 8.0, 1 mM EDTA (Sigma, P3803)
- Phase lock gel Heavy 1.5 mL (5PRIME, 2302810 or equivalent)
- 3 M sodium acetate pH 5.2
- Optional: In case the substrate will be labeled radioactively, use [ $\alpha$ - $^{32}$ P] deoxyadenosine 5'-triphosphate 10  $\mu$ Ci/ $\mu$ L (e.g., Hartmann Analytics, SRP-203) and Klenow Fragment (3'  $\rightarrow$  5' *exo*-) 5 units/ $\mu$ L (New England Biolabs, M0212). Use illustra-MicroSpin G-25 columns (GE Healthcare, 27-5325-01) or equivalent for reaction cleanup.
- Optional: In case DNA will be detected by staining, ethidium bromide (e.g., Merck, 111615), GelRed (Biotium, 41003), or equivalent dye can be used.

### 3.1.1.2 Procedure

The pUC19-based DNA substrate can be used in DNA end resection assays either unlabeled or labeled with  $^{32}\text{P}$ . Unlabeled “cold” DNA can be visualized by staining with ethidium bromide, GelRed, or a similar dye. Labeled “hot” DNA can be prepared by fill-in reaction with [ $\alpha$ - $^{32}\text{P}$ ] deoxyadenosine 5'-triphosphate and Klenow fragment of DNA polymerase I, and detected upon gel drying using standard radiography methods. In general, assays with radioactively labeled DNA are more sensitive and thus more suitable to detect intermediate degradative products.

1. Digest 25  $\mu\text{g}$  of pUC19 DNA with *Hind*III-HF according to manufacturer's recommendations. Incubate the reaction at 37°C for 1 h to cleave DNA and subsequently at 80°C for 20 min to inactivate the enzyme.
2. Purify the digested DNA using phenol–chloroform–isoamyl alcohol extraction. Add one reaction volume of phenol–chloroform–isoamyl alcohol to the digested vector and mix the solution vigorously by vortexing.
3. Isolate the aqueous (top) phase using phase lock gel tubes according to manufacturer's instructions. Determine the volume of the aqueous phase.
4. Add 2.5 volumes of 100% ethanol and 0.1 volumes of 3 M sodium acetate pH 5.2. Mix and incubate at  $-20^\circ\text{C}$  for 30 min.
5. Spin at 20,000  $\times g$  at 4°C for 30 min to precipitate DNA. Remove the supernatant and wash the pellet with 0.5 mL 70% ethanol.
6. Spin at 20,000  $\times g$  at 4°C for 15 min. Decant the supernatant and air-dry the pellet.
7. Resuspend the digested pUC19 in 150  $\mu\text{L}$  deionized nuclease-free water. Determine DNA concentration.
8. The steps below are optional. Use only in case substrate labeling with  $^{32}\text{P}$  is required.
9. Assemble a labeling reaction consisting of 2750 ng linearized pUC19, 3  $\mu\text{L}$  [ $\alpha$ - $^{32}\text{P}$ ] deoxyadenosine 5'-triphosphate, 1  $\mu\text{L}$  Klenow Fragment (3'  $\rightarrow$  5' exo-, final amount in reaction 5 units), 2.5  $\mu\text{L}$  NEB buffer 2 10  $\times$  (final concentration, 1  $\times$ ; 50 mM NaCl, 10 mM Tris-HCl pH 7.9, 10 mM MgCl<sub>2</sub>, 1 mM DTT) in a total reaction volume of 25  $\mu\text{L}$ . Incubate the labeling reaction at 37°C for 1 h. Heat-inactivate the reaction at 75°C for 20 min.
10. Separate labeled DNA from the rest of the reaction mixture using one illustra-MicroSpin G-25 column according to manufacturer's instructions.

11. Due to  $\sim 10\%$  loss of the linearized pUC19 on column and  $\sim 10\%$  increase of the sample volume upon purification, we consider the final concentration of the radiolabeled pUC19/*Hind*III substrate 50 nM.

### 3.1.2 Preparation of pOH-S-Based DNA Substrates (b)

#### 3.1.2.1 Buffers and Reagents

- Disposable illustra-MicroSpin G-25 columns (GE Healthcare, 27-5325-01)
- QIAquick Gel Extraction Kit (Qiagen, 28704)
- pOH-S vector (Sturzenegger et al., 2014)
- *Stu*I restriction endonuclease (New England Biolabs, R0187)
- Nt.BbvCI nicking endonuclease (10 units/ $\mu$ L, New England Biolabs, R0632)
- Nb.BbvCI nicking endonuclease (10 units/ $\mu$ L, New England Biolabs, R0631)
- Optional: [ $\alpha$ - $^{32}$ P] deoxythymidine 5'-triphosphate 10  $\mu$ Ci/ $\mu$ L (e.g., Hartmann Analytics, SRP-206), [ $\alpha$ - $^{32}$ P] cordycepin 5'-triphosphate 10  $\mu$ Ci/ $\mu$ L (PerkinElmer, NEG026250UC)

#### 3.1.2.2 Procedure

The pOH-S-based DNA substrate can be used in DNA end resection assays either unlabeled or labeled with  $^{32}$ P at the 3' end (to monitor 5' end resection). Unlabeled “cold” DNA can be visualized by staining with ethidium bromide, GelRed, or a similar dye. To radioactively label 5'-overhanged substrate, [ $\alpha$ - $^{32}$ P] deoxythymidine 5'-triphosphate and Klenow fragment of DNA polymerase I can be used similarly as described in Section 3.1.1. To radioactively label 3'-overhanged substrate, [ $\alpha$ - $^{32}$ P] cordycepin 5'-triphosphate and terminal transferase can be used as described in Section 2.1.1.3. Assays with radioactively labeled DNA are more sensitive and thus more suitable to detect intermediate degradative products in DNA end resection assays.

1. Digest 10  $\mu$ g of pOH-S DNA with *Stu*I (20 units per reaction) in a total of 55  $\mu$ L reaction volume. Incubate at 37°C for 1 h to cleave the DNA and at 65°C 20 min to inactivate the enzyme.
2. Add 2  $\mu$ L Nt.BbvCI (20 units) for creating 3' overhangs or Nb.BbvCI (20 units) for creating 5' overhangs. Incubate the reaction at 37°C for 2 h.
3. Add 270  $\mu$ L deionized nuclease-free water to the sample to reduce salt concentration in the reaction.

4. Heat the reaction at 85°C for 15 min. This step will inactivate the enzymes and denature short oligonucleotides resulting from nicking by Nt- or Nb.BbvCI at the tandem recognition sites. This step will not denature the full-length pOH-S plasmid DNA.
5. Add immediately 1.5 mL PB buffer from the QIAquick Gel Extraction Kit (Qiagen) and load directly on the spin column provided by QIAquick Gel Extraction Kit, centrifuge 1 min at 20,000 × *g*. The short oligonucleotides resulting from DNA cleavage by Nt/Nb.BbvCI will not be retained at this step.
6. Add 0.75 mL PE buffer from the QIAquick Gel Extraction Kit (Qiagen), centrifuge 1 min at 20,000 × *g*.
7. Add 50 μL water to elute the digested pOH-S vector, centrifuge 1 min at 20,000 × *g*.
8. Determine DNA concentration in the eluate.

**Note**

- Steps 2–4 can be excluded to prepare blunt-ended linear dsDNA substrate. This can be used as a control in experiments with overhanged DNA.

### 3.1.3 Expression and Purification of $\Phi$ C31 Integrase

The preparation of pAttP-S-based substrates requires recombinant  $\Phi$ C31 integrase (Smith et al., 2010), which is not available commercially. A brief protocol for the expression and purification of  $\Phi$ C31 is included below. The procedure involves expression of  $\Phi$ C31 in bacteria, followed by simple purification using a nickel-nitrilotriacetic acid (Ni-NTA) agarose resin. The affinity chromatography step exploits a 10 × his affinity tag at the N-terminus of  $\Phi$ C31. The average yield is ~6.6 mg from 1L *E. coli* culture (Fig. 5A).

#### 3.1.3.1 Equipment

- Sonicator (Bandelin, Sonopuls GM70) or equivalent.
- High speed centrifuge with compatible rotors capable of handling both low and high volumes at 4°C.

#### 3.1.3.2 Buffers and Reagents

- *E. coli* BL21(DE3) pLysS cells (Promega, L1195) or equivalent
- pHPhiC31Int expression vector (Jody Plank, Kowalczykowski laboratory, UC Davis)

- Disposable 5 mL polypropylene columns (ThermoFisher Scientific, 29922) or equivalent
- SOC medium: 2% tryptone, 0.5% yeast extract, 10 mM NaCl, 2.5 mM KCl, 10 mM MgCl<sub>2</sub>, 10 mM MgSO<sub>4</sub>, 20 mM glucose. Filter-sterilize.
- LB medium (AppliChem, A0954 or equivalent). Autoclave.
- LB Amp/Chlor: LB medium supplemented with 100 µg/mL ampicillin and 25 µg/mL chloramphenicol
- Isopropyl β-D-1-thiogalactopyranoside (IPTG, Sigma-Aldrich, I6758 or equivalent), prepare 0.1 M solution in water. Filter-sterilize.
- Lysis buffer: 20 mM HEPES pH 7.0, 500 mM NaCl, 5 mM β-mercaptoethanol (β-ME) (Sigma-Aldrich, M6250), 1 mM phenylmethane sulfonyl fluoride (PMSF) (AppliChem, A0999), 10 mM imidazole (Sigma-Aldrich, I202), 10% glycerol (AppliChem, A2926)
- Ni-NTA wash buffer I: 20 mM HEPES pH 7.0, 1 M NaCl, 5 mM β-ME, 1 mM PMSF, 10 mM imidazole, 10% glycerol
- Ni-NTA wash buffer II: 20 mM HEPES pH 7.0, 150 mM NaCl, 5 mM β-ME, 20 mM imidazole, 10% glycerol
- Ni-NTA elution buffer: 20 mM HEPES pH 7.0, 150 mM NaCl, 5 mM β-ME, 400 mM imidazole, 10% glycerol
- Ni-NTA agarose resin (Qiagen, 30230)

### 3.1.3.3 Procedure

1. Transform *E. coli* BL21(DE3) pLysS cells with 50 ng of pHPiC31Int plasmid using standard procedures. Resuspend the transformation mixture in 1 mL SOC medium and incubate at 37°C for 1 h.
2. Plate various dilutions on Amp/Chlor plates and incubate at 37°C overnight.
3. Pick a colony to inoculate 4 mL LB Amp/Chlor medium. Grow at 37°C overnight.
4. Inoculate 50 µL of the culture into four 2.8-L flasks containing 500 mL LB Amp/Chlor each. Grow the cultures at 30°C, shaking vigorously until the cultures reach optical density (at 600 nm) of ~0.6.
5. Induce the expression of the ΦC31 integrase with 0.5 mM IPTG, cool the culture briefly on ice and incubate overnight at 18°C while shaking vigorously.
6. Spin the cells at 5000 × g for 30 min and decant the supernatant. Freeze the cell pellets in liquid nitrogen and store the frozen pellets at -80°C.
7. All subsequent purification steps are carried out on ice or at 4°C.
8. Resuspend the pellet in 40 mL lysis buffer and lyse the cells by sonication.

9. Centrifuge the mixture at  $48,000 \times g$  for 30 min to obtain soluble extract. Keep a small aliquot of soluble extract for later analysis.
10. During centrifugation, preequilibrate Ni-NTA resin by gravity flow. In our example, we recommend a total of 2 mL (4 mL of 50% slurry) of Ni-NTA resin, loaded onto one 10-mL plastic disposable column. Wash the Ni-NTA resin first with water and then equilibrate with 15 mL lysis buffer.
11. Transfer the equilibrated Ni-NTA resin into a 50-mL conical tube. Add the soluble extract into the tube.
12. Incubate the suspension for 1 h with gentle agitation to allow  $\Phi$ C31 binding to the Ni-NTA resin.
13. Centrifuge the sample at  $2000 \times g$  for 2 min. Keep a small aliquot of the supernatant (Ni-NTA flow through) for later analysis.
14. Wash the Ni-NTA resin batch wise with Ni-NTA wash buffer I once, centrifuge as described earlier.
15. Transfer the Ni-NTA resin back into the plastic column.
16. Wash the resin with  $\sim 30$  mL Ni-NTA wash buffer I by gravity flow.
17. Wash the resin with  $\sim 10$  mL Ni-NTA wash buffer II by gravity flow.
18. Elute the bound proteins from the resin in 1 mL fractions of the Ni-NTA elution buffer. Avoid mixing of the resin during the elution step.
19. Determine protein concentration in the eluate fractions using a Bradford assay or equivalent.
20. Pool fractions containing the highest concentration of  $\Phi$ C31, aliquot, snap-freeze with liquid nitrogen, and store at  $-80^\circ\text{C}$ .
21. Analyze soluble extract, Ni-NTA flow through and Ni-NTA eluate by polyacrylamide gel electrophoresis (Fig. 5A).

**Note**

- The purity of  $\Phi$ C31 integrase is  $\sim 95\%$  in most cases, as estimated by polyacrylamide gel electrophoresis (Fig. 5A). As the next steps (see Section 3.1.4) are going to be carried out in a buffer containing EDTA that inhibits nucleases, and the reaction products are going to be extensively purified (see Section 3.1.4), this purity of  $\Phi$ C31 is sufficient and no additional chromatography steps are necessary.

**3.1.4 Preparation of pAttP-S-Based Substrates (c)**

The reaction involves  $\Phi$ C31-catalyzed site-specific recombination between two oligonucleotides annealed to form a DNA duplex containing the AttB site (and flanking sequences of choice) and a circular plasmid DNA containing the AttP site. The reaction product is plasmid-length

linear DNA with flanking sequences at DNA ends (Fig. 5B). The attB site within the oligonucleotides (top strand, minimal recognition site, GTGCCAGGGCGTGCCCTTGGGCTCCCCGGGCGCG) can be flanked by any desired sequence or DNA modification and/or radioactively labeled at 5' or 3' ends, as described in Section 2.1.1. The oligonucleotides PC210 and PC211 described in Section 2.4 contain the attB site and can be thus used to prepare plasmid-length dsDNA substrates with streptavidin-blocked DNA ends. The pAttP-S vector was prepared by inserting a sequence containing the attP site (top strand, GTAGTGCCCCAACTGGGGTAACCTTTGAGTTCTCTCAGTTGGGGCGTAG) into the *Hind*III site of pUC19 (Cannavo & Cejka, 2014).

#### 3.1.4.1 Equipment

- Apparatus for running horizontal agarose gels, such as Sub-Cell GT Cell (Bio-Rad, 1704403)

#### 3.1.4.2 Buffers and Reagents

- QIAquick Gel Extraction Kit (Qiagen, 28704) or QIAquick PCR Purification Kit (Qiagen, 28104), see below
- pAttP-S vector, containing the AttP recognition site (Cannavo & Cejka, 2014)
- Oligonucleotides PC210 and PC211 (containing the AttB recognition site and conjugated biotin at indicated positions, see Table 1), or any other oligonucleotides containing the AttB site
- Integrase reaction buffer 10 × (100 mM Tris-acetate pH 7.5, 10 mM EDTA, 1 M NaCl, 50 mM DTT)
- BSA (20 mg/mL, New England Biolabs, B9000 or equivalent)
- Stop solution (150 mM EDTA, 2% SDS, 30% glycerol, 1 mg/mL bromophenol blue)
- Proteinase K, recombinant, PCR grade (14–22 mg/mL, Roche, 03115828001 or equivalent)
- UltraPure agarose (ThermoFisher Scientific, 16500) or equivalent
- 10 × annealing buffer (0.5 M Tris-HCl pH 7.5, 100 mM MgCl<sub>2</sub>)
- Recombinant ΦC31 integrase, see Section 3.1.3

#### 3.1.4.3 Procedure

1. Anneal oligonucleotides PC210 and PC211: Mix 10 μL of oligonucleotide PC210 (10 μM stock concentration, final concentration 2 μM), 10 μL of oligonucleotide PC211 (10 μM stock concentration, final

- concentration  $2\ \mu\text{M}$ ), and  $5\ \mu\text{L}$   $10\times$  annealing buffer (final concentrations:  $50\ \text{mM}$  Tris-HCl pH 7.5,  $10\ \text{mM}$   $\text{MgCl}_2$ ). Bring the reaction volume up to  $50\ \mu\text{L}$  with deionized water.
2. Incubate the mixture at  $95^\circ\text{C}$  for 3 min. Turn off the heat block or oven to allow for slow cooling of the sample until it reaches room temperature (several hours to overnight).
  3. The final concentration of the duplex DNA substrate is  $2\ \mu\text{M}$  (in molecules).
  4. Set up an integrase reaction by mixing  $2\ \mu\text{L}$  integrase reaction buffer  $10\times$  (final concentrations  $10\ \text{mM}$  Tris-acetate pH 7.5,  $1\ \text{mM}$  EDTA,  $100\ \text{mM}$  NaCl,  $5\ \text{mM}$  DTT),  $1\ \mu\text{L}$  BSA ( $10\ \text{mg/mL}$ ),  $1600\ \text{ng}$  pAttP-S (corresponds to  $\sim 46\ \text{nM}$  final concentration, in molecules),  $2.1\ \mu\text{L}$  of the duplex DNA (final concentration  $210\ \text{nM}$ , in molecules,  $\sim 4.6$ -fold excess over plasmid DNA),  $\Phi\text{C31}$  integrase (amount to be determined empirically, see below) in a total reaction volume of  $20\ \mu\text{L}$ .
  5. Incubate at  $30^\circ\text{C}$  overnight.
  6. Terminate the reaction by adding  $2.5\ \mu\text{L}$  stop solution, incubate at  $37^\circ\text{C}$  for 1 h.
  7. To purify the reaction products, use either of the two methods described later.
    - a. In case the  $\Phi\text{C31}$ -catalyzed reaction was not very efficient and circular DNA is still present in the terminated sample, separate the reaction products on a 1% agarose gel. Excise the product band, corresponding to  $\sim 2.7\ \text{kbp}$ -long linear DNA, and purify the DNA using QIAquick Gel Extraction Kit according to manufacturer's recommendation.
    - b. In case the  $\Phi\text{C31}$ -catalyzed reaction was efficient, purify the reaction products using QIAquick PCR Purification Kit.
  8. Determine DNA concentration and store at  $-20^\circ\text{C}$ .

### Notes

- The specific activity of  $\Phi\text{C31}$  integrase needs to be determined empirically: Perform steps 1–7 scaled down to small volumes and test various amounts of the  $\Phi\text{C31}$  integrase preparation (see Fig. 5B). Analyze reaction products by agarose gel electrophoresis. Choose the lowest  $\Phi\text{C31}$  concentration that yields the maximal amount of linear DNA for future experiments.
- In most cases, the  $\Phi\text{C31}$  integrase reaction is very efficient ( $>95\%$  linear DNA), making purification described in step 7b sufficient for most applications. In case the integrase reaction is less efficient, or in case higher substrate purity is required, use steps described in 7a.

- If radioactive labeling is required, we recommend labeling the oligonucleotides prior to annealing and integrase reaction at the desired positions.

### 3.2 Protein Quality Control: DNA Unwinding Assay

As described in [Section 2.2](#), a nuclease assay should be performed with all purified recombinant proteins and/or nuclease-dead variants to ascertain that protein preparations are not contaminated with unrelated nucleases. As BLM, WRN, and the nuclease-dead variant of DNA2 (D277A) are DNA helicases, below we briefly describe a helicase assay that can be used to verify that the respective protein preparations are active.

#### 3.2.1 Equipment

- Horizontal gel electrophoresis system, such Sub-Cell GT Cell (Bio-Rad, 1704403)

#### 3.2.2 Buffers and Reagents

- Recombinant protein(s)
- BSA (20 mg/mL, New England Biolabs, B9000 or equivalent)
- 1 M DTT
- ATP disodium, crystalline (Amersham Biosciences, 27-1006-01 or equivalent)
- 1 M Tris-acetate pH 7.5
- Pyruvate kinase from rabbit muscle (25 units/ $\mu$ L, Sigma-Aldrich, P1506 or equivalent)
- 0.1 M phosphoenolpyruvate (Sigma, P0564 or equivalent)
- 1 M magnesium acetate
- Protein dilution buffer (25 mM Tris-HCl pH 7.5, 50 mM NaCl, 0.1 mg/mL BSA, 1 mM DTT)
- Stop solution (150 mM EDTA, 2% sodium dodecyl sulfate, 30% glycerol, 1 mg/mL bromophenol blue)
- Proteinase K, recombinant, PCR grade (14–22 mg/mL, Roche, 03115828001 or equivalent)
- 1  $\times$  TAE buffer (40 mM Tris, 20 mM acetic acid, 1 mM EDTA)
- UltraPure agarose (ThermoFisher Scientific, 16500) or equivalent
- Whatman cellulose chromatography paper DE81 (GE Healthcare, 3658-915), see note in [Section 2.1.2.2](#)
- DNA substrate, e.g., radiolabeled pUC19/*Hind*III, see [Section 3.1.1](#)

### 3.2.3 Procedure

1. Determine the number of samples to be analyzed. The volume of a single reaction is 15  $\mu\text{L}$ .
2. Prepare appropriate volume of reaction master mix containing: 25 mM Tris-acetate pH 7.5, 1 mM DTT, 0.1 mg/mL BSA, 1 mM ATP, 1 mM phosphoenolpyruvate, 80 units/mL pyruvate kinase, 2 mM magnesium acetate, DNA substrate (1 nM, in molecules, such as radiolabeled pUC19/*HindIII*, see [Section 3.1.1](#)) in nuclease-free water on ice.
3. If applicable, add recombinant RPA to the master mix. When using the pUC19/*HindIII* substrate, we recommend 215 nM RPA concentration (corresponding to  $\sim 100\%$  DNA coverage, assuming all DNA in the reaction was single-stranded and  $\sim 25$  nt-site size of RPA). RPA concentration can be adjusted as necessary.
4. Distribute 14  $\mu\text{L}$  master mix into each reaction tube on ice.
5. Add the respective recombinant protein (1–2  $\mu\text{L}$ , dilute if necessary with protein dilution buffer) to the reaction tube on ice. Mix the reaction by pipetting gently and incubate at 37°C for 30 min.
6. Stop each reaction by adding 5  $\mu\text{L}$  stop solution. Add 1  $\mu\text{L}$  proteinase K to each reaction and incubate at 37°C for 10 min.
7. Separate the reaction products on 1% agarose gel by electrophoresis in  $1\times$  TAE buffer. Loading smaller volumes ( $< 15\mu\text{L}$ ) leads to better DNA separation. Using Sub-Cell GT Cell (Bio-Rad), we recommend 100 V constant voltage ( $\sim 3\text{--}4\text{V/cm}$ ) until bromophenol blue runs  $\sim 8$  cm into the agarose gel,  $\sim 2$  h.
8. Place the agarose gel onto Whatman cellulose chromatography paper DE81 or equivalent (see note in [Section 2.1.2.2](#)). Place on top of  $\sim 10$ -cm thick stack of paper towels. Cover the agarose gel with a plastic wrap and a flat acrylic plate (or equivalent). Place a weight ( $\sim 3$  kg) on top of the plate. Squeeze the gel for 20 min.
9. Dry the gel for 1 h using a gel dryer. Expose the dried gel to storage phosphor screen and read the signal with a typhoon imager (see [Fig. 6](#)).

#### Notes

- The unwinding assay can be performed with other plasmid-based or oligonucleotide-based DNA substrates (e.g., Y-structure oligonucleotide-based DNA, see [Section 2.2.2](#)). If using oligonucleotide-based DNA substrate, use native polyacrylamide gel electrophoresis (see [Section 2.1.2.4](#)) to separate the reaction products. Also, when using oligonucleotide-based DNA in unwinding assays, we recommend supplementing the stop solution with 80-fold excess of unlabeled

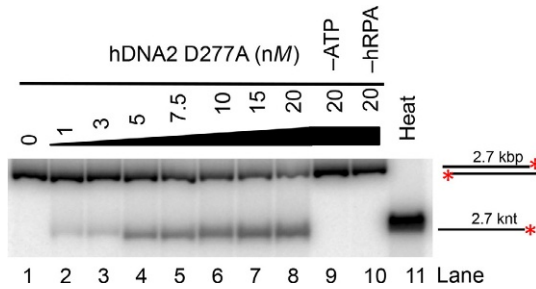


**Fig. 6** Agarose gel (1%) showing representative unwinding assay with various concentrations of nuclease-deficient DNA2 D277A (Section 3.2). 3'-end  $^{32}\text{P}$ -labeled dsDNA pUC19/*HindIII* substrate (2.7 kbp, Section 3.1.1). Heat, heat-denatured substrate marks ssDNA. \*, radioactive label. Experiment is similar to that published previously (Pinto et al., 2016).

oligonucleotide of the same sequence as the one radioactively labeled. This limits annealing of the unwound labeled oligonucleotide to the complementary strand upon deproteinization.

- If using unlabeled plasmid-length DNA as a substrate, use 100 ng for each reaction and stain the DNA with GelRed or equivalent. Radioactively labeled substrate however leads to better image quality and allows more precise quantitative analysis.
- Human RPA can melt dsDNA (Kemmerich et al., 2016). Do not exceed the recommended RPA concentration, or additionally supplement the reaction with salt and/or magnesium acetate. Always include a control reaction where only RPA has been added to the reaction mixture without the respective helicase. We recommend using RPA concentrations corresponding to 100% DNA coverage for both plasmid-length DNA substrates and oligonucleotide-based DNA substrates, assuming all DNA in the reaction was single-stranded and  $\sim 25$  nt-site size of RPA (Wold, 1997).
- Include a sample where DNA has been denatured by heating at  $95^\circ\text{C}$  for 5 min as a marker for ssDNA in all DNA unwinding assays.
- Do not terminate the reaction for more than 10 min; the short termination time reduces spontaneous annealing of unwound DNA products upon deproteinization.

### 3.3 DNA End Resection Assays With DNA2–BLM or DNA2–WRN

Below we describe a kinetic experiment that illustrates processing of the pUC19/*HindIII* substrate by DNA2, WRN, or the DNA2–WRN complex

in the presence of cognate human RPA. As in the examples above, the assay can be carried out in multiple different ways by using a variety of DNA substrates, protein concentrations, and buffer conditions. The assay presented below was chosen as it best demonstrates the synergy between DNA2 and WRN in dsDNA degradation (Pinto et al., 2016).

### 3.3.1 Equipment

- See equipment required for the substrate preparation and/or radioactive labeling (Section 3.1.1)
- Horizontal electrophoresis system, such as Sub-Cell GT Cell (Bio-Rad, 1704403)

### 3.3.2 Buffers and Reagents

- Recombinant proteins
- BSA (20 mg/mL, New England Biolabs, B9000 or equivalent)
- 1 M DTT
- ATP disodium, crystalline (Amersham Biosciences, 27-1006-01 or equivalent)
- 1 M Tris-acetate pH 7.5
- Pyruvate kinase from rabbit muscle 25 units/ $\mu$ L (Sigma-Aldrich, P1506 or equivalent)
- 0.1 M phosphoenolpyruvate (Sigma, P0564 or equivalent)
- 1 M magnesium acetate
- Protein dilution buffer (25 mM Tris-HCl pH 7.5, 50 mM NaCl, 0.1 mg/mL BSA, 1 mM DTT)
- DNA substrate (radiolabeled pUC19/*Hind*III, see Section 3.1.1)
- Stop solution (150 mM EDTA, 2% sodium dodecyl sulfate, 30% glycerol, 1 mg/mL bromophenol blue)
- Proteinase K, recombinant PCR grade (14–22 mg/mL, Roche, 03115828001 or equivalent)
- 1  $\times$  TAE buffer (40 mM Tris, 20 mM acetic acid, 1 mM EDTA)
- UltraPure agarose (ThermoFisher Scientific, 16500 or equivalent)
- Whatman cellulose chromatography paper DE81 (GE Healthcare, 3658-915) see note in Section 2.1.2.2.

### 3.3.3 Procedure

1. Prepare appropriate volume of reaction master mix containing: 25 mM Tris-acetate, 1 mM DTT, 0.1 mg/mL BSA, 1 mM ATP, 1 mM phosphoenolpyruvate, 80 units/mL pyruvate kinase, 2 mM magnesium acetate,

- 50 mM NaCl, 215 nM RPA, and 1 nM DNA substrate (in molecules) in nuclease-free water on ice.
- For each time-point sample, prepare a tube with 5  $\mu$ L stop solution.
  - Add recombinant WRN (100 nM final concentration) alone or DNA2 (30 nM final concentration) and WRN (100 nM final concentration) into the respective master mix on ice.
  - Remove 15  $\mu$ L reaction mix corresponding to the zero-minute time point and mix with 5  $\mu$ L stop solution. Place the tube on dry ice to freeze the sample.
  - Initiate the reaction by transferring the master mix tubes to 37°C.
  - Remove 15  $\mu$ L reaction mixture at each time-point and process as above (step 4).
  - Thaw the samples after collecting the last sample, add 1  $\mu$ L proteinase K to each reaction and incubate at 37°C for 10 min.
  - Separate the products on 1% agarose gel by electrophoresis (see Fig. 7). Follow the steps 7–9 from Section 3.2.3.

### Notes

- The reactions are strongly affected by NaCl concentration. Adjust the salt concentration in each reaction, considering the volume of recombinant protein and salt concentration in the protein storage buffer.
- Include a sample where DNA has been denatured by incubation at 95°C for 5 min as a marker for ssDNA.

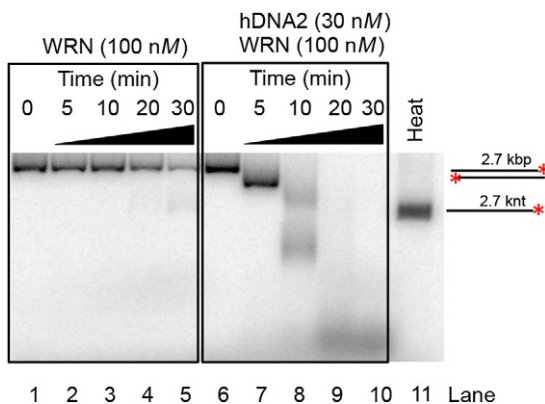


**Fig. 7** Agarose gel (1%) showing a representative kinetic long-range DNA end resection experiment with WRN (100 nM) and DNA2 (30 nM), lanes 6–10 (Section 3.3). DNA unwinding by WRN (100 nM) alone is shown in lanes 1–5. 3'-end  $^{32}$ P-labeled dsDNA pUC19/*Hind*III substrate (2.7 kbp, Section 3.1.1) was used. Heat, heat-denatured substrate marks ssDNA. \*, radioactive label. Experiment is similar to that published previously (Pinto et al., 2016).

## ACKNOWLEDGMENTS

We thank members of the Cejka laboratory (Elda Cannavo, Sean Howard, Giordano Reginato, Lepakshi Ranjha) for comments on the manuscript. We thank Jody Plank (formerly Kowalczykowski laboratory, UC Davis) for helpful discussions and initial setup of the  $\Phi$ C31 integrase reactions. The work was supported by grants from the Swiss National Science Foundation, European Research Council, and Swiss Cancer League to P.C.

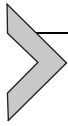
## REFERENCES

- Anand, R., Ranjha, L., Cannavo, E., & Cejka, P. (2016). Phosphorylated CtIP functions as a co-factor of the MRE11-RAD50-NBS1 endonuclease in DNA end resection. *Molecular Cell*, *64*(5), 940–950. <https://doi.org/10.1016/j.molcel.2016.10.017>.
- Bae, S. H., & Seo, Y. S. (2000). Characterization of the enzymatic properties of the yeast dna2 helicase/endonuclease suggests a new model for Okazaki fragment processing. *The Journal of Biological Chemistry*, *275*(48), 38022–38031. <https://doi.org/10.1074/jbc.M006513200>.
- Broderick, R., Nieminuszczy, J., Baddock, H. T., Deshpande, R. A., Gileadi, O., Paull, T. T., et al. (2016). EXD2 promotes homologous recombination by facilitating DNA end resection. *Nature Cell Biology*, *18*(3), 271–280. <https://doi.org/10.1038/ncb3303>.
- Cannavo, E., & Cejka, P. (2014). Sae2 promotes dsDNA endonuclease activity within Mre11-Rad50-Xrs2 to resect DNA breaks. *Nature*, *514*(7520), 122–125. <https://doi.org/10.1038/nature13771>.
- Cejka, P. (2015). DNA end resection: Nucleases team up with the right partners to initiate homologous recombination. *The Journal of Biological Chemistry*. <https://doi.org/10.1074/jbc.R115.675942>.
- Cejka, P., Cannavo, E., Polaczek, P., Masuda-Sasa, T., Pokharel, S., Campbell, J. L., et al. (2010). DNA end resection by Dna2-Sgs1-RPA and its stimulation by Top3-Rmi1 and Mre11-Rad50-Xrs2. *Nature*, *467*(7311), 112–116. <https://doi.org/10.1038/nature09355>.
- Chen, L., Trujillo, K. M., Van Komen, S., Roh, D. H., Krejci, L., Lewis, L. K., et al. (2005). Effect of amino acid substitutions in the rad50 ATP binding domain on DNA double strand break repair in yeast. *The Journal of Biological Chemistry*, *280*(4), 2620–2627. <https://doi.org/10.1074/jbc.M410192200>.
- Daley, J. M., Chiba, T., Xue, X., Niu, H., & Sung, P. (2014). Multifaceted role of the Topo III $\alpha$ -RMI1-RMI2 complex and DNA2 in the BLM-dependent pathway of DNA break end resection. *Nucleic Acids Research*, *42*(17), 11083–11091. <https://doi.org/10.1093/nar/gku803>.
- Daley, J. M., Niu, H., Miller, A. S., & Sung, P. (2015). Biochemical mechanism of DSB end resection and its regulation. *DNA Repair (Amst)*. <https://doi.org/10.1016/j.dnarep.2015.04.015>.
- Deshpande, R. A., Lee, J. H., Arora, S., & Paull, T. T. (2016). Nbs1 converts the human Mre11/Rad50 nuclease complex into an endo/exonuclease machine specific for protein-DNA adducts. *Molecular Cell*, *64*(3), 593–606. <https://doi.org/10.1016/j.molcel.2016.10.010>.
- Deshpande, R. A., Williams, G. J., Limbo, O., Williams, R. S., Kuhnlein, J., Lee, J. H., et al. (2014). ATP-driven Rad50 conformations regulate DNA tethering, end resection, and ATM checkpoint signaling. *The EMBO Journal*, *33*(5), 482–500. <https://doi.org/10.1002/emboj.201386100>.
- Garcia, V., Phelps, S. E., Gray, S., & Neale, M. J. (2011). Bidirectional resection of DNA double-strand breaks by Mre11 and Exo1. *Nature*, *479*(7372), 241–244. <https://doi.org/10.1038/nature10515>.

- Gravel, S., Chapman, J. R., Magill, C., & Jackson, S. P. (2008). DNA helicases Sgs1 and BLM promote DNA double-strand break resection. *Genes & Development*, 22(20), 2767–2772. <https://doi.org/10.1101/gad.503108>.
- Groth, A. C., Olivares, E. C., Thyagarajan, B., & Calos, M. P. (2000). A phage integrase directs efficient site-specific integration in human cells. *Proceedings of the National Academy of Sciences of the United States of America*, 97(11), 5995–6000. <https://doi.org/10.1073/pnas.090527097>.
- Hopkins, B. B., & Paull, T. T. (2008). The P. furiosus mre11/rad50 complex promotes 5' strand resection at a DNA double-strand break. *Cell*, 135(2), 250–260. <https://doi.org/10.1016/j.cell.2008.09.054>.
- Jackson, S. P., & Bartek, J. (2009). The DNA-damage response in human biology and disease. *Nature*, 461(7267), 1071–1078. <https://doi.org/10.1038/nature08467>.
- Keeney, S., & Kleckner, N. (1995). Covalent protein-DNA complexes at the 5' strand termini of meiosis-specific double-strand breaks in yeast. *Proceedings of the National Academy of Sciences of the United States of America*, 92(24), 11274–11278.
- Kemmerich, F. E., Daldrop, P., Pinto, C., Levikova, M., Cejka, P., & Seidel, R. (2016). Force regulated dynamics of RPA on a DNA fork. *Nucleic Acids Research*, 44(12), 5837–5848. <https://doi.org/10.1093/nar/gkw187>.
- Kowalczykowski, S. C. (2015). An overview of the molecular mechanisms of recombinational DNA repair. *Cold Spring Harbor Perspectives in Biology*, 7(11). <https://doi.org/10.1101/cshperspect.a016410>.
- Lammens, K., Bemeleit, D. J., Mockel, C., Clausing, E., Schele, A., Hartung, S., et al. (2011). The Mre11:Rad50 structure shows an ATP-dependent molecular clamp in DNA double-strand break repair. *Cell*, 145(1), 54–66. <https://doi.org/10.1016/j.cell.2011.02.038>.
- Larsen, N. B., & Hickson, I. D. (2013). RecQ helicases: Conserved guardians of genomic integrity. *Advances in Experimental Medicine and Biology*, 767, 161–184. [https://doi.org/10.1007/978-1-4614-5037-5\\_8](https://doi.org/10.1007/978-1-4614-5037-5_8).
- Lee, J. H., & Paull, T. T. (2004). Direct activation of the ATM protein kinase by the Mre11/Rad50/Nbs1 complex. *Science*, 304(5667), 93–96. <https://doi.org/10.1126/science.1091496>.
- Lee, J. H., & Paull, T. T. (2005). ATM activation by DNA double-strand breaks through the Mre11-Rad50-Nbs1 complex. *Science*, 308(5721), 551–554. <https://doi.org/10.1126/science.1108297>.
- Lengsfeld, B. M., Rattray, A. J., Bhaskara, V., Ghirlando, R., & Paull, T. T. (2007). Sae2 is an endonuclease that processes hairpin DNA cooperatively with the Mre11/Rad50/Xrs2 complex. *Molecular Cell*, 28(4), 638–651. <https://doi.org/10.1016/j.molcel.2007.11.001>.
- Levikova, M., Pinto, C., & Cejka, P. (2017). The motor activity of DNA2 functions as an ssDNA translocase to promote DNA end resection. *Genes & Development*, 31(5), 493–502. <https://doi.org/10.1101/gad.295196.116>.
- Liao, S., Guay, C., Toczylowski, T., & Yan, H. (2012). Analysis of MRE11's function in the 5'→3' processing of DNA double-strand breaks. *Nucleic Acids Research*, 40(10), 4496–4506. <https://doi.org/10.1093/nar/gks044>.
- Liao, S., Toczylowski, T., & Yan, H. (2008). Identification of the Xenopus DNA2 protein as a major nuclease for the 5'→3' strand-specific processing of DNA ends. *Nucleic Acids Research*, 36(19), 6091–6100. <https://doi.org/10.1093/nar/gkn616>.
- Liao, S., Toczylowski, T., & Yan, H. (2011). Mechanistic analysis of Xenopus EXO1's function in 5'-strand resection at DNA double-strand breaks. *Nucleic Acids Research*, 39(14), 5967–5977. <https://doi.org/10.1093/nar/gkr216>.
- Llorente, B., & Symington, L. S. (2004). The Mre11 nuclease is not required for 5' to 3' resection at multiple HO-induced double-strand breaks. *Molecular and Cellular Biology*, 24(21), 9682–9694. <https://doi.org/10.1128/MCB.24.21.9682-9694.2004>.

- Makharashvili, N., Tubbs, A. T., Yang, S. H., Wang, H., Barton, O., Zhou, Y., et al. (2014). Catalytic and noncatalytic roles of the CtIP endonuclease in double-strand break end resection. *Molecular Cell*, 54(6), 1022–1033. <https://doi.org/10.1016/j.molcel.2014.04.011>.
- Masuda-Sasa, T., Imamura, O., & Campbell, J. L. (2006). Biochemical analysis of human Dna2. *Nucleic Acids Research*, 34(6), 1865–1875. <https://doi.org/10.1093/nar/gkl070>.
- Miller, A. S., Daley, J. M., Pham, N. T., Niu, H., Xue, X., Ira, G., et al. (2017). A novel role of the Dna2 translocase function in DNA break resection. *Genes & Development*, 31(5), 503–510. <https://doi.org/10.1101/gad.295659.116>.
- Mimitou, E. P., & Symington, L. S. (2008). Sae2, Exo1 and Sgs1 collaborate in DNA double-strand break processing. *Nature*, 455(7214), 770–774. <https://doi.org/10.1038/nature07312>.
- Mimitou, E. P., & Symington, L. S. (2010). Ku prevents Exo1 and Sgs1-dependent resection of DNA ends in the absence of a functional MRX complex or Sae2. *The EMBO Journal*, 29(19), 3358–3369. <https://doi.org/10.1038/emboj.2010.193>.
- Neale, M. J., Pan, J., & Keeney, S. (2005). Endonucleolytic processing of covalent protein-linked DNA double-strand breaks. *Nature*, 436(7053), 1053–1057. <https://doi.org/10.1038/nature03872>.
- Nimonkar, A. V., Genschel, J., Kinoshita, E., Polaczek, P., Campbell, J. L., Wyman, C., et al. (2011). BLM-DNA2-RPA-MRN and EXO1-BLM-RPA-MRN constitute two DNA end resection machineries for human DNA break repair. *Genes & Development*, 25(4), 350–362. <https://doi.org/10.1101/gad.2003811>.
- Nimonkar, A. V., Ozsoy, A. Z., Genschel, J., Modrich, P., & Kowalczykowski, S. C. (2008). Human exonuclease 1 and BLM helicase interact to resect DNA and initiate DNA repair. *Proceedings of the National Academy of Sciences of the United States of America*, 105(44), 16906–16911. <https://doi.org/10.1073/pnas.0809380105>.
- Niu, H., Chung, W. H., Zhu, Z., Kwon, Y., Zhao, W., Chi, P., et al. (2010). Mechanism of the ATP-dependent DNA end-resection machinery from *Saccharomyces cerevisiae*. *Nature*, 467(7311), 108–111. <https://doi.org/10.1038/nature09318>.
- Paull, T. T. (2010). Making the best of the loose ends: Mre11/Rad50 complexes and Sae2 promote DNA double-strand break resection. *DNA Repair (Amst)*, 9(12), 1283–1291. <https://doi.org/10.1016/j.dnarep.2010.09.015>.
- Paull, T. T., & Gellert, M. (1998). The 3' to 5' exonuclease activity of Mre 11 facilitates repair of DNA double-strand breaks. *Molecular Cell*, 1(7), 969–979.
- Pinto, C., Kasaciunaite, K., Seidel, R., & Cejka, P. (2016). Human DNA2 possesses a cryptic DNA unwinding activity that functionally integrates with BLM or WRN helicases. *eLife*. <https://doi.org/10.7554/eLife.18574>.
- Sartori, A. A., Lukas, C., Coates, J., Mistrik, M., Fu, S., Bartek, J., et al. (2007). Human CtIP promotes DNA end resection. *Nature*, 450(7169), 509–514. <https://doi.org/10.1038/nature06337>.
- Shibata, A., Moiani, D., Arvai, A. S., Perry, J., Harding, S. M., Genois, M. M., et al. (2014). DNA double-strand break repair pathway choice is directed by distinct MRE11 nuclease activities. *Molecular Cell*, 53(1), 7–18. <https://doi.org/10.1016/j.molcel.2013.11.003>.
- Smith, M. C., Brown, W. R., McEwan, A. R., & Rowley, P. A. (2010). Site-specific recombination by phiC31 integrase and other large serine recombinases. *Biochemical Society Transactions*, 38(2), 388–394. <https://doi.org/10.1042/BST0380388>.
- Sturzenegger, A., Burdova, K., Kanagaraj, R., Levikova, M., Pinto, C., Cejka, P., et al. (2014). DNA2 cooperates with the WRN and BLM RecQ helicases to mediate long-range DNA end resection in human cells. *The Journal of Biological Chemistry*, 289(39), 27314–27326. <https://doi.org/10.1074/jbc.M114.578823>.
- Symington, L. S. (2016). Mechanism and regulation of DNA end resection in eukaryotes. *Critical Reviews in Biochemistry and Molecular Biology*, 51, 195–212. <https://doi.org/10.3109/10409238.2016.1172552>.

- Thangavel, S., Berti, M., Levikova, M., Pinto, C., Gomathinayagam, S., Vujanovic, M., et al. (2015). DNA2 drives processing and restart of reversed replication forks in human cells. *The Journal of Cell Biology*, 208(5), 545–562. <https://doi.org/10.1083/jcb.201406100>.
- Trujillo, K. M., Roh, D. H., Chen, L., Van Komen, S., Tomkinson, A., & Sung, P. (2003). Yeast xrs2 binds DNA and helps target rad50 and mre11 to DNA ends. *The Journal of Biological Chemistry*, 278(49), 48957–48964. <https://doi.org/10.1074/jbc.M309877200>.
- Trujillo, K. M., & Sung, P. (2001). DNA structure-specific nuclease activities in the *Saccharomyces cerevisiae* Rad50<sup>\*</sup>Mre11 complex. *The Journal of Biological Chemistry*, 276(38), 35458–35464. <https://doi.org/10.1074/jbc.M105482200>.
- Wang, A. T., Kim, T., Wagner, J. E., Conti, B. A., Lach, F. P., Huang, A. L., et al. (2015). A dominant mutation in human RAD51 reveals its function in DNA interstrand crosslink repair independent of homologous recombination. *Molecular Cell*, 59(3), 478–490. <https://doi.org/10.1016/j.molcel.2015.07.009>.
- Wang, H., Li, Y., Truong, L. N., Shi, L. Z., Hwang, P. Y., He, J., et al. (2014). CtIP maintains stability at common fragile sites and inverted repeats by end resection-independent endonuclease activity. *Molecular Cell*, 54(6), 1012–1021. <https://doi.org/10.1016/j.molcel.2014.04.012>.
- Williams, R. S., Moncalian, G., Williams, J. S., Yamada, Y., Limbo, O., Shin, D. S., et al. (2008). Mre11 dimers coordinate DNA end bridging and nuclease processing in double-strand-break repair. *Cell*, 135(1), 97–109. <https://doi.org/10.1016/j.cell.2008.08.017>.
- Wold, M. S. (1997). Replication protein A: A heterotrimeric, single-stranded DNA-binding protein required for eukaryotic DNA metabolism. *Annual Review of Biochemistry*, 66, 61–92. <https://doi.org/10.1146/annurev.biochem.66.1.61>.
- Yan, H., Toczylowski, T., McCane, J., Chen, C., & Liao, S. (2011). Replication protein A promotes 5'→3' end processing during homology-dependent DNA double-strand break repair. *The Journal of Cell Biology*, 192(2), 251–261. <https://doi.org/10.1083/jcb.201005110>.
- Zhou, Y., Caron, P., Legube, G., & Paull, T. T. (2014). Quantitation of DNA double-strand break resection intermediates in human cells. *Nucleic Acids Research*, 42(3), e19. <https://doi.org/10.1093/nar/gkt1309>.
- Zhu, Z., Chung, W. H., Shim, E. Y., Lee, S. E., & Ira, G. (2008). Sgs1 helicase and two nucleases Dna2 and Exo1 resect DNA double-strand break ends. *Cell*, 134(6), 981–994. <https://doi.org/10.1016/j.cell.2008.08.037>.



# Direct Quantitative Monitoring of Homology-Directed DNA Repair of Damaged Telomeres

Priyanka Verma<sup>2</sup>, Robert L. Dilley<sup>2</sup>, Melina T. Gyparaki,  
Roger A. Greenberg<sup>1</sup>

Basser Research Center for BRCA, Perelman School of Medicine, University of Pennsylvania,  
Philadelphia, PA, United States

<sup>1</sup>Corresponding author: e-mail address: rogergr@pennmedicine.upenn.edu

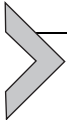
## Contents

|   |     |
|---|-----|
| 1. Introduction   | 108 |
| 2. Direct Detection of Break-Induced Telomere Synthesis                 | 109 |
| 2.1 BrdU Immunoprecipitation of Nascent Telomeres                       | 111 |
| 2.2 Single-Molecule Analysis of Nascent Telomeres                       | 115 |
| 3. In Vivo Imaging of DNA Double-Strand Break-Induced Telomere Mobility | 127 |
| 3.1 Materials   | 128 |
| 3.2 Procedure   | 128 |
| 3.3 Quantitative Analysis   | 129 |
| 3.4 Notes   | 130 |
| References  | 131 |

## Abstract

Homology-directed DNA repair (HDR) is an evolutionary conserved mechanism that is required for genome integrity and organismal fitness across species. While a myriad of different factors and mechanisms are able to execute HDR, all forms necessitate common steps of DNA damage recognition, homology search and capture, and assembly of a DNA polymerase complex to conduct templated DNA synthesis. The central question of what determines HDR mechanism utilization in mammalian cells has been limited by an inability to directly monitor the DNA damage response and products of repair as they arise from a defined genomic lesion. In this chapter, we describe several methodologies to delineate major steps of HDR during alternative lengthening of telomeres in human cells. This includes procedures to visualize interchromosomal telomere homology searches in real time and quantitatively detect HDR synthesis of nascent telomeres emanating from synchronous activation of telomere DNA double-strand breaks. We highlight the critical details of these methods and their applicability to monitoring HDR at telomeres in a broad variety of mammalian cell types.

<sup>2</sup> These authors contributed equally.



## 1. INTRODUCTION

Homology-directed DNA repair (HDR) is an evolutionary conserved DNA repair mechanism and critical determinant of genome integrity and organismal fitness. Indeed, inherited loss-of-function mutations within genes that mediate HDR are responsible for human syndromes that encompass developmental abnormalities, bone marrow failure, premature aging, and cancer predisposition (Prakash, Zhang, Feng, & Jasin, 2015). Conversely, aberrant gain of function recombination is tumor sustaining in ~15% of human cancers that utilize a poorly understood HDR mechanism for telomere maintenance known as alternative lengthening of telomeres (ALT) (Bryan, Englezou, Dalla-Pozza, Dunham, & Reddel, 1997; Bryan, Englezou, Gupta, Bacchetti, & Reddel, 1995; Dilley & Greenberg, 2015).

Despite clear differences in repair factor requirements and substrate preferences, all HDR variants necessitate several common steps. Recombination mediator proteins nucleate single-stranded overhangs for homology capture, followed by assembly of DNA polymerase complexes for templated synthesis. Canonical BRCA-Rad51 recombination involves strand invasion into duplex DNA to capture homology, while alternative HDR anneals single-stranded regions harboring as little as a few bases of homology (Bhowmick, Minocherhomji, & Hickson, 2016; Sfeir & Symington, 2015; Verma & Greenberg, 2016). Finally, a process that has been largely defined in yeast called break-induced replication (BIR) involves up to 100kb of DNA synthesis following homology capture (Anand, Lovett, & Haber, 2013; Costantino et al., 2014; Lydeard, Jain, Yamaguchi, & Haber, 2007; Saini et al., 2013; Wilson et al., 2013). Interestingly, yeast and human cells can utilize a BIR-like mechanism of HDR for telomere maintenance (Chen, Ijima, & Greider, 2001; Dilley et al., 2016; Lundblad & Blackburn, 1993; Lydeard et al., 2007; Roumelioti et al., 2016).

The central question of what determines HDR mechanism utilization in mammalian cells has been severely limited by an inability to directly monitor the DNA damage response and products of repair as they arise from a defined genomic lesion. While elegant reporter assays have been devised to monitor the products of recombination days after repair has been completed (Moynahan, Pierce, & Jasin, 2001; Pierce, Johnson, Thompson, & Jasin, 1999; Willis et al., 2014), none allow the dynamic quantification of HDR in real time. We have overcome this barrier using break-induced telomere synthesis as a model system to delineate major steps of noncanonical

HDR during ALT in human cells. The methodologies described later allow for direct visualization of telomere damage recognition, homology search and capture, and the products of HDR synthesis at an endogenous genomic location in mammalian cells.

## 2. DIRECT DETECTION OF BREAK-INDUCED TELOMERE SYNTHESIS

Direct detection of DNA synthesis *in vivo* relies on the incorporation of synthetic nucleoside analogs into replicating DNA. The methods described in this section utilize the analogs 5-bromo-2'-deoxyuridine (BrdU, Fig. 1A), 5-iodo-2'-deoxyuridine (IdU), 5-chloro-2'-deoxyuridine (CldU), and 5-ethynyl-2'-deoxyuridine (EdU), which can be detected using specific antibodies or click chemistry in the case of EdU. After pulsing cells with the analogs, the samples are processed by fluorescence microscopy or

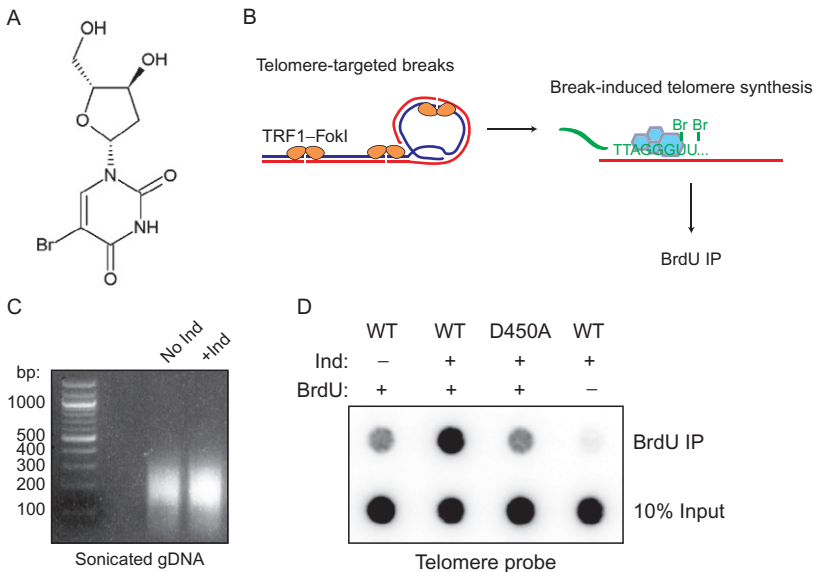


**Fig. 1** (A) Chemical structure of BrdU. (B) Schematic of BrdU incorporation into nascent telomeres after TRF1-FokI breaks. (C) Sample ethidium bromide-stained agarose gel of sonicated gDNA from U2OS cells induced with TRF1-FokI for 2 h. (D) Sample BrdU IP dot blot for telomere content using a  $^{32}\text{P}$ -labeled telomere oligonucleotide from U2OS cells induced with TRF1-FokI for 2 h. *BrdU*, 5-bromo-2'-deoxyuridine; *IP*, immunoprecipitation; *gDNA*, genomic DNA; *Ind*, induction of TRF1-FokI; *WT*, wild-type TRF1-FokI; *D450A*, nuclease-deficient TRF1-FokI.

immunoprecipitation (IP) in order to study the nascent DNA generated during the experiment.

When studying DNA repair synthesis, it is necessary to have a well-defined method of creating DNA damage. Examples include nucleases that directly cut DNA such as FokI or Cas9, as well as chemical compounds that create replication stress or DNA breaks. We use the telomere-specific nuclease (TRF1–FokI), which entails fusion of the telomere-binding protein TRF1 with the FokI endonuclease, for a multitude of reasons, not least of which is to gain insights into the mechanisms of break-induced telomere synthesis and ALT (Cho, Dilley, Lampson, & Greenberg, 2014; Dilley et al., 2016; Fig. 1B). Ectopic expression of TRF1–FokI results in robust induction of HDR-driven telomere synthesis in cells that utilize ALT or telomerase for telomere maintenance, making it broadly applicable to nearly any cell type of interest. Additionally, it is relatively easy to detect break-induced synthesis emanating from the telomere due to the high number of defined telomeric repeats throughout the genome. We suggest that the protocols described here can be adapted to study break-induced synthesis using different damaging agents at other genomic regions.

It is important to note that DNA synthesis due to S-phase replication of the genome may impact the ability to detect break-induced synthesis. As such, the signal to noise of the break-induced synthesis is critical. We have found several parameters to be important when planning experiments: the length and timing of the analog pulse, the cell cycle phase of the cell population, the length and synchrony of DNA damage, and the type of detection method used. We will present optimized conditions for detection of break-induced telomere synthesis after TRF1–FokI damage.

In this section, we focus on the novel assays adapted by our lab, namely BrdU IP and single-molecule fiber labeling to directly detect break-induced telomere synthesis. We also commonly employ routine immunofluorescence (IF) microscopy of intact cells labeled with BrdU. In our experience, results from BrdU IF experiments closely match those seen with other assays and therefore can serve as a validation. For a review of these methods, see Jackson and Cook (2008a, 2008b, 2008c). Recent studies have utilized cell microscopy, flow cytometry, and fiber labeling of thymidine analogs to detect break-induced synthesis after replication stress (Bhowmick et al., 2016; Costantino et al., 2014; Minocherhomji et al., 2015; Sotiriou et al., 2016) and at telomeres (Dilley et al., 2016; Min, Wright, & Shay, 2017; Roumelioti et al., 2016).

In addition to the direct measurement of analog incorporation during break-induced synthesis, assays designed to detect the repaired DNA products resulting from break-induced synthesis are also available. Developed in yeast, these assays have provided invaluable mechanistic insights into DNA repair pathways (Anand et al., 2013; Malkova & Ira, 2013). Since analogous systems in mammalian cells are lacking, the protocols described here provide new avenues of investigation into mammalian break-induced synthesis.

## 2.1 BrdU Immunoprecipitation of Nascent Telomeres

Isolation of DNA allows for many downstream applications such as southern blot, PCR, sequencing, electron microscopy, or in vitro reactions. BrdU IP has previously been used to study S-phase replication of human and yeast cells (Hansen et al., 2010; Viggiani, Knott, & Aparicio, 2010). We adapted these methods for the detection of nascent telomere sequences generated after TRF1–FokI breaks (Dilley et al., 2016; Fig. 1B). We prefer to visualize the nascent telomeres using a dot blot probed with radioactive telomeric repeat oligonucleotides (oligos), as described elsewhere for telomere ChIP and C-circle assays (Henson et al., 2009, 2017; Liu, Feng, & Ma, 2017). However, nonradioactive visualization using digoxigenin-labeled probes can also be used. Additionally, isolated nascent telomeres can be analyzed using PCR and next-generation sequencing methods (Cawthon, 2002; Lee et al., 2017). It is important to note that the DNA isolated after BrdU IP will be single-stranded, which may affect downstream applications.

In our experience, the success of this assay hinges on a tightly controlled damage system that is delivered to the majority of cells in synchrony. We use cell lines with a doxycycline (Dox)-inducible TRF1–FokI fused to the estrogen receptor to allow for control of expression and entry into the nucleus. Overnight addition of Dox, followed by a 2 h pulse of 4-hydroxytamoxifen (4-OHT) along with BrdU, generates robust telomere damage and nascent telomere synthesis (Dilley et al., 2016). The length of damage in this system is flexible since later time points yield similar results.

### 2.1.1 Equipment

- Covaris S220 sonicator and tubes or equivalent
- Standard agarose gel equipment
- Heat block
- End-over-end rotator
- Magnetic bead rack
- Bio-Dot Microfiltration Apparatus (Bio-Rad) or equivalent

- Amersham Hybond-N<sup>+</sup> nylon membrane (GE Healthcare)
- Stratagene UV Stratalinker 1800
- Radioactive workspace
- Standard hybridization oven and tubes for radioactive material
- Storage phosphor screen and cassette (GE Healthcare)
- STORM 860 Imager (Molecular Dynamics) or equivalent
- ImageQuant and Fiji for visualization and analysis

### 2.1.2 Buffers and Reagents

- IP buffer: 0.0625% (v/v) Triton X-100 in phosphate-buffered saline (PBS)
- Elution buffer: 1% (w/v) SDS in Tris-EDTA (TE) buffer
- Denaturation buffer: 0.5 N NaOH, 1.5 M NaCl
- Neutralization buffer: 0.5 M Tris, 1.5 M NaCl, pH adjusted to 7.0
- 20× Saline sodium citrate (SSC) pH adjusted to 7.0
- MasterPure DNA Purification Kit (Epicenter)
- PerfectHyb Plus Hybridization Buffer (Sigma)
- Anti-BrdU antibody (mouse B44, BD 347580)
- 10 mM BrdU stock dissolved in water
- ChIP DNA Clean & Concentrator Kit (Zymo)
- Protein G Magnetic Beads (Pierce)
- Bridging antibody (Active Motif)
- (TTAGGG)<sub>6</sub> or (CCCTAA)<sub>6</sub> telomere oligos resuspended at 10 μM
- T4 polynucleotide kinase (PNK) (NEB)
- ATP, [ $\gamma$ -<sup>32</sup>P] at 10 mCi/mL
- Illustra MicroSpin G-25 Columns (GE Healthcare)

### 2.1.3 Procedure

1. Induce damage: for our TRF1-FokI-inducible cells we add 40 ng/mL Dox for 16–24 h followed by 1 μM 4-OHT for 2 h.
2. Pulse cells with 100 μM BrdU for 2 h prior to collection. The pulse time can be adjusted from 30 min to 4 h if desired.
3. Collect cells and isolate genomic DNA (gDNA) using MasterPure DNA isolation kit. Resuspend gDNA in TE.
4. Shear gDNA into 100–300 bp fragments using a Covaris S220 sonicator. Check concentration and purity using NanoDrop. Fragment size should be checked by agarose gel electrophoresis (Fig. 1C).
5. Put 1–4 μg sheared gDNA in a safe-lock tube, add 5 μL of 10× PBS, and add sterile water to get 50 μL final volume. Denature for 10 min

- at 95°C and then cool in an ice-water bath. Save 10% inputs from original sheared gDNA.
6. Add 80  $\mu\text{L}$  of anti-BrdU antibody (2  $\mu\text{g}$ ) and 120  $\mu\text{L}$  of IP buffer to each denatured sample. Rotate overnight at 4°C. Samples incubated with anti-IgG serve as a control.
  7. Put 30  $\mu\text{L}$  per sample of protein G magnetic beads in a safe-lock tube (e.g., 300  $\mu\text{L}$  beads for 10 samples). Wash once and resuspend in original volume with 1  $\times$  PBS. Add 5  $\mu\text{L}$  of bridging antibody per 30  $\mu\text{L}$  beads. Mix by flicking and rotate for 1 h at 4°C.
  8. Add 30  $\mu\text{L}$  of prebound bead mixture to each IP sample. Rotate for 1 h at 4°C.
  9. Apply sample tubes to magnetic rack for at least 10 s. Aspirate supernatant. Wash 3  $\times$  with 1 mL of IP buffer, followed by one wash with 1 mL of TE. Only remove supernatant with pipet after TE wash. Be careful not to aspirate beads.
  10. Incubate beads with 50  $\mu\text{L}$  of elution buffer for 15 min at 65°C. Remove eluate to new tube. Repeat elution step and pool eluate.
  11. Clean eluate with CHIP DNA Clean & Concentrator Kit. Elute in 50  $\mu\text{L}$ .
  12. Dilute eluate, along with 10% inputs, to 100  $\mu\text{L}$  with freshly made 2  $\times$  SSC. Boil samples for 5 min at 95°C. Place on ice until ready to add to dot blot.
  13. Blot samples onto an Amersham Hybond-N<sup>+</sup> nylon membrane using Bio-Dot Microfiltration Apparatus according to manufacturer protocol.
  14. Place membrane face-up on a piece of filter paper soaked in denaturation buffer for 10 min. Move to a piece of filter paper soaked in neutralization buffer for 10 min. Place membrane on a dry piece of filter paper.
  15. UV cross link the membrane with 454 nm UV-C irradiation at 1200 J, rotate the membrane 90 degrees, and repeat.
  16. Place membrane in hybridization tube with 10 mL of Perfect-Hyb Plus hybridization buffer and prehybridize by rotating for 1 h at 37°C.
  17. While membrane is prehybridizing, prepare telomere probe. Combine 2  $\mu\text{L}$  of PNK buffer, 1  $\mu\text{L}$  of 10  $\mu\text{M}$  telomere or control oligo, and 1  $\mu\text{L}$  of T4 PNK. Move to radioactive workspace and add 3  $\mu\text{L}$  of 10 mCi/mL ATP, [ $\gamma$ -<sup>32</sup>P] and 13  $\mu\text{L}$  of sterile water. Incubate reaction for 45 min at 37°C.

18. Add 80  $\mu$ L of TE to labeling reaction. Purify 100  $\mu$ L of labeled oligo using an illustra MicroSpin G-25 Column. Add all 100  $\mu$ L of labeled oligo to hybridization tube. Rotate overnight at 37°C.
19. Wash membrane 2  $\times$  with  $\sim$ 30 mL of 2  $\times$  SSC, rotating for 20 min at 37°C both times.
20. In radioactive workspace, remove membrane using forceps, briefly place on filter paper, and then wrap tightly in polyvinyl wrapping film. Fold the edges over to make sure no remaining liquid leaks out. Place wrapped membrane in exposure cassette, add clean storage phosphor screen, and expose overnight.
21. Scan storage phosphor screen using STORM 860 with ImageQuant. Analyze image using Fiji or other image processing program (Fig. 1D).

### 2.1.4 Notes

- As a control, we usually use uninduced cells (no Dox or 4-OHT treatment). Alternatively, induction of a nuclease-defective mutant of TRF1–FokI (D450A) can be used. Other controls to include at least once are a no BrdU control as well as IgG IPs for all samples.
- To confirm telomere damage we prefer to perform IF staining of PCNA, 53BP1, or  $\gamma$ H2AX on fixed cells after TRF1–FokI induction. Colocalization of these factors with telomeres/TRF1–FokI should be clearly seen compared to uninduced cells. Damage can also be assessed by whole-cell western blot of  $\gamma$ H2AX or p-KAP1. Telomere pulsed-field gel electrophoresis will show a downward shift in the telomere smear.
- (TTAGGG)<sub>6</sub> oligos detect the C-rich telomere strand, whereas (CCCTAA)<sub>6</sub> oligos detect the G-rich telomere strand. We have not found any differences between results from these two probes. Although we mainly use 6  $\times$  oligos, 4  $\times$  oligos also yield the same results. For a control, we use a probe to Alu repeat sequences.  $\alpha$ -Satellite probes can also be used. These control probes should reveal constant levels of nascent DNA compared to the increases seen with telomere probes.
- After initial hybridization, membranes can be stripped and reprobed with another labeled oligo. To do this, incubate the membrane with boiling hot 0.1% SDS buffer with gentle rocking. Once the buffer cools to room temp, repeat 2–3 more times. Then proceed to prehybridization.
- We use Fiji to quantify images. Intensity values can be measured using a constant area circle with background subtraction. The dot blot macro can also be used. Quantifications should always be normalized to 10% input. An example dot blot is shown in Fig. 1D.

## 2.2 Single-Molecule Analysis of Nascent Telomeres

This approach, referred to as single-molecule analysis of replicating DNA (SMARD), was first developed to understand the duplication of the Epstein–Barr virus genome (Norio & Schildkraut, 2001) and is now commonly used to study the features of individual replication forks by labeling replicating DNA with two different thymidine analogs, CIdU and IdU. The technique involves pulsing cells with CIdU and IdU to allow for the differentiation of replication tracts generated at two different time points. CIdU and IdU can be distinguished using their corresponding antibodies generated in two different hosts. The combination of the two analogs has been extensively used to identify factors required for the protection and restart of the replication fork during S-phase replication (Breslin et al., 2006; Merrick, Jackson, & Diffley, 2004; Nieminuszczy, Schwab, & Niedzwiedz, 2016). An elegant study combined the use of CIdU and IdU with a third thymidine analog, EdU, which allowed the authors to demonstrate that replication can occur on either side of an adduct cross-linking two parental strands (Huang et al., 2013). Recently, the combination of the two different analogs was coupled with fluorescence in situ hybridization (FISH) to study the replication features of human and mouse telomeres (Drosopoulos, Kosiyatrakul, Yan, Calderano, & Schildkraut, 2012; Sfeir et al., 2009). We adapted this strategy to examine the nature of HDR DNA synthesis that occurs postinduction of DSBs at the telomeres (Dilley et al., 2016; Fig. 2).

### 2.2.1 Labeling of Nascent Telomeres Formed Postinduction of DSBs (Day 0–1)

#### 2.2.1.1 Reagents

- TRF1–FokI engineered cell lines and its respective media
- Doxycycline
- Thymidine analogues: IdU and CIdU

#### 2.2.1.2 Equipment

- Cell culture hood
- 37°C Cell incubator

#### 2.2.1.3 Procedure

1. Day 0: As discussed in the previous section, add doxycycline to a final concentration of 40 ng/mL to a 10-cm dish of 70% confluent cells for 16–20 h. For every cell line, include an uninduced control plate.

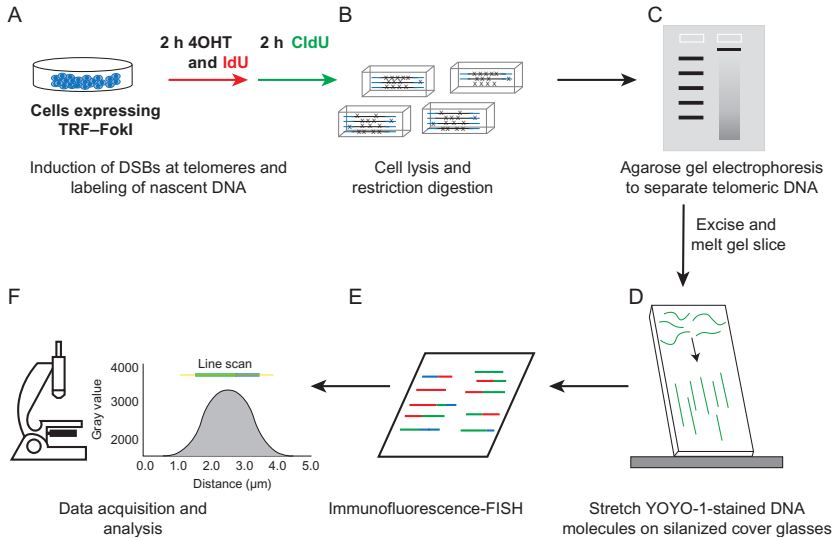


**Fig. 2** Overview of the SMARD assay to study break-induced telomere synthesis. (A) Induction of DSBs at the telomeres and labeling of nascent DNA by thymidine analogues: IdU and CldU. (B) Cell lysis and digestion of genomic DNA by *AluI* and *MboI*. The  $\times$  sign represents multiple restriction sites for the two enzymes in nontelomeric DNA. However, due to the GC-rich nature of telomeric DNA, most of the telomeres remain uncut by these two frequent cutters. (C) Agarose gel electrophoresis to separate the digested nontelomeric genomic DNA from the telomeres. (D) The isolated DNA is YOYO-1 stained and stretched onto silanized cover glasses. (E) Immunofluorescence-FISH to detect nascent telomeres. (F) Image acquisition and analysis.

- Day 1: After 16h of doxycycline treatment, add  $1\ \mu\text{M}$  4-OHT and  $30\ \mu\text{M}$  IdU to each plate and incubate the cells at  $37^\circ\text{C}$  for 2h. After 2h, remove the media, wash all plates twice with 10 mL PBS, and subsequently add medium containing  $30\ \mu\text{M}$  CldU. Incubate at  $37^\circ\text{C}$  for two additional hours.

## 2.2.2 Isolation of Telomeric DNA Formed Postinduction of DSBs (Day 1–4)

### 2.2.2.1 Reagents

- 0.25% Trypsin
- Phosphate buffer saline (PBS)
- 2% Agarose in PBS
- Tris-ethylenediaminetetraacetic acid (EDTA) (TE) buffer
- Disposable plug mold

- Solution for cell lysis: 100 mM EDTA +0.2% sodium deoxycholate (SDS) +1% sodium lauroyl sarcosine. Add 0.5 mL of proteinase K stock solution (20 mg/mL) to 50 mL of lysis buffer. Add proteinase K to lysis solution immediately before use
- Restriction enzymes: *MboI* and *AluI* and their respective buffer. If using *AluI* and *MboI* from New England Biolabs (NEB), use the CutSmart Buffer

#### 2.2.2.2 Equipment

- Cell culture hood
- Cell counter
- Benchtop centrifuge
- Heat block and 55°C water bath
- Tube rotator

#### 2.2.2.3 Procedure

1. Day 1: Prior to harvesting the cells, prepare 2% agarose in 1 × PBS and place in a 55°C water bath to maintain the agarose solution in a liquid state.
2. When ready to trypsinize, make 1 mL aliquots of the melted agarose in eppendorf tubes and place in a 70°C heat block.
3. Four hours after addition of 4-OHT, harvest the cells by trypsinization. Spin down the trypsinized cells at 200 × g and resuspend the cell pellet in 1 mL PBS. Proceed to cell counting.
4. Transfer 1 million cells to 1.5 mL eppendorf tubes and pellet down the cells at 200 × g.
5. Resuspend the cells in 50 μL of PBS. Incubate one sample at a time in the 70°C heat block for 30 s and then add 50 μL of 2% agarose to the cells, while the tube is still in the 70°C heat block. Immediately pipette up and down to mix.
6. Transfer the cell suspension to a plug holder by pipetting on one side until it is filled to the brim.
7. Once all the samples have been transferred to the plug holder, leave the plug holder at 4°C for ~20 min to allow the agarose to solidify.
8. Meanwhile, aliquot 1 mL of lysis solution into 1.5 mL amber-colored tubes.
9. Transfer the plugs to the lysis solution and incubate the tubes containing the cell plugs at 50°C overnight.
10. Day 2: Change the lysis solution and incubate the cell plugs at 50°C for an additional 24 h.

11. Day 3: Aspirate the lysis solution from the plugs and add 1 mL of TE buffer. This volume ensures that the plug is uniformly washed. Transfer the plug-containing tubes to a tube rotator. Rotate for 30 min at 30 rpm. Perform all subsequent washes on the tube rotator.
12. Next, perform one wash with 1 mL TE buffer containing 1 mM PMSF at 4°C for 60 min.
13. Perform two washes at room temperature (RT) with 1 mL TE buffer for 30 min each.
14. Wash once with 1 mL deionized water for 30 min at RT.
15. Equilibrate the plugs with 500  $\mu$ L of the 1  $\times$  CutSmart Buffer for 30 min at RT.
16. Replace with 500  $\mu$ L of fresh 1  $\times$  CutSmart Buffer and add *Mbo*I (100 units) and *Alu*I (100 units) to each plug. Digest the samples at 37°C for 16 h.

#### 2.2.2.4 Notes

1. The thymidine analogs are light sensitive. Avoid exposing the plugs to light.
2. After cell lysis, the plugs can be stored in TE buffer at 4°C for a couple of weeks. The buffer should be changed once or twice a week.

### 2.2.3 Purification of Telomeric DNA (Day 4–5)

#### 2.2.3.1 Reagents

- Ultrapure low melting point (LMP) agarose
- Agarose
- 0.5  $\times$  TBE (Tris/borate/EDTA buffer)
- $\beta$  Agarase-I
- YOYO-1 Iodide (491/509)
- Beta-mercaptoethanol ( $\beta$ ME)
- 5 M Sodium chloride (NaCl)

#### 2.2.3.2 Equipment

- Gel caster with a 1.5-mm comb and a powerpack
- Water bath at 55°C

#### 2.2.3.3 Steps

1. Day 4: In a cold room, cast a 0.7% LMP agarose gel in 0.5  $\times$  TBE containing ethidium bromide. Ensure that the comb is wide enough to

- hold the agarose plugs. A 1.5-mm wide comb is good enough for this purpose. The gel usually takes  $\sim 2$  h in the cold room to solidify.
2. Melt 1% agarose in  $0.5 \times$  TBE and place in  $55^\circ\text{C}$  water bath. This agarose will eventually be used to seal the wells of the gel.
  3. Once the gel is ready to load, aspirate the digestion mix off the plugs and add  $500 \mu\text{L}$  of  $0.5 \times$  TBE. Equilibrate for 5 min.
  4. Add  $0.5 \times$  TBE on the polymerized gel to help remove the comb. Try to be gentle as the gel is very fragile.
  5. Gently wash the wells with  $0.5 \times$  TBE and then aspirate the TBE.
  6. Using a blunt end forcep, insert the gel plugs into the wells.
  7. Use the melted 1% agarose to seal the wells.
  8. Cover the gel with aluminum foil and leave it for 5–10 min to allow the agarose to solidify.
  9. Carefully transfer the loaded gel to a running tank containing  $0.5 \times$  TBE and run at 20 V for 20–24 h at  $4^\circ\text{C}$ . Cover the lid with aluminum foil.
  10. Day 5: Prepare agarase digestion buffer:  $4.9 \text{ mL TE} + 100 \mu\text{L } 5 \text{ M NaCl} + 5 \mu\text{L } \beta\text{ME}$ .
  11. Due to the GC-rich nature of the telomeric region, telomeres are resistant to digestion by *AluI* and *MboI* restriction enzymes. Only non-telomeric gDNA is digested by these enzymes and will therefore run as a smear. On the other hand, undigested telomeres will run as an intact band (Fig. 3). Excise the telomere band, mince the gel piece, and remove any extra gel pieces. Transfer the gel piece to an amber-colored tube. Since this is a single-molecule assay, a small but brightly stained gel piece is ample. Additionally, the small size of the gel sample ensures complete digestion of the agarose in the subsequent step. The remaining gel pieces of the excised telomere band can be stored for weeks in agarase digestion buffer at  $4^\circ\text{C}$ .
  12. Add  $100 \mu\text{L}$  of the agarase digestion buffer to the gel piece. Make sure the gel piece is completely covered, else scale up the buffer volume.
  13. Incubate the eppendorf tubes containing the gel slice at  $45^\circ\text{C}$  for 5 min.
  14. Next, move the tubes to a  $69^\circ\text{C}$  heat block and incubate for 18 min ( $69^\circ\text{C}$  is close to the melting point of the LMP agarose).
  15. Equilibrate two tubes at a time on a  $45^\circ\text{C}$  heat block for 2 min and add  $3 \mu\text{L}$  of agarase by pipetting along the side of the tube. The tubes can be held in hand while adding agarase. Incubate the tubes at  $45^\circ\text{C}$  for 3 h. Once the agarose has melted, DNA is sensitive to shearing. Be gentle with the sample while handling and pipetting. Do not vortex.



**Fig. 3** Autoradiogram of an agarose gel hybridized with a  $^{32}\text{P}$ -telomeric probe. Lane 1: Undigested DNA from a U2OS cell line. Lane 2: DNA from U2OS cells digested with *AluI* and *MboI*. Lane 3: DNA from U2OS cells labeled with  $30\mu\text{M}$  IdU and  $30\mu\text{M}$  CIdU and digested with *AluI* and *MboI*. This lane shows that the incorporation of the thymidine analogue does not affect the digestion efficiency of the restriction enzymes.

**16.** After 3 h, place the tubes at RT. Gradually add  $10\mu\text{L}$  of  $\beta\text{ME}$  and  $0.4\mu\text{L}$  of  $1\text{mM}$  YOYO-1 stain along the sides of the tube and incubate overnight at RT in the dark.

#### 2.2.3.4 Notes

1. Avoid exposing the samples to light.
2. It is possible that gel pieces may remain after the 3 h digestion. In that situation, either extend the duration of the digestion or take the DNA from the top of the solution in the subsequent steps as the gel pieces will settle down.

3. To identify the location of the telomeric band on the gel, southern blot analysis using a telomeric probe can be performed.
4. We have tested the quality of the YOYO-1-stained DNA after a week of storage at RT and they look fine.

An autoradiogram of an agarose gel, hybridized with a  $^{32}\text{P}$ -labeled telomere probe, is shown in Fig. 3. It is a representative example of *AluI*- and *MboI*-digested gDNA sample from U2OS cells. Note that the gDNA runs as a smear and telomeric DNA runs as an intact band.

### 2.2.4 Slide Preparation (Day 5)

#### 2.2.4.1 Reagents

- 50 mm Cover glasses
- 1% SDS
- >98% Aminosilane solution (APTES)
- Conc. nitric acid ( $\text{HNO}_3$ )
- Conc. hydrochloric acid ( $\text{HCl}$ )
- Methanol
- Ethanol
- Saturated solution of sodium bicarbonate ( $\text{NaHCO}_3$ )

#### 2.2.4.2 Equipment

- Fume hood
- Digital orbital plate shaker
- Vacuum-sealed desiccator

#### 2.2.4.3 Procedure

1. Day 4: Soak the cover glasses in 1% SDS for an hour in a 10-cm glass petridish (3–4 cover glasses per dish).
2. Wash the cover glasses in the following order: 1% SDS solution, hot water, and  $2\times$  with RT water. Now transfer the slides to fresh glass petridishes.
3. Place a sheet of aluminum foil in a fume hood. Top the foil with saran wrap. Place the petridish containing the washed slides onto the saran wrap.
4. Combine  $\text{HNO}_3 + \text{HCl}$  (2:1) in the hood and immediately add to the slides. Carefully seal the petridish with saran wrap and leave the slides overnight in the fume hood.
5. Day 5: Using acid-resistant forceps, transfer the slides to a fresh petridish. Discard the acidic solution by neutralizing it with a saturated  $\text{NaHCO}_3$  solution.

6. Wash the coverslips thoroughly with distilled water three times for 3 min each by keeping the petridishes on an orbital shaker at 70 rpm.
7. After the third wash with water, perform two washes with methanol. Wipe any water on the cover or sides of the petridish by using a kimwipe. It is critical to ensure that there is no water during the aminosilanization step.
8. After the second methanol wash, add 20 mL of methanol to each dish and then add 440  $\mu\text{L}$  APTES dropwise to the cover glasses, while they are shaking in the petridish at 70 rpm. Incubate for exactly 1 h.
9. After an hour, wash once with methanol, three times with water, and then rinse with 95% ethanol. Each wash is at 70 rpm for 3 min.
10. Allow the cover glasses to dry by placing them in dark on a kimwipe with the aminosilated surface facing upward.
11. Transfer the cover glasses to a clean slide box and store them in the dark in a vacuum-sealed desiccator.

#### 2.2.4.4 Notes

1. It is highly recommended to make small aliquots of APTES and store in a vacuum-sealed desiccator. Do not reuse aliquots and discard APTES after 3 months of opening.
2. Aminosilization is sensitive to water. Ensure to remove any residual water before adding APTES.
3. Mixing at 70 rpm and the 1 h incubation are both crucial for proper aminosilization of the cover glasses.
4. It is always preferable to store the slides for at least a day before stretching the DNA fibers. Do not use slides that are more than 2 days old.

### 2.2.5 DNA Combing and Telomere FISH (Day 6)

#### 2.2.5.1 Reagents

- Frosted glass slides
- PAP pen for immunostaining
- Methanol + 0.1%  $\beta\text{ME}$
- Ethanol
- Formamide
- Blocking reagent for nucleic acids (Roche11096176001) dissolved in 100 mM maleic acid buffer pH 7.5
- 1 M Tris pH 7.5
- 100  $\mu\text{M}$  Biotin-OO- (CCCTAA)<sub>4</sub> locked nucleic acid (LNA) TelC probe (Exiqon)
- Denaturation solution: 0.1 N NaOH in 70% ethanol and 0.1%  $\beta\text{ME}$
- Fixation solution: 0.5% glutaraldehyde in the denaturation buffer

### 2.2.5.2 Equipment

- Wide-field microscope with a  $60\times/100\times$  objective
- $37^{\circ}\text{C}$  incubator

### 2.2.5.3 Procedure

1. Day 6: Take frosted slides and make hydrophobic boundaries along the edges using a PAP pen and allow to dry.
2. Take another set of frosted slides and flip the silanated cover glasses using forceps such that the aminosilated surface faces the slides. Also take care that the edge of these cover glasses aligns well with the slides.
3. Using a blunt-ended tip, pipette  $\sim 10\ \mu\text{L}$  from the central part of the YOYO-stained digestion tube and place the drop on the side of the coverslip by letting the drop touch the slide. Tilt the slide to approximately 45 degrees and allow the liquid to flow by capillary action. Take the slide to the scope and image at  $60\times$  or  $100\times$  to visualize the quality of the stretching. Fig. 4 shows examples of well (Fig. 4A) and poorly stretched (Fig. 4B) DNA fibers. The quality of DNA stretching mainly depends on the how well the cover glasses are silanized. If the cover glasses are not uniformly silanized and are too sticky, DNA tends to aggregate and does not spread well.

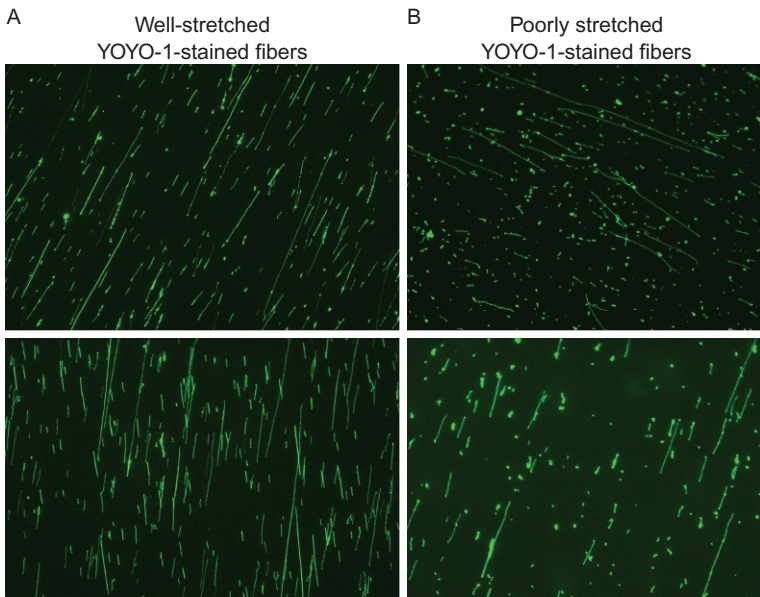


**Fig. 4** YOYO-1-stained DNA fibers stretched onto silanized coverslips. (A) Well-stretched DNA fibers. (B) Poorly stretched DNA fibers.

4. If the fibers look well stretched, flip back the coverslip on a kimwipe using a razor so that the side with the DNA faces upward. Next, clean the immersion oil by using an ethanol-soaked kimwipe and place the coverslip in a moisturized hybridization chamber. Cover the coverslip with methanol containing 0.1%  $\beta$ ME. Perform these steps for the rest of the samples.
5. Once all DNA samples are stretched, aspirate the methanol and add the denaturation buffer.
6. Two minutes before the end of the denaturation time, add glutaraldehyde to the denaturation buffer to a final concentration of 0.5%.
7. Remove the denaturation buffer and add the fixation buffer for 5 min.
8. Now perform a series of washes with 70%, 90%, and 100% ethanol. To perform these washes, incubate the cover glasses for 2 min with each ethanol solution, then aspirate and dry the coverslips before adding a more concentrated ethanol solution.
9. Remove ethanol as best as possible and then add methanol containing 0.1%  $\beta$ ME for 15 min.
10. Toward the end of this incubation period, make the hybridization buffer.

For 2 mL of hybridization buffer:

700  $\mu$ L Formamide

100  $\mu$ L Blocker

200  $\mu$ L 1 M Tris pH 7.5

2  $\mu$ L 100  $\mu$ M Biotinylated LNA TelC probe

998  $\mu$ L H<sub>2</sub>O

11. Pick each cover glass with forceps and vacuum it dry. Take the frosted slide with marked hydrophobic edges and spread 110  $\mu$ L of the hybridization buffer. Take the dried cover glass with the stretched DNA and flip it on the slide so that the DNA faces the hybridization mix. Bubbles may form but they will dissolve during the overnight incubation. Keep the slide in a humidified hybridization chamber. Repeat these steps for the other cover glasses and then leave the hybridization chamber overnight in a 37°C incubator.

#### 2.2.5.4 Notes

1. DNA is very sensitive to shearing and hence one needs to pipette and stretch the DNA fragments gently. We often cut the pointed ends of the micropipette tips to prevent DNA shearing during pipetting.

2. The time of denaturation is critical and needs to be optimized based on the length of the telomere. If the telomeres are long, extend the denaturation time. For telomeres isolated from U2OS and HeLa1.3 cells, a 9-min incubation time works well.
3. Glutaraldehyde is light sensitive and rapidly polymerizes in the presence of light. Turn off all lights before making the fixation solution and keep the lights off until the 70% ethanol wash.
4. We discard the glutaraldehyde bottle after 3–4 freeze thaw cycles.

### **2.2.6 Immunofluorescence Staining (Day 7)**

#### **2.2.6.1 Reagents**

- 3% BSA in PBS
- Alexa 405-conjugated streptavidin
- Alexa 568-conjugated antimouse and Alexa 488-conjugated antirat
- Anti-CIdU antibody (AbD Serotec)
- Anti-IdU antibody (Becton Dickinson)

#### **2.2.6.2 Procedure**

1. Day 7: Next morning, flip open the coverslip using a razor such that the DNA containing side faces up.
2. Cover the cover glasses with a solution of 4 × SSC containing 40% formamide for 3 min.
3. Wash the cover glasses with 1 × PBS containing 0.03% IGEPAL. Incubate for ~1–2 min.
4. Wash the cover glasses with 1 × PBS.
5. Remove PBS and add blocking buffer (3% BSA in PBS). Incubate for 30 min.
6. Aspirate the blocking buffer and add 200 μL of 1:250 dilution of Alexa 405 streptavidin antibody in blocking buffer and incubate for 30 min at RT.
7. Wash three times (5 min each) with 1 × PBS + 0.03% IGEPAL.
8. Add 200 μL of 1:45 dilution of antistreptavidin antibody in blocking buffer and incubate for 30 min at RT.
9. Wash three times (5 min each) with 1 × PBS + 0.03% IGEPAL.
10. To amplify the telomere FISH signal, repeat steps 6–9.
11. Add 200 μL of 1:45 diluted antistreptavidin, anti-IdU, and anti-CIdU and incubate for 1 h.
12. After three washes with 1 × PBS + 0.03% IGEPAL, add 1:250 dilution of Alexa 405 streptavidin, Alexa 568 antimouse, and Alexa 488 antirat and incubate for 1 h at RT.

13. Wash three times (5 min each) with  $1 \times$  PBS + 0.03% IGEPAL, followed by a wash with PBS.
14. To mount the cover glasses, aspirate any liquid from the cover glass to dry. Pipette 100  $\mu$ L of Prolong Gold antifade mounting media on a glass slide and mount the cover glass. Press the cover glass with a kimwipe gently to remove excess mounting media. Incubate the slide overnight at RT in the dark and allow the mounting media to harden.
15. The following morning, seal the edges of the coverslip with nail polish and allow the nail polish to dry at RT ( $\sim$ 30 min). The slides can be then stored at 4°C until imaging.

## 2.2.7 Image Acquisition, Analysis, and Interpretation

### 2.2.7.1 Equipment

- Wide-field fluorescence microscope with  $60 \times / 100 \times$  objective
- ImageJ
- GraphPad Prism 7 or other data analysis program

### 2.2.7.2 Procedure

1. Acquire images using a wide-field fluorescence microscope, which is set up for three-color imaging. Images can be acquired using either a  $60 \times$  or  $100 \times$  objective.
2. Open the image file with ImageJ.
3. *Quantification of the percent of nascent telomere fibers and interpretation of the differentially labeled telomere fibers:* In ImageJ, use the Image > Color > Channel tool to generate a composite image of the three colors. Percent of fiber labeled = (blue fibers labeled in green or red)/(total number of fibers in blue). The different types of labeling observed are depicted in Fig. 5A (schematic) and B (representative images).
4. *Measurement telomere fiber length:* In ImageJ, use the Straight-Line tool to measure the fiber length. Select Analyze > Plot Profile to obtain the length of the fibers in microns. Measure the length of blue fibers to retrieve the length of telomeres. Measure the length of red/green label overlapping with blue to obtain the length of nascent fibers. For converting microns to kilobases, 10 bp (equals one turn of the helix) has a linear length of 3.4 nm. Hence,  $0.26 \mu\text{m}$  corresponds to 1 kb of DNA.

### 2.2.7.3 Notes

1. For accuracy in length measurements, we do not quantify the length of fibers that are not straight.

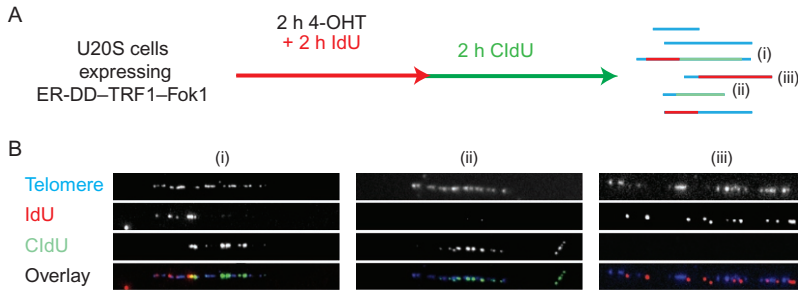
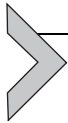


**Fig. 5** (A) Schematic of the labeling pattern observed on telomeres (blue) post labeling with IdU (red) and CldU (green). (B) Representative examples of telomeres (blue) tracts labeled with (i) both IdU and CldU (ii) CldU only (iii) IdU only.



### 3. IN VIVO IMAGING OF DNA DOUBLE-STRAND BREAK-INDUCED TELOMERE MOBILITY

Mobility increases following DNA damage have been previously described for both prokaryotes and eukaryotes, suggesting that such increases contribute to the repair of damage foci (Aten et al., 2004; Lesterlin, Ball, Schermelleh, & Sherratt, 2014). Mobility seems to play a particularly prominent role in DNA damage responses at telomeres (Cho et al., 2014; Dimitrova, Chen, Spector, & de Lange, 2008; Lottersberger, Karssemeijer, Dimitrova, & de Lange, 2015). Here, we describe an in vivo system to rapidly induce double-strand breaks at telomeres and simultaneously track their mobility.

Our system involves the use of a fusion protein containing domains TRF1, FokI, mCherry, and ER-DD for telomere localization, DSB generation, fluorescence tracking, and rapid protein induction, respectively. The mCherry-ER-DD-TRF1-FokI construct is transfected into cells, and its expression is induced using 4-OHT and Shield-1. The stabilized protein construct moves to the nucleus and accumulates onto telomeres within minutes, where it generates DSBs. The trajectories of the resulting mCherry foci can be followed over time using confocal microscopy. The nuclease-inactive FokI D450A variant of our construct can be used as a negative control since it does not cleave DNA and can therefore eliminate the possibility of telomere movement resulting from ectopic protein over-expression rather than DSB generation (Cho et al., 2014; Shanbhag, Rafalska-Metcalf, Balane-Bolivar, Janicki, & Greenberg, 2010; Tang et al., 2013).

### 3.1 Materials

- DMEM cell culture medium with GlutaMAX (ThermoFisher), supplemented with 10% bovine calf serum and 1% Penicillin/Streptomycin (Gibco)
- 6-Well culture plates (Sarstedt)
- LipoD293 transfection reagent (Signagen)
- 22 × 22 mm No 1.5 cover glass (Electron Microscopy Sciences)
- Incubator, 37°C and 5% CO<sub>2</sub>
- Leibovitz's L-15 medium with L-glutamine, without phenol red (ThermoFisher)
- 4-Hydroxytamoxifen (Sigma) at 1 mM stock concentration
- Shield-1 ligand (Clontech) at 0.5 mM stock concentration
- Inverted fluorescence microscope (DM6000, Leica Microsystems), equipped with a charge-coupled device camera (QuantEM 512C, Photometrics), a 100 × 1.4 NA objective, automated XYZ stage (Ludl Electronic Products), an X-LIGHT Confocal Imager (Crisel Electrooptical Systems), and a SPECTRA X Light Engine (Lumencor)
- Stagetop heating incubator (Tokai Hit)
- Magnetic coverslip mounting chamber (Chamlide CM-S22-1, LCI)
- MetaMorph software (Molecular Devices)
- ImageJ Fiji (NIH, <http://fiji.sc/>)
  - TrackMate plugin (<http://imagej.net/TrackMate>)
  - StackReg plugin (Dr. Philippe Thévenaz, EPFL)
- MATLAB software (MathWorks)
- Mean square displacement (MSD) analyzer scripts (Dr. Jean-Yves Tinevez, Institut Pasteur)
  - importTrackMateTracks (<https://github.com/fiji/TrackMate/blob/master/scripts/importTrackMateTracks.m>)
  - MSD analyzer (<https://github.com/tinevez/msdanalyzer>)

### 3.2 Procedure

1. Place 22 × 22 mm square glass coverslips into 6-well plates and sterilize under UV light for 15 min. Seed 200,000–250,000 cells in 2 mL culture media in the wells. Cells should be at 60%–90% confluence on the day of imaging.
2. Following 24 h of incubation, use the LipoD293 reagent and serum-free DMEM to transfect 1 μg of mCherry-ER-DD-TRF1-FokI plasmid into cells. Incubate cells for 16 h prior to protein induction.

3. Replace the culture media with fresh DMEM containing  $1\ \mu\text{M}$  Shield-1 and  $1\ \mu\text{M}$  4-OHT 1 h prior to mounting. Then, transfer the coverslips to a magnetic coverslip mounting chamber. Place 1 mL of prewarmed ( $37^\circ\text{C}$ ) L-15 media with  $1\ \mu\text{M}$  Shield-1 and  $1\ \mu\text{M}$  4-OHT on the coverslip. The mounting chamber should be loaded into a preequilibrated, humidified Tokai Hit stagetop incubator with the following settings: top heater  $41^\circ\text{C}$ , stage heater  $43^\circ\text{C}$ , lens heater  $37^\circ\text{C}$ , and an intrachamber temperature of  $37^\circ\text{C}$ .
4. Use the  $100\times$  objective to visualize mCherry-expressing nuclei. Using the MetaMorph software, select 10–12 stage positions for imaging. It is important to put the nucleus of interest at the center of the field of view as it is possible that cells migrate out of the stage view during imaging.
5. Acquire images as  $z$ -stacks of  $0.6\ \mu\text{m}$  interval for a total depth of 8–10  $\mu\text{m}$  which should be enough to cover the entire nucleus. Each stage position should be sequentially imaged for 2 min adding up to a total imaging time of 60 min.

### 3.3 Quantitative Analysis

The resulting images can be processed using the ImageJ software.

1. Load all  $z$ -stacks for a given stage position and obtain a maximum intensity projection of the  $z$ -stack set. U2OS cells are relatively flat, and therefore, the information contained in the  $x$ - $y$  plane is sufficient for quantitation of telomere mobility. Moreover, since the nuclei move and change shape during live-cell imaging, it is important to register the images (Thenevaz, Ruttimann, & Unser, 1998). Image registration is an algorithmic transformation which allows the alignment of the images in the series to the reference image. This can be achieved using the “scaled rotation” option of the StackReg plugin.
2. Telomere tracking is achieved using the TrackMate plugin in Fiji (Schindelin et al., 2012). For each image, the scale should be set to  $\mu\text{m}$  according to the pixel— $\mu\text{m}$  conversion ratio for the  $100\times$  objective on the microscope. The following settings should be used for the annotation of telomere foci: log detector, estimated blob diameter  $0.7\ \mu\text{m}$ , filter by contrast and quality. Manual corrections are often necessary when the algorithm fails to separate telomere foci that may overlap temporarily during imaging. Each track represents the movement of a telomere spot over the 60 min of imaging. Use the “simple LAP tracker” setting to establish the tracks in TrackMate with the following settings: linking

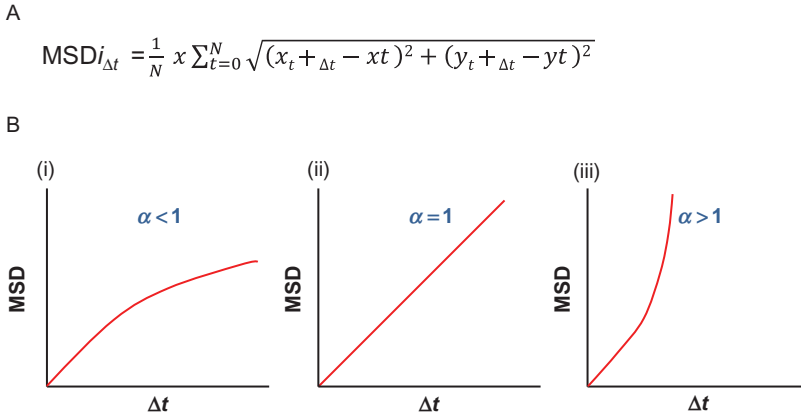


**Fig. 6** (A) Equation of mean square displacement (MSD) during  $\Delta t$  intervals for a particle  $i$  traveling in a 2D plane. (B) MSD plots of different classes of mobility. The equation,  $\text{MSD} = \Gamma t^\alpha$ , is used to provide a best fit curve for the MSD trajectories. Coefficient  $\Gamma$  indicates the magnitude of travel, while  $\alpha$  is a time-dependence coefficient which indicates the type of movement the particle exhibits. (i)  $\alpha$  Values of less than 1 indicate subdiffusion resulting from restriction to diffusion which would occur during molecular crowding in the nucleus. (ii)  $\alpha$  Values of 1 indicate Brownian diffusion. (iii)  $\alpha$  Values of greater than 1 indicate superdiffusive mobility. An  $\alpha$  value of 2 would be characteristic of a particle traveling in a directed manner (Guigas & Weiss, 2008; Marshall et al., 1997; Zajac, Goldman, Holzbaur, & Ostap, 2013).

max distance of  $2\ \mu\text{m}$ , gap-closing max distance of  $2\ \mu\text{m}$ , and gap-closing max frame gap of 2. Then, export the time and positional data generated from telomere tracking to an XML file for MATLAB analysis.

3. Import the track XML files into MATLAB using the importTrackMateTracks script.
4. Use the script, MSD analyzer, to perform a MSD analysis, which is a measure of the average distance that a particle travels (see equation in Fig. 6A) (Tarantino et al., 2014). In MSD analysis, MSD values are generated for each time interval. The MSD values at each time interval are averaged for all particles involved in the experiment and plotted on a graph of MSD on the  $y$ -axis and time interval on the  $x$ -axis (Fig. 6B). For example, for a 60-min experiment with 30 time points, where the time interval is 2 min, 29 interval square displacements are averaged.

### 3.4 Notes

Alternative analyses can also be used to quantify telomere mobility. For instance, counting the number of telomere merging events occurring per

nucleus per hour is a metric of the magnitude of telomere movement. A simpler approach would be to count the number of telomere foci at time 0 and compare it to the number of foci at the end of the sequence (Cho et al., 2014).

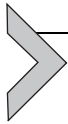
## REFERENCES

- Anand, R. P., Lovett, S. T., & Haber, J. E. (2013). Break-induced DNA replication. *Cold Spring Harbor Perspectives in Biology*, 5(12), a010397. <https://doi.org/10.1101/cshperspect.a010397>.
- Aten, J. A., Stap, J., Krawczyk, P. M., van Oven, C. H., Hoebe, R. A., Essers, J., et al. (2004). Dynamics of DNA double-strand breaks revealed by clustering of damaged chromosome domains. *Science*, 303(5654), 92–95. <https://doi.org/10.1126/science.1088845>.
- Bhowmick, R., Minocherhomji, S., & Hickson, I. D. (2016). RAD52 facilitates mitotic DNA synthesis following replication stress. *Molecular Cell*, 64(6), 1117–1126. <https://doi.org/10.1016/j.molcel.2016.10.037>.
- Breslin, C., Clements, P. M., El-Khamisy, S. F., Petermann, E., Iles, N., & Caldecott, K. W. (2006). Measurement of chromosomal DNA single-strand breaks and replication fork progression rates. *Methods in Enzymology*, 409, 410–425. [https://doi.org/10.1016/S0076-6879\(05\)09024-5](https://doi.org/10.1016/S0076-6879(05)09024-5).
- Bryan, T. M., Englezou, A., Dalla-Pozza, L., Dunham, M. A., & Reddel, R. R. (1997). Evidence for an alternative mechanism for maintaining telomere length in human tumors and tumor-derived cell lines. *Nature Medicine*, 3(11), 1271–1274.
- Bryan, T. M., Englezou, A., Gupta, J., Bacchetti, S., & Reddel, R. R. (1995). Telomere elongation in immortal human cells without detectable telomerase activity. *EMBO Journal*, 14(17), 4240–4248.
- Cawthon, R. M. (2002). Telomere measurement by quantitative PCR. *Nucleic Acids Research*, 30(10), e47–47. <https://doi.org/10.1093/nar/30.10.e47>.
- Chen, Q., Ijima, A., & Greider, C. W. (2001). Two survivor pathways that allow growth in the absence of telomerase are generated by distinct telomere recombination events. *Molecular and Cellular Biology*, 21(5), 1819–1827. <https://doi.org/10.1128/MCB.21.5.1819-1827.2001>.
- Cho, N. W., Dilley, R. L., Lampson, M. A., & Greenberg, R. A. (2014). Interchromosomal homology searches drive directional ALT telomere movement and synapsis. *Cell*, 159(1), 108–121. <https://doi.org/10.1016/j.cell.2014.08.030>.
- Costantino, L., Sotiriou, S. K., Rantala, J. K., Magin, S., Mladenov, E., Helleday, T., et al. (2014). Break-induced replication repair of damaged forks induces genomic duplications in human cells. *Science*, 343(6166), 88–91. <https://doi.org/10.1126/science.1243211>.
- Dilley, R. L., & Greenberg, R. A. (2015). ALTERNATIVE telomere maintenance and cancer. *Trends in Cancer*, 1(2), 145–156. <https://doi.org/10.1016/j.trecan.2015.07.007>.
- Dilley, R. L., Verma, P., Cho, N. W., Winters, H. D., Wondisford, A. R., & Greenberg, R. A. (2016). Break-induced telomere synthesis underlies alternative telomere maintenance. *Nature*, 539(7627), 54–58. <https://doi.org/10.1038/nature20099>.
- Dimitrova, N., Chen, Y. C., Spector, D. L., & de Lange, T. (2008). 53BP1 promotes non-homologous end joining of telomeres by increasing chromatin mobility. *Nature*, 456(7221), 524–528. <https://doi.org/10.1038/nature07433>.
- Drosopoulos, W. C., Kosiyatrakul, S. T., Yan, Z., Calderano, S. G., & Schildkraut, C. L. (2012). Human telomeres replicate using chromosome-specific, rather than universal, replication programs. *The Journal of Cell Biology*, 197(2), 253–266. <https://doi.org/10.1083/jcb.201112083>.

- Guigas, G., & Weiss, M. (2008). Sampling the cell with anomalous diffusion—The discovery of slowness. *Biophysical Journal*, *94*(1), 90–94.
- Hansen, R. S., Thomas, S., Sandstrom, R., Canfield, T. K., Thurman, R. E., Weaver, M., et al. (2010). Sequencing newly replicated DNA reveals widespread plasticity in human replication timing. *Proceedings of the National Academy of Sciences of the United States of America*, *107*(1), 139–144. <https://doi.org/10.1073/pnas.0912402107>.
- Henson, J. D., Cao, Y., Huschtscha, L. I., Chang, A. C., Au, A. Y. M., Pickett, H. A., et al. (2009). DNA C-circles are specific and quantifiable markers of alternative-lengthening-of-telomeres activity. *Nature Biotechnology*, *27*(12), 1181–1185. <https://doi.org/10.1038/nbt.1587>.
- Henson, J. D., Lau, L. M., Koch, S., Martin La Rotta, N., Dagg, R. A., & Reddel, R. R. (2017). The C-Circle Assay for alternative-lengthening-of-telomeres activity. *Methods (San Diego, Calif.)*, *114*, 74–84. <https://doi.org/10.1016/j.jymeth.2016.08.016>.
- Huang, J., Liu, S., Bellani, M. A., Thazhathveetil, A. K., Ling, C., de Winter, J. P., et al. (2013). The DNA translocase FANCM/MHF promotes replication traverse of DNA interstrand crosslinks. *Molecular Cell*, *52*(3), 434–446. <https://doi.org/10.1016/j.molcel.2013.09.021>.
- Jackson, D., & Cook, P. R. (2008a). Analyzing DNA replication I: Labeling animals, tissues, and cells with bromodeoxyuridine (BrdU). *Cold Spring Harbor Protocols*, 2008(9). pdb.prot5031–pdb.prot5031. <https://doi.org/10.1101/pdb.prot5031>.
- Jackson, D., & Cook, P. R. (2008b). Analyzing DNA replication II: Fixation and processing of tissues and cells labeled with bromodeoxyuridine (BrdU). *Cold Spring Harbor Protocols*, 2008(9). pdb.prot5032–pdb.prot5032. <https://doi.org/10.1101/pdb.prot5032>.
- Jackson, D., & Cook, P. R. (2008c). Analyzing DNA replication III: Antibody labeling of incorporated bromodeoxyuridine (BrdU) in tissues and cells. *Cold Spring Harbor Protocols*, 2008(9). pdb.prot5033–pdb.prot5033. <https://doi.org/10.1101/pdb.prot5033>.
- Lee, M., Napier, C. E., Yang, S. F., Arthur, J. W., Reddel, R. R., & Pickett, H. A. (2017). Comparative analysis of whole genome sequencing-based telomere length measurement techniques. *Methods (San Diego, Calif.)*, *114*, 4–15. <https://doi.org/10.1016/j.jymeth.2016.08.008>.
- Lesterlin, C., Ball, G., Schermelleh, L., & Sherratt, D. J. (2014). RecA bundles mediate homology pairing between distant sisters during DNA break repair. *Nature*, *506*, 249–253.
- Liu, F., Feng, X., & Ma, W. (2017). Analysis of telomere proteins by chromatin immunoprecipitation (ChIP). In H. Tsubouchi (Ed.), *DNA recombination: Vol. 1587*. (pp. 205–214). New York, NY: Springer New York. [https://doi.org/10.1007/978-1-4939-6892-3\\_19](https://doi.org/10.1007/978-1-4939-6892-3_19).
- Lottersberger, F., Karssemeijer, R. A., Dimitrova, N., & de Lange, T. (2015). 53BP1 and the LINC complex promote microtubule-dependent DSB mobility and DNA repair. *Cell*, *163*(4), 880–893.
- Lundblad, V., & Blackburn, E. H. (1993). An alternative pathway for yeast telomere maintenance rescues est1<sup>-</sup> senescence. *Cell*, *73*(2), 347–360.
- Lydeard, J. R., Jain, S., Yamaguchi, M., & Haber, J. E. (2007). Break-induced replication and telomerase-independent telomere maintenance require Pol32. *Nature*, *448*(7155), 820–823. <https://doi.org/10.1038/nature06047>.
- Malkova, A., & Ira, G. (2013). Break-induced replication: Functions and molecular mechanism. *Current Opinion in Genetics & Development*, *23*(3), 271–279. <https://doi.org/10.1016/j.gde.2013.05.007>.
- Marshall, W. F., Straight, A., Marko, J. F., Swedlow, J., Dernburg, A., Belmont, A., et al. (1997). Interphase chromosomes undergo constrained diffusional motion in living cells. *Current Biology*, *7*(12), 930–939.
- Merrick, C. J., Jackson, D., & Diffley, J. F. X. (2004). Visualization of altered replication dynamics after DNA damage in human cells. *The Journal of Biological Chemistry*, *279*(19), 20067–20075.

- Min, J., Wright, W. E., & Shay, J. W. (2017). Alternative lengthening of telomeres mediated by mitotic DNA synthesis engages break-induced replication processes. *Molecular and Cellular Biology*, 37(20), 00226–17.
- Minocherhomji, S., Ying, S., Bjerregaard, V. A., Bursomanno, S., Aleliunaite, A., Wu, W., et al. (2015). Replication stress activates DNA repair synthesis in mitosis. *Nature*, 528(7581), 286–290. <https://doi.org/10.1038/nature16139>.
- Moynahan, M. E., Pierce, A. J., & Jasin, M. (2001). BRCA2 is required for homology-directed repair of chromosomal breaks. *Molecular Cell*, 7(2), 263–272.
- Nieminszczy, J., Schwab, R. A., & Niedzwiedz, W. (2016). The DNA fibre technique—Tracking helicases at work. *Methods (San Diego, Calif.)*, 108, 92–98. <https://doi.org/10.1016/j.ymeth.2016.04.019>.
- Norio, P., & Schildkraut, C. L. (2001). Visualization of DNA replication on individual Epstein-Barr virus episomes. *Science (New York, NY)*, 294(5550), 2361–2364.
- Pierce, A. J., Johnson, R. D., Thompson, L. H., & Jasin, M. (1999). XRCC3 promotes homology-directed repair of DNA damage in mammalian cells. *Genes & Development*, 13(20), 2633–2638.
- Prakash, R., Zhang, Y., Feng, W., & Jasin, M. (2015). Homologous recombination and human health: The roles of BRCA1, BRCA2, and associated proteins. *Cold Spring Harbor Perspectives in Biology*, 7(4), a016600. <https://doi.org/10.1101/cshperspect.a016600>.
- Roumelioti, F.-M., Sotiriou, S. K., Katsini, V., Chiourea, M., Halazonetis, T. D., & Gagos, S. (2016). Alternative lengthening of human telomeres is a conservative DNA replication process with features of break-induced replication. *EMBO Reports*, 17(12), 1731–1737. <http://doi.org/10.15252/embr.201643169>.
- Saini, N., Ramakrishnan, S., Elango, R., Ayyar, S., Zhang, Y., Deem, A., et al. (2013). Migrating bubble during break-induced replication drives conservative DNA synthesis. *Nature*, 502(7471), 389–392. <https://doi.org/10.1038/nature12584>.
- Schindelin, J., Arganda-Carreras, I., Frise, E., Kaynig, V., Longair, M., Pietzsch, T., et al. (2012). Fiji: An open-source platform for biological-image analysis. *Nature Methods*, 9(7), 676–682.
- Sfeir, A., Kosiyatrakul, S. T., Hockemeyer, D., MacRae, S. L., Karlseder, J., Schildkraut, C. L., et al. (2009). Mammalian telomeres resemble fragile sites and require TRF1 for efficient replication. *Cell*, 138(1), 90–103. <https://doi.org/10.1016/j.cell.2009.06.021>.
- Sfeir, A., & Symington, L. S. (2015). Microhomology-mediated end joining: A back-up survival mechanism or dedicated pathway? *Trends in Biochemical Sciences*, 40(11), 701–714. <https://doi.org/10.1016/j.tibs.2015.08.006>.
- Shanbhag, N. M., Rafalska-Metcalf, I. U., Balane-Bolivar, C., Janicki, S. M., & Greenberg, R. A. (2010). ATM-dependent chromatin changes silence transcription in cis to DNA double-strand breaks. *Cell*, 141(6), 970–981.
- Sotiriou, S. K., Kamileri, I., Lugli, N., Evangelou, K., Da-Ré, C., Huber, F., et al. (2016). Mammalian RAD52 functions in break-induced replication repair of collapsed DNA replication forks. *Molecular Cell*, 64(6), 1127–1134. <https://doi.org/10.1016/j.molcel.2016.10.038>.
- Tang, J., Cho, N. W., Cui, G., Manion, E. M., Shanbhag, N. M., Botuyan, M. V., et al. (2013). Acetylation limits 53BP1 association with damaged chromatin to promote homologous recombination. *Nature Structural & Molecular Biology*, 20, 317–325.
- Tarantino, N., Tinevez, J. Y., Crowell, E. F., Boisson, B., Henriques, R., Mhlanga, M., et al. (2014). TNF and IL-1 exhibit distinct ubiquitin requirements for inducing NEMO-IKK supramolecular structures. *The Journal of Cell Biology*, 204(2), 231–245.
- Thenevez, P., Ruttimann, U. E., & Unser, M. (1998). A pyramid approach to subpixel registration based on intensity. *IEEE Transactions on Image Processing*, 7(1), 27–41.

- Verma, P., & Greenberg, R. A. (2016). Noncanonical views of homology-directed DNA repair. *Genes & Development*, 30(10), 1138–1154. <https://doi.org/10.1101/gad.280545.116>.
- Viggiani, C. J., Knott, S. R. V., & Aparicio, O. M. (2010). Genome-wide analysis of DNA synthesis by BrdU immunoprecipitation on tiling microarrays (BrdU-IP-chip) in *Saccharomyces cerevisiae*. *Cold Spring Harbor Protocols*, 2010(2). pdb.prot5385–pdb.prot5385. <https://doi.org/10.1101/pdb.prot5385>.
- Willis, N. A., Chandramouly, G., Huang, B., Kwok, A., Follonier, C., Deng, C., et al. (2014). BRCA1 controls homologous recombination at Tus/Ter-stalled mammalian replication forks. *Nature*, 510(7506), 556–559. <https://doi.org/10.1038/nature13295>.
- Wilson, M. A., Kwon, Y., Xu, Y., Chung, W.-H., Chi, P., Niu, H., et al. (2013). Pif1 helicase and Poldelta promote recombination-coupled DNA synthesis via bubble migration. *Nature*, 502(7471), 393–396. <https://doi.org/10.1038/nature12585>.
- Zajac, A. L., Goldman, Y. E., Holzbaur, E. L. F., & Ostap, E. M. (2013). Local cytoskeletal and organelle interactions impact molecular motor-driven early endosomal trafficking. *Current Biology*, 23(13), 1173–1180.



# Kinetic Analysis of the Exonuclease Activity of the Bacteriophage T4 Mre11–Rad50 Complex

Tibebe A. Teklemariam, Osvaldo D. Rivera, Scott W. Nelson<sup>1</sup>

Iowa State University, Ames, IA, United States

<sup>1</sup>Corresponding author: e-mail address: swn@iastate.edu

## Contents

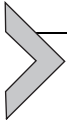
|   |     |
|---|-----|
| 1. Introduction                                   | 136 |
| 2. Assays Using Plasmids and PCR Products         | 138 |
| 2.1 Agarose Gel Electrophoresis                   | 138 |
| 2.2 Alkaline Agarose Gel Electrophoresis          | 139 |
| 2.3 Filter Binding and TLC Analysis               | 140 |
| 3. End-Labeled Oligonucleotide Substrates         | 142 |
| 4. Determining Exonuclease Polarity               | 146 |
| 5. 2-Aminopurine-Based Oligonucleotide Substrates | 148 |
| 6. Conclusions                                    | 153 |
| References  | 153 |

## Abstract

Bacteriophage T4 encodes orthologs of the proteins Rad50 (gp46) and Mre11 (gp47), which form a heterotetrameric complex (MR) that is responsible for host genome degradation and the processing of DNA ends for recombination-dependent DNA repair. In this chapter, we describe the ensemble methods currently employed by our laboratory to characterize the exonuclease activity of the T4 MR complex. DNA exonucleases play a vital role in maintaining the integrity of DNA through their participation in DNA repair pathways and as proofreaders for DNA polymerases. Methods for quantifying the general features of the exonuclease, and for determining steady-state kinetic parameters ( $K_m$ ,  $k_{cat}$ ), the polarity of exonuclease activity, and processivity are presented. These methods should be applicable to all DNA exonucleases, and to some extent endonucleases.

## ABBREVIATIONS

|              |                           |
|--------------|---------------------------|
| <b>2AP</b>   | 2-aminopurine             |
| <b>dsDNA</b> | double-stranded DNA       |
| <b>gp46</b>  | T4 Rad50                  |
| <b>gp47</b>  | T4 Mre11                  |
| <b>HDR</b>   | homology-directed repair  |
| <b>PEI</b>   | polyethyleneimine         |
| <b>sDNA</b>  | single-stranded DNA       |
| <b>TLC</b>   | thin-layer chromatography |



## 1. INTRODUCTION

DNA exonucleases are ubiquitous enzymes involved in a broad range of cellular processes. Primarily, exonucleases play a critical role in the maintenance of genomic material, as most DNA repair pathways rely on an exonuclease to excise damaged nucleotides (e.g., nucleotide excision repair, double-strand break (DSB) repair, base excision repair). Besides participating in DNA repair pathways, exonucleases are responsible for preventing mutagenesis by enhancing the fidelity of genomic replication. Many exonucleases act as proofreaders for replicative DNA polymerases, or take part in mismatch repair in the event that proofreading fails. As expected based on their central role in DNA metabolism, there are numerous diseases that are associated with mutations in exonuclease genes (Mason & Cox, 2012).

This chapter focuses on ensemble kinetic methods that have been used to characterize the exonuclease activity of the bacteriophage T4 MR complex. The MR complex, made up of the nuclease Mre11 and the ATPase Rad50, plays an important role in the initiation of DSB repair. DSBs can be caused by either physiological or pathological processes. Pathological DSBs are mainly caused by ionizing radiation and oxidative damage by cellular metabolites (Assenmacher & Hopfner, 2004; Chapman, Taylor, & Boulton, 2012; Deshpande, Lee, Arora, & Paull, 2016; Gobbini, Cassani, Villa, Bonetti, & Longhese, 2016; Lafrance-Vanasse, Williams, & Tainer, 2015). Defective DSB repair is a hallmark of many types of cancer and genotoxic chemicals that introduce DSBs are among the most commonly prescribed anticancer drugs (Broustas & Lieberman, 2014; Park, Chae, Kim, & Cho, 2011; Sung et al., 2014).

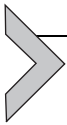
DSBs are repaired by one of two major pathways: homology-directed repair (HDR) and nonhomologous end joining. HDR involves extensive resection of 5' strands, which is initiated by the Mre11/Rad50/Nbs1 complex in mammals, the Mre11/Rad50/Xrs2 in yeast, and the Mre11/Rad50

complex in bacteriophage T4. The resection begins with endonucleolytic cleavage of the DNA by Mre11. This creates a nick on the 5' side of the DSB, which serves as an entry point for the 5' to 3' exonuclease Exo1 or Dna2 (Zhu, Chung, Shim, Lee, & Ira, 2008). The 5' to 3' exonuclease activity proceeding away from the DSB, combined with the 3' to 5' exonuclease activity of Mre11 proceeding toward the DSB, produces 3' single-stranded DNA (ssDNA) that is then bound by the recombinase protein (Kakarougkas & Jeggo, 2014; Lammens et al., 2011; Li et al., 2017). In addition to its DSB repair functions, the T4 phage MR complex is responsible for degradation of host genomic DNA to fuel the T4 replisome with deoxynucleotides for phage DNA synthesis (Mickelson & Wiberg, 1981). This noncanonical function for the T4 MR complex may be the physiological reason for its more rapid ATPase and exonuclease activities when compared with other MR complexes (Deshpande, Lee, & Paull, 2017; Herdendorf, Albrecht, Benkovic, & Nelson, 2011).

The MR complex is a heterotetramer made up of two dimers each of Mre11 and Rad50. The nuclease activities of Mre11 reside in the core phosphodiesterase domain (Hopfner et al., 2001). Adjacent to this is a capping domain that aids in distinguishing between ssDNA and double-stranded DNA (dsDNA), and is thought to guide its orientation into the nuclease active site (Williams et al., 2008, p. 11). Rad50 belongs to the ABC ATPase superfamily and the structural maintenance of chromosome family (Hopfner, 2003, p. 50). The walker A and B motifs of the Rad50 dimer fold on themselves to form the ATPase active site. Antiparallel coiled coils extend from the globular domain and are linked at their ends through a zinc ion bound by a completely conserved CXXC motif (Lammens et al., 2011). Rad50 is a slow ATPase, but its activity is stimulated by Mre11 and DNA (Deshpande et al., 2017; Herdendorf et al., 2011). Likewise, Rad50 stimulates the exonuclease activity of Mre11 (Herdendorf et al., 2011; Lafrance-Vanasse et al., 2015).

The reaction kinetics of exonucleases may not follow conventional Michaelis–Menten kinetics due to their processivity (or lack thereof) on polymeric substrates. Processivity as it pertains to an exonuclease is the ability to remove multiple nucleotides in a single binding event and is essentially the probability of the enzyme carrying out another catalytic cycle rather than dissociate from its DNA substrate. Partial processivity may give rise to unusual kinetic phenomenon depending on the type of DNA substrate used and how products are monitored in the assay (Rentergent, Driscoll, & Hay, 2016). For example, the effects of low processivity can be either enhanced or

suppressed by adjusting the enzyme-to-substrate ratio. At a low enzyme-to-substrate ratio, a modifier or amino acid mutation that alters the processivity will have a larger effect than at a higher enzyme-to-substrate ratio. Additionally, the effects of processivity can be further modified by the type of the assay that is employed. In the commonly used fluorescence assay that relies on the removal of the modified nucleotide 2-aminopurine (2AP) from the substrate, the position of the label has a large effect on how a processivity modifier is perceived. Similarly, the polarity of the exonuclease can lead to nonlinearity with respect to enzyme concentration when using positional labels. These issues will be discussed in detail using our efforts to characterize the bacteriophage T4 MR complex as an example.



---

## **2. ASSAYS USING PLASMIDS AND PCR PRODUCTS**

### **2.1 Agarose Gel Electrophoresis**

The simplest exonuclease assays are based on agarose gel electrophoresis combined with a dye-based visualization (Koontz, 2013). These assays can be useful in determining the broad features of an exonuclease early in the characterization process (Trujillo, Yuan, Lee, & Sung, 1998). The DNA substrate for these assays is often a purified PCR product or a plasmid that has been linearized with a DNA restriction enzyme. Specific restriction enzymes can be chosen to provide either blunt DNA ends or 5' or 3' ssDNA overhangs. The linearized plasmid can also be treated with alkaline phosphatase to test the effect of removing the 5' phosphate groups on the activity of the exonuclease. Similarly, with a PCR product, the primers used in the reaction can be synthesized with 5' phosphates included or the PCR product can be phosphorylated using T4 polynucleotide kinase and ATP. The kinetic assays are stopped-time using EDTA as a quencher of the reaction and the agarose gels are ran in  $1 \times$  TAE or  $0.5 \times$  TBE buffer in the absence of intercalating dye. After the gel has ran, it is stained with ethidium bromide or other dsDNA-specific dye and destained if necessary. Often both the substrate and a smear of shorter products can be observed on a gel and the length of the shorter products may provide some information regarding the processivity of the exonuclease, depending on the time points taken and the enzyme-to-substrate ratio used. At this stage in the characterization process, it is important to confirm that the observed exonuclease activity originates from the enzyme under investigation and not a copurifying contaminating exonuclease. The most direct way to do this is to generate an active site mutant that is expected to greatly decrease the exonuclease

activity. For T4 Mre11, we mutated two residues (His<sup>10</sup> and Asp<sup>48</sup>) that were predicted to be necessary for binding the essential divalent cations and exonuclease activity was reduced to a value below our detection limit. If the exonuclease being investigated is endogenously expressed, or sites for mutations cannot be easily predicted, then it is recommended that the exonuclease activity be closely followed through several steps of purification to confirm that the elution profile of the protein of interest (visualized by SDS-PAGE) exactly matches elution profile of the observed exonuclease activity. The initial characterization of the T4 MR complex relied on a linearized pGEM plasmid that was used to determine that the exonuclease activity of T4 Mre11 depends on the presence of Rad50 and ATP and that it strongly prefers Mn<sup>2+</sup> over Mg<sup>2+</sup> or Zn<sup>2+</sup> (Herdendorf et al., 2011; Fig. 1).

## 2.2 Alkaline Agarose Gel Electrophoresis

A more quantitative exonuclease assay that can be easily used to determine specific activities relies on the uniform labeling of a PCR product with [ $\alpha$ -<sup>32</sup>P] dNTPs (Herdendorf et al., 2011). In most cases, the label can be a single nucleotide (e.g., [ $\alpha$ -<sup>32</sup>P] dGTP) used in trace amounts relative to the unlabeled nucleotide. To avoid template-independent addition of dAMP to the 3' end of the PCR product, a thymine should be used at

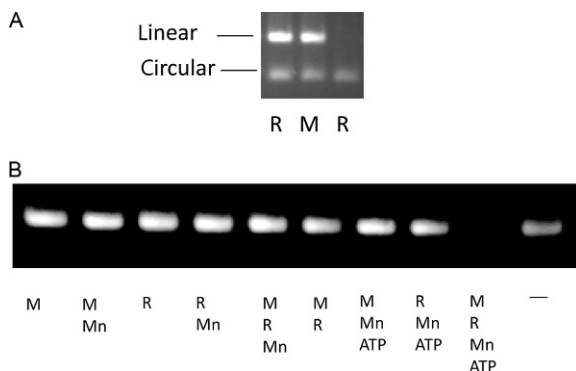


**Fig. 1** Nuclease reactions visualized with TAE-agarose gels. (A) Reactions with 0.4  $\mu$ g of circular and linearized forms of pGEM plasmid dsDNA using MnCl<sub>2</sub>, Rad50 (R), Mre11 (M), and ATP concentrations of 5 mM, 300 nM, 300 nM, and 2 mM, respectively. (B) Reactions with 0.4  $\mu$ g linearized pGEM dsDNA. The concentrations of MnCl<sub>2</sub> (Mn), Mre11 (M), Rad50 (R), and ATP were 5 mM, 300 nM, 300 nM, and 2 mM, respectively. Panels were reproduced with permission from Herdendorf, T. J., Albrecht, D. W., Benkovic, S. J., & Nelson, S. W. (2011). Biochemical characterization of bacteriophage T4 Mre11-Rad50 complex. *Journal of Biological Chemistry*, 286(4), 2382–2392. <https://doi.org/10.1074/jbc.M110.178871>.

the 5' end of the primer (Brownstein, Carpten, & Smith, 1996), or the PCR should be carried out with a proofreading DNA polymerase that has minimal 3' tailing activity. Again, if 5' phosphates are desired, they can be incorporated into the PCR primers during synthesis or the purified PCR product can be phosphorylated with T4 polynucleotide kinase and ATP. The concentration of the radioactive purified PCR product is determined using liquid scintillation counting of a small aliquot of a diluted sample of the reaction before and after PCR fragment purification. Once the concentration of dGMP in the sample is determined (if [ $\alpha$ - $^{32}$ P] dGTP is used), the concentration of nucleotides is calculated using the %GC content of the amplified PCR product and the concentration of DNA ends is determined using the calculated molecular weight of the PCR fragment. The concentration of DNA ends is usually is submicromolar; therefore, the assays are normally performed using a high enzyme-to-DNA ratio so that the observed rates are independent of protein concentration (e.g., 200 nM protein with 20 nM DNA ends). Again, this is a stopped time reaction and the reaction products are separated using alkaline agarose electrophoresis (Sambrook & Russell, 2006). We typically use 0.8% agarose prepared and ran in 30 mM NaOH and 5 mM EDTA. After running for approximately 16 h, the gel is removed from its tray and neutralized by soaking for 1 h in 1 L of 1  $\times$  TBE buffer at room temperature. The neutralized gel is then dried onto a sheet of DE81 paper using a 2-in. stack of paper towels to facilitate gel drying. After 4 h of drying with the paper towels, the gel and filter sheet are vacuum-dried for 1 h and then exposed to a Phosphorimager screen. After scanning the screen, the substrate and products are quantitated using ImageJ or similar software (Schneider, Rasband, & Eliceiri, 2012).

### 2.3 Filter Binding and TLC Analysis

Filter binding and thin-layer chromatography (TLC) assays are more rapid methods for analyzing reactions carried out with labeled DNA. The uniformly labeled PCR product substrate (discussed in the previous section) produces  $^{32}$ P-labeled dGMP as the product of the exonuclease reaction, which is easily separated from the much longer DNA substrate using a standard DNA DE81 filter binding assay (Brutlag & Kornberg, 1972) or TLC analysis using polyethyleneimine (PEI) cellulose plates (Merck Millipore) (Rajagopal & Lorsch, 2013). We prefer TLC analysis because of its ease of use, combined with its high accuracy and reproducibility, which is due to the simultaneous visualization of both substrates and products (Fig. 2A).

The total volume for these reactions can be quite low, on the order of a few microliters with only 0.5–1  $\mu\text{L}$  used per time point. The plates are developed in 300 mM KPi, pH 6.8, air dried, and exposed to a Phosphorimager screen for 30–60 min. The screen is then imaged and the spots are quantitated and analyzed using ImageJ (Schneider et al., 2012) or similar software. Fig. 2A shows an exonuclease assay examining the effect of ATP on the activity on the MR complex using a  $[\alpha\text{-}^{32}\text{P}]$  dGTP-labeled 1.9-kb PCR fragment. When adding nucleotides such as ATP, it is important to control for the stoichiometric binding of divalent cations by the nucleotide and adjust the concentration accordingly (to maintain a constant free cation concentration). Provided the exonuclease is specific for dsDNA, it is expected that at the

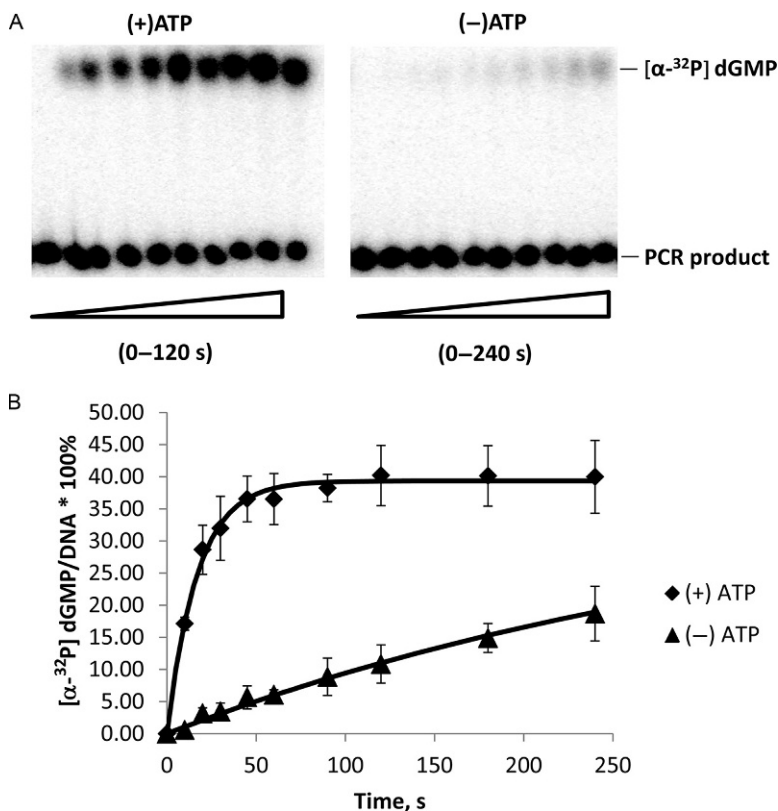
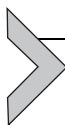


**Fig. 2** TLC plate-based exonuclease assays. The DNA substrate is a 1.9-kb PCR product uniformly labeled with  $[\alpha\text{-}^{32}\text{P}]$  dGMP. (A) The reaction contained 500 nM MR complex, 0.3 mM  $\text{Mn}^{2+}$ , and 5 mM  $\text{Mg}^{2+}$ . ATP, when present, was 2 mM. The degree of exonuclease activity in the presence or absence of ATP. The data were fit to a single-exponential equation.

completion of the reaction approximately half of the substrate will be degraded to mononucleotides. This is due to the exonuclease initiating from both ends and proceeding to remove nucleotides until they meet in the middle of the substrate, leaving half of the remaining DNA single stranded. The data points generated in the presence of ATP in Fig. 2B are well described by a single-exponential rise with a rate constant of  $\sim 0.06 \text{ s}^{-1}$ , which is then multiplied by half the number of bp in the DNA substrate (57 nts/s). In the absence of ATP, the observed exonuclease rate is much slower (2.6 nts/s), and an extended time course would be necessary to reach total substrate depletion. In this situation, rather than increasing the time of the assay, we increased the fitting accuracy of the single-exponential rate constant by fixing the amplitude of the exponential to that determined in the reaction performed in the presence of ATP (0.42).

Depending on the exonuclease under investigation, it may be possible to generate similar data as the uniformly  $^{32}\text{P}$ -labeled DNA substrate assay using fluorescent dyes that specifically bind to dsDNA. Tolun and Myers have successfully employed a continuous fluorescent assay to monitor the reaction of several exonucleases (Tolun & Myers, 2003). These authors surveyed several commercially available dsDNA dyes that show a strong preference for dsDNA over ssDNA and do not strongly inhibit the exonuclease when bound to the DNA substrate. Most dyes inhibited exonuclease I, but it was found that low concentrations of PicoGreen did not inhibit the exonuclease and had a large difference in fluorescent yield when bound to dsDNA compared to ssDNA. This assay is convenient and produces high-quality exonuclease kinetics in real time; however, it must be optimized for each exonuclease under investigation, and in some cases PicoGreen may be inhibitory even at very low concentrations. For the T4 MR complex, which is a moderately processive 3' to 5' exonuclease, we were unable to find conditions where the PicoGreen did not significantly reduce the exonuclease activity compared to the  $^{32}\text{P}$ -based assay described earlier.



### 3. END-LABELED OLIGONUCLEOTIDE SUBSTRATES

The resolution and ability to quantitate DNA using agarose gels is limited; therefore, when direct observation of the DNA substrate and products is beneficial, it is more common to use denaturing polyacrylamide gel electrophoresis (urea-PAGE) with short end-labeled oligonucleotides that can be synthesized by a commercial vendor (Albrecht, Herdendorf, & Nelson, 2012). The sequences of the oligonucleotides are under the

complete control of the investigator and they can be easily labeled at the 3' or 5' ends with fluorescent dyes during synthesis (Kricka, 2002). As with any modification of a substrate, control experiments must be performed to ensure that the attached fluorescent label does not reduce activity. It is not uncommon for proteins to have affinity for the attached dyes, which lowers the effective enzyme concentration. To determine if an enzyme has affinity for an appended dye, a fluorescence anisotropy assay can be used to determine the binding constants for the modified DNA and an unmodified DNA competitor (Heyduk, Ma, Tang, & Ebright, 1996). If it is determined that the enzyme has affinity for fluorescent dyes or increased detection sensitivity is required, 5'-<sup>32</sup>P end labeling can be performed using T4 polynucleotide kinase and [ $\gamma$ -<sup>32</sup>P] ATP. The oligonucleotide can be labeled as ssDNA, then annealed to its complementary strand or the complementary strands can be annealed prior to the PNK reaction. 3'-<sup>32</sup>P labeling requires the incorporation of a [ $\alpha$ -<sup>32</sup>P] dNTP using a DNA polymerase. In this case, the complementary strands need to be designed to leave a single nucleotide 5' overhang that will be filled in using the appropriate <sup>32</sup>P nucleotide. A proofreading-deficient DNA polymerase should be used and the DNA should be designed in such a way to avoid the use of dATP or dGTP, as many DNA polymerases that lack exonuclease activity will incorporate these nucleotides in a template-independent manner to make a single nucleotide 5' overhang (Fiala et al., 2007).

Special care should be taken in the sequence design for oligonucleotide-based exonuclease substrates. DNA sequences with the potential to form intramolecular hairpins and intermolecular dimers should be avoided. The activity of some exonucleases is dependent on the %GC content of their substrates, with higher GC leading to a slower exonuclease activity (van Oijen et al., 2003). This type of dependence suggests that melting of the basepair either prior to or after the exonucleolytic cut is at least partially rate-limiting under the conditions of the assay. It is therefore important to control the global %GC content of the substrate. If nothing is known regarding the GC dependence beforehand, the DNA substrate should be designed to match the %GC content of the organism in which it resides. Because the T4 MR complex is responsible for degrading the *Escherichia coli* genome (~50% GC) and acting on the bacteriophage T4 genome (34.5% GC), we have systematically examined the dependence of T4 MR complex on the %GC of the substrate (Teklemariam, unpublished observations). Surprisingly, we found that DNA sequences with a higher %GC content are better substrates for the T4 MR complex. We also found that transitions

between high and low GC tend to act as stall sites (e.g., a stretch of G/Cs followed by several Ts), highlighting the importance of controlling the local DNA sequence as well.

Depending on the length of the oligonucleotides used, it may be possible to directly determine the processivity of the exonuclease by a visual examination of the gel, or at a minimum, put a limit on its value (Subramanian, Rutvisuttinunt, Scott, & Myers, 2003). As an example, Fig. 3 shows an exonuclease reaction using a 50 bp dsDNA substrate that is labeled at both 5' ends with hexachlorofluorescein dye. Initially, several different fluorescent dyes were tested and their activity was compared to 5'  $^{32}\text{P}$ -labeled DNA substrate. We found that both Cy3- and Cy5-labeled substrates displayed lower activity compared to the  $^{32}\text{P}$ -labeled substrate, suggesting that the MR complex was directly binding to these labels. Additionally, charged dyes

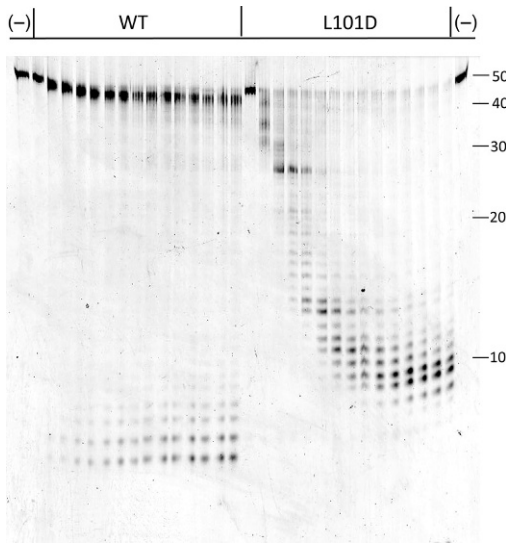


**Fig. 3** Example of a processive (WT) and nonprocessive (L101D) exonuclease reactions. The products are visualized on 16% urea-polyacrylamide gel. Each assay consisted of 0.3 mM  $\text{MnCl}_2$ , 100 nM Rad50, 105 nM Mre11, 2 mM ATP, and 1.3  $\mu\text{M}$  DNA substrate. Time points vary from 0 to 120 min. The *first* and *last* lanes are no protein controls and the approximate mobility of various DNA lengths is shown on the *right-hand* side of the gel. Figure was reproduced with permission from Albrecht, D. W., Herdendorf, T. J., & Nelson, S. W. (2012). Disruption of the bacteriophage T4 Mre11 dimer interface reveals a two-state mechanism for exonuclease activity. *Journal of Biological Chemistry*, 287(37), 31371–31381. <https://doi.org/10.1074/jbc.M112.392316>.

such as Cy3 and Cy5 should be avoided if possible, as they display aberrant migration patterns during electrophoresis when attached to oligonucleotides shorter than eight nucleotides (Killelea, Saint-Pierre, Ralec, Gasparutto, & Henneke, 2014). Fluorescein and hexachlorofluorescein were not inhibitory; therefore, hexachlorofluorescein was chosen due to its increased stability compared to fluorescein. The reactions shown in Fig. 3 were performed with a low enzyme-to-DNA ratio in the presence of ATP, so that at early time points the probability of binding to an intermediate product is minimal (referred to as “single-hit” conditions). Under these conditions, the product profile is a direct reporter of processivity (Bambara, Fay, & Mallaber, 1995). The exonuclease reaction carried out with a mutant MR complex that has a disrupted Mre11 dimer interface (L101D) indicates that the mutant has rendered the MR complex nonprocessive, as a progressive decrease in product length is seen as time increases. The ATP-dependent reaction using the wild-type MR complex does not exhibit this progressive decrease and only very short products are observed; therefore, the processivity in the presence of ATP is at least as long as the DNA substrate (50 bp) (Albrecht et al., 2012).

While determining processivity by direct visualization of the products under “single-hit” provides a good estimate of processivity, it may be preferable to determine the rate constants for forward translocation/exonuclease activity and product dissociation. Determining the rate constants for these steps in the catalytic cycle may be accomplished by global fitting of full progress curves using DNA substrates containing a 2AP probe located in at least two positions along the DNA substrate (the 2AP probe is discussed in detail in Section 5). Shown in Fig. 4 is an example of progress curve analysis of the MR complex acting on a 50 bp DNA substrate with 2AP probes located at the first and eight positions. The software DynaFit was used to numerically integrate a simple mechanism that includes association and dissociation rate constants for enzyme and DNA and a single combined rate constant for the translocation/exonuclease step ( $k_{\text{exo}}$ ) (Kuzmic, 2009; Reytor González, Cornell-Kennon, Schaefer, & Kuzmič, 2017). Processivity can be defined by the probability that the exonuclease performs another round of nucleotide removal instead of dissociating from the DNA (processivity =  $k_{\text{exo}} / (k_{\text{exo}} + k_2)$ ). The processivity of the MR complex under the conditions of this experiment (the absence of ATP) is 0.55, indicating that the enzyme has almost an equal probability of undergoing another round of catalysis as it does falling off the DNA, consistent with what has been observed using urea-PAGE analysis.

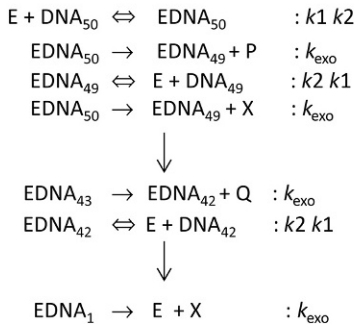
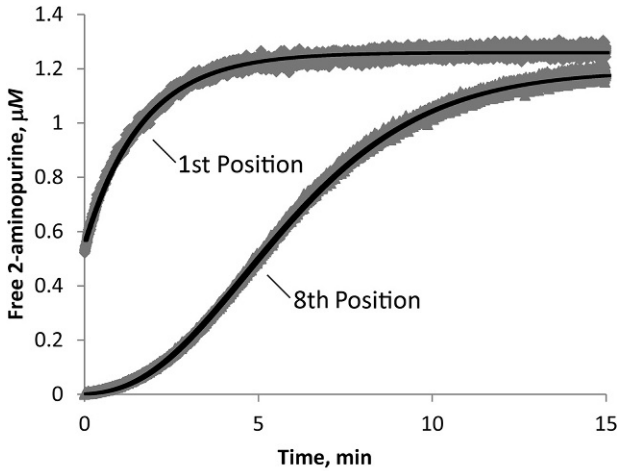
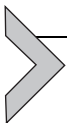


**Fig. 4** Global fitting of full progress curves with the 2-aminopurine probe in either the first and eight positions. The *gray points* and *black lines* represent the experimental data and the theoretical fits, respectively. The reactions were carried out in the absence of ATP with 400 nM MR complex and 1.3  $\mu\text{M}$  50 bp DNA substrate. The data were fit with the DynaFit program using the mechanism shown. The association rate ( $k_1$ ) was fixed at  $50 \mu\text{M}^{-1} \text{s}^{-1}$  and  $k_2$  and  $k_{\text{exo}}$  were determined to be  $2.68 \pm 0.05$  and  $3.28 \pm 0.03 \text{min}^{-1}$ .



#### 4. DETERMINING EXONUCLEASE POLARITY

The polarity of an exonuclease can be determined using several different biochemical assays. A straightforward method is separately  $^{32}\text{P}$  label a long DNA substrate (100–1000 bp, often a PCR product) at the 3' and 5' ends and follow the time course of the exonuclease reaction using a DE81-filter binding, PEI cellulose TLC, or urea-PAGE (Herdendorf et al., 2011; Trujillo & Sung, 2001). Labeling the 5' end is carried out using T4 PNK and  $[\gamma\text{-}^{32}\text{P}] \text{ATP}$ , whereas labeling of the 3' end is performed in two steps. In the first step, the terminal 3' nucleotide is removed using a

proofreading polymerase. The DNA sequence of the PCR primers must be chosen so that only a single nucleotide is removed by the proofreading polymerase (e.g., wild-type T4 DNA polymerase) when a specific deoxynucleotide is included in the reaction. For example, if a primer with the sequence 5'-AGACGTAGCGTATCGCAGGC is used, then a high concentration of dCTP (1–5 mM) should be included in the reaction to ensure that only the terminal 3' nucleotide is removed by the polymerase. After a brief incubation with the polymerase (~10 min at 37°C), the reaction is purified using phenol/chloroform extraction or commercial PCR clean up kit (the dCTP must be removed to avoid misincorporation in the next step). Next, an exonuclease-deficient DNA polymerase is added to the reaction, along with [ $\alpha$ - $^{32}\text{P}$ ] dTTP. After 10 min, 50  $\mu\text{M}$  unlabeled dTTP is added and the reaction is allowed to proceed for 10 additional minutes, followed by purification of the product. The DNA concentration is determined using scintillation counting as described earlier, except it is assumed that only two  $^{32}\text{P}$  labels per substrate are incorporated. If the end-labeled DNA used for the exonuclease assay is sufficiently long, then there will be a delay in the formation of the mononucleotide product on the end distal from the initiating end. In some cases, only a single type of end label will produce a labeled nucleotide monophosphate product because the complementary strands will melt as the exonuclease approaches the end of the substrate. This produces labeled ssDNA approximately 5–10 bases long that binds to DE81 filter paper or PEI cellulose in a similar fashion as the substrate.

If the reaction products are visualized using urea-PAGE, then the product profile often immediately suggests the polarity of the reaction. The T4 MR complex is a 3' to 5' exonuclease and the product pattern it produces is shown in Fig. 5. However, with highly active and processive exonucleases, it may be difficult to observe reaction intermediates that would normally be present when the enzyme initiates on the end distal to the label. In this situation, it is advantageous to employ 5'- and 3'-labeled oligonucleotide DNA substrates in combination with thiophosphoryl linkages at either end of the DNA. The activity of most exonucleases (including Mre11) is inhibited by thiophosphoryl groups. The thiophosphoryl groups enable the use of small oligonucleotide substrates and rapid analysis of the reaction via filter binding or PEI cellulose TLC. We examined the exonuclease activity of T4 MR by PEI cellulose TLC using four individual substrates (Fig. 6). Only the thiophosphoryl linkage at the 3' position inhibits the production of the  $^{32}\text{P}$ -labeled mononucleotide, consistent with a 3' to 5' exonuclease.

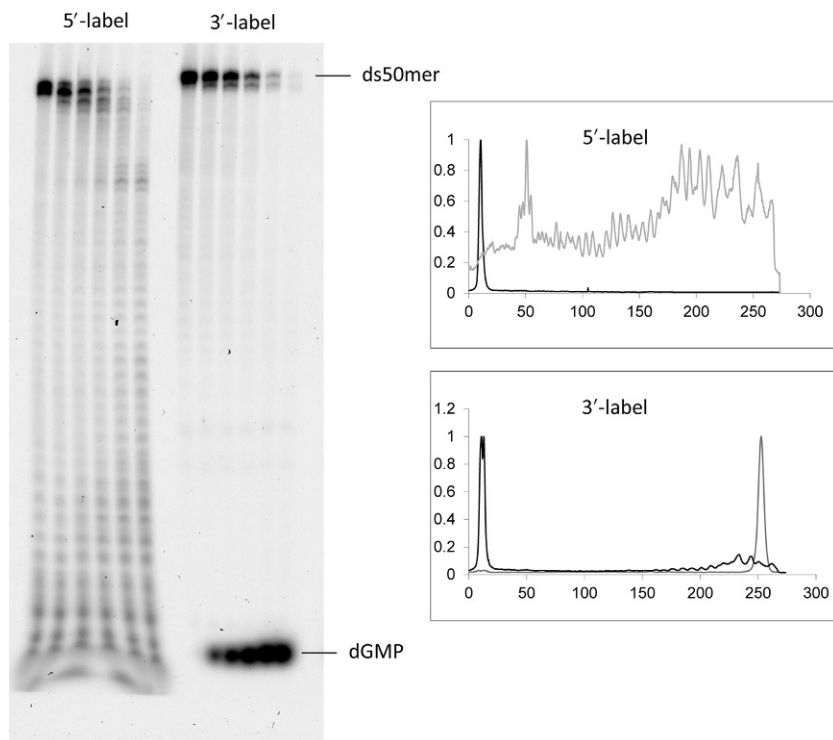


**Fig. 5** Analysis of the polarity of nuclease activity using 16% urea-PAGE. The reaction was carried out at 37°C, and the time points for each lane are 0, 0.5, 1, 2, 4, and 8 min. The concentrations of dsDNA, Mre11, Rad50, MnCl<sub>2</sub>, and ATP were 0.5 μM, 100 nM, 100 nM, 5 mM, and 2 mM, respectively. *Figure was reproduced with permission from Herdendorf, T. J., Albrecht, D. W., Benkovic, S. J., & Nelson, S. W. (2011). Biochemical characterization of bacteriophage T4 Mre11-Rad50 complex. Journal of Biological Chemistry, 286(4), 2382–2392. <https://doi.org/10.1074/jbc.M110.178871>.*



## 5. 2-AMINOPURINE-BASED OLIGONUCLEOTIDE SUBSTRATES

Perhaps the most convenient and informative exonuclease assays are based on the fluorescent base analog 2AP. The fluorescence of 2AP is quenched through base-stacking interactions so that when it is removed by the exonuclease, its fluorescent emission greatly increases (Frey, Sowers, Millar, & Benkovic, 1995; Jean & Hall, 2001). The 2AP base has been extensively used to indirectly report on the conformational changes that occur within the enzyme active site during the exonuclease reaction

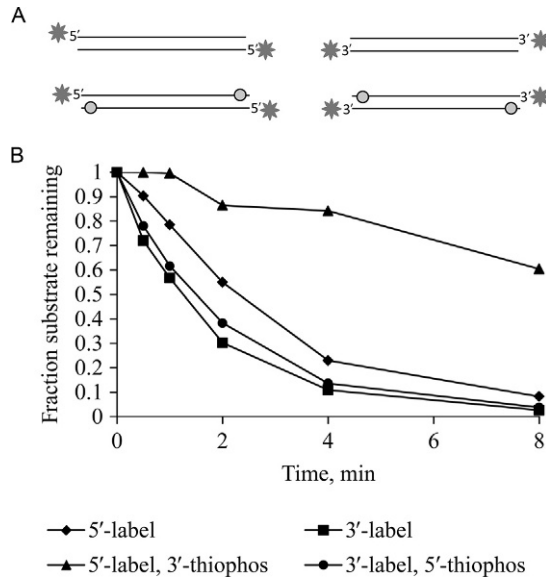


**Fig. 6** TLC-based assay for determination of exonuclease polarity. (A) Four DNA substrates utilized to determine exonuclease polarity. The  $^{32}\text{P}$  labels and thiophosphoryl groups are represented by the *gray stars* and *circles*, respectively. (B) Quantification of an exonuclease reaction carried out in the absence of ATP with 50 nM MR complex and 1.3  $\mu\text{M}$  DNA substrate.

and the kinetics of exonucleolytic removal of the base itself (Bloom et al., 1994; Frey et al., 1995). A major advantage of 2AP is that it can be easily incorporated into well-defined DNA substrates via oligonucleotide synthesis by several commercial vendors. The 2AP probe can be placed at any internal site or at the 3' or 5' end of the oligonucleotide. For determining simple comparative exonuclease activities, we incorporate the 2AP probe at the 3' end and refer to this as the first position. We have also used the first position 2AP DNA substrate to perform traditional steady-state kinetics under multiple turnover conditions to determine the kinetic constants and binding order of DNA and either  $\text{Mg}^{2+}$  or  $\text{Mn}^{2+}$  as a coactivator. In this case, we included a thiophosphoryl linkage between the second and third position of the substrate so that the MR complex dissociates from the DNA substrate rather than removing multiple nucleotides in a processive fashion. Steady-state nuclease assays were performed where the concentrations of DNA substrate and coactivating metal were varied at concentrations above and below their apparent affinity constants (Fig. 7). The initial

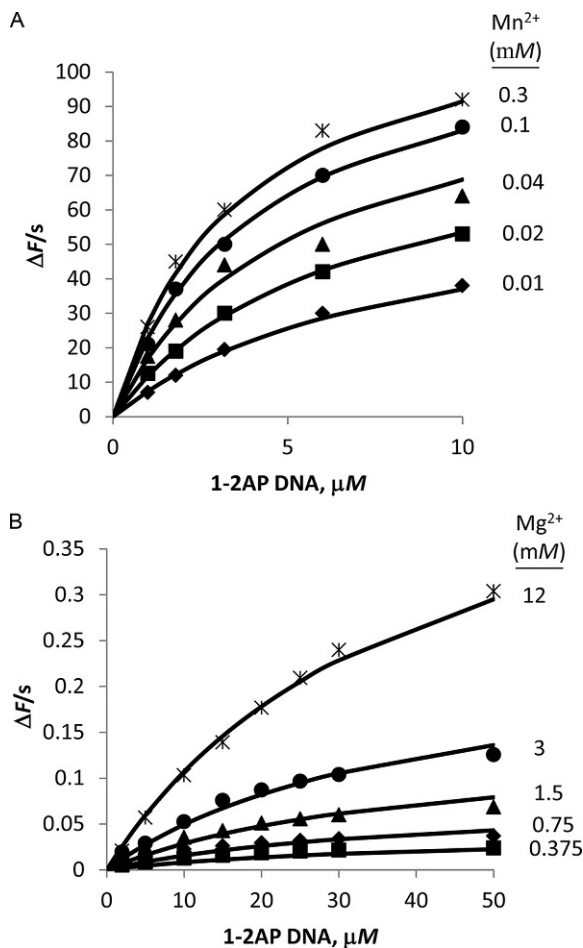


**Fig. 7** Kinetic mechanism of T4 MR complex excising a 2-aminopurine nucleotide from the first position in the presence of Mn<sup>2+</sup> (A) or Mg<sup>2+</sup> (B). Reactions were performed in the absence of ATP with 50 nM MR complex. The data were fit to a rapid equilibrium random mechanism and the determined values are found in [Table 1](#).

velocities were determined from the linear portion of each time course and the data were fit to four possible models using DynaFit software (BioKin Ltd.) (Kuzmic, 2009). In this analysis, DNA and the divalent metal cation are considered a substrate and an essential activator, respectively. The four models tested under the rapid equilibrium approximation were: (1) ordered addition with DNA binding first; (2) ordered addition with Mg<sup>2+</sup> binding first; (3) random addition with different affinities for the free and substrate-/activator-bound form of the enzyme; and (4) random addition with identical

affinities for the free and substrate-/activator-bound form of the enzyme (Segel, 1975). When  $Mg^{2+}$  is the activating metal, the statistical analysis indicated that the most plausible model is a random addition with identical affinities for the free enzyme and the single-substrate-/activator-bound form (Table 1). On the other hand, synergy is observed between the binding of  $Mn^{2+}$  and the DNA substrate such that the affinity for DNA binding to the  $Mn^{2+}$ -bound enzyme is threefold higher than in its absence (Table 1). The turnover number ( $k_{cat-Mn^{2+}}$ ) was  $57\text{ s}^{-1}$ , or about 65-fold higher than the  $Mg^{2+}$ -catalyzed reaction (Table 1).

The activity of the T4 MR complex using the first position 2AP DNA without the thiophosphoryl linkage as a substrate provided a hint that the complex might increase in processivity in the presence of ATP. On the basis of the gel-based assays that were previously performed, it was clear that ATP is a strong activator of T4 MR complex; however, using the first position substrate under multiple turnover conditions ( $[E] \gg [DNA]$ ), ATP became inhibitory. The simplest explanation for this observation is that ATP slows product dissociation. This could result from either a slow release of the  $n - 1$  product or from processive translocation/exonuclease activity of the complex along the DNA substrate, which prevents the enzyme from dissociating and rebinding to another DNA substrate. To distinguish between these possibilities, the 2AP probe can be moved to an internal site located some distance away from the DNA end. In the case of T4 MR complex, the observed exonuclease activity decreases relative to the first position 2AP and the presence of ATP now becomes strongly activating. As shown in Fig. 8A, the ratio of activities in the presence and absence of ATP increases

**Table 1** Steady-State Kinetic Parameters for T4 MR Complex Exonuclease Activity  
Activating Metal

| Parameter  | Activating Metal      |                             |
|------------|-----------------------|-----------------------------|
|            | $Mg^{2+}$ ( $\mu M$ ) | $Mn^{2+}$ Value ( $\mu M$ ) |
| $K_{ia}^a$ | $7700 \pm 600$        | $37 \pm 7$                  |
| $K_{im}^b$ | $39 \pm 4$            | $10 \pm 4$                  |
| $K_a^c$    | $7700 \pm 600$        | $11 \pm 3$                  |
| $K_m^d$    | $39 \pm 4$            | $3.2 \pm 0.4$               |
| $k_{cat}$  | $0.9 \pm 0.1$         | $56 \pm 2$                  |

<sup>a</sup> $K_{ia}$  is the dissociation constant for  $E + Mx^{2+} \leftrightarrow E - Mx^{2+}$ , where  $Mx^{2+}$  is  $Mg^{2+}$  or  $Mn^{2+}$ .

<sup>b</sup> $K_{im}$  is the dissociation constant for  $E + DNA \leftrightarrow E - DNA$ .

<sup>c</sup> $K_a$  is the dissociation constant for  $E - DNA + Mx^{2+} \leftrightarrow E - DNA - Mx^{2+}$ , where  $Mx^{2+}$  is  $Mg^{2+}$  or  $Mn^{2+}$ .

<sup>d</sup> $K_m$  is the dissociation constant for  $E - Mx^{2+} + DNA \leftrightarrow E - DNA - Mx^{2+}$ .

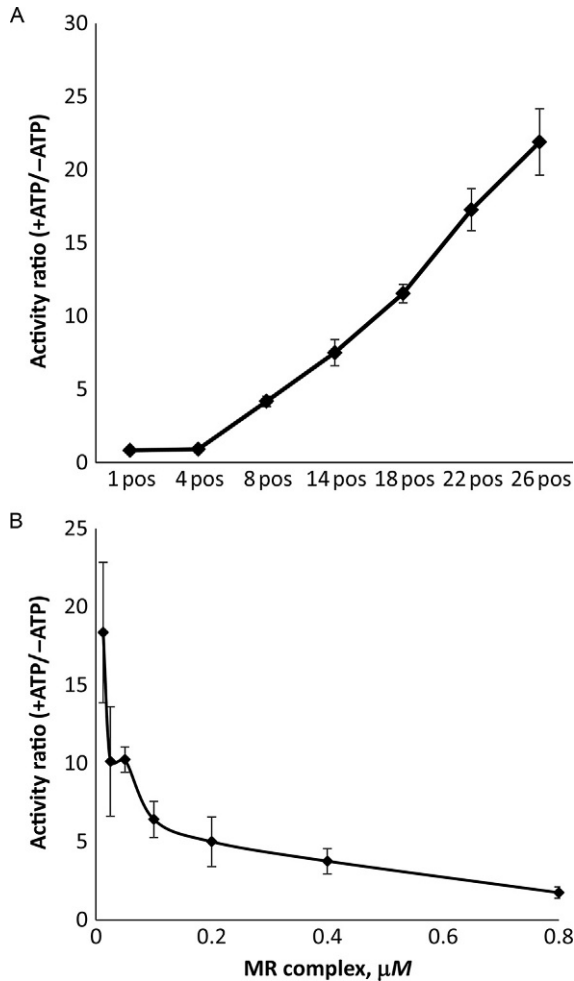
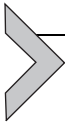


**Fig. 8** Effect of ATP on the processivity of the T4 MR complex. (A) The ratio of the exonuclease activity in the presence and absence of ATP with the 2-aminopurine probe located at the positions indicated on the x-axis. The concentration of the MR complex was held at 50 nM. (B) The ratio of the exonuclease activity in the presence and absence of ATP at various concentrations of the MR complex with the 2-aminopurine probe located at the 18th position. For both (A) and (B), the concentrations of dsDNA,  $MnCl_2$ ,  $MgCl_2$ , and ATP (when present) were 1.3  $\mu M$ , 0.3 mM, 5 mM, and 2 mM, respectively.

as the 2AP probe is moved away from the initiating 3' end of the DNA. This strongly suggests that ATP increases the activity of the MR complex by increasing its processivity. Consistent with the presence of processivity, when using a single internal 2AP at the 18th position, the activating effect

of ATP diminishes as the concentration of enzyme increases (Fig. 8B). Qualitatively, these data indicate that the T4 MR complex by itself has very limited processivity and that Rad50 enhances it through its ATPase activity.



## 6. CONCLUSIONS

Exonucleases play a vital role in maintaining the integrity of genomic DNA by participating in nearly all DNA repair pathways and by acting as proofreaders to increase the fidelity of DNA synthesis. Similar to DNA polymerases, there are a wide variety of activity assays that can be used to characterize the activity of DNA exonucleases. The ensemble assays presented here have been valuable tools in the characterization of the T4 MR complex and can easily be applied to most other DNA exonucleases. The T4 MR complex is a  $Mn^{2+}$ -dependent, ATP-activated 3' to 5' exonuclease. The primary effect of ATP binding and hydrolysis is to increase the processivity of the complex as it translocates along its DNA substrate. The assays described here can be used to characterize the effects of site-directed mutations or interaction with potential binding partners on DNA affinity, exonuclease rate, and processivity. The assays employing 2AP could easily be adapted to high-throughput format for the identification of inhibitors that could serve as potential drug candidates. DNA repair pathways are often upregulated in tumor cells treated with DNA-damaging agents and inhibition of specific exonucleases sensitizes cells to these agents (Chang et al., 2016; Rajecki et al., 2009; Wang et al., 2017; Xu et al., 2004).

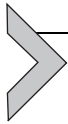
## REFERENCES

- Albrecht, D. W., Herdendorf, T. J., & Nelson, S. W. (2012). Disruption of the bacteriophage T4 Mre11 dimer interface reveals a two-state mechanism for exonuclease activity. *The Journal of Biological Chemistry*, 287(37), 31371–31381. <https://doi.org/10.1074/jbc.M112.392316>.
- Assenmacher, N., & Hopfner, K. P. (2004). MRE11/RAD50/NBS1: Complex activities. *Chromosoma*, 113(4), 157–166. <https://doi.org/10.1007/s00412-004-0306-4>.
- Bambara, R. A., Fay, P. J., & Mallaber, L. M. (1995). Methods of analyzing processivity. *Methods in Enzymology*, 262, 270–280.
- Bloom, L. B., Otto, M. R., Eritja, R., Reha-Krantz, L. J., Goodman, M. F., & Beechem, J. M. (1994). Pre-steady-state kinetic analysis of sequence-dependent nucleotide excision by the 3'-exonuclease activity of bacteriophage T4 DNA polymerase. *Biochemistry*, 33(24), 7576–7586.
- Broustas, C. G., & Lieberman, H. B. (2014). DNA damage response genes and the development of cancer metastasis. *Radiation Research*, 181(2), 111–130. <https://doi.org/10.1667/RR13515.1>.

- Brownstein, M. J., Carpten, J. D., & Smith, J. R. (1996). Modulation of non-templated nucleotide addition by Taq DNA polymerase: Primer modifications that facilitate genotyping. *BioTechniques*, 20(6), 1004–1006. 1008–1010.
- Brutlag, D., & Kornberg, A. (1972). Enzymatic synthesis of deoxyribonucleic acid. 36. A proofreading function for the 3' leads to 5' exonuclease activity in deoxyribonucleic acid polymerases. *The Journal of Biological Chemistry*, 247(1), 241–248.
- Chang, L., Huang, J., Wang, K., Li, J., Yan, R., Zhu, L., et al. (2016). Targeting Rad50 sensitizes human nasopharyngeal carcinoma cells to radiotherapy. *BMC Cancer*, 16, 190. <https://doi.org/10.1186/s12885-016-2190-8>.
- Chapman, J. R., Taylor, M. R. G., & Boulton, S. J. (2012). Playing the end game: DNA double-strand break repair pathway choice. *Molecular Cell*, 47(4), 497–510. <https://doi.org/10.1016/j.molcel.2012.07.029>.
- Deshpande, R. A., Lee, J. H., Arora, S., & Paull, T. T. (2016). Nbs1 converts the human Mre11/Rad50 nuclease complex into an endo/exonuclease machine specific for protein-DNA adducts. *Molecular Cell*, 64(3), 593–606. <https://doi.org/10.1016/j.molcel.2016.10.010>.
- Deshpande, R. A., Lee, J.-H., & Paull, T. T. (2017). Rad50 ATPase activity is regulated by DNA ends and requires coordination of both active sites. *Nucleic Acids Research*, 45(9), 5255–5268. <https://doi.org/10.1093/nar/gkx173>.
- Fiala, K. A., Brown, J. A., Ling, H., Kshetry, A. K., Zhang, J., Taylor, J.-S., et al. (2007). Mechanism of template-independent nucleotide incorporation catalyzed by a template-dependent DNA polymerase. *Journal of Molecular Biology*, 365(3), 590–602. <https://doi.org/10.1016/j.jmb.2006.10.008>.
- Frey, M. W., Sowers, L. C., Millar, D. P., & Benkovic, S. J. (1995). The nucleotide analog 2-aminopurine as a spectroscopic probe of nucleotide incorporation by the Klenow fragment of *Escherichia coli* polymerase I and bacteriophage T4 DNA polymerase. *Biochemistry*, 34(28), 9185–9192.
- Gobbini, E., Cassani, C., Villa, M., Bonetti, D., & Longhese, M. (2016). Functions and regulation of the MRX complex at DNA double-strand breaks. *Microbial Cell*, 3(8), 329–337. <https://doi.org/10.15698/mic2016.08.517>.
- Herdendorf, T. J., Albrecht, D. W., Benkovic, S. J., & Nelson, S. W. (2011). Biochemical characterization of bacteriophage T4 Mre11-Rad50 complex. *The Journal of Biological Chemistry*, 286(4), 2382–2392. <https://doi.org/10.1074/jbc.M110.178871>.
- Heyduk, T., Ma, Y., Tang, H., & Ebright, R. H. (1996). Fluorescence anisotropy: Rapid, quantitative assay for protein-DNA and protein-protein interaction. *Methods in Enzymology*, 274, 492–503.
- Hopfner, K. (2003). Rad50/SMC proteins and ABC transporters: Unifying concepts from high-resolution structures. *Current Opinion in Structural Biology*, 13, 249–255. [https://doi.org/10.1016/S0959-440X\(03\)00037-X](https://doi.org/10.1016/S0959-440X(03)00037-X).
- Hopfner, K. P., Karcher, A., Craig, L., Woo, T. T., Carney, J. P., & Tainer, J. A. (2001). Structural biochemistry and interaction architecture of the DNA double-strand break repair Mre11 nuclease and Rad50-ATPase. *Cell*, 105(4), 473–485.
- Jean, J. M., & Hall, K. B. (2001). 2-Aminopurine fluorescence quenching and lifetimes: Role of base stacking. *Proceedings of the National Academy of Sciences of the United States of America*, 98(1), 37–41. <https://doi.org/10.1073/pnas.011442198>.
- Kakarougkas, A., & Jeggo, P. A. (2014). DNA DSB repair pathway choice: An orchestrated handover mechanism. *British Journal of Radiology*, 87(1035). <https://doi.org/10.1259/bjr.20130685>.
- Killelea, T., Saint-Pierre, C., Ralec, C., Gasparutto, D., & Henneke, G. (2014). Anomalous electrophoretic migration of short oligodeoxynucleotides labelled with 5'-terminal Cy5 dyes. *Electrophoresis*, 35(14), 1938–1946. <https://doi.org/10.1002/elps.201400018>.

- Koontz, L. (2013). Agarose gel electrophoresis. *Methods in Enzymology*, 529, 35–45. <https://doi.org/10.1016/B978-0-12-418687-3.00004-5>.
- Kricka, L. J. (2002). Stains, labels and detection strategies for nucleic acids assays. *Annals of Clinical Biochemistry*, 39(Pt. 2), 114–129. <https://doi.org/10.1258/0004563021901865>.
- Kuzmic, P. (2009). DynaFit—A software package for enzymology. *Methods in Enzymology*, 467, 247–280. [https://doi.org/10.1016/S0076-6879\(09\)67010-5](https://doi.org/10.1016/S0076-6879(09)67010-5).
- Lafrance-Vanasse, J., Williams, G. J., & Tainer, J. A. (2015). Envisioning the dynamics and flexibility of Mre11–Rad50–Nbs1 complex to decipher its roles in DNA replication and repair. *Progress in Biophysics and Molecular Biology*, 117(2–3), 182–193. <https://doi.org/10.1016/j.pbiomolbio.2014.12.004>.
- Lammens, K., Bemeleit, D. J., Möckel, C., Clausing, E., Schele, A., Hartung, S., et al. (2011). The Mre11:Rad50 structure shows an ATP dependent molecular clamp in DNA double-strand break repair. *Cell*, 145(1), 54–66. <https://doi.org/10.1016/j.cell.2011.02.038>.
- Li, Y., Wang, J., Zhou, G., Lajeunesse, M., Le, N., Stawicki, B. N., et al. (2017). Nonhomologous end-joining with minimal sequence loss is promoted by the Mre11–Rad50–Nbs1–Ctp1 complex in *Schizosaccharomyces pombe*. *Genetics*, 206(1), 481–496.
- Mason, P. A., & Cox, L. S. (2012). The role of DNA exonucleases in protecting genome stability and their impact on ageing. *Age*, 34(6), 1317–1340. <https://doi.org/10.1007/s11357-011-9306-5>.
- Mickelson, C., & Wiberg, J. S. (1981). Membrane-associated DNase activity controlled by genes 46 and 47 of bacteriophage T4D and elevated DNase activity associated with the T4 *das* mutation. *Journal of Virology*, 40(1), 65–77.
- Park, Y. B., Chae, J., Kim, Y. C., & Cho, Y. (2011). Crystal structure of human Mre11: Understanding tumorigenic mutations. *Structure*, 19(11), 1591–1602. <https://doi.org/10.1016/j.str.2011.09.010>.
- Rajagopal, V., & Lorsch, J. R. (2013). ATP and GTP hydrolysis assays (TLC). *Methods in Enzymology*, 533, 325–334. <https://doi.org/10.1016/B978-0-12-420067-8.00025-8>.
- Rajecki, M., af Hallstrom, T., Hakkarainen, T., Nokisalmi, P., Hautaniemi, S., Nieminen, A. I., et al. (2009). Mre11 inhibition by oncolytic adenovirus associates with autophagy and underlies synergy with ionizing radiation. *International Journal of Cancer*, 125(10), 2441–2449.
- Rentger, J., Driscoll, M. D., & Hay, S. (2016). Time course analysis of enzyme-catalyzed DNA polymerization. *Biochemistry*, 55(39), 5622–5634. <https://doi.org/10.1021/acs.biochem.6b00442>.
- Reytor González, M. L., Cornell-Kennon, S., Schaefer, E., & Kuzmič, P. (2017). An algebraic model to determine substrate kinetic parameters by global nonlinear fit of progress curves. *Analytical Biochemistry*, 518, 16–24. <https://doi.org/10.1016/j.ab.2016.11.001>.
- Sambrook, J., & Russell, D. W. (2006). Alkaline agarose gel electrophoresis. *CSH Protocols*, 1, 2006.
- Schneider, C. A., Rasband, W. S., & Eliceiri, K. W. (2012). NIH image to ImageJ: 25 years of image analysis. *Nature Methods*, 9(7), 671–675.
- Segel, I. H. (1975). Rapid equilibrium bireactant and terreactant systems. In *Enzyme kinetics* (pp. 273–345). New York: John Wiley & Sons.
- Subramanian, K., Rutvisuttinun, W., Scott, W., & Myers, R. S. (2003). The enzymatic basis of processivity in lambda exonuclease. *Nucleic Acids Research*, 31(6), 1585–1596.
- Sung, S., Li, F., Park, Y. B., Kim, J. S., Kim, A.-K., Song, O.-K., et al. (2014). DNA end recognition by the Mre11 nuclease dimer: Insights into resection and repair of damaged DNA. *The EMBO Journal*, 33(20), 1–14. <https://doi.org/10.15252/emboj.201488299>.
- Tolun, G., & Myers, R. S. (2003). A real-time DNase assay (ReDA) based on PicoGreen fluorescence. *Nucleic Acids Research*, 31(18), e111.

- Trujillo, K. M., & Sung, P. (2001). DNA structure-specific nuclease activities in the *Saccharomyces cerevisiae* Rad50\**Mre11* complex. *The Journal of Biological Chemistry*, 276(38), 35458–35464. <https://doi.org/10.1074/jbc.M105482200>.
- Trujillo, K. M., Yuan, S. S., Lee, E. Y., & Sung, P. (1998). Nuclease activities in a complex of human recombination and DNA repair factors Rad50, *Mre11*, and p95. *The Journal of Biological Chemistry*, 273(34), 21447–21450. <https://doi.org/10.1074/jbc.273.34.21447>.
- van Oijen, A. M., Blainey, P. C., Crampton, D. J., Richardson, C. C., Ellenberger, T., & Xie, X. S. (2003). Single-molecule kinetics of lambda exonuclease reveal base dependence and dynamic disorder. *Science (New York, N.Y.)*, 301(5637), 1235–1238. <https://doi.org/10.1126/science.1084387>.
- Wang, Y., Gudikote, J., Giri, U., Yan, J., Deng, W., Ye, R., et al. (2017). RAD50 expression is associated with poor clinical outcomes after radiotherapy for resected non-small cell lung cancer. *Clinical Cancer Research: An Official Journal of the American Association for Cancer Research*, 24, 341–350. <https://doi.org/10.1158/1078-0432.CCR-17-1455>.
- Williams, R. S., Moncalian, G., Williams, J. S., Yamada, Y., Limbo, O., Shin, D. S., et al. (2008). *Mre11* dimers coordinate DNA end bridging and nuclease processing in double-strand-break repair. *Cell*, 135(1), 97–109. <https://doi.org/10.1016/j.cell.2008.08.017>.
- Xu, M., Myerson, R. J., Hunt, C., Kumar, S., Moros, E. G., Straube, W. L., et al. (2004). Transfection of human tumour cells with *Mre11* siRNA and the increase in radiation sensitivity and the reduction in heat-induced radiosensitization. *International Journal of Hyperthermia: The Official Journal of European Society for Hyperthermic Oncology, North American Hyperthermia Group*, 20(2), 157–162.
- Zhu, Z., Chung, W., Shim, E., Lee, S., & Ira, G. (2008). Sgs1 helicase and two nucleases Dna2 and Exo1 resect DNA double-strand break ends. *Cell*, 134(6), 981–994. <https://doi.org/10.1016/j.cell.2008.08.037>.



# Expression, Purification, and Biochemical Evaluation of Human RAD51 Protein

Shyamal Subramanyam<sup>2</sup>, Maria Spies<sup>1</sup>

University of Iowa Carver College of Medicine, Iowa City, IA, United States

<sup>1</sup>Corresponding author: e-mail address: maria-spies@uiowa.edu

## Contents

|  |     |
|--|-----|
| 1. Introduction  | 158 |
| 2. System for the Bacterial Expression of Human RAD51 Protein                              | 159 |
| 3. Equipment, Materials, and Reagents  | 160 |
| 3.1 Equipment  | 160 |
| 3.2 Materials Required   | 161 |
| 3.3 Oligonucleotides and DNA Substrates  | 162 |
| 3.4 Buffers and Solutions  | 162 |
| 4. Bacterial Expression of the RAD51 Protein From the pCH1/RAD51o Plasmid                  | 163 |
| 5. Purification of RAD51   | 164 |
| 6. FRET-Based DNA-Binding Assay to Measure ssDNA-Binding Activity of the RAD51 Recombinase | 167 |
| 7. Three-Strand DNA Strand Exchange Assay  | 170 |
| 8. Conclusions   | 175 |
| Acknowledgments  | 176 |
| References   | 176 |

## Abstract

The RAD51 DNA strand exchange protein plays an important role in maintaining the integrity of the human genome. It promotes homology-directed DNA repair by exchanging strands between the damaged and the intact DNA molecules. It also plays an important role in stabilizing distressed DNA replication forks. When overexpressed or misregulated, however, RAD51 contributes to “rogue,” genome destabilizing events that can lead to cancer, cell death, and to acquisition of chemotherapy resistance by cancerous cells. Human RAD51 is, therefore, an important and highly coveted anticancer drug target. Biochemical, biophysical, and structural studies of the human RAD51 and establishment of its structure–activity relationship require purification of large quantities of protein. In this

<sup>2</sup> Current address: Memorial Sloan-Kettering Cancer Center, New York, NY, United States

chapter we describe a robust method for expression and purification of human RAD51 and the methods for assessing its activity based on the single-strand DNA-binding stoichiometry and its capacity to carry out the DNA strand exchange reaction.



## 1. INTRODUCTION

The human RAD51 recombinase catalyzes the central step in homologous recombination (HR), which is an exchange of the DNA strands between two complementary DNA molecules (Baumann and West, 1998; Morrical, 2015). As a result, RAD51 is important for the accurate repair of DNA double strand breaks (DSB's), single-strand DNA (ssDNA) gaps, and stalled replication forks (Li & Heyer, 2008; Moynahan & Jasin, 2010). In addition to its HR function, RAD51 also protects damaged or stalled DNA replication forks from excessive nucleolytic degradation by the MRN complex (Kolinjivadi et al., 2017; Schlacher et al., 2011; Schlacher, Wu, & Jasin, 2012). Finally, as an integral member of the Fanconi Anemia pathway, RAD51 (FANCR) also plays an important role in repair of the DNA interstrand DNA crosslinks (ICLs) (Ameziane et al., 2015; Michl, Zimmer, & Tarsounas, 2016; Wang et al., 2015).

Despite numerous studies, significant gaps remain in our understanding of the assembly, dynamics, and regulation of the RAD51 nucleoprotein filament and mechanism of the DNA strand exchange reaction. Because of its important role in HR and because RAD51 overexpression contributes to radiation and chemotherapy resistance in a range of cancers, RAD51 has become an attractive drug target (see Budke, Lv, Kozikowski, & Connell, 2016; Hengel, Spies, & Spies, 2017 for recent reviews). Biochemical and biophysical analysis of RAD51, as well as drug discovery campaigns, requires robust methods for purification of the large quantities of this protein. Several methods have been developed for the purification and analysis of RAD51 (Baumann, Benson, Hajibagheri, & West, 1997; Benson, Stasiak, & West, 1994; Sigurdsson, Trujillo, Song, Stratton, & Sung, 2001). These methods for protein purification are generally complex and involve several supporting plasmids during expression. This is because the native *RAD51* gene sequence contains multiple rare codons, and the expression of soluble RAD51 also requires the presence of a chaperone. Additionally, biochemical studies of the RAD51 protein that require protein modifications, such as, for example, incorporation of artificial amino acids using amber suppressor systems to mimic tyrosine phosphorylation (Subramanyam, Ismail, Bhattacharya, & Spies, 2016; Xie, Supekova, & Schultz, 2007) or site-specific protein labeling using

genetically encoded aldehyde tags (Carrico, Carlson, & Bertozzi, 2007; Rabuka, Rush, Dehart, Wu, & Bertozzi, 2012), are not compatible with these protocols. Here, we describe a modified and highly optimized method for expression and purification of RAD51 that consistently yields large quantities of pure, functional protein using an *Escherichia coli* expression system while allowing the use of additional plasmids enabling incorporation of nonnatural amino acids or enzymatic modifications.



## 2. SYSTEM FOR THE BACTERIAL EXPRESSION OF HUMAN RAD51 PROTEIN

The RAD51 complementarity determining sequence (CDS) used here for RAD51 expression is optimized for *E. coli* codon usage, which is derived from the human RAD51, transcript variant 1 (NCBI RefSeq: [NM\\_002875](#)). This sequence has been cloned into the first multiple cloning site (MCS) of a pCOLA-Duet1 (Millipore Sigma) expression vector. The *E. coli* GroE operon has been cloned into the second MCS. The resulting plasmid is hereafter referred to as pCH1/RAD51o (Fig. 1A). The pCH1/RAD51o plasmid along with sequence information is available upon request from the Spies lab or from Addgene (#102562). We have also made variant of the pCH1 system that express RAD51 mutants, RAD51 containing a C-terminal 6xHis tag and RAD51 containing a recognition sequence for

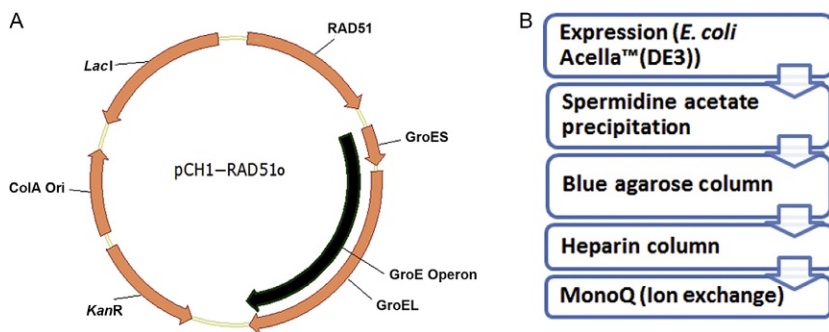


**Fig. 1** *E. coli* optimized expression system for human RAD51 protein. (A) The pCH1/RAD51o vector consists of an *E. coli* codon optimized CDS for the human RAD51 protein along with the *E. coli* GroE operon, which expresses the GroEL–GroE5 chaperone under the control of the T7 promoter and a ColA bacterial origin of replication. (B) Purification scheme for producing RAD51 protein involves expression of the protein in *E. coli* Acella (DE3) cells. After expression, the RAD51 protein is precipitated from the clarified lysate using spermidine acetate. The resuspended precipitate is then purified through affinity chromatography (blue agarose and heparin) followed by the anion exchange chromatography.

the formylglycine generating enzyme at the C-terminus. These constructs are available upon request.

The proteins are then expressed from the pCH1 vector in the Acella<sup>TM</sup> competent cells [ $F^- ompT hsdS_B(rB^- mB^-) gal dam$  (DE3)  $\Delta endA \Delta recA$ ] (EdgeBio Catalog#36795) which have the RecA protein completely deleted from their genome (Fig. 1). Note that while other bacterial strains can potentially be used for the RAD51 expression from the pCH1/RAD51o plasmid, these strains should not express native RecA recombinase. If present, bacterial RecA purifies with RAD51 and can affect the subsequent analysis.

The RAD51 protein, expressed in the Acella<sup>TM</sup> competent cells, is precipitated using spermidine acetate and then purified using chromatography based on Cibacron<sup>TM</sup> F3G-A (Blue) affinity followed by a Heparin column which removes any RAD51-bound DNA. The protein prep is then polished and concentrated using an anion exchange column (Fig. 1B). The detailed protocol is described later. This protocol does not require an affinity tag and instead depends on the specific properties of RAD51 and related RecA-like recombinases. The spermidine-mediated formation of microcrystals by the RecA family proteins was first reported for the bacterial RecA (Griffith & Shores, 1985) and latter was taken advantage in the human RAD51 purification (Baumann et al., 1997). The microcrystals readily formed in the presence of a polyamine spermidine can be separated from the rest of the cellular extract by centrifugation and dissolve in the presence of salt and/or phosphate. Besides aiding in the RAD51 purification, spermidine precipitation also removes *E. coli* nucleases that may otherwise contaminate the purify protein and interfere with the biochemical and biophysical analyses. Subsequent chromatographic steps also take advantage of the specific properties of recombinases. Cibacron Blue dye in the HiTrap<sup>TM</sup> Blue Agarose columns structurally resembles nucleotides, heparin offers a high affinity binding for the DNA-binding proteins, and Mono Q is a strong anion exchanger. Combined, the spermidine precipitation step followed by the three chromatographic steps yields highly pure, 100% active, nuclease-free RAD51 protein.



## 3. EQUIPMENT, MATERIALS, AND REAGENTS

### 3.1 Equipment

- 50-mL conical tubes
- 0.45- $\mu$ M syringe filters
- 0.2- $\mu$ M bottle top vacuum filters

Large agarose gel running apparatus  
Akta (GE) or BioLogic (BioRad) chromatography system  
ChemiDoc XRS (BioRad)  
Dialysis beakers  
Dialysis Tubing (10,000 MWCO)  
HiTrap™ Blue HP chromatography column (GE Life Sciences #17-0412-01)  
HiTrap™ Heparin HP chromatography column (GE Life Sciences #17-0406-01)  
MonoQ (5/50) Ion Exchange Column (GE Life Sciences #17-5166-01)  
Refrigerated floor standing centrifuge  
Oak Ridge Centrifuge tubes  
Shaker incubator  
Sonicator  
Temperature block/bath  
Micropipettors  
Micropipettor tips  
Fluorescence spectrophotometer equipped with a temperature controller and capable of simultaneously detecting fluorescence in two channels: We used Cary Eclipse (Agilent). Alternatively, a spectrofluorimeter from ISS or Shimadzu can be used. The assays described below also can be adapted for a multiwell plate format for use with a plate reader.  
UV–vis spectrophotometer  
Quartz or optical glass cuvettes for binding titrations (Starna)

### 3.2 Materials Required

Antifoam 204 (Sigma# A8311)  
Ammonium Sodium Phosphate Dibasic Tetrahydrate ( $\text{NaNH}_4\text{PO}_4$ ) (Sigma# 04266)  
*apa*LI (NEB# R0507)  
Bacto™ Tryptone (BD Biosciences)  
Bacto™ Yeast Extract (BD Biosciences)  
Chicken egg white lysozyme (Sigma# L7651)  
Dithiothreitol (DTT) (Sigma# D0632)  
Ethylenediaminetetraacetic acid, EDTA (Sigma# E9884)  
Glacial Acetic Acid  
Glycerol  
HEPES (Sigma# H4034)

Hydrochloric acid  
IPTG (EMD Millipore# 420322)  
Kanamycin sulfate from *Streptomyces kanamyceticus* (Sigma# K1377)  
Potassium Chloride (Sigma# P5405)  
Potassium Phosphate Monobasic (Sigma# P0662)  
Potassium Phosphate Dibasic (Sigma# P3786)  
Protease inhibitors (Roche# 11836170001)  
Proteinase K Solution (20 mg/mL) (Invitrogen/Life Technologies# AM2546)  
Sodium Chloride (NaCl)  
Sodium Dodecyl Sulfate (SDS)  
Sodium Hydroxide (Sigma# S5881)  
Sodium Thiocyanate (NaSCN) (Sigma# 251410)  
Spermidine (Sigma# S0266)  
SYBR<sup>®</sup> Gold Nucleic Acid Gel Stain (10,000 × Concentrate in DMSO) (Invitrogen/Life Technologies# S-11494)  
Trizma<sup>®</sup> Base (Sigma# T6066)  
Triton<sup>™</sup> X-100  
UltraPure<sup>™</sup> Agarose (Invitrogen/Life Technologies# 16500-100)

### 3.3 Oligonucleotides and DNA Substrates

The synthetic oligonucleotide used in the Förster resonance energy transfer (FRET)-based DNA extension assay can be commercially synthesized. We use PAGE purified oligonucleotides synthesized by IDT (Integrated DNA Technologies, Inc.). The dT<sub>60</sub> oligo we use has the Cy3 and Cy5 dyes separated by 25 nucleotides (5'-T<sub>5</sub>-Cy5-T<sub>25</sub>-Cy3-T<sub>30</sub>-3'). The oligonucleotides are resuspended in 10 mM Tris (pH 8.0) and stored at -20°C.

φX174 Virion ssDNA (NEB# N3023)

φX174 RFI dsDNA (NEB# N3021)

### 3.4 Buffers and Solutions

*Lysis Buffer:* 100 mM Tris-OAc (pH 7.5 at 23°C), 2 mM EDTA, 10% Glycerol (v/v), 1 mM DTT, Lysozyme (0.5 mg/mL), Protease Inhibitors, 0.1% Triton X-100

*Spermidine Acetate Buffer:* 20 mM Tris-OAc (pH 7.5 at 23°C), 7 mM Spermidine Acetate (pH 7.5), 5% Glycerol, 0.1 mM DTT

*T-150 Buffer:* 50 mM Tris-HCl (pH 7.5 at 23°C), 10% Glycerol, 150 mM NaCl, 1 mM DTT

*T-250 Buffer*: 50 mM Tris–HCl (pH 7.5 at 23°C), 10% Glycerol, 250 mM NaCl, 1 mM DTT

*T-300 Buffer*: 50 mM Tris–HCl (pH 7.5 at 23°C), 10% Glycerol, 300 mM NaCl, 1 mM DTT

*T-500 Buffer*: 50 mM Tris–HCl (pH 7.5 at 23°C), 10% Glycerol, 500 mM NaCl, 1 mM DTT

*T-600 Buffer*: 50 mM Tris–HCl (pH 7.5 at 23°C), 10% Glycerol, 600 mM NaCl, 1 mM DTT

*Blue-A Buffer*: 100 mM Potassium Phosphate (KPi) (pH 7.0 at 23°C), 5% Glycerol, 300 mM NaCl, 1 mM EDTA, 1 mM DTT

*Blue-B Buffer*: 100 mM Potassium Phosphate (KPi) (pH 7.0 at 23°C), 5% Glycerol, 2 M NaSCN, 1 mM EDTA, 1 mM DTT

*Buffer HA*: 20 mM HEPES–NaOH (pH 7.5 at 23°C), 5% Glycerol, 150 mM NaCl, 1 mM EDTA, 1 mM DTT

*Buffer HB*: 20 mM HEPES–NaOH (pH 7.5 at 23°C), 5% Glycerol, 2 M NaCl, 1 mM EDTA, 1 mM DTT

*FRET Buffer (Ca<sup>2+</sup>-ATP)*: 20 mM HEPES–KOH (pH 7.5 at 23°C), 5 mM CaCl<sub>2</sub>, 5 mM MgCl<sub>2</sub>, 150 mM KCl, 1 mM ATP, 1 mM DTT

*FRET Buffer (Mg<sup>2+</sup>-ATP)*: 20 mM HEPES–NaOH (pH 7.5 at 23°C), 150 mM NaNH<sub>4</sub>PO<sub>4</sub>, 2 mM MgCl<sub>2</sub>, 1 mM ATP, 1 mM DTT

0.5 M NaNH<sub>4</sub>PO<sub>4</sub> (this reagent tends to precipitate at room temperature during prolonged storage and is made fresh before use)

10% SDS

*Tris-Acetate-EDTA Buffer (TAE)*: 40 mM Trizma Base, 20 mM acetic acid, 1 mM EDTA

UltraPure™ Phenol:Chloroform:Isoamyl Alcohol (25:24:1, v/v) (Invitrogen/Life Technologies# 15593-031)

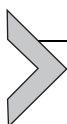
RPA Protein purified as described earlier (Henricksen, Umbricht, & Wold, 1994) and is also described in detail in Chapter “Single-molecule analysis of Replication Protein A–DNA interactions” by Bain, Fischer, Chen, and Wold of this volume.



## 4. BACTERIAL EXPRESSION OF THE RAD51 PROTEIN FROM THE PCH1/RAD51O PLASMID

**4.1** Inoculate two 10 mL LB cultures supplemented with 40 µg/mL Kanamycin with *E. coli* Acella™ (DE3)/pCH1–RAD51o. Incubate the cultures at 37°C overnight (~14 h) at 230 rpm.

- 4.2** Inoculate 8 mL of the overnight culture into 1 L of LB Broth supplemented with 40  $\mu\text{g}/\text{mL}$  Kanamycin and 300  $\mu\text{L}$  5% Antifoam 204. You will need two 1 L cultures. Incubate the inoculated cultures at 37°C at 230 rpm until the  $\text{OD}_{600}$  reaches 0.6–0.7 (~2.5 h). Induce the RAD51 expression with 0.1 mM IPTG (100  $\mu\text{L}$  of 1 M stock) followed by incubation at 37°C for 4 h. Higher IPTG concentrations result in an insoluble protein. Pellet the cells by centrifugation. We use the Sorvall Fiberlite™ F10–4x1000 LEX Rotor and spin cells at 10,500 rpm (20,600  $\times g$ ) for 20 min at 4°C. The pelleted cells can be stored at –80°C until further use. Typical yield is 2 g of cells per 1 L of culture.



## 5. PURIFICATION OF RAD51

All purification steps described below should be carried out on ice or at 4°C. All buffers should be prechilled and degassed (if air bubbles are observed).

- 5.1** *Day 1:* Take 4 g of the Acella™ (DE3)/pCH1–RAD51o cell pellet (from two 1 L cultures) from the –80°C and thaw on ice for 1 h. Resuspend the pellet in Lysis buffer (5 mL/g of cells) for 30 min at 4°C and lyse by sonication for about 4 min (Amplitude 40, 2 s pulse, 2 min timer repeated twice). Centrifuge the lysate. We use the Sorvall Fiberlite™ F21–8x50 fixed-angle rotor and spin the lysed cells at 18,000 rpm (38,759  $\times g$ ) for 1 h and 20 min at 4°C. Collect the clarified lysate and transfer it into a dialysis bag.
- 5.2** Dialyze the supernatant at 4°C in 500 mL of prechilled Spermidine Acetate Buffer (see [Section 3.4](#)) which needs to be replaced with fresh buffer after 3 h and then again after another 3 h. The final buffer change is kept overnight. While changing buffers, make sure to mix the precipitate by flipping the dialysis bag several times to distribute the forming precipitate throughout the buffer volume. This ensures uniform and efficient precipitation.
- 5.3** *Day 2:* Pellet the precipitated proteins by centrifugation at 18,000 rpm (38,759  $\times g$ ; Sorvall Fiberlite™ F21–8x50 fixed-angle rotor) for 20 min at 4°C.
- 5.4** Remove the supernatant and set aside. Resuspend the pellet in 10 mL T-150 buffer (see [Section 3.4](#)) using gentle pipetting on ice. Note that some fraction of the pellet will remain insoluble. Spin the pellet at 18,000 rpm (38,759  $\times g$ ; Sorvall Fiberlite™ F21–8x50 fixed-angle rotor) for 20 min at 4°C.

- 5.5** Remove the supernatant from the T-150 wash and set aside. Resuspend the pellet in 10 mL T-250 Buffer and spin at 18,000 rpm ( $38,759 \times g$ ; Sorvall Fiberlite™ F21-8x50 fixed-angle rotor) for 20 min at 4°C. It is important to note that these first two pellets be only partially solubilized. The RAD51 protein, if completely solubilized in these early fractions contains more impurities that are difficult to separate later. Repeat this step with 10 mL of T-300 and 5 mL of T-500 and T-600 Buffers. Analyze samples from all preserved supernatants by electrophoresis on a 12% SDS-PAGE to determine which fractions contain RAD51. Wild-type RAD51 is generally observed in T300, T500, and T600 fractions (Fig. 2A). Different mutants and modified forms of RAD51, however, may behave differently.
- 5.6** Pool the RAD51-containing fractions together. Combine the T600 fraction with the T300 and T500 fractions and filter the mixture through a 0.45- $\mu$ M syringe filter before loading the sample onto the blue column. This step must be done fast, just before loading onto the next column as pooled fractions tend to precipitate. Another option would be to load the samples individually.
- 5.7** Load the filtered sample onto three 5 mL HiTrap™ Blue Agarose columns (connected in series) cleaned with Blue-B Buffer and equilibrated with Blue-A Buffer (see Section 3.4).
- 5.8** Wash the columns with five-column volumes of Blue-A Buffer or until the absorbance signal stabilizes.
- 5.9** Elute the protein from the columns using a 60-mL 0–2 M NaSCN gradient in Blue-B Buffer at 5 mL/min. Collect 4 mL fractions. The wild-type RAD51 typically elutes before 800 mM NaSCN within the first 40% of the NaSCN gradient (Fig. 2B). Pool fractions containing RAD51 dialyze in 2 L of buffer HA overnight at 4°C.
- 5.10** *Day 3:* Filter the dialyzed RAD51 from step 5.9 to remove small precipitates (if any) and load onto three 5 mL HiTrap™ Heparin FF Columns using Buffer HA (see Section 3.4) as binding buffer. Wash the column with five-column volumes of loading buffer or until the absorbance signal has stabilized. Elute RAD51 with an 80 mL 150 mM–2 M NaCl gradient (Buffer HA–Buffer HB) at 5 mL/min (Fig. 2C). Collect 5 mL fractions.
- 5.11** Collect the fractions containing RAD51 and pool together to be dialyzed in 2 L of HA Buffer overnight at 4°C. The protein can be eluted over a longer gradient  $\sim$ 100 mL at this scale depending on separation

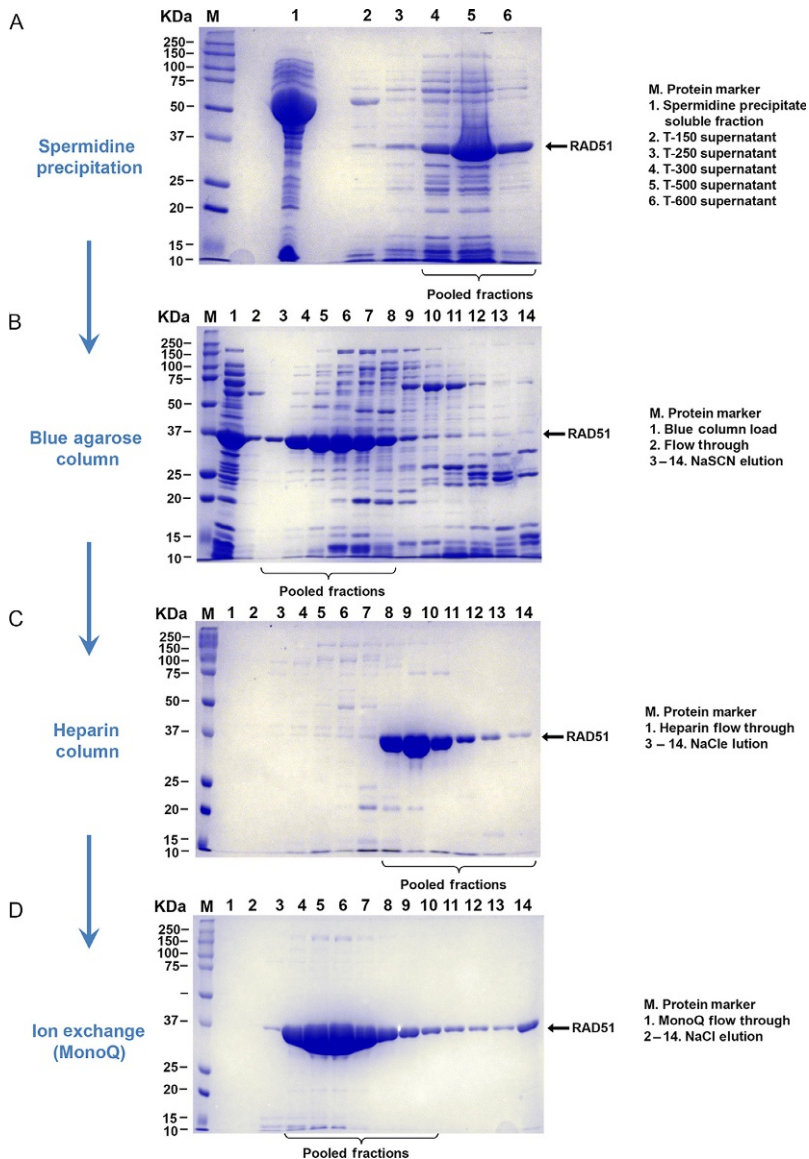
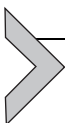


**Fig. 2** Step-by-step purification of RAD51 protein. (A) The clarified lysate is dialyzed overnight in spermidine acetate buffer. The precipitate is then selectively resuspended in increasing concentrations of sodium chloride. The RAD51 wild-type protein is generally soluble in salt concentrations above 300 mM. Any RAD51 protein found in fractions having lower salt concentrations is generally difficult to separate from other proteins in further purification steps. (B) Pooled fractions containing RAD51 from the spermidine precipitation are then passed through a Blue Agarose column. The RAD51 protein is eluted from the column using a sodium thiocyanate gradient. (C) Fractions containing RAD51 are then further loaded on a Heparin affinity column and RAD51 eluted using a sodium chloride gradient. (D) The protein is relatively pure at this step and is polished and concentrated using an MonoQ anion exchange step. Small fractions are collected during elution at this stage to minimized dilution of the RAD51 protein.

and column performance. It would be ideal to keep dialysis for approximately 12 h as the protein tends to precipitate when dialyzed longer.

- 5.12 Day 4: Filter the dialyzed fractions from the Heparin Column and load the protein a 1-mL MonoQ (5/50) Ion Exchange Column using Buffer HA as binding buffer followed by a linear NaCl salt gradient to 1.2 M over 8 mL to elute RAD51 and a final step up to 2 M over 10 mL at 1 mL/min. It is best to collect small fractions during this step  $\sim 0.3 \mu\text{L}$  (Fig. 2D). This allows us to retain fractions containing the highest concentrations of RAD51 while simultaneously separating the small impurities.
- 5.13 Pool the fractions containing human RAD51 and dialyze the purified protein overnight in HA buffer containing 10% glycerol at 4°C.
- 5.14 Day 5: The concentration of the protein measured spectrophotometrically at 280 nm using a molar extinction coefficient of  $14,900 M^{-1} \text{cm}^{-1}$ . The extinction coefficient for the mutant or tagged forms of the protein may be different and need to be calculated based on the changes in the sequence.
- 5.15 The protein can be aliquoted and flash frozen in liquid nitrogen. RAD51 should be thawed only once, as multiple cycles of freezing and thawing inactivate the protein. Therefore, we suggest making small (10–50  $\mu\text{L}$ ) aliquots.



## 6. FRET-BASED DNA-BINDING ASSAY TO MEASURE ssDNA-BINDING ACTIVITY OF THE RAD51 RECOMBINASE

The purification procedure prescribed above consistently yields fully active RAD51 protein. It is imperative, however, to confirm that each preparation of the protein is indeed 100% active. The percentage of the RAD51-specific activity can be derived from the ssDNA-binding stoichiometry. Similar to other RecA-family recombinases, the active form of human RAD51 is a regular, helical nucleoprotein filament formed on the ssDNA in the presence of ATP (Benson et al., 1994; Galkin et al., 2006; Ristic et al., 2005; Short et al., 2016; Xu et al., 2017). Each ATP-bound RAD51 protomer in the nucleoprotein filament occludes three nucleotides of ssDNA, and the ssDNA is extended approximately 1.6-fold relative to the B-form (Subramanyam et al., 2016; Subramanyam, Jones, Spies, & Spies, 2013; Xu et al., 2017).

Both of these properties can be assessed simultaneously as the change in the DNA extension upon the RAD51 binding can be followed using FRET (Clegg, 2002) between the FRET donor (Cy3) and FRET acceptor (Cy5) fluorophores incorporated into the DNA substrate (Grimme & Spies, 2011; Subramanyam et al., 2016, 2013). To determine the RAD51:ssDNA-binding stoichiometry we typically use a dT<sub>60</sub> ssDNA oligonucleotide internally labeled with Cy3 and Cy5 dyes (dT<sub>60</sub>-Cy3/Cy5). The two dyes are positioned 5 and 30 nucleotides from the 5' end of the dT<sub>60</sub> oligomer. The 25-nucleotide separation yields a high FRET signal ( $\sim 0.6$ ) for the protein-free ssDNA in the reaction buffer containing physiological concentrations of monovalent and divalent cations. Extension of the ssDNA to 1.6-fold over the B-form by the fully formed, ATP-bound RAD51 nucleoprotein results in a transition from a high FRET ( $\sim 0.6$ ) to a low FRET ( $\sim 0.2$ ) state (Fig. 3). To access the quality of the RAD51 prep, the assay is carried out under the stoichiometric-binding conditions (ssDNA is present at 600 nM nucleotides or 10 nM dT<sub>60</sub> molecules), where the FRET value increases linearly with each addition of RAD51 and then reaches saturation at 1 active RAD51 monomer per three nucleotides of ssDNA.

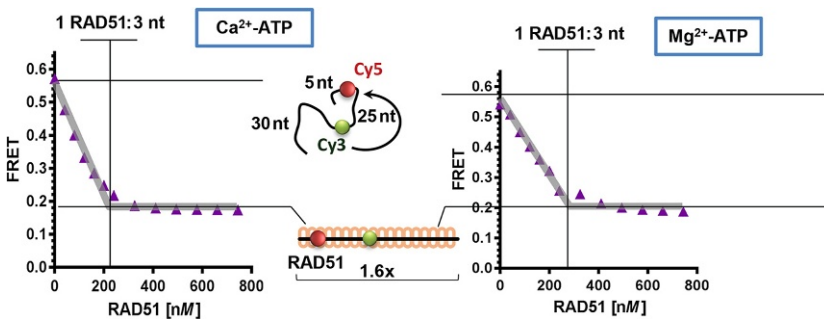


**Fig. 3** FRET-based DNA-binding and extension assay. The substrate for this assay is a poly dT<sub>60</sub> ssDNA oligomer, which is labeled internally with Cy3 (FRET donor) and Cy5 (FRET acceptor) fluorescent dyes separated by 25 nucleotides. Free ssDNA yields a high FRET due to the proximity of Cy3 and Cy5. Addition of RAD51 into the reaction mixture initiates nucleoprotein filament formation, which straightens and extends the oligomer, which is observed as a decrease in FRET as the two fluorophores move away from one another. The assay can be performed in conditions that permit ATP hydrolysis (Mg<sup>2+</sup>-ATP) or where ATP hydrolysis is inhibited (Ca<sup>2+</sup>-ATP). The biochemical characteristics of the wild-type RAD51 protein do not vary much between these two conditions but mutants with altered DNA-binding properties can be separated using this assay (Subramanyam et al., 2016).

The FRET-based ssDNA-binding assay can be carried out under two experimental regimes, in the buffer containing ammonium sodium phosphate where the RAD51 protein is allowed to hydrolyze ATP (Shim, Schmutte, Yoder, & Fishel, 2006; Subramanyam et al., 2016), or when the ATP hydrolysis (but not the ATP binding) is restricted due to the presence of  $\text{Ca}^{2+}$ . The wild-type RAD51 readily forms active nucleoprotein filaments on the 60-mer ssDNA oligonucleotide under both conditions. For the RAD51 mutant that may display lower binding affinity or a defective ssDNA binding to a relatively short ssDNA, we suggest using a  $\text{Ca}^{2+}$  condition, which promotes more regular and stable nucleoprotein filaments (Ristic et al., 2005).

### **Fluorimeter Settings for FRET-Based Binding Assays**

- 6.1 Cy3 excitation wavelength at 530 nm and emission wavelength at 565 nm.
- 6.2 Cy5 excitation wavelength at 630 nm and emission wavelength at 660 nm.
- 6.3 Excitation and emission slit widths set to 10 nm each.
- 6.4 PMT voltage set, so that the amplitude of the Cy3 signal is below 60% of the available scale.
- 6.5 The assays are carried out in kinetics mode with the Cy3 and Cy5 signals recorded every second. The kinetic mode allows one to monitor the change in the signal upon each RAD51 addition and to only analyze the data when the signal achieves equilibrium.

### **FRET DNA-Binding and Extension Assay Protocol**

- 6.6 Place fluorescence cuvette containing FRET reaction buffer (see Section 3.4) and allow the sample to equilibrate at 37°C. Zero the fluorimeter. Record the Cy3 and Cy5 baseline values for at least 1 min.
- 6.7 Add 600 nM nucleotides (10 nM molecules) of dT<sub>60</sub>-Cy3/Cy5 oligo into the cuvette, mix by pipetting and measure the Cy3 and Cy5 fluorescence values once the fluorescence has stabilized.
- 6.8 RAD51 protein is then titrated into the reaction with a proper mixing after each addition. For each addition, continue the recording until the equilibrium is achieved and the Cy3 and the Cy5 fluorescence stabilizes. Record the stable fluorescence signals for at least 1 min before making the next RAD51 addition.
- 6.9 Typical protein concentrations range from 40 nM to 1000 μM. Ideally, the total volume of the titrated protein should not exceed 10% of the reaction volume and the dilution should be factored in the final

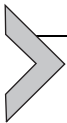
concentration of the titrations. We try to avoid pipetting extremely small volumes (<0.5  $\mu\text{L}$ ), to avoid pipetting errors.

- 6.10 For each RAD51 concentration select the period of at least 1 min of measurement before the next protein addition and record the average signals for Cy3 and Cy5 fluorescence.
- 6.11 Subtract the average baseline fluorescence from the average fluorescence recorded at each RAD51 concentration.
- 6.12 Resulting values for Cy3 and Cy5 fluorescence can be plotted as functions of RAD51 concentration. The FRET values are calculated as a fraction of donor acceptor intensity adjusted by correction factors (Grimme & Spies, 2011). For Cary Eclipse fluorescence spectrophotometer (Agilent) FRET between Cy3 and Cy5 dyes can be calculated using the equation:

$$\text{FRET} = \frac{4.2 * I_{\text{cy5}}}{4.2 * I_{\text{cy5}} + 1.7 * I_{\text{cy3}}}$$

The two correction factors account for the reduction in the measured fluorescence intensities due to the overall instrument detection efficiencies, quantum yield of the two dyes and the leakage between the donor and the acceptor channels (Ha et al., 1999; Joo & Ha, 2012).

- 6.13 The FRET values should saturate at a RAD51 concentration corresponding to  $\sim 1:3$  protein:nucleotides (Subramanyam et al., 2016, 2013) (Fig. 3).



## 7. THREE-STRAND DNA STRAND EXCHANGE ASSAY

The ssDNA binding by RAD51 described above is a prerequisite of all known RAD51 cellular function. The full functionality of the RAD51 protein can be further evaluated in a more delicate namesake (aka recombinase) activity of RAD51. In homologous recombination and homology-directed DNA repair, the RAD51 nucleoprotein filament performs an ATP-dependent homologous DNA pairing and DNA strand exchange reactions (Ciccia & Elledge, 2010; Mehta & Haber, 2014). The RAD51-mediated DNA strand exchange activity can be reconstituted in vitro in the so-called three strand DNA strand exchange reaction (Baumann, Benson, & West, 1996; Sigurdsson et al., 2001). The active RAD51 nucleoprotein filament is formed on  $\phi\text{X174}$  Virion ssDNA with the help of the ssDNA-binding protein RPA. The RAD51 nucleoprotein filament then pairs with and

invades a linear  $\phi$ X174 RFI double stranded (dsDNA) substrate. The strand exchange activity of RAD51 leads to the displacement of the complementary linear ssDNA from the dsDNA, forming a nicked circular product, through a series of joint molecule intermediates, all of which can easily be separated on an agarose gel (Sigurdsson et al., 2001; Subramanyam et al., 2016) (Fig. 4A). The reaction depends on the presence of the ssDNA-binding protein RPA, which, when added after RAD51, stimulates the DNA strand exchange by destabilizing remaining secondary structure in the ssDNA and by sequestering the displaced DNA strand. The assay, therefore, also reflects on the RPA functionality, as separation of function RPA mutants functional in DNA replication, but not recombination fail to support the formation of the nicked circular product (Chen, Subramanyam, Elcock, Spies, & Wold, 2016). Under conditions permitting ATP hydrolysis (i.e., in the buffer containing  $Mg^{2+}$ -ATP and  $NaNH_4PO_4$ ), RPA can be also added prior to RAD51. The yield of such RPA-first reaction is, however, significantly lower than that of the RAD51-first reaction due to the competition between the two proteins. The assays can also be carried out in the presence of  $Ca^{2+}$ -ATP, which activates RAD51 by preventing ATP hydrolysis (Bugreev & Mazin, 2004). These assays are described in detail in Chapter “Dissecting the recombination mediator activity of BRCA2 using biochemical methods” by von Nicolai, Ehlén, Martinez, and Carreira.

### Preparation of DNA Substrates

- 7.1 Linear double stranded DNA is prepared by digesting  $\phi$ X174 RFI dsDNA using the *Apa*LI restriction enzyme. We typically digest 60  $\mu$ g of dsDNA at a time.
- 7.2 The digested DNA is cleaned using Phenol:Chloroform:Isoamyl Alcohol extraction and precipitated using Isopropanol. Vigorous pipetting and vortexing the mixture should be avoided as it tends to shear the DNA. The DNA is resuspended in nuclease-free water and the concentration determined using  $A_{260}$  is then aliquoted and stored at  $-80^\circ C$ . Quality of the purified DNA is paramount as sheared DNA causes smearing in the gels and interferes with the results and quantitation of the strand exchange assay. All reagents used should be checked for the presence of nucleases.
- 7.3 Similarly,  $\phi$ X174 Virion concentration is measured using  $A_{260}$ .

### RAD51-First DNA Strand Exchange Reaction

- 7.4 Typical reaction volumes are 90  $\mu$ L which allows us to take five time points. All additions should be mixed by gentle pipetting as vigorous mixing or vortexing can shear the DNA substrates.

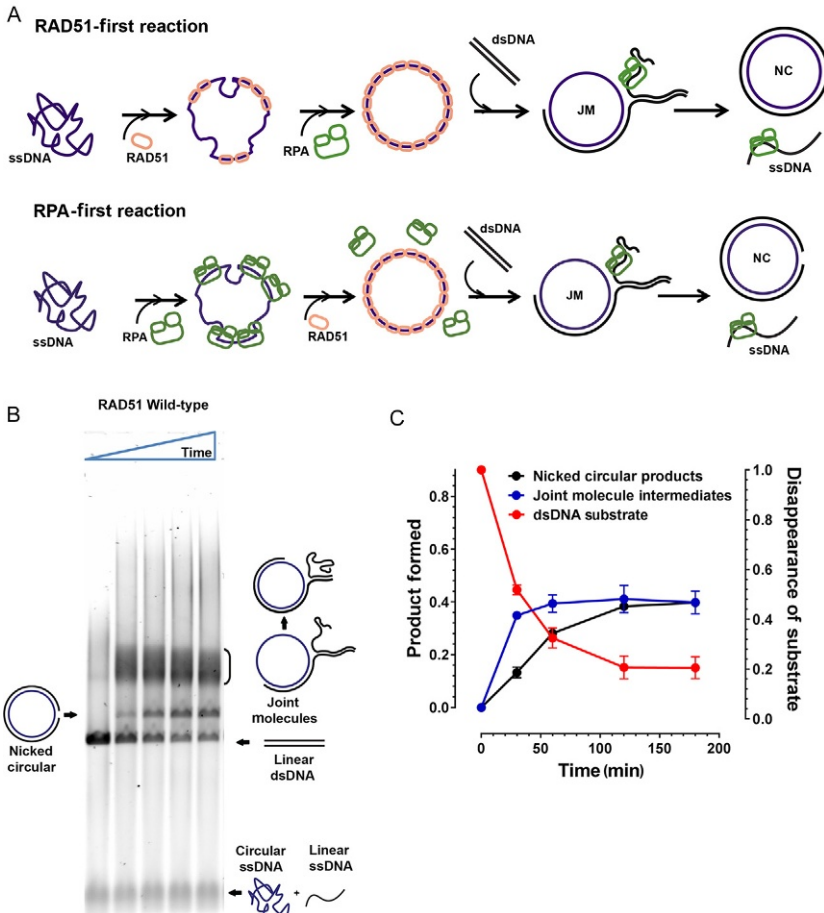


**Fig. 4** Three-Strand DNA strand exchange assay. (A) Active RAD51 nucleoprotein filament is formed on  $\phi$ X174 Virion circular ssDNA in reaction conditions permitting ATP hydrolysis followed by addition of RPA which helps remove secondary structures in the ssDNA allowing stable nucleoprotein filament formation. The RAD51 nucleoprotein then invades  $\phi$ X174 RFI linear dsDNA to form nicked circular dsDNA products through several joint molecule intermediates showing various stages of branch migration. The RPA also helps sequester any free displaced ssDNA following strand exchange thereby preventing a reverse reaction. (B) Typical agarose gel image from a strand exchange assay used to resolve the substrates, intermediates, and the products of the reaction over a time course of 0, 30, 60, 120, and 180 min. In reactions containing the wild-type protein, nicked circular products can be observed as early as 30 min. (C) Quantitation of the strand exchange assay gel showing appearance of nicked circular products (*black*) and joint molecules (*blue*) on the left Y axis. Disappearance of the linear dsDNA substrate (*red*) is quantitated on the right Y axis. Time in minutes is indicated on the X axis.

- 7.5 Prepare 4× strand exchange Reaction Buffer containing 80 mM HEPES–NaOH (pH 7.5 at 23°C), 40% Glycerol, 4 mM MgCl<sub>2</sub>, and 4 mM DTT.
- 7.6 Incubate 7.5 μM RAD51 with 30 μM (nucleotides) φX174 ssDNA (Note that all concentration are calculated for the final reaction volume of 90 μL) in the 1× strand exchange Reaction Buffer (20 mM HEPES–NaOH pH 7.5, 10% Glycerol, 1 mM MgCl<sub>2</sub>, and 1 mM DTT) for 5 min at 37°C.
- 7.7 Add 150 mM of Ammonium Sodium Phosphate (NaNH<sub>4</sub>PO<sub>4</sub>) and 2 μM RPA. Incubate the reaction for another 5 min.
- 7.8 Initiate the DNA strand exchange reaction by adding 15 μM (bp) of *Apa*LI-digested linear dsDNA. Further incubate the reaction at 37°C for the time course of the reaction (typically 180 min).
- 7.9 15 μL of the reaction can be drawn at different time points and deproteinized by addition of 0.8% SDS and proteinase K (800 μg/mL) followed by incubation at 37°C for 30 min. We usually take 0, 30, 60, 120, and 180 min time points.
- 7.10 The deproteinized samples are then loaded on a 0.9% TAE agarose gel and run at 3.5 V/cm overnight (about 14 h) at room temperature. In our experiments, the quality of Agarose and TAE seems to affect the result of the gels, and hence we always use UltraPure™ Agarose (see [Section 3.2](#)) and freshly prepared TAE buffer.

### **RPA-First DNA Strand Exchange Reaction**

The reaction scheme for the RPA-first reaction is overall similar to that for the RAD51-first reaction, except the order of RPA and RAD51 addition is reversed.

- 7.11 Prepare 4× strand exchange Reaction Buffer containing 80 mM HEPES–NaOH (pH 7.5 at 23°C), 40% Glycerol, 4 mM MgCl<sub>2</sub>, and 4 mM DTT.
- 7.12 Combine 2 μM RPA, 30 μM (nucleotides) φX174 ssDNA, and 150 mM of Ammonium Sodium Phosphate (NaNH<sub>4</sub>PO<sub>4</sub>) in the 1× reaction buffer (20 mM HEPES–NaOH pH 7.5, 10% Glycerol, 1 mM MgCl<sub>2</sub>, and 1 mM DTT) for 5 min at 37°C. Incubate for 5 min to form the RPA–ssDNA complex. (Note that all concentration are calculated for the final reaction volume of 90 μL.)
- 7.13 Initiate formation of the RAD51 nucleoprotein filament by adding 7.5 μM RAD51. Incubate the reaction for 5 min at 37°C.
- 7.14 Initiate the DNA strand exchange reaction by adding 15 μM (bp) of *Apa*LI digested Linear dsDNA is added and further incubated at 37°C for the time course of the reaction (typically 180 min).

**7.15** 15  $\mu\text{L}$  of the reaction can be drawn at different time points and deproteinized by addition of 0.8% SDS and Proteinase K (800  $\mu\text{g}/\text{mL}$ ) followed by incubation at 37°C for 30 min. We usually take 0, 30, 60, 120, and 180 min time points.

**7.16** The deproteinized samples are then loaded on a 0.9% TAE agarose gel and run at 3.5 V/cm overnight at room temperature. In our experiments, the quality of Agarose and TAE seems to affect the result of the gels, and hence we always use UltraPure™ Agarose (see Section 3.2) and freshly prepared TAE buffer.

### Visualization, Quantitation, and Interpretation of DNA Strand Exchange Data

**7.17** To visualize the products of the DNA strand exchange reaction, the agarose gel is stained with SYBR® Gold for 10 min and destained for 20 min in MilliQ  $\text{H}_2\text{O}$ . The gel can be visualized in a ChemiDoc XRS or equivalent imaging system by exciting the dye-nucleic acid complexes at 495 and 300 nm and recording the emission at 537 nm (Fig. 4B).

**7.18** The appearance of the nicked circular products can be quantitated using ImageJ software and normalized to the amount of initial linear dsDNA substrate. Draw equally sized rectangles around each band, measure the intensity of the band, and subtract the intensity of the same size rectangle placed in the empty lane of the gel (background). Determine the amount of the nicked circular product (%(nc)) as:

$$\%(nc(t)) = \frac{I_{nc}(t) - I_{bg}}{I_{dsDNA}(0) - I_{bg}} * 100,$$

where  $I_{nc}(t)$  is the intensity of the nicked circular band in the selected lane,  $I_{dsDNA}(0)$  is the intensity of the dsDNA band in the lane corresponding to the zero time point, and  $I_{bg}$  is the background intensity. Some image quantification software packages allow for an automated background correction. If this is the case, or if the background is negligibly low and there are no spare lanes on the gel, the background correction step can be omitted.

The amount of the unreacted dsDNA remaining in each lane is calculated as:

$$\%(dsDNA(t)) = \frac{I_{dsDNA}(t) - I_{bg}}{I_{dsDNA}(0) - I_{bg}} * 100,$$

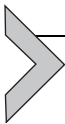
The nicked circular DNA and the linear dsDNA are the only two fully double-stranded species, as well as the species containing equivalent amount of DNA strands. Therefore, the intensities of the bands for these species can be compared directly.

**7.19** The appearance and clearance of the joint molecule intermediates can be estimated by subtracting the normalized intensity of the nicked circular products from the normalized intensity of the dsDNA for that lane (Subramanyam et al., 2016) (Fig. 4C).

$$\%(\text{jm}(t)) = \%(\text{dsDNA}(0)) - \%(\text{dsDNA}(t)) - \%(\text{nc}(t))$$

**7.20** The DNA strand exchange assay is generally performed in triplicate, and the results are plotted as standard error mean for the three independent experiments.

**7.21** Comparison of the kinetics of the appearance and disappearance of the major DNA species in the course of RAD51-first and RPA-first reactions allows to distinguish the two activities of RAD51, progression of the DNA strand exchange reaction (detected as clearance of the joint molecule intermediates in both reactions) and the RAD51 ability to compete with RPA (RPA-first reaction).



## 8. CONCLUSIONS

The *E. coli* Acella™ (DE3)/pCH1-RAD51o system can be used to produce large quantities of soluble human RAD51 protein. The purification scheme outlined earlier allows purification of RAD51 without the use of affinity tags, which may interfere with the recombinase functions or RAD51' other biochemical activities. The procedure takes 5 consecutive days, but is robust and straightforward. It can be readily extended to various RAD51 mutants and to the constructs containing tags, as well as recognition and labeling epitopes. The two assays that are routinely used in the validation of the RAD51 activity, the DNA-binding and the DNA strand exchange assays, follow the critical functional characteristics of the RecA-family recombinases, namely, the DNA-binding stoichiometry and the ssDNA extension within the recombinase nucleoprotein filament (FRET-based ssDNA-binding assay) and the DNA strand exchange reaction.

## ACKNOWLEDGMENTS

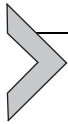
The authors' research is supported by National Institutes of Health (NIH) Grant GM108617 and by University of Iowa Holden Comprehensive Cancer Center Collaborative Pilot Grant NIH P30 CA086862 (to M.S.). The funders had no role in study design, data collection and analysis, decision to publish, or preparation of the manuscript. We thank members of the Spies lab and Dr. Marc Wold for critical reading of the manuscript and for valuable discussions.

## REFERENCES

- Ameziane, N., May, P., Haitjema, A., Van De Vrugt, H. J., Van Rossum-Fikkert, S. E., Ristic, D., et al. (2015). A novel Fanconi anaemia subtype associated with a dominant-negative mutation in RAD51. *Nature Communications*, *6*, 8829.
- Baumann, P., Benson, F. E., Hajibagheri, N., & West, S. C. (1997). Purification of human Rad51 protein by selective spermidine precipitation. *Mutation Research*, *384*, 65–72.
- Baumann, P., Benson, F. E., & West, S. C. (1996). Human Rad51 protein promotes ATP-dependent homologous pairing and strand transfer reactions in vitro. *Cell*, *87*, 757–766.
- Baumann, P., & West, S. C. (1998). Role of the human RAD51 protein in homologous recombination and double-stranded-break repair. *Trends in Biochemical Sciences*, *23*, 247–251.
- Benson, F. E., Stasiak, A., & West, S. C. (1994). Purification and characterization of the human Rad51 protein, an analogue of *E. coli* RecA. *EMBO Journal*, *13*, 5764–5771.
- Budke, B., Lv, W., Kozikowski, A. P., & Connell, P. P. (2016). Recent developments using small molecules to target RAD51: How to best modulate RAD51 for anticancer therapy? *ChemMedChem*, *11*, 2468–2473.
- Bugreev, D. V., & Mazin, A. V. (2004). Ca<sup>2+</sup> activates human homologous recombination protein Rad51 by modulating its ATPase activity. *Proceedings of the National Academy of Sciences of the United States of America*, *101*, 9988–9993.
- Carrico, I. S., Carlson, B. L., & Bertozzi, C. R. (2007). Introducing genetically encoded aldehydes into proteins. *Nature Chemical Biology*, *3*, 321–322.
- Chen, R., Subramanyam, S., Elcock, A. H., Spies, M., & Wold, M. S. (2016). Dynamic binding of replication protein a is required for DNA repair. *Nucleic Acids Research*, *44*, 5758–5772.
- Ciccia, A., & Elledge, S. J. (2010). The DNA damage response: Making it safe to play with knives. *Molecular Cell*, *40*, 179–204.
- Clegg, R. M. (2002). FRET tells us about proximities, distances, orientations and dynamic properties. *Journal of Biotechnology*, *82*, 177–179.
- Galkin, V. E., Wu, Y., Zhang, X. P., Qian, X., He, Y., Yu, X., et al. (2006). The Rad51/RadA N-terminal domain activates nucleoprotein filament ATPase activity. *Structure*, *14*, 983–992.
- Griffith, J., & Shores, C. G. (1985). RecA protein rapidly crystallizes in the presence of spermidine: A valuable step in its purification and physical characterization. *Biochemistry*, *24*, 158–162.
- Grimme, J. M., & Spies, M. (2011). FRET-based assays to monitor DNA binding and annealing by Rad52 recombination mediator protein. *Methods in Molecular Biology*, *745*, 463–483.
- Ha, T., Ting, A. Y., Liang, J., Caldwell, W. B., Deniz, A. A., Chemla, D. S., et al. (1999). Single-molecule fluorescence spectroscopy of enzyme conformational dynamics and cleavage mechanism. *Proceedings of the National Academy of Sciences of the United States of America*, *96*, 893–898.

- Hengel, S. R., Spies, M. A., & Spies, M. (2017). Small-molecule inhibitors targeting DNA repair and DNA repair deficiency in research and cancer therapy. *Cell Chemical Biology*, *24*, 1101–1119.
- Henricksen, L. A., Umbricht, C. B., & Wold, M. S. (1994). Recombinant replication protein A: Expression, complex formation, and functional characterization. *The Journal of Biological Chemistry*, *269*, 11121–11132.
- Joo, C., & Ha, T. (2012). Single-molecule FRET with total internal reflection microscopy. *Cold Spring Harbor Protocols*, *2012*(12), pdb.top072058.
- Kolinjivadi, A. M., Sannino, V., De Antoni, A., Techer, H., Baldi, G., & Costanzo, V. (2017). Moonlighting at replication forks—A new life for homologous recombination proteins BRCA1, BRCA2 and RAD51. *FEBS Letters*, *591*, 1083–1100.
- Li, X., & Heyer, W. D. (2008). Homologous recombination in DNA repair and DNA damage tolerance. *Cell Research*, *18*, 99–113.
- Mehta, A., & Haber, J. E. (2014). Sources of DNA double-strand breaks and models of recombinational DNA repair. *Cold Spring Harbor Perspectives in Biology*, *6*, a016428.
- Michl, J., Zimmer, J., & Tarsounas, M. (2016). Interplay between Fanconi anemia and homologous recombination pathways in genome integrity. *The EMBO Journal*, *35*, 909–923.
- Morrill, S. W. (2015). DNA-pairing and annealing processes in homologous recombination and homology-directed repair. *Cold Spring Harbor Perspectives in Biology*, *7*, a016444.
- Moynahan, M. E., & Jasin, M. (2010). Mitotic homologous recombination maintains genomic stability and suppresses tumorigenesis. *Nature Reviews. Molecular Cell Biology*, *11*, 196–207.
- Rabuka, D., Rush, J. S., Dehart, G. W., Wu, P., & Bertozzi, C. R. (2012). Site-specific chemical protein conjugation using genetically encoded aldehyde tags. *Nature Protocols*, *7*, 1052–1067.
- Ristic, D., Modesti, M., Van Der Heijden, T., Van Noort, J., Dekker, C., Kanaar, R., et al. (2005). Human Rad51 filaments on double- and single-stranded DNA: Correlating regular and irregular forms with recombination function. *Nucleic Acids Research*, *33*, 3292–3302.
- Schlacher, K., Christ, N., Siaud, N., Egashira, A., Wu, H., & Jasin, M. (2011). Double-strand break repair-independent role for BRCA2 in blocking stalled replication fork degradation by MRE11. *Cell*, *145*, 529–542.
- Schlacher, K., Wu, H., & Jasin, M. (2012). A distinct replication fork protection pathway connects Fanconi anemia tumor suppressors to RAD51-BRCA1/2. *Cancer Cell*, *22*, 106–116.
- Shim, K. S., Schmutte, C., Yoder, K., & Fishel, R. (2006). Defining the salt effect on human RAD51 activities. *DNA Repair*, *5*, 718–730.
- Short, J. M., Liu, Y., Chen, S., Soni, N., Madhusudhan, M. S., Shivji, M. K., et al. (2016). High-resolution structure of the presynaptic RAD51 filament on single-stranded DNA by electron cryo-microscopy. *Nucleic Acids Research*, *44*, 9017–9030.
- Sigurdsson, S., Trujillo, K., Song, B., Stratton, S., & Sung, P. (2001). Basis for avid homologous DNA strand exchange by human Rad51 and RPA. *The Journal of Biological Chemistry*, *276*, 8798–8806.
- Subramanyam, S., Ismail, M., Bhattacharya, I., & Spies, M. (2016). Tyrosine phosphorylation stimulates activity of human RAD51 recombinase through altered nucleoprotein filament dynamics. *Proceedings of the National Academy of Sciences of the United States of America*, *113*, E6045–E6054.
- Subramanyam, S., Jones, W. T., Spies, M., & Spies, M. A. (2013). Contributions of the RAD51 N-terminal domain to BRCA2-RAD51 interaction. *Nucleic Acids Research*, *41*, 9020–9032.

- Wang, A. T., Kim, T., Wagner, J. E., Conti, B. A., Lach, F. P., Huang, A. L., et al. (2015). A dominant mutation in human RAD51 reveals its function in DNA interstrand crosslink repair independent of homologous recombination. *Molecular Cell*, *59*, 478–490.
- Xie, J., Supekova, L., & Schultz, P. G. (2007). A genetically encoded metabolically stable analogue of phosphotyrosine in *Escherichia coli*. *ACS Chemical Biology*, *2*, 474–478.
- Xu, J., Zhao, L., Xu, Y., Zhao, W., Sung, P., & Wang, H. W. (2017). Cryo-EM structures of human RAD51 recombinase filaments during catalysis of DNA-strand exchange. *Nature Structural & Molecular Biology*, *24*, 40–46.



# Determining the RAD51-DNA Nucleoprotein Filament Structure and Function by Cryo-Electron Microscopy

Lingyun Zhao\*, Jingfei Xu\*, Weixing Zhao<sup>†</sup>, Patrick Sung<sup>†</sup>,  
Hong-Wei Wang<sup>\*,1</sup>

\*Ministry of Education Key Laboratory of Protein Sciences, Tsinghua-Peking Joint Center for Life Sciences, Beijing Advanced Innovation Center for Structural Biology, School of Life Sciences, Tsinghua University, Beijing, China

<sup>†</sup>Yale University, New Haven, CT, United States

<sup>1</sup>Corresponding author: e-mail address: hongweiwang@tsinghua.edu.cn

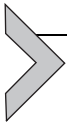
## Contents

|  |     |
|--|-----|
| 1. Introduction  | 180 |
| 2. Purification of hRAD51  | 183 |
| 3. Assembly of Presynaptic, Postsynaptic, and Arrested Synaptic Complexes        | 184 |
| 4. Negative Staining EM  | 185 |
| 5. Cryo-EM Sample Preparation  | 187 |
| 6. Cryo-EM Data Collection   | 188 |
| 7. Image Processing and Reconstruction   | 189 |
| 7.1 High-Resolution Cryo-EM Structures of Presynaptic and Postsynaptic Complexes | 189 |
| 7.2 Cryo-EM Structure of an Arrested Synaptic Complex                            | 193 |
| 8. Conclusion and Perspectives   | 195 |
| Acknowledgments  | 195 |
| References   | 196 |

## Abstract

Homologous recombination is a universal tool for DNA double-strand break and replication fork repair, and it is catalyzed by a highly conserved family of recombinases. In eukaryotes, Rad51 is the recombinase that catalyzes the pairing of homologous DNA molecules and the exchange of strands between the paired molecules. Rad51 assembles on single-stranded DNA (ssDNA) stemming from lesion processing to form a right-handed helical polymer that engages then samples double-stranded DNA (dsDNA) for homology. Upon matching with a homologous sequence, the Rad51-bound ssDNA invades the dsDNA, leading to the formation of a DNA joint with concomitant displacement of the strand of like polarity. The Rad51-DNA filaments are amenable to structural

studies using cryo-electron microscopy (cryo-EM). In particular, recent technical breakthroughs in cryo-EM have made it possible to define the structure and function of human RAD51 at near-atomic resolution. In this chapter, we describe our cryo-EM approach to capture the human RAD51 filament structures in various stages of catalysis. The approach may also be useful for related recombinases and other helical assemblies.



## 1. INTRODUCTION

Rad51 and its orthologs in prokaryotes help mediate homologous recombination (HR) and DNA repair reaction by catalyzing the pairing and exchange of strands between homologous DNA molecules (Amunugama & Fishel, 2012; Baumann, Benson, & West, 1996; Baumann & West, 1998; Shinohara, Ogawa, & Ogawa, 1992; Sung, 1994). These general recombinases function within the context of a highly ordered, right-handed protein polymer, referred to as the presynaptic filament, assembled on single-stranded DNA (ssDNA), that is generated via the nucleolytic processing of a primary lesion such as a DNA double-strand break (Galletto, Amitani, Baskin, & Kowalczykowski, 2006; Hilario, Amitani, Baskin, & Kowalczykowski, 2009; Ogawa, Yu, Shinohara, & Egelman, 1993; Sung & Klein, 2006; Yang, Yu, Seitz, Kowalczykowski, & Egelman, 2001; Yu, Jacobs, West, Ogawa, & Egelman, 2001). The initiation of homology search, complementary base pairing, and strand separation of the target homologous double-stranded DNA (dsDNA) occurs within the confines of the presynaptic filament (Bugreev & Mazin, 2004; Kowalczykowski, 1991; San Filippo, Sung, & Klein, 2008). ATP is required for the formation, maintenance, and functionality of the presynaptic filament (Baumann et al., 1996; San Filippo et al., 2008; Sung, 1994). In cells, timely assembly of the presynaptic filament is reliant on accessory factors termed “mediators,” which include Rad52 in yeast and the tumor suppressor BRCA2 in mammals (San Filippo et al., 2008).

Two distinct intermediates involving the Rad51 presynaptic filament have been described. The synaptic complex comprises the presynaptic filament and the incoming duplex DNA being aligned in homologous registry, with limited base pairing having been realized between the recombining DNA molecules (Bianco, Tracy, & Kowalczykowski, 1998). The postsynaptic complex represents a more advanced nucleoprotein intermediate in which extensive DNA strand exchange has occurred. A model that depicts the aforementioned nucleoprotein intermediates in HR is given in Fig. 1A.

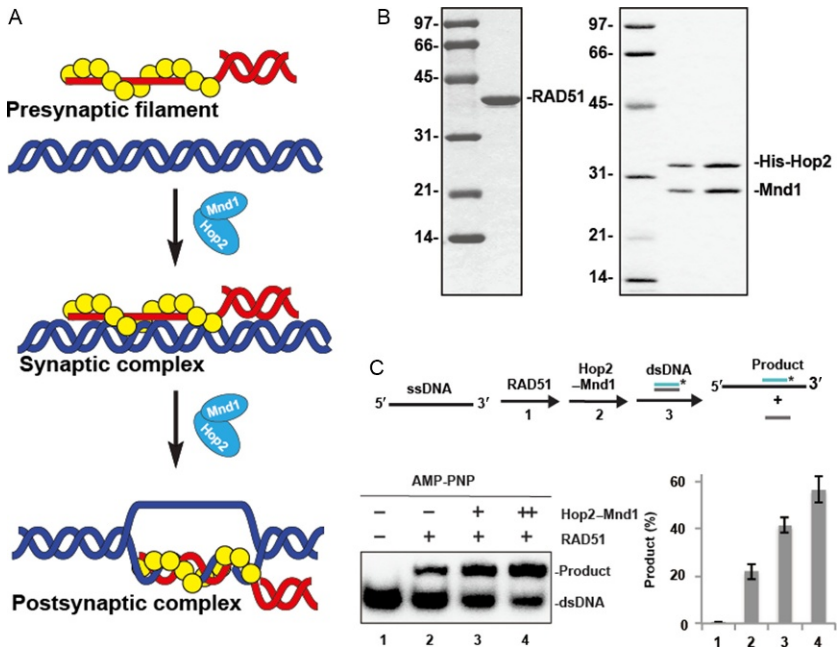


**Fig. 1** Intermediates in homologous DNA pairing and strand exchange mediated by hRAD51 in conjunction with Hop2-Mnd1. (A) hRAD51 (yellow circles) assembles on ssDNA for the presynaptic filament, which cooperates with Hop2-Mnd1 to search a dsDNA target for homology and then forms a synaptic complex with the latter. Transition into the postsynaptic state entails DNA strand exchange between the recombining to form a displacement loop, or D-loop. (B) Purity analysis of hRAD51 and mouse Hop2-Mnd1 by SDS-PAGE and Coomassie blue staining (Xu et al., 2017). (C) Schematic of the homologous DNA pairing and strand exchange reaction (upper) and results from a reaction that used hRAD51 in conjunction with Hop2-Mnd1 (lower, left). Quantification of data is also shown (lower, right) (Xu et al., 2017).

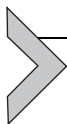
Previous studies on members of the conserved recombinase family, including analyses entailing X-ray crystallography and EM, have provided valuable information regarding the structure and function of these enzymes. Specifically, high-resolution X-ray crystal structures of the *E. coli* RecA protein and Rad51 from various organisms have furnished fine details of the ATP-binding pocket, the recombinase protomer-protomer interaction interface in the presynaptic filament, and the structure of the postsynaptic complex (Chen, Yang, & Pavletich, 2008; Conway et al., 2004; Pellegrini et al., 2002; Story, Weber, & Steitz, 1992; Wu, He, Moya, Qian, & Luo, 2004). While low-resolution EM structures have revealed the overall architecture of the recombinase assembly around DNA

molecules (Egelman, 2001; Sheridan et al., 2008; VanLoock et al., 2003; Yu et al., 2001), high resolution of the presynaptic, synaptic, and postsynaptic complexes that harbor human RAD51 (hRAD51) by cryo-EM is a recent development that we will cover later.

EM together with helical reconstruction represents an ideal structural tool in the determination of the filamentous nature of the recombinase assemblies. Recent technical advancement, such as the invention of the direct electron detector (Faruqi & Henderson, 2007; McMullan, Faruqi, Clare, & Henderson, 2014) and the implementation of new image processing algorithms (Brilot et al., 2012; Li et al., 2013; Scheres, 2012; Zheng et al., 2017), has rendered cryo-EM an exceptionally powerful approach for defining the structure and function of macromolecules in their native state at atomic or near-atomic resolution (Bai, McMullan, & Scheres, 2015; Cheng, Grigorieff, Penczek, & Walz, 2015; Nogales & Scheres, 2015). In this regard, we have developed protocols for the high-resolution structure determination of hRAD51 presynaptic and postsynaptic complexes and also for the medium-resolution reconstruction of the arrested synaptic state (Xu et al., 2017). This chapter describes these protocols in detail. It is our goal to make our methods and approach accessible to colleagues in the DNA repair and other fields.

Macromolecular helical assemblies fulfill divergent biological roles. Unique algorithms are available to define the properties of these assemblies. In fact, the first three-dimensional (3D) structure of a macromolecule assembly solved using EM, that of the extended tail of T4 bacteriophage, is a helical assembly (De Rosier & Klug, 1968). While the Fourier-Bessel helical reconstruction was the predominant algorithm for helical reconstruction for a few decades, iterative helical real space reconstruction (IHRSR) has since become the method of choice. This algorithm was initially implemented by Egelman and has been further refined in various software packages since then (Egelman, 2000, 2007). Briefly, IHRSR uses iterative projection matching to compare the segments from experimental EM images of helical assemblies with many projection images from a 3D reference model and searches for the best match to assign the optimal orientation angles of the experimental EM images. Then, the images are back-projected to generate an asymmetric 3D reconstruction. The helical parameters of the helical assembly are determined by the least-square self-correlation algorithm of the asymmetric 3D reconstruction and are imposed on the reconstruction to generate a symmetric 3D reference for the next iteration. The unique properties of a helical assembly would warrant the

convergence of the final solution if the initial reference or helical parameters are robust enough. The IHRSR algorithm been instrumental for solving the low-resolution structure of recombinase filaments (Egelman, 2001; VanLoock et al., 2003; Yu et al., 2001). Importantly, we have successfully combined advanced cryo-EM with the IHRSR algorithm to solve the structures of hRAD51 nucleoprotein complexes in different states of the homologous DNA and strand exchange reaction.

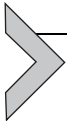


## 2. PURIFICATION OF hRAD51

Two isoforms of hRAD51, with Lys313 or Gln313, exist. These hRAD51 isoforms exhibit identical behavior during protein purification and in biochemical assays (Sigurdsson, Trujillo, Song, Stratton, & Sung, 2001). We have used the Gln313 isoform in our structural studies. The expression vector harboring the *hRAD51* gene is transformed into the RecA-deficient *E. coli* strain BLR (DE3) with pLysS. Single clones are picked from LB (Luria broth) agar plate containing 100  $\mu\text{g}/\text{mL}$  ampicillin, 34  $\mu\text{g}/\text{mL}$  chloramphenicol, and 12.5  $\mu\text{g}/\text{mL}$  tetracycline, inoculated into 40 mL LB with the above antibiotics, and cultured overnight at 37°C. Twenty milliliters of the culture are diluted into 1L fresh LB containing 100  $\mu\text{g}/\text{mL}$  ampicillin, 34  $\mu\text{g}/\text{mL}$  chloramphenicol, and cultured at 37°C until the optical density reaches 0.6–0.8 at 280 nm. The cells are treated with 1 mM IPTG at 37°C for 3–4 h to induce hRAD51 expression, harvested by centrifugation, and stored at –80°C.

All the protein purification steps are performed at 0–4°C. A 40-g *E. coli* cell pellet is resuspended in 200 mL breakage buffer (50 mM Tris–HCl pH 7.5, 1 M KCl, 0.5 M EDTA, 10% sucrose, 0.01% Igepal, 1 mM DTT, and the following protease inhibitors: aprotinin, chymostatin, leupeptin, and pepstatin A at 3  $\mu\text{g}/\text{mL}$  each, and 1 mM PMSF) and then subjected to sonication. The whole cell lysate is centrifuged at 100,000  $\times g$  for 1 h, and the supernatant is treated with ammonium sulfate at 40% saturation (0.242 g/mL). The precipitate is collected by centrifugation at 20,000  $\times g$  for 15 min. This procedure is repeated several more times until all the liquid is removed from the precipitate, which is then stored until further processing. For hRAD51 purification, the ammonium sulfate pellet is thawed on ice and centrifuged at 20,000  $\times g$  twice to remove residual liquid, then it is dissolved in 150 mL K buffer (20 mM  $\text{KH}_2\text{PO}_4$  pH 7.4, 10% glycerol, 0.5 mM EDTA, 0.01% Igepal, 1 mM DTT) and fractionated in a 40-mL Q-fast-flow Sepharose column with a 400-mL gradient from

200 to 600 mM KCl. The fractions (~380 mM KCl) are pooled, dialyzed against T buffer (25 mM Tris-HCl pH 7.5, 10% glycerol, 0.5 mM EDTA, 1 mM DTT) with 50 mM KCl for 90 min, before being fractionated in an 8 mL Macro-HAP (BioRad) column with a 120-mL gradient from 60 to 260 mM  $\text{KH}_2\text{PO}_4$ . The protein pool was dialyzed against T buffer as above and then fractionated in a 6-mL Source-Q column using an 80-mL gradient of 200–500 mM KCl. Fractions containing hRAD51, which elutes between 340 and 400 mM KCl, are pooled, dialyzed against T buffer, then fractionated in a 1-mL Mono-Q column with a 30-mL gradient of 200–450 mM KCl. Nearly homogeneous hRAD51 (Fig. 1B), eluting between 350 and 400 mM KCl, is concentrated to 1 mg/mL a Centricon-30K concentrator (Amicon) and stored in small aliquots (5–10  $\mu\text{L}$ ) at  $-80^\circ\text{C}$ . The recombinase activity of purified hRAD51 is tested in a strand exchange assay (Fig. 1C) (Chi, San Filippo, Sehorn, Petukhova, & Sung, 2007).



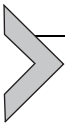
### 3. ASSEMBLY OF PRESYNAPTIC, POSTSYNAPTIC, AND ARRESTED SYNAPTIC COMPLEXES

The oligonucleotides used are listed in Table 1. For EM analysis, we omit bovine serum albumin and spermidine from the reaction as they would interfere with imaging. For presynaptic filament assembly, hRAD51 (2  $\mu\text{M}$ ) is incubated with either the 72-nt Oligonucleotide-1 or 150-nt Oligonucleotide-2 (6  $\mu\text{M}$  nucleotides) in reaction buffer (25 mM HEPES, pH 7.5, 25 mM KCl, 4 mM  $\text{MgCl}_2$ , and 4 mM AMP-PNP) at  $37^\circ\text{C}$  for 60 min. For generating the postsynaptic complex, presynaptic filaments formed on Oligonucleotide-2 is incubated with the mouse Hop2-Mnd1 complex (250 nM) purified as described in Chi et al. (2007) for 10 min, followed by the addition of the dsDNA substrate (5.1  $\mu\text{M}$  base pairs; prepared by annealing Oligonucleotide-2 and Oligonucleotide-3) and a 15-min incubation.

Capitalizing on the recent discovery that 8-nt of microhomology is sufficient for the presynaptic filament to engage dsDNA (Qi et al., 2015), we have been able to capture an intermediate corresponding to the transition from the synaptic stage to the postsynaptic complex. Specifically, we use a 72-nt ssDNA (Oligonucleotide-4) consisting of four 18-nt repeats to assemble presynaptic filaments, then allow the filaments to pair with an 18-bp dsDNA substrate (obtained by hybridizing Oligonucleotide-5 to Oligonucleotide-6) that bears 13-nt of homology to the repeats in Oligonucleotide-4. The reaction conditions are as described earlier.

**Table 1** DNA Oligonucleotides Used in This Study

| Oligo No.           | Sequence  |
|---------------------|---|
| Oligo 1<br>ssDNA    | 5'-TT<br>TT<br>TTTTTTTTTTTTTT-3'  |
| Oligo 2<br>dsDNA(-) | 5'-TAAATAAGATAAGGATAATACAAAATAAGT<br>AAATGAATAAACAGAGAAAATAAAGTAAAG<br>GATATAAAAAATGAACATAAAGAATAAGTA<br>AATGAATAAACATAATAGGAATAAATATA<br>GGAAATGAAATAAAGAGACATAAATAAGA-3'    |
| Oligo 3<br>dsDNA(+) | 5'-TCTTATTTATGTCTCTTTTATTTTCATTCC<br>TATATTTATTCCTATTATGTTTTATTCATT<br>TACTTATTCTTTATGTTTCATTTTTTATATC<br>CTTTACTTTATTTTCTCTGTTTATTCATTT<br>ACTTATTTTGTATTATCCTTATCTTATTTA-3' |
| Oligo 4<br>ssDNA    | 5'-TTTCCTATATTTATTCCTTTTCCTATATTT<br>ATTCCTTTTCCTATATTTATTCCTTTTCCT<br>ATATTTATTCCT-3'  |
| Oligo 5<br>dsDNA(-) | 5'-ATACGTAAATATAGGAAA-3'  |
| Oligo 6<br>dsDNA(+) | 5'-TTTCCTATATTTACGTAT-3'  |



## 4. NEGATIVE STAINING EM

We routinely test all samples by negative stain EM before conducting cryo-EM analysis, as it is a fast and cost-effective way to evaluate the homogeneity and quality of nucleoprotein filaments. Specifically, nucleoprotein filaments are embedded in a heavy-metal salt stain to yield good contrast. We use uranyl acetate to stain hRAD51-DNA assemblies, but suitable alternatives include ammonium molybdate, uranyl formate, and phosphotungstic acid.

Procedurally, a droplet of 3–5  $\mu\text{L}$  of a reaction mixture is loaded onto a glow-discharged carbon-coated grid (Zhongjingkeyi Company) for 1 min. After blotting with filter paper, the grid is immersed twice in a 40- $\mu\text{L}$  droplet of the staining solution (2% uranyl acetate) on Parafilm. The stain is removed from the grid by blotting with filter paper. Then, the grid is immersed in

another stain droplet for 1 min. Following stain removal, grids are dried in air for about 3 min. Grids thus prepared can be kept in the ambient environment away from dust for days or even months.

Negatively stained samples of hRAD51 presynaptic filaments as examined by transmission electron microscopy (TEM) are shown in Fig. 2A (assembled using AMP-PNP as the nucleotide cofactor and  $Mg^{2+}$ ) and Fig. 2B (assembled using ATP and  $Ca^{2+}$ ). These filaments appear as highly ordered helical structures with uniform density. In comparison, the use of ATP and  $Mg^{2+}$  leads to the formation of heterogeneous species, a large fraction of which correspond to either DNA-free ring-shaped hRAD51 oligomers or disordered filaments likely consisting of stacks of hRAD51

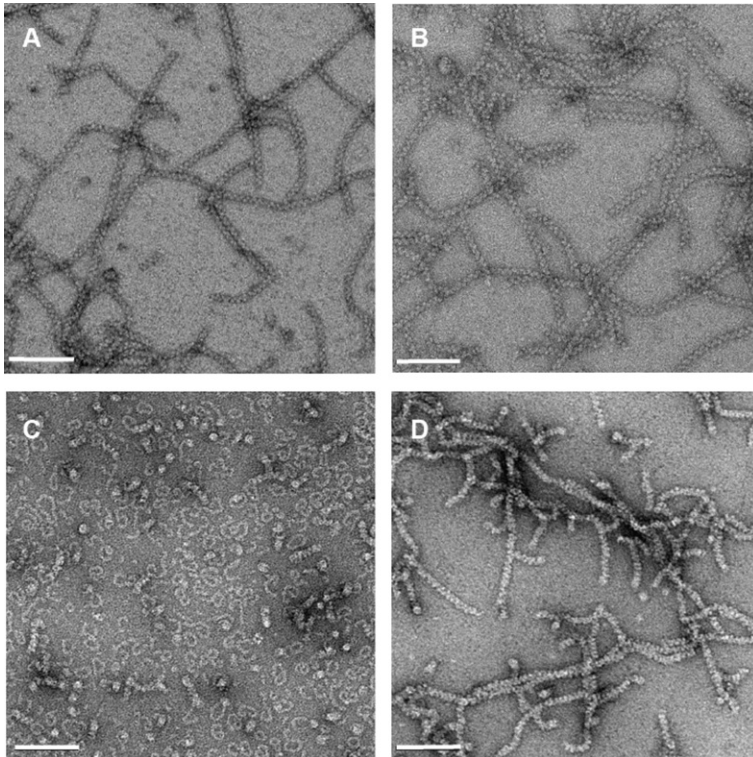


**Fig. 2** Negative staining EM micrographs of hRAD51 filaments. Presynaptic filaments of hRAD51 assembled with AMP-PNP and  $MgCl_2$  (A), with ATP and  $CaCl_2$  (B), or with ATP and  $MgCl_2$  (C). (D) A representative micrograph from a sample with bad batch of AMP-PNP for the RAD51 nucleoprotein filament assembly. The filaments appear as stacking of rings rather than in helical structures. The *scale bar* is 100 nm.

rings (Fig. 2C and D). We note that excessive or inadequate staining of the hRAD51 nucleoprotein filaments invariably affects how well the filaments can be visualized by TEM.



## 5. CRYO-EM SAMPLE PREPARATION

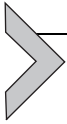
Once the quality of nucleoprotein filaments has been evaluated by TEM, they are ready for cryo-EM applications. There are different grid types for these applications, including a choice of metallic material (e.g., copper, gold, or molybdenum) and diverse mesh and hole sizes. We use Cu R1.2/1.3 400 mesh grids (Quantifoil) in our hRAD51 work.

The grids are first subjected to “glow discharging” to render their surface hydrophilic. When liquid is placed on the glow-discharged grid, it spreads evenly and, upon blotting, forms a film as thin as just tens of nanometers. The grid is immediately plunged into liquid ethane or propane cooled at liquid nitrogen temperature so that the liquid film becomes converted into vitreous ice that embeds the macromolecules. The hydrophilicity of the grid surface and the macromolecule’s properties can exert a strong influence on the distribution and thickness of the ice. In practice, we use a plasma cleaner (Harrick Plasma PDC-32G) to glow discharge the Quantifoil grids for 30 s at low intensity and prepare the cryo-EM specimens using a semiautomatic plunge instrument, the Vitrobot Mark IV (FEI Company).

The following is a typical protocol for preparing cryo-EM specimens of hRAD51 nucleoprotein filaments.

1. Turn on the Vitrobot and set the humidity to 100%, temperature to 16°C, blot-time to 3.5 s, and blot-force to -2. The optimal settings need to be predetermined for different machines and samples, especially for the blot-time and blot-force values.
2. Prepare the cryogen. Fill the container with liquid nitrogen around the cryogen cup until the cup is cooled below the boiling point of liquid nitrogen (when the liquid nitrogen stops bubbling violently). Fill the precooled cryogen cup completely with pure ethane gas at a controlled speed so that the ethane liquidizes in the cup.
3. Secure a glow-discharged EM grid with the Vitrobot tweezers and mount the tweezers to the Vitrobot’s arm.
4. Apply 4  $\mu$ L of reaction mixture containing RAD51 nucleoprotein filaments onto the carbon side of the EM grid and start the blotting and plunging process immediately on the Vitrobot.

5. Transfer the vitrified grid into a storage box in liquid nitrogen. Avoid exposure of the grid to atmospheric moisture during transfer.
6. Keep the grid storage box in a liquid nitrogen cryo-storage dewar.



## 6. CRYO-EM DATA COLLECTION

We evaluate the quality of the cryo-EM specimen by two criteria: (1) the concentration and stability of the filaments, (2) the ice thickness (the ideal thickness is just above the diameter of the filament) and uniformity across the grid. Fig. 3A and B illustrates a representative cryo-EM specimen of hRAD51 nucleoprotein filaments with uniform and proper ice thickness at low magnification and high magnification, respectively. In contrast, the

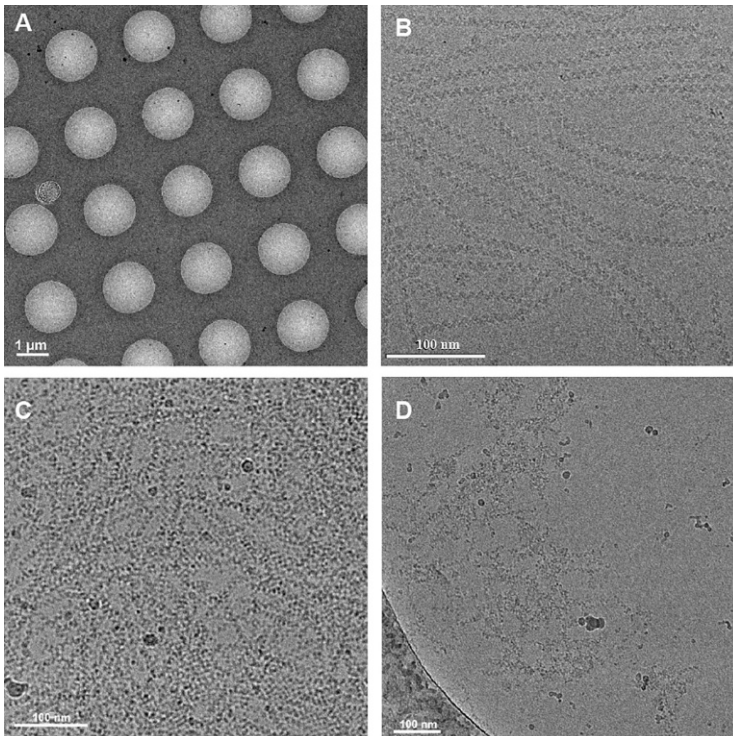
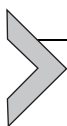


**Fig. 3** Representative cryo-EM micrographs of hRAD51 presynaptic filaments. (A) Shows cryo-EM samples of hRAD51 with uniform and proper ice thickness under low magnification. (B) Corresponds to the high magnification exposure in (A). (C) The filaments are too dense in the sample for data analysis. (D) An example of helical filaments that are not evenly distributed or are partially disassembled or denatured.

filaments are too dense in Fig. 3C and badly distributed or partially damaged by the air/water interface in Fig. 3D. For specimens that meet the quality criteria, we collect a small dataset comprising a few hundreds of micrographs and perform preliminary image processing such as reference-free two-dimensional (2D) classification as described in Section 7, so as to evaluate the structural homogeneity and sample quality. Large datasets of the specimens are then collected for generating 2D class averages to reveal detailed features and shapes.

For high-resolution cryo-EM data collection, the electron dose and defocus value are optimized to obtain the best possible signal, while minimizing radiation damage to the structure. In our structural studies of hRAD51 nucleoprotein filaments, grids are examined in a Titan Krios (FEI) microscope operated at the acceleration voltage of 300 kV and equipped with a K2 Summit direct electron detector device (Gatan). We collect data manually at a nominal magnification of 22,500 with the super resolution mode of the K2 camera, thus yielding a pixel size of 0.653 Å, with the UCSF-Image4 user interface (Li, Zheng, Agard, & Cheng, 2015). The specimen is exposed for a total duration of 8 s at a dose rate of  $\sim 6.2$  electrons per Å<sup>2</sup> per second as movie stacks each containing 32 frames with 0.25 s per frame. The defocus value for data collection ranges from  $-1.5$  to  $-2.5$  μm.



## 7. IMAGE PROCESSING AND RECONSTRUCTION

### 7.1 High-Resolution Cryo-EM Structures of Presynaptic and Postsynaptic Complexes

We use the IHRSR algorithm for the 3D reconstruction of hRAD51 filaments. We have been following the two workflows illustrated in Fig. 4A in the reconstructions. The procedural details are as follows.

The collected 32-frames movie stacks are subject to MotionCorr1 (Li et al., 2013) for whole frame-based motion correction and binned twofold. The program generates a drift-corrected sum of each movie stack, which is subsequently processed as a micrograph. For each micrograph, the CTF parameters are determined using the CTFFIND3 program (Mindell & Grigorieff, 2003) and the filaments with various length in each micrograph are manually picked using the program e2helixboxer.py within EMAN2 (Tang et al., 2007). Segments of each helical filament are extracted from overlapping boxes with a dimension of 256 pixels and 230 pixels along the helical axis. Two independent software packages are used to perform the IHRSR structural determination of the same dataset, one in SPIDER

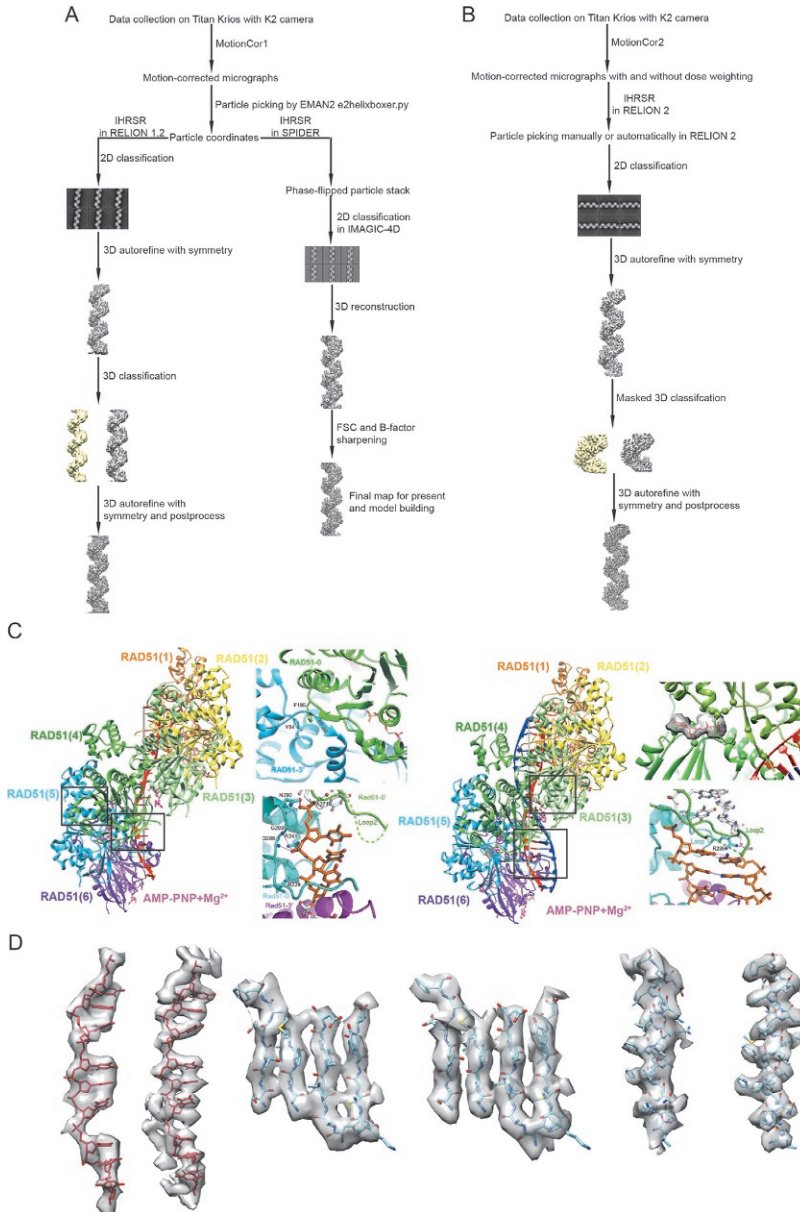


**Fig. 4** Workflow and results for high-resolution structure determination of the hRAD51 presynaptic and postsynaptic filaments (Xu et al., 2017). (A) The old method for the reconstruction of presynaptic and postsynaptic complexes. The reconstruction process is in SPIDER or a modified version of RELION 1.2. (B) The new RELION 2.0 reconstruction method. (C) The atomic model of the hRAD51 presynaptic (*left*) and postsynaptic (*right*)

and the other in a modified version of RELION 1.2 (Clemens, Ge, Lee, Horwitz, & Zhou, 2015; Frank et al., 1996; Scheres, 2012).

In the SPIDER reconstruction method, we reextract the picked particles from the micrographs that are CTF phase-flipped to generate a new particle stack. Reference-free 2D classification of the particles is performed in IMAGIC-4D package (van Heel, Harauz, Orlova, Schmidt, & Schatz, 1996) to screen for particles whose class averages show clear secondary structural information for further processing. The selected particles are then aligned iteratively in a SPIDER IHRSR script that incorporates the projection matching, searching for helical symmetry and symmetry imposing steps (Ge & Zhou, 2011). The initial model for the IHRSR script is generated with randomly assigned Euler angle and initial helical parameters of  $\Delta\varphi = 56.8$  degrees and  $\Delta z = 15.7 \text{ \AA}$  (a parameter set determined previously from negative staining EM analysis). The iterations proceed until the helical parameters and 3D reconstruction converge to a stable solution. As the particles are phase-flipped, the converged 3D map is corrected for the CTF amplitude calculated by dividing the map with the summation of the absolute values of CTF amplitude from all the micrographs and is further sharpened with an arbitrary B-factor of  $\sim 250 \text{ \AA}^2$ . The resolutions of the final reconstructions are estimated with Fourier shell correlation (FSC) 0.5 criterion between two reconstructions from randomly separated halves of the dataset.

In the RELION reconstruction method, the workflow in a modified version of RELION 1.2 implemented IHRSR is very similar to that of most single particle analysis (Clemens et al., 2015). We import the box file to RELION and extract particles from the micrographs. The particle stack is subjected to run reference-free 2D classification to exclude bad particles. The initial model used for 3D reconstruction/classification is a map low-pass filtered to  $60 \text{ \AA}$  resolution from the SPIDER reconstruction method.

---

filament built from high-resolution reconstructions. To the right of the presynaptic model, the *upper-right inset* shows the two conserved protomer-protomer interfaces in hRAD51, while the *lower-right* one presents the nucleotide triplet interaction with hRAD51 in the presynaptic state. To the right of the postsynaptic model, the *upper-right inset* shows an AMP-PNP buried in two neighboring hRAD51 and the *lower-right inset* exhibits the complementary strand in the postsynaptic complex interacting with Arg235. (D) Comparison of representative EM densities from the reconstructions by the old method (*left*) and the new method (*right*) docked with their corresponding atomic models. They are DNA density, four selected  $\beta$ -strand and one  $\alpha$ -helix from *left* to *right*, respectively.

The difference between 3D classification and autorefinement for helical structures and regular single particle is that at the end of each iteration, the program would search and impose helical symmetry for the asymmetric volume. After rounds of classification and autorefinement, we obtain the converged reconstructions that are similar to those calculated using the SPIDER method. To estimate the resolutions of the maps accurately, a soft mask covering three adjacent monomers are applied to the two volumes independently reconstructed from two randomly selected halves of the dataset, between which the “gold-standard” FSC is calculated. The resolutions are estimated according to the “gold-standard” FSC 0.143 criterion. Then, the maps are postprocessed in RELION 1.2 to manually filter to the real resolution and sharpened through applying a B-factor of about  $-250 \text{ \AA}^2$ .

Using the above-mentioned methods, we have achieved near-atomic resolution structures of hRAD51 in both the presynaptic and postsynaptic states at the resolution of  $\sim 4.4$  and  $\sim 4.5 \text{ \AA}$ , respectively. These structures share very similar helical parameters with a  $\sim 15.8 \text{ \AA}$  helical rise and  $56.77$  degrees twist, corresponding to  $6.3$  hRAD51 protomers per turn with a pitch of  $100 \text{ \AA}$ . These structures are of high enough resolution to permit the building of atomic models of the nucleoprotein complexes. An independent study from the Venkataraman’s group of the hRAD51 presynaptic filament reports results that are very similar to ours (Short et al., 2016). The available structures reveal key features of the hRAD51 complexes, especially the hRAD51 protomer/protomer interaction interface mediated by the ATP-binding pocket, the BRAC2-like beta-strand lateral interaction, association of hRAD51 with the phosphate backbone of DNA, and triplet base pairing in the matching of homologous ssDNA and dsDNA (Fig. 4C). The structures also furnish compelling evidence for the evolutionary conservation of nucleoprotein complexes involving hRAD51 and *E. coli* RecA. Both recombinases extend the bound ssDNA to  $\sim 1.5$  times the pitch of B-form DNA and organize neighboring DNA bases in discrete triplets in the presynaptic state. Moreover, the RecA/hRAD51 structures provide insights into how the complementary DNA strand in the duplex partner is paired with the stretched and triplet-clustered ssDNA. Importantly, our analysis has shown that Arginine-235 in hRAD51 interacts with and stabilizes the complementary strand in the postsynaptic complex (Fig. 4C). This finding may explain why the mutation of Arginine-235 in hRAD51 leads to the impairment of recombinase activity (Prasad, Yeykal, & Greene, 2006; Reymer, Frykholm, Morimatsu, Takahashi, & Nördén, 2009).

In our attempt to improve the resolution of the hRAD51 presynaptic filament, we have reprocessed the original dataset using the latest image processing algorithms (Fig. 4B). First, the motion-corrected 32-frames movie stacks are further aligned with smaller patches in MotionCor2 (Zheng et al., 2017) to generate two micrographs, one being the motion-corrected sum while the other dose-weighted sum. Second, the motion-corrected sum is used to perform CTF estimation with CTFFIND4 (Rohou & Grigorieff, 2015) or Gctf (Zhang, 2016) to speedup and improve the precision of the calculation. Third, particles are extracted from the dose-weighted sums, as the signal-to-noise ratio is increased in a new version of RELION 2 that implements the helical processing routine in a more user-friendly and robust fashion (He & Scheres, 2017). The workflow is almost the same as our general single-particle reconstruction protocol. A unique feature of RELION 2 is that it allows the picking of helical particles. Since RELION 2 supports acceleration by GPU (Kimanius, Forsberg, Scheres, & Lindahl, 2016), the refinement to a high-resolution structure can be completed with a single 8-GPU workstation within a few days. For more details on the helical reconstruction in RELION, see He and Scheres (2017).

Using the new procedure, we have been able to improve the resolution of the hRAD51 presynaptic filament from 4.4 to 3.6 Å using the same dataset. Within the refined structure, the major features are maintained, while some side chains are better resolved than in the previous reconstruction (Fig. 4D).

## 7.2 Cryo-EM Structure of an Arrested Synaptic Complex

We have modified our procedure for 3D reconstruction in order to accommodate the unique properties of the arrested synaptic complex. As there may exist structural differences within every 18-nt DNA repeat with six consecutive hRAD51 protomers, we have developed an algorithm to reconstruct the complex in hexameric repeats (Fig. 5A). This algorithm is inspired by the strategy developed for the reconstruction of microtubules (Zhang & Nogales, 2015). Particles are picked from the motion-corrected micrographs and extracted with overlapping boxes, 400 pixels long with 90 pixels' shift (corresponding to the pitch of the hexamer) along the helical axis between neighboring particles. The SPIDER reconstruction approach used in the presynaptic and postsynaptic reconstruction is applied to find the converged helical parameters of the arrested synaptic complex. Meanwhile, FREALIGN is employed for the 3D reconstruction (Grigorieff, 2007).

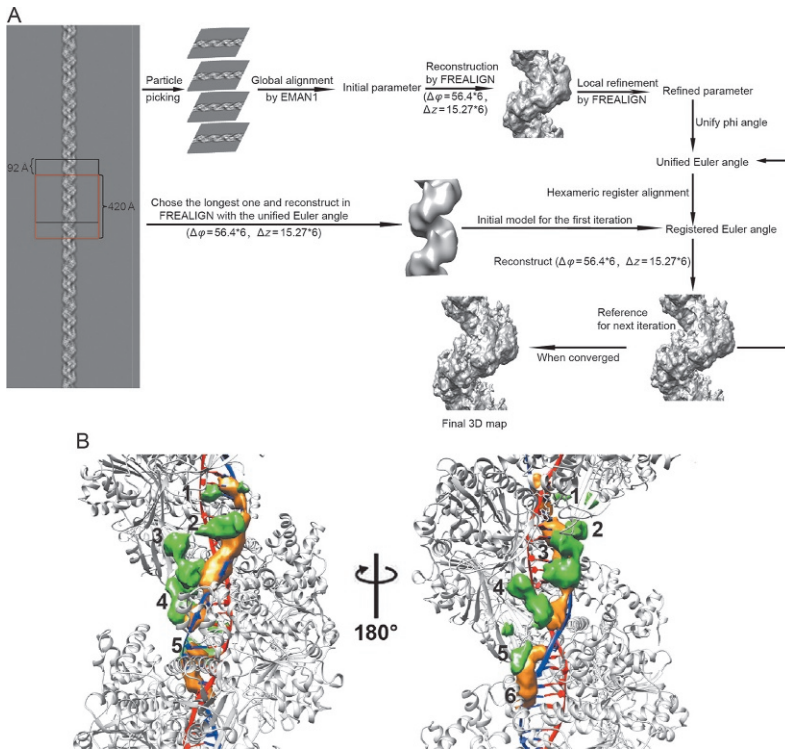
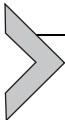


**Fig. 5** Structure of hRAD51 in the arrested synaptic state (Xu et al., 2017). (A) Workflow of the reconstruction for the arrested synaptic complex with hexameric hRAD51 protomers as an asymmetric unit. (B) The difference maps of the arrested synaptic complex subtracted by the atomic model of presynaptic complex (orange) and postsynaptic complex (green). The extra densities in green likely correspond to the displaced DNA strand.

The global parameters are obtained from the classesbymra program in EMAN (Ludtke, Baldwin, & Chiu, 1999) against the projections of reconstruction from SPIDER. Two rounds of local refinement are performed to accurately assign the Euler angle of each particle.

Next, the azimuthal angles of the particles from the same filament are reassigned to a unified series of values that are consistent with the helical symmetry of the structure, which we call “unify phi.” We then choose the particles from the longest filament and reconstruct the 3D volume with the hexameric hRAD51 protomer as the asymmetric unit, which is then used as reference to align all other filaments. As the specially designed dsDNA has a unique homologous pattern on the invading strand, it is important to align different filaments to ensure that the starting point within

consecutive hexameric hRAD51 protomers remains the same. There exist six possibilities that the particles from one filament could match with the reference, among which only one possibility with the highest cross-correlation value is correct (Zhang & Nogales, 2015). We calculate the crosscorrelation scores for each filament in all six possibilities and select the highest score as the reference register. We refer to the procedure as “register search.” We employ the most possible register of each filament to reconstruct a new map to serve as the reference for the next iteration. After several iterations, the Euler angles of each particle become stable, and the final reconstruction of the synaptic complex is obtained in FREALIGN. Using the above procedure, a 12-Å structure of the arrested synaptic complex can be obtained. Upon subtracting the atomic model of the presynaptic or postsynaptic complex from the map of the arrested complex, an extra density is clearly present in the first four hRAD51 protomers within the hexameric repeat (Fig. 5B). These results indicate that DNA strand exchange proceeds normally until the heterologous sequence is encountered. Therefore, the structure captures a state in which the DNA strand displaced as a consequence of DNA strand exchange is held by the secondary DNA-binding site of hRAD51.



## 8. CONCLUSION AND PERSPECTIVES

We have established versatile methods for determining the helical nucleoprotein filament structures of recombinases. With these methods, we have succeeded in solving the structures of hRAD51 in complex with ssDNA/dsDNA in the presynaptic and postsynaptic states at near-atomic resolution. These methods are applicable to studies of other recombinases such as the meiosis-specific Dmc1. Furthermore, the methods provide a useful tool to examine the structure and function of the myriad of accessory factors that regulate the dynamics and catalytic potential of the recombinase filaments, and also to elucidate the mechanism of action of chemical reagents designed to attenuate or enhance the activity of Rad51.

## ACKNOWLEDGMENTS

The authors thank J.L. Lei, Y.J. Xu for maintenance of the cryo-EM facility in the National Protein Science Facility (Beijing) at Tsinghua University, T. Yang for support in high-performance computation, and X.M. Li for help in data collection. We are grateful to E. Egelman for advice, to T. Baker for distributing the IHRSR scripts in the SPIDER package, and to P. Ge and Z.H. Zhou for distributing the IHRSR-incorporated version of RELION 1.2. Our laboratories are supported by the National Science Foundation of

China (Grant 31270765), the Key Research and Development Program of MOST (Grant 2016YFA0501100), and the Beijing Municipal Science & Technology Commission (Grant Z161100000116034) to H.-W.W., additional funding from the National Science Foundation of China (Grant 31700654) to L.Z., and by the US National Institutes of Health (Grants CA168635, ES007061, and CA220123) to P.S.

## REFERENCES

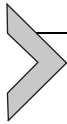
- Amunugama, R., & Fishel, R. (2012). Homologous recombination in eukaryotes. *Progress in Molecular Biology and Translational Science*, 110, 155–206. <https://doi.org/10.1016/B978-0-12-387665-2.00007-9>.
- Bai, X., McMullan, G., & Scheres, S. H. W. (2015). How cryo-EM is revolutionizing structural biology. *Trends in Biochemical Sciences*, 40(1), 49–57. <https://doi.org/10.1016/j.tibs.2014.10.005>.
- Baumann, P., Benson, F. E., & West, S. C. (1996). Human Rad51 protein promotes ATP-dependent homologous pairing and strand transfer reactions in vitro. *Cell*, 87(4), 757–766.
- Baumann, P., & West, S. C. (1998). Role of the human RAD51 protein in homologous recombination and double-stranded-break repair. *Trends in Biochemical Sciences*, 23(7), 247–251.
- Bianco, P. R., Tracy, R. B., & Kowalczykowski, S. C. (1998). DNA strand exchange proteins: A biochemical and physical comparison. *Frontiers in Bioscience*, 3, D570–D603.
- Brilot, A. F., Chen, J. Z., Cheng, A., Pan, J., Harrison, S. C., Potter, C. S., et al. (2012). Beam-induced motion of vitrified specimen on holey carbon film. *Journal of Structural Biology*, 177(3), 630–637. <https://doi.org/10.1016/j.jsb.2012.02.003>.
- Bugreev, D. V., & Mazin, A. V. (2004).  $\text{Ca}^{2+}$  activates human homologous recombination protein Rad51 by modulating its ATPase activity. *Proceedings of the National Academy of Sciences of the United States of America*, 101(27), 9988–9993. <https://doi.org/10.1073/pnas.0402105101>.
- Chen, Z., Yang, H., & Pavletich, N. P. (2008). Mechanism of homologous recombination from the RecA-ssDNA/dsDNA structures. *Nature*, 453(7194), 489.
- Cheng, Y., Grigorieff, N., Penczek, P. A., & Walz, T. (2015). A primer to single-particle cryo-electron microscopy. *Cell*, 161(3), 438–449. <https://doi.org/10.1016/j.cell.2015.03.050>.
- Chi, P., San Filippo, J., Sehorn, M. G., Petukhova, G. V., & Sung, P. (2007). Bipartite stimulatory action of the Hop2-Mnd1 complex on the Rad51 recombinase. *Genes & Development*, 21(14), 1747–1757.
- Clemens, D. L., Ge, P., Lee, B.-Y., Horwitz, M. A., & Zhou, Z. H. (2015). Atomic structure of T6SS reveals interlaced array essential to function. *Cell*, 160(5), 940–951. <https://doi.org/10.1016/j.cell.2015.02.005>.
- Conway, A. B., Lynch, T. W., Zhang, Y., Fortin, G. S., Fung, C. W., Symington, L. S., et al. (2004). Crystal structure of a Rad51 filament. *Nature Structural & Molecular Biology*, 11(8), 791.
- De Rosier, D. J., & Klug, A. (1968). Reconstruction of three dimensional structures from electron micrographs. *Nature*, 217(5124), 130–134.
- Egelman, E. H. (2000). A robust algorithm for the reconstruction of helical filaments using single-particle methods. *Ultramicroscopy*, 85(4), 225–234.
- Egelman, E. H. (2001). Does a stretched DNA structure dictate the helical geometry of RecA-like filaments? *Journal of Molecular Biology*, 309(3), 539–542. <https://doi.org/10.1006/jmbi.2001.4686>.
- Egelman, E. H. (2007). The iterative helical real space reconstruction method: Surmounting the problems posed by real polymers. *Journal of Structural Biology*, 157(1), 83–94.

- Faruqi, A., & Henderson, R. (2007). Electronic detectors for electron microscopy. *Current Opinion in Structural Biology*, 17(5), 549–555.
- Frank, J., Radermacher, M., Penczek, P., Zhu, J., Li, Y., Ladjadj, M., et al. (1996). SPIDER and WEB: Processing and visualization of images in 3D electron microscopy and related fields. *Journal of Structural Biology*, 116(1), 190–199. <https://doi.org/10.1006/jsbi.1996.0030>.
- Galletto, R., Amitani, I., Baskin, R. J., & Kowalczykowski, S. C. (2006). Direct observation of individual RecA filaments assembling on single DNA molecules. *Nature*, 443(7113), 875.
- Ge, P., & Zhou, Z. H. (2011). Hydrogen-bonding networks and RNA bases revealed by cryo electron microscopy suggest a triggering mechanism for calcium switches. *Proceedings of the National Academy of Sciences of the United States of America*, 108(23), 9637–9642. <https://doi.org/10.1073/pnas.1018104108>.
- Grigorieff, N. (2007). FREALIGN: High-resolution refinement of single particle structures. *Journal of Structural Biology*, 157(1), 117–125. <https://doi.org/10.1016/j.jsb.2006.05.004>.
- He, S., & Scheres, S. H. W. (2017). Helical reconstruction in RELION. *Journal of Structural Biology*, 198(3), 163–176. <https://doi.org/10.1016/j.jsb.2017.02.003>.
- Hilario, J., Amitani, I., Baskin, R. J., & Kowalczykowski, S. C. (2009). Direct imaging of human Rad51 nucleoprotein dynamics on individual DNA molecules. *Proceedings of the National Academy of Sciences of the United States of America*, 106(2), 361–368.
- Kimanius, D., Forsberg, B. O., Scheres, S. H. W., & Lindahl, E. (2016). Accelerated cryo-EM structure determination with parallelisation using GPUs in RELION-2. *eLife*, 5, e18722. <https://doi.org/10.7554/eLife.18722>.
- Kowalczykowski, S. C. (1991). Biochemistry of genetic recombination: Energetics and mechanism of DNA strand exchange. *Annual Review of Biophysics and Biophysical Chemistry*, 20, 539–575. <https://doi.org/10.1146/annurev.bb.20.060191.002543>.
- Li, X., Mooney, P., Zheng, S., Booth, C. R., Braunfeld, M. B., Gubbens, S., et al. (2013). Electron counting and beam-induced motion correction enable near-atomic-resolution single-particle cryo-EM. *Nature Methods*, 10(6), 584–590. <https://doi.org/10.1038/nmeth.2472>. <http://www.nature.com/nmeth/journal/v10/n6/abs/nmeth.2472.html#supplementary-information>.
- Li, X., Zheng, S., Agard, D. A., & Cheng, Y. (2015). Asynchronous data acquisition and on-the-fly analysis of dose fractionated cryoEM images by UCSFImage. *Journal of Structural Biology*, 192(2), 174–178. <https://doi.org/10.1016/j.jsb.2015.09.003>.
- Ludtke, S. J., Baldwin, P. R., & Chiu, W. (1999). EMAN: Semiautomated software for high-resolution single-particle reconstructions. *Journal of Structural Biology*, 128(1), 82–97. <https://doi.org/10.1006/jsbi.1999.4174>.
- McMullan, G., Faruqi, A. R., Clare, D., & Henderson, R. (2014). Comparison of optimal performance at 300 keV of three direct electron detectors for use in low dose electron microscopy. *Ultramicroscopy*, 147, 156–163. <https://doi.org/10.1016/j.ultramicro.2014.08.002>.
- Mindell, J. A., & Grigorieff, N. (2003). Accurate determination of local defocus and specimen tilt in electron microscopy. *Journal of Structural Biology*, 142(3), 334–347. [https://doi.org/10.1016/S1047-8477\(03\)00069-8](https://doi.org/10.1016/S1047-8477(03)00069-8).
- Nogales, E., & Scheres, S. H. (2015). Cryo-EM: A unique tool for the visualization of macromolecular complexity. *Molecular Cell*, 58(4), 677–689. <https://doi.org/10.1016/j.molcel.2015.02.019>.
- Ogawa, T., Yu, X., Shinohara, A., & Egelman, E. H. (1993). Similarity of the yeast RAD51 filament to the bacterial RecA filament. *Science (New York, NY)*, 259(5103), 1896–1899.
- Pellegrini, L., Yu, D. S., Lo, T., Anand, S., Lee, M., Blundell, T. L., et al. (2002). Insights into DNA recombination from the structure of a RAD51-BRCA2 complex. *Nature*, 420(6913), 287–293. <https://doi.org/10.1038/nature01230>.

- Prasad, T. K., Yeykal, C. C., & Greene, E. C. (2006). Visualizing the assembly of human Rad51 filaments on double-stranded DNA. *Journal of Molecular Biology*, 363(3), 713–728. <https://doi.org/10.1016/j.jmb.2006.08.046>.
- Qi, Z., Redding, S., Lee, J. Y., Gibb, B., Kwon, Y., Niu, H., et al. (2015). DNA sequence alignment by microhomology sampling during homologous recombination. *Cell*, 160(5), 856–869.
- Reymer, A., Frykholm, K., Morimatsu, K., Takahashi, M., & Nordén, B. (2009). Structure of human Rad51 protein filament from molecular modeling and site-specific linear dichroism spectroscopy. *Proceedings of the National Academy of Sciences of the United States of America*, 106(32), 13248–13253. <https://doi.org/10.1073/pnas.0902723106>.
- Rohou, A., & Grigorieff, N. (2015). CTFFIND4: Fast and accurate defocus estimation from electron micrographs. *Journal of Structural Biology*, 192(2), 216–221. <https://doi.org/10.1016/j.jsb.2015.08.008>.
- San Filippo, J., Sung, P., & Klein, H. (2008). Mechanism of eukaryotic homologous recombination. *Annual Review of Biochemistry*, 77(1), 229–257. <https://doi.org/10.1146/annurev.biochem.77.061306.125255>.
- Scheres, S. H. W. (2012). RELION: Implementation of a Bayesian approach to cryo-EM structure determination. *Journal of Structural Biology*, 180(3), 519–530. <https://doi.org/10.1016/j.jsb.2012.09.006>.
- Sheridan, S. D., Yu, X., Roth, R., Heuser, J. E., Sehorn, M. G., Sung, P., et al. (2008). A comparative analysis of Dmc1 and Rad51 nucleoprotein filaments. *Nucleic Acids Research*, 36(12), 4057–4066. <https://doi.org/10.1093/nar/gkn352>.
- Shinohara, A., Ogawa, H., & Ogawa, T. (1992). Rad51 protein involved in repair and recombination in *S. cerevisiae* is a RecA-like protein. *Cell*, 69(3), 457–470.
- Short, J. M., Liu, Y., Chen, S., Soni, N., Madhusudhan, M. S., Shivji, M. K., et al. (2016). High-resolution structure of the presynaptic RAD51 filament on single-stranded DNA by electron cryo-microscopy. *Nucleic Acids Research*, 44(19), 9017–9030.
- Sigurðsson, S., Trujillo, K., Song, B., Stratton, S., & Sung, P. (2001). Basis for avid homologous DNA strand exchange by human Rad51 and RPA. *The Journal of Biological Chemistry*, 276(12), 8798–8806. <https://doi.org/10.1074/jbc.M010011200>.
- Story, R. M., Weber, I. T., & Steitz, T. A. (1992). The structure of the *E. coli* recA protein monomer and polymer. *Nature*, 355(6358), 318–325.
- Sung, P. (1994). Catalysis of ATP-dependent homologous DNA pairing and strand exchange by yeast RAD51 protein. *Science*, 265(5176), 1241–1244.
- Sung, P., & Klein, H. (2006). Mechanism of homologous recombination: Mediators and helicases take on regulatory functions. *Nature Reviews. Molecular Cell Biology*, 7(10), 739.
- Tang, G., Peng, L., Baldwin, P. R., Mann, D. S., Jiang, W., Rees, I., et al. (2007). EMAN2: An extensible image processing suite for electron microscopy. *Journal of Structural Biology*, 157(1), 38–46. <https://doi.org/10.1016/j.jsb.2006.05.009>.
- van Heel, M., Harauz, G., Orlova, E. V., Schmidt, R., & Schatz, M. (1996). A new generation of the IMAGIC image processing system. *Journal of Structural Biology*, 116(1), 17–24. <https://doi.org/10.1006/jsbi.1996.0004>.
- VanLoock, M. S., Yu, X., Yang, S., Lai, A. L., Low, C., Campbell, M. J., et al. (2003). ATP-mediated conformational changes in the RecA filament. *Structure*, 11(2), 187–196. [https://doi.org/10.1016/S0969-2126\(03\)00003-0](https://doi.org/10.1016/S0969-2126(03)00003-0).
- Wu, Y., He, Y., Moya, I. A., Qian, X., & Luo, Y. (2004). Crystal structure of archaeal recombinase RadA. *Molecular Cell*, 15(3), 423–435. <https://doi.org/10.1016/j.molcel.2004.07.014>.
- Xu, J., Zhao, L., Xu, Y., Zhao, W., Sung, P., & Wang, H.-W. (2017). Cryo-EM structures of human recombinase RAD51 filaments in the catalysis of DNA strand exchange. *Nature Structural & Molecular Biology*, 24(1), 40.

- Yang, S., Yu, X., Seitz, E. M., Kowalczykowski, S. C., & Egelman, E. H. (2001). Archaeal RadA protein binds DNA as both helical filaments and octameric rings. *Journal of Molecular Biology*, *314*(5), 1077–1085.
- Yu, X., Jacobs, S. A., West, S. C., Ogawa, T., & Egelman, E. H. (2001). Domain structure and dynamics in the helical filaments formed by RecA and Rad51 on DNA. *Proceedings of the National Academy of Sciences of the United States of America*, *98*(15), 8419–8424. <https://doi.org/10.1073/pnas.111005398>.
- Zhang, K. (2016). Gctf: Real-time CTF determination and correction. *Journal of Structural Biology*, *193*(1), 1–12. <https://doi.org/10.1016/j.jsb.2015.11.003>.
- Zhang, R., & Nogales, E. (2015). A new protocol to accurately determine microtubule lattice seam location. *Journal of Structural Biology*, *192*(2), 245–254. <https://doi.org/10.1016/j.jsb.2015.09.015>.
- Zheng, S. Q., Palovcak, E., Armache, J.-P., Verba, K. A., Cheng, Y., & Agard, D. A. (2017). MotionCor2: Anisotropic correction of beam-induced motion for improved cryo-electron microscopy. *Nature Methods*, *14*(4), 331–332. <https://doi.org/10.1038/nmeth.4193>. <http://www.nature.com/nmeth/journal/v14/n4/abs/nmeth.4193.html#supplementary-information>.

This page intentionally left blank



# Observation and Analysis of RAD51 Nucleation Dynamics at Single-Monomer Resolution

Shyamal Subramanyam<sup>\*,2</sup>, Colin D. Kinz-Thompson<sup>†</sup>,  
Ruben L. Gonzalez Jr.<sup>†,1</sup>, Maria Spies<sup>\*,1</sup>

<sup>\*</sup>University of Iowa Carver College of Medicine, Iowa City, IA, United States

<sup>†</sup>Columbia University, New York, NY, United States

<sup>1</sup>Corresponding authors: e-mail address: rlg2118@columbia.edu; maria-spies@uiowa.edu

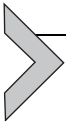
## Contents

|   |     |
|---|-----|
| 1. Introduction   | 202 |
| 2. Observing RAD51 Nucleation on ssDNA Using Total Internal Reflection Fluorescence Microscopy  | 206 |
| 2.1 Total Internal Reflection Fluorescence Microscope   | 206 |
| 2.2 Preparation of Fluorophore-Labeled DNA Substrates   | 207 |
| 2.3 Preparation of Reagents for Single-Molecule Experiments   | 209 |
| 2.4 Oxygen-Scavenging System  | 210 |
| 2.5 Surface Passivation and Functionalization, and Tethering of the DNA Substrates  | 211 |
| 2.6 Acquisition of Single-Molecule Data for Equilibrium-Binding Experiments   | 213 |
| 2.7 Acquisition of Single-Molecule Kinetic Data for Preequilibrium Experiments  | 214 |
| 2.8 Extracting and Organizing Single-Molecule Fluorescence Trajectories   | 214 |
| 3. Ensemble Analysis of Single-Molecule Data  | 217 |
| 3.1 Preparing $E_{\text{FRET}}$ Histograms  | 217 |
| 4. Real-Time Observation and Analysis of RAD51 Nucleation Using ebFRET  | 219 |
| 4.1 Using Hidden Markov Models to Analyze Single-Molecule Data  | 219 |
| 4.2 Using ebFRET to Determine the Set of HMMs That Are Consistent With an Entire Population of $E_{\text{FRET}}$ Trajectories                       | 223 |
| 4.3 Selecting the HMM That Best Describes the Entire Population of $E_{\text{FRET}}$ Trajectories and Analyzing the Corresponding Kinetic Mechanism | 225 |
| 5. Conclusions  | 227 |
| Acknowledgments   | 229 |
| References  | 229 |

<sup>2</sup> Present address: Memorial Sloan-Kettering Cancer Center, New York, NY, United States.

## Abstract

Human RAD51 promotes accurate DNA repair by homologous recombination and is involved in protection and repair of damaged DNA replication forks. The active species of RAD51 and related recombinases in all organisms is a nucleoprotein filament assembled on single-stranded DNA (ssDNA). The formation of a nucleoprotein filament competent for the recombination reaction, or for DNA replication support, is a delicate and strictly regulated process, which occurs through filament nucleation followed by filament extension. The rates of these two phases of filament formation define the capacity of RAD51 to compete with the ssDNA-binding protein RPA, as well as the lengths of the resulting filament segments. Single-molecule approaches can provide a wealth of quantitative information on the kinetics of RAD51 nucleoprotein filament assembly, internal dynamics, and disassembly. In this chapter, we describe how to set up a single-molecule total internal reflection fluorescence microscopy experiment to monitor the initial steps of RAD51 nucleoprotein filament formation in real-time and at single-monomer resolution. This approach is based on the unique, stretched-ssDNA conformation within the recombinase nucleoprotein filament and follows the efficiency of Förster resonance energy transfer ( $E_{\text{FRET}}$ ) between two DNA-conjugated fluorophores. We will discuss the practical aspects of the experimental setup, extraction of the FRET trajectories, and how to analyze and interpret the data to obtain information on RAD51 nucleation kinetics, the mechanism of nucleation, and the oligomeric species involved in filament formation.



## 1. INTRODUCTION

The RAD51 DNA strand-exchange protein (recombinase) is critical for the stability of the human genome. It is a key player in homologous recombination, which provides the most accurate means to repair such deleterious DNA lesions as double-strand DNA breaks, interstrand DNA cross-links, and collapsed replication forks (Ameziane et al., 2015; Li & Heyer, 2008; Michl, Zimmer, & Tarsounas, 2016; Moynahan & Jasin, 2010). RAD51 also helps to maintain the integrity of damaged replication forks (Kolinjivadi et al., 2017; Schlacher et al., 2011; Schlacher, Wu, & Jasin, 2012). It is important for the cell, however, to maintain an exact balance in the amount and engagement of RAD51, as both its dearth and overabundance can have deleterious consequences. RAD51 overexpression and misregulation, for example, promote genome instability and allow cancerous cells to develop resistance to radiation and DNA-damaging drugs used in chemotherapy (reviewed in Budke, Lv, Kozikowski, & Connell, 2016; Klein, 2008). Both the recombination- and replication-associated functions of RAD51 depend on the RAD51 nucleoprotein filament assembled on single-stranded DNA (ssDNA). In recombination, the RAD51

nucleoprotein filament catalyzes the reciprocal exchange of DNA sequences between the damaged and template molecules. In DNA replication, RAD51 protects stalled replication forks from excessive nucleolytic degradation by the MRE11 nuclease via a mechanism that may or may not involve the exchange of DNA strands (Kolinjivadi et al., 2017; Schlacher et al., 2011, 2012). The ability to selectively manipulate the two functions of the RAD51 nucleoprotein filament can have significant biomedical implications, but it requires knowledge regarding how RAD51 nucleoprotein filaments assemble on the recombination and replication intermediates, and whether the two types of RAD51 nucleoprotein filaments have distinct mechanistic or structural features that can be selectively manipulated. Such information can be obtained through the quantitative analysis, at the single-molecule level, of the kinetics of the RAD51 nucleoprotein filament assembly.

Human RAD51 is a member of the highly conserved family of ATP-dependent recombinases. Recombinases from all species, including bacteriophage UvsX, bacterial RecA, archaeal RadA, yeast Rad51, and human RAD51 share significant structural and functional similarities. A conserved feature of these RecA-like recombinases is that the active, ATP-bound form of the recombinase assembles on the ssDNA into a right-handed, helical nucleoprotein filament (i.e., a presynaptic filament). The formation of a nucleoprotein competent for DNA strand-exchange reaction requires a bound nucleotide cofactor, either ATP or a nonhydrolyzable ATP analog. Each recombinase monomer within the filament occludes three nucleotides of ssDNA, and the ssDNA within the active form of the filament is extended approximately 1.6-fold beyond its B-form (Benson, Stasiak, & West, 1994; Galkin et al., 2005; Qiu et al., 2013; Ristic et al., 2005; Short et al., 2016; Subramanyam, Jones, Spies, & Spies, 2013; Xu et al., 2016). Crystallographic studies of bacterial RecA (Chen, Yang, & Pavletich, 2008) and high-resolution electron microscopy (EM) studies of human RAD51 (Short et al., 2016; Xu et al., 2016) revealed the remarkably conserved and very unusual structure of the recombinase-extended ssDNA within the presynaptic filament. In each triplet base, the ssDNA extension is not uniform, with the inner triplet bases maintaining stacking interactions and a near-B-DNA conformation, while the backbone between the adjacent triplet bases exhibits significant local stretching ( $\sim 8 \text{ \AA}$ ). The inactive (e.g., ADP-bound) form of the RecA or RAD51 nucleoprotein filament is shorter and more compressed compared to the active, ATP-bound state (Yu, Jacobs, West, Ogawa, & Egelman, 2001). Universal organization of the extended DNA structure within the active recombinase filament is

likely to be important for the processes of homology search and DNA strand exchange. Indeed, recent single-molecule studies from the Greene lab (Qi et al., 2015) revealed that homology sampling, at least during the very initial steps in the DNA strand-exchange reaction, proceeds in three-nucleotide steps, and the fidelity of the recombinase-mediated DNA strand-exchange reaction being defined by the subsequent stabilization of DNA triplet bases.

While the overall conservation of the nucleoprotein filament is striking, the idiosyncratic features of the recombinases from different species are manifold. These include the mechanism of nucleoprotein filament assembly. All recombinases are believed to form the presynaptic filament by a nucleation event that is followed by filament growth (Chabbert, Cazenave, & Helene, 1987) (Fig. 1A). The rates, cooperativity, and mechanisms of the nucleation and growth phases define the segments' lengths within the nucleoprotein filament, which may in turn have significant influence on the mechanism of homology search and the DNA strand-exchange reaction, as well as on the requirement for, and sensitivity to, different recombination mediators, various auxiliary proteins, and antirecombinases. Scanning force microscopy studies revealed a diversity of shapes, lengths, and regularities in the organization of human RAD51 nucleoprotein filaments assembled in the presence of different nucleotide cofactors, with more regular filaments corresponding to the conditions that promote the DNA strand-exchange reaction (Ristic et al., 2005).

Several single-molecule approaches have been developed for the analysis of recombinase nucleoprotein filament formation, dynamics, and disassembly (see Bell & Kowalczykowski, 2016; Candelli, Modesti, Peterman, & Wuite, 2013 for relatively recent comprehensive reviews). Each of these approaches provides uniquely valuable information on different aspects of this process. The optical (Amitani, Liu, Dombrowski, Baskin, & Kowalczykowski, 2010; Bell & Kowalczykowski, 2016) or magnetic tweezers (Arata et al., 2009; Ristic et al., 2005; van der Heijden et al., 2007) experiments that monitor RecA or RAD51 nucleoprotein formation by following the changes in the mechanical properties of the DNA molecule have sufficiently high resolution to detect binding or dissociation of individual recombinase molecules. These analyses, however, cannot unambiguously separate ssDNA extension arising from multiple nucleation sites. Additionally, tension exerted on the DNA may affect nucleoprotein filament formation and dynamics. Visualization of fluorophore-labeled RecA (Forget & Kowalczykowski, 2012) and RAD51 (Candelli et al., 2014; Forget & Kowalczykowski, 2010) forming nucleoprotein filaments on

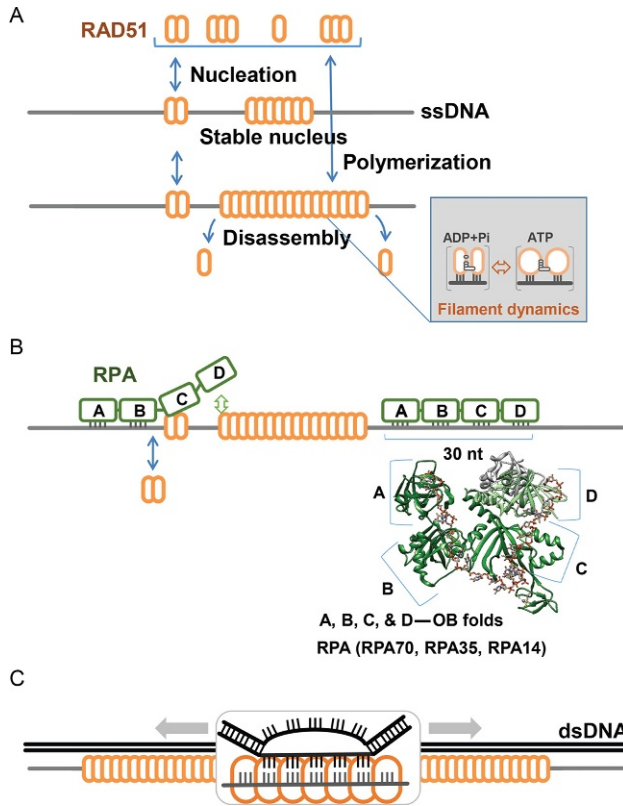
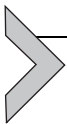


**Fig. 1** Dynamics of human RAD51 nucleation. (A) Reversible nucleation of RAD51 onto ssDNA. Human RAD51 binds ssDNA in an ATP-dependent manner (Tomblin, Shim, & Fishel, 2002). The ATP-bound RAD51 nucleoprotein assembles on ssDNA by first forming a stable nucleus, which can grow to form longer RAD51 nucleoprotein filaments in the polymerization phase. Both the RAD51 filament nucleation and polymerization are dynamic processes. Each RAD51 monomer within the filament binds three nucleotides forming the active pairing unit in the DNA strand-exchange reactions. Hydrolysis of ATP lowers the RAD51 affinity for ssDNA and leads to turnover or disassembly of the nucleoprotein filament. (B) To form nucleoprotein filaments and perform strand invasion and recombinase activities within the cell, human RAD51 has to compete with replication protein A (RPA), the ssDNA-binding protein. The stability of the RAD51 nucleus and its extension define the capacity of RAD51 to favorably compete with RPA. (C) The strand invasion and homology search by the RAD51 nucleoprotein filament allows it to invade homologous duplex DNA, resulting in a displacement loop structure that can be used as a primer for synthesis of DNA using the intact duplex as a template, resulting in accurate repair of damaged DNA.

DNA molecules extended by hydrodynamic flow or optical tweezers provided information on the kinetics of filament nucleation and growth originating from distinct nuclei. The drawback of these experiments is that they require “dipping” of the DNA molecule into the solution of fluorescently labeled recombinase and, therefore, only provide discrete snapshots of the reaction. Power analysis of the time dependence of filament length is used to deduce the oligomeric species involved in the nucleation and growth phases. The two phases can be distinguished by performing several cycles of “dipping” and observation. [Candelli et al. \(2014\)](#), for example, showed that the RAD51 nucleoprotein filaments grow on ssDNA from heterogeneous nuclei ranging in size from oligomers to dimers and even monomers. This assay, however, is blind to the dynamics of the nucleation step per se. These initial steps of recombinase filament formation can instead be observed and analyzed using a Förster resonance energy transfer (FRET)-based single-molecule assay enabled by total internal reflection fluorescence microscopy (TIRFM). Here, a FRET donor (typically Cy3) and a FRET acceptor (typically Cy5) are incorporated into the DNA substrate, which is then immobilized on the surface of a TIRFM observation flow cell. Binding and dissociation of the recombinase results in increases and decreases to the length of the DNA, respectively, which in turn causes decreases and increases in the FRET efficiency ( $E_{\text{FRET}}$ ) signal (a measure of nonradiative energy transfer from the FRET donor to the FRET acceptor), respectively. This approach has been applied to study RecA ([Joo et al., 2006](#)), yeast Rad51 ([Qiu et al., 2013](#)), and human RAD51 ([Subramanyam, Ismail, Bhattacharya, & Spies, 2016](#)) nucleation on ssDNA. These studies showed that while nucleation by RecA and yeast Rad51 occurs mainly via addition of RecA ([Joo et al., 2006](#)) or Rad51 ([Qiu et al., 2013](#)) monomers, human RAD51 nucleates on the ssDNA primarily via addition of RAD51 dimers ([Subramanyam et al., 2016](#)). In this chapter, we provide a protocol for the observation, analysis, and interpretation of human RAD51 filament formation by single-molecule FRET (smFRET).



## **2. OBSERVING RAD51 NUCLEATION ON ssDNA USING TOTAL INTERNAL REFLECTION FLUORESCENCE MICROSCOPY**

### **2.1 Total Internal Reflection Fluorescence Microscope**

TIRFM provides a convenient system to observe fluorophore-labeled molecules tethered to the surface of a passivated, functionalized observation

flow cell. The basic TIRF microscope comes in three main types: prism based, objective based, and micromirror based (see [Axelrod, 2008](#); [Larson et al., 2014](#) for detailed descriptions of these types of microscopes). The single-molecule RAD51 filament formation assay can be performed using any of the three microscope configurations. For FRET-based measurements, a single excitation source is sufficient, but the emission signal needs to be recorded in a dual-view system, which separates the emission of the FRET donor and FRET acceptor. Our TIRF-FRET setup uses Cy3 as a donor fluorophore (excited by a 532 nm, DPSS Laser; Coherent Inc.) and Cy5 as an acceptor fluorophore. An evanescent wave generated by total internal reflection of the laser source specifically illuminates molecules that are tethered to the surface of the observation flow cell ( $<100$  nm) ([Axelrod, 2008](#); [Bain, Wu, & Spies, 2016](#)). The scattered light is removed using a Cy3/Cy5 dual band-pass filter (Semrock, FF01-577/690) in the emission optical path. Images are chromatically separated into Cy3 image (using a Chroma ET605/70m filter) and Cy5 image (using a Chroma ET700/75m filter) using a 630-nm dichroic mirror inside the dual-view system (DV2; Photometrics) ([Fig. 2A](#)). An evanescent wave generated by total internal reflection of the laser source specifically illuminates molecules that are tethered to the surface of the slide ( $<100$  nm) ([Axelrod, 2008](#); [Bain et al., 2016](#)) ([Fig. 2B](#)).

## 2.2 Preparation of Fluorophore-Labeled DNA Substrates

DNA oligonucleotides can be site-specifically labeled with a wide range of fluorophores compatible with most single-molecule TIRFM setups and are available for purchase through commercial companies like IDT, MWG, Operon, etc. In order to visualize the RAD51 nucleoprotein filaments using our FRET-based assay and TIRF microscope, a DNA substrate labeled with a Cy3 donor fluorophore and a Cy5 acceptor fluorophore is prepared and immobilized on the surface of the observation flow cell. A biotin-Neutravidin interaction is used for tethering the substrate to the surface. Therefore, the substrate has to contain a biotin moiety in addition to two fluorophores. The Cy3 and Cy5 fluorophores are positioned such that there will be a sufficient, appreciable change in the  $E_{\text{FRET}}$  signal upon binding of RAD51 to the substrate. We use a biotinylated oligonucleotide substrate that is composed of two ssDNA oligonucleotides. The first is a short anchor oligo containing the Cy5 fluorophore at the 5' and the biotin tag at the 3' end (5Cy5-Bot18-3Bio 5'Cy5-GCCTCGCTGCCGTCGCCA-3'Bio) is used to tether the DNA to the surface of the observation flow cell. The second oligonucleotide contains a complementary sequence to the anchor

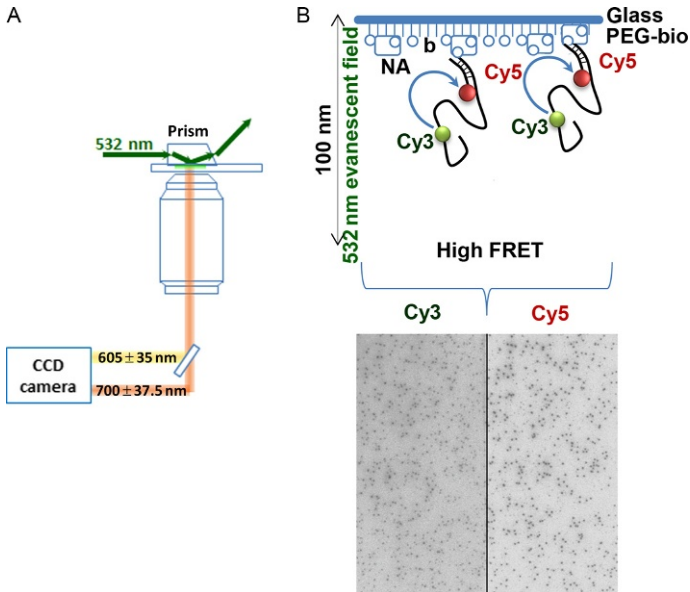


**Fig. 2** Observing the RAD51 nucleoprotein filament formation by TIRFM. (A) Typical layout of a prism-based TIRF microscope. A 532 nm laser is used as an excitation source. Fluorescence emission from the Cy3 and Cy5 fluorophores is separated in the dual view, and the split image of the flow cell surface is projected onto the CCD camera. (B) A poly dT(60) ssDNA substrate is tethered to the surface of a passivated quartz slide functionalized with biotin through the biotin–Neutravidin interaction. The evanescent wave produced by total internal reflection illumination excites the Cy3 fluorophore incorporated into the surface-tethered DNA substrate. Both Cy3 and Cy5 emissions are observed in separate channels. The *dark spots* in the microscope field of view below show the distribution of fluorescent molecules on the flow cell surface. The *black line* separates the Cy3 and Cy5 channels. Intensities of the Cy3 and Cy5 dyes incorporated into the individual DNA molecules are tracked over time by recording movies over the course of the experiment.

oligo followed by a poly(dT) sequence containing the Cy3 fluorophore. Constructing the substrate from two oligonucleotides is advantageous as they are less expensive to synthesize compared to a single oligonucleotide containing the donor, the acceptor, and the biotin. Another advantage of the two-oligonucleotide design is that the length of the poly(dT) sequence can be varied, along with the location of the Cy3 donor (Joo et al., 2006), simply by synthesizing different complementary oligonucleotides with the desired changes. In our assay, we use a poly(dT<sub>60</sub>) with the Cy3 fluorophore internally positioned 21 bases from the end of the complementary sequence. The resulting oligonucleotide is referred to as Top18-(T21)Cy3(T39)

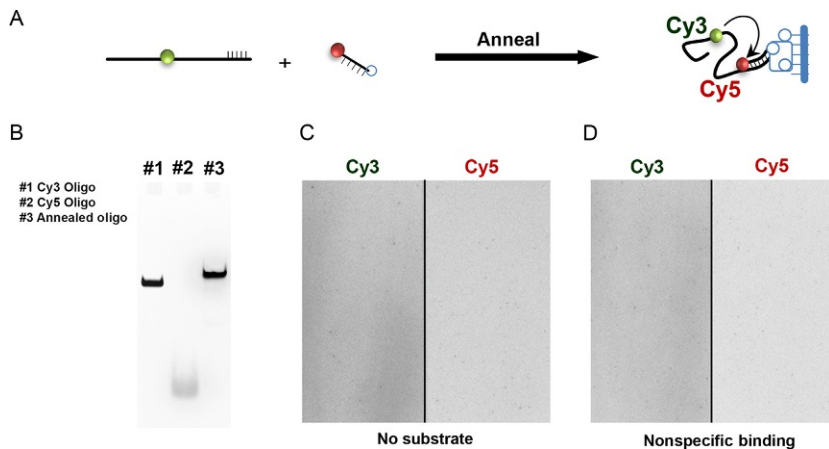


**Fig. 3** Preparation and tethering of fluorophore-labeled DNA substrates. (A) Scheme for annealing of the Cy3- and Cy5-labeled oligos to generate the DNA substrate used for the single-molecule RAD51-binding experiment. (B) PAGE gel used to verify the annealing of the two ssDNA substrates. (C and D) Image of a flow cell illuminated by evanescent wave produced by total internal reflection of the 532 nm, DPSS laser source (Cy3 excitation). The absence of appreciable fluorescent spots in both the Cy3 (left) and Cy5 (right) channels confirms that there is no nonspecific binding on introduction of the annealed substrate.

(TGGCGACGGCAGCGAGGCTTTTTTTTTTTTTTTTTTTTTTTT/iCy3/TT). The two oligonucleotides are annealed in a 1:1 *M* ratio (500 nM each) in annealing buffer (10 mM Tris, pH 8.0, 100 mM NaCl, 0.1 mM EDTA) by heating the solution to 95°C in a heat block for 5 min and allowing it to cool down to room temperature in a dark chamber (Fig. 3A). The annealed oligos can be analyzed on an 8% TAE-PAGE gel (Fig. 3B), aliquoted as required for a single experiment, and stored at -80°C.

### 2.3 Preparation of Reagents for Single-Molecule Experiments

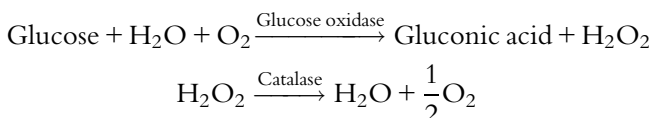
The following reagents need to be prepared for all single-molecule experiments. Attention to detail while preparing these solutions is required, as they are critical to the proper immobilization of substrates and the photostability of the organic fluorophores while performing experiments.

**2.3.1. 0.2 mg/mL Neutravidin**—Mix 2 mg of Neutravidin (Thermo Fisher catalog # 31000) with 10 mL of phosphate-buffered saline (Thermo Fisher catalog # 10010023). Do not vortex. Aliquot the solution and store the aliquots at 4°C, where they will be stable for use for up to a month.

- 2.3.2.** *24 mM Trolox (6-hydroxy-2,5,7,8-tetramethylchroman-2-carboxylic acid)*—Add 60 mg Trolox powder (Sigma catalog #391913) directly to 10 mL Milli-Q water in 15-mL sterilized tube. Before Trolox dissolves, add 60  $\mu\text{L}$  of 2 M NaOH ( $\sim 12 \text{ mM}$ ). Shake the solution few times by hand and incubate at 25°C for approximately 60 h on a rotary shaker under a fluorescent lamp. Monitor Trolox solubilization and the color of solution. The solution should turn cloudy after incubation, can be filtered using a 0.2- $\mu\text{m}$  syringe filter, and can be stored at 4°C and used for up to 1 month. NaOH is added because the Trolox solubilization results in a drop in pH (pH 3–4), and higher solubility can be achieved by dissolving Trolox in a solution with neutral pH, rather than in acidic medium. A good preparation of Trolox has a yellow color and an  $\text{OD}_{350}$  of  $>0.12$ . The higher peak at 400 nm corresponds to the ability of Trolox to more effectively quench excited triplet states of the fluorophores that can lead to photoblinking and photobleaching, thus resulting in extended visualization times with minimal photophysical side effects (Ha & Tinnefeld, 2012).
- 2.3.3.** *1  $\times$  Bovine serum albumin (BSA)*—Mix 10 mg of BSA (Sigma catalog #A7030) in 1 mL of T50 buffer (10 mM Tris pH 8.0, 50 mM NaCl). Mix and centrifuge the solution for 1 min at 4°C at 1000  $\times$  g. The solution can be stored at 4°C for a month.
- 2.3.4.** *100  $\times$  Gloxy (glucose oxidase–catalase)*—Prepare 40 mg/mL catalase (Sigma catalog #E3289) solution in T50 buffer. Weigh 10 mg glucose oxidase (Sigma catalog #G2133) and add 90  $\mu\text{L}$  of T50 buffer. Add 10  $\mu\text{L}$  of the catalase solution. Mix the two by tapping; do not vortex. Centrifuge the solution for 1 min at 1000  $\times$  g and collect the supernatant. The solution can be stored at 4°C for a month.

## 2.4 Oxygen-Scavenging System

Employing an enzymatic oxygen-scavenging system such as gloxy system effectively reduces photobleaching. In addition, using Trolox, a vitamin E analog, further eliminates photoblinking and reduces photobleaching. Gloxy is one of the most popular oxygen-scavenging systems in use today. It employs glucose oxidase and catalase to remove molecular oxygen by oxidizing glucose (Shi, Lim, & Ha, 2010) (see reaction scheme below).



## 2.5 Surface Passivation and Functionalization, and Tethering of the DNA Substrates

The poly(dT) partial overhang substrate is annealed to the anchor oligomer in annealing buffer as described earlier. Surface-passivated and functionalized TIRFM observation flow cells are prepared by chemically treating the quartz microscope slide and borosilicate glass coverslip components of the flow cells with detergents and strong alkali (potassium hydroxide) followed by aminosilanation (uniformly coating the slide with negative charge) and coating the reaction surface with a mixture of mPEG (polyethylene glycol) and biotinylated PEG. The coated slide and coverslips can be stored in nitrogen-dried, vacuum-sealed, conical tubes at  $-20^{\circ}\text{C}$ . Before use, the tubes are equilibrated to room temperature for about 20 min in a dark chamber to prevent condensation onto the treated surface. The passivated and functionalized slides and coverslips are then assembled into flow cells using double-sided tape and epoxy (detailed procedures for cleaning, passivating, functionalizing, and assembling the flow cells can be found in [Bain et al., 2016](#); [Joo & Ha, 2012a](#)) and depicted in [Fig. 4](#). This procedure reduces the nonspecific binding of proteins and nanoscopic impurities in buffers that might autofluoresce. In the absence of any DNA substrate, no more than four to five fluorescent spots should be observed in the field of view ( $57\ \mu\text{m} \times 150\ \mu\text{m}/256 \times 512$  pixels) ([Fig. 3C](#)). Higher abundance of nonspecific fluorescent spots may stem from imperfections in the quartz or borosilicate glass, contaminants in the solutions, or from air pollution. Inject  $50\ \mu\text{M}$  of the annealed DNA substrate in one  $100\ \mu\text{L}$  of T50 buffer (Tris pH 8.0,  $50\ \text{mM}$  NaCl) into the flow cell to test the quality of the surface passivation and functionalization. Since the flow cell has not yet been treated with Neutravidin, addition of the fluorophore-labeled DNA should not, at this step, change the number of fluorescent spots, thereby indicating the absence of nonspecific adsorption of the DNA to the surface of the flow cell ([Fig. 3D](#)). One hundred microliters (reaction volume) of  $0.2\ \text{mg}/\text{mL}$  Neutravidin is then added to the flow cell. In the case of flow experiments, we use  $300\ \mu\text{L}$  of  $0.2\ \text{mg}/\text{mL}$  Neutravidin. After 3-min incubation at room temperature, excess Neutravidin is washed out of the flow cell using  $300\ \mu\text{L}$  T50 buffer. Fifty picomolar annealed DNA substrate is added to the imaging buffer ( $24\ \text{mM}$  Trolox,  $20\ \text{mM}$  HEPES pH 7.5,  $2\ \text{mM}$   $\text{MgCl}_2$ , 0.8% glucose,  $150\ \text{mM}$   $\text{NaNH}_4\text{PO}_4$ ,  $1\ \text{mM}$  ATP,  $1\ \text{mM}$  DTT,  $0.1\ \text{mg}/\text{mL}$  BSA,  $0.04\ \text{mg}/\text{mL}$  catalase, and  $1\ \text{mg}/\text{mL}$  glucose oxidase ( $1 \times$  gloxy)) and flowed into the reaction chamber. Excess DNA substrate is washed out by flowing in  $300\ \mu\text{L}$  of fresh imaging buffer.

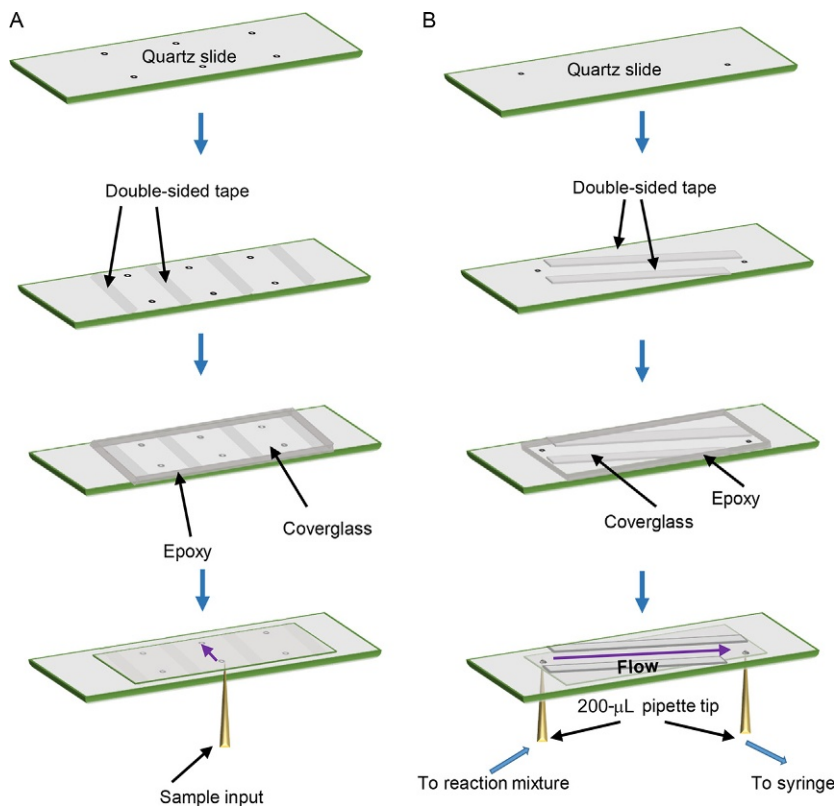


**Fig. 4** Assembly of flow cells for TIRFM imaging. (A) To prepare flow cells for equilibrium TIRFM experiments, a set of quartz microscope slides are drilled and, together with corresponding borosilicate glass coverslips, are passivated and functionalized with a mixture of mPEG and biotinylated PEG as described in Section 2.5. Double-sided tape is applied to each slide to mark out three flow cells per slide. A passivated and functionalized coverslip is then applied onto the slide, covering the predrilled holes. The edges of the coverslip are then sealed with epoxy. Once dry, excess epoxy is removed from the slide to make sure it lies flat on a table with the coverslip facing down. Samples can be pipetted into the flow cell from one direction using a 200- $\mu$ L pipette while the excess sample flows out of the predrilled hole at the other end and absorbed by a clean absorbent tissue. Note that the flow cell is placed on prism-type TIRFM with the coverslip facing down while the sample is introduced from the top, whereas the figure shows an inverted scheme with introduction of the sample from the bottom in order to clearly depict assembly of the flow cell. (B) Preparation of flow cells for pre-equilibrium experiments is similar as described earlier with the following differences. Holes in the slide are predrilled in a diagonal direction and the double-sided tape is placed such that a long flow cell is created along the diagonal of the slide. The coverslip is placed onto the slide and sealed with epoxy in a manner similar to that for the equilibrium flow cells. 200- $\mu$ L pipette tips, attached to flow tubing, are glued to the ports. One end of the tube is inserted into the reaction mixture and is drawn out at the other end, through the flow cell using a syringe. The solution can be exchanged by pausing flow and placing the tubing into another sample tube before reestablishing flow.

For experiments performed under flow, we use a similar experimental protocol, except 75 pM of the DNA substrate is used instead of 50 pM. The concentration of the annealed substrate is calibrated such that there is sufficient spacing between the observed fluorescent spots and no overlap between the diffraction-limited fluorescent spots corresponding to the individual molecules. Too high a density of surface-tethered molecules may lead to errors during image analysis, or may preclude the extraction of the trajectories (see later). The optimal density corresponds to approximately three to five hundred molecules in the field of view (Fig. 2B).

## 2.6 Acquisition of Single-Molecule Data for Equilibrium-Binding Experiments

The construction of the imaging chambers for the flow experiments is depicted in (Fig. 4B). To initiate the RAD51 filament formation, RAD51 (in imaging buffer) is added at various concentrations into the flow cell containing the immobilized DNA substrates. For equilibrium experiments, the sample is equilibrated for  $\sim 5$  min prior to imaging and the recording is started when the system has fully equilibrated.

Single-molecule data are acquired using an Andor iXon EMCCD camera, using software written in Visual C++ (available at <https://cplc.illinois.edu/software/>). Movies are recorded in the \*.pma format which is analyzed by the IDL suite (ITT Visual Information Solutions) (see later), using customized scripts (available upon request from the Spies lab). For equilibrium experiments, 40 movies, of 15-s duration each (100 ms time resolution, 400 background value, and 1600 data scalar), are recorded using a gain of 230 at a 532 nm laser power of 45.6 mW. These short movies are used to measure the equilibrium state of the entire system. The recorded movies contain Cy3 and Cy5 fluorescence intensities for all of the molecules in the field of view over each frame recorded. These time-based changes in the fluorescence intensities of the donor and acceptor fluorophores at a specified location are referred to as *fluorescence trajectories*. These fluorescence trajectories correspond to single fluorescent molecules and are extracted from the movies using IDL scripts. If the surface-tethered DNA substrates are separated further than the diffraction limit (ensured by the low ratio of biotinylated to nonbiotinylated PEG molecules and the concentrations of the Neutravidin and biotinylated molecules during surface immobilization reaction) and in the absence of nonspecific binding, each fluorescence trajectory can be attributed to the binding of RAD51 (or the absence of binding of RAD51) to a single, surface-tethered DNA molecule.

## 2.7 Acquisition of Single-Molecule Kinetic Data for Preequilibrium Experiments

For measuring preequilibrium dynamics of RAD51 nucleation events, 3-min movies are recorded to capture all events of RAD51 nucleation on ssDNA. The main differences between these preequilibrium experiments and the equilibrium experiments described in the previous section are that the RAD51 protein sample is flowed into a modified flow cell (Fig. 4B). We begin recording the movie with the DNA tethered to the surface, but no RAD51 present. After 10s from the beginning of the movie, we flow the RAD51 protein sample into the flow cell. Otherwise we use the same recording conditions as described for the equilibrium experiments.

## 2.8 Extracting and Organizing Single-Molecule Fluorescence Trajectories

To extract single-molecule fluorescence trajectories and to correlate signals from the donor and acceptor channels, we use an smFRET data acquisition and analysis package which can be downloaded from the University of Illinois Center for the Physics of Living Cells website (<https://cplc.illinois.edu/software/>). Note that this package requires the IDL suite, an IDL script, movie files with \*.pma extension,  $512 \times 512$  pixels frames (containing the donor and the acceptor channels,  $256 \times 512$  pixels each), and a mapping file. The mapping file, which is essential to accurately align the donor and acceptor channels, should be recorded within a week of the experimental data recording using a flow cell that is sparsely populated with beads that fluoresce in both donor and acceptor channels. The IDL script uses the mapping file to correlate fluorescent spots in the donor channel with the corresponding fluorescent spots in the acceptor channel and then uses this alignment to identify the locations in the field of view that contain individual, surface-tethered DNA molecules labeled with both Cy3 and Cy5 fluorophores. For the FRET-based experiments with surface-tethered DNA molecules, only the first 10 frames are usually used to map the location of the molecules. It is expected that each acceptable molecule will generate a circular, diffraction-limited fluorescent spot whose fluorescence intensity has a Gaussian distribution and is present in both channels. The images are first analyzed in the Cy3 channel, and the location of the individual molecules is identified as two-dimensional Gaussian peaks of fluorescence intensity by comparing the fluorescence around the bright spot in two circles, with diameters of 6 and 8 pixels. Then, the corresponding location in the

Cy5 channel is checked for the presence of an acceptable Gaussian peak. Peaks that are deformed or present only in one channel are ignored, as these either stem from imperfections in the quartz microscope slide or the borosilicate glass coverslip or are due to two molecules located too close to one another. The selected peaks are marked for extracting the fluorescence trajectories. Fluorescence trajectories represent the time-based changes in the Cy3 and Cy5 fluorescence intensity of each individual molecule over time.

Several hundred individual fluorescence trajectories are extracted from each recorded video and visualized. Fluorescence trajectories can be visualized using customized MATLAB<sup>®</sup> (The MathWorks, Inc.) scripts (available upon request from the Spies lab) and can be used to generate the corresponding  $E_{\text{FRET}}$  trajectories using the following equation to calculate  $E_{\text{FRET}}$ :

$$E_{\text{FRET}} = \frac{1}{\left(1 + \gamma \frac{I_{\text{Cy3}}}{I_{\text{Cy5}}}\right)}$$

where  $I_{\text{Cy3}}$  and  $I_{\text{Cy5}}$  are the sensitized emission intensity of the donor and acceptor, respectively (Ha, 2001). The measured raw intensities of the donor and acceptor channels must be corrected by measuring the percentage of fluorescence bleedthrough from the donor channel to the acceptor channel (denoted as  $\beta$ ). The donor bleedthrough is then subtracted from the acceptor channel intensities and added back to the donor intensity.

The  $\beta$  on the optical setup of the TIRF microscope and can be determined by immobilizing an oligonucleotide substrate labeled only with the fluorescent donor (in our experiments, this is Cy3). Movies are recorded until all the Cy3 molecules are completely photobleached such that there are no spots visible in either the donor or acceptor channels. The fluorescence trajectories are extracted from the movies as described earlier. Residual background intensities after the photobleaching step are subtracted from the fluorescence intensity values for both the donor and acceptor fluorescence trajectories (Fig. 5). Using the background-corrected fluorescence trajectories, average values of the Cy3 intensity before and after Cy3 photobleaching are picked out for each fluorescence trajectory. Similar values are obtained for Cy5 after Cy3 photobleaching. The change in the background-corrected donor intensity ( $\Delta I_{\text{D}}$ ) corresponds to the difference between the Cy3 intensities before and after photobleaching. The change in the background-corrected acceptor intensity ( $\Delta I_{\text{DA}}$ ) corresponds to the difference in Cy5 intensities before and after Cy3 (donor) photobleaching.

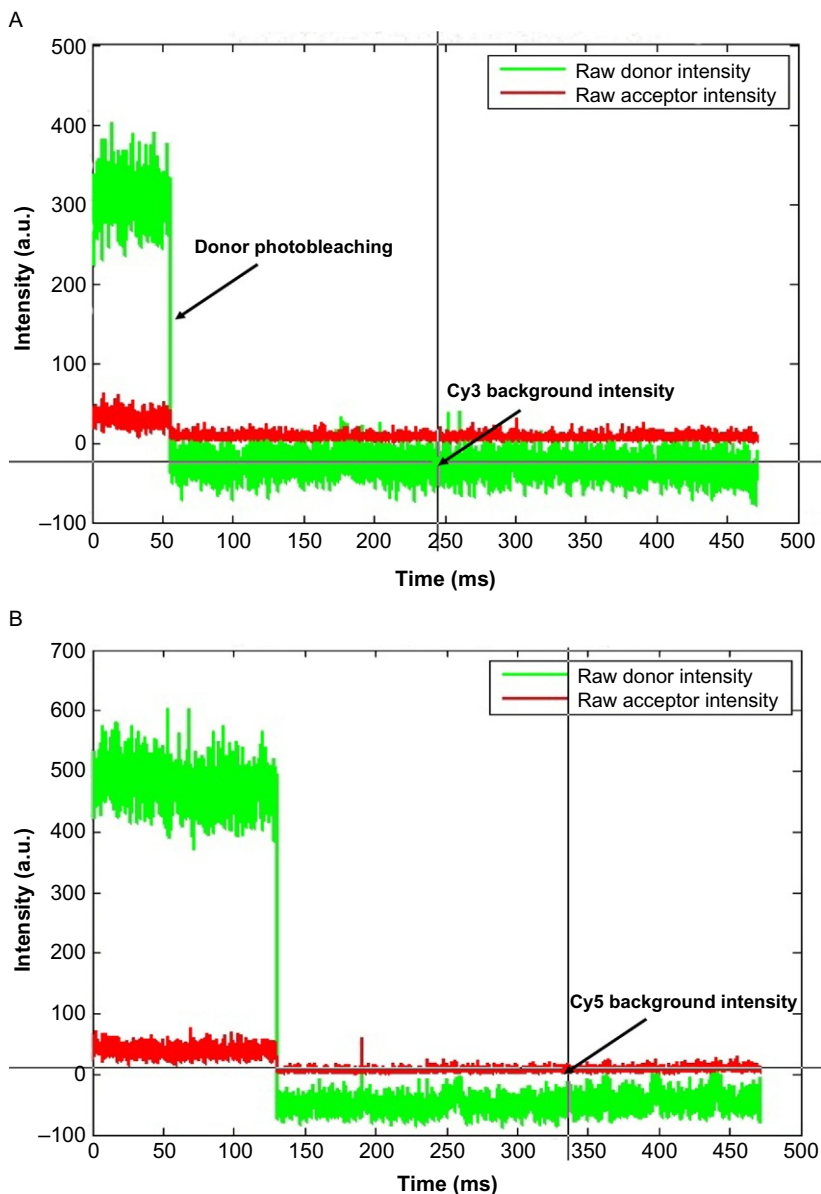


**Fig. 5** Background correction and measurement of donor bleedthrough. (A and B) Fluorescence trajectories for the Cy3 and Cy5 channels of surface-tethered Cy3-labeled ssDNA molecules showing single-step photobleaching events. Donor and acceptor background intensities are measured by recording the values of Cy3 and Cy5 intensities after the Cy3 molecule has photobleached (shown in *crosshairs*). The background intensity values are averaged for several molecules in a movie to account for small fluorescence changes in the local environment of the molecules. The drop in the intensity of the Cy5 trajectory as the Cy3 fluorophore undergoes photobleaching corresponds to the amount of donor bleedthrough from the Cy3 channel to the Cy5 channel. This is measured as a fraction and defined as the ratio of the change in the background-corrected acceptor intensity to the change in the background-corrected donor intensity ( $\beta = \Delta I_{DA} / \Delta I_D$ ).

The ratio (i.e., the percentage of donor intensity that bleeds into the acceptor channel upon donor excitation (Ha, 2001)) is calculated to get the donor bleedthrough for that fluorescence trajectory (i.e.,  $\beta = \Delta I_{DA} / \Delta I_D$ ). Averaging the donor bleedthrough values for several such fluorescence trajectories gives us the donor bleedthrough intensity for the optical setup. For our experimental system, the donor bleedthrough correction was measured to be 7%. Applying this correction, we get the equation for  $E_{\text{FRET}}$  given below:

$$E_{\text{FRET}} = \frac{(I_{\text{Cy5}}^* - \beta)}{(I_{\text{Cy5}}^* - \beta) + \gamma(I_{\text{Cy3}}^* + \beta)}$$

where  $I_{\text{Cy5}}^*$  and  $I_{\text{Cy3}}^*$  are the background-corrected acceptor and donor intensities, respectively.  $\gamma = 1$  is a parameter and parameter value representing the relative detection efficiencies and quantum yields of the donor and acceptor fluorophores.  $\gamma$  can be determined by calculating the ratio in the change of the acceptor intensity,  $\Delta I_{\text{Cy5}}$ , to the change of the donor intensity,  $\Delta I_{\text{Cy3}}$ , upon acceptor photobleaching ( $\gamma = \Delta I_{\text{Cy5}} / \Delta I_{\text{Cy3}}$ ) (Joo & Ha, 2012b; Roy, Hohng, & Ha, 2008).



### 3. ENSEMBLE ANALYSIS OF SINGLE-MOLECULE DATA

Ensemble analysis of RAD51 filament formation is a useful method to quickly determine many of the physicochemical properties of the equilibrium-bound state of the RAD51 filament. For example, it can be used to identify the number of equilibrium states, stoichiometric information, and relative affinities. For the RAD51 wild-type protein, two major states are observed (Fig. 6A), one corresponding to free DNA and the other representing the fully extended nucleoprotein filament (Fig. 6A). Intermediate states might be observed in mutants harboring deficiencies in the binding of short oligonucleotides, or those that have nucleation defects. These generally manifest in broadening of the peaks, or the appearance of new, intermediate peaks, in an  $E_{\text{FRET}}$  histogram.

#### 3.1 Preparing $E_{\text{FRET}}$ Histograms

All fluorescence trajectories extracted from the 15-s movies are background-corrected such that intensities for photobleached donor and acceptor are always zero. To generate FRET histograms, we use a MATLAB<sup>®</sup> script

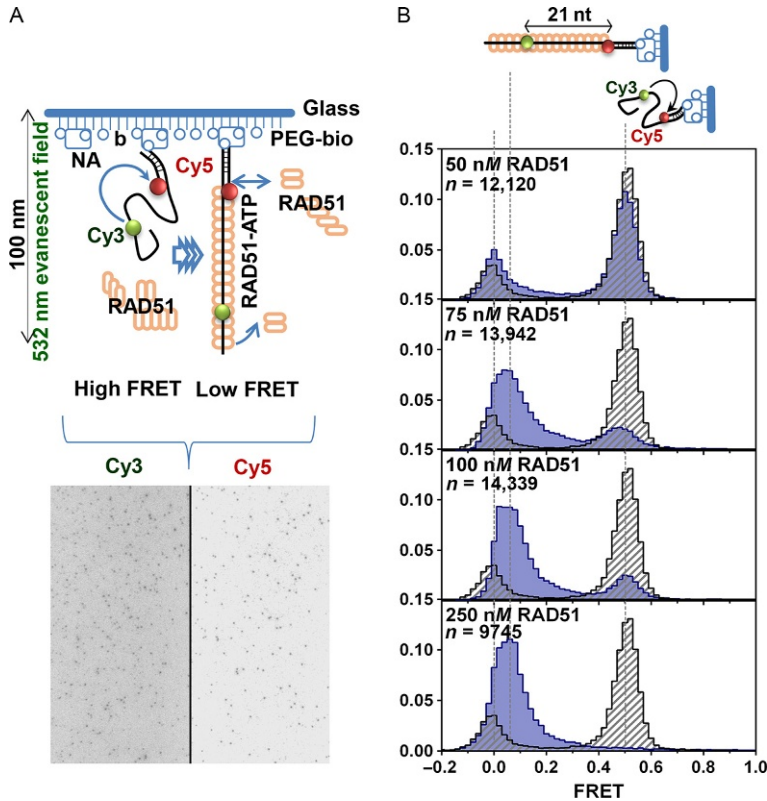
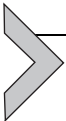


**Fig. 6** Single-molecule experiments to visualize equilibrium distributions of the RAD51–DNA FRET states. (A) Single-molecule TIRFM experiment visualizing binding of RAD51 protein onto an ssDNA FRET substrate. In the absence of RAD51 binding, the acceptor Cy5 fluorophore on the substrate DNA is excited via FRET (High  $E_{FRET}$ ). Upon binding to ssDNA, RAD51 extends the ssDNA substrate leading to a decrease in  $E_{FRET}$  and reduction in Cy5 emission with a corresponding increase in Cy3 intensity (Low  $E_{FRET}$ ). The *dark spots* in the microscope field of view below show the distribution of fluorescent molecules on the flow cell surface. The *black line* separates the Cy3 and Cy5 channels. Both Cy3 and Cy5 emission can be tracked simultaneously using a dual-view system. Changes in Cy3 and Cy5 intensities as RAD51 binds the ssDNA substrate can be tracked over time by recording movies over the course of the experiment. (B) Analysis of the equilibrium ssDNA binding using single-molecule TIRFM.  $E_{FRET}$  distributions in the presence of the indicated concentrations of RAD51 overlaid with  $E_{FRET}$  distributions in the absence of protein. Unbound ssDNA (*gray*) yields a peak in the histogram centered at the  $E_{FRET}$  value of  $\sim 0.5$ , while fully extended RAD51 nucleoprotein filament (*blue*) yields a peak in the histogram centered at an  $E_{FRET}$  value  $\sim 0.1$ . Concentrations of RAD51, as well as the number of molecules used to build each histogram are indicated in each panel.

(available upon request) in which five frames from each movie are included in the calculation of the  $E_{\text{FRET}}$  values for each molecule and for all molecules in the movie, and to bin and plot these values as a normalized  $E_{\text{FRET}}$  histogram. The MATLAB<sup>®</sup> script allows us to set cutoff values for acceptable fluorescence intensities to exclude experimental artifacts like autofluorescent aggregates or light-scattering artifacts. The number of bins in the histogram can also be adjusted for the dataset (we have optimized this value to 80 bins, but this can be changed). The program outputs the absolute, as well as normalized, counts per bin, which can be used to create  $E_{\text{FRET}}$  histogram plots in other programs such as GraphPad Prism (GraphPad software). Under our experimental conditions, unbound ssDNA molecules yield a peak in the histogram that is centered at an  $E_{\text{FRET}}$  value of  $\sim 0.5$ , while fully extended RAD51 nucleoprotein filament yields a peak in the histogram that is centered at an  $E_{\text{FRET}}$  value of  $\sim 0.1$   $E_{\text{FRET}}$  value (Fig. 6B). The progression of complete binding and elongation of the ssDNA substrate can be visualized by varying the RAD51 concentration in the reactions. Molecules in which the acceptor (Cy5) undergoes premature photobleaching represent a small fraction of the histogram ( $<3\%$ ) centered on the 0  $E_{\text{FRET}}$  value (Fig. 6B).



## 4. REAL-TIME OBSERVATION AND ANALYSIS OF RAD51 NUCLEATION USING ebFRET

### 4.1 Using Hidden Markov Models to Analyze Single-Molecule Data

The data collected in time-dependent, single-molecule experiments are signal vs time trajectories (i.e., the  $E_{\text{FRET}}$  trajectories in the current case), which are measurements of the signal from an individual molecule (i.e., the ssDNA labeled with Cy3 and Cy5 fluorophores in the current case) or macromolecular complex (i.e., the RAD51 nucleoprotein filament in the current case) taken at consecutive time points. Analysis of these signal trajectories involves correlating the values of the signal at different time points to the underlying conformational dynamics of the individual molecule (Kinz-Thompson, Bailey, & Gonzalez, 2016). Unfortunately, despite being sensitive enough to report on individual molecules, the signal trajectories collected using most single-molecule techniques are relatively noisy, and this confounds the ability to correlate the signal values to the underlying dynamics. Currently, the most popular approach for inferring the dynamics of the individual molecule from the noisy, observed signal trajectory is to use

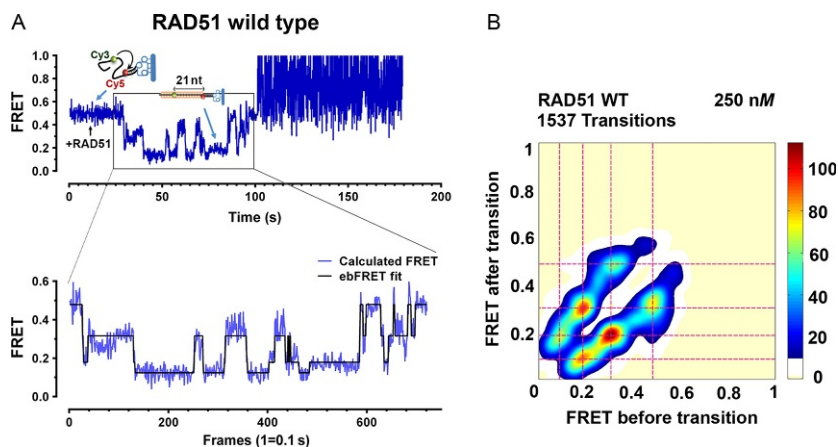


**Fig. 7** Analysis of human RAD51 nucleation using hidden Markov models. (A) Representative  $E_{\text{FRET}}$  trajectories from preequilibrium experiments visualizing step-wise RAD51 nucleation onto ssDNA in real time. RAD51 wild-type protein is added to the flow cell at  $t \sim 10$  s. The region of the trajectory that includes the first observed transition and all subsequent transitions until one of the fluorophores photobleaches (*gray box*); or the transitions stop occurring (i.e., equilibrium is achieved) or the recording is terminated. The remainder of the  $E_{\text{FRET}}$  trajectory is excluded from the HMM analysis. The *black lines* overlaying the  $E_{\text{FRET}}$  trajectory (*blue*) represent the idealized  $E_{\text{FRET}}$  trajectory from the HMM that best describes the  $E_{\text{FRET}}$  trajectory, which describes the nucleation of the 21-base (nucleotide distance between the Cy3 and Cy5 fluorophores) ssDNA substrate through four distinct states. (B) Transition density plot (TDP) showing the transition densities corresponding to each state for the wild-type RAD51 protein nucleation. 1537 transitions were analyzed from 85 molecules at a concentration of 250 nM RAD51. Warmer colors (*red*) indicate more frequent transitions. The frequency scale is shown on the *right* of the TDP.

a hidden Markov model (HMM) (Bishop, 2006). Conceptually, HMMs posit that each data point in a signal trajectory corresponds to an unobserved (i.e., hidden) underlying state of the molecule, and that, at each time point, the hidden state has a certain probability of transitioning to a different hidden state for the next time point (cf., Fig. 7A). By determining the HMMs that are consistent with an observed signal trajectory, one can determine the number of underlying hidden states, the signal values corresponding to those states, and the probability of transitioning between those states (i.e., the rate constants for transitions between the states).

As described in the previous section, the donor and acceptor fluorescence trajectories that are observed in an smFRET experiment are used to calculate  $E_{\text{FRET}}$  trajectories. Because  $E_{\text{FRET}}$  is a proxy for the distance between the donor and acceptor fluorophore, the hidden states in an  $E_{\text{FRET}}$

trajectory correspond to conformational states of the underlying molecule. Consequently, an HMM analysis of an  $E_{\text{FRET}}$  trajectory provides a structure-based interpretation of the dynamics of the individual molecule corresponding to that  $E_{\text{FRET}}$  trajectory, which was measured in the smFRET experiment. There are many software packages that are appropriate for the analysis of  $E_{\text{FRET}}$  trajectories using HMMs (e.g., QuB (Qin, Auerbach, & Sachs, 2000), HaMMMy (McKinney, Joo, & Ha, 2006), vbFRET (Bronson, Fei, Hofman, Gonzalez, & Wiggins, 2009; Bronson, Hofman, Fei, Gonzalez, & Wiggins, 2010), or ebFRET (van de Meent, Bronson, Wiggins, & Gonzalez, 2014; van de Meent, Bronson, Wood, Gonzalez, & Wiggins, 2013)), and these primarily differ in the approach with which they determine which HMM(s) are consistent with the observed  $E_{\text{FRET}}$  trajectory being analyzed. Many of these packages, including QuB (Qin et al., 2000) and HaMMMy (McKinney et al., 2006), utilize the maximum-likelihood approach, which yields the one HMM that best “fits” the  $E_{\text{FRET}}$  trajectory. This approach ignores the fact that, statistically, multiple HMMs will be consistent with an  $E_{\text{FRET}}$  trajectory. Perhaps more importantly, because the HMM with the best “fit” (i.e., the largest likelihood value) is the one in which each data point in the  $E_{\text{FRET}}$  trajectory has been assigned to a unique hidden state, determining an HMM using a maximum-likelihood approach may overfit the number of hidden states in an  $E_{\text{FRET}}$  trajectory. To avoid these shortcomings of using maximum-likelihood-based approaches, a Bayesian inference-based approach has been developed that can be used to find the range of HMMs that are consistent with an  $E_{\text{FRET}}$  trajectory, while simultaneously avoiding overfitting (Bishop, 2006; Bronson et al., 2009, 2010; van de Meent et al., 2014, 2013). Both vbFRET and its successor, ebFRET, use this statistically rigorous, Bayesian inference-based approach to analyze  $E_{\text{FRET}}$  trajectories with HMMs (Bronson et al., 2009, 2010; van de Meent et al., 2014, 2013). Regardless of the approach that is used, determining the HMMs corresponding to the hundreds to thousands of  $E_{\text{FRET}}$  trajectories that comprise a single smFRET experiment allows one to gain enough statistical insight so as to infer the kinetic scheme and set of parameters governing the behavior of the population of individual molecules that have been observed in the experiment.

A relatively new, yet powerful, approach to analyzing the hundreds to thousands of  $E_{\text{FRET}}$  trajectories collected in an smFRET experiment is to simultaneously analyze the entire population of  $E_{\text{FRET}}$  trajectories corresponding to a single experimental dataset. Conventionally, software programs such as QuB (Qin et al., 2000), HaMMMy (McKinney et al., 2006),

and vbFRET (Bronson et al., 2009, 2010) analyze each  $E_{\text{FRET}}$  trajectory in a dataset separately, with each  $E_{\text{FRET}}$  trajectory yielding its own HMM. A significant disadvantage of such an approach is that the results from the HMM(s) that are determined from the analysis of one  $E_{\text{FRET}}$  trajectory in a dataset will not inform on the HMM(s) that will be consistent with another  $E_{\text{FRET}}$  trajectory within the entire population of  $E_{\text{FRET}}$  trajectories in the dataset. Nonetheless, the ultimate goal of these analyses is most often to generate a unified description of the entire population of individual molecules. Thus, the ideal approach would be one in which the entire population of  $E_{\text{FRET}}$  trajectories in a dataset are simultaneously analyzed with a so-called hierarchical HMM, which accounts for the different types of  $E_{\text{FRET}}$  trajectories that are observed across the entire population of  $E_{\text{FRET}}$  trajectories in a dataset. As such, this approach determines the consensus HMM(s) that are consistent with the dynamics of the entire population of individual molecules (van de Meent et al., 2014, 2013). Such a hierarchical HMM approach enables one to quantitatively characterize the structural and/or dynamic heterogeneity that is frequently present across an entire population of molecules (e.g., the scenario in which an unlabeled ligand binds to and alters the dynamics of the molecules, thereby resulting in two subpopulations of molecules, and therefore  $E_{\text{FRET}}$  trajectories, which differ in terms of their dynamics). Equally as important, a hierarchical HMM approach also provides the consensus kinetic scheme and set of parameters that governs the behavior of the entire population of molecules that is observed in the single experimental dataset (e.g., even in cases where a rarely sampled conformational state is not observed in every  $E_{\text{FRET}}$  trajectory, the consensus kinetic scheme and parameter set that are obtained from a hierarchical HMM approach will include this conformational state). In a step that moves the field closer to such a hierarchical HMM approach, the ebFRET software package utilizes the same Bayesian inference-based approach that is used in vbFRET to find the HMMs that are consistent with each  $E_{\text{FRET}}$  trajectory, but, in a second step, it then uses this information to find the consensus HMM(s) that are consistent with the entire population of  $E_{\text{FRET}}$  trajectories in the dataset (van de Meent et al., 2014, 2013). In the following sections, we describe how we have used ebFRET to determine the consensus HMMs and corresponding kinetic mechanism that best describes the entire population of  $E_{\text{FRET}}$  trajectories obtained from smFRET experiments reporting on the nucleation of human RAD51 nucleoprotein filaments.

## 4.2 Using ebFRET to Determine the Set of HMMs That Are Consistent With an Entire Population of $E_{\text{FRET}}$ Trajectories

In preparation to run ebFRET, download the ebFRET program from <http://ebfret.github.io> onto your local computer, open MATLAB<sup>®</sup>, select the **Set Path** button from the main interface, select the **Add Folder** button, and then select the **ebFRET-gui/src** folder that was downloaded onto your local computer; note that bolded text denotes MATLAB<sup>®</sup>- and ebFRET-specific terminology. These steps will point MATLAB<sup>®</sup> to the ebFRET code. Although it is not necessary, we suggest using a computer containing multiple processors and running ebFRET on several of these processors to speed up the calculation times; to do so, run the MATLAB<sup>®</sup> command `parpool('local',num_proc)`, where the `num_proc` variable is the number of processors to be used. The ebFRET interface can then be launched by running the MATLAB<sup>®</sup> command `gui = ebFRET()`. Donor and acceptor fluorescence trajectories can then be loaded into ebFRET by selecting the **Load** item from the **File** menu, and selecting the files containing the donor and acceptor fluorescence trajectories using the **Raw donor-acceptor time series (.dat)** file option. If desired, donor and acceptor fluorescence trajectories obtained from separate smFRET experiments can be analyzed together by loading the additional donor and acceptor fluorescence trajectory files, and choosing the option **Keep** in the subsequent dialog box. Although ebFRET loads donor and acceptor fluorescence trajectories, the program will first calculate the  $E_{\text{FRET}}$  trajectories corresponding to the loaded donor and acceptor fluorescence trajectories and then analyze the subsequent  $E_{\text{FRET}}$  trajectories. Because the  $E_{\text{FRET}}$  values that would be calculated for data points corresponding to times when the donor fluorophore is photoblinked or photobleached are undefined (i.e.,  $E_{\text{FRET}} = 0/(0+0)$ ), these data points must be removed prior to calculation of the  $E_{\text{FRET}}$  trajectories. Although this can be accomplished using ebFRET by selecting the **Remove Photo-bleaching** item from the **Analysis** menu, in the case of our analysis of RAD51 nucleation dynamics, we used a custom MATLAB<sup>®</sup> script (available upon request from the Spies lab) to trim the beginning of the  $E_{\text{FRET}}$  trajectories to remove the wait time before binding of the first RAD51, and also to trim the end of the  $E_{\text{FRET}}$  trajectories to include only those times before donor or acceptor fluorophore photobleaching.

After setting up ebFRET, HMMs can be determined by setting the **Min** and **Max** variables in the main ebFRET interface to the minimum and maximum number of states to be considered, respectively, and clicking the **Run**

button in the same interface. An analysis in progress can be interrupted by selecting the **Stop** button, and the entire ebFRET session can be saved by selecting the **Save** item in the **File** menu. Saved sessions can be reloaded by selecting the **Load** item in the **File** menu and using the **ebFRET saved session (.mat)** file type. Running ebFRET entails a search for the parameters that yield the highest probability of the data being generated by a particular HMM. This probability is often referred to as the “evidence” of the model. Notably, however, ebFRET actually uses a lower bound to the evidence, which is often just referred to as the “lower bound.” If the parameter search is run long enough, ebFRET is guaranteed to find the parameters that yield the highest lower bound. However, in practice, it is not usually possible to run the parameter search for as long as would be required to achieve this guaranteed outcome. Thus, in practice, the parameter search is typically stopped when the value of the lower bound converges and thus effectively stops increasing. ebFRET determines what this stopping point is by detecting the point in the parameter search at which the relative increase of the lower bound is less than the value that is specified by the **Precision** variable in main ebFRET interface; for a robust parameter search, a value for the precision of less than  $10^{-6}$  is recommended, which is even less than the default value. Additionally, the parameter search process is repeated a number of times, specified by the **Restarts** variable in the main ebFRET interface. Each parameter search runs with different starting parameter values in order to increase the probability of rapidly finding the parameter values that will result in the highest lower bound; for a robust analysis, a value for the restarts of at least 10 is recommended, which is greater than the default value.

When ebFRET is finished running, the results can be obtained by selecting the **Export** item from the **File** menu and then selecting the **Analysis Summary** item. This will export a “comma separated value,” .csv, file to your local computer that can be opened using any spreadsheet program. This .csv file contains three sections of results entitled **Lower\_Bound**, **Statistics**, and **Parameters**. The **Lower\_Bound** section contains statistics describing the lower bounds on a per trajectory and per data point level. The **Statistics** section summarizes the data points assigned to each of the different states, including the fraction of data points assigned to each state (**Occupancy**), the  $E_{\text{FRET}}$  values of the data points assigned to each state (**Observation**), and the number and probability of transitioning from each state to each of the other states (**Transitions**). It is worth noting that, in these calculations, ebFRET inherently accounts for the uncertainty of assigning a data point to each of the different states. The **Parameters** section

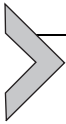
provides the values of the variables that describe the consensus HMM(s) that are consistent with the ensemble of  $E_{\text{FRET}}$  trajectories that were analyzed (i.e., the so-called hyperparameters), including the mean of the  $E_{\text{FRET}}$  distribution corresponding to each state (**Center**), the width of the  $E_{\text{FRET}}$  distribution corresponding to each state reported as an inverse variance (**Precision**), the number of time points spent in each state (**Dwell\_Time**), and the probability of transitioning from each state to each of the other states (**Transition\_Matrix**).

### 4.3 Selecting the HMM That Best Describes the Entire Population of $E_{\text{FRET}}$ Trajectories and Analyzing the Corresponding Kinetic Mechanism

After an ebFRET run is complete, the user must choose between the resulting HMMs in order to determine the corresponding kinetic mechanism (i.e., the number of states and the rates of transitions between those states) that best describes the  $E_{\text{FRET}}$  trajectories that were analyzed. Because ebFRET is a Bayesian method, the HMM that generates the highest lower bound will be the HMM, and thus kinetic mechanism, that best describes the  $E_{\text{FRET}}$  trajectories. In order to compare the lower bounds of the various HMMs, we recommend using either the sum of the lower bound of all the trajectories (i.e., **Total**), or the mean and standard deviation (i.e., **Mean** and **Std**) of the lower bounds of all the trajectories as a metric for whether one of the HMMs yields a distinctly higher lower bound. Ideally, a plot of the lower bounds vs the increasing number of states in the HMMs will exhibit a peaked lower bound at some specific complexity (i.e., specific number of states). However, because the amount of information in a population of  $E_{\text{FRET}}$  trajectories to be analyzed is sometimes not enough to make the distinction between the lower bounds obvious, we find that the lower bounds in such plots sometimes plateau rather than peak. This can make it difficult to select the kinetic mechanism that best describes the  $E_{\text{FRET}}$  trajectories. In such a case, we advocate for parsimony such that the HMM that has the lowest complexity (i.e., the lowest number of states) within the plateaued region of the plot is selected as the HMM that best describes the  $E_{\text{FRET}}$  trajectories; this will avoid overfitting and overinterpretation of the data. In the analysis of RAD51 nucleation dynamics, the lower bounds plateaued starting with the HMM that was composed of four states, so we therefore used this four-state HMM in the subsequent analysis. With four distinct conformational states of the nucleating filament, this suggests that the nucleating species of RAD51 is a dimer (Subramanyam et al., 2016).

Once an HMM has been selected, information about the kinetic mechanism of interest can be obtained by calculating rate constants for transitions from each state to the other states. For the rate constant for the transition from generic states  $i$  to  $j$ , denoted  $k_{ij}$ , this calculation can be performed with the formula  $k_{ij} = -\ln(1 - P_{ij})/\tau$ , where  $P_{ij}$  is the transition probability for the transition from state  $i$  to  $j$ , which is an element of the transition matrix located in **Transition\_Matrix** entry of the **Analysis Summary**, and  $\tau$  is the time resolution of the dataset in units of seconds (see [Kinz-Thompson et al., 2016](#) for additional details). Further insights relating to the kinetic mechanism of interest can be obtained by generating a transition density plot (TDP). A TDP is a contour surface plot that reports the relative frequencies of transitions between different states by plotting the  $E_{\text{FRET}}$  at each time point on the  $x$ -axis vs the  $E_{\text{FRET}}$  at each subsequent time point on the  $y$ -axis ([Fig. 7B](#)). TDPs allow us to better understand the underlying kinetic mechanism by providing a visual representation of which states transition into which other states and the relative frequencies with which these transitions occur. Notably, in smFRET experiments in which the molecules of interest do not undergo frequent conformational changes, the molecules predominantly remain in the same  $E_{\text{FRET}}$  state during the majority of the  $E_{\text{FRET}}$  trajectories. Consequently, the relative frequencies of the consecutive time points in which no transitions occur (i.e., the on-diagonal peaks in the TDP) can dominate the TDP and obscure the relative frequencies of the consecutive time points in which transitions do occur (i.e., the off-diagonal peaks in the TDP). However, because the HMM that has been selected as best describing the  $E_{\text{FRET}}$  trajectories contains all of the information that is required to determine when transitions do occur, we can use the selected HMM to generate a TDP that plots only the  $E_{\text{FRET}}$  values of those steps in which consecutive time points undergo a transition. This is done by generating a TDP using the “idealized”  $E_{\text{FRET}}$  trajectories, or “Viterbi paths,” which are generated by turning each  $E_{\text{FRET}}$  value in an  $E_{\text{FRET}}$  trajectory into the average  $E_{\text{FRET}}$  value of the corresponding hidden state determined by the HMM (black line in [Fig. 7A](#)). The idealized  $E_{\text{FRET}}$  trajectories can be exported as a .dat file from ebFRET by selecting the **Export** item from the **File** menu, then selecting the **Traces** item, defining the filename, toggling off all of the **channels** except the **Viterbi Mean** channel, and then setting the **Number of States** variable such that it corresponds to the HMM that has been selected. Once the idealized  $E_{\text{FRET}}$  trajectories have been generated, a TDP can be generated by downloading a custom MATLAB<sup>®</sup> script called **plot\_TDP.m** from <http://ebfret.github.io> onto

your local computer, and running the script using the MATLAB<sup>®</sup> command **plot\_TDP('filename.dat')**, where **filename.dat** corresponds to the .dat file containing the idealized  $E_{\text{FRET}}$  trajectories; further instructions for running this script can be found at <http://ebfret.github.io>. As was seen in the TDP of the  $E_{\text{FRET}}$  trajectories of RAD51 nucleation dynamics using an HMM containing four states, high transition frequencies were only observed between states corresponding to adjacent  $E_{\text{FRET}}$  values (Fig. 7B). Also, we note that this behavior was independent of the number of states that were used to determine the HMM (e.g., eight states), and no substantial differences in the TDP are observed for HMMs with more than four states. Therefore, TDPs are a robust analysis method that are relatively independent of the results of an HMM.



## 5. CONCLUSIONS

Nucleation of the RAD51 filament on ssDNA is a critical step in the formation of the active species in homologous recombination and even slight deviations toward either a more or a less stable RAD51 filament, as well as slight differences in the filament nucleation and growth kinetics may cause aberrant recombination or an unstable RAD51 nucleoprotein filament. In this chapter, we discussed the analysis of human RAD51 nucleoprotein filament formation using a FRET-based assay enabled by TIRF microscopy. This assay takes advantage of the recombinase-stretched ssDNA within the active form of the RAD51 filament, which allows the experimenter to monitor a dynamic, stepwise formation of a stable RAD51–ssDNA complex by following the ssDNA extension. The experiment is carried out by first imaging a protein-free, surface-tethered DNA decorated with the Cy3 (FRET donor) and Cy5 (FRET acceptor) dyes separated by 21 nucleotides of ssDNA and then flowing in RAD51. FRET-based studies require positioning of the donor and acceptor fluorophores within 25 nucleotides from one another within the substrate that typically does not exceed 100 nucleotides in length. Such substrates allow formation of relatively short nucleoprotein filaments (up to 30–35 monomers of RAD51), which coincidentally corresponds to an average segment size within discontinuous RAD51 filaments formed under conditions permitting ATP hydrolysis (Holthausen, Wyman, & Kanaar, 2011). A flow experiment, like the one described in this chapter, follows the very first steps in the RAD51 nucleoprotein filament assembly, namely, a formation of a stable nucleus from which the filament can then grow. In the case of human RAD51 under

conditions permitting ATP hydrolysis, filament nucleation occurs through a dynamic association and dissociation of RAD51 dimers (Subramanyam et al., 2016). Similar approaches have been applied to other RecA-family recombinases (including yeast Rad51 protein (Qiu et al., 2013), and RecA (Joo et al., 2006)), albeit with different kinetics and via different oligomeric species.

The utility of the assay described in this chapter is that it can be readily extended to other experimental conditions. Nucleoprotein filament formation can be monitored, for example, in the presence of  $\text{Ca}^{2+}$ , where RAD51 can bind ATP and forms an extended active nucleoprotein filament, but cannot hydrolyze ATP (Bugreev & Mazin, 2004) and where it forms longer and less dynamic filaments (Holthausen et al., 2011), or in the presence of different small-molecule modulators of the RAD51–ssDNA interaction (see Hengel, Spies, & Spies, 2017 for review). The partial duplex DNA substrate described here can be substituted with the DNA substrates resembling various DNA repair intermediates and stalled replication forks that are expected to attract RAD51 in the cell. Analysis of RAD51 dynamics on different DNA substrates can help to parse out the differences and similarities between the RAD51 nucleoprotein filaments acting in homology-directed DNA repair and in stabilization of DNA replication forks. Additionally, various posttranslationally modified forms of RAD51 can be examined. We have shown recently that RAD51 phosphorylated at Tyr54 has a low affinity for ssDNA, but forms the nucleoprotein filament with higher cooperativity (Subramanyam et al., 2016). RAD51, however, is subject to numerous post-translational modifications, including tyrosine phosphorylation by the c-Abl kinase at Y54 and Y315 residues, tyrosine phosphorylation by the Arg kinase, threonine phosphorylation on T309 by the CHK1 kinase, SUMOylation by UBL1 (Popova, Henry, & Fleury, 2011), and ubiquitylation mediated by the FBH1 helicase (Chu et al., 2015). How these modifications affect the dynamics of nucleoprotein filament assembly and stability remains to be determined. More importantly, the RAD51–DNA interactions are controlled by the recombination mediator BRCA2, by RAD51 paralogs and Shu complex (Godin, Sullivan, & Bernstein, 2016; Prakash, Zhang, Feng, & Jasin, 2015; Zelensky, Kanaar, & Wyman, 2014), by antirecombinogenic DNA helicases (Daley, Gaines, Kwon, & Sung, 2014), and by the heteroduplex rejection machinery (Spies & Fishel, 2015). These modulators of RAD51 activity or their individual RAD51-interacting domains can be incorporated into the FRET-based, single-molecule experiments described here. Given the flexibility with which it can be adapted to pursue all of these experimental

avenues, the assay described in this chapter should become a powerful tool in the field's effort to build a comprehensive mechanistic description of RAD51 nucleoprotein filament formation, the most critical step in homologous recombination and an important step in the maintenance of robust and accurate DNA replication. With the increasing availability of single-molecule TIRFM instrumentation and the robust data analysis routine afforded by ebFRET (van de Meent et al., 2014), we expect this FRET-based analysis of the RAD51 nucleoprotein filament formation and stability to be extended to many conditions, RAD51 mutants, and RAD51 nucleoprotein filament modulators.

## ACKNOWLEDGMENTS

The authors' research is supported by National Institutes of Health (NIH) Grant GM108617 and by University of Iowa Holden Comprehensive Cancer Center Collaborative Pilot Grant NIH P30 CA086862 to M.S., and NIH Grants GM084288 and GM 119386 to R.L.G. C.D. K.-T. was supported by the Department of Energy Office of Science Graduate Fellowship Program (DOE SCGF), made possible in part by the American Recovery and Reinvestment Act of 2009, administered by ORISE-ORAU under contract number DE-AC05-06OR23100, as well as by Columbia University's NIH Training Program in Molecular Biophysics (T32-GM008281). The funders had no role in study design, data collection and analysis, decision to publish, or preparation of the manuscript. We thank Colleen Caldwell and Fletcher Bain for critical reading of the manuscript and for valuable discussions.

## REFERENCES

- Ameziane, N., May, P., Haitjema, A., van de Vrugt, H. J., van Rossum-Fikkert, S. E., Ristic, D., et al. (2015). A novel Fanconi anaemia subtype associated with a dominant-negative mutation in RAD51. *Nature Communications*, 6, 8829.
- Amitani, I., Liu, B., Dombrowski, C. C., Baskin, R. J., & Kowalczykowski, S. C. (2010). Watching individual proteins acting on single molecules of DNA. In G. W. Nils (Ed.), *Methods in enzymology*. Academic Press.
- Arata, H., Dupont, A., Miné-Hattab, J., Disseau, L., Renodon-Cornière, A., Takahashi, M., et al. (2009). Direct observation of twisting steps during Rad51 polymerization on DNA. *Proceedings of the National Academy of Sciences of the United States of America*, 106, 19239–19244.
- Axelrod, D. (2008). Total internal reflection fluorescence microscopy. In L. Wilson & P. Matsudaira (Eds.), *Methods in cell biology*. Academic Press. chapter 7.
- Bain, F. E., Wu, C. G., & Spies, M. (2016). Single-molecule sorting of DNA helicases. *Methods*, 108, 14–23.
- Bell, J. C., & Kowalczykowski, S. C. (2016). Mechanics and single-molecule interrogation of DNA recombination. *Annual Review of Biochemistry*, 85, 193–226.
- Benson, F. E., Stasiak, A., & West, S. C. (1994). Purification and characterization of the human Rad51 protein, an analogue of *E. coli* RecA. *EMBO Journal*, 13, 5764–5771.
- Bishop, C. M. (2006). *Pattern recognition and machine learning*. Springer.
- Bronson, J. E., Fei, J., Hofman, J. M., Gonzalez, R. L., & Wiggins, C. H. (2009). Learning rates and states from biophysical time series: A Bayesian approach to model selection and single-molecule FRET data. *Biophysical Journal*, 97, 3196–3205.

- Bronson, J. E., Hofman, J. M., Fei, J., Gonzalez, R. L., & Wiggins, C. H. (2010). Graphical models for inferring single molecule dynamics. *BMC Bioinformatics*, *11*, S2.
- Budke, B., Lv, W., Kozikowski, A. P., & Connell, P. P. (2016). Recent developments using small molecules to target RAD51: How to best modulate RAD51 for anticancer therapy? *ChemMedChem*, *11*, 2468–2473.
- Bugreev, D. V., & Mazin, A. V. (2004). Ca<sup>2+</sup> activates human homologous recombination protein Rad51 by modulating its ATPase activity. *Proceedings of the National Academy of Sciences of the United States of America*, *101*, 9988–9993.
- Candelli, A., Holthausen, J. T., Depken, M., Brouwer, I., Franker, M. A., Marchetti, M., et al. (2014). Visualization and quantification of nascent RAD51 filament formation at single-monomer resolution. *Proceedings of the National Academy of Sciences of the United States of America*, *111*, 15090–15095.
- Candelli, A., Modesti, M., Peterman, E. J., & Wuite, G. J. (2013). Single-molecule views on homologous recombination. *Quarterly Reviews of Biophysics*, *46*, 323–348.
- Chabbert, M., Cazenave, C., & Helene, C. (1987). Kinetic studies of recA protein binding to a fluorescent single-stranded polynucleotide. *Biochemistry*, *26*, 2218–2225.
- Chen, Z., Yang, H., & Pavletich, N. P. (2008). Mechanism of homologous recombination from the RecA-ssDNA/dsDNA structures. *Nature*, *453*, 489–494.
- Chu, W. K., Payne, M. J., Beli, P., Hanada, K., Choudhary, C., & Hickson, I. D. (2015). FBH1 influences DNA replication fork stability and homologous recombination through ubiquitylation of RAD51. *Nature Communications*, *6*, 5931.
- Daley, J. M., Gaines, W. A., Kwon, Y., & Sung, P. (2014). Regulation of DNA pairing in homologous recombination. *Cold Spring Harbor Perspectives in Biology*, *6*, a017954.
- Forget, A. L., & Kowalczykowski, S. C. (2010). Single-molecule imaging brings Rad51 nucleoprotein filaments into focus. *Trends in Cell Biology*, *20*, 269–276.
- Forget, A. L., & Kowalczykowski, S. C. (2012). Single-molecule imaging of DNA pairing by RecA reveals a three-dimensional homology search. *Nature*, *482*, 423–427.
- Galkin, V. E., Esashi, F., Yu, X., Yang, S., West, S. C., & Egelman, E. H. (2005). BRCA2 BRC motifs bind RAD51-DNA filaments. *Proceedings of the National Academy of Sciences of the United States of America*, *102*, 8537–8542.
- Godin, S. K., Sullivan, M. R., & Bernstein, K. A. (2016). Novel insights into RAD51 activity and regulation during homologous recombination and DNA replication. *Biochemistry and Cell Biology*, *94*, 407–418.
- Ha, T. (2001). Single-molecule fluorescence resonance energy transfer. *Methods*, *25*, 78–86.
- Ha, T., & Tinnefeld, P. (2012). Photophysics of fluorescent probes for single-molecule biophysics and super-resolution imaging. *Annual Review of Physical Chemistry*, *63*, 595–617.
- Hengel, S. R., Spies, M. A., & Spies, M. (2017). Small-molecule inhibitors targeting DNA repair and DNA repair deficiency in research and cancer therapy. *Cell Chemical Biology*, *24*, 1101–1119.
- Holthausen, J. T., Wyman, C., & Kanaar, R. (2011). Regulation of DNA strand exchange in homologous recombination. *DNA Repair*, *9*, 1264–1272.
- Joo, C., & Ha, T. (2012a). Preparing sample chambers for single-molecule FRET. *Cold Spring Harbor Protocols*, 2012. <https://doi.org/10.1101/pdb.prot071530>.
- Joo, C., & Ha, T. (2012b). Single-molecule FRET with total internal reflection microscopy. *Cold Spring Harbor Protocols*, 2012. <https://doi.org/10.1101/pdb.top072058>.
- Joo, C., Mckinney, S. A., Nakamura, M., Rasnik, I., Myong, S., & Ha, T. (2006). Real-time observation of RecA filament dynamics with single monomer resolution. *Cell*, *126*, 515–527.
- Kinz-Thompson, C. D., Bailey, N. A., & Gonzalez, R. L. (2016). Precisely and accurately inferring single-molecule rate constants. *Methods in Enzymology*, *581*, 187–225.
- Klein, H. L. (2008). The consequences of Rad51 overexpression for normal and tumor cells. *DNA Repair (Amst)*, *7*, 686–693.

- Kolinjivadi, A. M., Sannino, V., de Antoni, A., Techer, H., Baldi, G., & Costanzo, V. (2017). Moonlighting at replication forks—A new life for homologous recombination proteins BRCA1, BRCA2 and RAD51. *FEBS Letters*, *591*, 1083–1100.
- Larson, J., Kirk, M., Drier, E. A., O'Brien, W., Mackay, J. F., Friedman, L. J., et al. (2014). Design and construction of a multiwavelength, micromirror total internal reflectance fluorescence microscope. *Nature Protocols*, *9*, 2317.
- Li, X., & Heyer, W. D. (2008). Homologous recombination in DNA repair and DNA damage tolerance. *Cell Research*, *18*, 99–113.
- McKinney, S. A., Joo, C., & Ha, T. (2006). Analysis of single-molecule FRET trajectories using hidden Markov modeling. *Biophysical Journal*, *91*, 1941–1951.
- Michl, J., Zimmer, J., & Tarsounas, M. (2016). Interplay between Fanconi anemia and homologous recombination pathways in genome integrity. *The EMBO Journal*, *35*, 909–923.
- Moynahan, M. E., & Jasin, M. (2010). Mitotic homologous recombination maintains genomic stability and suppresses tumorigenesis. *Nature Reviews. Molecular Cell Biology*, *11*, 196–207.
- Popova, M., Henry, S., & Fleury, F. (2011). Posttranslational modifications of Rad51 protein and its direct partners: Role and effect on homologous recombination-mediated DNA repair. In I. Kruman (Ed.), *DNA repair*. Rijeka, Croatia: InTech.
- Prakash, R., Zhang, Y., Feng, W., & Jasin, M. (2015). Homologous recombination and human health: The roles of BRCA1, BRCA2, and associated proteins. *Cold Spring Harbor Perspectives in Biology*, *7*, a016600.
- Qi, Z., Redding, S., Lee, J. Y., Gibb, B., Kwon, Y., Niu, H., et al. (2015). DNA sequence alignment by microhomology sampling during homologous recombination. *Cell*, *160*, 856–869.
- Qin, F., Auerbach, A., & Sachs, F. (2000). A direct optimization approach to hidden Markov modeling for single channel kinetics. *Biophysical Journal*, *79*, 1915–1927.
- Qiu, Y., Antony, E., Doganay, S., Ran Koh, H., Lohman, T. M., & Myong, S. (2013). Srs2 prevents Rad51 filament formation by repetitive motion on DNA. *Nature Communications*, *4*, 2281.
- Ristic, D., Modesti, M., van der Heijden, T., van Noort, J., Dekker, C., Kanaar, R., et al. (2005). Human Rad51 filaments on double- and single-stranded DNA: Correlating regular and irregular forms with recombination function. *Nucleic Acids Research*, *33*, 3292–3302.
- Roy, R., Hohng, S., & Ha, T. (2008). A practical guide to single-molecule FRET. *Nature Methods*, *5*, 507–516.
- Schlacher, K., Christ, N., Siaud, N., Egashira, A., Wu, H., & Jasin, M. (2011). Double-strand break repair-independent role for BRCA2 in blocking stalled replication fork degradation by MRE11. *Cell*, *145*, 529–542.
- Schlacher, K., Wu, H., & Jasin, M. (2012). A distinct replication fork protection pathway connects Fanconi anemia tumor suppressors to RAD51-BRCA1/2. *Cancer Cell*, *22*, 106–116.
- Shi, X., Lim, J., & Ha, T. (2010). Acidification of the oxygen scavenging system in single-molecule fluorescence studies: In situ sensing with a ratiometric dual-emission probe. *Analytical Chemistry*, *82*, 6132–6138.
- Short, J. M., Liu, Y., Chen, S., Soni, N., Madhusudhan, M. S., Shivji, M. K. K., et al. (2016). High-resolution structure of the presynaptic RAD51 filament on single-stranded DNA by electron cryo-microscopy. *Nucleic Acids Research*, *44*, 9017–9030.
- Spies, M., & Fishel, R. (2015). Mismatch repair during homologous and homeologous recombination. *Cold Spring Harbor Perspectives in Biology*, *7*, a022657.
- Subramanyam, S., Ismail, M., Bhattacharya, I., & Spies, M. (2016). Tyrosine phosphorylation stimulates activity of human RAD51 recombinase through altered nucleoprotein

- filament dynamics. *Proceedings of the National Academy of Sciences of the United States of America*, 113, E6045–E6054.
- Subramanyam, S., Jones, W. T., Spies, M., & Spies, M. A. (2013). Contributions of the RAD51 N-terminal domain to BRCA2-RAD51 interaction. *Nucleic Acids Research*, 41, 9020–9032.
- Tomblin, G., Shim, K. S., & Fishel, R. (2002). Biochemical characterization of the human RAD51 protein. II. Adenosine nucleotide binding and competition. *Journal of Biological Chemistry*, 277, 14426–14433.
- van de Meent, J.-W., Bronson, J. E., Wiggins, C. H., & Gonzalez, R. L., Jr. (2014). Empirical Bayes methods enable advanced population-level analyses of single-molecule FRET experiments. *Biophysical Journal*, 106, 1327–1337.
- van de Meent, J.-W., Bronson, J. E., Wood, F., Gonzalez, R. L., Jr., & Wiggins, C. H. (2013). In *Hierarchically-coupled hidden Markov models for learning kinetic rates from single-molecule data*. *Proceedings of the 30th international conference on machine learning*.
- van der Heijden, T., Seidel, R., Modesti, M., Kanaar, R., Wyman, C., & Dekker, C. (2007). Real-time assembly and disassembly of human RAD51 filaments on individual DNA molecules. *Nucleic Acids Research*, 35, 5646–5657.
- Xu, J., Zhao, L., Xu, Y., Zhao, W., Sung, P., & Wang, H.-W. (2016). Cryo-EM structures of human RAD51 recombinase filaments during catalysis of DNA-strand exchange. *Nature Structural & Molecular Biology*, 24, 40.
- Yu, X., Jacobs, S. A., West, S. C., Ogawa, T., & Egelman, E. H. (2001). Domain structure and dynamics in the helical filaments formed by RecA and Rad51 on DNA. *Proceedings of the National Academy of Sciences of the United States of America*, 98, 8419–8424.
- Zelensky, A., Kanaar, R., & Wyman, C. (2014). Mediators of homologous DNA pairing. *Cold Spring Harbor Perspectives in Biology*, 6, a016451.



# TIRF-Based Single-Molecule Detection of the RecA Presynaptic Filament Dynamics

Sung H. Kim<sup>1</sup>

School of Biological Science, Institute of Molecular Biology and Genetics, Seoul National University, Seoul, Republic of Korea

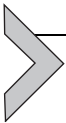
<sup>1</sup>Corresponding author: e-mail address: kahutia@snu.ac.kr

## Contents

|   |     |
|---|-----|
| 1. Introduction   | 234 |
| 1.1 RecA Presynaptic Filament and Homologous Recombination          | 234 |
| 1.2 Why SM-FRET?  | 235 |
| 2. Total Internal Reflection Fluorescence-Based SM-FRET Measurement | 236 |
| 2.1 Total Internal Reflection Fluorescence Microscopy               | 236 |
| 2.2 DNA Labeling and Sample Preparation                             | 237 |
| 2.3 DNA Immobilization and Single-Molecule FRET Measurement         | 239 |
| 2.4 SM-FRET Data Analysis   | 240 |
| 3. Nucleation   | 241 |
| 3.1 DNA Design and Buffer Condition                                 | 241 |
| 3.2 Experimental Procedure  | 242 |
| 3.3 Real-Time Observation of RecA Filament Nucleation               | 242 |
| 4. End-Dependent Presynaptic Filament Dynamics                      | 243 |
| 4.1 DNA Design and Buffer Conditions                                | 244 |
| 4.2 Experimental Procedure for the 5'End Dynamics                   | 244 |
| 4.3 Experimental Procedure for the 3'End Dynamics                   | 244 |
| 4.4 Monomer Binding and Dissociation at the End of RecA Filament    | 245 |
| 5. Protein Scaffold Shift Within Presynaptic Filament               | 246 |
| 5.1 DNA Design  | 246 |
| 5.2 Experimental Procedure  | 247 |
| 5.3 Phase Detection of Individual RecA Filaments and Scaffold Shift | 248 |
| 6. ATP-Dependent Conformational Change                              | 248 |
| 6.1 DNA Design and Buffer Condition                                 | 249 |
| 6.2 Experimental Procedure  | 250 |
| 6.3 Real-Time Observation of Conformational Transitions             | 250 |
| 7. Conclusions  | 251 |
| Acknowledgment  | 251 |
| References  | 251 |

## Abstract

RecA is a key protein in homologous DNA repair process. On a single-stranded (ss) DNA, which appears as an intermediate structure at a double-strand break site, RecA forms a kilobase-long presynaptic filament that mediates homology search and strand exchange reaction. RecA requires adenosine triphosphate as a cofactor that confers dynamic features to the filament such as nucleation, end-dependent growth and disassembly, scaffold shift along the ssDNA, and conformational change. Due to the complexity of the dynamics, detailed molecular mechanisms of functioning presynaptic filament have been characterized only recently after the advent of single-molecule techniques that allowed real-time observation of each kinetic process. In this chapter, single-molecule fluorescence resonance energy transfer assays, which revealed detailed molecular pictures of the presynaptic filament dynamics, will be discussed.



---

## 1. INTRODUCTION

### 1.1 RecA Presynaptic Filament and Homologous Recombination

RecA is an adenosine triphosphate (ATP)-dependent DNA repair protein that catalyzes the DNA strand exchange reaction in homologous recombination (Bianco, Tracy, & Kowalczykowski, 1998; Kowalczykowski, 2000; Lusetti & Cox, 2002). When double-strand break (DSB) occurs, RecA-loading machineries such as RecBCD and RecFOR first appear at the site and process the broken DNA to make a long ss-overhang (Dillingham & Kowalczykowski, 2008; Michel, Boubakri, Baharoglu, LeMasson, & Lestini, 2007; Spies, Dillingham, & Kowalczykowski, 2005). RecA proteins are then loaded on to the ssDNA and form a helical structured filament (Chen, Yang, & Pavletich, 2008). This presynaptic filament grows to several kilobases by addition of RecA monomers at the ends of the filament (Galletto, Amitani, Baskin, & Kowalczykowski, 2006; Joo et al., 2006). The ssDNA lies along the central axis of the filament such that the bases of the ssDNA are exposed to the solvent for homology searching and pairing (Fig. 1A) (Chen et al., 2008). After finding a homology, the filament serves as a scaffold for strand exchange between the homologous strands. Finally, RecA disassembles from the DNA and DNA polymerases are recruited to the site to synthesize DNA.

RecA monomers within the presynaptic filament continuously hydrolyze ATP regardless of their position (Brenner et al., 1987), conferring dynamic features to the filament (Fig. 1B): (1) cooperative nucleation and

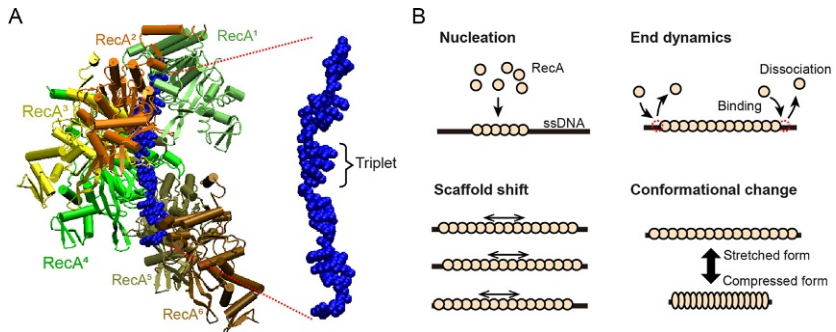


**Fig. 1** RecA presynaptic filament structure and dynamics. (A) Crystal structure of RecA filament with embedded ssDNA. Six monomers that make one turn of the helical pitch are drawn in *different colors* (PDB: 3CMU). The ssDNA (*blue*) is highlighted with its triplet structure. (B) The RecA presynaptic filament dynamics.

disassembly (Joo et al., 2006), (2) monomer binding and dissociation at the filament ends (Galletto et al., 2006; Joo et al., 2006), (3) protein scaffold shift along ssDNA (Kim et al., 2017), and (4) structural transitions between the active (stretched) and inactive (compressed) forms, resulting in length shortening (compression) of the filament by 1.5-folds (Chen et al., 2008; Egelman & Stasiak, 1993). Albeit these dynamic features, the kilobase-long presynaptic filament needs to be stably bound to DNA and keeps its active conformation for fast homology search and strand exchange reaction. Therefore, the presynaptic filament dynamics is tightly regulated by many factors such as pH, ATP concentration, and substrate DNA sequences (Kim et al., 2017, 2014; Kim, Joo, Ha, & Kim, 2013; Kim, Park, Joo, Kim, & Ha, 2015). For a comprehensive understanding of this complex dynamics, it is necessary to dissect each kinetic process separately from others. Single-molecule (SM) fluorescence resonance energy transfer (FRET) has been proven to be an ideal method for studying complex dynamics processes (Ha, Kozlov, & Lohman, 2012). In this chapter, several SM-FRET assays specifically designed for each kinetic process will be discussed.

## 1.2 Why SM-FRET?

FRET is an energy transfer mechanism that occurs between two fluorescent dye molecules in close proximity (typically within 10 nm). When the absorption spectrum of a dye (donor) overlaps with the emission spectrum of another dye (acceptor), the energy absorbed by the donor upon excitation can be transferred nonradiatively to the acceptor, which will then emit

fluorescence instead of the donor. The efficiency of the energy transfer, which can be measured by the ratio between the donor and acceptor intensities, depends sensitively on the distance between the two dyes. Therefore, FRET can be used as a nanoscale molecular ruler to measure the interdyer distance. In application, a molecule of interest, such as DNA or protein, is labeled with a donor and an acceptor at two different positions so that the structural change in the molecule of interest can be reported by FRET efficiency changes between the dyes.

Unlike typical biochemical assays, which measure ensemble-averaged properties of molecules, SM measurement can separately monitor individual functioning molecules in real time. Owing to this unique capability, detailed kinetic information in complex biological processes can be obtained. Consequently, since its first introduction (Ha et al., 1996), SM-FRET has been extensively used to study detailed mechanisms of biomolecules in function (Ha et al., 2012; Joo, Balci, Ishitsuka, Buranachai, & Ha, 2008).



## **2. TOTAL INTERNAL REFLECTION FLUORESCENCE-BASED SM-FRET MEASUREMENT**

### **2.1 Total Internal Reflection Fluorescence Microscopy**

For SM-FRET measurement, total internal reflection fluorescence (TIRF) microscopy is a practical choice because (1) it has intrinsically low background noise for detection of weak fluorescence signal from single molecules, and (2) it allows in-parallel observation of several hundreds of single molecules (Roy, Hohng, & Ha, 2008). Two types of TIRF microscopy are widely used for SM-FRET measurement: prism-type TIRF and objective-type TIRF. All the experimental procedures described in this chapter assume prism-type TIRF, but objective-type TIRF can also be used. Detailed practical information on how to build prism- and objective-type TIRF microscopes for single-molecule experiment can be found elsewhere (Roy et al., 2008; Selvin & Ha, 2008).

Schematic of prism-type TIRF microscope is shown in Fig. 2A. The TIRF microscope is built around a commercial inverted microscope (IX51 or IX71, Olympus). A flow chamber containing fluorescently labeled sample is placed on the inverted microscope and a prism made of quartz or suprasil (Pellin-Broca Prism, CVI Laser Optics) is placed on top of the chamber. The gap between the chamber and the prism is filled with a drop of immersion oil for index matching. For Cy3–Cy5 FRET pair, which is used throughout this chapter, 532 nm laser with output power  $>25$  mW is used

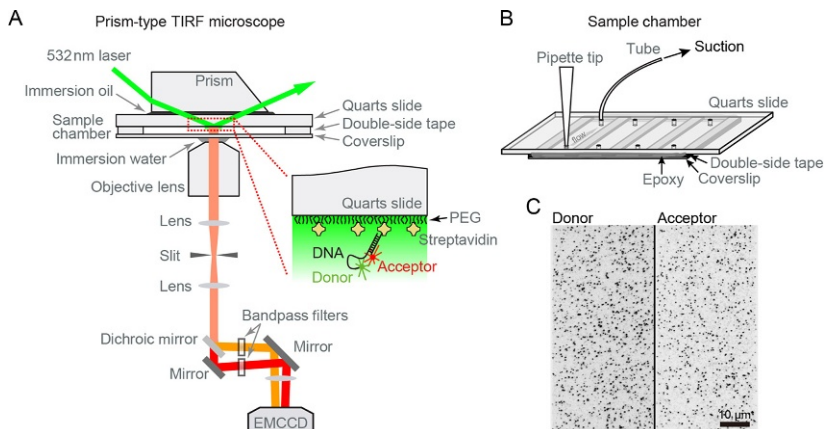


**Fig. 2** TIRF microscopy and sample chamber. (A, B) Schematic of prism-type TIRF microscopy (A) and microfluidic sample chamber (B). (C) An example of single-molecule fluorescence image. The image is divided such that donor fluorescence is imaged on the *left half* of the CCD area and acceptor fluorescence from the same surface area is imaged on the *right half*.

as a light source. The laser beam is sent from the side of the prism such that total internal reflection occurs at the sample surface (inner surface of the flow chamber). Dye molecules on the surface are then excited by the evanescent field and fluorescence lights emitted by the dyes are collected by an objective lens (Olympus, NA 1.2 water immersion). The field of view for single-molecule imaging is adjusted with a slit positioned at the first image plane of the microscope. After the slit, the fluorescence light is collimated again and spectrally separated into the donor (Cy3) and acceptor (Cy5) channels by using a dichroic mirror (cutoff wavelength at 630 nm). A band pass filter is placed at each fluorescence channel to eliminate scattered laser light and the fluorescence images are recorded by using an electron-multiplying charge-coupled device camera (iXon 897, Andor) that is suitable for low-light detection with single-photon sensitivity. The donor and acceptor images are mapped for colocalization as described by Roy et al. (2008). Typically, the exposure time is set to 100 ms or so depending on how fast the dynamics of interest is.

## 2.2 DNA Labeling and Sample Preparation

### 2.2.1 Fluorescence Labeling of DNA

Labeling positions of Cy3 and Cy5 pairs (PA13101 and PA15101, GE Healthcare) should be carefully chosen such that the interdy distance is

in the FRET-sensitive region (2–8 nm). Synthetic oligonucleotides with amine-modified thymine bases or dye and biotin conjugation can be purchased from commercial vendors such as IDT (Integrated DNA Technologies, Inc.). Amine-modified oligos can be labeled following the protocol provided by the vendor. Briefly, the oligos is dissolved in sodium tetraborate buffer (100 mM, pH 9.2). Typically, the concentration of the oligo is 10–100  $\mu\text{M}$ . 5- to 10-time molar excess of the dyes with a reactive NHS ester group is then mixed with the oligo and incubates for 6 h with gentle agitation at room temperature. Unreacted dyes are removed by ethanol precipitation and the labeling efficiency can be checked by measuring the concentration of the oligo and dye by absorptions. For amine-NHS ester reaction, labeling efficiency is more than 90%.

### 2.2.2 Buffers and Reagents

- *T50 buffer*
  - 10 mM Tris-HCl pH 8.0
  - 50 mM NaCl
- *RecA reaction buffer*
  - 25 mM Tris-Acetate (Tris-OAc), pH 7.5
  - 100 mM NaOAc ( $\text{NaCH}_3\text{COO}$ )
  - 10 mM  $\text{Mg}(\text{OAc})_2$  ( $\text{Mg}(\text{CH}_3\text{COO})_2$ )
  - 1 mM ATP

For single-molecule fluorescence imaging, following reagents are added to the RecA reaction buffer to stabilize photo stability of the dyes.

- *Imaging reagents I*
  - 2 mg/mL 6-hydroxy-2,5,7,8-tetramethylchroman-2-carboxylic acid (Trolox)
  - 1 mg/mL glucose oxidase
  - 0.4% (w/v) glucose
  - 0.04 mg/mL catalase

Alternatively, protocatechuate-3,4-dioxygenase (PCD)/protocatechuic acid (PCA) oxygen-scavenging system can be used instead of glucose oxidase system (Aitken, Marshall, & Puglisi, 2008).

- *Imaging reagents II*
  - 2 mg/mL 6-hydroxy-2,5,7,8-tetramethylchroman-2-carboxylic acid (Trolox)
  - 2.5 mM PCA
  - 50 nM PCD

### 2.2.3 Flow Chamber

Fluorescently labeled biomolecules with a Cy3 (donor)–Cy5 (acceptor) pair are immobilized on the inner surface of a flow chamber made by sandwiching a quartz slide and a coverslip with a double sticky tape (Fig. 2B). Holes in the quartz slide serve as inlet and outlet of the flow channel. The quartz slide and coverslip are precoated with polyethylene glycol (PEG, mPEG-SVA MW 5000, Laysan Bio) to suppress nonspecific binding of DNA and proteins. For DNA immobilization, small amount (1%–2%) of biotinylated PEG (biotin-PEG-SVA, MW 5000, Laysan Bio) is mixed (Chandradoss et al., 2014). If the sample buffer pH is lower than 7.4, where nonspecific binding of DNA to the PEG surface increases significantly, additional surface passivation with 10 mM DST (disuccinimidyl tartrate) in sodium bicarbonate buffer for an hour is required.

## 2.3 DNA Immobilization and Single-Molecule FRET Measurement

Before each experiment, 60  $\mu\text{L}$  of 0.2 mg/mL of streptavidin (Sigma) is injected into the chamber and incubated for 5 min. The amount of samples described in following sections assumes 20  $\mu\text{L}$  of chamber capacity and should be rescaled if different chamber capacity is used. After streptavidin incubation, flow 100  $\mu\text{L}$  of 10 pM partial duplex DNA in *T50 buffer* into the sample chamber and incubate for 3 min. Wash the chamber with 100  $\mu\text{L}$  of *T50 buffer* and inject another 100  $\mu\text{L}$  *T50 buffer* carrying *imaging agents I*. Place the sample chamber on the TIRF microscope setup and adjust camera settings to achieve maximum S/N ratio following instructions from the camera vendor. Typically, we observe 300–500 fluorescence spots in the field of view (see Fig. 2C). If the surface density is too low, repeat the DNA immobilization step with increased DNA concentration. If too high, prepare a new sample chamber and immobilize the DNA with lower DNA concentration.

Typically, we obtain two types of SM-FRET data: (1) FRET time traces of individual single molecules and (2) ensemble FRET histograms of single molecules. SM-FRET time trace shows how FRET efficiency changes over time; thus it is useful to track structural dynamics of individual molecules. SM-FRET histogram is useful to visualize population distribution of heterogeneous samples, which are often indistinguishable in bulk ensemble measurement. For FRET time-trace measurement, take three long movies (typically for 1–10 min) with 100 ms frame time under continuous 532 nm illumination. If the dyes photo-bleach too fast during the

measurement, which is seen as disappearance of the fluorescence spots, reduce the excitation laser power such that at least 50% of the dyes survive during the measurement. For SM-FRET histogram measurement, take 10-framed movies with 100 ms frame time from 10 different surface areas.

## 2.4 SM-FRET Data Analysis

Fluorescence from a single dye molecule is imaged as a point spread function (PSF) across a few pixels on a CCD image (Fig. 2C). To find positions of fluorescent molecules, first 10 frames of each movie are averaged and subjected to a thresholds algorithm that finds intensity peaks larger than the background noise level by at least five times. Once we identify positions of all the molecules in both the donor and acceptor images, molecules that appear in both images are selected as FRET pairs. Fluorescence intensity of each molecule is determined by summing the surrounding pixel intensities of a peak within a distance twice of FWHM of the PSF. Then the intensities of the selected pairs are extracted out from all the remaining frames to obtain intensity time traces of the donor and acceptor for each molecule.

FRET efficiency,  $E(t)$ , is calculated by the ratio of the acceptor intensity to the total intensity:

$$E(t) = \frac{F_A(t)}{F_A(t) + \gamma \times F_D(t)}$$

Here,  $F_D(t)$  and  $F_A(t)$  are the fluorescence intensities of the donor and acceptor molecules at time  $t$ , respectively.  $\gamma$  accounts differences in intrinsic brightness of the donor and the acceptor, which is approximately 1 for the Cy3–Cy5 pair. In practice, small fraction (leakage,  $L$ ) of the donor signal is measured in the acceptor channel due to a spectral overlap of the two dyes. The leakage fraction can be directly determined by using a sample labeled with only donor dye. The corrected FRET efficiency is then,

$$E(t) = \frac{F_A(t) - L \times F_D(t)}{F_A(t) + F_D(t)}$$

To visualize the FRET population distribution, we determine FRET values of all the single molecules observed in the 10-framed short movies (see Section 2.3) and build an SM-FRET histogram. SM-FRET analysis codes used in this chapter are written in Matlab and are freely available upon request.

### 3. NUCLEATION

Although RecA loading is tightly regulated by RecA-loading machineries such as RecBCD and RecFOR, RecA alone can spontaneously nucleate on an ssDNA to form a small patch of a filament (Bell, Plank, Dombrowski, & Kowalczykowski, 2012; Galletto et al., 2006; Joo et al., 2006; van Loenhout, van der Heijden, Kanaar, Wyman, & Dekker, 2009). This spontaneous nucleation requires simultaneous binding of two to six monomers to a nucleation site. The de novo filament is, however, unstable and can easily disassemble from the ssDNA unless it grows to a longer filament by addition of more monomers at its ends. The nucleation frequency and the stability of the de novo filament are dependent on the substrate DNA sequence (Kim et al., 2013). In this section, we describe a real-time SM-FRET assay that measures the nucleation and disassembly processes of the RecA filament.

#### 3.1 DNA Design and Buffer Condition

To observe the filament nucleation process on an ssDNA, we use a partial duplex DNA with a short 5' ss-overhang of which length is 18–21 nt (Fig. 3A). The ss-overhang is long enough for binding of five to six RecA monomers but too short for further growth. The partial duplex DNA is made by hybridizing (1) 5'-Cy5-GCC TCG CTG CCG TCG CCA-biotin-3' and (2) 5'-TGG CGA CGG CAG CGA GGC-N<sub>n</sub>-Cy3-3', where N<sub>n</sub> indicates a sequence of *n* nucleotides on which a RecA filament forms. Typically, N<sub>n</sub> sequence is designed as a repeat of three nucleotides

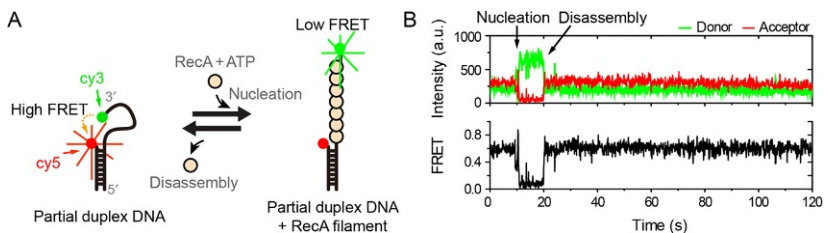


**Fig. 3** RecA nucleation and disassembly. (A) Schematic of DNA design for nucleation process. (B) An example of SM fluorescence (*top panel*) and FRET (*bottom panel*) time traces.

because a RecA monomer interacts with three nucleotides within the filament. To observe the nucleation process independent of the substrate sequence, polythymine is a preferential choice due to its lack of secondary structure.

RecA protein can be purchased from New England Biolabs (M0249) and used without further purification. Nucleation is performed with 1  $\mu\text{M}$  RecA and 1 mM ATP in *RecA reaction buffer* at room temperature. For real-time measurement, *imaging reagents I* is also included in the reaction buffer.

### 3.2 Experimental Procedure

- i. Prepare a sample chamber and immobilize DNA as described in [Section 2.2](#).
- ii. Inject 100  $\mu\text{L}$  of *RecA Reaction buffer* carrying 1  $\mu\text{M}$  RecA, 1 mM ATP, and *Imaging reagents I* into the chamber and incubate for 5 min.
- iii. Place the sample chamber on the TIR microscope setup and take a 5-min-long movie with 100 ms frame rates.
- iv. Repeat measurements for at least three different surface areas.

### 3.3 Real-Time Observation of RecA Filament Nucleation

An example of the single-molecule FRET trace is shown in [Fig. 3B](#). Initially, the molecule shows high FRET efficiency ( $\sim 0.7$ ), reflecting relatively short dye-to-dye distance due to the flexible ssDNA overhang. Nucleation of RecA filament makes the ss-overhang stretched, increasing the dye-to-dye distance. A nucleation step is observed as an abrupt change in the FRET time trace ([Fig. 3B](#), indicated by an arrow), implying that five to six RecA monomers bind simultaneously within the experimental time resolution. As the filament cannot grow due to the spatial confinement, it disassembles and the FRET efficiency recovers back to the bare DNA state. Again, the abrupt FRET change indicates cooperative disassembly of the bound monomers. Useful parameters that can be obtained from the SM-FRET measurements are nucleation frequency and dwell time of the de novo filament. Typically, in a 5-min-long time trace, one or two nucleation events occur and, therefore, nucleation events should be collected from all the molecules observed for statistical analysis. As nucleation frequency and dwell time determine overall stability of the RecA filament, these parameters are useful to find a preferential condition for RecA filament formation.

## 4. END-DEPENDENT PRESYNAPTIC FILAMENT DYNAMICS

After a successful nucleation, a RecA filament grows to several kilobases by addition of monomers at its ends (Joo et al., 2006). The growth occurs mainly toward 3' end side of the substrate DNA (Register & Griffith, 1985). While this elongation process stabilizes the presynaptic filament on its substrate ssDNA, bound monomers at the ends can dissociate from the filament upon ATP hydrolysis, resulting in filament destabilization. These perpetual binding and dissociation of monomers put the filament end in dynamic equilibrium in which the kinetic rates of the two processes determine overall growth or disassembly of the filament. It has been shown that the binding rate at 3' end is larger than that of 5' end by two orders of magnitude, while the dissociation rate is similar regardless of polarity, resulting in the asymmetric growth toward 3' end (Joo et al., 2006). Consequently, these kinetic rates are tightly controlled by many factors such as pH and substrate DNA sequence (Kim et al., 2013, 2015). In this section, we describe SM-FRET assays that separately measure the binding and dissociation process at each end of the RecA filament (Fig. 4).

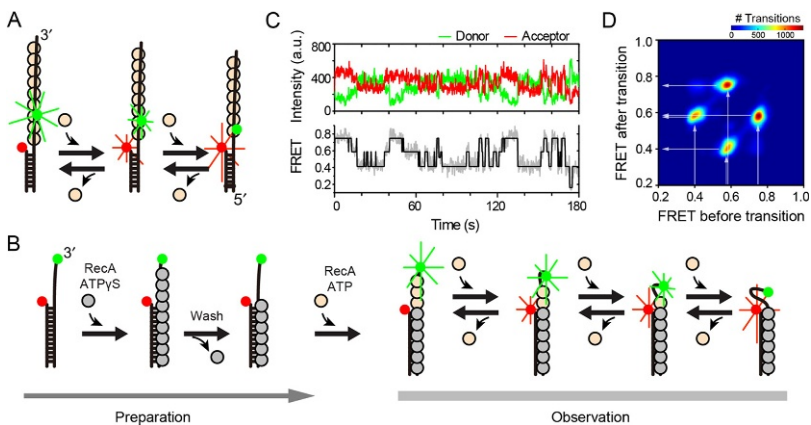


**Fig. 4** End-dependent monomer binding and dissociation. (A) Schematic of the partial duplex DNA for 5' end dynamics. (B) DNA design and experimental scheme of 3' end dynamics. (C) An example of SM fluorescence (*top panel*) and FRET (*bottom panel*) time traces measured at 5' end of the RecA filament. FRET states defined by using HMM are shown in *black (bottom panel)*. (D) An example of TDP plot for the 5' end dynamics measured with 10 nt dye separation. Three FRET states are observed for the cases of 0, 1, and 2 monomers occupation between the dye pair.

## 4.1 DNA Design and Buffer Conditions

To observe the monomer binding and dissociation process at 5' end of the RecA filament, a dye pair is placed near the junction of a partial duplex DNA with 3' ss-overhang (Fig. 4A). The partial duplex DNA is made by hybridizing (1) a 3'-biotinylated 18 nt-long oligo with Cy5 labeled at its 5' end (5'-Cy5-GCC TCG CTG CCG TCG CCA-biotin-3') and (2) a 78 nt-long oligo with internally labeled Cy3 (5'-TGG CGA CGG CAG CGA GGC (dT)<sub>10</sub>-T\*-(dT)<sub>49</sub>-3'), where T\* denotes an amine-labeled thymine base for Cy3 labeling. Note that Cy3 is separated by 10 nt from the Cy5 when hybridized. The 10 thymine bases between the dye pairs can be replaced with other sequence combinations to study the influence of the substrate sequence dependency on the monomer binding and disassembly (Kim et al., 2014). The reaction buffer condition is the same with that used in Section 3.

For 3' end dynamics, a partial duplex DNA (Fig. 4B) with a relatively short ss-overhang (10 nt) is used. The acceptor dye is placed at the junction of the partial duplex and the donor is placed at the end of the ss-overhang. The partial duplex DNA is made by hybridizing (1) a 3'-biotinylated 18 nt-long oligos with Cy5 labeled at its 5' end (5'-Cy5-GCC TCG CTG CCG TCG CCA-biotin-3') and (2) a Cy3-labeled 10 nt-long polythymine strand with 18 bases of complementary sequences to the biotinylated oligo at 5' end (5'-TGG CGA CGG CAG CGA GGC (dT)<sub>10</sub>-Cy3). The reaction buffer condition is the same with that used in for 5' end dynamics except the RecA concentration which is reduced down to 10 nM.

## 4.2 Experimental Procedure for the 5' End Dynamics

- i. Prepare a sample chamber and immobilize DNA as described in Section 2.2.
- ii. Flow 100  $\mu$ L *RecA reaction buffer* carrying 1  $\mu$ M RecA and 1 mM ATP and incubate for 5 min.
- iii. Take 10-frame-long movies with 100 ms frame time.
- iv. Take a movie for 3–5 min at 100 ms frame time.

## 4.3 Experimental Procedure for the 3' End Dynamics

- i. Prepare a sample chamber and immobilize DNA as described in Section 2.2.
- ii. Inject 100  $\mu$ L *RecA reaction buffer* carrying 1  $\mu$ M RecA and 1 mM ATP $\gamma$ S and incubate for 5 min.

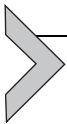
- iii. Take 10-frame-long movies with 100 ms frame time and build a FRET histogram of the ATP $\gamma$ S-RecA filament.
- iv. Wash the chamber by flowing 300  $\mu$ L *RecA reaction buffer* without RecA and ATP and incubate for 30 min. In the absence of free RecA and ATP in solution, the RecA monomers bound on the ss-overhang with ATP $\gamma$ S would slowly disassemble, whereas the monomers bound on the double stranded (ds) would not (Fig. 4B). The remaining ATP $\gamma$ S/dsDNA filament is stable for several hours in *RecA reaction buffer* and therefore can be used for a stable nucleated filament that can grow into the ss-overhang of the partial duplex DNA.
- v. Check the FRET distribution as is done in (iii). The FRET population should show high FRET state as the filament on ss-overhang disassembles. If the ATP $\gamma$ S-RecA filament population remains at this step repeat the washing step in (iv) until all the ATP $\gamma$ S-RecA filament population disappears.
- vi. Flow 100  $\mu$ L *RecA reaction buffer* carrying 10 nM RecA and 1 mM ATP and incubate for 5 min. Note that 10 nM of RecA is 100 times lower than that used in Section 3. Therefore, de novo nucleation on the ssDNA does not occur in this condition and FRET change solely reflects filament growth and shrinkage from the ATP $\gamma$ S/dsDNA filament.
- vii. Take a movie for 3–5 min at 100 ms time resolution.

#### 4.4 Monomer Binding and Dissociation at the End of RecA Filament

Monomer binding and dissociation events can be observed as abrupt changes in SM-FRET time traces of individual RecA filament. When a RecA monomer binds to ssDNA, it occupies three bases and keeps the region stretched, effectively increasing the interdye distance. When the dye pairs are 10 nt apart, three RecA monomers can bind between the dyes. Therefore, there are four FRET states depending on the number of bound RecA monomers (Joo et al., 2006). In case of the 5' end dynamics, however, up to two monomers were observed to bind with the partial duplex DNA design possibly due to spatial hindrance of the nearby double-strand DNA (Joo et al., 2006). An example of SM-FRET time trace is given in Fig. 4C, which shows transitions between three FRET states. The transitions are best observed when the binding and dissociation rates are similar so that the filament end is in dynamic equilibrium. Thus, if the observed trace shows bias

to either high or low FRET states, RecA concentration in the buffer should be adjusted to change the binding rate.

To quantitatively determine transition rates between the states, Hidden Markov Method (HMM) is used. HMM assumes that the transitions between the states follow Markovian process, i.e., random transition that depends solely on the kinetic rates and current state of the system. Details of the method applied to SM-FRET data analysis are well established (Abraham, Ram, Chao, Ward, & Ober, 2009; Lee, 2009; McKinney, Joo, & Ha, 2006) and an analysis program is freely available at <http://ha.med.jhmi.edu>. An example of SM-FRET time trace together with its most-likely estimation of the FRET states using HMM is shown in Fig. 4C. Once all the transitions are identified from the SM traces, a transition density plot (TDP) is built to classify the transitions (Fig. 4D), from which the kinetic rate of each transition can be determined (McKinney et al., 2006).



## 5. PROTEIN SCAFFOLD SHIFT WITHIN PRESYNAPTIC FILAMENT

RecA monomers within a presynaptic filament continuously hydrolyze ATP, but only the monomers situated at the end of the filament can disassemble (Brenner et al., 1987; Shan, Bork, Webb, Inman, & Cox, 1997). Because the RecA filament is, in fact, capable of finding and pairing of the homology without ATP hydrolysis (Kowalczykowski & Krupp, 1995; Menetski, Bear, & Kowalczykowski, 1990), it has long been an open question why the internally located monomers also consume ATP energy which is seemingly too wasteful. Recently, a novel ATP-dependent internal dynamics, in which the RecA protein scaffold moves relatively to its substrate ssDNA, has been directly observed by using SM-FRET (Kim et al., 2017). Through this scaffold shift process, two fragmented filaments can be connected to each other, which is essential in making a kilobase long seamless filament. Consequently, scaffold shift is tightly regulated by the substrate ssDNA sequence containing the recombination hot spot, Chi.

### 5.1 DNA Design

For observation of internal dynamics of RecA filament, a dye pair is placed in the middle of an ss-overhang of a partial duplex DNA (Fig. 5A). The partial duplex DNA is made by hybridizing (1) a 3'-biotinylated 18 nt-long oligo (5'-GCC TCG CTG CCG TCG CCA-biotin-3') and (2) a double-labeled

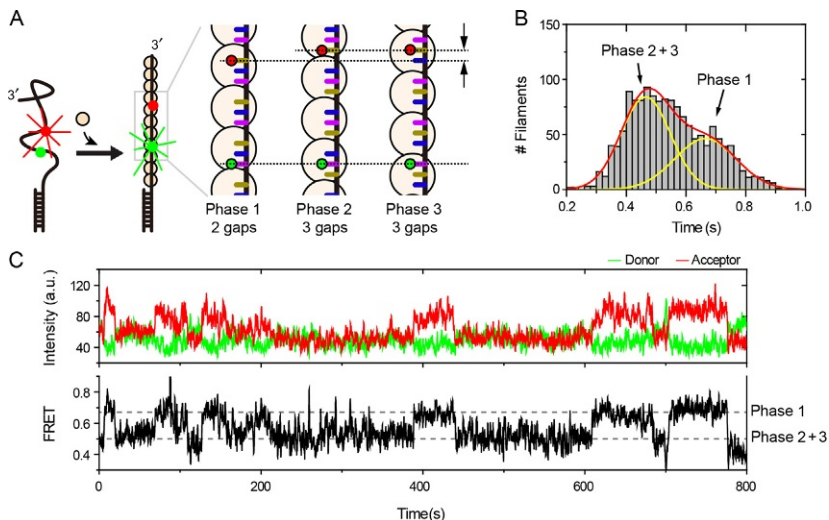


**Fig. 5** Protein scaffold shift along the substrate DNA. (A) Schematic of the DNA design for internal filament dynamics. The dye pairs are separated by 8 nt. (B) SM-FRET histogram obtained from RecA filament formed on the internally labeled FRET pair with 8 nt separation. (C) An example of SM-FRET time traces that shows transition between the two FRET states identified in (B). *Dashed lines* are eye guides for FRET states.

oligo with amine groups ( $5'$ -TGG CGA CGG CAG CGA GGC (dT) $_{29}$ -T $^*$ -(dT) $_n$ -T $^*$ -(dT) $_{29-n}$ -3'), where  $n$  is either 7, 8, or 9 and T $^*$  denotes the amine-modified thymine. Before hybridization, the two amino groups are randomly labeled with Cy3 or Cy5 by reacting with an equimolar mixture of Cy3 and Cy5. Therefore, only half of the DNA sample would have both the donor and acceptors. To study the influence of the substrate DNA sequence, thymine sequences near the dye-labeling sites can be modified as desired.

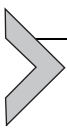
## 5.2 Experimental Procedure

- i. Prepare a sample chamber and immobilize DNA as described in [Section 2.2](#).
- ii. Flow 100  $\mu$ L *RecA* reaction buffer carrying 1  $\mu$ M RecA and 1 mM ATP and incubate for 5 min.
- iii. Take 10-frame-long movies with 100 ms frame time from 10 different surface areas.
- iv. Take a movie for 10 min at 100 ms frame time.

### 5.3 Phase Detection of Individual RecA Filaments and Scaffold Shift

The experimental design for a direct observation of protein scaffold shift is based on a unique structure of the ssDNA lying at the central axis of the RecA filament (Chen et al., 2008; Kim et al., 2017). The bases of the ssDNA are grouped into base triplets (three bases) each of which is occupied by a RecA monomer, while neighboring triplets are separated by a large gap (Fig. 1A). Therefore, there are three RecA-binding modes (hereafter referred as “phase”) depending on grouping of the bases or positioning of gaps (Volodin & Camerini-Otero, 2002; Volodin, Smirnova, Bocharova, & Camerini-Otero, 2003). For example, if we index the bases with numbers from 3'end, phase 1 can be defined as to have one to three bases into a triplet, four to six bases to another, and so on. In phase 2, two to four bases are grouped together, leaving the first base unoccupied. Phase 3 is then to group 3–5, 6–8, and so on. Note that the relative position of the protein scaffold for each phase is shifted by 1 or 2 nt.

The phase of the RecA filament can be detected by SM-FRET. If a dye pair is placed on the ssDNA in the middle of the filament with 9 nt separation (which is multiple of 3), there are always three gaps regardless of the phase. However, when the dye pairs are separated by 8 or 10 nt (which are not multiple of 3), the number of gaps between the dyes changes depending on the phase of the filament. An example case of 8 nt separation is shown in Fig. 5A, in which two gaps exist between the dyes in phase 1, while three gaps are in phases 2 and 3. Because a gap is generated by extra elongation of phosphate backbone of the ssDNA (Chen et al., 2008), the length difference due to different number of gaps can be picked up by FRET. A representative example of SM-FRET histogram shows two distinct populations at  $E \sim 0.46$  and  $E \sim 0.64$  with the population ratio of 2:1 (Fig. 5B). SM-FRET time trace shows the transition between these two FRET states, showing phase transition via protein scaffold shift (Fig. 5C). This scaffold shift requires energy from ATP hydrolysis and tightly regulated by substrate DNA sequence (Kim et al., 2017).



## 6. ATP-DEPENDENT CONFORMATIONAL CHANGE

RecA filament adapts two conformations depending on nucleotide cofactor state (Bell, 2005; Chen et al., 2008; Story, Weber, & Steitz, 1992). With ATP, RecA forms a stretched (active) filament with a helical

pitch length of 9.4 nm. With ADP or without any nucleotide cofactor, it forms a compressed (inactive) filament with a helical pitch length of 7.5 nm. In an ATP-rich environment, RecA maintains the stretched conformation for homology search and strand exchange. When the ATP concentration decreases, RecA filament changes its conformation to compressed form. Therefore, it is critical for cells to keep the RecA filament in the stretched form when DSB occurs. Decades of efforts have been dedicated to characterize the two conformations and transitions between them. Electron microscopy and X-ray crystallography have provided high-resolution images of the two conformations (Chen et al., 2008; Egelman & Stasiak, 1986; Story & Steitz, 1992; Story et al., 1992; Yu & Egelman, 1992). SM approaches including optical and magnetic tweezers and DNA curtain have observed conformational change in real time (Hilario, Amitani, Baskin, & Kowalczykowski, 2009; Nishinaka, Doi, Hara, & Yashima, 2007; Robertson et al., 2009; van Loenhout et al., 2009), yet these studies were limited by low spatial resolution and unable to investigate detailed molecular mechanisms behind the conformational change. To overcome these limitations, an SM-FRET assay is designed for a real-time observation with high spatial resolution in the nanometer scale and used to study the detailed molecular mechanism of the conformational transition (Kim et al., 2014).

## 6.1 DNA Design and Buffer Condition

To observe conformational transition of the RecA filament, we use a similar partial duplex DNA used in Section 5. The interdyde distance is set to 9 nt such that the FRET is insensitive to the scaffold shift seen in Section 5 and faithfully reflects conformational transitions (Fig. 6A). The partial

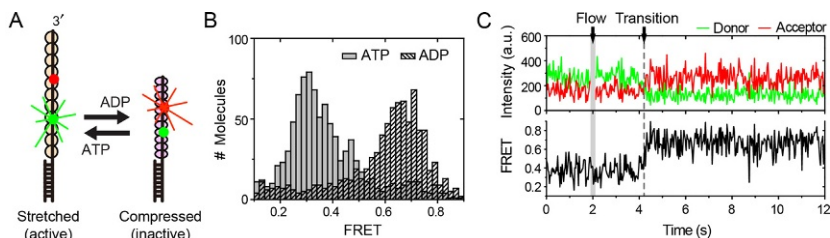


**Fig. 6** Cooperative conformational change of RecA filament. (A) Schematic of conformational change of RecA filament upon nucleotide exchange. The dye pairs are separated by 9 nt. (B) SM-FRET histograms obtained in the presence of ATP (gray bars) or ADP (shaded bars). (C) An example of the SM fluorescence and FRET time traces. Buffer exchange was given at  $t = 2$  s and a transition is observed at  $\sim 4$  s.

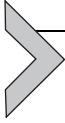
duplex DNA is made by hybridizing (1) a 3'-biotinylated 18 nt-long oligo (5'-GCC TCG CTG CCG TCG CCA-biotin-3') and (2) a double-labeled oligo with amine groups (5'-TGG CGA CGG CAG CGA GGC (dT)<sub>29</sub>-T\*-(dT)<sub>8</sub>-T\*-(dT)<sub>21</sub>-3'). T\* denotes the amine-modified thymine which is randomly labeled with Cy3 or Cy5 as described in [Section 5.1](#). To study the influence of the substrate DNA sequence, thymine sequences near the dye-labeling sites can be modified as desired. The reaction buffer condition is the same with that used in [Section 3](#).

## 6.2 Experimental Procedure

- i. Prepare a sample chamber and immobilize DNA as described in [Section 2.2](#).
- ii. Flow 100  $\mu\text{L}$  *RecA reaction buffer* carrying 1  $\mu\text{M}$  RecA and 1 mM ATP and incubate for 5 min.
- iii. Take 10-frame-long movies with 100 ms frame time from 10 different surface areas.
- iv. Prepare 100  $\mu\text{L}$  *RecA reaction buffer* carrying 1  $\mu\text{M}$  RecA and 1 mM ADP for buffer exchange in the next step.
  - v. Start taking a 1-min-long movie with 100 ms frame time. 2 s after the recoding starts, flow the buffer prepared in step (iv) into the chamber.
- vi. Take 10-frame-long movies with 100 ms frame time from 10 different surface areas.

## 6.3 Real-Time Observation of Conformational Transitions

Representative examples of SM-FRET histogram measured from the RecA filament formed with ATP or ADP are shown in [Fig. 6B](#). Initially with ATP, the RecA filament shows low FRET efficiency peaked at  $E \sim 0.3$ , reflecting the stretched ssDNA of the filament. After ATP is replaced by ADP via buffer exchange, the filament shows high FRET state at  $E \sim 0.65$  as the filament is compressed. The conformational transition is recorded in the SM-FRET time trace as an abrupt increase of FRET efficiency ([Fig. 6C](#)). The abrupt FRET change implies that the conformational change happens within the experimental time resolution (100 ms) via cooperative transition of the RecA monomers ([Kim et al., 2014](#)). Note that the flow is given at 2 s, while the transition occurs at  $\sim 4$  s, indicating that RecA does not change its conformation immediately after the buffer exchange but wait for a while for hydrolysis of bound ATP molecules.



## 7. CONCLUSIONS

SM-FRET has been proven to be a powerful technique to study the molecular mechanism of protein-mediated dynamics owing to its capability of dissecting complex kinetic processes. In this chapter, TIFR-based SM-FRET assays that unveil the complex molecular mechanisms of the RecA presynaptic filament dynamics are described with detailed experimental procedures. Each kinetic process happening in the RecA presynaptic filament is separately controlled and measured, providing detailed molecular pictures of the intrinsically dynamic nucleoprotein complex. The findings from these assays enabled a comprehensive understanding on how RecA presynaptic filament maintains its active state despite its dynamic properties. The experimental frameworks illustrated in this chapter can be used to study the molecular mechanisms of synaptic and postsynaptic filament of RecA. Also, these methodologies are applicable for other proteins that interact with DNA making a nucleoprotein complex.

## ACKNOWLEDGMENT

S.H.K. was funded by the National Creative Research Initiative Program (Center for Single-Molecule Systems Biology, NRF-2011-0018352) of the National Research Foundation.

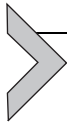
## REFERENCES

- Abraham, A. V., Ram, S., Chao, J., Ward, E. S., & Ober, R. J. (2009). Quantitative study of single molecule location estimation techniques. *Optics Express*, *17*, 23352–23373.
- Aitken, C. E., Marshall, R. A., & Puglisi, J. D. (2008). An oxygen scavenging system for improvement of dye stability in single-molecule fluorescence experiments. *Biophysical Journal*, *94*, 1826–1835.
- Bell, C. E. (2005). Structure and mechanism of Escherichia coli RecA ATPase. *Molecular Microbiology*, *58*, 358–366.
- Bell, J. C., Plank, J. L., Dombrowski, C. C., & Kowalczykowski, S. C. (2012). Direct imaging of RecA nucleation and growth on single molecules of SSB-coated ssDNA. *Nature*, *491*, 274–278.
- Bianco, P. R., Tracy, R. B., & Kowalczykowski, S. C. (1998). DNA strand exchange proteins: A biochemical and physical comparison. *Frontiers in Bioscience*, *3*, D570–603.
- Brenner, S. L., Mitchell, R. S., Morrical, S. W., Neuendorf, S. K., Schutte, B. C., & Cox, M. M. (1987). recA protein-promoted ATP hydrolysis occurs throughout recA nucleoprotein filaments. *The Journal of Biological Chemistry*, *262*, 4011–4016.
- Chandradoss, S. D., Haagsma, A. C., Lee, Y. K., Hwang, J. H., Nam, J. M., & Joo, C. (2014). Surface passivation for single-molecule protein studies. *Journal of Visualized Experiments*, *86*, e50549.
- Chen, Z. C., Yang, H. J., & Pavletich, N. P. (2008). Mechanism of homologous recombination from the RecA-ssDNA/dsDNA structures. *Nature*, *453*, 489–494.
- Dillingham, M. S., & Kowalczykowski, S. C. (2008). RecBCD enzyme and the repair of double-stranded DNA breaks. *Microbiology and Molecular Biology Reviews*, *72*, 642–671.

- Egelman, E. H., & Stasiak, A. (1986). Structure of helical RecA-DNA complexes. Complexes formed in the presence of ATP-gamma-S or ATP. *Journal of Molecular Biology*, *191*, 677–697.
- Egelman, E. H., & Stasiak, A. (1993). Electron-microscopy of RecA-DNA complexes—2 different states, their functional-significance and relation to the solved crystal-structure. *Micron*, *24*, 309–324.
- Galletto, R., Amitani, I., Baskin, R. J., & Kowalczykowski, S. C. (2006). Direct observation of individual RecA filaments assembling on single DNA molecules. *Nature*, *443*, 875–878.
- Ha, T., Enderle, T., Ogletree, D. F., Chemla, D. S., Selvin, P. R., & Weiss, S. (1996). Probing the interaction between two single molecules: Fluorescence resonance energy transfer between a single donor and a single acceptor. *Proceedings of the National Academy of Sciences of the United States of America*, *93*, 6264–6268.
- Ha, T., Kozlov, A. G., & Lohman, T. M. (2012). Single-molecule views of protein movement on single-stranded DNA. *Annual Review of Biophysics*, *41*, 295–319.
- Hilario, J., Amitani, I., Baskin, R. J., & Kowalczykowski, S. C. (2009). Direct imaging of human Rad51 nucleoprotein dynamics on individual DNA molecules. *Proceedings of the National Academy of Sciences of the United States of America*, *106*, 361–368.
- Joo, C., Balci, H., Ishitsuka, Y., Buranachai, C., & Ha, T. (2008). Advances in single-molecule fluorescence methods for molecular biology. *Annual Review of Biochemistry*, *77*, 51–76.
- Joo, C., McKinney, S. A., Nakamura, M., Rasnik, I., Myong, S., & Ha, T. (2006). Real-time observation of RecA filament dynamics with single monomer resolution. *Cell*, *126*, 515–527.
- Kim, S. H., Ahn, T., Cui, T. J., Chauhan, S., Sung, J., Joo, C., et al. (2017). RecA filament maintains structural integrity using ATP-driven internal dynamics. *Science Advances*, *3*, e1700676.
- Kim, S. H., Joo, C., Ha, T., & Kim, D. (2013). Molecular mechanism of sequence-dependent stability of RecA filament. *Nucleic Acids Research*, *41*, 7738–7744.
- Kim, S. H., Park, J., Joo, C., Kim, D., & Ha, T. (2015). Dynamic growth and shrinkage govern the pH dependence of RecA filament stability. *PLoS One*, *10*, e0115611.
- Kim, S. H., Ragunathan, K., Park, J., Joo, C., Kim, D., & Ha, T. (2014). Cooperative conformational transitions keep RecA filament active during ATPase cycle. *Journal of the American Chemical Society*, *136*, 14796–14800.
- Kowalczykowski, S. C. (2000). Initiation of genetic recombination and recombination-dependent replication. *Trends in Biochemical Sciences*, *25*, 156–165.
- Kowalczykowski, S. C., & Krupp, R. A. (1995). DNA-strand exchange promoted by RecA protein in the absence of ATP: Implications for the mechanism of energy transduction in protein-promoted nucleic acid transactions. *Proceedings of the National Academy of Sciences of the United States of America*, *92*, 3478–3482.
- Lee, T. H. (2009). Extracting kinetics information from single-molecule fluorescence resonance energy transfer data using hidden markov models. *The Journal of Physical Chemistry B*, *113*, 11535–11542.
- Lusetti, S. L., & Cox, M. M. (2002). The bacterial RecA protein and the recombinational DNA repair of stalled replication forks. *Annual Review of Biochemistry*, *71*, 71–100.
- McKinney, S. A., Joo, C., & Ha, T. (2006). Analysis of single-molecule FRET trajectories using hidden Markov modeling. *Biophysical Journal*, *91*, 1941–1951.
- Menetski, J. P., Bear, D. G., & Kowalczykowski, S. C. (1990). Stable DNA heteroduplex formation catalyzed by the Escherichia coli RecA protein in the absence of ATP hydrolysis. *Proceedings of the National Academy of Sciences of the United States of America*, *87*, 21–25.
- Michel, B., Boubakri, H., Baharoglu, Z., LeMasson, M., & Lestini, R. (2007). Recombination proteins and rescue of arrested replication forks. *DNA Repair (Amst)*, *6*, 967–980.

- Nishinaka, T., Doi, Y., Hara, R., & Yashima, E. (2007). Elastic behavior of RecA-DNA helical filaments. *Journal of Molecular Biology*, 370, 837–845.
- Register, J. C., 3rd, & Griffith, J. (1985). The direction of RecA protein assembly onto single strand DNA is the same as the direction of strand assimilation during strand exchange. *The Journal of Biological Chemistry*, 260, 12308–12312.
- Robertson, R. B., Moses, D. N., Kwon, Y., Chan, P., Chi, P., Klein, H., et al. (2009). Structural transitions within human Rad51 nucleoprotein filaments. *Proceedings of the National Academy of Sciences of the United States of America*, 106, 12688–12693.
- Roy, R., Hohng, S., & Ha, T. (2008). A practical guide to single-molecule FRET. *Nature Methods*, 5, 507–516.
- Selvin, P. R., & Ha, T. (2008). *Single-molecule techniques: A laboratory manual*. Cold Spring Harbor, NY: Cold Spring Harbor Laboratory Press.
- Shan, Q., Bork, J. M., Webb, B. L., Inman, R. B., & Cox, M. M. (1997). RecA protein filaments: End-dependent dissociation from ssDNA and stabilization by RecO and RecR proteins. *Journal of Molecular Biology*, 265, 519–540.
- Spies, M., Dillingham, M. S., & Kowalczykowski, S. C. (2005). Translocation by the RecB motor is an absolute requirement for {chi}-recognition and RecA protein loading by RecBCD enzyme. *The Journal of Biological Chemistry*, 280, 37078–37087.
- Story, R. M., & Steitz, T. A. (1992). Structure of the recA protein-ADP complex. *Nature*, 355, 374–376.
- Story, R. M., Weber, I. T., & Steitz, T. A. (1992). The structure of the E. coli recA protein monomer and polymer. *Nature*, 355, 318–325.
- van Loenhout, M. T., van der Heijden, T., Kanaar, R., Wyman, C., & Dekker, C. (2009). Dynamics of RecA filaments on single-stranded DNA. *Nucleic Acids Research*, 37, 4089–4099.
- Volodin, A. A., & Camerini-Otero, R. D. (2002). Influence of DNA sequence on the positioning of RecA monomers in RecA-DNA cofilaments. *The Journal of Biological Chemistry*, 277, 1614–1618.
- Volodin, A. A., Smirnova, E. A., Bocharova, T. N., & Camerini-Otero, R. D. (2003). Phasing of RecA monomers on quasi-random DNA sequences. *FEBS Letters*, 546, 203–208.
- Yu, X., & Egelman, E. H. (1992). Direct visualization of dynamics and co-operative conformational changes within RecA filaments that appear to be associated with the hydrolysis of adenosine 5'-O-(3-thiotriphosphate). *Journal of Molecular Biology*, 225, 193–216.

This page intentionally left blank



# The RadA Recombinase and Paralogs of the Hyperthermophilic Archaeon *Sulfolobus solfataricus*

Michael L. Rolfsmeier, Cynthia A. Haseltine<sup>1</sup>

School of Molecular Biosciences, Washington State University, Pullman, WA, United States

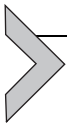
<sup>1</sup>Corresponding author: e-mail address: chaseltine@wsu.edu

## Contents

|   |     |
|---|-----|
| 1. Introduction   | 256 |
| 1.1 Recombinase Function  | 256 |
| 1.2 The RecA Family Paralogs  | 256 |
| 2. Biochemical Approaches to Study of the <i>S. solfataricus</i> SsoRadA Protein and Its Paralogs | 258 |
| 3. Methods Shared Across Protocols  | 259 |
| 3.1 Growth of <i>E. coli</i> and Induction for Protein Expression                                 | 259 |
| 3.2 Preparation of Cell Sonicate  | 260 |
| 3.3 Dialysis Tubing Preparation   | 260 |
| 3.4 Protein Concentration Using PEG   | 261 |
| 3.5 End-Labeling Oligonucleotides With <sup>32</sup> P  | 261 |
| 4. Heterologous Protein Purification  | 261 |
| 4.1 Purification of Heterologous SsoRadA  | 262 |
| 4.2 Purification of Heterologous SsoRal1  | 264 |
| 4.3 Purification of Heterologous SsoRal2  | 267 |
| 4.4 Purification of Heterologous SsoRal3  | 270 |
| 5. ATPase Activity Assays   | 272 |
| 5.1 Thin-Layer Chromatography   | 272 |
| 5.2 Coupled Spectrophotometric Assay  | 274 |
| 6. DNA and ATP Binding Assays   | 276 |
| 6.1 Gel Shift   | 276 |
| 6.2 Filter Binding  | 278 |
| 7. Mechanistic Recombination Assays   | 279 |
| 7.1 Strand Invasion (D-Loop)  | 279 |
| 7.2 Strand Exchange   | 281 |
| 8. Summary and Conclusion   | 282 |
| References  | 283 |

## Abstract

Repair of DNA double-strand breaks is a critical function shared by organisms in all three domains of life. The majority of mechanistic understanding of this process has come from characterization of bacterial and eukaryotic proteins, while significantly less is known about analogous activities in the third, archaeal domain. Despite the physical resemblance of archaea to bacteria, archaeal proteins involved in break repair are remarkably similar to those used by eukaryotes. Investigating the function of the archaeal version of these proteins is, in many cases, simpler than working with eukaryotic homologs owing to their robust nature and ease of purification. In this chapter, we describe methods for purification and activity analysis for the RadA recombinase and its paralogs from the hyperthermophilic acidophilic archaeon *Sulfolobus solfataricus*.



---

## 1. INTRODUCTION

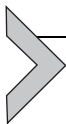
### 1.1 Recombinase Function

Homologous recombination (HR) is a universal approach for repairing DNA double-strand breaks (DSBs). While meiotic DSBs are generally programmed, those that arise during mitotic growth are often the result of replication errors or mutational events, both of which contribute to overall genome instability. In all domains of life, recombinases are central to the HR process and the main strand exchange protein is referred to by different names depending on the organism. In bacteria it is RecA, in eukaryotes it is Rad51, and in archaea it is RadA. All these RecA family proteins have conserved catalytic Walker box A and B domains and are ssDNA-dependent NTPases. These recombinases are responsible for catalyzing strand invasion and exchange during HR. To perform these functions, the recombinase must first assemble on ssDNA and form a nucleoprotein filament. The nucleoprotein filament can exist in either an inactive, nucleotide triphosphate-minus form or an active, nucleotide triphosphate-bound active form where the cofactor is typically ATP.

### 1.2 The RecA Family Paralogs

A number of proteins with similarity to RecA family recombinases have been identified and many of these paralogs have been shown to participate in HR. In *Escherichia coli*, the RadA protein (not to be confused with the archaeal RadA recombinase) is a RecA paralog that can bind to ssDNA and stimulate branch migration to increase the rate of HR (Cooper & Lovett, 2016). In *Saccharomyces cerevisiae*, the Rad55 and Rad57 proteins

are paralogs of Rad51 recombinase and act as a complex in presynapsis, assisting Rad51 in forming more continuous filaments by reducing RPA ssDNA binding affinity (Paques & Haber, 1999; Sung, 1997; Sung, Trujillo, & Van Komen, 2000) while stabilizing the nucleoprotein filament and counteracting activity of the Srs2 antirecombinase (Liu et al., 2011). The RFS-1/RIP-1 paralog complex of *Caenorhabditis elegans* is also involved in presynapsis, remodeling the Rad51 nucleoprotein filament via an end-capping mechanism to yield a flexible conformation that facilitates strand exchange (Taylor et al., 2015, 2016). Humans also encode multiple Rad51 paralogs: Rad51B, Rad51C, Rad51D, XRCC2, and XRCC3. These proteins function in multisubunit complexes to enhance HR (Albala et al., 1997; Cartwright, Tambini, Simpson, & Thacker, 1998; Dosanjh et al., 1998; Liu et al., 1998; Rice, Smith, Bullrich, Havre, & Kmiec, 1997). Archaea that are members of the euryarchaeal branch encode a single RadA recombinase paralog, RadB. RadB is characterized by a KHR motif and can interact with the Holiday junction cleavage protein (Guy et al., 2006; Komori, Miyata, Daiyasu, et al., 2000; Komori, Miyata, DiRuggiero, et al., 2000). For halophiles within this branch, this protein has been implicated as a recombination mediator that induces a conformational change in RadA protein, promoting nucleoprotein filament formation (Wardell et al., 2017). Crenarchaeal members of the *Sulfolobus* genus encode multiple RadA paralogs. *Sulfolobus islandicus* has two identified paralogs that have been implicated in DNA repair through deletion studies (Liang et al., 2013). Three paralogs have been identified in *Sulfolobus tokodaii* and some of these may individually function positively through displacement of the single-stranded DNA binding protein to promote nucleoprotein filament formation, while others act as antirecombinases via inhibition of RadA activity (Sheng, Li, Jiao, Ni, & Shen, 2008; Sheng, Zhu, Wei, Ni, & Shen, 2008; Wang et al., 2012). *Sulfolobus solfataricus* encodes three paralogs named for their similarity to the RadA protein: SsoRal1, SsoRal2, and SsoRal3 (Rolfmeier, Laughery, & Haseltine, 2010). SsoRal1 has ssDNA-stimulated ATPase activity, binds ssDNA, and acts to stabilize the SsoRadA nucleoprotein filament (Graham, Rolfmeier, & Haseltine, 2013). SsoRal3 also functions to stabilize the SsoRadA nucleoprotein filament, but differs from SsoRal1 in that it changes its DNA binding preferences depending on nucleotide availability; in the presence of ATP it binds ssDNA, but in its absence, it instead binds dsDNA with high affinity (Graham & Haseltine, 2013). The role of the SsoRal2 protein in HR is as yet undefined; however, it is a DNA-independent ATPase that directly interacts with both SsoRal1 and SsoRal3 (Corey Knadler & Cynthia Haseltine, unpublished results).



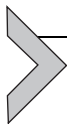
## 2. BIOCHEMICAL APPROACHES TO STUDY OF THE *S. SOLFATARICUS* SsoRadA PROTEIN AND ITS PARALOGS

One of the reasons the archaeal SsoRadA recombinase and its paralogs are an attractive choice for study is that they have significant similarity to the eukaryotic recombinases and paralogs. Archaea employ a number of proteins and pathways that strongly resemble those found in eukaryotes; this is especially true for DNA information processes including transcription, replication, and repair. Additionally, SsoRadA and its paralogs are exceptionally easy to purify heterologously and are remarkably robust, retaining activity after extended incubation at high temperature as well as after storage at 4°C for months.

We have produced overexpression vectors for heterologous protein production in *E. coli* for SsoRadA and all three of the *S. solfataricus* paralogs (Corey Knadler & Cynthia Haseltine, unpublished results; [Graham & Haseltine, 2013](#); [Graham et al., 2013](#)). In all cases, the vectors have been from the pET group and expression is IPTG inducible. The cloning design we employed was simple, with the start of the gene directionally fused into the vector. In our experience, good background expression strains for soluble expression are either CodonPlus or Rosetta.

Protein purification in all cases includes an early heat treatment step, where the cell sonicate is incubated at 80°C to precipitate most mesophilic *E. coli* proteins, while the thermophilic overexpressed protein remains soluble. In addition to removing a majority of contaminating *E. coli* proteins, the heat step also effectively inactivates nucleases that will degrade DNA substrates used in protein activity assays. Inactivation of nucleases can be verified by incubating purified protein with radiolabeled oligonucleotides and dsDNA substrates and evaluating degradation by acrylamide gel ([Haseltine & Kowalczykowski, 2009](#)).

Because *S. solfataricus* is both a thermophile and an acidophile, temperature and pH must be considered when designing experimental assays. We have found that pHs from ~5.5 to 7.5 are generally sufficient for high levels of activity, with the optimum varying for each individual protein. While these proteins, like most thermophilic proteins, are broad range and have activity from room temperature to over 90°C, we have found that the optimal activity for the recombinant proteins is generally in the 70–80°C range.



### 3. METHODS SHARED ACROSS PROTOCOLS

A number of methods are repeatedly used for the following protocols. In consideration of space, these methods are listed here and will be referred to in the individual protocols where they are needed. Unless otherwise indicated, all procedures are performed at room temperature.

- Equipment list
  - Super speed centrifuge
  - SLA 3000 rotor
  - Branson 250 Sonifier (or similar)
  - FPLC or peristaltic pump
  - Dialysis tubing (MWCO 6000–8000) and clips
  - Glass baking dish

#### 3.1 Growth of *E. coli* and Induction for Protein Expression

1. Transform expression construct of interest (e.g., SsoRadA in a pET vector) into an *E. coli* expression strain (e.g., Rosetta) and plate for single colonies. Note: expression constructs for SsoRadA, SsoRal1, SsoRal2, and SsoRal3 are available upon request from the corresponding author of this chapter. Expression constructs for the coupled ATPase assay should be requested from Wigley (Seybert, Scott, Scaife, Singleton, & Wigley, 2002).
2. Select a single colony transformant and grow as a small overnight (2–5 mL) culture in rich medium with appropriate antibiotics at 37°C with shaking.
3. Use this starter culture to inoculate a larger volume of media in a flask (500 mL to 1 L) containing appropriate antibiotics. Grow to an OD<sub>600</sub> of 0.8–1.0 at 37°C with shaking.
4. Add IPTG to 1 mM final concentration and allow induction of expression to proceed for ~3 h.
5. Harvest cells by centrifugation at 10,000 × *g*. Discard spent media.
6. Remove pellet using a flexible household kitchen spatula and deposit on preweighed plastic wrap in approximately 1 g quantities. Fold over plastic wrap to completely enclose on all sides. Label with tape, including weight of cell pellet, and place directly in –80°C freezer. Store frozen until needed.

### 3.2 Preparation of Cell Sonicate

Sonicate the resuspended cells  $5 \times 30$  s at 20% output using a Branson 250 sonifier (or similar). Ensure at least 90% sonication by visually examining the sonicate microscopically. This step not only lyses any *E. coli* cells that remain intact after freezing but also disrupts protein:DNA and protein:protein complexes. Incomplete sonication can significantly reduce the final protein yield.

### 3.3 Dialysis Tubing Preparation

Use gloves throughout the procedure. Multiple lengths of tubing can be prepared at once in advance and stored until needed.

1. Cut dialysis tubing into sections corresponding roughly with the volume it should accommodate, allowing an extra 0.5–1 in. at each end to accommodate the dialysis tubing clips.
2. Soak the tubing in distilled water until pliable.
3. Boil the tubing with stirring for 10 min in 5%  $\text{NaHCO}_3$  (wt/vol), 1 mM EDTA solution in a glass beaker. This is most easily accomplished on a heated stir plate. Make sure that the buffer completely covers the tubing and do not allow the stir bar to bump into the tubing. To keep the tubing from drying out while boiling (since it tends to rise to the surface), it is helpful to place either another, smaller glass beaker or glass Petri dish lid on the surface of the liquid where it will press the tubing down into the buffer (see Fig. 1).

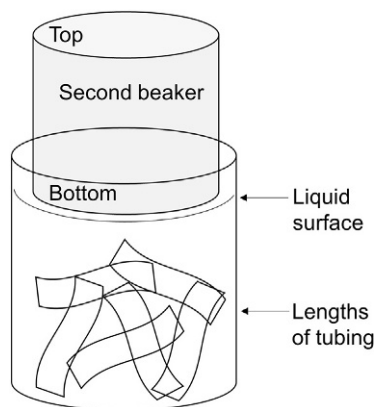


**Fig. 1** Schematic of dialysis tubing boiling setup. A large beaker is filled with buffer (*bottom of figure*). The tubing is kept submerged in this lower beaker during boiling by placing a second, smaller beaker *right-side up* on the surface of the buffer.

4. Transfer the tubing to a beaker filled with distilled H<sub>2</sub>O and then rinse the inside and outside of the tubing thoroughly with distilled water.
5. Store the boiled tubing at 4°C in 50% ETOH. Before use, rinse the individual length of tubing thoroughly with distilled H<sub>2</sub>O both inside and out to remove the ETOH.

### 3.4 Protein Concentration Using PEG

Concentrate protein at room temperature by placing samples or selected fractions in preprepared MWCO 6000–8000 dialysis tubing (see [Section 3.3](#)) with clips at either end. Spread dry PEG 20,000 in a shallow layer in a glass dish. Place the tubing on top of the PEG layer and cover with additional PEG. Monitor the concentration process visually until it reaches the desired volume. Wash the exterior of the tubing extensively with distilled H<sub>2</sub>O to remove residual PEG, which can inhibit downstream applications.

### 3.5 End-Labeling Oligonucleotides With <sup>32</sup>P

Prepare labeling reactions containing 100 μM nucleotides of the selected oligonucleotide in a 20 μL volume in a microfuge tube. Include oligonucleotide, 1 × T4 polynucleotide kinase buffer (NEB), 2 μL α-labeled <sup>32</sup>P ATP, and 200U T4 Polynucleotide kinase (NEB). Incubate the tube for 1 h at 37°C and then heat inactivate the enzyme for 10 min at 70°C. Store at –20°C.



## 4. HETEROLOGOUS PROTEIN PURIFICATION

The SsoRadA protein is 342 amino acids in length and approximately 35.9 kDa in size. This purification protocol differs significantly from the purification approach used in the earliest report of this protein ([Seitz, Brockman, Sandler, Clark, & Kowalczykowski, 1998](#)). We constructed a new expression vector using pET3a, greatly simplified the purification procedure, and performed all steps at room temperature. The resulting purified heterologous protein is, curiously, slightly larger when visualized by Coomassie gel than that reported by Seitz et al. and shows significantly higher ATPase, strand invasion, and strand exchange activity ([Michael Rolfmeier & Cynthia Haseltine, unpublished results; Rolfmeier & Haseltine, 2010](#)).

## 4.1 Purification of Heterologous SsoRadA

### 4.1.1 Equipment

- Microfuge
- Heating block or water bath
- Vortex mixer
- Blue column (1 mL HiTrap from GE Healthcare)
- Q anion exchange column (1 mL HiTrap from GE Healthcare)
- Acrylamide gel electrophoresis apparatus (BioRad or similar)
- Light box

### 4.1.2 Buffers and Reagents

- Sonication buffer: 20 mM Tris-Cl, pH 7.5, 1 mM EDTA, 500 mM NaCl, 10% glycerol
- Dilution buffer: 20 mM Tris-Cl, pH 7.5, 1 mM EDTA, 10% glycerol
- Equilibration buffer: 20 mM Tris-Cl, pH 7.5, 1 mM EDTA, 100 mM NaCl, 10% glycerol
- Step gradient buffers:
  - 20 mM Tris-Cl, pH 7.5, 1 mM EDTA, 100 mM NaCl, 10% glycerol
  - 20 mM Tris-Cl, pH 7.5, 1 mM EDTA, 200 mM NaCl, 10% glycerol
  - 20 mM Tris-Cl, pH 7.5, 1 mM EDTA, 400 mM NaCl, 10% glycerol
  - 20 mM Tris-Cl, pH 7.5, 1 mM EDTA, 600 mM NaCl, 10% glycerol
  - 20 mM Tris-Cl, pH 7.5, 1 mM EDTA, 800 mM NaCl, 10% glycerol
  - 20 mM Tris-Cl, pH 7.5, 1 mM EDTA, 1 M NaCl, 10% glycerol
  - 20 mM Tris-Cl, pH 7.5, 1 mM EDTA, 1.5 M NaCl, 10% glycerol
  - 20 mM Tris-Cl, pH 7.5, 1 mM EDTA, 2 M NaCl, 10% glycerol

### 4.1.3 Procedure

Begin with frozen, expressed cell pellet prepared as described in [Section 3](#).

1. Thaw pellet at room temperature in a 50-mL conical tube with sonication buffer at a ratio of 5 mL buffer for each 1 g of cell pellet. Vortex to completely resuspend the entire cell pellet.
2. Sonicate the cell pellet as described in [Section 3](#).
3. Heat treat the sonicate for 20 min at 80°C in a heat block. Vortex thoroughly after the first 10 min. It may be helpful to aliquot the sonicate into several smaller tubes to better fit the heat block available. This step will heat denature a majority of the mesophilic *E. coli* proteins, while the thermophilic protein remains soluble in solution.
4. Pellet the sonicate by centrifuging for 15 min at 13.3krpm in a bench-top microfuge at room temperature. Transfer the supernatant to fresh

tubes and repeat the spin. Transfer the supernatant to a fresh tube and discard the pellets. The supernatant will contain soluble, thermostable proteins. These will include the heterologous archaeal protein as well as some *E. coli* proteins, primarily heat-shock proteins.

5. Dilute the sonicate supernatant with dilution buffer to adjust the NaCl concentration to 100 mM.
6. All chromatography steps are performed at room temperature. Wash the Blue column with 5–10 column volumes of filtered, degassed distilled H<sub>2</sub>O to remove the storage buffer.
7. Equilibrate the column with 10 column volumes of equilibration buffer.
8. Prefilter the clarified sonicate using a 0.45- $\mu$ m filter (it is convenient to use a syringe filter for this) and load on the Blue column. Wash with 5–10 column volumes of equilibration buffer.
9. Perform a step gradient from 200 mM to 2 M NaCl with the listed buffers and 5 column volumes per elution. Collect 1 or 5 mL fractions. Wash the column with an additional 5 column volumes following the last elution. Finally, wash the salt off the column with 10 column volumes of Nanopure H<sub>2</sub>O and then store the column in 20% ETOH.
10. Check fractions visually using 10% separating/4% stacking tricine gels as described in [Price and Shand \(2000\)](#). The majority of SsoRadA elutes from 600 mM to 2 M NaCl. For an example, see [Fig. 2](#).
11. Pool selected fractions and dialyze against equilibration buffer, two changes of at least a 100-fold excess buffer volume at room temperature.

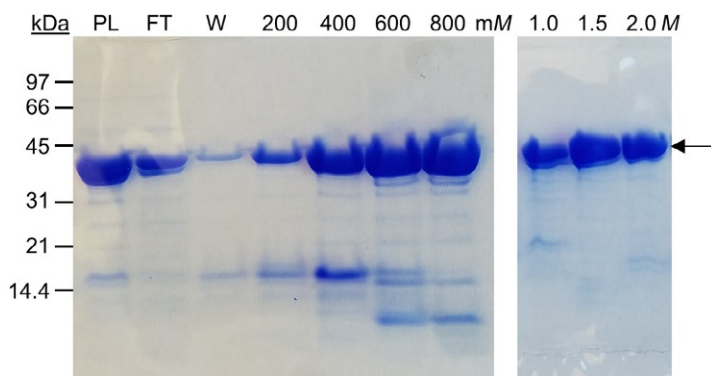


**Fig. 2** Visualization of SsoRadA protein elution from the Blue column. 10  $\mu$ L of 5 mL fractions collected from step elution ranging from 200 mM to 2 M NaCl. PL is preload material, FT is flow through, and W is wash. The arrow indicates the position of SsoRadA on the gels.

12. Wash ETOH from Q column with 5–10 column volumes of equilibration buffer.
13. Load the pooled, dialyzed fractions on the column and then wash with additional 5–10 column volumes of equilibration buffer.
14. Perform a step gradient from 200 mM to 600 mM NaCl with the listed buffers and 5 column volumes per elution. Collect 0.5–1.0 mL fractions. Wash the column with 10 column volumes of 2 M buffer following the last elution to remove any residual protein. Finally, wash the salt off the column with 10 column volumes of Nanopure H<sub>2</sub>O and store the column in 20% ETOH.
15. Check fractions by Coomassie-stained gel using 10% separating/4% stacking tricine gels as in step 10.
16. Pool SsoRadA protein-containing fractions and concentrate using PEG as described in Section 3. Dialyze against equilibration buffer, two buffer changes of at least a 100-fold excess of the pooled fraction volume at room temperature.
17. Aliquot concentrated, dialyzed protein in 100  $\mu$ L volumes in microfuge tubes. Flash freeze using a dry ice/ETOH bath and store at  $-80^{\circ}\text{C}$ .

#### 4.1.4 Notes

1. The SsoRadA protein overexpresses very well in *E. coli*, resulting in large quantities of protein (see Fig. 2 for example). Be careful to not over-concentrate the protein as it will irreversibly aggregate.
2. A thawed frozen aliquot of protein will maintain activity for at least a month with storage at  $4^{\circ}\text{C}$ .

## 4.2 Purification of Heterologous SsoRal1

The SsoRal1 protein is encoded by the open reading frame Sso2452 in the *S. solfataricus* P2 genome. It is 262 amino acids in length and is approximately 30.3 kDa in size.

### 4.2.1 Protocol-Specific Equipment

- Tube rotator
- EconoColumn (BioRad)
- HiTrap Q FF column (1 mL, GE Healthcare)
- HiTrap SP FF column (1 mL, GE Healthcare)

### 4.2.2 Buffers and Reagents

- Sonication buffer: 20 mM Tris–Cl, pH 8.0, 1 mM EDTA, 50 mM NaCl, 10% glycerol
- ssDNA cellulose and HiTrap Q FF equilibration buffer: 20 mM Tris–Cl, pH 8.0, 1 mM EDTA, 50 mM NaCl, 10% glycerol
- ssDNA cellulose resin (GE Healthcare)
- 1 × TE: 10 mM Tris–Cl, pH 8.0, 1 mM EDTA
- ssDNA cellulose and HiTrap Q FF step gradient buffers:
  - 20 mM Tris–Cl, pH 8.0, 1 mM EDTA, 100 mM NaCl, 10% glycerol
  - 20 mM Tris–Cl, pH 8.0, 1 mM EDTA, 200 mM NaCl, 10% glycerol
  - 20 mM Tris–Cl, pH 8.0, 1 mM EDTA, 400 mM NaCl, 10% glycerol
  - 20 mM Tris–Cl, pH 8.0, 1 mM EDTA, 600 mM NaCl, 10% glycerol
  - 20 mM Tris–Cl, pH 8.0, 1 mM EDTA, 1 M NaCl, 10% glycerol
- HiTrap SP FF equilibration buffer: 10 mM NaPO<sub>4</sub>, pH 7.2, 1 mM EDTA, 50 mM NaCl, 10% glycerol
- HiTrap SP FF step gradient buffers:
  - 10 mM NaPO<sub>4</sub>, pH 7.2, 1 mM EDTA, 100 mM NaCl, 10% glycerol
  - 10 mM NaPO<sub>4</sub>, pH 7.2, 1 mM EDTA, 200 mM NaCl, 10% glycerol
  - 10 mM NaPO<sub>4</sub>, pH 7.2, 1 mM EDTA, 300 mM NaCl, 10% glycerol
  - 10 mM NaPO<sub>4</sub>, pH 7.2, 1 mM EDTA, 400 mM NaCl, 10% glycerol
  - 10 mM NaPO<sub>4</sub>, pH 7.2, 1 mM EDTA, 500 mM NaCl, 10% glycerol
  - 10 mM NaPO<sub>4</sub>, pH 7.2, 1 mM EDTA, 600 mM NaCl, 10% glycerol
  - 10 mM NaPO<sub>4</sub>, pH 7.2, 1 mM EDTA, 1 M NaCl, 10% glycerol

### 4.2.3 Procedure

Begin with a frozen, expressed cell pellet prepared as described in [Section 3](#).

1. Resuspend the frozen cell pellet in sonication buffer. Add *N*-lauryl sarcosine to 0.25%. Dissolve one Roche EDTA-free protease inhibitor tablet in 500  $\mu$ L Nanopure H<sub>2</sub>O and add 250  $\mu$ L to resuspended cell pellet. Additionally, add PMSF to a final concentration of 1 mM. Follow steps 1–4 of [Section 3](#) to produce cell sonicate.
2. After sonication, add the remaining 250  $\mu$ L of EDTA-free protease inhibitor and readd PMSF to a final concentration of 1 mM.
3. Dialyze the sonicate 2 × 2 h each against at least a 100-fold excess of ssDNA cellulose equilibration buffer. This will effectively remove the *N*-lauryl sarcosine.
4. Heat treat the dialyzed sonicate 20 min at 80°C, vortexing thoroughly after 10 min. It is very important that the sonicate is dialyzed to remove

the *N*-lauryl sarcosine prior to heat treatment; heating in the presence of this detergent will irreversibly inactivate SsoRal1.

5. Clarify the heat-treated sonicate for 15 min at 13.3krpm in a microfuge at room temperature. Transfer the supernatant to a fresh tube, reheat treat for 15 min at 80°C, and respin for 15 min at 13.3krpm in a microfuge at room temperature. Transfer the supernatant to a fresh tube and discard all pellets.
6. Mix the clarified sonicate with approximately 15–20 mL of ssDNA cellulose that has been prewashed with  $1 \times$  TE four times and equilibrated two times with equilibration buffer.
7. Bind SsoRal1 to ssDNA resin overnight ( $\sim$ 8–12 h) at room temperature with mixing using rotator.
8. Pour the SsoRal1-bound ssDNA cellulose resin into an EconoColumn and collect the flow through.
9. Wash the column with 4 column volumes of equilibration buffer.
10. Elute protein using a step gradient: first with 2 column volumes of ssDNA cellulose equilibration buffer and then 2 column volumes of each of the ssDNA cellulose step gradient buffers from low to high NaCl concentration (200–600 mM NaCl). Finally wash with 4 column volumes of ssDNA cellulose step gradient buffer containing 1 M NaCl.
11. Check all fractions and washes for the SsoRal1 protein by Coomassie-stained gel using 10% separating/4% stacking tricine gels prepared as in [Price and Shand \(2000\)](#). Most of the SsoRal1 protein should elute in the 200 and 400 mM NaCl fractions.
12. Pool SsoRal1 protein-containing fractions and concentrate with PEG as described in [Section 3](#).
13. Dialyze against sonication buffer  $1 \times$  for 2 h and  $1 \times$  overnight at room temperature.
14. Wash ETOH from a HiTrap Q FF column using 5–10 column volumes of Nanopure H<sub>2</sub>O using a peristaltic pump. Equilibrate the column with 10 column volumes of sonication buffer at 1.0 mL/min.
15. Load pooled, dialyzed protein on HiTrap Q column at 0.5 mL/min. Wash with 5–10 column volumes of sonication buffer.
16. Elute protein in a step gradient of 4 mL volumes of HiTrap Q step gradient buffers from 100 to 400 mM NaCl at 1.0 mL/min. Finally, wash the column with 10 column volumes of HiTrap Q step gradient buffer containing 1 M NaCl at 1.0 mL/min.
17. Wash salt out of column with 10 column volumes Nanopure H<sub>2</sub>O and store in 20% ETOH.

18. Check all fractions and washes for the SsoRal1 protein by Coomassie-stained gel using 10% separating/4% stacking tricine gels as in step 11. The majority of SsoRal1 should elute in the flow through and low salt wash.
19. Pool SsoRal1-containing fractions and concentrate with PEG as described in [Section 3](#). Dialyze against HiTrap SP FF equilibration buffer in at least a 100-fold excess  $1 \times$  for 2 h and  $1 \times$  overnight at room temperature.
20. Wash ETOH from a HiTrap SP FF column with 5–10 volumes of Nanopure H<sub>2</sub>O. Equilibrate the column with 10 column volumes of HiTrap SP FF equilibration buffer at 1.0 mL/min with a peristaltic pump.
21. Load pooled, dialyzed material on HiTrap SP column at 0.5 mL/min. Wash the column with 5–10 column volumes of HiTrap SP equilibration buffer at 1.0 mL/min.
22. Elute protein in a step gradient of 4 mL volumes of HiTrap SP step gradient buffers from 100 to 600 mM NaCl at 1.0 mL/min. Finally, wash the column with 10 column volumes of HiTrap SP step gradient buffer containing 1 M NaCl at 1.0 mL/min.
23. Wash salt out of column with 10 column volumes of Nanopure H<sub>2</sub>O and store in 20% ETOH.
24. Check all fractions for SsoRal1 on 10% separating/4% stacking tricine gel as in step 11. The majority of the SsoRal1 protein should elute in the 200–400 mM NaCl-containing fractions.
25. Pool SsoRal1-containing fractions and concentrate using PEG as described in [Section 3](#). Dialyze against sonication buffer in at least a 100-fold excess  $1 \times$  for 2 h and  $1 \times$  overnight at room temperature.
26. Aliquot dialyzed protein into 50–100  $\mu$ L volumes, flash freeze with dry ice/ETOH bath, and store at  $-80^{\circ}\text{C}$ .

#### 4.2.4 Notes

1. A thawed aliquot of protein will maintain the activity for at least a month with storage at  $4^{\circ}\text{C}$ .

### 4.3 Purification of Heterologous SsoRal2

The SsoRal2 protein is encoded by the open reading frame Sso0777 in the *S. solfataricus* P2 genome. It is 175 amino acids in length and is approximately 19.8 kDa in size. This purification protocol is specific for an N-terminal 6xHis-Tagged version of SsoRal2.

### 4.3.1 Equipment

- IMAC column (GE Healthcare)
- MonoQ 5/50 (GE Healthcare)
- HiTrap Chelating (GE Healthcare)

### 4.3.2 Buffers and Reagents

- Sonication buffer: 20 mM Tris–Cl, pH 7.5, 1 M NaCl, 10% glycerol
- Nickel column elution buffer: 20 mM Tris–Cl, pH 7.5, 1 M NaCl, 0.5 M imidazole, 10% glycerol
- Dialysis buffer #1: 20 mM Tris–Cl, pH 7.5, 100 mM NaCl, 10% glycerol
- Gradient elution buffers:
  - 20 mM Tris–Cl, pH 7.5, 10% glycerol
  - 20 mM Tris–Cl, pH 7.5, 2 M NaCl, 10% glycerol
- Dialysis buffer #2: 20 mM Tris–Cl, pH 7.5, 1 M NaCl, 10% glycerol

### 4.3.3 Procedure

Begin with a frozen, expressed cell pellet prepared as described in [Section 3](#).

1. Resuspend the frozen cell pellet in sonication buffer. Add *N*-lauryl sarcosine to 0.25%. Dissolve one Roche EDTA-free protease inhibitor tablet in 500  $\mu$ L Nanopure H<sub>2</sub>O and add 250  $\mu$ L to resuspended cell pellet. Additionally, add PMSF to a final concentration of 1 mM. Produce cell sonicate as described in [Section 3](#).
2. After sonication, add the remaining 250  $\mu$ L of EDTA-free protease inhibitor and read PMSF to a final concentration of 1 mM.
3. Clarify the sonicate for 15 min at 13.3 krpm in a microfuge at room temperature. Transfer the supernatant to a fresh tube and respin for 15 min at 13.3 krpm in a microfuge at room temperature. Transfer the supernatant to a fresh tube and discard all pellets.
4. Filter the supernatant through a 0.45- $\mu$ m pore syringe filter.
5. Load the clarified sonicate on a 3-mL IMAC column that has been nickel charged following the manufacturer's directions.
6. Wash the column with 5 column volumes sonication buffer.
7. Elute the column with 2 column volumes of IMAC nickel column elution buffer.
8. Check all fractions and washes for the SsoRal2 protein by Coomassie-stained gel using 10% separating/4% stacking tricine gels as in [Price and Shand \(2000\)](#).
9. Pool SsoRal2 protein-containing fractions.
10. Dialyze against dialysis buffer #1, 1  $\times$  for 2 h and 1  $\times$  overnight at room temperature.

11. Wash ETOH from a MonoQ 5/50 column using 5–10 column volumes of Nanopure H<sub>2</sub>O. Equilibrate the column with 10 column volumes of dialysis buffer #1.
12. Load pooled, dialyzed protein on MonoQ 5/50 column at 0.3 mL/min. Wash the column with 3 column volumes of dialysis buffer #1 at 0.5 mL/min.
13. Elute protein in a 25-mL gradient from 100–500 mM NaCl using the gradient elution buffers at 0.5 mL/min. Finally, wash the column with 10 column volumes of the gradient elution buffer containing 2 M NaCl at 0.5 mL/min.
14. Wash the salt out of the column with 10 column volumes Nanopure H<sub>2</sub>O and store in 20% ETOH.
15. Check all fractions and washes for the SsoRal2 protein by Coomassie-stained gels using 10% separating/4% stacking tricine gels as in step 8. SsoRal2 should elute at the beginning of the gradient.
16. Pool SsoRal2-containing fractions and dialyze against dialysis buffer #2 in at least a 100-fold excess 1 × for 2h and 1 × overnight at room temperature.
17. Wash the ETOH from a HiTrap Chelating column that has been precharged with nickel with 5–10 volumes of Nanopure H<sub>2</sub>O. Equilibrate the column with 10 column volumes of dialysis buffer #2 at 1.0 mL/min with a peristaltic pump.
18. Load pooled, dialyzed material on HiTrap Chelating column at 0.5 mL/min. Wash the column with 5–10 column volumes of dialysis buffer #2 at 1.0 mL/min.
19. Elute the protein in 3 mL of nickel column elution buffer at 1.0 mL/min.
20. Wash salt out of column with 10 column volumes of Nanopure H<sub>2</sub>O and store in 20% ETOH.
21. Check all fractions for SsoRal2 on 10% separating/4% stacking tricine gel as in step 8.
22. Pool SsoRal2-containing fractions and concentrate using PEG as described in [Section 2](#). Dialyze against dialysis buffer #1 in at least a 100-fold excess 1 × for 2h and 1 × overnight at room temperature.
23. Aliquot dialyzed protein into 50–100 μL volumes, flash freeze with dry ice/ETOH bath, and store at –80°C.

#### 4.3.4 Notes

1. Thawed aliquots of this protein should retain activity for 1–3 months at 4°C.

## 4.4 Purification of Heterologous SsoRal3

The SsoRal3 protein is encoded by the open reading frame Sso1861 in the *S. solfataricus* P2 genome. It is 283 amino acids in length and is approximately 34.3 kDa in size.

### 4.4.1 Equipment

- FPLC
- MonoQ column (5/50 from GE Healthcare)

### 4.4.2 Buffers and Reagents

- Sonication buffer: 20 mM Tris–Cl, pH 7.5, 1 M NaCl, 10% glycerol
- Blue Sepharose equilibration buffer: 20 mM Tris–Cl, pH 7.5, 200 mM NaCl, 10% glycerol
- Gradient elution buffers:
  - 20 mM Tris–Cl, pH 7.5, 10% glycerol
  - 20 mM Tris–Cl, pH 7.5, 2 M NaCl, 10% glycerol
- Dialysis buffer: 20 mM Tris–Cl, pH 7.5, 100 mM NaCl, 10% glycerol
- MonoQ equilibration buffer: 20 mM Tris–Cl, pH 7.5, 50 mM NaCl, 10% glycerol

### 4.4.3 Procedure

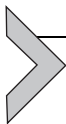
Begin with a frozen, expressed cell pellet prepared as described in [Section 3](#).

1. Resuspend the frozen cell pellet in sonication buffer. Add *N*-lauryl sarcosine to 0.25%. Dissolve one Roche EDTA-free protease inhibitor tablet in 500  $\mu$ L Nanopure H<sub>2</sub>O and add 250  $\mu$ L to resuspended cell pellet. Produce cell sonicate as described in [Section 3](#).
2. After sonication, add the remaining 250  $\mu$ L of EDTA-free protease inhibitor. Dialyze the sonicate 2  $\times$  2 h each against at least a 100-fold excess of Blue Sepharose equilibration buffer. This will effectively remove the *N*-lauryl sarcosine.
3. Heat treat the dialyzed sonicate 20 min at 80°C, vortexing thoroughly after 10 min. It is very important that the sonicate is dialyzed to remove the *N*-lauryl sarcosine prior to heat treatment; heating in the presence of this detergent will irreversibly inactivate SsoRal3.
4. Clarify the heat-treated sonicate for 15 min at 13.3 krpm in a microfuge at room temperature. Transfer the supernatant to a fresh tube, reheat treat for 15 min at 80°C, and respin for 15 min at 13.3 krpm in a microfuge at room temperature. Transfer the supernatant to a fresh tube and discard all pellets. Filter supernatant through a 0.45- $\mu$ m filter.

5. Wash the ETOH from the Blue Sepharose column with 5–10 column volumes of Nanopure H<sub>2</sub>O. Equilibrate the column with 8–10 column volumes of Blue Sepharose equilibration buffer.
6. Load the clarified sonicate on the column at 0.1 mL/min. Wash the column with 3 column volumes of equilibration buffer at 0.2 mL/min.
7. Develop the column with a 40-mL gradient from 200 mM NaCl to 800 mM NaCl using the Blue Sepharose elution buffers at 0.5 mL/min. Collect 1 mL fractions.
8. Wash the column with 5 column volumes of 2 M NaCl-containing elution buffer. Wash salt out of column with 8–10 column volumes Nanopure H<sub>2</sub>O and store column in 20% ETOH.
9. Check all fractions for SsoRal3 using 10% separating/4% stacking tricine gels as described in [Price and Shand \(2000\)](#). Pool SsoRal3-containing fractions and dialyze against dialysis buffer in at least a 100-fold excess 2 × for 2 h at room temperature.
10. Wash the ETOH from a MonoQ column with Nanopure H<sub>2</sub>O and equilibrate with 8–10 column volumes of MonoQ equilibration buffer.
11. Load the pooled, dialyzed material on the MonoQ column at 0.2 mL/min. Wash the column with 3–5 column volumes dialysis buffer at 0.2 mL/min.
12. Develop the column using a 25-mL gradient of 100–700 mM NaCl using the gradient elution buffers at 0.4 mL/min. Collect 1 mL fractions.
13. Wash the column with 5 column volumes of the 2 M NaCl-containing gradient elution buffer.
14. Finally, wash the salt out of the column with 5–10 column volumes of Nanopure H<sub>2</sub>O and store in 20% ETOH.
15. Check all fractions for SsoRal3 protein with Coomassie-stained gels using 10% separating/4% stacking tricine gels as in step 9.
16. Pool protein-containing fractions and concentrate with PEG as described in [Section 3](#) if necessary.
17. Aliquot the protein into 50–100 μL volumes, flash freeze with dry ice/ETOH bath, and store at –80°C.

#### 4.4.4 Notes

1. Thawed aliquots of protein will maintain activity for at least a month with storage at 4°C.



## 5. ATPase ACTIVITY ASSAYS

### 5.1 Thin-Layer Chromatography

This assay is particularly useful when testing a number of different buffer conditions, using cofactors that could inhibit other assays (for example, the coupled assay described in [Section 5.2](#)), or when there are only small concentrations of protein available.

#### 5.1.1 Equipment

- Thin-layer chromatography tank
- PEI Cellulose F TLC plates (EMD Chemicals)
- Phosphorimager screen (Molecular Dynamics)
- Typhoon or Storm phosphorimager (or similar)
- Thermal cycler with a heated lid
- Forceps or tweezers

#### 5.1.2 Buffers and Reagents

- Nanopure water to prerun the PEI cellulose plates
- Development solution: 1 M formic acid, 250 mM LiCl
- 10× reaction buffer: 400 mM HEPES, pH 7.0, 100 mM MgOAc
- ATP (GE Healthcare) resuspended as a 300 mM stock in Nanopure water
- ATP reagent: 40 mM ATP from 300 mM stock with 1:50  $^{32}\text{P}$  gamma-ATP (3000 Ci/mmol) added

#### 5.1.3 Procedure

1. Wearing gloves, cut PEI cellulose plate with clean, dry scissors to a size appropriate for experiment. Write on the plate surface with pencil lightly and sparingly to indicate the location to apply individual samples and separate lanes. In general, lanes 0.5 cm wide and 5 cm long work well. It may be helpful to leave a blank lane in between each sample. See [Fig. 3](#).
2. Prepare experimental samples containing 1× reaction buffer and add ATP reagent to a final concentration of 4  $\mu\text{M}$ . This does not have to be done on ice and can be done at room temperature using a microfuge rack. Assays typically can contain a range of DNA concentrations, depending on the desired final protein:DNA stoichiometry. Be sure

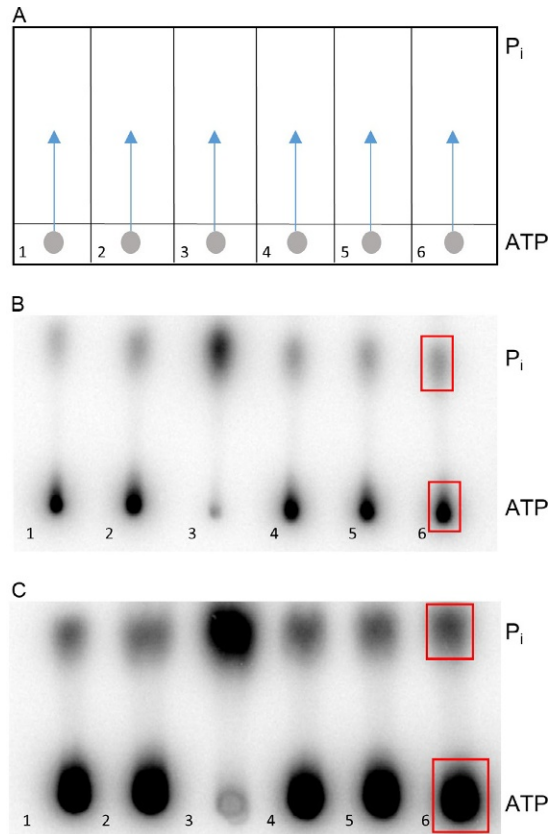


**Fig. 3** Thin-layer chromatography to detect ATPase activity. (A) Schematic representation of a chromatography plate, pencil lines, and spot locations. Buffer migration direction is indicated by *arrows* and the location of ATP and  $P_i$  are indicated. (B) and (C) Actual results after chromatographic separation. In (B), the plate is properly exposed and boxes are shown to indicate regions selected for densitometry. In (C), the plate has been over-exposed and as a result, activity measured will be artificially low.

to include a reaction that excludes the recombinase/paralog as a control to determine background spontaneous degradation of ATP.

3. Incubate reactions at  $65^{\circ}\text{C}$  in a thermal cycler with a heated lid. Time-courses for activity can be produced by preparing larger reaction volumes and removing samples for chromatography.
4. Pulse-spin reaction tubes to ensure no material remains on the inside of the lid; open carefully. Spot  $5\ \mu\text{L}$  samples from the reactions 1.0 cm from the bottom of the plate.

5. Using forceps, place the plates in TLC tank (using forceps) with 0.5 cm of development solution in the bottom. If you are using a wider tank and there is a risk of the plate falling face-down into the development solution, be extra careful when placing the plates in the tank. If the plate face contacts the development solution, no data will be obtainable from that plate.
6. Allow solution front to reach the top of the plate. You may see a yellow edge at the solution front and it may be uneven or wavy. If you have prerun the plate with Nanopure water prior to chromatography, this yellow edge will have no effect on separation. If the plate was not prerun, the yellow edge will be darker (sometimes more brown) and samples will generally not separate well.
7. Using forceps, remove the plates from the TLC tank and set face up on lab paper to dry completely.
8. Wrap the plates in plastic wrap and expose to a Molecular Dynamics phosphorimaging screen. Expose for an appropriate time to visualize individual spots. The length of time will depend on the level of decay of the isotope.
9. Image the plates using a Phosphorimager and quantitate the activity using densitometry software such as ImageQuant TL software.

### 5.1.4 Notes

1. Follow radiation safety procedures as are required at your institution.

## 5.2 Coupled Spectrophotometric Assay

This assay is a thermophilic, continuous coupled spectrophotometric method that permits real-time determination of ATPase activity (Seybert et al., 2002). ATPase activity is directly proportional to and is measured by the conversion of NADH to NAD. See Fig. 4 for diagram of coupled reaction, sample raw output data, and final graphed result example. Lactate dehydrogenase (LDH) and pyruvate kinase (PK) are from *Thermotoga maritima* and are prepared in advance for use as stocks as described in Seybert et al. (2002).

### 5.2.1 Equipment

- Spectrophotometer capable of real-time absorbance readings (preferably multicell) with a temperature controller.
- Quartz cuvettes (microcuvettes are preferable) that read in the UV light range.

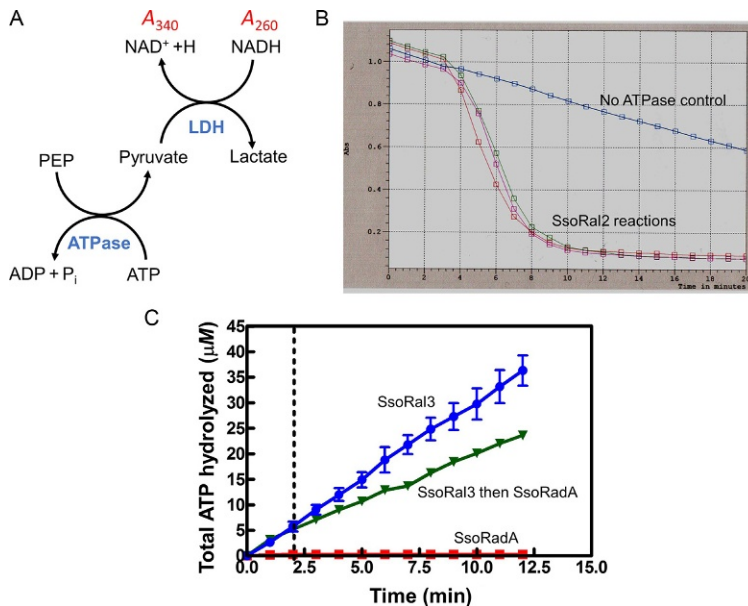


**Fig. 4** Thermophilic coupled ATPase assay. (A) ATP hydrolysis activity of the ATPase correlated directly with the loss of absorbance of NADH at 340nm. (B) Raw results of a coupled assay performed with SsoRal2 in triplicate showing the loss of NADH absorbance over time. (C) Example of coupled assay data plotted as ATP hydrolyzed over time. Note that for the *green line (inverted triangles)*, SsoRadA was added at the 2-min mark, while the assay was underway. Note that this assay was performed at suboptimal conditions for SsoRadA to better visualize the mediator effect of the paralog in conjunction with the recombinase.

### 5.2.2 Buffers and Reagents

- ATP (GE Healthcare) resuspended as a 300 mM stock in Nanopure water
- NADH (Sigma) resuspended as a 20 mM stock in Nanopure water
- Coupled assay reaction buffer: 40 mM HEPES, pH 7.0, 20 mM MgOAc, 250  $\mu\text{M}$  NADH, 2 mM phosphoenol pyruvate (Sigma), 15 U LDH, 15 U PK,  $\phi\text{X174}$  virion DNA (generally 3–10  $\mu\text{M}$  nucleotides), ATP (generally 0.5–5 mM), SsoRadA, or paralog protein (generally 1–5  $\mu\text{M}$ )

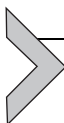
### 5.2.3 Procedure

1. Turn on the spectrophotometer, warm the lamps, turn on the temperature controller, and select or edit the kinetics program. Detect absorbance change at 340 nm.

2. Set up the coupled ATPase reactions on ice except for the protein (or except for the ATP or DNA if initiating the reaction with those components).
3. Transfer the reactions to the cuvettes, place them in the warmed cuvette holder, and start the program, beginning the incubation at temperature.
4. At the 2-min mark, add the protein (or initiating factor) to the cuvettes.
5. Monitor the reaction progress on the spectrophotometer computer screen.
6. Collect assay data and save as an electronic file.
7. Calculate activity (rate of ADP production/NADH loss) using the Beer–Lambert equation and the molar extinction coefficient for NADH ( $\epsilon_{340} = 6220 \text{ M}^{-1} \text{ cm}^{-1}$ ).

### 5.2.4 Notes

1. Coupled ATPase assays are generally performed in the 70–80°C range.
2. Additional reagents may be added to reactions under way by simply pipetting into the cuvette. For example, we commonly add other proteins to assess their impact on reaction rates (see Fig. 4C).



---

## 6. DNA AND ATP BINDING ASSAYS

### 6.1 Gel Shift

#### 6.1.1 Equipment

- Vertical gel rig with cooling (Owl P2DS)
- Power supply (300 V)
- Temperature controller for gel rig
- Thermal cycler with a heated lid
- Slab gel dryer
- Pump
- Slab gel dryer condenser unit
- Phosphorimager screen (Molecular Dynamics) or X-ray film and developer
- Storm 845
- Whatman 3 M filter paper
- DEAE ion exchange chromatography paper (if available)

#### 6.1.2 Buffers and Reagents

- Gel shift sample buffer (final concentration): 20 mM HEPES, pH 7.0, 10 mM MgOAc, 50  $\mu\text{g}/\text{mL}$  BSA, NaCl (generally 100 mM but may use higher or lower concentration, ranging from 50 mM to 1 or 2 M)

- ATP (GE Healthcare, resuspended as a 300 mM stock in Nanopure water)
- $^{32}\text{P}$ -labeled ssDNA oligonucleotide of choice (generally 60–100 bases)—see [Section 3](#)
- Purified SsoRadA recombinase or paralog(s)
- $1 \times$  TBE: 0.089 M Tris–borate, 0.089 M boric acid, 0.002 M EDTA
- $6 \times$  DNA loading dye: 0.025% bromophenol blue in 30% glycerol

### 6.1.3 Procedures

1. Pour the vertical gel(s) as per the manufacturer's recommendations. For most applications, we use 7.5% acrylamide gels in  $1 \times$  TBE buffer. Cool the gel rig using the temperature controller. If this sort of controller is unavailable, the gel can also be run in a cold room or a chromatography refrigerator.
2. Set up gel shift reactions on ice in 20  $\mu\text{L}$  volumes using gel shift sample buffer with desired concentration of salt, 10 mM ATP, and 10  $\mu\text{M}$  nucleotides  $^{32}\text{P}$ -labeled ssDNA oligonucleotide. Protein can be used in varying concentrations, generally 0.5–5.0  $\mu\text{M}$ .
3. Incubate the reactions 10–15 min at 70–80°C (depending on ATPase optimum of recombinase/paralog used) in the thermal cycler. Remove samples to rack to cool at room temperature. Add DNA loading dye to  $1 \times$ .
4. Rinse the gel wells and prerun the gel 15 min at 30 mA before loading samples. Take care when loading to go slowly and deposit the sample at the bottom of the well. This will yield sharper shift bands on the final gel and reduce smearing.
5. Electrophorese samples at 25 mA (50 mA for 2 gels together) for 1 h.
6. Recover gel from plates and place on filter paper. Dry using three layers of Whatman 3 M paper on the slab gel dryer.
7. Cover gel(s) dried onto the filter paper (keep all three layers) in plastic wrap and expose to a phosphorimaging screen. Expose for an appropriate time to visualize bands; this will be dependent on the age of the isotope. Scan the phosphorimaging screen with a Storm 845 (GE Healthcare). Quantitate band intensity using ImageQuant TL software.

### 6.1.4 Notes

1. The choice of protein and ssDNA concentrations should be pre-determined using the stoichiometries established from the ATPase activity for that protein.
2. Follow all radiation safety regulations as dictated by your institution.

3. To accurately quantitate band intensity, it is necessary to account for all signals. Historically, this has been accomplished by drying gels onto Whatman DEAE ion exchange chromatography paper, which prevented signal loss by capturing nucleotides on the paper. The problem is amplified with smaller DNA substrates. Whatman DEAE chromatography paper has been discontinued, making quantitation of these kinds of experiments more challenging. We have found that using three layers of Whatman paper retains virtually all of the signal during gel drying. You may wish to establish that your specific drying apparatus and filter paper setup are sufficient to retain signal.

## 6.2 Filter Binding

### 6.2.1 Equipment

- 13 mm diameter Buchner funnel
- 13 mm Millipore MF filters, 0.45- $\mu$ m pore size
- A trap hooked up to a vacuum line or pump
- Scintillation counter
- Forceps
- Thermal cycler or reliable heat source that limits condensation on the inside lid of microfuge tubes
- Scintillation fluid
- Scintillation vials

### 6.2.2 Buffers and Reagents

- Assay buffer: 40 mM HEPES, pH 7.0, 10 mM MgCl<sub>2</sub>, 50 mM KCl, 2  $\mu$ M (20 pmol) SsoRadA, 1–100  $\mu$ M ATP (as needed—ATP is spiked 1:20 with alpha-labeled <sup>32</sup>P ATP—3000 Ci/mmol)
- Wash buffer: 40 mM HEPES, pH 7.0, 20 mM MgCl<sub>2</sub>, 50 mM KCl
- Alpha-labeled <sup>32</sup>P ATP—3000 Ci/mmol

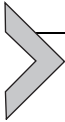
### 6.2.3 Procedure

1. Set up binding reactions in assay buffer.
2. Incubate reactions for 15 min at 80°C.
3. Place a filter in a Buchner funnel positioned above the trap and pretreat with wash buffer (about 350  $\mu$ L). Apply the vacuum.
4. Stop the vacuum, load the reaction on the center of the filter, and then restore the vacuum.
5. Wash the filter three times with 1 mL wash buffer.

6. Release the vacuum and, using forceps, transfer the filter to a scintillation vial containing 5 mL scintillation fluid.
7. When all filters from all the reactions have been placed in vials, transport the vials to the scintillation counter.
8. Count the radioactive signal for all vials using a program designed to detect  $^{32}\text{P}$ .
9. Graph the results as ATP concentration (*X*-axis) vs detected counts (*Y*-axis).

#### 6.2.4 Notes

1. Sample variation in this assay is not uncommon, so it is very important to set up all reactions in at least triplicate.
2. To determine ATP binding in the presence of ssDNA, we include  $0.7\ \mu\text{M}$  nucleotides of unlabeled oligonucleotide in each reaction.



---

## 7. MECHANISTIC RECOMBINATION ASSAYS

### 7.1 Strand Invasion (D-Loop)

Recombination can be separated into individual steps including strand invasion and subsequent exchange. This assay addresses only the first of these, wherein the nucleoprotein filament invades a double-stranded molecule and seeks homologous sequences. Highly efficient reactions will demonstrate a D-loop “cycle” over a time-course, where the nucleoprotein filament will invade and then proceed to dissociate (Shibata, Ohtani, Iwabuchi, & Ando, 1982).

#### 7.1.1 Equipment

- Thermal cycler or high-temperature incubator that reduces condensation
- Slab gel dryer
- Pump
- Slab gel dryer condenser unit
- Phosphorimager screen (Molecular Dynamics)
- Storm 845 (GE Healthcare)
- Vertical gel rig with cooling (Owl P2DS)

#### 7.1.2 Buffers and Reagents

- $10\times$  reaction buffer:  $250\text{mM}$  Tris–acetate pH 7.5,  $1\text{mg/mL}$  BSA,  $100\text{mM}$  MgOAc
- 10% SDS

- 0.5 M EDTA, pH 8.0
- Proteinase K (20 mg/mL)
- 50× TAE—242 g Tris, 18.61 g EDTA, 57.1 mL glacial acetic acid, distilled H<sub>2</sub>O to 1 L
- Covalently closed circular DNA plasmid—it is absolutely critical that this plasmid is prepared using a nondenaturing method. Qiagen kits (or similar) will leave regions of the plasmid denatured and will ultimately cause high, nonprotein-mediated, spontaneous D-loop formation which are false positives for activity. We use a sucrose gradient method for preparation as previously described (Graham & Haseltine, 2013).
- 5' <sup>32</sup>P-labeled oligonucleotide with homology to the plasmid (prepared as in the kinase reaction in Section 3)
- 6× loading dye: 30% glycerol with bromophenol blue at 0.25% (wt/vol)

### 7.1.3 Procedure

1. Pour a 1.2% agarose gel in 1× TAE.
2. Set up reactions in 1× reaction buffer with 0.9 μM nucleotides oligonucleotide, 0.6 μM SsoRadA, and 2 mM ATP.
3. Incubate the samples for 5 min at 65°C to form the nucleoprotein filament.
4. Add 30 μM bp plasmid DNA and incubate further at 65°C. We generally perform time-courses.
5. After desired time-point, stop the reaction by adding 1.5 μL 10% SDS and 0.5 μL 0.5 M EDTA, pH 8.0, and 10 μg proteinase K.
6. Incubate for 20 min at 65°C to deproteinize.
7. Add loading gel to a final 1× concentration to each reaction.
8. Load the reactions on 1.2% agarose, 1× TAE gel, and electrophorese for 110 min at 90 V while running the cooling apparatus.
9. After completion of electrophoresis, recover the gel and dry on 3 layers of Whatman 3 M paper using a slab gel dryer.
10. Cover the gel with plastic wrap and expose to a Molecular Dynamics phosphorimaging screen. Expose for an appropriate time to visualize bands; this will be dependent on the age of the isotope.
11. Visualize the image with a Storm 845 (GE Healthcare) phosphorimager and quantitate the data using ImageQuant TL software.

### 7.1.4 Notes

1. Follow all radiation safety regulations as dictated by your institution.

## 7.2 Strand Exchange

This assay will evaluate the ability of the recombinase/paralog to catalyze or influence not only strand invasion but also strand exchange events. While strand exchange assays using oligonucleotides are popular, we have found that with thermophilic proteins and high-temperature conditions that methodology is generally uninformative due to duplex denaturation over short substrates. The assay described here instead uses plasmid length substrates to mitigate the problem.

### 7.2.1 Equipment

- Horizontal gel rig
- Power supply
- Gel documentation system
- Quantitation software
- Thermal cycler (or high-temperature incubator that reduces condensation)

### 7.2.2 Buffers and Reagents

- 10 × strand exchange buffer: 300 mM MES, pH 6.5, 500 μg/mL BSA, 100 mM MgOAc
- Linearized dsDNA: *Pst*I digested φX174 RF DNA (NEB) in a 400 mM stock
- Circular ssDNA: φX174 virion DNA (NEB)
- ATP (GE Healthcare, resuspended as a 300 mM stock in Nanopure water)
- 6 × loading dye: 30% glycerol with bromophenol blue at 0.25% (wt/vol)

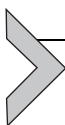
### 7.2.3 Procedure

1. Pour a 1.0% agarose 1 × TAE gel (use a 12 cm × 15 cm gel or larger).
2. Prerun the gel 15 min at 30 V and rinse out the wells prior to loading.
3. Prepare strand exchange reactions in 25 μL volumes containing: 1 × strand exchange buffer, 2.5 mM ATP, 33 μM φX174 virion DNA, and 11 μM recombinase or paralog (or mixture of these).
4. Incubate the reactions for 5 min at 80°C to allow nucleoprotein filament formation.
5. Add linear dsDNA to a final concentration of 33 μM and then continue incubation at 80°C for preferred time. We generally observe full-strand exchange with SsoRadA after 30–60 min depending on the stoichiometry.
6. Stop the reactions by addition of EDTA to 10 mM, 10 μg proteinase K, and SDS to 0.6%. Incubate the stopped reactions for 20 min at 65°C.

7. Add loading dye to the deproteinized reactions at a final  $1 \times$  concentration and separate the reaction products by electrophoresis using a 1.0% agarose,  $1 \times$  TAE gel run for 16 h at 30 V.
8. After electrophoresis, soak the gel in 50 mM EDTA with shaking for 1 h.
9. Wash the gel in Nanopure (or distilled) water for 60–90 min, changing the water every 20 min.
10. Stain the gel in freshly prepared 5  $\mu\text{g}/\text{mL}$  ethidium bromide (in water) for 1 h.
11. Capture an image of the gel with your gel documentation system.
12. Quantitate DNA using appropriate quantitation software.

### 7.2.4 Notes

1. Pour the agarose gel while it is still very hot to achieve the best resolution of products.
2. A long, slow gel run is crucial for resolution of the reaction products. A quick, rushed gel will not yield useful data.
3. Longer reaction incubation times will unavoidably result in some loss of ssDNA, both input material and the displaced strand, due to heat and acid hydrolysis. This can be partially alleviated by including the SsoSSB (single-strand DNA binding protein) in the reaction, but addition of this protein will alter reaction kinetics for strand exchange due to the need for its displacement prior to nucleoprotein filament formation.



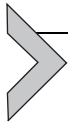
## 8. SUMMARY AND CONCLUSION

Their long-term stability and robust nature make the *S. solfataricus* recombinase and its paralogs attractive targets for biochemical analysis. These proteins are all remarkably easy to purify and, with the establishment and optimization of the methods described in this chapter, their functions in recombination and overall genome stability mechanisms are becoming apparent. The crenarchaeal group within the archaeal branch of life is deeply rooted, suggesting a close evolutionary relationship between the *Sulfolobales* and eukaryotes. This connection is supported by the remarkable similarity of the SsoRadA and its paralogs to eukaryotic Rad51 and its paralogs. As mechanistic details of the activity of these *S. solfataricus* proteins have emerged, it has become increasingly apparent that despite physical similarity to bacteria, this organism can truly serve as a model for understanding basic molecular functions shared with eukaryotes.

## REFERENCES

- Albala, J. S., Thelen, M. P., Prange, C., Fan, W., Christensen, M., Thompson, L. H., et al. (1997). Identification of a novel human RAD51 homolog, RAD51B. *Genomics*, *46*(3), 476–479. <https://doi.org/10.1006/geno.1997.5062>.
- Cartwright, R., Tambini, C. E., Simpson, P. J., & Thacker, J. (1998). The XRCC2 DNA repair gene from human and mouse encodes a novel member of the recA/RAD51 family. *Nucleic Acids Research*, *26*(13), 3084–3089.
- Cooper, D. L., & Lovett, S. T. (2016). Recombinational branch migration by the RadA/Sms paralog of RecA in *Escherichia Coli*. *eLife*, *5*, e10807. <https://doi.org/10.7554/eLife.10807>.
- Dosanjh, M. K., Collins, D. W., Fan, W., Lennon, G. G., Albala, J. S., Shen, Z., et al. (1998). Isolation and characterization of RAD51C, a new human member of the RAD51 family of related genes. *Nucleic Acids Research*, *26*(5), 1179–1184.
- Graham, W. J. T., & Haseltine, C. A. (2013). A recombinase paralog from the hyperthermophilic crenarchaeon *Sulfolobus solfataricus* enhances SsoRadA ssDNA binding and strand displacement. *Gene*, *515*(1), 128–139. <https://doi.org/10.1016/j.gene.2012.11.010>.
- Graham, W. J. T., Rolfsmeier, M. L., & Haseltine, C. A. (2013). An archaeal RadA paralog influences presynaptic filament formation. *DNA Repair (Amst)*, *12*(6), 403–413. <https://doi.org/10.1016/j.dnarep.2013.03.003>.
- Guy, C. P., Haldenby, S., Brindley, A., Walsh, D. A., Briggs, G. S., Warren, M. J., et al. (2006). Interactions of RadB, a DNA repair protein in archaea, with DNA and ATP. *Journal of Molecular Biology*, *358*(1), 46–56. <https://doi.org/10.1016/j.jmb.2006.02.010>.
- Haseltine, C. A., & Kowalczykowski, S. C. (2009). An archaeal Rad54 protein remodels DNA and stimulates DNA strand exchange by RadA. *Nucleic Acids Research*, *37*(8), 2757–2770. <https://doi.org/10.1093/nar/gkp068>.
- Komori, K., Miyata, T., Daiyasu, H., Toh, H., Shinagawa, H., & Ishino, A. Y. (2000). Domain analysis of an archaeal RadA protein for the strand exchange activity. *The Journal of Biological Chemistry*, *275*(43), 33791–33797. <https://doi.org/10.1074/jbc.M004556200>.
- Komori, K., Miyata, T., DiRuggiero, J., Holley-Shanks, R., Hayashi, I., Cann, I. K., et al. (2000). Both RadA and RadB are involved in homologous recombination in *Pyrococcus furiosus*. *The Journal of Biological Chemistry*, *275*(43), 33782–33790. <https://doi.org/10.1074/jbc.M004557200>.
- Liang, P. J., Han, W. Y., Huang, Q. H., Li, Y. Z., Ni, J. F., She, Q. X., et al. (2013). Knock-outs of RecA-like proteins RadC1 and RadC2 have distinct responses to DNA damage agents in *Sulfolobus islandicus*. *Journal of Genetics and Genomics*, *40*(10), 533–542. <https://doi.org/10.1016/j.jgg.2013.05.004>.
- Liu, N., Lamerdin, J. E., Tebbs, R. S., Schild, D., Tucker, J. D., Shen, M. R., et al. (1998). XRCC2 and XRCC3, new human Rad51-family members, promote chromosome stability and protect against DNA cross-links and other damages. *Molecular Cell*, *1*(6), 783–793.
- Liu, J., Renault, L., Veaute, X., Fabre, F., Stahlberg, H., & Heyer, W. D. (2011). Rad51 paralogues Rad55–Rad57 balance the antirecombinase Srs2 in Rad51 filament formation. *Nature*, *479*(7372), 245–248. <https://doi.org/10.1038/nature10522>.
- Paques, F., & Haber, J. E. (1999). Multiple pathways of recombination induced by double-strand breaks in *Saccharomyces cerevisiae*. *Microbiology and Molecular Biology Reviews*, *63*(2), 349–404.
- Price, L. B., & Shand, R. F. (2000). Halocin S8: A 36-amino-acid microhalocin from the haloarchaeal strain S8a. *Journal of Bacteriology*, *182*(17), 4951–4958.
- Rice, M. C., Smith, S. T., Bullrich, F., Havre, P., & Kmiec, E. B. (1997). Isolation of human and mouse genes based on homology to REC2, a recombinational repair gene from the fungus *Ustilago maydis*. *Proceedings of the National Academy of Sciences of the United States of America*, *94*(14), 7417–7422.

- Rolfsmeier, M. L., & Haseltine, C. A. (2010). The single-stranded DNA binding protein of *Sulfolobus solfataricus* acts in the presynaptic step of homologous recombination. *Journal of Molecular Biology*, *397*, 31–45.
- Rolfsmeier, M. L., Laughery, M. F., & Haseltine, C. A. (2010). Repair of DNA double-strand breaks following UV damage in three *Sulfolobus solfataricus* strains. *Journal of Bacteriology*, *192*(19), 4954–4962. <https://doi.org/10.1128/JB.00667-10>.
- Seitz, E. M., Brockman, J. P., Sandler, S. J., Clark, A. J., & Kowalczykowski, S. C. (1998). RadA protein is an archaeal RecA protein homolog that catalyzes DNA strand exchange. *Genes & Development*, *12*(9), 1248–1253.
- Seybert, A., Scott, D. J., Scaife, S., Singleton, M. R., & Wigley, D. B. (2002). Biochemical characterisation of the clamp/clamp loader proteins from the euryarchaeon *Archaeoglobus fulgidus*. *Nucleic Acids Research*, *30*(20), 4329–4338.
- Sheng, D., Li, M., Jiao, J., Ni, J., & Shen, Y. (2008). Co-expression with RadA and the characterization of stRad55B, a RadA paralog from the hyperthermophilic crenarchaea *Sulfolobus tokodaii*. *Science in China. Series C, Life Sciences*, *51*(1), 60–65. <https://doi.org/10.1007/s11427-008-0008-x>.
- Sheng, D., Zhu, S., Wei, T., Ni, J., & Shen, Y. (2008). The in vitro activity of a Rad55 homologue from *Sulfolobus tokodaii*, a candidate mediator in RadA-catalyzed homologous recombination. *Extremophiles*, *12*(1), 147–157. <https://doi.org/10.1007/s00792-007-0113-y>.
- Shibata, T., Ohtani, T., Iwabuchi, M., & Ando, T. (1982). D-loop cycle. A circular reaction sequence which comprises formation and dissociation of D-loops and inactivation and reactivation of superhelical closed circular DNA promoted by recA protein of *Escherichia Coli*. *The Journal of Biological Chemistry*, *257*(23), 13981–13986.
- Sung, P. (1997). Yeast Rad55 and Rad57 proteins form a heterodimer that functions with replication protein A to promote DNA strand exchange by Rad51 recombinase. *Genes & Development*, *11*(9), 1111–1121.
- Sung, P., Trujillo, K. M., & Van Komen, S. (2000). Recombination factors of *Saccharomyces cerevisiae*. *Mutation Research*, *451*(1–2), 257–275.
- Taylor, M. R., Spirek, M., Chaurasiya, K. R., Ward, J. D., Carzaniga, R., Yu, X., et al. (2015). Rad51 paralogs remodel pre-synaptic Rad51 filaments to stimulate homologous recombination. *Cell*, *162*(2), 271–286. <https://doi.org/10.1016/j.cell.2015.06.015>.
- Taylor, M. R., Spirek, M., Jian Ma, C., Carzaniga, R., Takaki, T., Collinson, L. M., et al. (2016). A polar and nucleotide-dependent mechanism of action for RAD51 paralogs in RAD51 filament remodeling. *Molecular Cell*, *64*(5), 926–939. <https://doi.org/10.1016/j.molcel.2016.10.020>.
- Wang, L., Sheng, D., Han, W., Huang, B., Zhu, S., Ni, J., et al. (2012). *Sulfolobus tokodaii* RadA paralog, stRadC2, is involved in DNA recombination via interaction with RadA and Hjc. *Science China. Life Sciences*, *55*(3), 261–267. <https://doi.org/10.1007/s11427-012-4292-0>.
- Wardell, K., Haldenby, S., Jones, N., Liddell, S., Ngo, G. H. P., & Allers, T. (2017). RadB acts in homologous recombination in the archaeon *Haloferax volcanii*, consistent with a role as recombination mediator. *DNA Repair (Amst)*, *55*, 7–16. <https://doi.org/10.1016/j.dnarep.2017.04.005>.



# Reconstituting the 4-Strand DNA Strand Exchange

Olga M. Mazina, Alexander V. Mazin<sup>1</sup>

Drexel University College of Medicine, Philadelphia, PA, United States

<sup>1</sup>Corresponding author: e-mail address: avm28@drexel.edu

## Contents

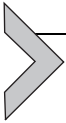
|  |     |
|--|-----|
| 1. Introduction  | 286 |
| 2. Preparation of DNA Substrates for 4-Strand DNA Exchange | 288 |
| 2.1 Preparation of Gapped DNA Substrate                    | 288 |
| 2.2 Labeling of Linear dsDNA                               | 295 |
| 3. Preparation of Joint Molecules                          | 297 |
| 3.1 Preparation of 3'-Joint Molecules                      | 297 |
| 3.2 Preparation of 5'-Joint Molecules                      | 299 |
| 3.3 Deproteinization and Purification of Joint Molecules   | 299 |
| 4. Branch Migration of Joint Molecules                     | 300 |
| 4.1 4-Strand DNA Branch Migration by hRad51                | 300 |
| 4.2 4-Strand DNA Branch Migration by <i>E. coli</i> RecA   | 302 |
| 5. Summary and Conclusion                                  | 303 |
| Acknowledgments  | 304 |
| References   | 304 |
| Further Reading  | 305 |

## Abstract

Proteins of the Rad51 family play a key role in homologous recombination by carrying out DNA strand exchange. Here, we present the methodology and the protocols for the 4-strand exchange between gapped circular DNA and homologous linear duplex DNA promoted by human Rad51 and *Escherichia coli* RecA orthologs. This reaction includes formation of joint molecules and their extension by branch migration in a polar manner. The presented methodology may be used for reconstitution of the medial-to-late stages of homologous recombination in vitro as well as for investigation of the mechanisms of branch migration by helicase-like proteins, e.g., Rad54, BLM, or RecQ1.

## ABBREVIATIONS

|              |                                     |
|--------------|-------------------------------------|
| <b>bp</b>    | base pair                           |
| <b>BSA</b>   | bovine serum albumin                |
| <b>dsDNA</b> | double-stranded DNA                 |
| <b>DTT</b>   | 1,4-Dithiothreitol                  |
| <b>nt</b>    | nucleotide                          |
| <b>RPA</b>   | replication protein A               |
| <b>SSB</b>   | single-stranded DNA-binding protein |
| <b>ssDNA</b> | single-stranded DNA                 |



## 1. INTRODUCTION

The recombinases of the Rad51 family, which include eukaryotic Rad51 and Dmc1, bacterial RecA, and archaeal RadA orthologs, promote DNA strand exchange between homologous DNA molecules (Kowalczykowski, 2015). In this reaction, Rad51–ssDNA filament invades the homologous duplex DNA to produce a joint molecule, in which the incoming ssDNA forms a heteroduplex with the complementary DNA strand displacing the identical strand of the duplex. Rad51 recombinases can promote extension of joint molecules via a kinetically and mechanistically distinct reaction, known as 3-strand branch migration. Experimental data indicate that branch migration is driven by cycles of recombinase dissociation, reassociation, and polymerization on the displaced ssDNA of joint molecules directed toward the ssDNA–dsDNA junction (Rossi, Mazina, Bugreev, & Mazin, 2011). Consequently, the branch migration activity depends on ATP hydrolysis which requires for dissociation of Rad51 recombinases from DNA (Kowalczykowski, 1991). In contrast, the Rad51 DNA strand exchange activity does not require protein dissociation from DNA and can be carried out in the presence of nonhydrolyzable ATP analogs. The polarity of branch migration is determined by the direction of the recombinase polymerization on the displaced ssDNA strand; e.g., it is 5′–3′ for RecA and 3′–5′ for hRad51 (Konforti & Davis, 1992; Kowalczykowski, 1991; Rossi et al., 2011).

When DNA heteroduplex extension reaches the ssDNA–dsDNA junction on the invading tailed dsDNA strand, the 3-stranded joint molecule is converted into a 4-stranded crossover junction, known as the Holliday junction (Fig. 1). Rad51 recombinases can promote migration of Holliday junctions (Cunningham, DasGupta, Shibata, & Radding, 1980; Murayama,

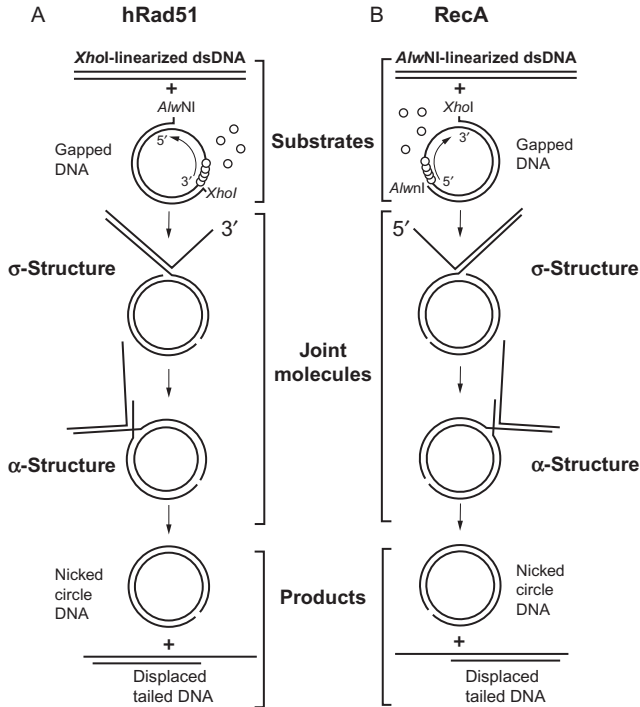


**Fig. 1** The scheme of 4-strand exchange reaction promoted by hRad51 and *E. coli* RecA. (A) Joint molecules with the 3'-ssDNA displaced strand are produced by hRad51 using gapped DNA and *XhoI*-linearized pBS II SK(+) dsDNA. (B) Joint molecules with the 5'-ssDNA displaced strand are produced by RecA using gapped DNA and *AlwNI*-linearized pBS II SK(+) dsDNA. Curved arrows show the direction of polymerization of hRad51 (3' → 5') and RecA (5' → 3') on the ssDNA region of gapped DNA to initiate the reactions.

Kurokawa, Mayanagi, & Iwasaki, 2008; Murayama, Tsutsui, & Iwasaki, 2011; Robu, Inman, & Cox, 2001; Rossi, Mazina, Bugreev, & Mazin, 2010; West, Cassuto, Murselim, & Howard-Flanders, 1980), although with a lower efficiency than specialized helicase-like branch migration proteins, e.g., RuvAB or Rad54 (Mazina, Rossi, Deakyne, Huang, & Mazin, 2012). The 4-strand branch migration activity is mechanistically similar to the 3-strand branch migration and strictly depends on ATP hydrolysis.

Here, we describe reconstitution of the 4-strand DNA exchange, between circular dsDNA containing a region of ssDNA (gapped DNA) and homologous linear dsDNA (Fig. 1). The DNA strand exchange (invasion) step is initiated at the single-stranded gap to produce joint molecules ( $\sigma$ -structures) that are then extended by 3-strand branch migration. As the reaction proceeds beyond the gap, joint molecules are converted into

$\alpha$ -structures that undergo 4-strand branch migration to produce nicked circular DNA and displaced tailed dsDNA products (Fig. 1). We describe the use of human Rad51 and *Escherichia coli* RecA which promote the 4-strand DNA exchange with the opposite polarities, the 3'-5' and 5'-3', respectively (Fig. 1). The described methodology can be applied for studies of branch migration promoted by Rad51 recombinases (Rossi et al., 2011), and also by helicase-like proteins, e.g., Rad54, BLM, or RecQ1 (Mazina et al., 2012).



## 2. PREPARATION OF DNA SUBSTRATES FOR 4-STRAND DNA EXCHANGE

### 2.1 Preparation of Gapped DNA Substrate

The preparation of gapped circular DNA takes several days and includes the following steps (Fig. 2): (i) digestion of plasmid DNA with two restriction enzymes to produce a dsDNA fragment that is shorter than the original plasmid DNA by several hundred bp (the size of the future gap); (ii) isolation of the dsDNA fragment by agarose gel electrophoresis, its excision from the gel and electroelution; (iii) denaturation of the purified dsDNA fragment and its annealing to circular ssDNA to produce gapped DNA; (iv) purification of the gapped DNA by agarose gel electrophoresis, followed by gel excision and electroelution.

Duplex and circular ssDNA may be derived from ssDNA bacteriophages (e.g., M13,  $\phi$ X174), or from phagemids (e.g., pBS II). The phagemids are smaller in size and preferable for preparation of gapped DNA, because the efficiency of DNA elution from agarose gels decreases significantly with the increase in DNA size.

#### 2.1.1 Equipment

- Standard agarose gel running setup (Bio-Rad Wide Mini-Sub Cell GT)
- AlphaImager 3400 gel documentation station (Alpha Innotech)
- Vortex-2 Genie (Scientific Industries)
- Low-speed benchtop centrifuge
- Heat blocks or water baths set at 37°C and 65°C
- UV lamp
- Electroelution apparatus: Schleicher&Schuell Elutrap (Whatman)
- Micro Bio-Spin 6 columns (Bio-Rad, cat# 732-6221)
- 50- $\mu$ L quartz cuvettes (Agilent Technologies, cat# 5062-2496)

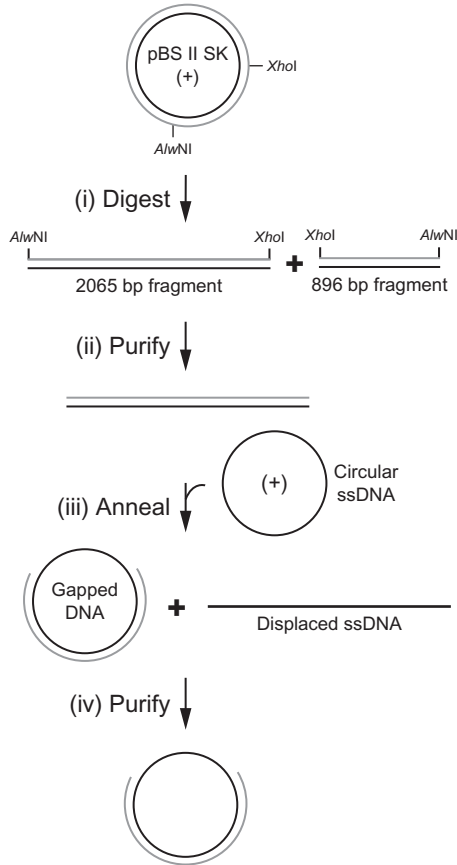


**Fig. 2** Construction of gapped DNA. (i) pBS II SK(+) plasmid DNA is cleaved with *XhoI* and *AlwNI* restriction endonucleases. (ii) The 2065 bp *XhoI*–*AlwNI* dsDNA fragment is purified by electrophoresis in agarose gels, then (iii) denatured and annealed to circular ssDNA to produce gapped DNA. (iv) Finally, the gapped DNA is purified by electrophoresis in agarose gels.

### 2.1.2 Buffers and Reagents

- NanoPure water
- *XhoI* restriction endonucleases (NEB)
- *AlwNI* restriction endonucleases (NEB)
- Bovine serum albumin (BSA), 20 mg/mL (NEB, cat# B9000S)
- Ethanol 200 proof
- TAE buffer: 40 mM Tris, 20 mM acetic acid, 1 mM EDTA, pH 8.0
- TE buffer: 10 mM Tris–HCl, 1 mM EDTA, pH 8.0

- Agarose, Type I-A, Low-EEO (Sigma cat# A0169) for analytical electrophoresis
- Agarose, Certified Molecular Biology (Bio-Rad cat# 161-3101) for purification of dsDNA and gapped DNA molecules by electroelution
- 1-kb DNA ladder Molecular Weight Marker
- 10× DNA loading buffer for agarose gels (0.25% bromophenol blue, 50% glycerol, 1 mM EDTA, pH 8.0)
- Ethidium bromide staining solution, 2 µg/mL in water
- 1-Butanol ≥99.4% ACS reagent (Sigma cat# 360465)
- 10× annealing buffer: 250 mM Tris-acetate, pH 7.5, 500 mM NaCl
- Formamide ≥99.5% (Sigma cat# F9037)

### 2.1.3 Procedure for Preparation of Linear dsDNA Fragment

Carry out the cleavage of pBS II SK (+) plasmid dsDNA with *Xho*I and *Alu*NI restriction endonucleases. Next, separate the 2065 and 896 bp dsDNA fragments (Fig. 2i) by agarose gel electrophoresis. Excise the 2065 bp dsDNA fragment from the gel and electroelute it. Note: load not more than 60 µg of pBS II SK (+) plasmid DNA per a 10 × 15 × 0.5-cm agarose gel. To scale up dsDNA fragment preparation use larger gels or multiple gels.

1. Take two 1.5-mL Eppendorf test tubes. In each tube, mix 30 µg pBS II SK (+), 30 µL 10× NEBuffer 2, 3 µL BSA (10 mg/mL), 6 µL *Xho*I (20 units/µL), and water to 300 µL. Next steps are described for each 300 µL reaction.
2. Incubate reaction mixture at 37°C for 1 h.
3. Test completeness of *Xho*I digestion. To do that, withdraw 1 µL (100 ng of DNA) out of the reaction mixture and combine it with 5 µL TE buffer (pH 8.0) premixed with 1 µL of 10× DNA loading buffer. Continue the incubation of the remaining 299 µL at 37°C until the test will confirm full digestion.
4. Load DNA samples onto a 6-cm long 0.8% agarose gel and run analytical gel electrophoresis. Use intact pBS II SK (+) plasmid DNA (100 ng) and a 1-kb DNA ladder as migration markers.
5. Stain the gel with ethidium bromide for 30 min at room temperature, destain for 30 min in a large volume of water, and visualize using an AlphaMager gel documentation station.
6. If *Xho*I digest is incomplete, check completeness of *Xho*I digestion again after 2 h from the beginning of the reaction. If *Xho*I digest is complete, heat the reaction at 65°C for 20 min to inactivate *Xho*I, and then

- cool it on ice. Prepare *Xho*I-linearized DNA sample as described in step 3 and keep at  $-20^{\circ}\text{C}$ . This sample will be used later as a marker during test for completeness of *Alu*NI digestion.
7. Precipitate *Xho*I-linearized DNA with ethanol. To do that, add  $15\ \mu\text{L}$  of  $5\ \text{M}$  NaCl to  $300\ \mu\text{L}$  of reaction mixture (to  $300\ \text{mM}$  including  $50\ \text{mM}$  NaCl in  $1\times$  NEB buffer 2), mix well, and then add  $800\ \mu\text{L}$  of ethanol. Mix and incubate at  $-20^{\circ}\text{C}$  for at least 1 h (or overnight).
  8. Centrifuge at  $>16,000\ \text{g}$  for 30 min at  $4^{\circ}\text{C}$ , discard the supernatant, and dry the pellet. Resuspend the pellet ( $30\ \mu\text{g}$ ) in reaction mixture, containing  $261\ \mu\text{L}$  of water and  $30\ \mu\text{L}$  of  $10\times$  NEBuffer 4, and then add  $9\ \mu\text{L}$  of *Alu*NI (10 units/ $\mu\text{L}$ ).
  9. Perform steps 3–8, except that the pellet has to be resuspended in  $150\ \mu\text{L}$  of TE buffer (pH 8.0) and proceed to purification of the 2065 bp DNA fragment.
  10. Add  $22\ \mu\text{L}$  of DNA loading buffer to each of the two DNA samples, combine them (total volume  $344\ \mu\text{L}$ ) and load onto a 1.1% agarose gel ( $10\times 15\times 0.5\ \text{cm}$ ). Modify a standard 20-well comb using a tape to create a 5-well comb with 2 preparative wells ( $\sim 50\ \text{mm}$  wide) and 3 analytical wells (5 mm wide) (Fig. 3A). Load  $7\ \mu\text{L}$  samples in each of the analytical wells (lanes A, C, and E), split the remaining  $323\ \mu\text{L}$  between two preparative wells (lanes B and D). Run the gel in TAE buffer at  $1.7\ \text{V}/\text{cm}$  for 13–14 h at room temperature. No ethidium bromide should be present in the gel or the running buffer since any residual ethidium bromide in the DNA sample will inhibit subsequent DNA strand exchange.
  11. Following electrophoresis, excise lanes A, C, and E from the gel and stain them with ethidium bromide. Reassemble the gel and visualize it under a UV lamp, revealing two bands. Using lanes A, C, and E as markers, excise the sections of agarose containing the 2065 bp DNA fragment from lanes B and D (dashed white boxes in Fig. 3A).
  12. Place two agarose gel slices into one Schleicher and Schuell Elutrap following the manufacturer's instructions. The DNA is extracted by electroelution at  $150\ \text{mA}$  for 4 h using TAE buffer. To increase the yield of extracted DNA do second elution at  $150\ \text{V}$  for 4 h or at  $75\ \text{V}$  overnight.
  13. Concentrate the recovered DNA in each eluate ( $500\text{--}930\ \mu\text{L}$ ) to  $\sim 200\ \mu\text{L}$  by extraction with 1-butanol. To do that, add equal volume of 1-butanol, mix well, and separate two phases by centrifugation in a benchtop centrifuge. Discard the upper phase. Repeat this step until the volume of DNA solution reaches  $\sim 200\ \mu\text{L}$ . Precipitate the DNA by adding 1/10 volume of  $3\ \text{M}$  sodium acetate, pH 7.0, and 2.5 volumes of ethanol. Incubate for at

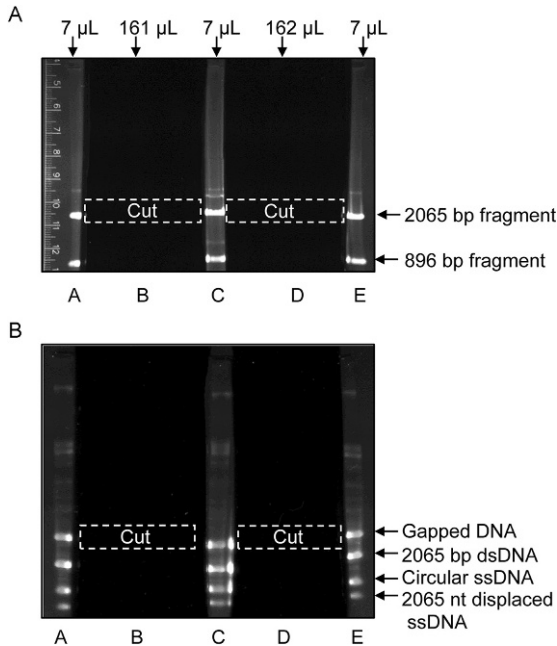


**Fig. 3** Purification of the 2065 bp *XhoI*–*AluNI* dsDNA fragment of pBS II SK(+) (A) and the gapped DNA (B) by electrophoresis in agarose gels. (A) After electrophoresis, lanes A, C, and E are excised from the gel and stained with ethidium bromide to visualize the DNA bands. Using these bands as markers, the area of the gel with the 2065 bp dsDNA fragment (A) and with the gapped DNA (B) is cut out of lanes B and D (dashed white boxes), and then the DNA is extracted from the gel by electroelution.

least 1 h (or overnight) at  $-20^{\circ}\text{C}$ . Centrifuge at  $>16,000 \times g$  for 30 min at  $4^{\circ}\text{C}$ , dry the pellets, and resuspend each in  $20 \mu\text{L}$  of TE buffer. Because 1-butanol extraction increases salt concentration in DNA samples, desalting is needed. Combine the DNA from eluate #1 and #2 ( $\sim 40 \mu\text{L}$ ) and pass it through a Micro-BioSpin 6 column equilibrated with  $10 \text{ mM}$  Tris–HCl, pH 8.0. Determine the DNA concentration on a spectrophotometer at 260 nm (usually at 1:40 dilution) using  $50\text{-}\mu\text{L}$  cuvettes and the ratio of 1 unit  $\text{OD}_{260} = 50 \mu\text{g}/\text{mL}$ . Good yields are in the range of  $20\text{--}27 \mu\text{g}$  of dsDNA ( $\sim 40\%$  of the theoretical yield).

14. Check the quality of the purified 2065 bp dsDNA fragment (Fig. 4, lane 3) as described in steps 3 and 5. Run a sample of *XhoI*–*AluNI* digested pBS II K (+) plasmid DNA ( $100 \text{ ng}$ ) and a 1-kb DNA ladder along with the purified 2065 bp dsDNA fragment ( $2 \mu\text{L}$  or  $\sim 100 \text{ ng}$ ) to judge its purity and concentration.

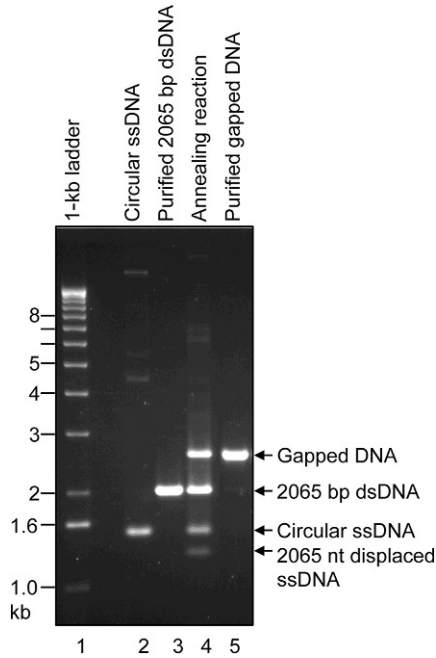


**Fig. 4** Analysis of the DNA substrates, intermediates, and gapped DNA product by electrophoresis in a 1.4% agarose gel. Lane 1: 1-kb DNA ladder. Lane 2, 3, and 5: purified circular ssDNA pBS II SK (+) (100 ng), 2065 bp dsDNA (125 ng), and gapped DNA (125 ng), respectively. Lane 4: DNA products of the annealing reaction (415 ng).

### 2.1.4 Procedure of Preparation of Gapped DNA

Prepared circular ssDNA of pBS II SK (+) as described in [Sambrook and Russell \(2001\)](#). Because pBluescript II can be secreted from *E. coli* cells in a circular ssDNA form only in the presence of VCSM13 helper phage, a small amount of this phage ssDNA (~6 kb) is always present in the pBluescript II ssDNA preparation.

1. Perform a trial small-scale annealing reaction (22  $\mu$ L) to determine the optimum ratio between circular ssDNA and dsDNA fragment for the maximal gapped DNA yield. Typically, 1  $\mu$ g of linear duplex fragment is mixed with 1, 1.5, and 2  $\mu$ g of circular pBS II SK (+) ssDNA in 1  $\times$  annealing buffer and 50% formamide.
2. Incubate the mixture for 5 min at 75°C, vortex, spin the tube for 2 s in a low-speed benchtop centrifuge just to collect the liquid, and continue the incubation for another 5 min to denature the dsDNA fragment.
3. Carry out annealing at room temperature for at least 3 h (or overnight).

4. To analyze DNA after annealing, withdraw 5  $\mu\text{L}$  (450–680 ng) from each reaction mixture, combine with 4  $\mu\text{L}$  TE buffer (pH 8.0) pre-mixed with 1  $\mu\text{L}$  of  $10\times$  DNA sample buffer and load on a 10-cm long 1.4% agarose gel along with circular ssDNA (100 ng) and purified 2065 bp dsDNA fragment (100 ng). DNA samples can be stored at  $-20^\circ\text{C}$  and used later as a marker (Fig. 4, lane 4) for testing the quality of purified gapped DNA.
5. Based on the obtained result, prepare a large-scale annealing reaction. Take two 1.5-mL Eppendorf tubes. Typically, in each tube we mix 17  $\mu\text{g}$  of the linear dsDNA fragment, 17  $\mu\text{g}$  of circular ssDNA ( $\sim 1.4$ -fold excess in terms of DNA molecules), 37.4  $\mu\text{L}$   $10\times$  annealing buffer, 188  $\mu\text{L}$  of formamide (99.5%), and water to 374  $\mu\text{L}$ .
6. Perform annealing reaction as described in steps 2 and 3.
7. Precipitate DNA in each annealing reaction by adding 34  $\mu\text{L}$  of 3 *M* sodium acetate, pH 7.0, and 1020  $\mu\text{L}$  of ethanol. Mix and incubate at  $-20^\circ\text{C}$  for at least 1 h (or overnight).
8. Centrifuge at  $>16,000\times g$  for 30 min at  $4^\circ\text{C}$ , dry the pellets, and resuspend each pellet in 150  $\mu\text{L}$  of TE buffer (pH 8.0).
9. Perform electrophoresis as in Section 2.1.3, step 10, except that percentage of an agarose gel has to be 1.4% to improve the separation of the DNA products.
10. Following electrophoresis, excise lanes A, C, and E and stain them with ethidium bromide (Fig. 3B). Reassemble the gel and visualize it under a UV lamp, to reveal four major bands. Using DNA in lanes A, C, and E as markers, excise the uppermost band (the gapped DNA) from lanes B and D (dashed white boxes in Fig. 3B). Be precise when cutting out this band, it is easy to pick up the 2065 bp dsDNA that migrates slightly faster than the gapped DNA.
11. Electroelute the DNA, as in Section 2.1.3, step 12.
12. Concentrate DNA from the eluates #1 and #2 (500–930  $\mu\text{L}$ ) to 100–150  $\mu\text{L}$  with 1-butanol as in Section 2.1.3, step 13.
13. Determine the final concentration of gapped DNA on a spectrophotometer at 260 nm (usually at dilution 1:10) using 50- $\mu\text{L}$  cuvettes and the ratio  $1 \text{ OD}_{260} = 45 \mu\text{g}/\text{mL}$ . Good yields are in the range 8–10  $\mu\text{g}$  of gapped DNA.
14. Check the quality of purified gapped DNA by electrophoresis in a 10-cm long 1.4% agarose gel (Fig. 4, lane 5). Run a sample of the small-scale annealing reaction (5  $\mu\text{L}$  containing 450 ng of DNA) (Fig. 4, lane 4) along with the purified gapped DNA (100 ng) to judge its purity.

### 2.1.5 Notes

We do not cleave pBS II SK (+) plasmid dsDNA simultaneously with *Xho*I and *Alu*NI, although both enzymes are active in NEBuffer 2. First, the mobilities of pBS II SK (+) supercoiled plasmid DNA and 2065 bp dsDNA fragment are similar making it difficult to judge the completeness of digestion. Second, *Alu*NI is more active in NEBuffer 4. After *Alu*NI digest, we precipitate DNA with ethanol to remove salt from the sample and to reduce its volume. This allows to have more sharp DNA bands during preparative gel electrophoresis, and therefore to minimize the width of the gel slices. Reduction of reaction volume during *Alu*NI digest will increase the DNA concentration above 100  $\mu\text{g}/\text{mL}$  that results in an incomplete digestion regardless of restriction endonuclease concentration and incubation time. During the gel excision step, be sure to minimize the width of the gel slices, as an excess of agarose will decrease the recovery of DNA. After removing the bands, stain the remainder of the gel with ethidium bromide to determine how successful the band excision was. Minor bands that migrate slower than the gapped DNA likely represent VCSM13 helper phage DNA (Fig. 4, lane 4).

## 2.2 Labeling of Linear dsDNA

For quantification of the 4-strand reaction, use  $^{32}\text{P}$ -labeled DNA joint molecules. Also, these joint molecules need to be suitable for branch migration in either the 5'–3' or the 3'–5' direction (Fig. 1). For this purpose, we prepare *Xho*I- and *Alu*NI-linearized dsDNA molecules labeled with  $^{32}\text{P}$  at the 5'- and 3'-end, respectively.

### 2.2.1 Equipment

- Equipment is as in [Section 2.1.1](#)

### 2.2.2 Buffers and Reagents

- Shrimp Alkaline Phosphatase (USB cat# 70092Y)
- [ $\gamma$ - $^{32}\text{P}$ ] ATP 6000 Ci/mmol, 10 mCi/mL (Perkin Elmer cat# BLU002Z250UC)
- T4 polynucleotide kinase (NEB cat# M0201S)
- Terminal deoxynucleotidyl transferase (NEB cat# M0315S).
- [ $\alpha$ - $^{32}\text{P}$ ] dCTP 6000 Ci/mmol, 10 mCi/mL (Perkin Elmer cat# BLU013Z)
- Other buffers and reagents are as in [Section 2.1.2](#)

### 2.2.3 Procedure of <sup>32</sup>P-Labeling of *Xho*I-Linearized pBS II SK(+) dsDNA at the 5'-End

The ssDNA region of gapped DNA is defined by the *Alu*NI and *Xho*I restriction sites of pBS II SK (+). The ssDNA of the gap runs in a 5'–3' direction from the *Alu*NI to the *Xho*I site (Fig. 1). To produce joint molecules with a 3'-displaced ssDNA, pBS II SK (+) plasmid DNA needs to be digested with *Xho*I (Fig. 1A). *Xho*I creates a 5'-protruding DNA end that can readily be <sup>32</sup>P-labeled with T4 polynucleotide kinase.

1. Mix in a tube 10 µg of pBS II SK (+) plasmid DNA, 10 µL of 10 × NEBuffer 2, 10 µL of BSA (1 mg/mL), 2 µL of *Xho*I (20 units/µL), 2 µL of Shrimp Alkaline Phosphatase (1 unit/µL), and water to 100 µL. The phosphatase removes the 5' terminal phosphate group left on DNA ends after *Xho*I digestion, producing the OH-end suitable for incorporation of <sup>32</sup>P label.
2. Prepare *Xho*I-linearized dsDNA as in Section 2.1.3, steps 2–8, except that the pellet has to be resuspended in 20 µL of Tris–HCl, pH 8.0, to give a DNA concentration ~0.5 µg/µL.
3. Radiolabel 5 µg of *Xho*I-linearized pBS II SK (+) DNA in a 40-µL reaction mixture containing 100 µCi of [ $\gamma$ -<sup>32</sup>P] ATP (10 mCi/mL), 1 × T4 polynucleotide kinase buffer, and 2 units of T4 polynucleotide kinase. Incubate the reaction for 1 h at 37°C, and then inactivate the enzyme for 20 min at 65°C. Remove unincorporated [ $\gamma$ -<sup>32</sup>P] ATP using a Micro-BioSpin 6 column equilibrated with 10 mM Tris–HCl, pH 8.0, as described by the manufacturer.
4. Determine the DNA concentration on a spectrophotometer at 260 nm (usually at dilution 1:10) using 50-µL cuvettes and the ratio 1 OD<sub>260</sub> = 50 µg/mL.

### 2.2.4 Procedure of <sup>32</sup>P-Labeling of *Alu*NI-Linearized pBS II SK(+) dsDNA at the 3'-End

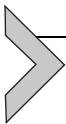
Joint molecules can also be constructed with a 5'-end displaced ssDNA strand using pBS II SK (+) linear dsDNA produced by *Alu*NI (Fig. 1B). *Alu*NI generates DNA ends with 3' overhangs, which may be 3' radio-labeled with terminal deoxynucleotidyl transferase.

1. Mix in 100 µL reaction 10 µg of pBS II SK (+) plasmid DNA, 10 µL of 10 × NEBuffer 4, and 4 µL of *Alu*NI (10 units/µL).
2. Prepare *Alu*NI-linearized dsDNA as in Section 2.1.3, steps 2–8, except that the pellet has to be resuspended in 20 µL of Tris–HCl, pH 8.0, to give a DNA concentration ~0.5 µg/µL.

3. Radiolabel 5  $\mu\text{g}$  of *Alw*NI-linearized pBS II K (+) plasmid DNA in a 40- $\mu\text{L}$  mixture containing 16  $\mu\text{Ci}$  of [ $\alpha$ - $^{32}\text{P}$ ] dCTP (10 mCi/mL) and terminal deoxynucleotidyl transferase (10 units) in cacodylate buffer as described by the manufacturer.
4. Incubate the reaction for 15 min at 37°C, then inactivate the enzyme for 10 min at 75°C. Remove unincorporated [ $\alpha$ - $^{32}\text{P}$ ] dCTP using a MicroBioSpin 6 column equilibrated with 10 mM Tris-HCl, pH 8.0, as described by the manufacturer.
5. Determine the DNA concentration on a spectrophotometer at 260 nm (usually at dilution 1:10) using 50- $\mu\text{L}$  cuvettes and the ratio 1  $\text{OD}_{260} = 50 \mu\text{g/mL}$ .

### 2.2.5 Notes

The number of incorporated nucleotide residues depends on the ratio 3' DNA ends:dNTP. We use 5.2 pmol of 3'-DNA ends and 2.6 pmol of [ $\alpha$ - $^{32}\text{P}$ ] dCTP. Under these conditions, dCTP and dGTP provide smaller number of incorporated nucleotide residues per a DNA end (1–3 nt) than dATP or dTTP (1–5 nt), and therefore are preferable. [ $\alpha$ - $^{32}\text{P}$ ] ddNTP that allows only a single nucleotide incorporation is even better, though is more expensive.



## 3. PREPARATION OF JOINT MOLECULES

We use hRad51 and RecA to prepare joint molecules with different polarities, as substrates for the 4-strand branch migration. Optimal conditions for the joint molecule preparation need to be determined for specific stocks of the proteins, gapped DNA, and  $^{32}\text{P}$ -labeled linear duplex DNA. For this purpose, conduct small-scale reactions (10  $\mu\text{L}$ ), as described in [Section 3.1.3](#), varying the concentrations of DNA and the proteins. Using optimal conditions scale-up the reaction to 90  $\mu\text{L}$ .

### 3.1 Preparation of 3'-Joint Molecules

#### 3.1.1 Equipment

- Typhoon FLA 7000 Phosphor imaging system (GE Healthcare)
- Whatman DE81 chromatography paper (GE Healthcare cat# 3658-915) or Amersham Hybond-N<sup>+</sup> membrane (GE Healthcare cat# RPN1520B)
- Illustra MicroSpin S-400 HR column (GE Healthcare cat# 27-5140-01)
- Other equipment is as in [Section 2.1.1](#)

### 3.1.2 Buffers and Reagents

- hRad51 was purified as described (Sigurdsson, Trujillo, Song, Stratton, & Sung, 2001)
- Human Replication protein A (hRPA) was purified as described (Henricksen, Umbricht, & Wold, 1994)
- Proteinase K, 20 mg/mL (Roche cat# 03115828001)
- Rad51 strand exchange buffer: 25 mM Tris-acetate, pH 7.5, 275 mM NaCl, 2 mM ATP, 1 mM MgCl<sub>2</sub>, 1 mM CaCl<sub>2</sub>, 1 mM DTT, and 100 µg/mL BSA
- 3 × deproteinization buffer: 4.8 mg/mL proteinase K, 3% SDS, 18% glycerol, and 0.03% bromophenol blue
- Other buffers and reagents are as in [Section 2.1.2](#)

### 3.1.3 Procedure of Preparation of 3'-Joint Molecules

hRad51 polymerizes on ssDNA preferentially in the 3'–5' direction (Fig. 1A) and promotes strand exchange between gapped DNA and linear dsDNA in the same direction, generating the displaced 3'-ssDNA strand.

1. To prepare joint molecules with a 3'-displaced ssDNA strand (90 µL final volume), mix 20 µM (nt) gapped DNA with 5 µM hRad51 in Rad51 strand exchange buffer. Incubate for 10 min at 37°C, then add 0.4 µM hRPA, incubate for another 10 min, and finally add 20 µM (nt) <sup>32</sup>P-labeled *Xho*I-linearized dsDNA to initiate joint molecule formation. Incubate the mixture for 2 h at 37°C.
2. Withdraw a 10-µL aliquot to estimate the extent of joint molecule formation. Incubate the remaining 80 µL for another 20 h, and then freeze it in dry ice. Store the 80 µL at –80°C.
3. Mix the 10 µL aliquot with 5 µL of 3 × deproteinization buffer. Incubate for 15 min at 37°C to deproteinize DNA products.
4. Separate the reaction products by electrophoresis in a 1.5% agarose gel (10 × 15 × 0.5 cm). Run the gel in TAE buffer at 5 V/cm for 1.5 h at room temperature.
5. Dry the gel on DE81 chromatography paper.
6. Visualize and quantify <sup>32</sup>P-labeled products using Typhoon FLA 7000 Phosphor imaging system. If the yield is in the range of 50%–60%, the joint molecules can be purified (see [Section 3.3](#)) and used for testing branch migration activities.

## 3.2 Preparation of 5'-Joint Molecules

### 3.2.1 Equipment

- Equipment is as in [Section 3.1.1](#).

### 3.2.2 Buffers and Reagents

- RecA protein (USB cat# 70028Z)
- ssDNA-binding protein (SSB) (USB cat# 70032Y)
- RecA strand exchange buffer: 35 mM Tris-HCl, pH 7.5, 3 mM ATP, 15 mM MgCl<sub>2</sub>, 2 mM DTT, and 100 µg/mL BSA
- Phosphocreatine (Sigma cat# P7936)
- Creatine phosphokinase (CalBiochem cat# 2384)
- Other buffers and reagents are as in [Section 3.1.2](#)

### 3.2.3 Procedure for Preparation of 5'-Joint Molecules

RecA polymerizes on ssDNA preferentially in the 5'–3' direction ([Fig. 1B](#)) and promotes strand exchange in the 5'–3' direction, generating the displaced 5'-ssDNA strand.

1. To prepare joint molecules with a 5'-ssDNA displaced strand (90 µL final volume), mix 20 µM (nt) of gapped DNA with 4 µM RecA in RecA strand exchange buffer supplemented with 10 mM phosphocreatine, and 10 units/mL creatine phosphokinase (an ATP regeneration system). Incubate for 5 min at 37°C, then add 0.33 µM SSB, incubate for another 1 min, and finally add 20 µM (nt) <sup>32</sup>P-labeled *Alu*NI-linearized dsDNA to initiate joint molecule formation. Incubate for 10 min at 37°C.
2. Withdraw a 10-µL aliquot for the analysis and freeze the remaining 80 µL of the reaction on dry ice. Store at –80°C.
3. Estimate the extent of joint molecule formation in a 1.5% agarose gel as described in [Section 3.1.3](#), steps 3–6. If the yield is in the range of 50%–60%, the joint molecules can be purified (see [Section 3.3](#)) and used for testing branch migration activities.

## 3.3 Deproteinization and Purification of Joint Molecules

### 3.3.1 Equipment

- Equipment is the same as in [Section 3.1.1](#).

### 3.3.2 Buffers and Reagents

- 0.5 M EDTA (pH 8.0)
- Other buffers and reagents are as in [Section 3.1.2](#)

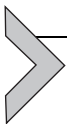
### 3.3.3 Procedure of Deproteinization and Purification of Joint Molecules

1. Following joint molecule formation (by hRad51 or RecA), add 8  $\mu\text{L}$  10% SDS and 8  $\mu\text{L}$  20 mg/mL proteinase K to the reaction mixture (80  $\mu\text{L}$ ), mix well, and incubate for 15 min at 37°C to deproteinize DNA, and then add 2  $\mu\text{L}$  98 mM EDTA, pH 8.0, to chelate  $\text{Ca}^{2+}$  or  $\text{Mg}^{2+}$ .
2. Prepare two S-400 Spin columns by equilibrating them with 30 mM Tris-acetate, pH 7.5, as described by the manufacturer.
3. Pass deproteinized joint molecules (98  $\mu\text{L}$ ) through first S-400 Spin column, and then apply the recovered eluate #1 (98–100  $\mu\text{L}$ ) to the second S-400 Spin column.
4. Add 2–10 mM  $\text{MgCl}_2$  to the recovered eluate #2 to inhibit spontaneous branch migration and store at  $-20^\circ\text{C}$ . The concentration of the purified joint molecules (typically 0.5–1 nM molecules) can be calculated by comparing their radioactivity to a known amount of  $^{32}\text{P}$ -labeled dsDNA after electrophoresis on the same gel.

### 3.3.4 Notes

As a control, always determine the extent of protein-independent (spontaneous) joint molecule formation by replacing Rad51/RecA with their storage buffers.

Passage of deproteinized joint molecules through the second S-400 Spin column is essential to remove all SDS traces, which can still be present in the eluate after the first column.



## 4. BRANCH MIGRATION OF JOINT MOLECULES

### 4.1 4-Strand DNA Branch Migration by hRad51

In the presence of  $\text{Ca}^{2+}$  and ATP, hRad51 forms a stable filament that promotes formation of joint molecules, but not their branch migration. Thus, the joint molecules will accumulate, reaching the maximum at 22 h. To increase the yield of joint molecules further, 2 mM ATP may be replaced with 2 mM dATP. In the presence of 2 mM dATP, only tiny amounts of branch migration products (nicked circular dsDNA and displaced tailed dsDNA) can be detected after 20 h of incubation (Fig. 5A, lane 3). 4-Strand branch migration is initiated by  $\text{Ca}^{2+}$  depletion with EGTA, yielding ~36% of products at 20 h of incubation (Fig. 5A, lane 4).

#### 4.1.1 Equipment

- Equipment is as in [Section 3.1.1](#)

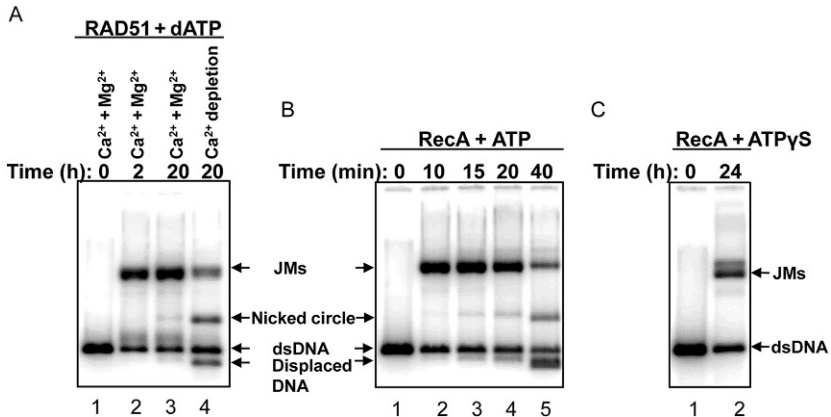


**Fig. 5** 4-strand branch migration of nondeproteinized joint molecules by hRad51 (5  $\mu$ M) (A) or RecA (4  $\mu$ M) (B). Reaction scheme is shown in Fig. 1. dsDNA was <sup>32</sup>P-labeled. (A) Ca<sup>2+</sup> stimulates joint molecule formation but inhibits branch migration by hRad51. The reaction was carried out in the presence of 1 mM Ca<sup>2+</sup> and 1 mM Mg<sup>2+</sup> for 2 h (lane 2) as described in Section 3.1.3, except that 2 mM ATP was replaced with 2 mM dATP. The reaction mixture was divided between two test tubes. In the first, incubation was continued for another 20 h (lane 3). In the second, EGTA (1.2 mM, pH 8.0) was added to deplete Ca<sup>2+</sup> and incubation continued for 20 h (lane 4). (B) RecA promotes strand exchange and 4-strand branch migration under the same reaction conditions as described in Section 3.2.3. Time course of the RecA-promoted 4-strand exchange reaction (lanes 1–5). (C) In the presence of 4 mM Mg<sup>2+</sup> and 1 mM ATPγS, RecA (12  $\mu$ M) promotes joint molecule formation, but not their branch migration (lane 2).

#### 4.1.2 Buffers and Reagents

- 0.5 M EGTGA, pH 8.0
- Rad51 branch migration buffer: 30 mM Tris-acetate, pH 7.5, 350 mM NaCl, 2 mM ATP, 10 mM MgCl<sub>2</sub>, 1 mM DTT, and 100  $\mu$ g/mL BSA
- Other buffers and reagents are as in Section 3.2.2

#### 4.1.3 Procedure for Initiation of hRad51 4-Strand Branch Migration on Nondeproteinized 3'-Joint Molecules

1. Set up 90  $\mu$ L of 4-strand exchange reaction as described in Section 3.1.1, step 1. Incubate the mixture for 2 h at 37°C.
2. Withdraw a 10- $\mu$ L aliquot to estimate the extent of joint molecule formation.
3. To initiate branch migration mix the remaining 80  $\mu$ L with 2  $\mu$ L of 50 mM EGTGA, pH 8.0, and continue incubation at 37°C.
4. Withdraw 10  $\mu$ L aliquots at desirable time points and analyze DNA products as in Section 3.1.3, steps 3–6 (Fig. 5A, lane 4).

#### 4.1.4 Procedure for Reinitiation of hRad51 Branch Migration on Purified 3'-Joint Molecules

For hRad51, initiation of 4-strand (forward) branch migration on purified 3'-joint molecules requires 1–10 mM  $Mg^{2+}$ , an ATP regeneration system, elevated concentrations of NaCl (350 mM) and hRad51 (10  $\mu M$ ).  $Ca^{2+}$  inhibits the reaction. Purified 5'-joint molecules support only 3-strand (reverse) branch migration that leads to disruption of joint molecules into the original DNA substrates ( $^{32}P$ -labeled linear dsDNA and unlabeled gapped DNA).

1. Mix 0.3–0.5 nM (molecules) 3'-joint molecules in Rad51 branch migration buffer, supplemented with 8 mM phosphocreatine, and 8 units/mL creatine phosphokinase (an ATP regeneration system). Initiate the reaction by the addition of RAD51 (10  $\mu M$ ) and carry it out at 37°C.
2. Withdraw 10  $\mu L$  aliquots at desirable time points and analyze DNA products as in [Section 3.1.3](#), steps 3–6.

#### 4.2 4-Strand DNA Branch Migration by *E. coli* RecA

RecA forms dynamic filament in the presence of  $Mg^{2+}$ , which promotes both strand exchange and branch migration. Branch migration converts joint molecules into 4-strand Holliday junctions and drives them further into nicked circular DNA and displaced tailed DNA products ([Fig. 1B](#)). The 10-min reaction time represents a compromise allowing for the largest accumulation of joint molecules ([Fig. 5B](#), lane 2) before the branch migration products become visible ([Fig. 5B](#), lanes 3–5). To produce joint molecules with RecA, but without initiating branch migration, 3 mM ATP can be replaced with 1 mM ATP $\gamma$ S ([Fig. 5C](#), lane 2). In this case, the ATP regeneration system needs to be omitted, RecA concentration increased to 12  $\mu M$ ,  $MgCl_2$  concentration decreased to 4 mM, and the reaction time increased from 10 min to 24 h. However, even at 24 h, the yield of RecA-promoted joint molecules in the presence of ATP $\gamma$ S is half as high as in the presence of ATP (30% vs 60%).

##### 4.2.1 Equipment

- Equipment is the same as in [Section 3.1.1](#)

##### 4.2.2 Buffers and Reagents

- RecA branch migration buffer: 30 mM Tris-HCl, pH 7.5, 10 mM  $MgCl_2$ , 2 mM DTT, and 2 mM ATP
- Other buffers and reagents are as in [Section 3.2.2](#)

### 4.2.3 Procedure of Re-Initiation of RecA Branch Migration on Purified 5'-Joint Molecules

For RecA, initiation of 4-strand (forward) branch migration on purified 5'-joint molecules requires the same conditions as the standard 4-strand branch migration. RecA promotes the 4-strand branch migration with the rate approximately 11-fold faster than hRad51.

Purified 3'-joint molecules support only reverse branch migration that leads to disruption of joint molecules into the original DNA substrates (<sup>32</sup>P-labeled linear dsDNA and unlabeled gapped DNA).

1. Mix 0.3–0.5 nM (molecules) 5'-joint molecules in RecA branch migration buffer, supplemented with 10 mM phosphocreatine, and 10 units/mL creatine phosphokinase (an ATP regeneration system). Initiate the reaction by the addition of RecA (4 μM) and carry it out at 37°C.
2. Withdraw 10-μL aliquots at desirable time points and analyze DNA products as in [Section 3.1.3](#), steps 3–6.

### 4.2.4 Notes

Branch migration of joint molecules can proceed either in the forward (DNA 4-strand branch migration) or the reverse direction (3-strand reaction). This direction is determined by (1) the polarity of the displaced ssDNA strand in the joint molecules and (2) by the intrinsic polarity of branch migration protein. As a control, always determine the extent of protein-independent (spontaneous) branch migration by replacing your branch migration protein with its storage buffer.



## 5. SUMMARY AND CONCLUSION

Here, we describe the methodology and the protocols for preparation of the joint molecules with the opposite polarities, which can be used to study the mechanisms of branch migration of Holliday junctions promoted by different proteins that play an important role in homologous recombination and DNA repair. The described basic design of these joint molecules can be further modified, e.g., by incorporation the regions of heterology ([Mazina et al., 2012](#)). In addition, these joint molecules may serve as substrates for structure-specific endonucleases that are responsible for cleavage of Holliday junctions.

## ACKNOWLEDGMENTS

We thank Kritika Hanamshet and Nadish Goyal for the feedback on this protocol. We acknowledge funding from the National Cancer Institute of the National Institutes of Health (NIH) Grant numbers CA188347, P30CA056036 (to A.V.M.) and from Drexel Coulter Program (to A.V.M.) for supporting this work. The authors declare no conflicts of interests.

## REFERENCES

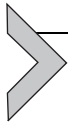
- Cunningham, R. P., DasGupta, C., Shibata, T., & Radding, C. M. (1980). Homologous pairing in genetic recombination: recA protein makes joint molecules of gapped circular DNA and closed circular DNA. *Cell*, *20*(1), 223–235.
- Henricksen, L. A., Umbricht, C. B., & Wold, M. S. (1994). Recombinant replication protein A: Expression, complex formation, and functional characterization. *The Journal of Biological Chemistry*, *269*(15), 11121–11132.
- Konforti, B. B., & Davis, R. W. (1992). ATP hydrolysis and the displaced strand are two factors that determine the polarity of RecA-promoted DNA strand exchange. *Journal of Molecular Biology*, *227*(1), 38–53.
- Kowalczykowski, S. C. (1991). Biochemistry of genetic recombination: Energetics and mechanism of DNA strand exchange. *Annual Review of Biophysics and Biophysical Chemistry*, *20*, 539–575.
- Kowalczykowski, S. C. (2015). An overview of the molecular mechanisms of recombinational DNA repair. *Cold Spring Harbor Perspectives in Biology*, *7*(11), a016410. <https://doi.org/10.1101/cshperspect.a016410>.
- Mazina, O. M., Rossi, M. J., Deakyn, J. S., Huang, F., & Mazin, A. V. (2012). Polarity and bypass of DNA heterology during branch migration of Holliday junctions by human RAD54, BLM, and RECQ1 proteins. *The Journal of Biological Chemistry*, *287*(15), 11820–11832. <https://doi.org/10.1074/jbc.M112.341347>.
- Murayama, Y., Kurokawa, Y., Mayanagi, K., & Iwasaki, H. (2008). Formation and branch migration of Holliday junctions mediated by eukaryotic recombinases. *Nature*, *451*(7181), 1018–1021.
- Murayama, Y., Tsutsui, Y., & Iwasaki, H. (2011). The fission yeast meiosis-specific Dmc1 recombinase mediates formation and branch migration of Holliday junctions by preferentially promoting strand exchange in a direction opposite to that of Rad51. *Genes and Development*, *25*(5), 516–527. <https://doi.org/10.1101/gad.1997511>.
- Robu, M. E., Inman, R. B., & Cox, M. M. (2001). RecA protein promotes the regression of stalled replication forks in vitro. *Proceedings of the National Academy of Sciences of the United States of America*, *98*(15), 8211–8218.
- Rossi, M. J., Mazina, O. M., Bugreev, D. V., & Mazin, A. V. (2010). Analyzing the branch migration activities of eukaryotic proteins. *Methods*, *51*(3), 336–346. <https://doi.org/10.1016/j.ymeth.2010.02.010>.
- Rossi, M. J., Mazina, O. M., Bugreev, D. V., & Mazin, A. V. (2011). The RecA/RAD51 protein drives migration of Holliday junctions via polymerization on DNA. *Proceedings of the National Academy of Sciences of the United States of America*, *108*(16), 6432–6437. <https://doi.org/10.1073/pnas.1016072108>.
- Sambrook, J., & Russell, D. W. (Eds.), (2001). In *Molecular cloning: A laboratory manual*. : Vol. 1. (pp. 1.65–1.68) (3rd ed.). Cold Spring Harbor, NY: Cold Spring Harbor Laboratory Press.
- Sigurdson, S., Trujillo, K., Song, B., Stratton, S., & Sung, P. (2001). Basis for avid homologous DNA strand exchange by human Rad51 and RPA. *The Journal of Biological Chemistry*, *276*(12), 8798–8806.

West, S. C., Cassuto, E., Mursalim, J., & Howard-Flanders, P. (1980). Recognition of duplex DNA containing single-stranded regions by recA protein. *Proceedings of the National Academy of Sciences of the United States of America*, 77, 2569–2573.

### **FURTHER READING**

Mazina, O. M., & Mazin, A. V. (2004). Human Rad54 protein stimulates DNA strand exchange activity of hRad51 protein in the presence of Ca<sup>2+</sup>. *The Journal of Biological Chemistry*, 279(50), 52042–52051.

This page intentionally left blank



# Purification of *Saccharomyces cerevisiae* Homologous Recombination Proteins Dmc1 and Rdh54/Tid1 and a Fluorescent D-Loop Assay

Yuen-Ling Chan, Douglas K. Bishop<sup>1</sup>

University of Chicago, Chicago, IL, United States

<sup>1</sup>Corresponding author: e-mail address: dbishop@uchicago.edu

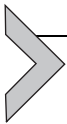
## Contents

|  |     |
|--|-----|
| 1. Introduction                                    | 308 |
| 2. Overexpression of Dmc1                          | 310 |
| 2.1 General Comments                               | 310 |
| 2.2 Equipment, Buffers, and Reagents               | 311 |
| 2.3 Expression Procedure                           | 311 |
| 3. Purification of Dmc1                            | 312 |
| 3.1 General Comments                               | 312 |
| 3.2 Equipment                                      | 313 |
| 3.3 Buffers and Reagents                           | 313 |
| 3.4 Procedure                                      | 314 |
| 3.5 FPLC Ion Exchange Chromatography               | 316 |
| 3.6 Notes  | 316 |
| 4. D-Loop Assay Using Fluorescent Dye-Tagged ssDNA | 317 |
| 4.1 Buffers and Reagents                           | 318 |
| 4.2 Procedure                                      | 319 |
| Acknowledgment                                     | 319 |
| References   | 319 |

## Abstract

Budding yeast Dmc1 is a member of the RecA family of strand exchange proteins essential for homologous recombination (HR) during meiosis. Dmc1 mediates the steps of homology search and DNA strand exchange reactions that are central to HR. To achieve optimum activity, Dmc1 requires a number of accessory factors. Although methods for purification of Dmc1 and many of its associated factors have been described (Binz, Dickson, Haring, & Wold, 2006; Busygina et al., 2013; Chan, Brown, Qin, Handa, & Bishop, 2014; Chi et al., 2006; Cloud, Chan, Grubb, Budke, & Bishop, 2012; Nimonkar, Amitani,

Baskin, & Kowalczykowski, 2007; Van Komen, Macris, Sehorn, & Sung, 2006), Dmc1 has been particularly difficult to purify because of its tendency to aggregate. Here, we provide an alternative and simple high-yield purification method for recombinant Dmc1 that is active and responsive to stimulation by accessory factors. The same method may be used for purification of recombinant Rdh54 (a.k.a. Tid1) and other HR proteins with minor adjustments. We also describe an economical and sensitive D-loop assay for strand exchange proteins that uses fluorescent dye-tagged, rather than radioactive, ssDNA substrates.



## 1. INTRODUCTION

In eukaryotic cells, Dmc1 is essential for, and functions specifically during, meiosis. During meiosis, chromosomes are replicated and undergo homologous recombination (HR) (Brown & Bishop, 2014). Meiotic recombination is then initiated by programmed double-strand DNA breaks which are processed by a group of specific proteins and nucleases to generate 5'-duplex junctions with 3'-single-stranded DNA (ssDNA) overhangs. In *Saccharomyces cerevisiae*, Dmc1 with the help of associated factors binds ssDNA to form nucleoprotein filaments. These filaments, in turn, search the genome for homologous DNA sequences. Once a homologous sequence is found, Dmc1 then catalyzes strand invasion and strand exchange, resulting in a heteroduplex with a displaced strand called the displacement loop (D-loop). The *in vitro* D-loop assay models the *in vivo* reaction using ssDNA oligo as substrate for the assembly of nucleoprotein filaments by Dmc1 (or other recombinases) together with a negatively supercoiled plasmid that carries a sequence identical to that of the oligo. After strand exchange, the ssDNA forms a heteroduplex inside the plasmid resulting in a D-loop (Fig. 1A). The D-loop assay is one of the most commonly used biochemical functional assays for recombinases.

Genetic and biochemical studies have provided many insights into the mechanism of HR. Purified HR proteins in native or recombinant forms have facilitated many of these biochemical studies. However, some recombination proteins, including budding yeast Dmc1, are difficult to purify. The key challenge for purification of Dmc1 is its tendency to aggregate. The Rad54 family translocase Rdh54/Tid1 (Brown & Bishop, 2014) is also difficult to purify because of its instability; proteolysis tends to occur during purification. This chapter describes an alternative method for purification of (His)<sub>6</sub>-tagged versions of Dmc1 and Rdh54/Tid1 proteins (Fig. 2A).

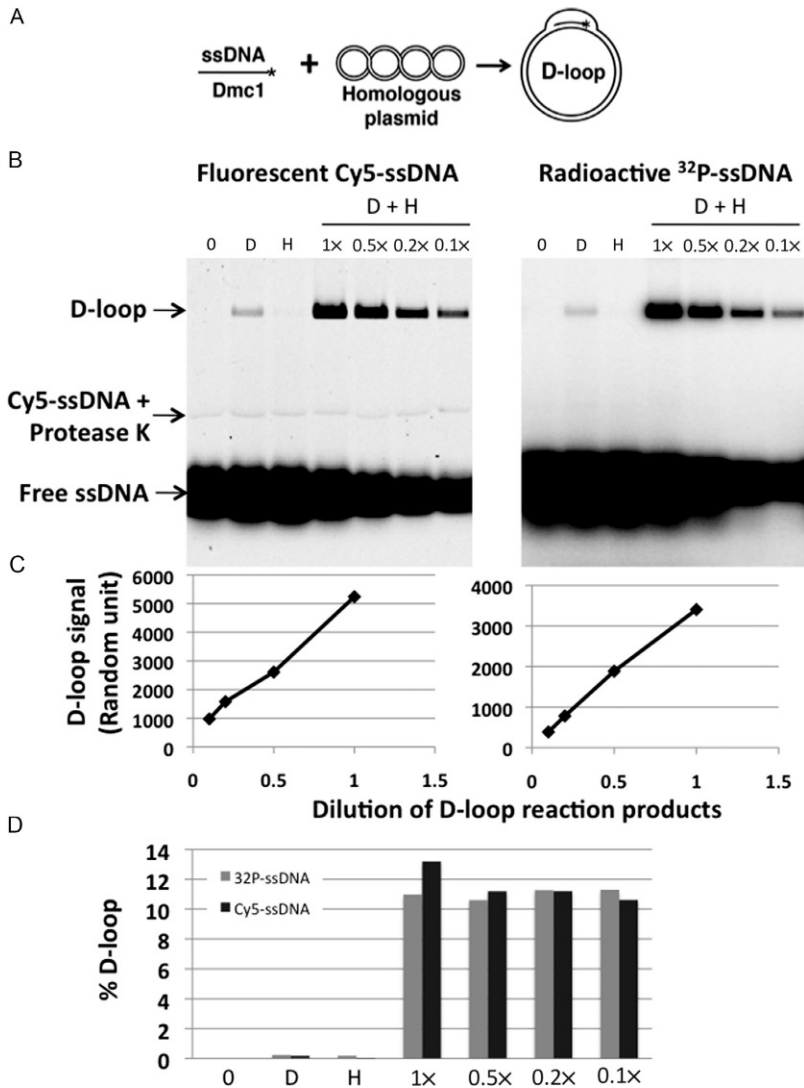


**Fig. 1** Comparison of D-loop assays using Cy5-ssDNA vs  $^{32}\text{P}$ -ssDNA. (A) Cartoon of the D-loop assay. (B) Hop2-Mnd1 (H) stimulation of Dmc1 (D) D-loop formation using both fluorescent Cy5-ssDNA and radioactive  $^{32}\text{P}$ -ssDNA in the same reaction mixture. Equal amount (15 nM each) of the two ssDNAs were added to the reaction. The "0" lane has no protein. After the D-loop formation step, the reaction mixture was diluted by half, 5-fold, and 10-fold using reaction buffer. The dilution step was followed by deproteinization and other steps. After gel electrophoresis, the agarose gel was first imaged directly for Cy5 signal in Typhoon 9200 Imager. Subsequently, the same gel was dried onto a positively charged membrane and exposed to an image plate overnight. The radioactive signal from the image plate was acquired using the same Imager. (C) The signal of D-loop bands from diluted reactions in (B) were quantified and plotted. (D) The D-loop activity of the reactions are plotted.

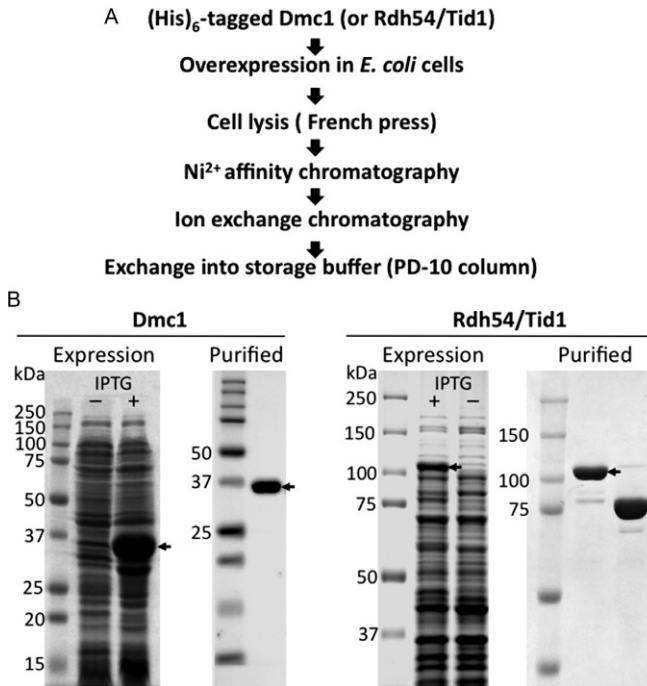
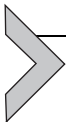


**Fig. 2** (A) A flow chart showing steps of the two-column method in the purification of (His)<sub>6</sub>-tagged Dmc1 and Rdh54/Tid1. (B) Overexpression and purification of Dmc1 and Rdh54/Tid1 proteins. Lysates from Rosetta(DE3)pLysE *E. coli* cells before and after induction of expression by IPTG were analyzed on 12% SDS-PAGE for Dmc1 and 8% for Rdh/Tid1. Gel staining was with Coomassie Brilliant Blue. The purified proteins (2 μg Dmc1 [37 kDa], 2.5 μg Rdh54/Tid1 [105 kDa]) were analyzed on separate gels. Arrows indicate the position of Dmc1 and Rdh54/Tid1; an asterisk indicates the position of the 75 kDa C-terminal Rdh54/Tid1 fragment (4 μg fragment). The intact Rdh54/Tid1 was separated from the truncated protein by Mono S column.

We have also used modest modification of the same approach to purify other HR proteins and believe the method is broadly applicable to other (His)<sub>6</sub>-tagged DNA-binding proteins. We also describe a fluorescent dye-based D-loop assay for functional studies of HR proteins.



## 2. OVEREXPRESSION OF Dmc1

### 2.1 General Comments

Dmc1 is overexpressed from the plasmid pNRB150 (Hong, Shinohara, & Bishop, 2001) (available upon request) that has pET11a as its backbone. Dmc1 is (His)<sub>6</sub>-tagged at its N-terminal, and the (His)<sub>6</sub>-tagged protein

has been demonstrated to be expressed at normal levels during meiosis following targeting into yeast cells, where it functions normally (Hong et al., 2001). The recombinant protein is expressed from a T7 promoter. Overexpression of Dmc1 is toxic to *Escherichia coli* cells, thus the following protocol is optimized for induction of high levels of expression with minimum impact of toxicity on protein yield. Section 2.3 has been applied to Rdh54/Tid1 and other proteins with adjustment of the concentration of IPTG, temperature, and the duration of induction.

## 2.2 Equipment, Buffers, and Reagents

- Standard shaker that holds baffled flask and allows temperature control
- Six 2.8-L baffled flasks
- Luria broth (LB) (10 g Bacto-tryptone, 5 g yeast extract, and 10 g NaCl per liter, adjust to pH 7–7.5 with NaOH, sterilized)
- 40% glucose, 100 mg/mL ampicillin, 34 mg/mL chloramphenicol, 5 M NaCl
- Centrifuge with rotor for 0.5-L (FiberLite F10) or 1-L bottles (Sorvall H6000A)
- Standard SDS-PAGE gel apparatus, 12% SDS-PAGE gels

## 2.3 Expression Procedure

Dmc1 is overexpressed in the *E. coli* strain Rosetta(DE3)pLysS (Novagen, chloramphenicol<sup>+</sup>)

1. Transform Rosetta(DE3)pLysS competent cells with pNRB150 (Ampicillin<sup>+</sup>). Grow cells on agar plates containing 100 µg/mL ampicillin and 34 µg/mL chloramphenicol at room temperature till the colonies are ~2 mm in diameter (in about 2–3 days). Or, include 1% glucose in agar plates if cells are to be grown at 37°C. (NB: glucose is necessary for suppressing expression from the T7 promoter carried by pET11.)
2. *Starting culture*: In a 2-L flask, inoculate 600 mL LB (supplemented with 1% glucose, 100 µg/mL ampicillin, 17 µg/mL chloramphenicol) with about 20 colonies. Let the culture stand at room temperature overnight.
3. Next morning, grow cells in a shaker at 37°C (230–250 rpm) for 1.5 h or until  $A_{600}$  reaches 0.5–0.7.
4. Inoculate each liter LB (supplemented with 1% glucose, 100 µg/mL ampicillin, 17 µg/mL chloramphenicol) in a 2.8-L baffled flask. Add a sufficient volume of starting culture to make the starting  $A_{600}$  of the medium around 0.05. This is typically between 50 and 90 mL of starting

- culture per flask. Grow cells in a shaker at 37°C (230–250 rpm) for about 2–2.5 h or until  $A_{600}$  reach 0.7–1.0. Save 1 mL culture for SDS-PAGE gel analysis.
5. Induce expression of Dmc1 by adding 0.5 mL of 1 M IPTG per liter culture (final concentration of 0.5 mM IPTG). After 1 h induction at 37°C, adjust the shaker temperature to 30°C and allow temperature to taper down slowly from 37°C to 30°C while still shaking and continue cell growth for another 1 h, i.e., a total of 2 h induction. Save 1 mL induced culture for SDS-PAGE gel analysis.
  6. Harvest cells by centrifugation at 5000 rpm (Sorvall H6000A rotor) for 20 min at 4°C. Wash cell pellets by suspending cells in Cell lysis buffer (25 mM sodium phosphate buffer, pH 7.5 + 1 mM dithiothreitol (DTT) + 1 M NaCl + 50 mM imidazole; see details later) and combine cells from all 6 L cultures (yield about 12 g cells) into one bottle. Centrifuge cells again and store the cell pellet at –20°C. Proceed to purification within 1 week. Store cells at –80°C if longer storage is required.
  7. Analyze protein extracts from cultures above to determine the expression level of Dmc1 using a 12% SDS-PAGE gel. In general, 150  $\mu$ L aliquots of the culture, taken before and after induction by IPTG, should be adequate for gel analysis.



### 3. PURIFICATION OF Dmc1

#### 3.1 General Comments

Purification of Dmc1 and many of its associated factors have been described (Binz, Dickson, Haring, & Wold, 2006; Busygina et al., 2013; Chan, Brown, Qin, Handa, & Bishop, 2014; Chi et al., 2006; Cloud, Chan, Grubb, Budke, & Bishop, 2012; Nimonkar, Amitani, Baskin, & Kowalczykowski, 2007; Van Komen, Macris, Sehorn, & Sung, 2006). Purification of Dmc1 has proven difficult because of its tendency to aggregate. The method described here includes techniques developed to avoid aggregation. Some practical suggestions on the purification of Dmc1: (a) try to achieve a high level of protein expression while avoiding the formation of inclusion bodies (i.e., avoiding conditions that result in an insoluble form of the protein that goes to the pellet when the extract is cleared by centrifugation); (b) overload  $\text{Ni}^{2+}$  resin to encourage specific his-tagged protein binding and minimize nonspecific protein binding; 1 mL  $\text{Ni}^{2+}$  resin binds about 30 mg of (His)<sub>6</sub>-tagged Dmc1; (c) reduce protein concentration after elution from  $\text{Ni}^{2+}$  column to no more than 4–5 mg/mL to avoid

aggregation of Dmc1; (d) use high salt in the lysis buffer to release Dmc1 from *E. coli* genomic DNA; (e) wash the protein-bound Ni<sup>2+</sup> resin excessively before elution, to remove DNA and protein contaminants, in particular DNA nucleases and helicases; (f) avoid concentrating Dmc1 by centricon because the protein tends to bind to the membrane; (g) avoid dialysis of Dmc1 because it is likely to either precipitate or stick to dialysis membrane; (f) avoid detergents in the buffer as these may affect biochemical assays.

The protein overexpression and purification protocols detailed here have been adopted for Rdh54/Tid1 (details are provided later).

### 3.2 Equipment

- Bio-Rad glass Econo-column
- Dounce glass homogenizer (40 mL, Kontes Glass Co.)
- French press (or other equipment for the efficient lysis of bacterial cells)
- Standard SDS-PAGE gel apparatus, 12% SDS-PAGE gels
- Ultracentrifuge
- Type 60 or Type 70 titanium rotor (Beckmann) or equivalent
- Rotisserie apparatus
- Ni<sup>2+</sup> Sepharose High Performance resin (GE Healthcare) or equivalent resin
- FPLC system (Bio-Rad or equivalent system)
- Mono Q column (1 mL resin, GE HealthCare, HR 5/50 GL)
- PD-10 desalting column containing Sephadex G-25 resin (GE Healthcare)

### 3.3 Buffers and Reagents

- 2 × Sodium phosphate buffer (2 × buffer P), pH 7.5: 50 mM buffer containing 2 mM DTT and 20% glycerol
- 2 × Tris-HCl buffer, pH 7.5 (2 × buffer T): 50 mM buffer containing 2 mM DTT and 20% glycerol
- 5 M NaCl
- 2 M imidazole (adjust to pH 7.4 with HCl)
- Cell lysis buffer P: (1 × buffer P) + 1 M NaCl + 50 mM imidazole (NB: low concentration imidazole is added to minimize binding of host cell proteins)

- Protease inhibitor cocktail tablet (EDTA-free, Roche protease inhibitor cocktail tablet. Add one tablet per 50–100 mL Cell lysis buffer immediately before use)
- Wash buffer T: (1 × buffer T) + 0.5 M NaCl + 30 mM or 50 mM imidazole (detail later)
- Elution buffer T: (1 × buffer T) + 0.5 M NaCl + 80 mM, or 350 mM, or 500 mM imidazole (detail later)
- Storage buffer T: (1 × buffer T) + 0.5 M NaCl + 1 mM EDTA + 10% glycerol

### 3.4 Procedure

#### 3.4.1 Cell Lysate Preparation at 4°C

To frozen cell pellet from 6 L culture, add 120 mL ice-cold Cell lysis buffer P plus protease inhibitors and allow cells to thaw on ice. Resuspend cells using a Dounce homogenizer until no cell clumps remain. Then lyse cells using a French press; repeat three passes at 18,000–20,000 psi. Centrifuge the lysate at 120,000 × *g* (use Beckman rotor Type60 or Type70) for 30 min at 4°C. Collect the clear supernatant and avoid cell debris. If debris is observed, filter the lysate through a 0.45 μm low protein binding membrane (e.g., Millipore Stericup).

#### 3.4.2 Batch/Gravity Flow Ni<sup>2+</sup> Column Purification

Perform all steps at 4°C or in the cold room. Save 50 μL sample from each step for SDS-PAGE gel analysis.

1. *Ni<sup>2+</sup> resin preparation:* Wash Ni<sup>2+</sup> resin with double-distilled water and equilibrate resin with Cell lysis buffer P (without protease inhibitors) as suggested by the manufacturer. Use about 0.7 mL packed Ni<sup>2+</sup> resin for lysate from 1 L cell culture if the expression is estimated to be ~20 mg. Equilibrate resin with 15 mL of Cell lysis buffer P in a 50-mL centrifuge tube for 10 min on a rotisserie apparatus at low speed. Pellet resin in a clinical centrifuge for 1 min.
2. *Protein binding to resin:* Add the cleared lysate to the buffer equilibrated Ni<sup>2+</sup> resin. Gently rotate the sample on a rotisserie at low speed for 1 h at 4°C. After binding, pellet resin in a clinical centrifuge for 1 min, remove almost all of the supernatant without disturbing the resin pellet. The resin will change color from light blue to gray when bound with protein. Proceed to wash the resin.

3. *Batch-wash the resin* with 45 mL Cell lysis buffer P + 50 mM imidazole for 1 min with gentle shaking. Centrifuge as in step 2 above. Repeat batch-wash once more.
4. *Gravity Ni<sup>2+</sup> column wash*: Resuspend resin in ~5 mL Wash buffer T + 30 mM imidazole. Transfer the resin mixture into a glass Econo-column (~1.5 cm diameter) with an end cap in place. Allow resin to settle in the column for about 5 min. Remove end cap and allow buffer to drain till it reaches the top of the resin bed. Avoid air bubbles, gently layer 5 mL Wash buffer T + 30 mM imidazole onto the top of the resin. Set up a continuous buffer siphon system for auto-wash by gravity and change buffer sequentially as follows:
  - a. 40–50 column volume (CV) of Wash buffer T + 30 mM imidazole
  - b. 10–20 CV Wash buffer T + 50 mM imidazole(NB: this extensive washing procedure is critical for purity; we discourage the temptation to reduce wash volumes).
5. *Protein elution*: Manually elute his-tagged Dmc1 by the following steps, and collect 1–1.5 mL fractions (depending on the size of Ni<sup>2+</sup> column), elute till  $A_{280}$  reaches baseline:
  - a. 5 CV, Elution buffer T + 80 mM imidazole
  - b. 10 CV, Elution buffer T + 300 mM imidazole
  - c. 5 CV, Elution buffer T + 500 mM imidazole
6. Read  $A_{280}$  of the fractions. A NanoDrop apparatus is particularly convenient for this purpose. Dilute peak fractions containing high Dmc1 concentration to about 4–5 mg/mL using Storage buffer T as soon as possible after elution to avoid Dmc1 precipitating out of solution.
7. Analyze fractions (10–20  $\mu$ L per fraction) on a 12% SDS-PAGE gel. Pool peak fractions according to protein purity as revealed by the SDS gel.
8. Typically, Dmc1 is estimated to be near 95% homogeneity after just the Ni<sup>2+</sup> resin column (Fig. 2B). If no further purification step needs to be taken, proceed to remove imidazole and exchange Dmc1 into Storage buffer T using a PD-10 or equivalent column according to manufacturer's instructions. Store the purified protein at  $-80^{\circ}\text{C}$ .

### 3.4.3 Cleaning and Storage of Ni<sup>2+</sup> Resin Column

Ni<sup>2+</sup> Sepharose high performance resin can be reused 7–9 times without regeneration.

After the last elution step, wash the column sequentially with 5 CV of Wash buffer T containing 500 mM imidazole; 5 CV of distilled water;

5 CV of 20% ethanol containing 0.05% sodium azide. Cap the top and bottom of column and store it in the cold room.

### 3.5 FPLC Ion Exchange Chromatography

If Dmc1 is still not pure enough after the  $\text{Ni}^{2+}$  resin step, proceed to Mono Q anion exchange column for additional purification at 4°C.

#### 3.5.1 Buffers and Reagents

- Buffer A1 = 1 × buffer T
- Buffer B1 = 1 × buffer T + 1 M KCl

#### 3.5.2 Procedure

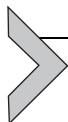
1. Exchange about 20 mg Dmc1 eluted from the  $\text{Ni}^{2+}$  column into (buffer A1 + 200 mM KCl) using PD-10 column which also removes the imidazole.
2. Equilibrate a Mono Q column with 5–10 CV of (buffer A1 + 200 mM KCl).
3. Load the sample onto Mono Q.
4. Using FPLC software, set automated program as follows: Wash the column with 10 CV (buffer A1 + 200 mM KCl). Elute Dmc1 with a 30 mL linear gradient of 200–800 mM KCl or 20%–80% buffer B1 at 0.8–1 mL/min, collect 1 mL fractions.
5. Analyze proteins in peak fractions on a 12% SDS-PAGE gel. The prominent peak should contain intact Dmc1 which is eluted at ~350 mM KCl. Pool fractions containing Dmc1, exchange into storage buffer by the PD10 column, keep Dmc1 concentration below 4–5 mg/mL, and store aliquots at –80°C.

### 3.6 Notes

The overall yield of near-homogenous Dmc1 is around 7 mg/L culture. Dmc1 is a stable protein that sustains full D-loop activity for 3–5 freeze/thaw cycles when stored at concentrations higher than 30  $\mu\text{M}$  at –80°C. Nonetheless, the purified protein should be stored in aliquots and minimize the number of freeze/thaw cycles.

The concentration of Dmc1 may be determined spectrophotometrically using a molar extinction coefficient of 11,520  $\text{M}^{-1} \text{cm}^{-1}$  at 280 nm; molecular weight of (His)<sub>6</sub>-tagged Dmc1 is 37.4 kDa; use the ratio of molecular weight to molar extinction coefficient to convert Dmc1  $A_{280}$  to concentration in mg/mL. For Dmc1, 1  $A_{280} = 3.25 \text{ mg/mL}$ .

Budding yeast Rdh54/Tid1 can be overexpressed from pET21a-Tid1 (Chi et al., 2006); the protein is (His)<sub>6</sub>-tagged at the C-terminal and purified by the two-column method described here with modification of the FPLC step. After the first step of Ni<sup>2+</sup> resin, the partially purified Rdh54/Tid1 should be further purified by FPLC on Mono S column instead of Mono Q because Rdh54/Tid1 is a basic protein. The protocol for Mono S will be the same as for Mono Q described earlier except a different buffer is required. Buffer A2 = 25 mM potassium phosphate buffer, pH 7.5 + 1 mM DTT + 10% glycerol; buffer B2 = buffer A2 + 1 M KCl. Rdh54/Tid1 is eluted at ~360 mM KCl. Full-length Rdh54/Tid1 is relatively stable in our hands and also could sustain about three cycles of freeze/thaw without compromising its activity. The yield of intact Rdh54/Tid1 (Fig. 2B) was 1.3 mg from 6 L culture (~12 g cells). As mentioned previously, Rdh54/Tid1 is prone to proteolysis and has a tendency to be truncated into smaller size proteins. A 75 kDa protein fragment that is missing its N-terminal is often recovered in substantial quantity after the Ni + affinity step. This fragment is separated from the full-length protein by the Mono S column (Fig. 2B).



#### 4. D-LOOP ASSAY USING FLUORESCENT DYE-TAGGED ssDNA

The D-loop assay is one of the most common biochemical assays for characterizing the activity of RecA-type of recombinases. Perhaps the most commonly used version of the D-loop assay uses radioactively labeled (<sup>32</sup>P) ssDNA oligos. Here, we introduce a method that replaces the <sup>32</sup>P-ssDNA substrate with a fluorescent dye Quasar670-labeled ssDNA. Fluorescent dye Quasar670 (LGC BioSearch Technologies) is a Cy5 (Cyanine 5) analog that renders bright signal suitable for detection using the 633 or 647 nm laser lines.

We have compared the feasibility of Quasar670-ssDNA (alias Cy5-ssDNA) to <sup>32</sup>P-ssDNA in D-loop assays (Fig. 1). In this assay, equal amounts of Cy5-ssDNA and <sup>32</sup>P-ssDNA were mixed and used as substrate for Dmc1. The assay results showed that Cy5-ssDNA assay is comparable in sensitivity to the <sup>32</sup>P-ssDNA assay. D-loop band signals remain linear when reaction products were diluted by half, 5-fold, and 10-fold (Fig. 1C). The D-loop activity (the D-loop yield expressed as a percentage of input plasmid DNA) is similar using either <sup>32</sup>P-ssDNA or Cy5-ssDNA (Fig. 1B and D). The advantages of Cy5-ssDNA over <sup>32</sup>P-ssDNA are (a) Cy5-ssDNA is

very stable when stored at  $-20^{\circ}\text{C}$  in contrast to  $^{32}\text{P}$ -ssDNA which rapidly loses radioactivity (half-life is 14.3 days); typically a preparation of  $^{32}\text{P}$ -labeled ssDNA is only suitable for use in the D-loop assay for 2 weeks. A 200 nmol synthesis of Quasar670-ssDNA is sufficient for  $\sim 75,000$  D-loop reactions (10  $\mu\text{L}$  reaction with Cy5-ssDNA at 30 nM). The cost of Cy5-ssDNA is about 100 times cheaper than  $^{32}\text{P}$ -ssDNA. (b) Comparing gel images, the Cy5 method yields bands that are sharper than those produced by  $^{32}\text{P}$ -ssDNA. (c) After electrophoresis, the agarose gel can be imaged directly for Cy5 fluorescence signal without any further gel manipulation. That is, there is no loss of D-loop assay product signal. When  $^{32}\text{P}$ -ssDNA is used, the agarose gel must be dried onto a positively charged membrane (to capture and retain small DNA oligos), the dried gel is then exposed to image plate for a period of time before imaging. Some loss of D-loop or ssDNA signal can occur during transfer of DNAs to the filter, reducing reproducibility. It should also be noted that positively charged membranes, such as from Roche Diagnostics, or DE81 from Whatman, are quite expensive ( $\$6$ – $10$  per membrane of 10 cm  $\times$  15 cm per gel) and add significantly to the cost of the  $^{32}\text{P}$  method. Overall the fluorescence version of the D-loop assay gives better resolution, is far more convenient, and is much less costly than the  $^{32}\text{P}$  method.

A typical D-loop assay that assesses the Dmc1 activity stimulated by its accessory factor Hop2-Mnd1 using Cy5-ssDNA will be described later.

#### 4.1 Buffers and Reagents

- D-loop assay reaction buffer: 25 mM Tris-HCl, pH 7.5; 1 mM dithiothreitol, 5 mM MgCl<sub>2</sub>, 3 mM ATP, 250 nM CaCl<sub>2</sub>, 100  $\mu\text{g}/\text{mL}$  BSA.
- Quasar670-ssDNA (or Cy5-ssDNA): 5' Quasar670-modified 90 mer ssDNA oligo, stored in 10 mM Tris-HCl, pH 7.5; final concentration in assay is 30 nM (i.e., 2.7  $\mu\text{M}$  nucleotides), ordered from LGC BioSearch Technologies. 90 mer ssDNA sequence:  
5'AAAAGGCCTCTAGGTTCCCTTTGTTACTTCTTCTGCCG  
CCTGCTTCAAACCGCTAACAATACCTGGGCCACCA  
CACCGTGTGCATTCGTA.
- Final concentrations of yeast proteins: Dmc1, 3  $\mu\text{M}$ ; Hop2-Mnd1, 0.5  $\mu\text{M}$ .
- Plasmid pRS306 with homologous sequence to Cy5-ssDNA: negatively supercoiled, purified by standard protocol using cesium chloride equilibrium gradient and without dsDNA denaturation with NaOH during cell lysis; final concentration of plasmid molecules is 5 nM in assay.

- Deproteinization solution: equal volume of 10% SDS and 10 mg/mL protease K.
- Gel, gel buffer, and electrophoresis buffer: 0.9% agarose gel (10 cm × 14.5 cm) in 1 × TAE (40 mM Tris–HCl, pH 7.5, 5 mM sodium acetate, 1 mM EDTA).
- Gel loading buffer: 25 mM Tris–HCl, pH 7.5; 50% glycerol, no dye.

## 4.2 Procedure

1. Mixture A: in an 8  $\mu$ L reaction volume, mix 2  $\mu$ L D-loop reaction buffer (5 × stock), 4  $\mu$ L double-distilled water, 1  $\mu$ L of Dmc1 (30  $\mu$ M stock), and 1  $\mu$ L of Cy5-ssDNA (300 nM stock). Incubate the mixture in a water bath at 37°C for 5 min.
2. Mixture B: mix 1  $\mu$ L Hop2-Mnd1 (5  $\mu$ M stock) with 1  $\mu$ L plasmid pRS306 (50 nM stock), incubate at room temperature for 3 min.
3. Add Mixture A to Mixture B; incubate at 37°C for 20 min to form D-loops.
4. Add 2  $\mu$ L of deproteinization solution, incubate at 37°C for 5 min.
5. Add 2  $\mu$ L gel loading buffer. Make sure there is no dye in the buffer because many dyes fluoresce and interfere with the Cy5 signal.
6. Load the mixture onto agarose gel and resolve the DNA species at room temperature by electrophoresis at 8 V/cm for 1 h 45 min.
7. Image the gel directly for Cy5 fluorescence signal using the 647–670 nm laser line at 570 PMT in a Typhoon 9200 Imager or the equivalent. At this PMT value, both the D-loop band and the unreacted ssDNA band are at the linear range, i.e., the signals are under saturation.

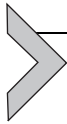
## ACKNOWLEDGMENT

This work was supported by the National Institutes of Health (grant GM050936 from NIGMS to D.K.B.).

## REFERENCES

- Binz, S. K., Dickson, A. M., Haring, S. J., & Wold, M. S. (2006). Functional assays for replication protein A (RPA). *Methods in Enzymology*, 409, 11–38.
- Brown, M. S., & Bishop, D. K. (2014). DNA strand exchange and RecA homologs in meiosis. *Cold Spring Harbor Perspectives in Biology*, 7, a016659.
- Busygina, V., Gaines, W. A., Xu, Y., Kwon, Y., Williams, G. J., Lin, S.-W., et al. (2013). Functional attributes of the *Saccharomyces cerevisiae* meiotic recombinase Dmc1. *DNA Repair*, 12, 707–712.
- Chan, Y.-L., Brown, M. S., Qin, D., Handa, N., & Bishop, D. K. (2014). The third exon of the budding yeast meiotic recombination gene HOP2 is required for calcium-dependent

- and recombinase Dmc1-specific stimulation of homologous strand assimilation. *Journal of Biological Chemistry*, 289, 18076–18086.
- Chi, P., Kwon, Y., Seong, C., Epshtein, A., Lam, I., Sung, P., et al. (2006). Yeast recombination factor Rdh54 functionally interacts with the Rad51 recombinase and catalyzes Rad51 removal from DNA. *Journal of Biological Chemistry*, 281, 26268–26279.
- Cloud, V., Chan, Y.-L., Grubb, J., Budke, B., & Bishop, D. K. (2012). Rad51 is an accessory factor for Dmc1-mediated joint molecule formation during meiosis. *Science*, 337, 1222–1225.
- Hong, E. L., Shinohara, A., & Bishop, D. K. (2001). *Saccharomyces cerevisiae* Dmc1 protein promotes renaturation of single-strand DNA (ssDNA) and assimilation of ssDNA into homologous super-coiled duplex DNA. *The Journal of Biological Chemistry*, 276, 41906–41912.
- Nimonkar, A. V., Amitani, I., Baskin, R. J., & Kowalczykowski, S. C. (2007). Single molecule imaging of Rdh54, a Rad54 homolog that translocates on duplex DNA and can disrupt joint molecules. *The Journal of Biological Chemistry*, 282, 30776–30784.
- Van Komen, S., Macris, M., Sehorn, M. G., & Sung, P. (2006). Purification and assays of *Saccharomyces cerevisiae* homologous recombination proteins. *Methods in Enzymology*, 408, 445–463.



# Probing Dynamic Assembly and Disassembly of Rad51 Tuned by Srs2 Using smFRET

Yupeng Qiu\*, Hye Ran Koh\*,<sup>†</sup>, Sua Myong\*,<sup>1</sup>

\*Johns Hopkins University, Baltimore, MD, United States

<sup>†</sup>Chung-Ang University, Seoul, South Korea

<sup>1</sup>Corresponding author: e-mail address: smyong1@jhu.edu

## Contents

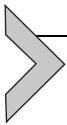
|   |     |
|---|-----|
| 1. Filament Formation by Rad51  | 322 |
| 1.1 Monitoring Rad51 Filament Formation by TIRFM: FRET Histogram, Time Trace, and TDP | 322 |
| 1.2 Determining Rad51-Binding Size for the Filament Formation                         | 326 |
| 1.3 The Directionality of Rad51 Filament Formation: 5'–3' vs 3'–5'                    | 326 |
| 2. ATP-Dependent Activity of Srs2 on DNA  | 328 |
| 2.1 The Repetitive Motion of Srs2 on ssDNA: Immobilized DNA vs Immobilized Protein    | 329 |
| 2.2 The Unwinding Activity of Srs2 on DNA   | 332 |
| 2.3 The DNA Tail Length Dependence: The Repetitive Motion vs the Unwinding Activity   | 335 |
| 3. The Srs2 Activity on the Rad51 Filament  | 339 |
| 3.1 The Antirecombinase Activity of Srs2 on Rad51 vs RecA Filament                    | 339 |
| 3.2 The Unwinding Activity of Srs2 on the Rad51 Filament                              | 342 |
| 4. Conclusions  | 343 |
| References  | 343 |

## Abstract

The integrity of DNA is critical for sustaining the life of any living organism, as DNA is a reservoir of its genetic information. However, DNA is continuously damaged by either normal metabolic pathways or environmental insults such as ultraviolet exposure or chemicals. Double-stranded DNA break is one of the most common types of DNA damage that requires activation of homologous recombination (HR) pathway mediated by Rad51 in eukaryotes (Paques & Haber, 1999; Symington, 2002). Rad51 protein forms a helical nucleoprotein filament on resected DNA to initiate homology search but also can interact with other single-stranded DNA (ssDNA)-binding proteins including Srs2. Srs2, a well-known antirecombinase in HR, is an ATP-dependent 3'–5' DNA helicase in the budding yeast *Saccharomyces cerevisiae* as well as an ssDNA translocase. It

disrupts Rad51 filaments, preventing HR (Krejci et al., 2003; Le Breton et al., 2008; Veaute et al., 2003).

In the following text, we provide detailed experimental platforms employed to investigate the activity of Rad51 and Srs2 using single-molecule Forster resonance energy transfer and protein-induced fluorescence enhancement. First, we demonstrate how to detect Rad51 filament formation to address the binding site size binding kinetic of the Rad51, as well as the directionality of the filament formation. Next, we explain how to visualize ATP-dependent translocation and unwinding activities of Srs2 on DNA. Lastly, we demonstrate the filament forming activity by Rad51 which is counteracted by the filament removal activity of Srs2.



## 1. FILAMENT FORMATION BY Rad51

The first step in studying DNA repair by homologous recombination (HR) via Rad51 in eukaryotes (Paques & Haber, 1999; Symington, 2002) is to form a stable Rad51 filament on a double-stranded DNA break (DSB) DNA mimic. The formation of a stable Rad51 filament requires single-stranded DNA (ssDNA) long enough for the formation of a nucleation cluster. Here, we show the steps in obtaining that threshold ssDNA length.

### 1.1 Monitoring Rad51 Filament Formation by TIRFM: FRET Histogram, Time Trace, and TDP

To capture the process of filament formation using single-molecule Forster resonance energy transfer (smFRET), we prepared doubly labeled partial duplex DNA (pdTDNA) molecules and immobilized them to a PEG-coated quartz surface via biotin–neutravidin interaction (Fig. 1A). The partial duplex was prepared with two fluorophores, an FRET pair of a donor and an acceptor, at the two ends of ssDNA where protein filament is expected to form as shown in Fig. 1A. In our experiments, we used the Cy3–Cy5 FRET pair. The dyes and biotin-labeled oligonucleotides were purchased from Integrated DNA Technologies (Coralville, IA, USA). For internally labeled oligos, they were ordered with an amino modifier dT and subsequently labeled using Cy3 monofunctional NHS esters (GE Healthcare, Princeton, NJ, USA). The donor dye is excited with a 532-nm solid-state laser (75 mW, Coherent CUBE) and emitted signals are captured by an EMCCD camera (iXon DU-897ECS0-#BV; Andor Technology) using a custom C++ program. The data are processed by IDL software and analyzed using homemade Matlab codes. All homemade

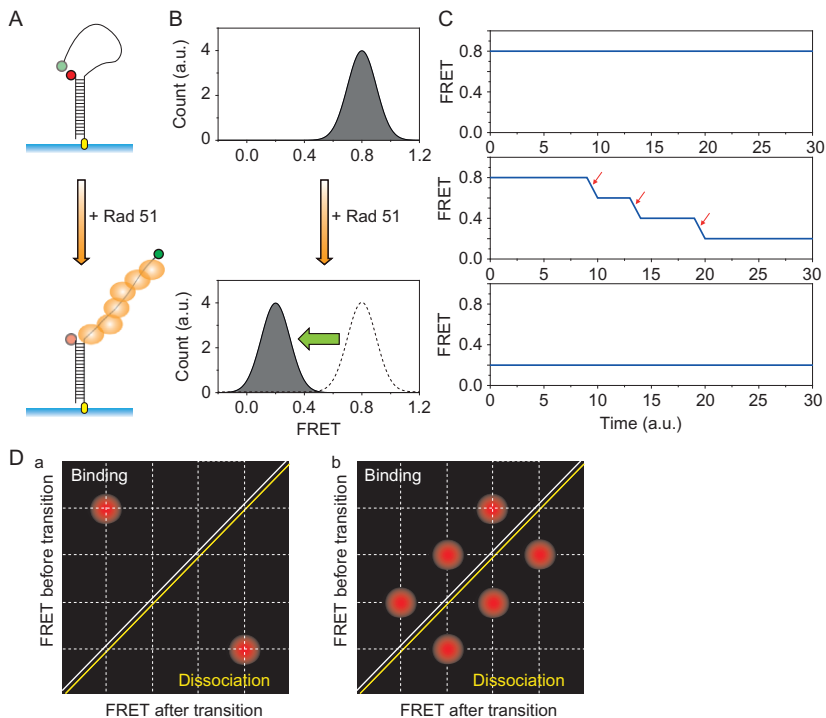


**Fig. 1** How to monitor the filament formation using smFRET assay. (A) The labeling orientation in a partial duplex DNA to study filament formation using smFRET. (B) Typical FRET histogram showing the filament formation with the transition from high FRET efficiency to low FRET efficiency. (C) FRET time trace shows the filament forming process in real time as a stepwise FRET decrease as shown in the *middle panel*. (D) Typical transition density plot to show the stepwise FRET decrease caused by filament formation: (a) monomer binding (b) three Rad51 binding.

codes can be found in the smFRET package available at the Center for the Physics of Living Cells (<https://cplc.illinois.edu/software/>, Biophysics Department, University of Illinois at Urbana–Champaign). Before the filament formation, we expect high FRET efficiency due to the proximity between the donor and an acceptor resulting from highly flexible ssDNA (Murphy, Rasnik, Cheng, Lohman, & Ha, 2004). As the Rad51 filament forms along ssDNA, the distance between the two dyes increases, generating low FRET. Therefore, the transition from high FRET efficiency to low FRET efficiency is a clear proxy for filament formation (Fig. 1A). This FRET change can be analyzed in three ways: FRET histogram, time traces, and transition density plot (TDP), which we will explain one by one here.

### 1.1.1 FRET histogram

FRET histogram is generated before and after Rad51 addition to show the filament formation of Rad51 on the ssDNA in the following way:

- (1) Incubate NeutrAvidin (0.05 mg/mL) to a PEG-coated surface (Roy, Hohng, & Ha, 2008) for 5 min
- (2) Rinse with T50 buffer (Tris 10 mM (pH 7.5), NaCl 50 mM) and add 50–100 pM\* of the partial duplex DNA to the surface, wait for 5 min. (\*This low concentration is critical to achieve the single-molecule density. Each field of view of  $25 \times 75 \mu\text{m}^2$  yields approximately 300–400 single-molecule fluorescence spots.)
- (3) Rinse with T50 and add an imaging buffer (50 mM Tris-HCl (pH 7.5), 50 mM NaCl, 10 mM  $\text{MgCl}_2$ , 1 mM ATP with an oxygen-scavenging system containing 0.8% v/v dextrose, 1 mg/mL glucose oxidase, 0.03 mg/mL catalase, and 1% v/v 2-mercaptoethanol (Roy et al., 2008)).
- (4) Record 15–20 short movies (20–50 frames per movie at 100 ms/frame) in different areas of the imaging field. This ensures collecting FRET values from 5000 to 6000 molecules spread out through the imaging surface. Short movies are recommended to prevent photo-bleaching of fluorophores.
- (5) The average FRET efficiencies are obtained from the initial 10–20 frames in these short movies, and the FRET histogram is built using homemade Matlab code. The histogram is binned into 80 equally spaced containers. This is the reference histogram before the filament formation.
- (6) Add 1  $\mu\text{M}$  of Rad51 in its reaction buffer and incubate the mixture for 5–10 min to allow for filament formation.
- (7) As before, record 15–20 short movies (20–50 frames per movie at 100 ms/frame).
- (8) Do the step (5) for the movies taken in step (7) and compare the FRET histograms.
- (9) If the FRET peak obtained at step (8) did not shift significantly from the reference FRET histogram obtained at step (5), increase the concentration of Rad51 and repeat steps (6)–(8).
- (10) At approximately 1  $\mu\text{M}$  Rad51 concentration, we expect to observe a clear transition from high FRET to low FRET peak shift as shown in Fig. 1B.
- (11) By performing the filament formation in varying length of ssDNA from 10 to 20 nts, the length of DNA required for stable filament nucleation can be determined. For Rad51, a minimum of

18 nucleotide was required for stable filament formation, deduced from a complete shift in FRET peak.

### 1.1.2 FRET time trace

After we confirm the filament formation by FRET histogram, we obtain FRET time traces from the individual molecules to track the filament formation in real-time. This provides the kinetics of filament formation as well as the maximum detectable steps of Rad51 binding. This information can aid in the determination of the binding site size of each Rad51 monomer on ssDNA in [Section 1.2](#). Here is the procedure to obtain FRET time traces for measuring filament formation by Rad51.

- (1) In order to capture the real-time binding kinetic, Rad51 needs to be added after the data acquisition begins, i.e., after the movie recording is started.
- (2) Take two–three long movies (1800 frames per movie at 100 ms/frame) for the sample prepared at step (3) above, which should show step-wise FRET decrease as shown in the middle panel of [Fig. 1C](#), reporting on the successive binding of Rad51 monomers to ssDNA. FRET trajectories are extracted by IDL software and analyzed by homemade Matlab codes as previously described. The time trace is displayed as Cy3 and Cy5 signals over time, and FRET is calculated using the equation 
$$\text{FRET} = \frac{\text{Cy5}}{\text{Cy3} + \text{Cy5}}.$$
- (3) Confirm that you can observe a steady FRET efficiency over the time course as shown in the upper panel of [Fig. 1C](#).
- (4) Take one–two additional long movies to check if there is any additional decrease of FRET.
- (5) If you observe any additional FRET changes in step (4), repeat step (3) at the longer exposure time and lower excitation power to capture the whole FRET changes upon the addition of Rad51 in one movie. The duration of movies can be selected to suite the kinetic parameters expected for the particular reaction. For this case, 2–3 min was sufficient to observe majority of DNA molecules to transition to low FRET state.

### 1.1.3 Transition density plot

We obtain about 400 FRET time traces per movie, which renders thousands of FRET transitions, which can be combined to build TDP. TDP is a 2D cluster map used to represent many FRET transition events as a density plot as shown in [Fig. 1D](#). Each population (red circle in [Fig. 1D](#)) reflects one FRET transition composed of FRET value before transition on  $\gamma$ -axis

and FRET value after transition on  $x$ -axis. The colormap of the circle should be a heatmap that reflects the density of the FRET values. In case of Rad51 filament formation, FRET changes from high-to-low, resulting in a position in the upper diagonal area, while filament dissociation will be at the lower diagonal area. Fig. 1Da shows the example of traces with only one type of reversible FRET transition, and Fig. 1Db shows the TDP expected for FRET time traces with the stepwise three step FRET transition as shown in Fig. 1C (middle). In order to extract the information of FRET transition from FRET time traces, we do HaMMY (McKinney, Joo, & Ha, 2006), which is an automated algorithm used to analyze the number of FRET states in the time traces without any predefined FRET states. The distribution of TDP spots indicates the stability of each bound state, i.e., stably bound state will have a higher density in the upper diagonal section than in the corresponding lower diagonal space.

## 1.2 Determining Rad51-Binding Size for the Filament Formation

One of the fundamental questions inherent to the filament forming process is the binding size or occupancy of a monomeric protein. The binding size of Rad51 monomer on the ssDNA during filament formation can be determined by applying the protein on varying lengths of ssDNA FRET construct. We prepared doubly labeled partial duplexes as shown in Fig. 1A with 10–20 nucleotide long ssDNA. For the proteins that do not have a sequence specificity for binding, poly deoxythymidine (poly T) sequence is ideal because it does not form any secondary structure by itself. We added Rad51 to T10, 13, 15, 18, and 20 and obtained time traces (Fig. 2A) with which TDP for each substrate was generated. In TDP (Fig. 2B), we find several transition populations along the diagonal line of TDP, which implies the sequential FRET change during the filament formation by Rad51. The maximum number of transitions in the upper diagonal area of TDP is interpreted as number of monomers contributing to filament formation. We observed three for T10, four for T13, and five clusters for T15, suggesting that monomeric Rad51 binds to three nucleotides (Qiu et al., 2013).

## 1.3 The Directionality of Rad51 Filament Formation: 5'–3' vs 3'–5'

In addition to the binding size, the directionality involved in the filament formation is another inherent property of Rad51, especially in light of its native substrate, the resected DNA which possesses 3'-tailed ssDNA end.

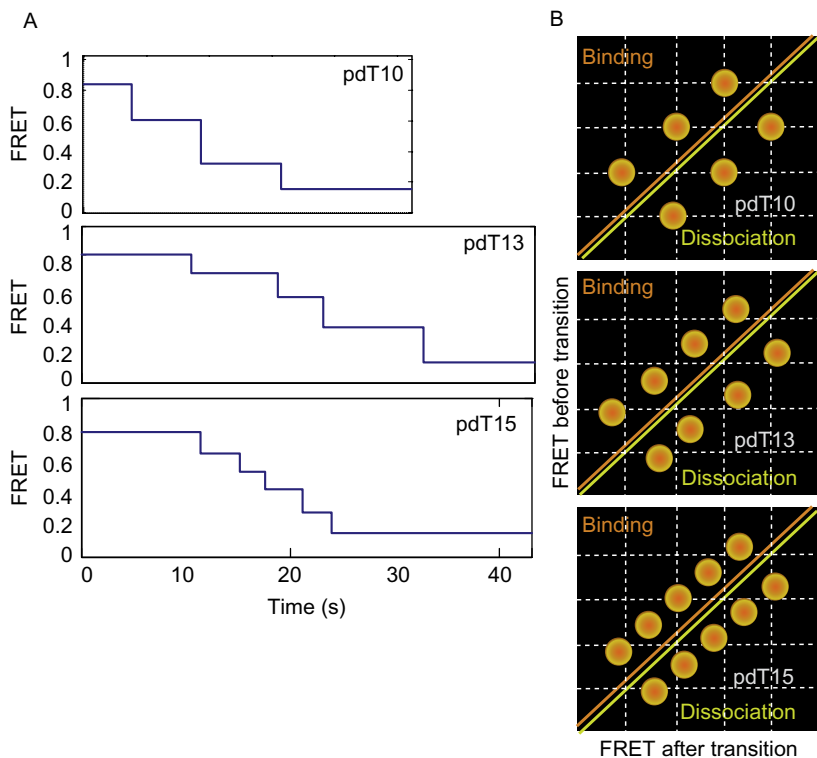


**Fig. 2** Rad51 filament formation steps for DNA of various tail lengths. (A) Example FRET time traces showing stepwise decrease as each Rad51 protein binds onto DNA. (B) Example TDP plots showing FRET transition populations that correspond to the sequential binding of Rad51 monomers on ssDNA.

While smFRET assay enables visualizing steps involved in filament formation by Rad51 seen as sequential FRET decrease, the directionality of the filament formation is not revealed because both 3′–5′ and 5′–3′ filament formations are expected to yield the same result. We took advantage of an alternate single-molecule approach, termed protein-induced fluorescence enhancement (PIFE), in which the intensity of fluorophore increases when protein binds in its vicinity (Antony et al., 2009; Fischer & Lohman, 2004; Hwang, Kim, & Myong, 2011; Myong et al., 2009). In order to distinguish the directionality between 5′–3′ and 3′–5′, we prepared two DNA substrates with different Cy3 position as shown in Fig. 3, one with Cy3 dye near to the duplex-ssDNA junction (substrate A) and the other with Cy3 near the 3′ free end of ssDNA (substrate B). Using the same TIRF microscope, we can conduct single-molecule assay, only collecting fluorescence from the Cy3

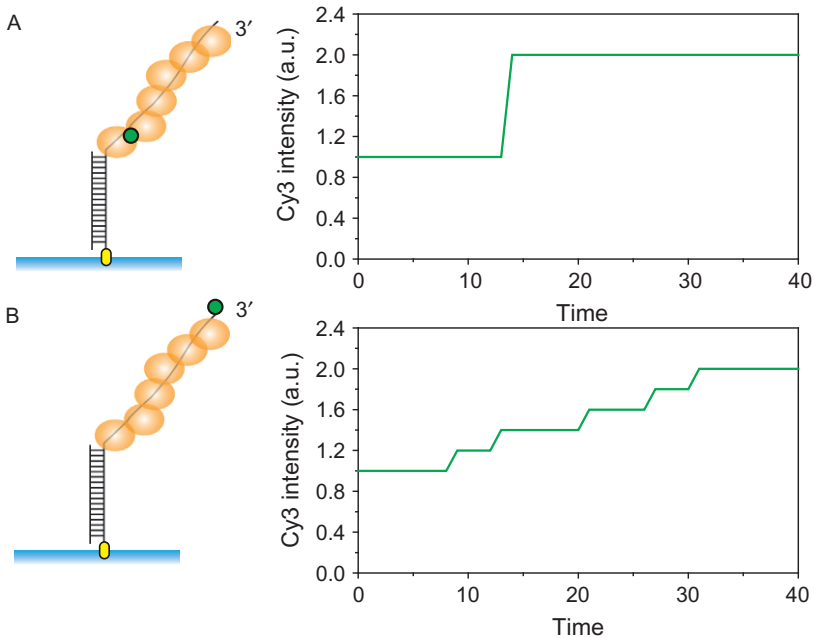
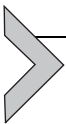


**Fig. 3** PIFE assay for testing the directionality of filament formation. The expected Cy3 intensity time trace in the case of 5′–3′ filament formation on the DNA substrate labeled with Cy3 (A) near to the 5′ duplex-ssDNA junction and (B) at 3′ end.

channel. If Rad51 nucleoprotein filament forms in the 5′–3′ direction, we expect the Cy3 intensity of substrate A to jump initially with no subsequent changes and Cy3 intensity of substrate B to show stepwise increase to high intensity value. Likewise, the 3′–5′ filament formation is expected to yield the opposite trend. We observed result in agreement with the former prediction, i.e., single intensity jump of Cy3 for substrate A, and stepwise intensity increase of Cy3 for substrate B, suggesting the 5′–3′ directionality for Rad51 filament formation.



## 2. ATP-DEPENDENT ACTIVITY OF Srs2 ON DNA

In addition to its role as the antirecombinase for opposing Rad51 formation during HR (Krejci et al., 2003; Le Breton et al., 2008; Veaute et al., 2003), Srs2 is a helicase belonging to the super family (SF)1 (Krejci et al., 2004). In this section, we present the experimental procedures to investigate the behavior of Srs2 on partial duplex DNA (Qiu et al., 2013), which

includes translocation along ssDNA as well as duplex DNA unwinding activity. For [Sections 2 and 3](#), we used a well-characterized C-terminal deletion mutant, Srs2<sup>CΔ276</sup>, in all experiments unless stated otherwise. This truncated mutant exhibits ATP-driven translocation and antirecombinase activity similar to that of the wild-type protein ([Antony et al., 2009](#); [Lytle et al., 2014](#)) and we refer to it as Srs2 from here on.

## 2.1 The Repetitive Motion of Srs2 on ssDNA: Immobilized DNA vs Immobilized Protein

The translocation activity of Srs2 is thought to contribute to its antirecombinase function ([Antony et al., 2009](#)). To probe the translocation activity of Srs2 on immobilized DNA, we used the identical partial duplex DNA construct used in Rad51 assay above, i.e., consisting of 18 base pairs of dsDNA and a 3'-ssDNA tail consisting of 20 deoxythymidine ([Fig. 4A](#)). As before, the FRET value for DNA only is steady mid-FRET level. The addition of Srs2 (5 nM) and ATP (1 mM) induced FRET shift to lower level, consistent with the expected occupancy of Srs2 on ssDNA. In addition, the single-molecule time trace displayed repetitive FRET fluctuation, suggesting dynamic conformational fluctuation of ssDNA induced by Srs2. We performed the reciprocal assay in which Srs2 protein was surface immobilized and FRET DNA (nonbiotinylated) added, which confirmed that the FRET fluctuation observed above represents activity of a single Srs2 monomer.

### 2.1.1 FRET Histogram

- (1) The DNA construct is tethered to the imaging surface and FRET value are taken using the method in [Section 1](#), steps (1)–(5) for the formation of the reference FRET histogram ([Fig. 4B](#), dark gray histogram).
- (2) Add 5 nM of Srs2 to the imaging buffer listed in [Section 1](#), and add the mixture to the imaging surface. Image immediately after and make another FRET histogram based on 15–20 images.
- (3) Compare the postreaction FRET histogram with the reference histogram ([Fig. 4B](#), light gray histogram). The two FRET peaks tell us that the ssDNA tail now exists in two conformations.
- (4) If there is no difference from the reference FRET histogram, check if the proteins are still active via an ATPase assay or a bulk unwinding assay and increase protein concentration.

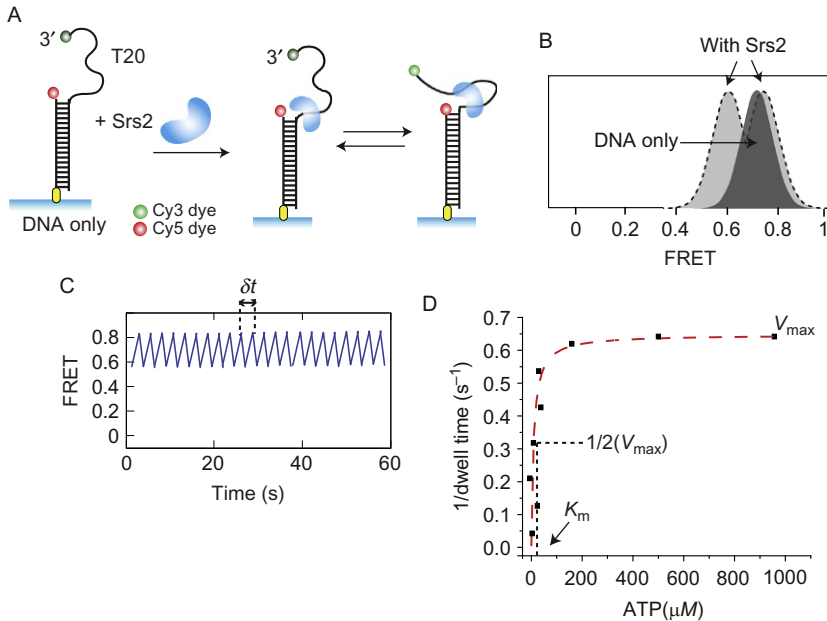


**Fig. 4** How to monitor Srs2 translocation activity on immobilized DNA using smFRET. (A) Experimental schematics of FRET DNA used to monitor Srs2 translocation. (B) Example FRET histogram showing DNA only FRET peak and peak shifts after binding and activity of Srs2. (C) Example FRET trace showing FRET fluctuations resulting from Srs2 translocation on DNA. (D) Example Michaelis–Menten curve constructed using rates calculated from ATP concentrations varying from 1  $\mu\text{M}$  to 1 mM.

### 2.1.2 FRET time traces

After confirming Srs2 interacting with the ssDNA, we can examine the FRET time traces to analyze the frequency and amplitude of the FRET fluctuations.

- (1) After adding the Srs2 reaction mixture to the DNA sample as previously mentioned, take several long movies, each lasting 2–3 min (exposure time of 100 ms). After each movie, move to a new area to continue recording. Check the overall average intensity decay of each movie over time to make sure that the recorded fluorophores did not photobleach too quickly.
- (2) The time traces should exhibit a periodic, rapid FRET fluctuations between mid and low FRET value (Fig. 4C). Such FRET fluctuation continues as long as 15 min.
- (3) The number of time traces generated from each movie should be similar, given that the slide surface was evenly coated by the same density of

DNA. If molecules disappear over time, it is likely due to high Srs2 concentration that induce DNA unwinding.

- (4) ATP concentration can be reduced to slow down Srs2 activity on DNA.
- (5) Subsequently, obtain the rate ( $V$ ) of Srs2 translocation at each ATP concentration by measuring the peak-to-peak dwell time ( $\delta t$ ) between each of the fluctuation peaks (Fig. 4C). Using the Michaelis–Menten equation  $v = \frac{V_{max}[ATP]}{K_m + [ATP]}$ ,  $K_m$ , the amount of ATP required for the reaction to reach half of maximum velocity can be obtained (Fig. 4D).

### 2.1.3 Tethered monomer Srs2

To check if the FRET fluctuation arises from a monomeric Srs2 protein, we can tether individual Srs2 to the imaging surface. In this case, Srs2 has  $9 \times$  histidine tags, which can be tethered with a NeutrAvidin–biotin–tris-NTA linkage (Lata, Gavutis, Tampe, & Piehler, 2006). Alternate approaches include flag tag to anti-flag and hexahistidine tag to antiHis antibody pairing (Qiu et al., 2017). Nonbiotinylated partial duplex FRET DNA is added to the surface tethered Srs2 to test the monomer protein activity (Fig. 5A). Since the protein is not labeled, the only time we should see FRET signal

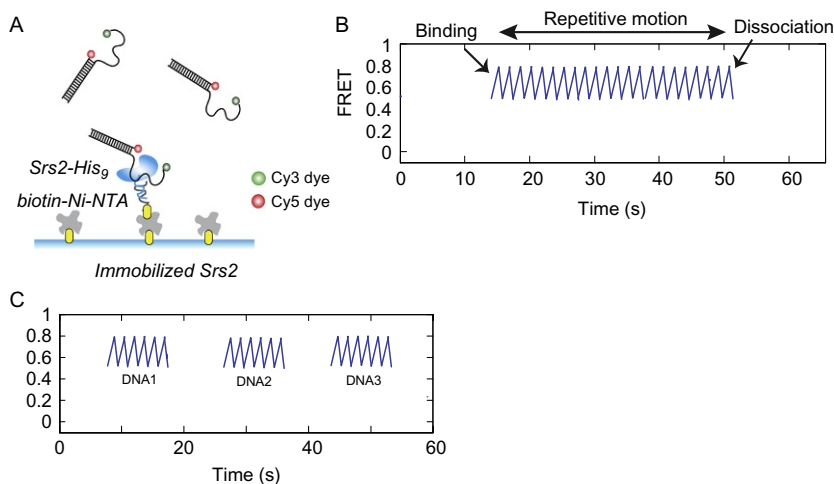


**Fig. 5** How to perform the immobilized protein experiment for Srs2 translocation. (A) Experimental schematic showing Srs2 tethered to the surface and acting on nonbiotinylated FRET DNA. (B) Example FRET trace showing FRET fluctuation of Srs2 on DNA. (C) Example FRET trace showing multiple DNA binding to the same Srs2 consecutively. Resulting in multiple FRET fluctuation segments.

in the time trace is when the FRET DNA is bound to Srs2 (Fig. 5B). Here is the procedure for the tethered protein experiment.

- (1) Add NeutrAvidin to the PEG surface as before.
- (2) Mix biotin-tris-NTA (20 nM) with NiCl<sub>2</sub> (50 nM) in T50 buffer and incubate on ice for 15 min.
- (3) Add biotin-Ni-NTA mixture to the slide surface and incubate for 10 min at room temperature.
- (4) Add 0.5–1 nM Srs2 (in T50 buffer) to the slide surface and incubate for another 5 min at room temperature.
- (5) Add nonbiotinylated DNA substrates in imaging buffer to initiate the reaction.
- (6) Take two–three long movies for the time trace analysis.
- (7) Compare the time traces with the previously obtained time traces of Srs2 translocating on immobilized DNA, does the FRET fluctuations look similar? Does it fluctuate in the same FRET range?
- (8) You may also observe bursts of such FRET fluctuation within a single long movie (Fig. 5C). This is an indication that Srs2 does not stay bound on the ssDNA, but rather only remains for a limited time before dissociating (Qiu et al., 2013).

## 2.2 The Unwinding Activity of Srs2 on DNA

Since Srs2 is a helicase protein, it is capable of unwinding double-stranded DNA (dsDNA) with a 3'-ssDNA tail (>12 nucleotides) if used in a high enough concentration (Krejci et al., 2004). For our protein prep (Qiu et al., 2013), Srs2 with a threshold concentration of 20 nM or more will unwind partial duplex DNA in our experiments.

### 2.2.1 Srs2 unwinds dsDNA

We use a partial duplex DNA construct with fluorescent dye locations such that both dyes are located at the junction of the substrate (Fig. 6A). For the dye at the 5' end of the 18mer strand, it can be ordered directly from IDTDNA with the dye attached. For the dye at the junction on the complementary strand consisting of poly-dT and 18mer, since it is internally labeled, the dye should not be placed on the sugar-phosphate backbone as that can interfere with protein binding/translocation.

- (1) Immobilize the DNA substrate to the PEG surface as described previously. Check that you have at least 400 fluorescent spots in each imaging plane.

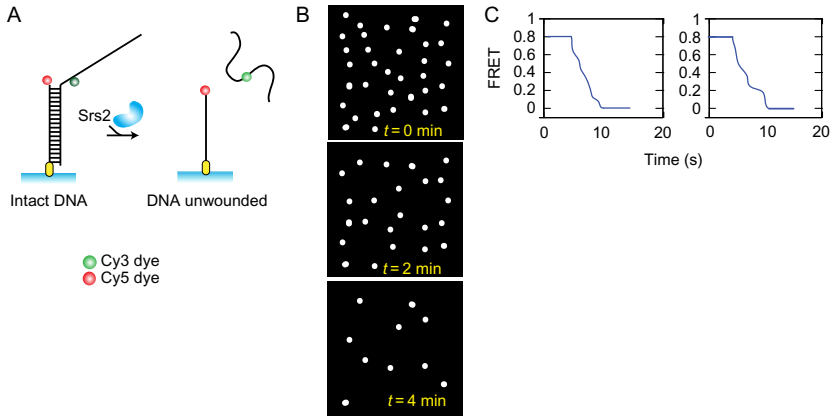


**Fig. 6** How to monitor Srs2 unwinding of naked DNA. (A) Experimental schematic of DNA construct used to monitor Srs2 unwinding. Note that unwinding results in the release of the Cy3 strand. (B) Fluorescent Cy3 spots disappear over time as observed in the experimental channel. (C) Example FRET traces showing the unwinding of DNA going from high FRET to low FRET.

- (2) Begin taking a long movie (2–3 min).
- (3) While the movie is recording, flow in 20 nM of Srs2 to the imaging buffer and add the mixture to the DNA substrates. Be careful not to jostle the imaging plane or introduce bubbles to the reaction chamber.
- (4) Active unwinding is expected to result in rapid disappearance of fluorescence spots over time (Fig. 6B), which do not recover even after you switch to a new imaging area. This is not caused by photobleaching, but rather by the release of the nonbiotinylated DNA strand with Cy3 due to Srs2 unwinding (Fig. 6A). FRET signal is lost after the nonbiotinylated DNA strand departs.
- (5) Continue to take two–three long movies afterward, or until most of the fluorescence spots have disappeared. This will allow you to capture the maximum number of unwinding time traces.
- (6) Examine the time traces, you should see very brief, stepwise FRET transitions from high to low FRET (Fig. 6C). Also note that this transition takes <10s and FRET signal does not recover, confirming Srs2 unwinding.
- (7) If you did not see visual evidence of unwinding, increase Srs2 concentration and make sure the DNA substrate that you are using has a 3'-ssDNA tail that is at least 12 nucleotides long.

### 2.2.2 Srs2 resolves Trinucleotide repeat structure

A less known function of Srs2 is its ability to resolve trinucleotide repeat (TNR) hairpins during DNA replication. These TNR hairpins arise from expanded regions of particular triplet repeat sequences (Mirkin, 2007) that can form secondary DNA hairpin structure (Cleary, Nichol, Wang, & Pearson, 2002) and are linked to many neurodegenerative diseases (Freudenreich, Stavenhagen, & Zakian, 1997; Gatchel & Zoghbi, 2005; Mirkin, 2006; Mirkin & Mirkin, 2014). Srs2 was found through a series of genetic screening to be a potential inhibitor of TNR hairpins (Anand et al., 2012; Bhattacharyya & Lahue, 2004; Dhar & Lahue, 2008; Kerrest et al., 2009). In our study, we found that Srs2 is able to specifically unfold the TNR hairpins repetitively (Qiu, Niu, Vukovic, Sung, & Myong, 2015). For this experiment, a special substrate is designed such that it has a hairpin consisting of a number of repeats of CNG (where  $N$  can be any of the four nucleotides) in the dsDNA region and a 3' ssDNA tail long enough for Srs2 loading (Fig. 7A). The fluorescent dye pair is located at the “opening” of the hairpin to monitor Srs2’s hairpin unfolding activity. The experimental procedure is as follows:

- (1) The DNA should be annealed in a magnesium buffer (10 mM MgCl<sub>2</sub>, 10 mM Tris-HCl (pH 8.0)) to facilitate the formation of the hairpin structure. Biotinylated and nonbiotinylated oligonucleotides in a 1:2 M ratio in the magnesium buffer to achieve a final concentration of 10 μM. The mixture is then incubated at 95°C for 2 min followed by slow cooling to room temperature to complete the annealing reaction in just under 2<sup>o</sup>h. The annealed DNA should be diluted to 10 nM and stored at -20°C for use in single-molecule imaging.

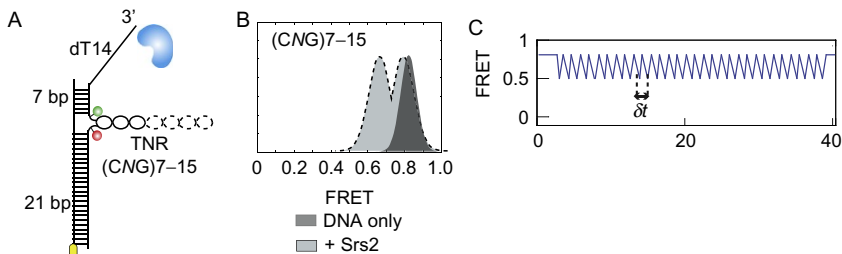


**Fig. 7** Testing Srs2 on TNR hairpins structures. (A) Schematic of DNA used, the hairpin repeat can have different sequences as well as different number of repeats. (B) Example FRET histogram of Srs2 opening up the hairpin. (C) Example FRET trace showing the FRET fluctuations resulting from repetitively opening of the hairpin by Srs2.

- (2) Immobilize the DNA substrate on the PEG slide as previously described.
- (3) Using the TNR imaging buffer (40 mM Tris-HCl (pH 7.5), 50 mM KCl, 2 mM MgCl<sub>2</sub>, 1 mM ATP with an oxygen-scavenging system containing 0.8% v/v dextrose, 1 mg/mL glucose oxidase, 0.03 mg/mL catalase, and 1% v/v 2-mercaptoethanol (Roy et al., 2008)), take 10–20 short movies (~2s each) and assemble the FRET histogram. The properly annealed DNA should exhibit a high FRET peak (Fig. 7B, dark gray histogram), confirming the presence of the hairpin.
- (4) Add 10 nM of Srs2 with the TNR imaging buffer to the tethered hairpin DNA, take two–three long movies and then 10–20 short movies to obtain FRET histogram (Fig. 7B, light gray histogram) and FRET traces (Fig. 7C).
- (5) Collect the dip-to-dip dwell time ( $\delta t$ ) as shown (Fig. 7C) for all four nucleotide variations of CNG while keeping the number of repeats at 11. You will find that as the dwell time is increase in the order of C=A<T<G. By changing the middle nucleotide sequence, the strength of the hairpin seemed to have changed such that the stronger the hairpin, the more difficult it is for Srs2 to open it.
- (6) Measure the total duration of the FRET fluctuations, you will find that the total duration of FRET fluctuations is similar among all four nucleotide sequences, suggesting that Srs2 will work on the hairpin for the same amount of time regardless of the TNR sequence.
- (7) Next, keep the TNR sequence as CAG, but vary the number of repeats in the hairpin from 7 to 15 repeats. Perform the same experiment.
- (8) Repeat step (5) for the hairpin structures in (7). Notice that now  $\delta t$  increases as the number of repeats lengthens, suggesting that TNR hairpin is stronger for longer repeats.
- (9) Repeat step (6) for the hairpin structures in (7). Notice that the total duration of FRET fluctuations is not affected by the change in the number of TNR repeats.

## 2.3 The DNA Tail Length Dependence: The Repetitive Motion vs the Unwinding Activity

### 2.3.1 Srs2 displays repetitive motion on ssDNA at ss-ds junction

The concentration of the Srs2 protein determines whether or not the dsDNA will be unwound by the helicase. When the protein concentration is below the unwinding threshold (<20 nM), Srs2 will simply translocate on the ssDNA near the junction (Qiu et al., 2013). We can study the

mechanism responsible for this repetitive translocation by testing Srs2 on varying length of ssDNA tail:

- (1) Repeat the procedure from [Section 2.1](#) for immobilized DNA, but replace the DNA construct used with other tail lengths ([Fig. 8A](#)).
- (2) Compare the FRET histograms made from Srs2 on each tail lengths. The two-peak FRET histogram moves toward lower FRET and eventually disappear as ssDNA tail lengthens ([Fig. 8B](#)), suggesting that as Srs2 translocate near the junction, thus the FRET signal subsides on longer DNA strands.
- (3) Observe the individual FRET traces obtained for each length and measure the peak-to-peak dwell time as before. The dwell time does not increase past a length of 20 nucleotides on the ssDNA tail ([Fig. 8](#)), suggesting length-independent translocation mechanism, i.e., localized to near junction ([Qiu et al., 2013](#)).
- (4) To investigate the mechanism further, we prepared three DNA tail lengths: T30, 40, and 50, with fixed Cy3 dye positions ([Fig. 8D](#)).
- (5) The obtained data, i.e., all three exhibiting very similar FRET histograms and FRET traces ([Fig. 8E](#)) with similar very dwell times ([Fig. 8F](#)) suggest that Srs2 translocates near the junction of the DNA substrate ([Qiu et al., 2013](#)). Most likely, Srs2 scrunches well-defined length of short ssDNA, followed by release and this process repeats itself, powered by ATP.

To further test the location of Srs2 on ssDNA, we labeled the DNA construct with a donor dye (Cy3) at either the junction or the 3' end of the ssDNA, then we labeled the protein with the acceptor dye (ATTO 647N) and add it to the immobilized DNA construct ([Fig. 9A](#)). We used DNA constructs with ssDNA tail length ranging from T20 to T40. Here is the procedure for using the protein with a Ni-NTA-ATTO 647N dye ([Grunwald et al., 2011](#)):

- (1) Mix Srs2 and dye at a ratio of 1:1.5 (5 and 7.5 nM, respectively) with imaging buffer and 2 mM dithiothreitol, incubated at room temperature for 5 min.
- (2) Add the mixture to the immobilized DNA and image as before. Collect FRET histograms and FRET traces for analysis.
- (3) Compare the FRET histograms and traces for the DNA with the dye at the junction vs the dye at the 3' ssDNA tail ([Fig. 9B and C](#)). Note that the FRET histogram with the junction-dye DNA does not change nor exhibit the double FRET peak regardless of the tail length while the tail labeled T20 shows two FRET peaks

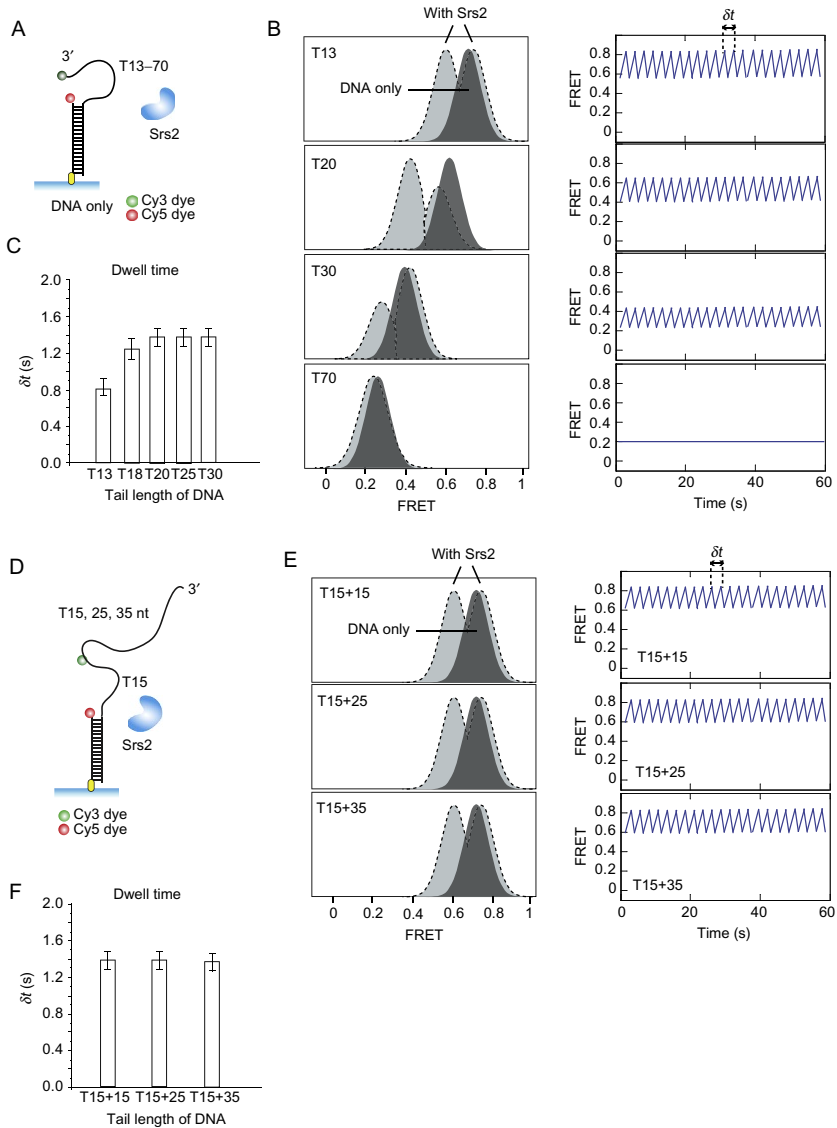


**Fig. 8** Localizing the position of Srs2 using different DNA tail lengths. (A) Schematic of partial duplex DNA with varied tail lengths. (B) Example FRET histogram and traces of Srs2 translocating on each tail length. (C) Example peak-to-peak dwell time measurements of FRET fluctuations for each tail length. (D) Schematic of partial duplex DNA with the internal Cy3 dye fixed at the same tail length. (E) Example FRET histogram and traces of Srs2 translocating on the DNA shown in (D). (F) Example peak-to-peak dwell time measurements of the FRET fluctuations shown in (E).

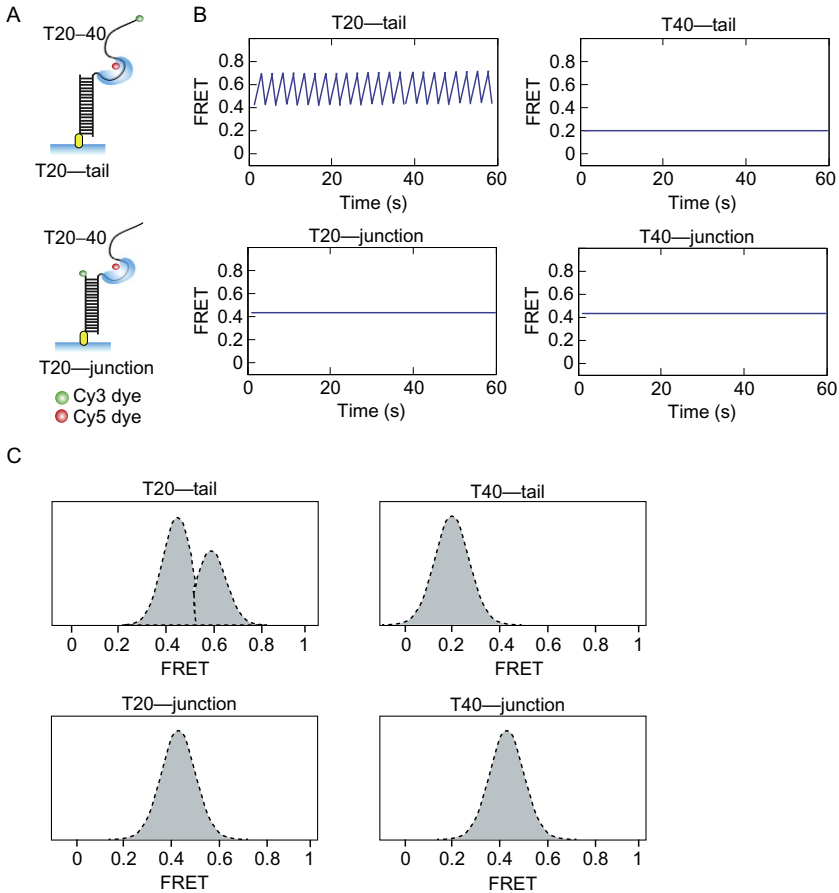


**Fig. 9** Localizing Srs2 position using labeled protein. (A) Schematics of labeled DNA and protein. (B) Example FRET traces showing fluctuations at one Cy3 dye location and steady FRET at the other Cy3 dye location. (C) Example FRET histograms showing multiple FRET peaks at one Cy3 dye location and a steady, mid-FRET peak at the other location.

and fluctuating FRET signal (Fig. 9B and C), supporting the mechanism of Srs2 that situates itself at the junction and scrunches short segment of ssDNA repetitively.

### 2.3.2 Unwinding rate of Srs2 on naked ssDNA is tail length-dependent

When the concentration of Srs2 surpasses the unwinding threshold, likely multimers of Srs2 bound to ssDNA will lead to unwinding of dsDNA (Krejci et al., 2004). We varied the tail length of the ssDNA to see if it affected the rate of dsDNA unwinding.

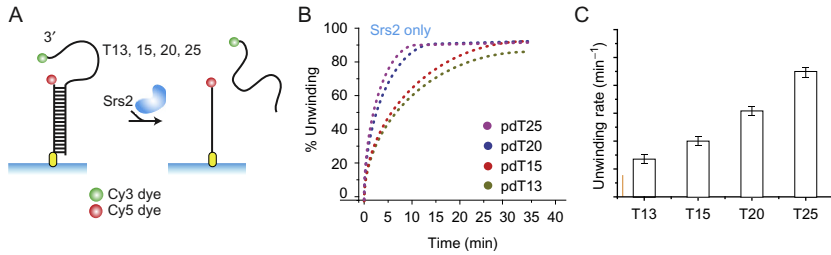


**Fig. 10** Monitoring Srs2 unwinding naked DNA with various tail lengths. (A) Schematic of DNA used. (B) Plot of Cy3 spot counting (as % unwound) over time for various DNA tail lengths. (C) Unwinding rates as calculated from (B) show faster unwinding rate as DNA tail lengths.

- (1) Start with the DNA substrate with the same sequence design and dye placements as the DNA from [Section 2.1](#) for immobilized DNA, but vary the tail length from T13 to T25 ([Fig. 10A](#)). Immobilize them to the PEG surface as before and record the number of Cy3 spots, this is the preunwound DNA count.
- (2) Apply 200 nM of Srs2 in imaging buffer to the immobilized DNA. Take short sequential movies in different imaging surface to track the status of unwinding. As the nonbiotinylated Cy3 strand is released via Srs2 unwinding DNA, the number of Cy3 spots should decrease as unwinding proceeds. Continue to image until majority of Cy3 signal disappears to ensure that unwinding is complete.
- (3) Convert the Cy3 count (intact DNA count) to unwinding % and plot against time for all tail length tested ([Fig. 10B](#)). The rate of unwinding increase as a function of tail length ([Fig. 10C](#)).



### 3. THE Srs2 ACTIVITY ON THE Rad51 FILAMENT

#### 3.1 The Antirecombinase Activity of Srs2 on Rad51 vs RecA Filament

##### 3.1.1 Srs2 cannot disassemble a RecA filament

Srs2 is a unique antirecombinase protein in yeast in that it is highly specific to the removal of Rad51 filaments via direct interaction ([Antony et al., 2009](#); [Colavito et al., 2009](#)). To test for its specificity for Rad51, we tested the removal of RecA (bacterial homolog of Rad51) filaments by Srs2 ([Fig. 11A](#)) in the following way.

- (1) A stable RecA filament ([Joo et al., 2006](#)) is formed when the protein is mixed at 1  $\mu$ M with RecA imaging buffer (100 mM NaAc, 25 mM

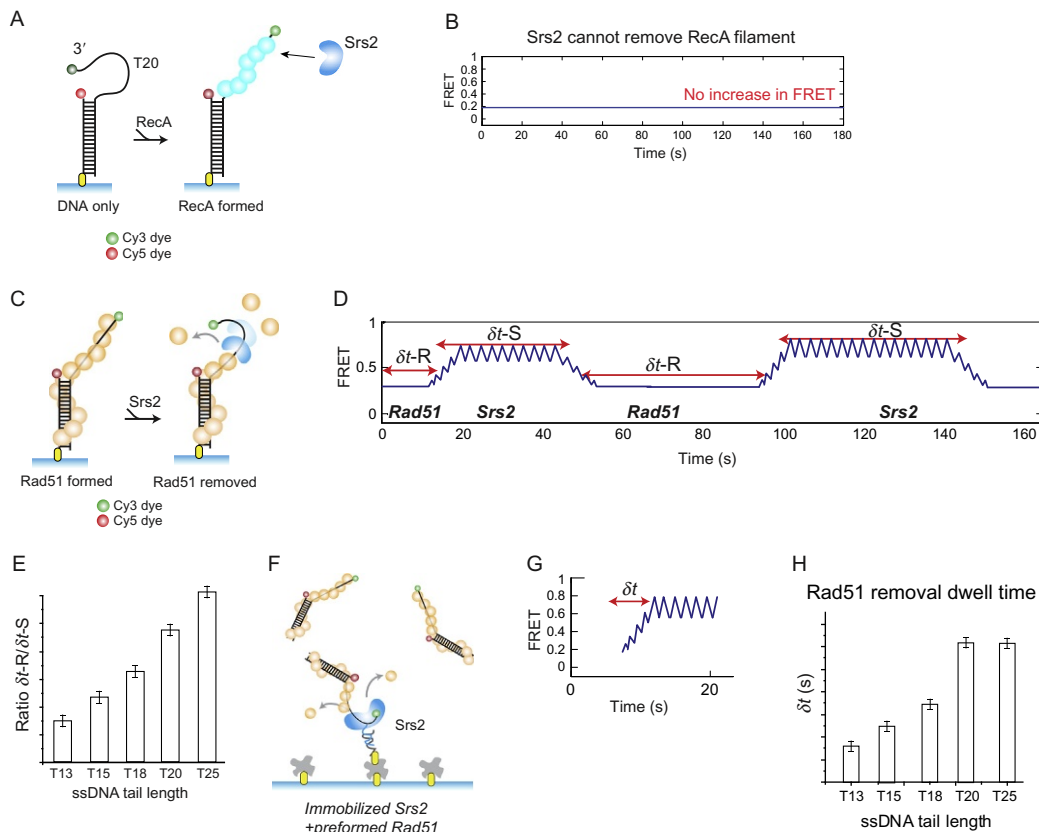


**Fig. 11** Removal of RecA/Rad51 filaments by Srs2. (A) Schematic of RecA filament formation and removal on DNA by Srs2. (B) Example FRET trace showing no FRET recovery, suggest that Srs2 cannot remove RecA. (C) Schematic of Rad51 filament formation and removal on DNA by Srs2. (D) Example FRET trace showing multiple events of Rad51 removal and reformation in the presence of Srs2. (E) Ratio of Rad51 filament formation and Srs2 clearance for each tail length. (F) Schematic of tethered monomer Srs2 removing Rad51 filament. (G) Example FRET trace showing a single event of Rad51 removal by Srs2. (H) Comparing the time it takes for Rad51 removal for various DNA tail lengths.

Tris-HCl (pH 7.5), 10mM MgAc, 1mM ATP with an oxygen-scavenging system containing 0.8% v/v dextrose, 1 mg/mL glucose oxidase, 0.03 mg/mL catalase, and 1% v/v 2-mercaptoethanol), and added to a flow chamber that had pdT20 DNA FRET construct immobilized on imaging surface (see [Section 1.1](#) for immobilization procedure).

- (2) FRET histogram for RecA filament should be similar to that of the Rad51 filament ([Fig. 1B](#)) on the same DNA substrate.
- (3) Mix 200 nM of Srs2 with the RecA imaging buffer and add to the RecA filament, begin taking long movies (>3 movies) for FRET traces and then short movies for FRET histogram building.
- (4) There should be no (<5%) FRET fluctuations in the individual FRET traces ([Fig. 11B](#)), and no FRET histogram shift because Srs2 does not disassemble RecA filaments.

### 3.1.2 Srs2 anti-recombinase activity

We then test the same removal condition for Srs2 with Rad51 filaments formed on various ssDNA tail lengths.

- (1) Form a stable Rad51 filament ([Fig. 11C](#)) with the procedure outlined in [Section 1.1](#). Confirm with FRET histogram. Please note that Rad51 filament will also grow around the dsDNA but the growth rate is much slower than on the ssDNA, resulting in a net-growth direction of 5'-3' ([Qiu et al., 2013](#)).
- (2) Add Srs2 (200 nM) to the Rad51 filament ([Fig. 11C](#)), begin taking long movies (>3 movies) for FRET traces and then short movies for FRET histogram building.
- (3) Examine the FRET traces. You should see low FRET signal followed by FRET fluctuations leading to high FRET. This is an indication of Rad51 filament removal by Srs2. You may also see a repetitive pattern of high-to-low then low-to-high FRET fluctuations ([Fig. 11D](#)), indicating a dynamic exchange between Rad51 filament reformation and Srs2 clearance.
- (4) Repeat the procedure for T13 to T25 tail lengths. Measure the ratio between Rad51 filament formation and Srs2 clearance ( $\frac{\delta I - R}{\delta I - S}$ ) for each tail length and compare. You should see that the ratio increases as the ssDNA tail lengthens ([Fig. 11E](#)), signifying the improved stability of Rad51 filament, which makes it resistant to Srs2 mediated removal.

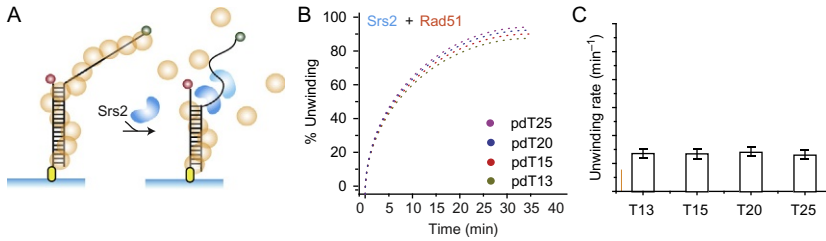


**Fig. 12** Monitoring Srs2 unwinding Rad51 filament-covered DNA with various tail lengths. (A) Experimental Schematic. (B) Plot of Cy3 spot counting (as % unwound) over time for various DNA tail lengths. (C) Unwinding rates as calculated from (B) shows similar unwinding rate regardless of DNA tail lengths.

### 3.1.3 Monomer Srs2 is able to remove Rad51 filament

Srs2 removal of Rad51 filament can also be done with immobilized protein (Fig. 11F), this allows us to measure the time it takes for the initial removal of the Rad51 filament.

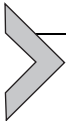
- (1) Follow the procedure in Section 2.1 to tether 10 nM of Srs2 proteins to the PEG surface.
- (2) Preform the Rad51 filament on nonbiotinylated DNA construct by incubating 1  $\mu\text{M}$  of Rad51 protein with DNA in Rad51 imaging buffer. Incubate at room temperature for 15 min.
- (3) Add the mixture to the tethered protein and record long movies for FRET trace analysis.
- (4) Measure the time ( $\delta t$ ) it took to go from the lowest FRET to the highest FRET in the trace (Fig. 11G), this is the duration for Rad51 filament removal by Srs2.
- (5) Repeat steps (1)–(4) for T13 to T25 ssDNA tail lengths. Compare the Rad51 removal times, the comparison should show again, that it is more difficult for Srs2 to remove Rad51 filaments formed on longer ssDNA tail lengths (Fig. 11H).

## 3.2 The Unwinding Activity of Srs2 on the Rad51 Filament

In the previous section, we have established that the unwinding activity of Srs2 on naked DNA is dependent on the length of the 3' ssDNA tail (Qiu et al., 2013). We then test Srs2 on filament-covered DNA (Fig. 12A) to see if the presence of Rad51 deters unwinding.

- (1) Immobilize partial duplex DNA to the PEG surface as before.
- (2) Add 1  $\mu\text{M}$  Rad51 in imaging buffer to form a stable Rad51 filament. Begin taking a short movie immediately and count the Cy3 spots. This is the number of filament covered DNA before unwinding.

- (3) Repeat step (2) from Section 2.3, part 2 for the counting of Cy3 spots during unwinding.
- (4) Repeat steps (1)–(3) for ssDNA tail lengths from T13 to T25. Then plot the Cy3 counts for each tail length vs time (Fig. 12B). First, you should see that the unwinding rates for all filament-covered DNA are substantially lower than the unwinding rate obtained in the absence of Rad51. Second, the unwinding rate is the same regardless of the ssDNA tail length (Fig. 12C). These findings suggest that Rad51 filament plays a protective role in DNA unwinding by resisting the unwinding activity by Srs2.



## 4. CONCLUSIONS

Here, we present a comprehensive, step-by-step procedure in which the interaction between Rad51 (recombinase) and Srs2 (antirecombinase) can be studied using single-molecule FRET and PIFE. The high sensitivity of the single-molecule assays allows us to monitor the association and activity of a single protein in real-time, which is impossible for many ensemble-type measurements. The ability to tether single proteins to the imaging surface is especially useful for resolving a monomer driven activity. The ability to detect protein binding with no protein modification, enabled by PIFE is an easy way to detect any directionally biased intensity increase (Qiu et al., 2013; Qiu & Myong, 2016). Developing and combining different single-molecule technique have allowed us to uncover mechanistic details of many proteins including DNA/RNA-binding proteins, helicases and other motor proteins (Koh, Kidwell, Ragunathan, Doudna, & Myong, 2013; Myong et al., 2009; Myong, Rasnik, Joo, Lohman, & Ha, 2005; Park et al., 2010), and chromatin remodelers (Qiu et al., 2017).

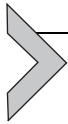
## REFERENCES

- Anand, R. P., Shah, K. A., Niu, H., Sung, P., Mirkin, S. M., & Freudenreich, C. H. (2012). Overcoming natural replication barriers: Differential helicase requirements. *Nucleic Acids Research*, 40(3), 1091–1105. <https://doi.org/10.1093/nar/gkr836>.
- Antony, E., Tomko, E. J., Xiao, Q., Krejci, L., Lohman, T. M., & Ellenberger, T. (2009). Srs2 disassembles Rad51 filaments by a protein-protein interaction triggering ATP turnover and dissociation of Rad51 from DNA. *Molecular Cell*, 35(1), 105–115. <https://doi.org/10.1016/j.molcel.2009.05.026>.
- Bhattacharyya, S., & Lahue, R. S. (2004). *Saccharomyces cerevisiae* Srs2 DNA helicase selectively blocks expansions of trinucleotide repeats. *Molecular and Cellular Biology*, 24(17), 7324–7330. <https://doi.org/10.1128/MCB.24.17.7324-7330.2004>.
- Cleary, J. D., Nichol, K., Wang, Y. H., & Pearson, C. E. (2002). Evidence of cis-acting factors in replication-mediated trinucleotide repeat instability in primate cells. *Nature Genetics*, 31(1), 37–46. <https://doi.org/10.1038/ng870>.

- Colavito, S., Macris-Kiss, M., Seong, C., Gleeson, O., Greene, E. C., Klein, H. L., et al. (2009). Functional significance of the Rad51-Srs2 complex in Rad51 presynaptic filament disruption. *Nucleic Acids Research*, 37(20), 6754–6764. <https://doi.org/10.1093/nar/gkp748>.
- Dhar, A., & Lahue, R. S. (2008). Rapid unwinding of triplet repeat hairpins by Srs2 helicase of *Saccharomyces cerevisiae*. *Nucleic Acids Research*, 36(10), 3366–3373. <https://doi.org/10.1093/nar/gkn225>.
- Fischer, C. J., & Lohman, T. M. (2004). ATP-dependent translocation of proteins along single-stranded DNA: Models and methods of analysis of pre-steady state kinetics. *Journal of Molecular Biology*, 344(5), 1265–1286. <https://doi.org/10.1016/j.jmb.2004.10.004>.
- Freudenreich, C. H., Stavenhagen, J. B., & Zakian, V. A. (1997). Stability of a CTG/CAG trinucleotide repeat in yeast is dependent on its orientation in the genome. *Molecular and Cellular Biology*, 17(4), 2090–2098.
- Gatchel, J. R., & Zoghbi, H. Y. (2005). Diseases of unstable repeat expansion: Mechanisms and common principles. *Nature Reviews. Genetics*, 6(10), 743–755. <https://doi.org/10.1038/nrg1691>.
- Grunwald, C., Schulze, K., Giannone, G., Cognet, L., Lounis, B., Choquet, D., et al. (2011). Quantum-yield-optimized fluorophores for site-specific labeling and super-resolution imaging. *Journal of the American Chemical Society*, 133(21), 8090–8093. <https://doi.org/10.1021/ja200967z>.
- Hwang, H., Kim, H., & Myong, S. (2011). Protein induced fluorescence enhancement as a single molecule assay with short distance sensitivity. *Proceedings of the National Academy of Sciences of the United States of America*, 108(18), 7414–7418. <https://doi.org/10.1073/pnas.1017672108>.
- Joo, C., McKinney, S. A., Nakamura, M., Rasnik, I., Myong, S., & Ha, T. (2006). Real-time observation of RecA filament dynamics with single monomer resolution. *Cell*, 126(3), 515–527. <https://doi.org/10.1016/j.cell.2006.06.042>.
- Kerrest, A., Anand, R. P., Sundararajan, R., Bermejo, R., Liberi, G., Dujon, B., et al. (2009). SRS2 and SGS1 prevent chromosomal breaks and stabilize triplet repeats by restraining recombination. *Nature Structural & Molecular Biology*, 16(2), 159–167. <https://doi.org/10.1038/nsmb.1544>.
- Koh, H. R., Kidwell, M. A., Ragunathan, K., Doudna, J. A., & Myong, S. (2013). ATP-independent diffusion of double-stranded RNA binding proteins. *Proceedings of the National Academy of Sciences of the United States of America*, 110(1), 151–156. <https://doi.org/10.1073/pnas.1212917110>.
- Krejci, L., Macris, M., Li, Y., Van Komen, S., Villemain, J., Ellenberger, T., et al. (2004). Role of ATP hydrolysis in the antirecombinase function of *Saccharomyces cerevisiae* Srs2 protein. *The Journal of Biological Chemistry*, 279(22), 23193–23199. <https://doi.org/10.1074/jbc.M402586200>.
- Krejci, L., Van Komen, S., Li, Y., Villemain, J., Reddy, M. S., Klein, H., et al. (2003). DNA helicase Srs2 disrupts the Rad51 presynaptic filament. *Nature*, 423(6937), 305–309.
- Lata, S., Gavutis, M., Tampe, R., & Piehler, J. (2006). Specific and stable fluorescence labeling of histidine-tagged proteins for dissecting multi-protein complex formation. *Journal of the American Chemical Society*, 128(7), 2365–2372. <https://doi.org/10.1021/ja0563105>.
- Le Breton, C., Dupaigne, P., Robert, T., Le Cam, E., Gangloff, S., Fabre, F., et al. (2008). Srs2 removes deadly recombination intermediates independently of its interaction with SUMO-modified PCNA. *Nucleic Acids Research*, 36(15), 4964–4974. <https://doi.org/10.1093/nar/gkn441>.
- Lytle, A. K., Origanti, S. S., Qiu, Y., VonGermeten, J., Myong, S., & Antony, E. (2014). Context-dependent remodeling of Rad51-DNA complexes by Srs2 is mediated by a specific protein-protein interaction. *Journal of Molecular Biology*, 426(9), 1883–1897. <https://doi.org/10.1016/j.jmb.2014.02.014>.

- McKinney, S. A., Joo, C., & Ha, T. (2006). Analysis of single-molecule FRET trajectories using hidden Markov modeling. *Biophysical Journal*, *91*(5), 1941–1951. <https://doi.org/10.1529/biophysj.106.082487>.
- Mirkin, S. M. (2006). DNA structures, repeat expansions and human hereditary disorders. *Current Opinion in Structural Biology*, *16*(3), 351–358. <https://doi.org/10.1016/j.sbi.2006.05.004>.
- Mirkin, S. M. (2007). Expandable DNA repeats and human disease. *Nature*, *447*(7147), 932–940. <https://doi.org/10.1038/nature05977>.
- Mirkin, E. V., & Mirkin, S. M. (2014). To switch or not to switch: At the origin of repeat expansion disease. *Molecular Cell*, *53*(1), 1–3. <https://doi.org/10.1016/j.molcel.2013.12.021>.
- Murphy, M. C., Rasnik, I., Cheng, W., Lohman, T. M., & Ha, T. (2004). Probing single-stranded DNA conformational flexibility using fluorescence spectroscopy. *Biophysical Journal*, *86*(4), 2530–2537. [https://doi.org/10.1016/S0006-3495\(04\)74308-8](https://doi.org/10.1016/S0006-3495(04)74308-8).
- Myong, S., Cui, S., Cornish, P. V., Kirchhofer, A., Gack, M. U., Jung, J. U., et al. (2009). Cytosolic viral sensor RIG-I is a 5'-triphosphate-dependent translocase on double-stranded RNA. *Science*, *323*(5917), 1070–1074. <https://doi.org/10.1126/science.1168352>.
- Myong, S., Rasnik, I., Joo, C., Lohman, T. M., & Ha, T. (2005). Repetitive shuttling of a motor protein on DNA. *Nature*, *437*(7063), 1321–1325. <https://doi.org/10.1038/nature04049>.
- Paques, F., & Haber, J. E. (1999). Multiple pathways of recombination induced by double-strand breaks in *Saccharomyces cerevisiae*. *Microbiology and Molecular Biology Reviews*, *63*(2), 349–404.
- Park, J., Myong, S., Niedziela-Majka, A., Lee, K. S., Yu, J., Lohman, T. M., et al. (2010). PcrA helicase dismantles RecA filaments by reeling in DNA in uniform steps. *Cell*, *142*(4), 544–555. <https://doi.org/10.1016/j.cell.2010.07.016>.
- Qiu, Y., Antony, E., Doganay, S., Koh, H. R., Lohman, T. M., & Myong, S. (2013). Srs2 prevents Rad51 filament formation by repetitive motion on DNA. *Nature Communications*, *4*, 2281. <https://doi.org/10.1038/ncomms3281>.
- Qiu, Y., Levandosky, R. F., Chakravarthy, S., Patel, A., Bowman, G. D., & Myong, S. (2017). The Chd1 chromatin remodeler shifts nucleosomal DNA bidirectionally as a monomer. *Molecular Cell*, *68*(1), 76–88. e76. <https://doi.org/10.1016/j.molcel.2017.08.018>.
- Qiu, Y., & Myong, S. (2016). Single-molecule imaging with one color fluorescence. *Methods in Enzymology*, *581*, 33–51. <https://doi.org/10.1016/bs.mie.2016.08.011>.
- Qiu, Y., Niu, H., Vukovic, L., Sung, P., & Myong, S. (2015). Molecular mechanism of resolving trinucleotide repeat hairpin by helicases. *Structure*, *23*(6), 1018–1027. <https://doi.org/10.1016/j.str.2015.04.006>.
- Roy, R., Hohng, S., & Ha, T. (2008). A practical guide to single-molecule FRET. *Nature Methods*, *5*(6), 507–516. <https://doi.org/10.1038/nmeth.1208>.
- Symington, L. S. (2002). Role of RAD52 epistasis group genes in homologous recombination and double-strand break repair. *Microbiology and Molecular Biology Reviews*, *66*(4), 630–670 [table of contents].
- Veaute, X., Jeusset, J., Soustelle, C., Kowalczykowski, S. C., Le Cam, E., & Fabre, F. (2003). The Srs2 helicase prevents recombination by disrupting Rad51 nucleoprotein filaments. *Nature*, *423*(6937), 309–312.

This page intentionally left blank



# The Recombination Mediator BRCA2: Architectural Plasticity of Recombination Intermediates Revealed by Single-Molecule Imaging (SFM/TIRF)

Arshdeep Sidhu\*, Dejan Ristic\*, Humberto Sánchez†, Claire Wyman\*,<sup>1</sup>

\*Erasmus University Medical Center, Rotterdam, The Netherlands

†Kavli Institute of Nanoscience, Faculty of Applied Sciences, Delft University of Technology, Delft, The Netherlands

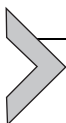
<sup>1</sup>Corresponding author: e-mail address: c.wyman@erasmusmc.nl

## Contents

|  |     |
|--|-----|
| 1. Introduction  | 348 |
| 2. Organization and Architectural Plasticity of Protein and DNA–Protein Assemblies: Single-Molecule SFM Imaging    | 350 |
| 2.1 Sample Quality   | 351 |
| 2.2 Tip–Sample Interaction   | 351 |
| 2.3 Surface Properties of the Substrate  | 353 |
| 3. SFM Imaging to Reveal and Quantify Protein Architectural Plasticity   | 354 |
| 3.1 Notes  | 356 |
| 3.2 Image Analysis   | 356 |
| 4. SFM Analysis of RAD51 Filament and Joint Molecules  | 358 |
| 4.1 RAD51 Filament Formation for SFM Imaging and Analysis  | 359 |
| 4.2 Notes  | 360 |
| 4.3 Joint Molecule Formation   | 362 |
| 4.4 Notes  | 362 |
| 4.5 Analysis   | 363 |
| 5. Identifying Specific Proteins in Complex Structures by Fluorescence: BRCA2–RAD51 Complexes Analyzed by TIRF–SFM | 364 |
| 5.1 Tips for SFM–TIRF Imaging  | 367 |
| 5.2 Notes  | 367 |
| 5.3 Image Analysis and Quantification  | 369 |
| 6. Conclusions   | 371 |
| References   | 371 |

## Abstract

Cellular functions are defined by dynamic assembly, rearrangement, and disassembly of biomolecules to achieve control and specificity. As an example, effective DNA repair is brought about by the concerted action of several DNA processing proteins. Both changes in the structure of individual proteins and in the arrangement of multiple proteins together (referred to here as architecture) are inherent to biological function. These dynamic changes are exemplified in the breast cancer susceptibility protein 2 (BRCA2). BRCA2 is a DNA repair protein that undergoes changes in its own structure and affects changes in molecular architecture with partners during homologous recombination (HR) repair of DNA double strand breaks. These challenging features of BRCA2 protein, its size and predicted stretches of intrinsically disordered regions, have made it difficult to determine the structural consequences and mechanistic importance of interactions between full-length BRCA2 with RAD51 and other HR proteins. In this chapter, we describe scanning force microscopy (SFM)-based approaches to study DNA–protein complexes involved in HR, the architectural plasticity of full-length BRCA2, and the dynamic reorganization of these molecular components associated with essential steps of HR.



## 1. INTRODUCTION

DNA lesions caused by a number of extrinsic and intrinsic factors challenge genomic integrity on a daily basis. DNA double strand DNA breaks (DSBs) are potentially one of the most toxic DNA lesions. Incorrect repair of DSBs can result in point mutations, small deletion mutations, or more dramatically in chromosomal translocations, which are common precursors to neoplastic transformation. Most of the incurred DSBs are repaired by homologous recombination (HR) or nonhomologous end joining repair pathways. The choice of repair pathway depends on the phase of cell cycle and the availability of a homologous chromosome for repair. HR repair is essential for supporting replication and is the most accurate mechanism for repair of DSBs (Mehta & Haber, 2014; van Gent, Hoeijmakers, & Kanaar, 2001).

HR repair requires the coordinated action of many DNA repair proteins including RAD50, Mre11, NBS1, RPA, RAD51 (and its paralogs), RAD52, BRCA1, BRCA2, DSS1, and RAD54. Some of these proteins, like MRE11, RAD51, have catalytic function in the repair process while others, like NBS1, RPA, BRCA2, have regulatory or structural roles (Stracker, Theunissen, Morales, & Petrini, 2004). Precisely coordinated intermolecular protein interactions among these proteins are essential for

maintaining an error-free genome. Detailed understanding of molecular interactions and their structural consequences in HR repair can contribute important insight needed to design new therapeutic strategies and manage pathologies in, for instance, cancers where the role of HR in genomic (in)stability is linked to both causes and cures.

The protein-protein interactions in the HR repair pathways have been studied by a variety of biochemical, structural, biophysical, and single-molecule approaches (Jensen, Carreira, & Kowalczykowski, 2010; Modesti et al., 2007; Sanchez, Kertokalio, van Rossum-Fikkert, Kanaar, & Wyman, 2013; Sanchez et al., 2017; Shahid et al., 2014; Thorslund et al., 2010; Yang et al., 2002; Yang, Li, Fan, Holloman, & Pavletich, 2005). Nevertheless, it remains difficult to define dynamic changes in molecular structure and complex architecture. Although X-ray crystallography and NMR provide atomic resolution, both these techniques require high concentration of protein and are limited by intrinsic structural flexibility of the proteins and architectural variability of the complexes being analyzed. Protein and DNA molecules are nanoscale entities whose molecular interactions can be determined by techniques that visualize single molecules. Single-molecule imaging by scanning force microscopy (SFM) and (cryo-) EM have been used successfully with full-length proteins to reveal nanoscale structures and molecular characteristic of several DNA repair complexes (Sanchez et al., 2013, 2017; Shahid et al., 2014; Thorslund et al., 2010). SFM does not require the class averaging of thousands of single-molecule projections needed in cryo-EM to reconstruct a 3D particle image and therefore reveals structural information on each individual molecule/complex observed. This yields rich information on all conformation of complexes in a mixture and their distributions in variable but defined conditions provide additional information on dynamic arrangement.

SFM imaging is well suited for analysis of conformational flexibility of proteins and architectural variability of their complexes. Recent advances combining fluorescence microscopy with SFM topography significantly broaden the possible applications. Individual protein or DNA components in complex assemblies can be identified and quantified based on signals from fluorescent tags. This can provided essential new information on molecular composition and architecture of multicomponent complexes. This chapter focuses on the SFM-based approaches to study protein-protein and protein-DNA interactions at molecular resolution in the context of HR repair. We introduce methods developed so far to obtain additional information by combining total internal reflection fluorescence (TIRF) microscopy with SFM.

We focus on the breast cancer susceptibility protein 2, BRCA2, to investigate the role of conformational dynamics in interaction with RAD51. BRCA2 is an essential mediator of RAD51, required for localizing RAD51 to sites of DNA damage and exchanging RPA for RAD51 on single-stranded DNA in need of HR repair (Jensen et al., 2010; Kolinjivadi et al., 2017; Prakash, Zhang, Feng, & Jasin, 2015). BRCA2 consists of 3418 amino acids including domains that interact with RAD51, PALB2, DNA, and other partners, but notably also large stretches predicted to be intrinsically disordered regions (IDRs). From a practical point of view, protein purification requires expression in mammalian cells and typically yields are rather low, in the range of micrograms of protein from a liter of culture (Jensen et al., 2010; Sanchez et al., 2017). Given these features BRCA2 is ideally suited for SFM-based studies. A typical SFM imaging experiment requires only tens of microliters volume of sample in standard biochemical buffers at nanogram per microliter concentrations. The images obtained provide nanometer resolution information on shape, size, and volume of the objects in the sample, where volume correlates linearly with molecular mass (Moreno-Herrero et al., 2005; Ratcliff & Erie, 2001; Wyman, Rombel, North, Bustamante, & Kustu, 1997). Thus, single-molecule imaging of proteins and protein complexes by SFM can determine the distribution of conformations and multimerization state of protein in physiologically relevant buffer conditions. TIRF microscopy can be combined with SFM to identify specific proteins in complex structures by fluorescent labels and single-molecule localization. Although technically challenging, combined TIRF–SFM provides richer data and is an exciting advance for studying dynamic multicomponent processes such as HR.



---

## **2. ORGANIZATION AND ARCHITECTURAL PLASTICITY OF PROTEIN AND DNA–PROTEIN ASSEMBLIES: SINGLE-MOLECULE SFM IMAGING**

SFM imaging, in brief, includes sample deposition onto a substrate, which is then scanned by a sharp tip to generate images. Primary factors that determine the quality of SFM imaging include the sample quality, tip–sample interactions, and substrate. In the following paragraphs we discuss how these three primary factors affect the quality of SFM imaging with respect to the DNA repair complexes we study:

## 2.1 Sample Quality

For SFM experiments sample quality involves two aspects, *purity* and *concentration*. Purity is important because any material in the sample with a size of a few Angstroms up to 100 nm can severely compromise image quality. Impurities larger than 100 nm impede imaging altogether. Therefore, all the buffers and consumables involved in sample preparation should be “nanoscopically” clean, prepared with pure components, if necessary filtered but not autoclaved. Concentration of the molecules of interest and their affinity for the substrate will determine coverage, density of objects of interest in the images obtained. Ideal sample coverage results in individual molecular species that can be recognized but are not overlapping. The goal is to be able to unambiguously identify molecules/complexes of interest and to have sufficient examples recorded in a reasonable number of scan images (Fig. 1). Coincidental colocalization of, for instance, monomers/dimers due to crowding can appear as potential larger oligomers complicating or preventing analysis of oligomerization (Fig. 1B and C). Normally, about 1–2 ng/ $\mu\text{L}$  of protein in the mixture to be deposited is sufficient for imaging. However, when studying protein complexes and interactions, the concentration of the components should be at least a magnitude higher than the affinity of their interaction ( $K_d$ ), which may then require dilution in the deposition step. Buffer conditions are usually determined by the interactions being studied based on prior biochemical analysis. A range of standard biochemical reactions conditions is suitable for SFM sample preparation allowing deposition of complexes directly from biochemically active conditions.

## 2.2 Tip–Sample Interaction

SFM imaging modes are categorized based on the extent of tip–sample interaction as contact, tapping, and true noncontact mode. We use almost exclusively tapping mode SFM and refer only to this imaging mode here. One of the unavoidable aspects of tip–sample interactions is convolution of the size of the molecules being imaged and the size and shape of the scanning tip apex. Using standard tips with  $\sim 10$  nm radius this typically results in exaggerated X–Y dimensions for biomolecules such as DNA (Fuentes-Perez, Dillingham, & Moreno-Herrero, 2013; van Raaij, Segers-Nolten, & Subramaniam, 2006; Yang, Vesenka, & Bustamante, 1996). Short range tip–sample and tip–substrate interactions, attraction and repulsion, result

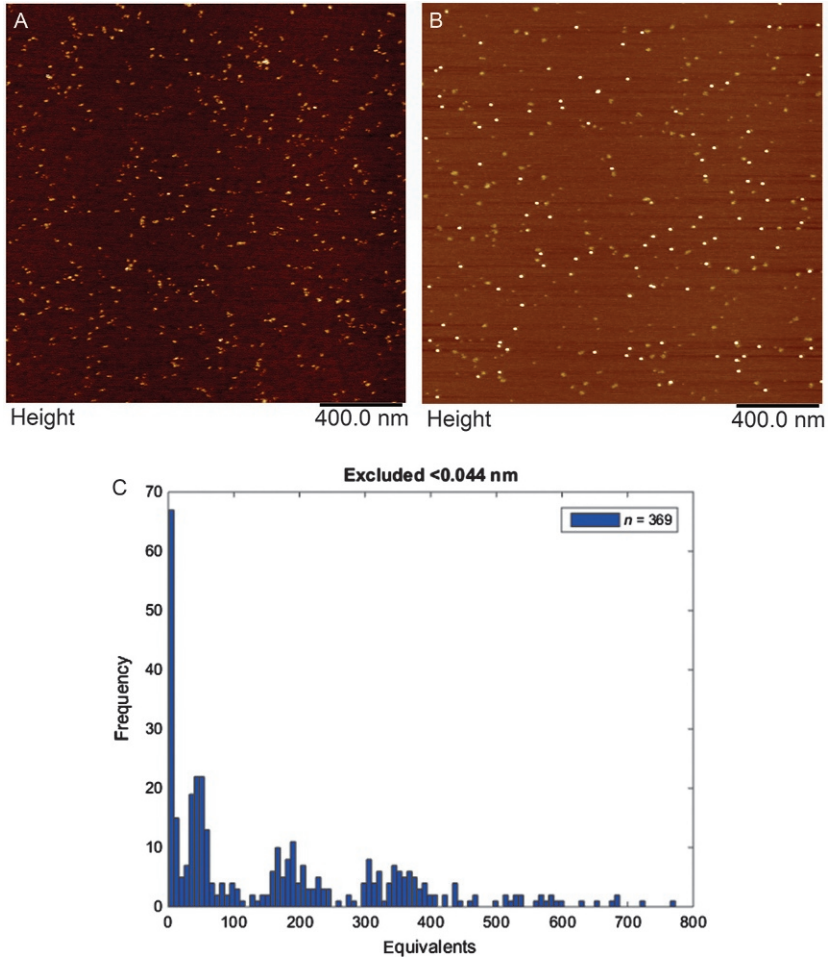


**Fig. 1** Examples of effect of crowding and higher concentration on SFM imaging. (A) A crowded SFM image of Aldolase molecules. It is not possible to discern single molecules in the image. (B) SFM image of catalase at high concentration that shows multimerization. (C) Volumetric analysis of (B) using SFMedges (module of SFMetrics) showing distinct populations of multimers.

in distortions in absolute height of biomolecules (Fig. 2). Relative height is however a very reliable measurement. In experiments measuring volume it is crucial to use the same tip and system scanning parameters constant when comparing two samples (Fuentes-Perez et al., 2013). The height and width of double-stranded DNA can be used as a convenient standard for

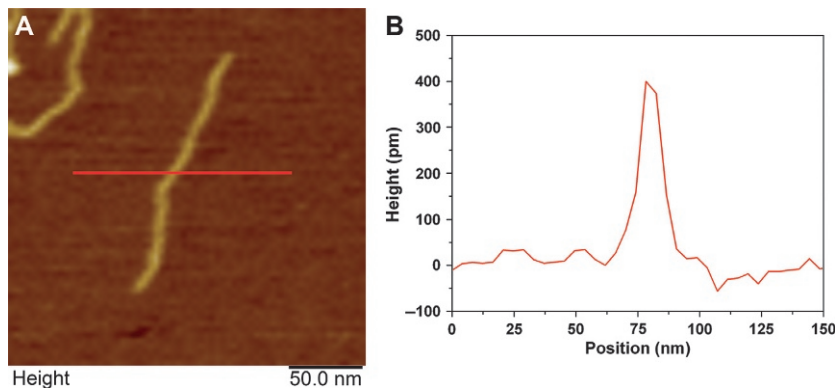


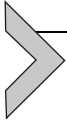
**Fig. 2** Image showing the effect of convolution in SFM imaging. Note the difference in the height ( $\sim 0.4$  nm) and width ( $\sim 12$  nm) of a linear DNA molecule. Horizontal line in (A) corresponds to the cross-sectional profile shown in (B).

comparison between images. As a final note, the tip can become contaminated with material from the surface resulting in poorer image quality and requiring replacement with a new tip.

### 2.3 Surface Properties of the Substrate

Ideally the dynamic rearrangement of proteins, protein–protein complexes, and protein–DNA complexes required for biological function is captured during deposition for SFM imaging as a variety of conformations or architectures. This is achieved by deposition on to a suitable surface from solutions compatible with biochemical activity (or as close as practical). Sample deposition, washing and drying, is usually rapid (typically  $>30$  s for washing and drying) to maintain distribution from solution as close as possible. A number of different substrates like mica, HOPG, glass coverslips, atomically flat gold layers, etc., have been explored for SFM imaging (Chada et al., 2015; Cisneros, Muller, Daud, & Lakey, 2006; Rahman, Neff, Green, & Norton, 2016). All of the methods described here use mica as a substrate because of its ease of use, compatibility with biochemical buffers for deposition and flatness. Mica is an aluminosilicate mineral that can easily be cleaved, using an adhesive tape, to expose an atomically flat surface. This surface has a net negative charge compatible with interaction of molecules in aqueous buffers (Maslova, Gerasimova, & Forsling, 2004). Chemical modification of the surface is not needed for the methods described here.

Chemical modification of the surface can complicate imaging and analysis as it increases surface roughness, decreasing imaging quality and it can bias the distribution of molecular conformations adhering to the surface. In addition for TIRF–SFM clarity of mica is also very important because the substrate has to be transparent in addition to being flat.



### 3. SFM IMAGING TO REVEAL AND QUANTIFY PROTEIN ARCHITECTURAL PLASTICITY

All proteins require flexibility for function, and the extent of flexibility varies from a few atoms at enzymatic catalytic sites to large domain reorientations needed for mechanical work. At one end of this spectrum are proteins with few or no structured element(s), designated as intrinsically disordered proteins (IDPs), where binding partners often impose structure and function are linked to the disordered–structured transitions (Uversky, 2016). The variable conformations of IDPs, and proteins with intrinsically disordered domains/regions (IDRs), make it difficult to study their structural features by methods that rely on averaging over many identical/similar molecules or complexes (i.e., X-ray crystallography, NMR, cryo-EM). Single-molecule techniques reveal structural information on individual molecules or complexes allowing different conformations or architectural arrangements to be observed and characterized. This additionally allows valuable quantification of the distribution of the different structural forms. BRCA2, for example, contains regions predicted to be intrinsically disordered thorough out the protein sequence (Sanchez et al., 2017). Indeed, SFM and TIRF–SFM have proven particularly valuable for studying BRCA2, revealing molecular plasticity, unexpected variable multimeric assemblies, and dramatic architectural reorganization upon interactions with binding partners (Sanchez et al., 2017). We describe procedures specifically for imaging and analyzing BRCA2 (general methods and some variations are described in Grosbart, Ristic, Sanchez, & Wyman, 2018).

#### Equipment

1. SFM capable of tapping mode operation (e.g., Multimode Nanoscope or Dimension series from Bruker or similar instrument).
2. SFM tips (e.g., Silicon Pointprobe: NHC-W, 310–371 kHz, 42 N/m from Nanosensors).

3. Standard molecular biology/biochemistry equipment for protein/DNA analysis.
4. Filtered (0.22  $\mu\text{m}$ ) supply of air or  $\text{N}_2$  gas.

### Buffers and Reagents

1. Sample buffer for BRCA2: 22 mM HEPES (pH 8.2), 2.5% glycerol, 112 mM NaCl, 0.12 mM EDTA, 0.25 mM DTT.
2. Deposition buffer: 10 mM HEPES buffer pH 8.2, 10 mM  $\text{MgCl}_2$ .
3. 1 M spermidine solution, filtered through a 0.22- $\mu\text{m}$  filter.

### Other Supplies

1. SFM sample disc: metal  $\text{\O}$  12 mm (e.g., from EMS or as supplied with the instrument).
2. Mica discs  $\text{\O}$  10 mm, Muscovite-V1 to V5 quality (from EMS). The required mica disc can be punched out of a mica sheet using a punch and die set.
3. Clear adhesive tape (e.g., 3M Scotch™ tape).
4. Strong adhesive compatible with metal surface (e.g., “super glue”).
5. Lint-free wipes (e.g., Kim wipes).

### Procedure

1. Thaw BRCA2 protein sample briefly on ice and dilute with HEPES sample buffer to a final composition of 10–25 ng BRCA2, 22 mM HEPES (pH 8.2), 2.5% glycerol, 112 mM NaCl, 0.12 mM EDTA, 0.25 mM DTT in a reaction volume of 20  $\mu\text{L}$ .
2. Incubate sample at 37°C for 30 min without shaking.
3. Prepare substrate for sample deposition, glue mica to metal with superglue (can be done ahead of time and kept indefinitely).
4. Cleave the mica surface by applying clear adhesive tape and peeling off to expose a clean and atomically flat surface.
5. Deposit 10–20  $\mu\text{L}$  of protein sample on the mica and incubate for 1 min at room temperature.
  - a. Optionally add spermidine to the sample to a concentration of 50  $\mu\text{M}$  before deposition. Spermidine is a polyamine and carries a positive charge, which helps in adsorption of sample to the negatively charged mica surface. In case sample adsorption appears poor, adding spermidine may increase the amount of protein absorbed.

6. After incubation, wash the sample three times ( $\sim 500\mu\text{L}$  each) with MilliQ grade water. Hold the metal disc by the edge at an angle, using a pair of tweezers, and gently add drops of water with a pipette.
7. Remove excess water by tilting the sample and blotting by the corner of a lint-free wipe.
8. Dry the sample in a gentle stream of filtered air for a minute or so until all visible water has evaporated or been blown off.
9. Mount the metal disc in the SFM and image using Tapping mode, or equivalent, according to instrument instructions.

### 3.1 Notes

1. A standard sample or marker with features of known dimensions (such as double-stranded DNA or protein with known dimensions at a concentration in the range of  $1\text{--}5\text{ ng}/\mu\text{L}$ , or lower if the sample of interest is already fairly dense on the surface) should be included in the scanning regimen to ensure reliable images, check tip, and allow optimizing scanning parameters.
2. Lower scan rates usually provide better images. A typical feature of high scan rate is the shadowing of the particles in a flattened image.
3. For good resolution the pixel size should be smaller than the size of features of interest. Routine scan size for single-molecule imaging varies between  $1 \times 1$ ,  $2 \times 2$ , and up to  $5 \times 5\mu\text{m}$  at 512–1024 pixels per line. Larger scan size gives a better overview of the sample but lacks resolution. At 512 pixels/line or higher resolution the scan rate should be between 0.5 and 1 Hz for best images. This is balanced to be practical, based on the number of images that need to be collected, as slower scan rates increase the time to collect each image. e.g.,  $2 \times 2\mu\text{m}$  image at 512 pixels/line at 1 Hz takes about 8 min for image acquisition, while same image at 0.5 Hz takes about 15–17 min.

### 3.2 Image Analysis

Raw data SFM images usually have significant tilt in the nm range and, depending on the scanner, often have bowing where the edges are higher than the center. These elements of background slope are corrected by flattening the image using plane-fitting options of the image analysis software, usually standard with the instruments. The flattened images can be further analyzed by standard instrument analysis software packages, like NanoScope analysis from Bruker, JPKSPM data processing from JPK, IGOR Pro from

Asylum Research, etc., or by third party software like SPIP, Gwyddion, WSxM, Image SXM, Femtoscan online, etc. Additionally, custom scripts can be written with specific tool set for high-throughput custom image analysis. We use SFMetrics, a Matlab-based open-licensed set of routines for analysis of protein and DNA molecules (<http://cluster15.erasmusmc.nl/TIRF-SFM-scripts>) (Sanchez & Wyman, 2015).

### **3.2.1 Quantification of Molecular Structure and Architectural Features From SFM Images**

Standard SFM image is a topographic or height image with Angstrom resolution in the  $z$  coordinate. Depending on the SFM instrument, additional channels of amplitude error and phase may be available as well. Because the  $z$  scale in amplitude error and phase image is not calibrated, the topographic image is the most useful for quantitative experiments with SFM. In topographic images the objects observed are defined by lateral ( $x$ ,  $y$ ) and height ( $z$ ) measurements. This can be used to quantify size by volume and other parameters representing conformational plasticity of flexibility and irregular molecules.

### **3.2.2 Volumetric Analysis**

SFM measured volume correlates with molecular mass, and the volume distribution of molecule in a given solution condition is a very useful parameter to measure size and consequently multimerization state (Ratcliff & Erie, 2001; Wyman et al., 1997). Volume of protein and DNA molecules can be conveniently determined, for example, by SFMetrics in a semiautomated, high-throughput manner (Sanchez & Wyman, 2015). It is often useful to also collect images of an easily identifiable protein with known volume, like RNA polymerase, as a reference to quantify multimerization of complex protein like BRCA2 (Sanchez et al., 2017). Volume of objects of interest can be determined in SFMetrics by importing an image flattened by plane-fitting as described earlier, then applying a user-defined threshold to define objects above background and sum the volume of each pixel included in the object (Sanchez & Wyman, 2015). When one threshold is applied to an entire image or image set, volumes can be determined in a high-throughput manner.

### **3.2.3 Conformational Flexibility**

The various shapes of molecules or molecular complexes observed in SFM images are a rich source of information on conformational flexibility that can

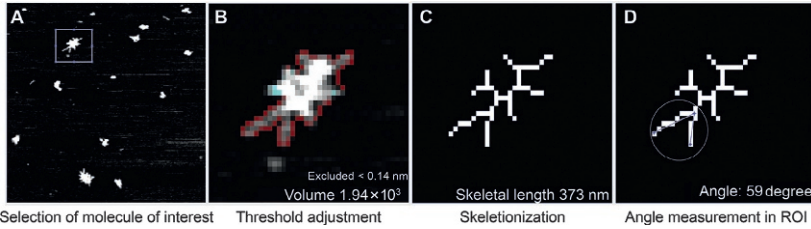
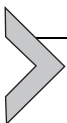


**Fig. 3** Overview of conformational analysis of BRCA2 molecule by SFMetrics. (A) First the molecule of interest is selected and (B) a user-defined threshold is selected to calculate volume. (C) The molecule is skeletonized and (D) desired angles are measured.

be quantified. Standard image analysis often defines objects by the minimal oval that encloses them to provide parameters such as length (major axis), width (minor axis), and ellipticity. These standard parameters often fail to capture or accurately quantify important features of proteins and their complexes with DNA. It is important to look carefully at any image set of interest and identify the features that appear to be correlated with differences in function or conditions. Methods to quantify these often have to be developed. We have for instance observed changes in BRCA2 structure, apparent variability in condensed or extended forms, in response to different conditions that can be quantified in SFMetrics (Sanchez et al., 2017). For BRCA2 in this case we could correlate extension/compaction with different conditions by conveniently combining parameters measured in SFMetrics. Object volume was coupled to skeleton length and to angles defining arrangement of component junctions to more completely quantitatively characterize the shape of a molecule. Skeleton length measures compaction or extension of an object as the minimum number of continuous pixels needed to cover the whole structure after “skeletonization.” Irregularly shaped molecules are often depicted by branched skeleton (Fig. 3), where the angle between branches can provide a robust unbiased signature of conformation.



#### 4. SFM ANALYSIS OF RAD51 FILAMENT AND JOINT MOLECULES

As a mediator of homologous recombination BRCA2 interacts with and affects RAD51, RAD51–DNA filaments, and RAD51–mediated DNA joint molecules. To understand these interactions we will describe SFM and TIRF–SFM analysis of these multicomponent assemblies. Directly determining the arrangement of proteins and DNA in complexes representing staged steps in strand exchange during HR has proven uniquely valuable

for understanding how this process works. A family of highly conserved DNA strand exchange proteins catalyze the defining reactions of HR: homology search, strand invasion, and joint molecule formation. Our work considers the human protein, RAD51. All strand exchange proteins form nucleoprotein filaments on single-stranded DNA, which is the active complex responsible for subsequent steps of recognizing homologous sequence in a double-stranded DNA strand and catalyzing strand exchange between these two. Novel mechanistic insight into the mechanism and control of HR has been revealed from defining the arrangement of RAD51–DNA filaments correlated to reaction conditions, specific RAD51 variants or mutant forms, as well as effect of recombination mediators crucial for filament formation. Here we describe how we have applied SFM imaging to analyze filament formation, the structure of the filaments, and joint molecules. SFM imaging experiments work best when the object of interest (filaments of joint molecules) is efficiently formed and deposited while unwanted molecules/structures (excess free protein or free DNA, aggregates, etc.) are minimized. We describe here our experience with specific emphasis on aspects that are essential to allow efficient, coherent image collection while preserving authentic (biochemical) function for RAD51 filaments and joint molecules.

#### 4.1 RAD51 Filament Formation for SFM Imaging and Analysis

Human RAD51 was expressed and purified as described (Modesti et al., 2007).

##### Equipment and Other Supplies

1. SFM capable of tapping mode operation (e.g., Multimode Nanoscope or Dimension series from Bruker).
2. SFM tip (e.g., Silicon Pointprobe: NHC-W, 310–371 kHz, 42 N/m from Nanosensors).
3. Standard molecular biology/biochemistry equipment for protein/DNA analysis.
4. Filtered (0.22  $\mu\text{m}$ ) supply of air or  $\text{N}_2$  gas.

##### Buffers and Reagents

1. Reaction buffer: 25–50 mM HEPES or Tris–HCl pH 7.5, 2–5 mM  $\text{CaCl}_2$ , 1–2 mM ATP (buffered to pH 7.5), 30–50 mM KCl, 1 mM DTT.
2. Deposition buffer: 10 mM HEPES–KOH pH 7.5, 10 mM  $\text{MgCl}_2$ .

## Procedure

1. Thaw RAD51 aliquot on ice.
2. Prepare filament formation reaction with  $7.5\ \mu\text{M}$  DNA (bp or nucleotide concentration). Although specific length of DNA may be needed for some experiments, best results are achieved with DNA ranging from 300 to 1000 nt/bp),  $2.5\ \mu\text{M}$  RAD51 in reaction buffer in  $10\ \mu\text{L}$  volume.
3. Incubate at  $37^\circ\text{C}$  for 10 min.
4. Dilute the reaction 3–10 times in deposition buffer, deposit  $10\ \mu\text{L}$  onto freshly cleaved mica, and incubate at room temperature 15 s.
5. After incubation wash mica once with about  $500\ \mu\text{L}$  of MilliQ water.
6. Remove excess water by tilting the sample and blotting by the corner of a lint-free wipe.
7. Dry the sample in a gentle stream of filtered air for a minute or so until all visible water has evaporated or been blown off.
8. Mount the metal disc in the SFM and image using Tapping mode, or equivalent, according to instrument instructions.

## 4.2 Notes

1. Optimal monovalent salt concentration for the filament formation reaction is 30–50 mM, which is usually contributed by protein storage buffer. If desired to make the reaction more efficient or accommodate the amount of protein needed, the concentration of monovalent salt can be adjusted to 100–200 mM.
2. Concentration of  $\text{CaCl}_2$  is usually two times the concentration of ATP, for e.g., 2 mM  $\text{CaCl}_2$  and 1 mM ATP; however, slightly higher concentrations like 5 mM  $\text{CaCl}_2$  and 2 mM ATP can also be used. In these conditions stable filaments in the ATP bound form are observed. Using  $\text{MgCl}_2$  or a mixture  $\text{CaCl}_2$  and  $\text{MgCl}_2$  allows (some) ATP hydrolysis and dynamic filaments which appear irregular with respect to arrangement and amount of protein bound.
3. The degree of dilution with deposition buffer is determined empirically for each reaction and depends to some extent on the length of DNA used. Ideally 5–10 (fewer for longer DNA, e.g., 1–2 kbp, more for shorter DNA, e.g., 200–800 bp) nonoverlapping filaments will be observed in each  $2 \times 2\ \mu\text{m}$  image. It is most efficient to deposit several dilutions at once, make quick test scans, and use the one that has best distribution of molecules of interest.
4. In these conditions RAD51 forms filaments on both circular and linear DNA as well as on ss- and ds-DNA. Since filaments on circular DNA frequently collapse on themselves, linear ss- or ds-DNA is more frequently used in SFM experiments (Fig. 4).

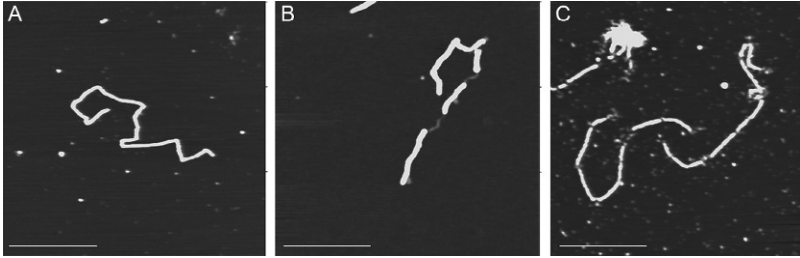


**Fig. 4** Examples of RAD51 filament formation on ds-DNA substrates. (A) Regular filaments on linear ds-DNA (3901 bp). (B) Partial filament on linear ds-DNA (3901 bp). (C) Irregular filaments on linear ds-DNA (3901 bp). Scale bar 500 nm.

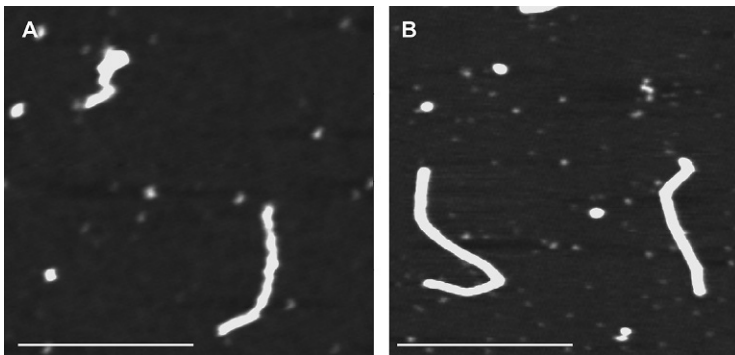


**Fig. 5** Examples of RAD51 filament formation. (A) Irregular filaments on linear ss-DNA (1000 nt). (B) Regular filaments on 3' tailed substrate (1031 nt ss- + 200 bp ds-DNA). Scale bar 500 nm.

5. Under these conditions, ATP + Ca<sup>2+</sup> with 3 bp/nt DNA per monomer, RAD51 forms stable and highly regular filaments that completely cover ds-DNA. The amount of RAD51 has to be carefully titrated for each batch of protein produced. Suboptimal amounts of RAD51 result in partial filaments that tend to cluster/aggregate and complicate analysis (Fig. 4C). This undesired effect can be minimized by addition of 100 mM (final concentration in reaction) K<sub>2</sub>SO<sub>4</sub> or (NH<sub>4</sub>)<sub>2</sub>SO<sub>4</sub> to the filament formation reaction with additional incubation for 10 min at 37°C before deposition. For such reaction, deposit 10 μL directly onto freshly cleaved mica without dilution with deposition buffer. On the other hand, excess protein not bound in filaments will bind to mica resulting in background roughness which can interfere with interpretation and analysis.
6. RAD51 filaments on ss-DNA tend to be more irregular. In order to produce as complete filaments as possible, excess of RAD51 protein can be used (2–1 nucleotide per monomer). Also, incubation time can be increased to 30 min. Filament formation on ss-DNA can be enhanced if the DNA is partially ds- with a ss-tail (Ristic et al., 2005) (Fig. 5).

## 4.3 Joint Molecule Formation

### Buffers and Reagents

1. Reaction buffer: 25–50 mM HEPES or Tris–HCl pH 7.5, 2–5 mM  $\text{CaCl}_2$ , 1–2 mM ATP (buffered to pH 7.5), 30–50 mM KCl, 1 mM DTT.
2. 1 M  $\text{K}_2\text{SO}_4$ .
3. Wash buffer: 10 mM HEPES–KOH pH 7.5, 100 mM KCl.
4. Deposition buffer: 10 mM HEPES–KOH pH 7.5, 10 mM  $\text{MgCl}_2$ .

### Procedure

1. Prepare filament formation reaction with 7.5  $\mu\text{M}$  DNA (nucleotide concentration), 2.5  $\mu\text{M}$  RAD51 in reaction buffer in 10  $\mu\text{L}$  volume.
2. To form joint molecules prepare a reaction with 1–3  $\mu\text{M}$  ds-DNA (bp concentration) in reaction buffer, add 2–3  $\mu\text{L}$  of the ss-DNA filament formation (from step 1) reaction to 10  $\mu\text{L}$  total volume. Incubate for 15 min at 37°C.
3. Add  $\text{K}_2\text{SO}_4$  to 100 mM and incubate for an additional 10 min at 37°C.
4. Deposit this reaction directly onto freshly cleaved mica and incubate for 15 s at room temperature.
5. Wash with  $\sim 500 \mu\text{L}$  of wash buffer, to remove free DNA not captured as joint molecules.
6. Remove excess water by tilting the sample and blotting by the corner of a lint-free wipe.
7. Add 10  $\mu\text{L}$  deposition buffer to the mica to enable DNA to attach.
8. After 5 s, wash mica with  $\sim 500 \mu\text{L}$  of MilliQ water and dry in a filtered stream of air or  $\text{N}_2$  gas.
9. Remove excess water by blotting with the corner of a lint-free wipe.
10. Dry the sample in a gentle stream of filtered air for a minute or so until all visible water has evaporated or been blown off.
11. Mount the metal disc in the SFM and image using Tapping mode, or equivalent, according to instrument instructions.

## 4.4 Notes

1. In vitro joint molecule formation is very sensitive to reaction conditions for filament formation. Filaments can be formed on ss-DNA or, with more success, on 3'-tailed substrates with partial ss- and partial ds-DNA. DNA with longer 3' tail (1000 nt vs 300 nt) pairs more efficiently with homologous template (Wright & Heyer, 2014) (Fig. 6).

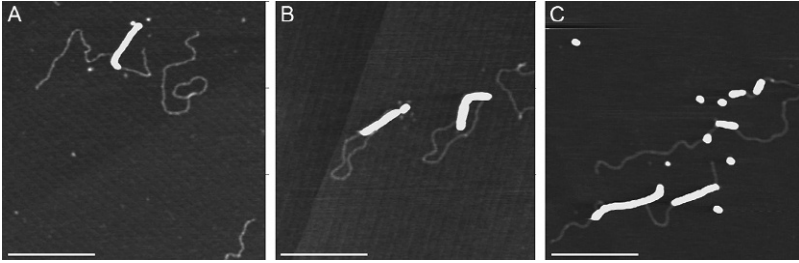


**Fig. 6** Examples of joint molecule formation. (A) With linear homologous template (3901 bp) 3' tailed substrate = 505 bp ds-region and 289 nt 3' overhang. (B) With circular sc homologous template (3901 bp) 3' tailed substrate = 505 bp ds-region and 289 nt 3' overhang. (C) Difficulties in joint molecule formation if excess RAD51 ss-DNA present in filament formation reaction. Filaments formed on 3' tailed substrate (1031 nt ss- + 200 bp ds-DNA). Template is 3901 bp ds-DNA (pDR6/Xmnl). Scale bar 500 nm.

However, longer 3' ss-DNA tail makes it challenging to form fully extended filaments.

2. The amount of RAD51 in the reaction is critical as free protein tends to bind homologous DNA template and complicates subsequent analysis. Optimal ratio for the reaction is three nucleotides or bp of DNA, in the filament formation step, per monomer of RAD51. Careful titration of each batch of RAD51 is usually required.
3. Circular as well as linear DNA can be used as the homologous ds-DNA partner. Efficiency of joint molecules formation is higher with circular DNA. If subsequent analysis will include measuring the position of joint molecule pairing, linear ds-DNA should be used. A defined position of the homologous sequence with respect to the DNA ends allows measuring parameters such as position and length of pairing (Ristic, Kanaar, & Wyman, 2011).

## 4.5 Analysis

To determine the effect of recombination mediators, reaction conditions or specific amino acid mutations in RAD51 on filament formation (Grigorescu et al., 2009; Holthausen et al., 2011), there are a number of parameters that can be analyzed from SFM images.

1. DNA extension upon filament formation can be determined by measuring contour length of visualized filaments. Comparison with contour length of bare DNA and RAD51 filaments on the same bp length of DNA indicates that bound DNA is extended up to  $1.5 \times B$  form length for complete continuous filaments.

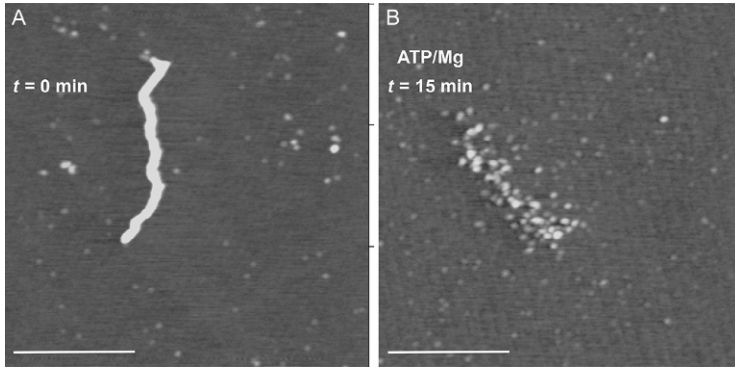
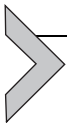


**Fig. 7** Example of filament disassembly upon changing buffer conditions. (A) RAD51 filament formed on ds-DNA, 1.8 kb, in ATP+CaCl<sub>2</sub> conditions, where ATP hydrolysis is inhibited. (B) Partially disassembled RAD51 filament on ds-DNA, 1.8 kb, after buffer exchange allowing ATP hydrolysis on mica for the indicated time. Scale bar 500 nm.

2. The continuity and stiffness of filaments can also be quantified by determining the apparent persistence length of filaments based on well-known relationship between the end-to-end distance and contour length (Modesti et al., 2007).
3. Regularity or continuity of filaments is also identified by positions where protein is lacking, detected as “gaps” in the height profile or kinks in filament trajectory (Modesti et al., 2007; Ristic et al., 2011, 2005).
4. Even while immobilized on mica, RAD51 retains its ability to hydrolyze ATP and disassemble from DNA (Fig. 7). This can be analyzed by buffer exchange on mica. After deposition in conditions that do not allow ATP hydrolysis, bulk liquid is removed by wicking with a tissue from the mica edge and replaced by 10  $\mu$ L of reaction buffer including ATP and MgCl<sub>2</sub>. At defined time points after buffer addition and incubation at room temperature the mica is washed and dried as described earlier for SFM imaging (Ristic et al., 2005).



## 5. IDENTIFYING SPECIFIC PROTEINS IN COMPLEX STRUCTURES BY FLUORESCENCE: BRCA2–RAD51 COMPLEXES ANALYZED BY TIRF–SFM

Conventional SFM images as we describe here provide information on shape and size of objects but cannot identify individual specific proteins in complex structures that simply get bigger and more variable as additional components are added. However, recent advances combining SFM with

other imaging modalities (Dazzi et al., 2012; Ebenstein, Gassman, Kim, & Weiss, 2009; Sanchez et al., 2013), especially with fluorescence, can identify specific molecular constituents and provide coherent quantitative analysis of multimolecular assemblies. We have developed methods to successfully analyze the complex molecular machinery of HR. Here we describe molecular complexes of BRCA2 and RAD51, using SFM coupled to TIRF microscopy. The sample preparation for TIRF–SFM experiment is more challenging, in comparison to regular SFM. Most notably, for fluorescent imaging the sample needs to be optically transparent and for SFM atomically flat at the same time. In addition, for optimal excitation of the fluorophores from the evanescent field (generated due to total internal reflection) on a composite substrate of glass coverslip and mica, the mica layer needs to be just a few basal layers thick. However, important protein–protein and protein–DNA interaction parameters can uniquely be obtained, justifying the additional sample preparation complexity. Considering the example of BRCA2–RAD51 interaction, TIRF–SFM was used to determine the number of RAD51 molecules interacting per BRCA2 molecule under different solution conditions. In addition we determined the amount of BRCA2 and RAD51 that interact with ss-DNA in different conditions representing stages of filament formation. Sequential changes in the stoichiometry of biomolecules, interactions in a multicomponent process, can help elucidate the mechanism steps of the processes.

Full-length BRCA2 was purified as described (Jensen et al., 2010; Sanchez et al., 2017). Human RAD51 was expressed and purified as described (Modesti et al., 2007). Purified RAD51 was labeled, one fluorophore per monomer, with AF 488 at C319 using thiol maleimide chemistry. The fluorescent signal indicated the presence of RAD51, and calibrated intensity was used to determine number of monomers.

## Equipment

1. SFM instrument coupled with a TIRF microscope (e.g., Nanowizard II scanner from JPK with Nikon TE 2000U microscope). In combined SFM–TIRF microscopy, it is essential that the optical and topographic image overlay with nm precision. This can be achieved by the instrument overlaying software (e.g., JPK DirectOverlay™) but requires custom workflows for more precision, such as those we have developed which provide up to 40 nm alignment accuracy (Sanchez, Kanaar, & Wyman, 2010).
2. UV lamp for curing adhesive.

## Buffers and Reagents

1. Sample buffer: 12.5 mM HEPES pH 8.2, 4 mM Tris-HCl pH 7.5, 3.25% glycerol, 125 mM NaCl, 65 mM KCl, 0.4 mM DTT, 0.17 mM EDTA.
2. Deposition buffer: 10 mM HEPES-KCl pH 8.2, 10 mM MgCl<sub>2</sub>.
3. 0.25% Sodium tetrahydridoborate solution (aq. w/v).
4. Fluorescent fiducial markers (e.g., 0.04 μm Ø TransFluoSpheres, 488/645, from Invitrogen).
5. Electron microscopy grade glutaraldehyde, in single use glass ampules.

## Other Supplies

1. 10-mm Ø mica discs, Muscovite-V1 quality (e.g., from EMS). The required mica disc can be punched out of a mica sheet using a punch and die set.
2. 24-mm Ø clean glass coverslips, round, #0 (0.08–0.12 mm) (e.g., from Menzel-Gläser).
3. Optical adhesive (e.g., NOA88 from Norland products).
4. Clear adhesive tape (e.g., 3M Scotch™ tape).
5. Lint-free wipes (e.g., Kim wipes).

## Procedure

1. Prepare mica substrate for sample deposition: For TIRF microscopy the sample should be optically transparent. This can be achieved by using an assembly of glass coverslip and thin mica. The mica discs are typically punched out of 0.15 to 0.21-mm or 0.26 to 0.31-mm thick mica sheets. Muscovite-V1 is the clearest quality of mica with no color or inclusion; however, at the supplied thickness it is too thick for TIRF microscopy.
  - a. Using a scalpel tip, split the mica disc into thinner sections.
  - b. Attach the thin mica disc on the glass coverslip with optical adhesive.
  - c. After curing of the adhesive, cleave the mica further to make it just a few atomic layer thick. Cleaving mica to such transparency and thickness is tricky and needs practice.
  - d. Next, treat the mica surface with 0.25% sodium tetrahydridoborate solution (aq. w/v) at room temperature for 20 min, to reduce background fluorescence signal. Rinse with MilliQ water.
2. Form BRCA2-RAD51 complexes by incubating 25 nM BRCA2 with 600 nM RAD51, fluorescently labeled as described (Modesti et al., 2007), in sample buffer for 30 min at 37°C.
3. Add glutaraldehyde to a final concentration of 0.12% to crosslink the protein sample and incubate for additional 5 min at 37°C.

- a. Fixation or crosslinking of the sample should be avoided as much as possible to visualize native protein–protein or protein–DNA interactions. In some cases we observe significantly reduced background for crosslinked vs noncrosslinked samples. Alternatively when potentially dynamic or short-lived reactions are to be observed, crosslinking effectively freezes a snapshot representing the mixture of molecular complexes present in a reaction.
4. Add 50 mM Tris–HCl pH 7.5 to quench excess glutaraldehyde.
5. Dilute sample 20–200 times in deposition buffer to reduce background fluorescence from free RAD51.
6. Add 3 pM TranFluospheres fiducial markers.
7. Deposit 20  $\mu$ L of this sample on the prepared mica substrate. Adsorb for 1 min. Rinse the mica with about 1 mL of MilliQ water and dry in stream of filtered air. Image with TIRF–SFM (see Fig. 8 for schematic overview of TIRF–SFM work flow).
8. Obtain a TIRF optical image of the fluorescent signal at wavelength appropriate for imaging the fiducials.
9. Obtain a TIRF optical image of the fluorescent signal at a wavelength appropriate for imaging the sample. We typically collect a stack of exposures from this sample field, 300 frames, each as 300 ms exposures.
10. Collect SFM topographic image of the same area.

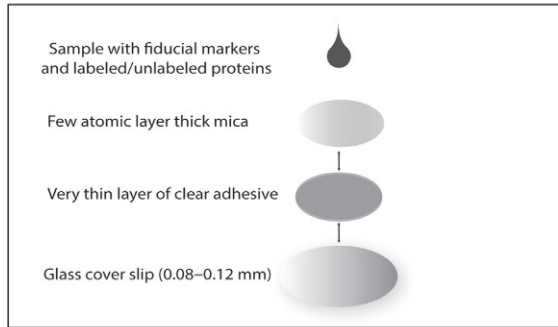
## 5.1 Tips for SFM–TIRF Imaging

1. Optimal density of the sample is crucial for reliable TIRF–SFM data. While SFM provides nanometer resolution, TIRF resolution is diffraction limited. Therefore, the (fluorescent) proteins or complexes must be distributed so that their fluorescent signals do not overlap. Typically molecules should be  $>250$  nm apart (Fig. 9).
2. Large scan sizes (e.g.,  $35 \times 35 \mu\text{m}$ ) provide optimal overlay of SFM and TIRF images.
3. To maintain high resolution in terms of pixel size and slow scan rate for good image quality. We have best success collecting such large topographic images overnight.
4. There should be at least three fiducial markers in a given field of view for precise alignment of fluorescence and SFM image (Fig. 10).

## 5.2 Notes

1. NOA 88 cures at long wavelength UV light (315–395 nm) with an optimum at 365 nm.
2. There should be no air bubbles between the mica and the glass coverslip.

## Sample preparation



## Imaging

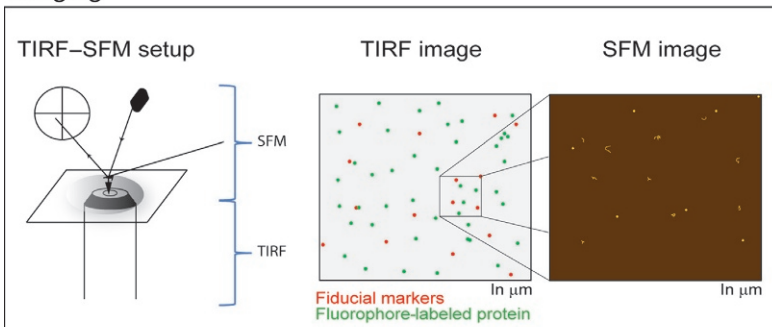


## Image processing

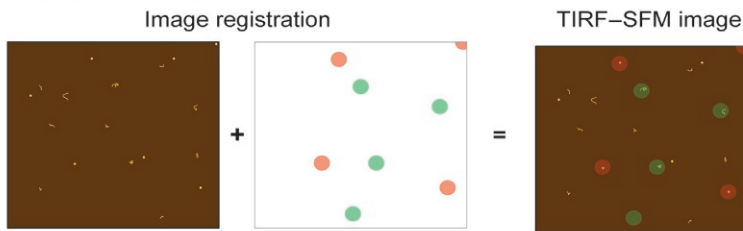


**Fig. 8** Overview of steps in experiments applying TIRF-SFM imaging. Schematic representation of sample preparation steps, image collection aspects, and required post collection image processing to create merged fluorescent and topographic data.

3. The excitation wavelength of the sample fluorophore and the fiducial markers should not overlap to avoid photobleaching of the sample while focusing.
4. Obtaining large size scans at high resolution require several hours to overnight to collect. A microscopy environment that limits vibrations and noise is required.

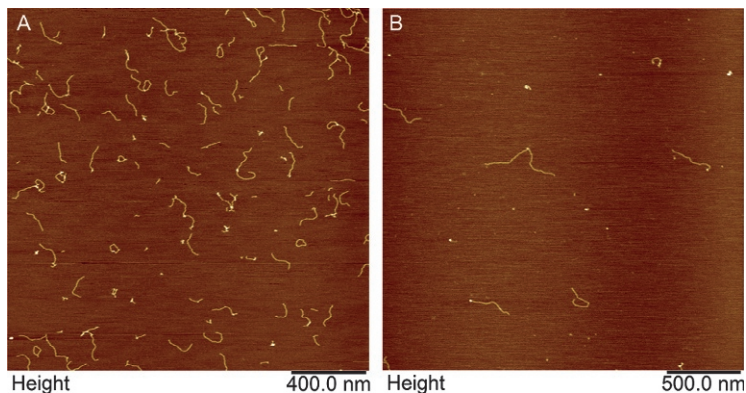


**Fig. 9** Representative image, example of DNA molecules, comparing optimal mica coverage for (A) SFM and (B) TIRF–SFM imaging where molecules/complexes with potential fluorescent signals have to be separated by  $>200$  nm.

### 5.3 Image Analysis and Quantification

Analysis of the TIRF–SFM data requires the following general steps: Locate the position of the fiducials and the sample from the fluorescence signals, register TIRF and SFM images, and quantify the amount of fluorescence for each ROI (for detailed description, see [Sanchez et al., 2013](#)). The topographic SFM image can be used to analyze objects with respect their size and shape as described in previous sections. The addition of fluorescence localization and fluorescence intensity adds considerable functional information for multicomponent complexes such as BRCA2–RAD51. We have used this to analyze the role of BRCA2 in setting up RAD51 filaments in collaboration with other HR proteins for eventual DNA strand exchange.

1. Determine the locations of each fluorescent signal (ROI) by accumulating the signal from sets of 10 consecutive frames, (3s total exposure time) in a single frame; repeat for frames 2–11, etc., until all frames have been accounted for.
2. From each ROI, the position is calculated by fitting the fluorescent signal, summed over 10 frames, with a two-dimensional Gaussian function (nonlinear least-squares method) to determine the mean of this intensity distribution. This operation is repeated with the next 10 consecutive frames until last frame acquired, generating a cloud of positions per ROI. Finally, from each ROI, both from the fiducials and sample, the centroid of the cluster can be estimated from a normal fitting.
3. Register TIRF and SFM images by matching the “optical” centroid with the “topographic” center of mass of the fiducials ([Fig. 10](#)). This will produce a matrix with the scaling ( $S$ ) and translation factor ( $T$ ) needed for the sample.

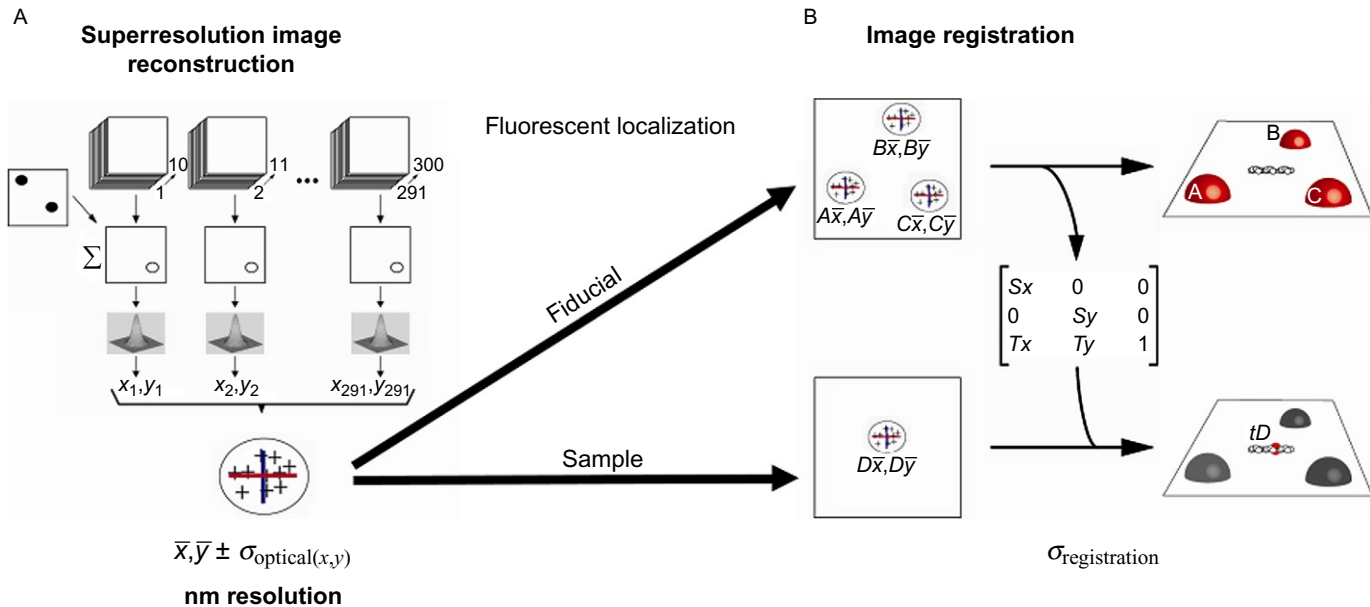
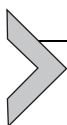


**Fig. 10** Flowchart illustrating steps in TIRF-SFM image processing for registration and eventual analysis. (A) The fluorescent signals coming from the fiducials and the sample are separately processed (collected at different wavelengths). The X-Y coordinates of the fluorescent source are calculated from the point spread function from the sum of 10 frames, and the uncertainty for this localization is determined based on the cloud as indicated in the summed image by the large “+” sign (vertical = uncertainty in Y and horizontal = uncertainty in X). (B) The location of the fiducials as determined in (A) is mapped onto their topographic center of mass (objects labeled A, B, and C) to create a transformation matrix which is then applied to the sample fluorescent localization to determine their position with respect to the sample topographic image (object labeled D).

4. Quantify the number of fluorophores per ROI based on stepwise photobleaching, calibrated by the signal from a single fluorophores:
  - a. Correct individual frames for background and select ROIs.
  - b. Extract from each ROI the intensity ( $N$ ) trace over time.
  - c. Variations in intensity can be estimated with a step fitting algorithm (Kersemaekers et al., 2006; van Mameren et al., 2009) and the intensity of a single fluorophore defined as the average step size for each ROI. This number ( $\Delta N$ ) divided by the maximum  $N$  in the ROI represents the number of fluorophores. It is useful to calibrate this type of measurement with objects with a known number of fluorophores, for example, a stoichiometrically labeled protein(complex) defined by size based on SFM volume.



## 6. CONCLUSIONS

SFM-based approaches provide unique information probing the nanoscale properties of biomolecules. Most importantly they help to bridge the gap between the atomic resolution structural studies and the cell-based microscopic studies. Because only low concentrations of proteins are needed, SFM is an indispensable practical tool to study hard to purify proteins and their complexes. In addition the advantage of observing, categorizing, and quantifying all examples in a sample reveals conformational plasticity and multimerization under various conditions. SFM-based approaches have also been especially useful in elucidating DNA protein interactions for complex multistep biological processes like HR repair. Stoichiometry and assembly–disassembly of proteins into DNA-based multi-molecular complexes can be accurately investigated by staging reactions based on biochemically defined conditions. Fluorescence–coupled SFM in TIRF mode allows identifying one or more protein molecule(s) with fluorescent dyes thus combining the versatility of fluorescence with accuracy and ease of SFM to study molecular reactions at single-molecule resolution.

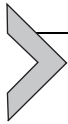
## REFERENCES

- Chada, N., Sigdel, K. P., Gari, R. R., Matin, T. R., Randall, L. L., & King, G. M. (2015). Glass is a viable substrate for precision force microscopy of membrane proteins. *Scientific Reports*, 5, 12550. <https://doi.org/10.1038/srep12550>.
- Cisneros, D. A., Muller, D. J., Daud, S. M., & Lakey, J. H. (2006). An approach to prepare membrane proteins for single-molecule imaging. *Angewandte Chemie (International Edition in English)*, 45(20), 3252–3256. <https://doi.org/10.1002/anie.200504506>.

- Dazzi, A., Prater, C. B., Hu, Q., Chase, D. B., Rabolt, J. F., & Marcott, C. (2012). AFM-IR: Combining atomic force microscopy and infrared spectroscopy for nanoscale chemical characterization. *Applied Spectroscopy*, *66*(12), 1365–1384. <https://doi.org/10.1366/12-06804>.
- Ebenstein, Y., Gassman, N., Kim, S., & Weiss, S. (2009). Combining atomic force and fluorescence microscopy for analysis of quantum-dot labeled protein-DNA complexes. *Journal of Molecular Recognition*, *22*(5), 397–402. <https://doi.org/10.1002/jmr.956>.
- Fuentes-Perez, M. E., Dillingham, M. S., & Moreno-Herrero, F. (2013). AFM volumetric methods for the characterization of proteins and nucleic acids. *Methods*, *60*(2), 113–121. <https://doi.org/10.1016/j.ymeth.2013.02.005>.
- Grigorescu, A. A., Vissers, J. H., Ristic, D., Pigli, Y. Z., Lynch, T. W., Wyman, C., et al. (2009). Inter-subunit interactions that coordinate Rad51's activities. *Nucleic Acids Research*, *37*(2), 557–567. <https://doi.org/10.1093/nar/gkn973>.
- Grosbart, M., Ristic, D., Sanchez, H., & Wyman, C. (2018). Imaging of DNA and protein by SFM and combined SFM-TIRF microscopy. *Methods in Molecular Biology*, *1665*, 259–280. [https://doi.org/10.1007/978-1-4939-7271-5\\_14](https://doi.org/10.1007/978-1-4939-7271-5_14).
- Holthausen, J. T., van Loenhout, M. T., Sanchez, H., Ristic, D., van Rossum-Fikkert, S. E., Modesti, M., et al. (2011). Effect of the BRCA2 CTRD domain on RAD51 filaments analyzed by an ensemble of single molecule techniques. *Nucleic Acids Research*, *39*(15), 6558–6567. <https://doi.org/10.1093/nar/gkr295>.
- Jensen, R. B., Carreira, A., & Kowalczykowski, S. C. (2010). Purified human BRCA2 stimulates RAD51-mediated recombination. *Nature*, *467*(7316), 678–683. <https://doi.org/10.1038/nature09399>.
- Kersemakers, J. W., Munteanu, E. L., Laan, L., Noetzel, T. L., Janson, M. E., & Dogterom, M. (2006). Assembly dynamics of microtubules at molecular resolution. *Nature*, *442*(7103), 709–712. <https://doi.org/10.1038/nature04928>.
- Kolinjivadi, A. M., Sannino, V., de Antoni, A., Techer, H., Baldi, G., & Costanzo, V. (2017). Moonlighting at replication forks—A new life for homologous recombination proteins BRCA1, BRCA2 and RAD51. *FEBS Letters*, *591*(8), 1083–1100. <https://doi.org/10.1002/1873-3468.12556>.
- Maslova, M. V., Gerasimova, L. G., & Forsling, W. (2004). Surface properties of cleaved mica. *Colloid Journal*, *66*(3), 322–328. <https://doi.org/10.1023/B:COLL.0000030843.30563.c9>.
- Mehta, A., & Haber, J. E. (2014). Sources of DNA double-strand breaks and models of recombinational DNA repair. *Cold Spring Harbor Perspectives in Biology*, *6*(9), a016428. <https://doi.org/10.1101/cshperspect.a016428>.
- Modesti, M., Ristic, D., van der Heijden, T., Dekker, C., van Mameren, J., Peterman, E. J., et al. (2007). Fluorescent human RAD51 reveals multiple nucleation sites and filament segments tightly associated along a single DNA molecule. *Structure*, *15*(5), 599–609. <https://doi.org/10.1016/j.str.2007.04.003>.
- Moreno-Herrero, F., de Jager, M., Dekker, N. H., Kanaar, R., Wyman, C., & Dekker, C. (2005). Mesoscale conformational changes in the DNA-repair complex Rad50/Mre11/Nbs1 upon binding DNA. *Nature*, *437*(7057), 440–443. <https://doi.org/10.1038/nature03927>.
- Prakash, R., Zhang, Y., Feng, W., & Jasin, M. (2015). Homologous recombination and human health: The roles of BRCA1, BRCA2, and associated proteins. *Cold Spring Harbor Perspectives in Biology*, *7*(4), a016600. <https://doi.org/10.1101/cshperspect.a016600>.
- Rahman, M., Neff, D., Green, N., & Norton, M. L. (2016). DNA origami reorganizes upon interaction with graphite: Implications for high-resolution DNA directed protein patterning. *Nanomaterials (Basel)*, *6*(11), E196. <https://doi.org/10.3390/nano6110196>.
- Ratcliff, G. C., & Erie, D. A. (2001). A novel single-molecule study to determine protein-protein association constants. *Journal of the American Chemical Society*, *123*(24), 5632–5635. <https://doi.org/10.1021/ja005750n>.

- Ristic, D., Kanaar, R., & Wyman, C. (2011). Visualizing RAD51-mediated joint molecules: Implications for recombination mechanism and the effect of sequence heterology. *Nucleic Acids Research*, 39(1), 155–167. <https://doi.org/10.1093/nar/gkq766>.
- Ristic, D., Modesti, M., van der Heijden, T., van Noort, J., Dekker, C., Kanaar, R., et al. (2005). Human Rad51 filaments on double- and single-stranded DNA: Correlating regular and irregular forms with recombination function. *Nucleic Acids Research*, 33(10), 3292–3302. <https://doi.org/10.1093/nar/gki640>.
- Sanchez, H., Kanaar, R., & Wyman, C. (2010). Molecular recognition of DNA-protein complexes: A straightforward method combining scanning force and fluorescence microscopy. *Ultramicroscopy*, 110(7), 844–851. <https://doi.org/10.1016/j.ultramic.2010.03.002>.
- Sanchez, H., Kertokallio, A., van Rossum-Fikkert, S., Kanaar, R., & Wyman, C. (2013). Combined optical and topographic imaging reveals different arrangements of human RAD54 with presynaptic and postsynaptic RAD51–DNA filaments. *Proceedings of the National Academy of Sciences of the United States of America*, 110(28), 11385–11390. <https://doi.org/10.1073/pnas.1306467110>.
- Sanchez, H., Paul, M. W., Grosbart, M., van Rossum-Fikkert, S. E., Lebbink, J. H. G., Kanaar, R., et al. (2017). Architectural plasticity of human BRCA2–RAD51 complexes in DNA break repair. *Nucleic Acids Research*, 45(8), 4507–4518. <https://doi.org/10.1093/nar/gkx084>.
- Sanchez, H., & Wyman, C. (2015). SFMetrics: An analysis tool for scanning force microscopy images of biomolecules. *BMC Bioinformatics*, 16, 27. <https://doi.org/10.1186/s12859-015-0457-8>.
- Shahid, T., Soroka, J., Kong, E. H., Malivert, L., McIlwraith, M. J., Pape, T., et al. (2014). Structure and mechanism of action of the BRCA2 breast cancer tumor suppressor. *Nature Structural and Molecular Biology*, 21(11), 962–968. <https://doi.org/10.1038/nsmb.2899>.
- Stracker, T. H., Theunissen, J. W., Morales, M., & Petrini, J. H. (2004). The Mre11 complex and the metabolism of chromosome breaks: The importance of communicating and holding things together. *DNA Repair (Amst)*, 3(8–9), 845–854. <https://doi.org/10.1016/j.dnarep.2004.03.014>.
- Thorslund, T., McIlwraith, M. J., Compton, S. A., Lekomtsev, S., Petronczki, M., Griffith, J. D., et al. (2010). The breast cancer tumor suppressor BRCA2 promotes the specific targeting of RAD51 to single-stranded DNA. *Nature Structural and Molecular Biology*, 17(10), 1263–1265. <https://doi.org/10.1038/nsmb.1905>.
- Uversky, V. N. (2016). p53 proteoforms and intrinsic disorder: An illustration of the protein structure-function continuum concept. *International Journal of Molecular Sciences*, 17(11), E1874. <https://doi.org/10.3390/ijms17111874>.
- van Gent, D. C., Hoeijmakers, J. H., & Kanaar, R. (2001). Chromosomal stability and the DNA double-stranded break connection. *Nature Reviews. Genetics*, 2(3), 196–206. <https://doi.org/10.1038/35056049>.
- van Mameren, J., Modesti, M., Kanaar, R., Wyman, C., Peterman, E. J., & Wuite, G. J. (2009). Counting RAD51 proteins disassembling from nucleoprotein filaments under tension. *Nature*, 457(7230), 745–748. <https://doi.org/10.1038/nature07581>.
- van Raaij, M. E., Segers-Nolten, I. M., & Subramaniam, V. (2006). Quantitative morphological analysis reveals ultrastructural diversity of amyloid fibrils from alpha-synuclein mutants. *Biophysical Journal*, 91(11), L96–98. <https://doi.org/10.1529/biophysj.106.090449>.
- Wright, W. D., & Heyer, W. D. (2014). Rad54 functions as a heteroduplex DNA pump modulated by its DNA substrates and Rad51 during D loop formation. *Molecular Cell*, 53(3), 420–432. <https://doi.org/10.1016/j.molcel.2013.12.027>.
- Wyman, C., Rombel, I., North, A. K., Bustamante, C., & Kustu, S. (1997). Unusual oligomerization required for activity of NtrC, a bacterial enhancer-binding protein. *Science*, 275(5306), 1658–1661.

- Yang, H., Jeffrey, P. D., Miller, J., Kinnucan, E., Sun, Y., Thoma, N. H., et al. (2002). BRCA2 function in DNA binding and recombination from a BRCA2-DSS1-ssDNA structure. *Science*, *297*(5588), 1837–1848. <https://doi.org/10.1126/science.297.5588.1837>.
- Yang, H., Li, Q., Fan, J., Holloman, W. K., & Pavletich, N. P. (2005). The BRCA2 homologue Brh2 nucleates RAD51 filament formation at a dsDNA-ssDNA junction. *Nature*, *433*(7026), 653–657. <https://doi.org/10.1038/nature03234>.
- Yang, G. L., Vesenka, J. P., & Bustamante, C. J. (1996). Effects of tip-sample forces and humidity on the imaging of DNA with a scanning force microscope. *Scanning*, *18*(5), 344–350.



# Single-Molecule Dynamics and Localization of DNA Repair Proteins in Cells

Maarten W. Paul\*, Alex N. Zelensky\*, Claire Wyman\*,<sup>†</sup>  
Roland Kanaar\*,<sup>1</sup>

\*Department of Molecular Genetics, Cancer Genomics Center Netherlands, Erasmus University Medical Center, Rotterdam, The Netherlands

<sup>†</sup>Department of Radiation Oncology, Erasmus University Medical Center, Rotterdam, The Netherlands

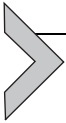
<sup>1</sup>Corresponding author: e-mail address: r.kanaar@erasmusmc.nl

## Contents

|  |     |
|--|-----|
| 1. Introduction  | 376 |
| 2. Generating Cells With Endogenously Expressed Fusion Proteins for Live-Cell Imaging                            | 378 |
| 2.1 Fluorescent Proteins   | 378 |
| 2.2 Self-ligating Tags   | 380 |
| 2.3 Genomic Engineering by HR and CRISPR/Cas9-Induced DSBs   | 380 |
| 2.4 Protocol: Engineering sgRNA for <i>S. pyogenes</i> Cas9, and Donor Construct for C-Terminal HaloTag Knock-In | 382 |
| 2.5 Protocol: CRISPR/Cas9-Stimulated Gene Targeting in Mouse ES Cells  | 385 |
| 2.6 Protocol: Preparing Cells for Imaging  | 387 |
| 3. Mobility Assays   | 389 |
| 3.1 Fluorescence Recovery After Photobleaching   | 389 |
| 3.2 Fluorescence Correlation Spectroscopy  | 389 |
| 3.3 Single-Particle Tracking   | 390 |
| 3.4 Protocol: Live-Cell Particle Tracking Using HiLo Illumination Microscopy                                     | 393 |
| 3.5 Data Analysis: Tracking Individual Fluorescent Particles in Live Cells and Characterizing (Im)mobility       | 394 |
| 4. Relative Position of Proteins in DSB Foci   | 396 |
| 4.1 Super-Resolution Microscopy  | 396 |
| 4.2 Protocol: Dual-Color Super-Resolution Imaging of Nuclear Proteins  | 399 |
| 4.3 Data Analysis: Dual-Color SMLM   | 401 |
| 4.4 Single-Molecule Colocalization Analysis  | 402 |
| 5. Conclusion/Perspective  | 403 |
| References   | 404 |

## Abstract

Direct observation of individual protein molecules in their native environment, at nanometer resolution, in a living cell, in motion is not only fascinating but also uniquely informative. Several recent major technological advances in genomic engineering, protein and synthetic fluorophore development, and light microscopy have dramatically increased the accessibility of this approach. This chapter describes the procedures for modifying endogenous genomic loci to producing fluorescently tagged proteins, their high-resolution visualization, and analysis of their dynamics in mammalian cells, using DNA repair proteins BRCA2 and RAD51 as an example.



## 1. INTRODUCTION

Among the different pathways to repair DNA double-strand breaks (DSBs) homologous recombination (HR) is considered the most faithful mechanism, making use of an intact homologous DNA template to restore the information lost to the lesion. Among the many proteins involved in repair of broken DNA the recombinase RAD51 is essential for homology recognition and strand invasion of the homologous DNA template, most often provided by the sister chromatid. In higher eukaryotes, the displacement of RPA and loading of RAD51 onto the resected single-strand (ss) DNA ends of the break is facilitated by BRCA2 (Prakash, Zhang, Feng, & Jasin, 2015). BRCA2 is a large multidomain protein that can interact with multiple RAD51 protomers per BRCA2 molecule. The localization of BRCA2 and consequently RAD51 to a DSB is regulated by the interactions of BRCA2 with PALB2 and its interactor BRCA1. The localization of these HR proteins is also cell cycle regulated, since the sister chromatid required for HR-mediated DSB repair limits the process to S and G2 of the cell cycle. In S phase HR, and thus BRCA2 and RAD51 function, is also essential to underpin DNA replication by rescuing stalled and broken replication forks (Schlacher et al., 2011).

Delivery of proteins to the right place, at the right time, at the site of damage, occurs through diffusion, followed by stabilization of interactions between the different proteins and/or the DNA substrate. In case a lesion is repaired through HR, RAD51 needs to be faithfully delivered to the ssDNA at the DSB, while complex formation on undamaged chromatin needs to be prevented. The interaction of BRCA2 with RAD51 potentially prevents interaction of RAD51 with the undamaged DNA while diffusing in the nucleus. Analysis of the mobility of endogenous BRCA2 and RAD51

in living cells showed that BRCA2 and RAD51 diffuse together as a oligomeric complex before engaging with DNA damage (Fig. 1) (Reuter et al., 2014). The BRCA2 complex is transiently immobilized, and upon damage induction an increase in immobilization of BRCA2 is observed. Measurement of the mobility of endogenous fluorescently tagged proteins in living cells allows quantitative analysis of how DNA repair proteins end up and engage at the sites of damage. By employing different techniques (fluorescence correlation spectroscopy (FCS), fluorescence recovery after photobleaching (FRAP), and single-particle tracking) proteins can be studied at a range of timescales, from milliseconds to minutes (Reuter et al., 2014; Van Royen et al., 2014). All visualization techniques in live cells require the proteins to be tagged so that they can be made to emit a fluorescent signal. To ensure proper regulation of expression and native concentration

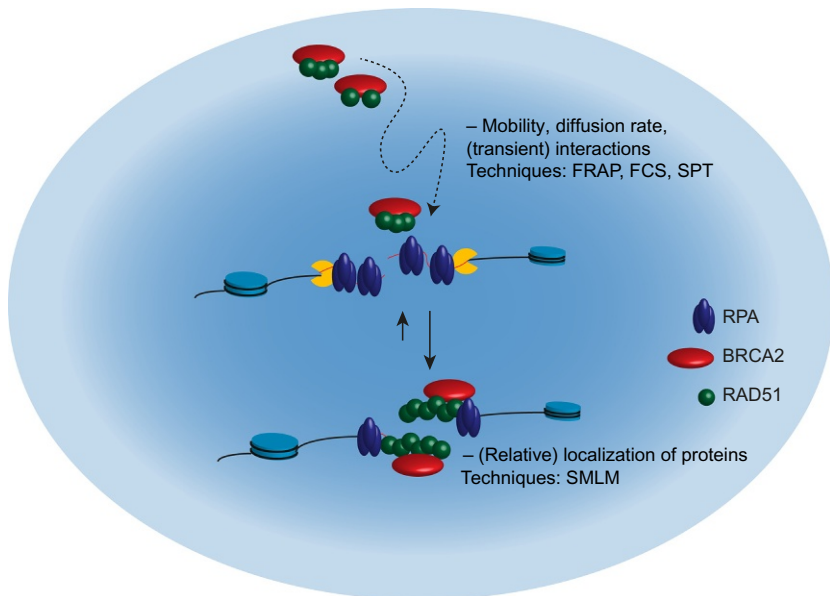
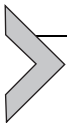


**Fig. 1** Studying the dynamics and localization of BRCA2 and RAD51 molecules in intact cells. BRCA2 and RAD51 diffuse as a complex throughout the nucleus. To analyze the dynamics and diffusion of proteins in living cells different fluorescence-based assays are available. Upon engagement of BRCA2 and RAD51 with the sites of DNA damage the complex possibly reorganizes. The organization of the proteins at the sites of damage can be studied by super-resolution techniques. *FCS*, fluorescence correlation spectroscopy; *FRAP*, fluorescence recovery after photobleaching; *SIM*, structured illumination microscopy; *SMLM*, single-molecule localization microscopy; *SPT*, single-particle tracking.

of the proteins to preserve their stoichiometry relative to their interacting partners, the tagged proteins should be expressed from their endogenous locus. Using CRISPR/Cas9-mediated integration of a protein tag encoding DNA sequence at the proper gene locus has become straightforward.

After the site of damage has been marked by signaling proteins, it is processed for repair. This involves the accumulation of some of the HR repair proteins in high local concentration, which can be observed under the microscope as nuclear foci. The protein distribution within the DSB foci is difficult to assess with conventional fluorescence microscopy because of the small size of the foci and the large number of proteins present in the foci. Advances in super-resolution microscopy make it feasible to determine the organization of the protein molecules at the sites of damage, providing a high-resolution map of individual DSB foci. The relative positioning of different proteins can provide mechanistic insights into the function of proteins at the DSB, and help to better define the nature of DSB foci. For example, why do so many copies of proteins accumulate when only a few proteins are needed to act on the DNA? Upon association with the DSB BRCA2 can displace RPA and deliver RAD51 on to the DNA. The BRCA2–RAD51 complex might reorganize to release RAD51 from BRCA2, which then allows RAD51 to employ its function. Using single-molecule localization microscopy (SMLM) we indeed observed that BRCA2 and RAD51, while complexed before the engagement of damage, are to a large extent separated inside a DSB focus (Sánchez et al., 2017) (Fig. 1).

In this chapter, we describe recent genome manipulation techniques to precisely modify mammalian cells such that they encode (fluorescently) tagged and mutant proteins from endogenous loci. Subsequently, we discuss the acquisition and analysis of the mobility of these fluorescently tagged proteins. Finally, we describe how SMLM can be used to analyze the organization of DSB foci.



---

## **2. GENERATING CELLS WITH ENDOGENOUSLY EXPRESSED FUSION PROTEINS FOR LIVE-CELL IMAGING**

### **2.1 Fluorescent Proteins**

Detecting the fluorescence of tagged proteins at the endogenous level, especially for proteins with a low expression level, can be demanding. Therefore, it is important to consider the most optimal fluorophores for the experiments. The different microscopy-based mobility assays available

such as, FRAP, FCS, and particle tracking have specific demands of fluorescent (protein) tags, but several common characteristics can be defined. The most important characteristics of the fluorescent probes are brightness, photostability, and blinking behavior. The brightness is the product of the number of photons the fluorescent dye can absorb and the fraction of these photons that results in fluorescence decay. The brighter the individual molecules are, the easier it is to detect them. The photostability of the protein defines how much light the molecule can absorb before it bleaches and loses its fluorescence. A third characteristic is blinking of the fluorescent molecule; when molecules are excited by light there is a chance they temporarily become nonfluorescent. For all different mobility assays blinking is an important factor to take into account when performing the analysis. The optimized version of GFP (EGFP) is in many cases a good choice to be used for different assays; as a fluorescent protein it is relatively bright, photostable, and its blinking behavior is well defined. YFP is another option which is useful for FCS due to its different blinking behavior compared to GFP, and can also be used in FRAP and particle tracking. Orange and red fluorescent proteins, such as mCherry and mOrange, are often less bright and photostable and therefore less suitable for these assays; however, fluorescent proteins are under continuous development and optimized for different properties (Cranfill et al., 2016).

Single-particle tracking requires fluorescent molecules which are bright and preferably can be followed as long as possible. GFP and its variants can be used to follow individual proteins (or clusters) under the microscope. This, however, is restricted to proteins which are expressed at a sufficient low concentration such that the signals of the individual particles can be distinguished. BRCA2 is present at an estimated concentration between 3 and 15 nM. At a concentration below 10 nM particles will be on average sufficiently far apart to be detected individually (Reuter et al., 2014). Additionally, proteins present in a multimeric form, as is the case for BRCA2, can be more easily followed by particle tracking because of the brighter signals resulting from multiple proteins in the clusters. This also reduces the number of overlapping signals, since the effective concentration of diffusing particles is reduced. For many other proteins which are present at a higher concentration the signals of molecules will overlap and extensive bleaching is required before individual molecules can be detected or tracked. A possible solution is to use photoactivatable (PA-GFP, PA-mCherry) or photoconvertible proteins (PS-CFP2, mEos2, mMaple3). This makes it possible to track a few proteins at a time while using photoconversion to

continuously photoactivate a few additional proteins. It is important to realize that when using photoactivatable proteins the cells are nonfluorescent before imaging, which makes it challenging to locate cells of interest. In addition, photoconvertible proteins such as mEos2 and mMaple3 have lower brightness and photostability compared to EGFP (Wang, Moffitt, Dempsey, Xie, & Zhuang, 2014). Although they have been used for particle tracking, the fast bleaching causes the observed tracks to be short.

## 2.2 Self-ligating Tags

To overcome the limited brightness and stability of fluorescent proteins for single-particle tracking self-ligating tags such as SNAP-tag and HaloTag allow incorporation of bright organic dyes (Keppler, Pick, Arrivoli, Vogel, & Johnsson, 2004; Los et al., 2008). These tags are expressed as fusion proteins in cells, but require the addition of fluorescent dyes to the cell medium right before image acquisition. By controlling the amount of dye added to the cells it is possible to label only a fraction of all fusion proteins present, making it easier to track individual molecules. Several studies using self-ligating tags to analyze the dynamics of nuclear proteins have already demonstrated these advantages (Hansen, Pustova, Cattoglio, Tjian, & Darzacq, 2017; Liu et al., 2014; Stracy, Uphoff, Garza de Leon, & Kapanidis, 2014; Zhen et al., 2016). SNAP-tag and HaloTag are compatible labeling techniques and can be used together for dual-color imaging. While deciding on which tag to use for a particular study, it is important to realize the origins of the tags. For example, the SNAP-tag is a mutant version of the human O6-alkylguanine-DNA alkyl transferase (AGT) DNA repair protein, which interacts with BRCA2 (Philip et al., 2008), and therefore may not be the most optimal tag for use in the study of HR proteins. The HaloTag instead is based on the bacterial haloalkane dehalogenase protein. Finally, it is important to keep in mind that not all SNAP-tag and HaloTag ligands are cell permeable. Recently improved cell-permeable dyes have been developed, as SNAP-tag and HaloTag ligands (Grimm et al., 2015), which in our hands work very well for particle tracking.

## 2.3 Genomic Engineering by HR and CRISPR/Cas9-Induced DSBs

The optimal setting for studying the natural behavior of a protein is when the fluorescently tagged form is expressed from the endogenous locus and is the

only form present in the cell. This can be achieved by inserting a sequence encoding the tag into the coding sequence of the gene, most commonly in front of the stop codon or after the start codon. Until recently such precise modification of genomic DNA was challenging to the point of being impractical, and surrogate approaches relying on overproduction of tagged ectopic copies of the protein coding sequence were prevalent. Although useful information could be obtained, large deviations from physiological concentration of the protein due to overexpression can lead to major artifacts due to effects on solubility and more importantly stoichiometric imbalances due to intricate macromolecular ensembles and pathways. These tradeoffs became obsolete with the advent of RNA-guided nucleases (Cas9 and other proteins from the bacterial CRISPR immunity systems), which greatly increase the efficiency of precise genome modification, and are easily accessible.

Tag integration into genomic DNA can be performed via HR with a donor encoding the desired fusion sequence, flanked by regions of homology that will guide the insertion of the fusion by HR. This HR reaction needs to be triggered by a lesion in the locus (a DSB or a replication problem). This trigger events occurs with a very low probability naturally resulting in absolute frequencies  $>10^{-5}$  of the desired outcome. Specific DSB induction with a programmable nuclease such as CRISPR/Cas9 increases the frequency by several orders of magnitude. Under the most optimal circumstances (high efficiency of transfection, DSB induction, favorable genetic context, etc.) the probability can reach tens of percent, and cells carrying the modification can be screened for. However, enrichment for the modified cell population by selection or sorting is generally required, especially if homozygous targeting is pursued. The least invasive enrichment method is FACS, since in our context modified alleles often produce fluorescent cells. For this to be feasible in practice the tagged protein must be sufficiently abundant and bright to allow the FACS instrument to separate the positive cell population from background. When this is not the case, as for most DNA repair proteins we study (BRCA2, RAD54, PALB2, BRCA1) that are tagged with various natural and enhanced fluorescent proteins (GFP, Venus, mEos2, etc.), or if the tag is photoactivatable, addition of a selectable marker can be a solution. Alternatively, chemical fluorophores for self-ligating tags fluoresce much brighter and can provide enough separation for FACS.

If enrichment by FACS is not an option, targeted allele can be made selectable by the addition of an antibiotic resistance protein. Expression

can be dependent on the activity of the promoter of the target gene or the promoter of the antibiotic resistance gene itself. The former approach has the advantage that no antibiotic resistance will be expressed if the cassette integrates ectopically, which occurs with a  $10^{-3}$ – $10^{-4}$  frequency. Coexpression with the target gene can be achieved using a self-cleaving 2A peptide (Szymczak et al., 2004) or via an internal ribosome entry site (IRES), and is more straightforward when the tag is at the C-terminus of the target.

The CRISPR/Cas9 RNA-guided nucleases truly revolutionized genetics and there is no shortage of excellent publications on the subject (Doudna & Charpentier, 2014; Wright, Nunez, & Doudna, 2016), so we will only briefly touch on the design choices we made. As tag insertion does not generally remove any sequence from the target locus, and the target for CRISPR/Cas9 must not be present in the donor, options for choosing a gRNA target sequence are limited. This can be further limited when the guidelines for optimal gRNA design are followed. In our experience with selectable HR donors, the only two requirements for CRISPR/Cas9 target sequence choice are the presence of the PAM sequence (NGG) and the absence of perfect matches for the gRNA elsewhere in the genome. Another design decision is the size of homology arms. We generally aim to have >1.5 kb for each arm, as there is no advantage to having less for HR donor construct engineering from PCR-amplified fragments using isothermal Gibson assembly (Gibson et al., 2009), and longer homologies positively correlate with the frequency and fidelity of recombination. Much shorter homologies (>200 bp), which can be produced by chemical synthesis, thus avoiding two PCRs and reducing the number of fragments in the donor assembly, have been successfully used in human cells (Natsume, Kiyomitsu, Saga, & Kanemaki, 2016).

## **2.4 Protocol: Engineering sgRNA for *S. pyogenes* Cas9, and Donor Construct for C-Terminal HaloTag Knock-In**

### **2.4.1 Equipment**

- PCR machine

### **2.4.2 Reagents**

- Q5 high-fidelity DNA polymerase (NEB M0491)
- Genomic DNA from the destination cells
- pSpCas9(BB)-2A-Puro (PX459) V2.0 (Addgene plasmid # 62988) (Ran et al., 2013); pUC18 or related high-copy vector

- DNA template for Halo-2A-Neo-stop cassette amplification (available from the authors)
- 2 × Gibson assembly mix, commercial (NEB) or homemade
- Competent *E. coli* cells

### 2.4.3 Primer Design and Construct Assembly

1. Locate the *S. pyogenes* Cas9 PAM consensus sequence (NGG) nearest to the stop codon. Use Off-Spotter (Pliatsika & Rigoutsos, 2015) or a similar tool to assess the number of potential unwanted target sites for the potential gRNA (20 bp upstream of the PAM).
2. Follow the protocol by Ran et al. to clone sgRNA as annealed oligonucleotides into *Bbs*I-digested pX459 or the steps below to clone using the Gibson assembly method, which we use as it can be adapted to clone multiple sgRNA expression cassettes into one construct (Ran et al., 2013).
  - a. Digest PX459 with *Afl*III and *Xba*I and gel-purify both fragments (433 bp and 8.7 kb). Use the 433-bp fragment diluted to 10 ng/μL and use 1 μL of this as template for PCR. Use the 8.7-kb fragment as linearized target vector in Gibson assembly.
  - b. Perform two 25-μL PCRs using primer combinations listed in Table 1, Q5 polymerase and the recommended PCR protocol, 60°C annealing temperature, 30 s extension, 35 cycles.
  - c. Mix in a PCR tube 1 μL 8.7-kb *Xba*I-*Afl*III fragment of PX459, 1 μL of each of the two PCR products, 3 μL 2 × Gibson assembly mix. Incubate for 1.5 h in a PCR block set to 50°C.
  - d. Chill the reaction on ice and transform everything into 50–100 μL competent *E. coli* cells.
3. Design primers to amplify the homology arms, Halo-2A-Neo cassette and the vector backbone. If the target sequence for sgRNA is not disrupted by tag insertion, the primer for the homology arm containing it needs to include a noncoding substitution disrupting the PAM sequence (Fig. 2B). Perform PCRs using Q5 polymerase and analyze the products on a gel. If amplification was specific and equally efficient, no further purification or concentration adjustment is normally necessary. In this case mix in a PCR tube 1 μL of each of the four PCR products, add equal volume of the 2 × Gibson mix, incubate for 1.5 h at 50°C, and transform everything into 100 μL competent *E. coli* cells. Screen plasmid mini-preps from 5 to 10 colonies using diagnostic restriction digestion.

**Table 1** Oligonucleotide Sequences

| <b>Name</b>         | <b>Sequence</b>  | <b>PCR</b> |
|---------------------|--|------------|
| U6-F (universal)    | tgctggccttttgctcacatgtgaggcctatttcccatgattcc   | gRNA-#1    |
| sgRNA-R             | nnnnnnnnnnnnnnnnnnnnCGGTGTTTCGTCCTTTCCAC<br>n—reverse complement of the target sequence  | gRNA-#1    |
| sgRNA-F             | NNNNNNNNNNNNNNNNNNNNNGTTTTAGAGCTAGAAATAGCAAG<br>N—20 nt target sequence  | gRNA-#2    |
| sgRNA-R (universal) | tgtaacgggtacctctagaCAAGTAGAGTCAGGTAAGCTAAAAAAgcccactcgg  | gRNA-#2    |
| Halo-2A-Neo-F       | N <sub>18-25</sub> GCAGAAATCGGTACTGGCTT<br>N—last 18–25 bases at the 3' end of the left homology arm (melting temperature $\geq 50^\circ\text{C}$ )  | Cassette   |
| Halo-2A-Neo-R       | n <sub>18-25</sub> TCGCCTTCTTGACGAGTTCTTCTGA<br>n—reverse complement of the first 18–25 bases at the 5' end of the right homology arm                | Cassette   |
| Vector-F            | N <sub>18-25</sub> TTCCAGTCGGGAAACCTGTC<br>N—last 18–25 bases at the 3' end of the right homology arm (melting temperature $\geq 50^\circ\text{C}$ ) | Vector     |
| Vector-R            | n <sub>18-25</sub> ATAAACAAATAGGGGTTCCGC<br>n—reverse complement of the first 18–25 bases at the 5' end of the left homology arm                     | Vector     |

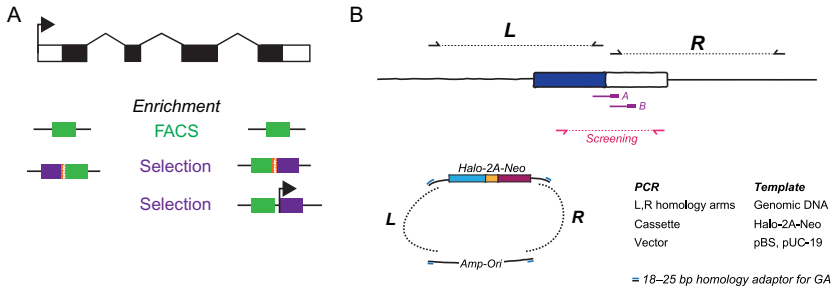


**Fig. 2** Cloning of donor vectors, Cas9/gRNAs, and generation/selection of cell lines. (A) Different tagging strategies and compatible enrichment methods. Tag (green) can be inserted at the N- or C-terminus of a protein encoded by the gene (shown above as exon splicing scheme; coding sequence represented by filled portion). An optional selection marker is shown in purple; its expression is achieved via creation of bicistronic transcript (via IRES or 2A peptide—yellow line) or from independent promoter (arrow). Stop codons are shown as red lines. (B) Assembly of the donor construct for insertion of a Halo-2A-tag at the end of the coding sequence (blue rectangle) in front of the 3'-UTR (white rectangle). Two alternative gRNA target sequences are shown below the gene diagram. Target A is disrupted by insertion of the tag, target B is not, so one of the homology arms (shown above the exon diagram as dotted lines and arrows for the primers used to amplify them from genomic DNA) has to be modified to eliminate the PAM for gRNA B. Vector assembly is shown below.

- Design a pair of primers amplifying a 200–400-bp region containing the HaloTag insertion point. Design a control amplicon elsewhere in the part of the genome that will not be affected by the targeting.

## 2.5 Protocol: CRISPR/Cas9-Stimulated Gene Targeting in Mouse ES Cells

### 2.5.1 Equipment

- GenePulser XCell electroporator (BioRad)
- PCR machine

### 2.5.2 Reagents

- Complete mouse ES media: 250 mL DMEM (Lonza BioWhittaker Cat. BE12-604F/U1, with Ultraglutamine 1, 4.5 g/L glucose), 200 mL DMEM conditioned by exposure to a confluent monolayer of buffalo rat liver (BRL) cells in T175 flask, 50 mL FCS, 5 mL nonessential amino acids (Lonza), 200 U/mL penicillin, 200 µg/mL streptomycin, 89 µM β-mercaptoethanol, 1000 U/mL leukemia inhibitory factor
- 0.1% Porcine gelatin in water (autoclaved) for coating plates
- PBS (Lonza)

- 0.5% Trypsin/0.2% EDTA (Lonza)
- Electroporation cuvettes (BTX, 2 mm gap)
- Mouse ES cells
- Selection antibiotic: puromycin (Invivogen), hygromycin B (Roche), or G418
- MyTaq Red Mix (Bioline)
- Cell lysis buffer (compatible with direct PCR): 50 mM KCl, 10 mM Tris-HCl pH 9, 0.1% Triton X-100 in water. Store at room temperature. Add proteinase K to 0.15 mg/mL before use

### 2.5.3 Transfection

1. Prepare 10 cm cell culture dishes coated with 10 mL gelatin solution for at least 10 min.
2. Trypsinize and count the cells. Resuspend in growth media to  $3.75 \times 10^7$  per mL.
3. Mix in the electroporation cuvette 15  $\mu$ g of the sgRNA/Cas9 expression construct, 15  $\mu$ g donor construct, and 400  $\mu$ L of the cell suspension. Prepare a negative control reaction where cognate sgRNA is replaced by one that cuts in a location other than the targeted gene, or by an empty pX459 vector.
4. Electroporate the cells (118 V, 1200  $\mu$ F,  $\infty$   $\Omega$ , exponential decay) and seed 90% and 10% into two 10 cm dishes in 10 mL media.
5. Next day add selection antibiotic (1.5  $\mu$ g/mL puromycin, 200  $\mu$ g/mL G418, or 200  $\mu$ g/mL hygromycin B). Continue selection for 8 days, changing media as appropriate (every 2 days in the 90% plate) until colonies form.
6. Verify that colony numbers are  $>10\times$  higher in the matching sgRNA-donor combination plate than in the negative control.

### 2.5.4 Colony Picking and Genotyping

1. Prepare two 96-well cell culture plates. Gelatinize one of the cell culture plates and fill with 200  $\mu$ L growth media per well. Pipette 50  $\mu$ L trypsin-EDTA per well of the other cell culture dish.
2. Select the plate with optimal colony density (90% or 10%). Rinse the cells with twice with PBS and refill with 20 mL PBS.
3. Place a microscope in the cell culture hood. With a P20 pipette tip pick a colony and transfer into the 96-well plate with 50  $\mu$ L trypsin-EDTA; repeat for 24–48 colonies.

4. With a multichannel pipette add 100  $\mu\text{L}$  media to the wells with trypsinized colonies in 96-well plate. Pipette up and down several times to resuspend. Transfer  $\sim 40 \mu\text{L}$  into the 96-well plate for maintenance, and the rest into a 96-well PCR dish for genotyping.
5. Place the maintenance 96-well plate in the incubator.
6. Spin down the PCR plate for 5 min at 200 rcf. Turn the plate over and shake a few times to remove the media. Add 200  $\mu\text{L}$  PBS, spin down for 5 min at 200 rcf, and shake out the wash.
7. With a multichannel pipette add 30  $\mu\text{L}$  of cell lysis buffer per well. Seal the plate and incubate at 60°C for 1 h in a PCR machine, then at 95°C for 10 min to stop the cell lysis.
8. Dilute the cell lysate with 100  $\mu\text{L}$  MQ. Use 5  $\mu\text{L}$  per genotyping PCR.
9. Assemble genotyping PCRs on ice: 8  $\mu\text{L}$  MyTaq mix, 5  $\mu\text{L}$  diluted cell lysate, 0.75  $\mu\text{L}$  of 5  $\mu\text{M}$  stock of each of the two primers amplifying a region within the target and each of the two control primers (3  $\mu\text{L}$  primer solutions in total). Prepare a mastermix containing everything by the template, pipette 11  $\mu\text{L}$  per PCR well, add the lysates. Include wild-type (parental) cell line DNA and no template reactions as controls.
10. Perform genotyping PCRs: 95°C 5 min, [95°C 30 s, 60°C 30 s, 72°C 30 s]  $\times$  35, 72°C 5 min, 15°C hold. Run 7.5  $\mu\text{L}$  of the reaction on a 2% agarose TBE gel. Loss of the target band while the control band is present indicates homozygous knock-in clones.
11. Passage 6–10 potential homozygous knock-in clones and 2–3 clones where the target amplicon is still present into 6-well plate to expand. Regenotype and verify by immunoblotting against the target protein and the tag.

## 2.6 Protocol: Preparing Cells for Imaging

### 2.6.1 Equipment

- Coulter Counter (Z2, Beckman Coulter)

### 2.6.2 Reagents

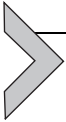
- Mouse ES cells with endogenously expressing fluorescent protein fusions
- $\mu$ -Slide 8 Well Glass Bottom # 1.5H (170  $\pm$  5  $\mu\text{m}$ ) (Ibidi)
- Laminin from mouse Engelbreth-Holm-Swarm (EHS) sarcoma (Roche)
- PBS (Lonza)
- 0.5% Trypsin/0.2% EDTA (Lonza)
- 5  $\mu\text{M}$  stock HaloTag ligand (TMR, JF549, or SiR) dissolved in DMSO

- ES cell imaging medium
  - 90 mL FluoroBrite DMEM media (ThermoFisher Scientific)
  - 10 mL Fetal calf serum
  - 2 mL 4 mM Ultra/L-glutamine (Lonza)
  - 1 mL 10 mM NEAA (Lonza)
  - 1 mL Pen/strep (Lonza)
  - 100  $\mu$ L 0.7% 2-Mercaptoethanol solution in water, sterile filtered
  - 10  $\mu$ L Leukemia inhibitory factor,  $10^6$  U/mL
- Dilute laminin (Roche) 1:40 in PBS, use 40  $\mu$ L of the solution per well of the multiwell dish.
- Add a 40  $\mu$ L of the diluted laminin (Roche) solution drop to the individual wells of the dish. Incubate the dish either for at least 1 h at 37°C or leave it overnight at 4°C. Avoid evaporation of the laminin on the coverslips.
- The day before experiment trypsinize the cells from the plate and count the cells using the cell counter. Seed 20,000–30,000 ES cells per well of the glass slide dish. Leave the cells overnight to properly attach to the glass.
- Optionally treat the cells with ionizing radiation or damaging agents such as HU or MMC.
- Replace complete ES cell medium with ES imaging medium, wash the cells twice with PBS to get rid of the phenol red in the medium. When performing HaloTag labeling this step can be omitted and labeling with the HaloTag ligand can be started directly.
- Prepare sufficient imaging medium (300  $\mu$ L medium per well) with HaloTag ligand, at a 5 nM final concentration.
- Replace the existing cell medium with labeling medium and incubate for 30 min.
- Wash twice with PBS and replace with fresh imaging medium (without HaloTag ligand).
- After 15 min wash with PBS and again replace with imaging medium.
- Repeat washing again after 15 min and keep cells in imaging medium.
- Proceed to the microscope.

### 2.6.3 Notes

- Coating the glass with laminin (or other extracellular proteins) instead of gelatin will result in nicely attached cells which allows to acquire better images.

- The concentration HaloTag ligand has to be optimized based on the protein concentration to obtain the right concentration of labeled protein and finally being able to detect single molecules under the microscope.
- It takes some time for the unreacted HaloTag ligands to be released by the cells; therefore, it is important to take sufficient time between the washing steps.



## 3. MOBILITY ASSAYS

### 3.1 Fluorescence Recovery After Photobleaching

An established assay to determine the mobility of proteins is FRAP. Studying the dynamics of HR proteins by FRAP established that different DNA repair proteins can exhibit very different dynamic behavior and levels of immobilization after damage induction (Essers, Houtsmuller, & Kanaar, 2006; Essers et al., 2002). FRAP relies on analysis of the recovery of fluorescent signal in a region of the cell, where the fluorescence has been bleached away. The fluorescent intensity in the region is recorded over time. The rate and the amount of recovery of the fluorescent signal provide information on diffusion rate and (transient) immobilization. For reproducible results with FRAP the normalized recovery curves of multiple cells are averaged. Although FRAP can be used to determine qualitative differences between conditions, quantitative analysis of the fluorescence recovery is challenging because the recovery of the fluorescence is dependent on many factors (size of the region, shape of the laser beam) and consequently requires advanced computer simulations to fully understand and validate (Geverts, van Royen, & Houtsmuller, 2015). It is therefore challenging to obtain absolute quantitative data such as diffusion constants and residence times from FRAP data alone.

### 3.2 Fluorescence Correlation Spectroscopy

FCS is an alternative for measuring protein mobility. It is very useful for studying fast dynamics of proteins, while sampling only a very small volume in the cell using a confocal microscope. Recording the temporal fluctuations of fluorescence emission inside the confocal volume gives information on the rate at which proteins are moving in and out of the illumination spot. The temporal fluctuations can then be analyzed by the autocorrelation function to determine diffusion constants of the proteins. Using reference

solutions with known diffusion rates it is possible to determine the excitation volume precisely, which will help to reliably determine the diffusion coefficients. In addition to movement of the proteins in and out of the excitation volume, blinking of the molecules during the recording affects the result of the analysis. The GFP blinking rate is similar to the diffusion rate of many proteins, making it difficult to estimate the diffusion constant using GFP (Haupts, Maiti, Schwille, & Webb, 1998). YFP on the other hand exhibits faster blinking rates which enables separation of the blinking component from the component of free diffusing protein (Reuter et al., 2014). FCS is a very powerful technique to determine diffusion rates and protein concentrations of free moving proteins; however, immobilization of proteins inside the excitation volume complicates analysis of the data. Furthermore, like with FRAP the obtained information is an average of all proteins and does not provide information about the individual proteins.

### 3.3 Single-Particle Tracking

When applying specific illumination schemes, the fluorescence of individual molecules can be distinguished under a microscope. Although a modern EM-CCD or sCMOS camera is required, single-molecule tracking can be done on a relative simple widefield/TIRF microscope setup. For high-resolution microscopy, in particular single-molecule imaging, it is necessary to reduce background and out-of-focus fluorescence as much as possible. To compensate for the high background in epifluorescence optical sectioning can be applied to reduce the total excitation volume (Fig. 3A). Total internal reflection (TIRF) is frequently used to obtain a thin excitation volume of about 200 nm just above the coverslip (Fig. 3B). For imaging inside the cell, for example, in the cell nucleus this will not work. As an alternative for TIRF, we use highly inclined and laminated optical sheet (HiLo) illumination to illuminate the nucleus in a thin slice of a few micrometers in thickness (Tokunaga, Imamoto, & Sakata-Sogawa, 2008) (Fig. 3C). Using a smaller incidence angle than TIRF a beam of excitation light is created illuminating a slice in the cell. To further enhance optical sectioning more advanced systems have become available that use very thin light sheets; however, these techniques require advanced microscopes and more challenging sample preparation.

The detected individual molecules need to be spatially separated (effective fluorophore concentration of less than 10 nM), which can be achieved by imaging proteins at low concentration or by using photoactivation to

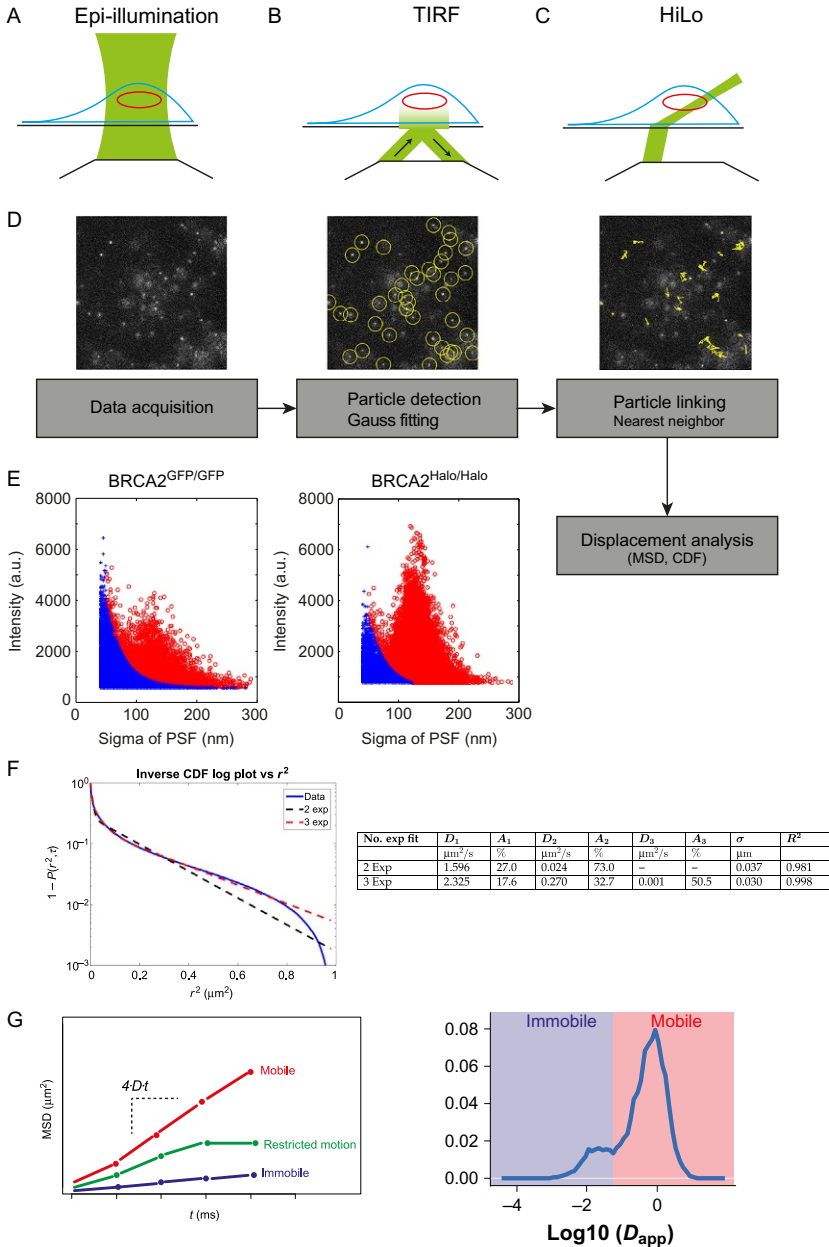


**Fig. 3** Investigation of protein mobility by single-particle tracking. Different modes of illumination are available for single-particle tracking. (A) The most straightforward mode is epifluorescence, illuminating the sample from below and detecting the fluorescence using the same microscope objective. (B) By changing the position of the illumination

*(Continued)*

detect only a subset of the molecules at a time (Manley et al., 2008). Subsequently, the position of the individual molecules can be determined at high accuracy. In living cells these molecules will diffuse, allowing to follow single molecules in time. The displacements of the molecules can be used to calculate their mobility. The mean square displacement (MSD) or cumulative distribution function (CDF) of the particle displacements presumably undergoing Brownian motion can then be used to estimate the diffusion coefficient.

Particle tracking can also be used to quantify binding and dissociation kinetics (e.g., binding of a protein to a relatively immobile cellular component) of molecules in cells. The dynamic behavior of the individual molecules is representative of dynamics of the entire population and more importantly provides details of individual function that is lost in methods that determine values based on population averages. Single-particle tracking can distinguish subpopulations of molecules that exhibit a specific type of mobility.

---

**Fig. 3—cont'd** laser with respect to the objective, the light comes out at an angle, total internal reflection (TIRF) microscopy. When the angle is large enough, the light is reflected at the glass–medium interface. The remaining evanescent wave creates a thin illumination layer just above the coverslip. (C) Highly inclined and laminated optical sheet (HiLo) illumination; when applying the light at a slightly smaller angle a sheet of light is created, which illuminates only part of the cell. Compared to TIRF this allows imaging of the cell further away from the coverslip. (D) Workflow for single-particle tracking. After data acquisition individual molecules are localized with high localization precision using 2D Gaussian fitting. Subsequently, the localized molecules that are found in subsequent frames are linked together by nearest-neighbor linking, resulting in single-particle tracks. These tracks can then be used to extract dynamic information describing the mobility of the proteins. (E) Scatter plots showing the distribution of the fitted sigma of the point spread function (PSF) against the intensity of the molecules. The distribution can be used to separate background signals from true single particles, by assuming that the noise is distributed exponential (*blue*) while the true single particles have a Gaussian distribution. The first plot shows the distribution when using GFP fusions for tracking BRCA2, while the second plot shows the distribution from a video recorded using HaloTag (JF549) fused to BRCA2. (F) Example of the analysis of single-particle data using the inverse cumulative distribution function (CDF). All displacements from all tracks are put together to get a distribution of displacements. The squared displacements are then used to fit a multiexponential function to the data. From this function, multiple diffusion coefficients can be extracted together with the fraction of the molecules exhibiting this diffusion rate. (G) Mean square displacement analysis of the single-particle tracks. When tracks are sufficiently long, the mean square displacement of individual tracks can be used to extract the apparent diffusion constant for that molecule. When this analysis is done for all tracks in the data set, a distribution of diffusion rates can be obtained, showing at what rate the different molecules diffuse.

Camera acquisition speed limits the maximum diffusion rate that can be detected by single-particle tracking. Molecules that move too fast will be blurred out during the time the camera is exposed or molecules might move too far to unambiguously link in tracks. Since BRCA2 and RAD51 diffuse relatively slowly as oligomeric complexes an exposure time of 30 ms is sufficient to track nearly all the diffusing molecules (diffusion constant of about  $1.5 \mu\text{m}^2/\text{s}$ ). There is also a lower limit of movement that can be detected, which depends on the localization precision for determining the position of a molecule (10–30 nm). Molecules that move less than the localization precision within the exposure time are considered immobile. Increasing the exposure time allows to discriminate better between mobile and immobile molecules and additionally can be used to quantify the (transient) residence times.

### **3.4 Protocol: Live-Cell Particle Tracking Using HiLo Illumination Microscopy**

#### **3.4.1 Equipment**

- Inverted TIRF microscope with temperature-controlled stage and objective at 37°C, as well as 5% CO<sub>2</sub>
  - EM-CCD camera Andor iXon DU 897, 512 × 512 pixels
  - 30 mW 405 nm, 100 mW 488, 561, and 633 nm lasers

#### **3.4.2 Imaging**

- Use a fixed frame acquisition time, the chosen acquisition speed depends on the diffusion rate of the protein under investigation; for BRCA2 we use an acquisition time of 30 ms. A higher frame rate allows tracking of faster moving molecules, but requires more laser power to see the individual molecules.
- Use a constant laser power during acquisition, at the same time avoid using too much laser power as this results in shorter tracks, due to bleaching and blinking.
- With HiLo illumination imaging it is important to properly adjust the TIRF angle and focus until the best signal-to-noise ratio is achieved. For every imaged nucleus, the TIRF angle might slightly change.
- Before starting the actual acquisition make sure individual molecules are visible. If necessary apply a short prebleaching to avoid having overlapping single molecules in the video.

- Record an image stream of several 100–1000s of frames. This depends on stability of the dyes used for imaging. For BRCA2 with the HaloTag we can acquire at least 2000 frames per nucleus.

### 3.4.3 Notes

- When using HaloTag-JF549, and possibly also for other dyes, one can use low 405 nm light to reactivate the dyes from a dark state. This will help to image a cell for a longer time while acquiring sufficient single-molecule tracks for the entire movie.

## 3.5 Data Analysis: Tracking Individual Fluorescent Particles in Live Cells and Characterizing (Im)mobility

Analysis of particle tracking data consists of several steps, which are first of all detection and localization of fluorescent particles at subpixel precision in the raw data. This is followed by linking of the fluorescent particles in subsequent frames to obtain tracks. For this procedure, we use the freely available SOS Plugin in ImageJ/Fiji (<http://www.smal.ws/wp/software/sosplugin/>). The obtained track data can then be used to extract dynamic information. These steps will be discussed below (Fig. 3D).

### 3.5.1 Detection and Localization

To detect and localize the single molecules from the images, several parameters have to be set in the software. Many of these parameters need to be adjusted manually until most single molecules in the images are detected by the software, without taking background signals along. An important parameter is the minimum spot intensity to only select the signals which are clearly above the background. Additionally, it is important to set the correct values for the minimum and maximum standard deviation of the Gaussian fit. These values can be obtained by measuring the point spread function (PSF) of the microscope, for example, by recording the signal of 100 nm fluorescent beads. Avoid using too small numbers for the minimum standard deviation, values below 1 pixel potentially allows fitting of a signal to single noise pixels.

When tracking BRCA2-GFP we observed that we could improve the separation of the background noise from true single molecules by fitting a combined exponential and Gaussian function to the distribution of detected intensity and the standard deviation of the fitted (Fig. 3E). Using a routine in MATLAB<sup>®</sup> we remove the detected particles under the exponential function, before linking of the observed particles together. We can clearly see

that there is a difference in the intensity of molecules labeled with GFP or HaloTag-JF549 (Fig. 3E). The increased intensity of the HaloTag-JF549 signal makes it easier to separate the true signals from the background.

### 3.5.2 Tracking Linking Distance

When the signals are detected, the next step is to link the positions of the molecules in time. We use nearest-neighbor linking with a distance threshold to build the tracks. One needs to define the maximum distance the particles can travel between two frames. It is important to set this value as small as practical, maximum a few hundred nanometers, because too large distances will result in linking different molecules into the same track.

### 3.5.3 CDF/MSD Analysis

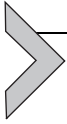
Analysis of the track data can be done in scripting software such as R or MATLAB<sup>®</sup>. For nuclear proteins, it is often most interesting to quantify the fractions of proteins that exhibit different mobilities, from immobilized presumably on chromatin to free diffusing in the nucleoplasm. If only short tracks, of only several steps, are obtained, a good approach is to pool all displacements in the data set and present them as a histogram. This histogram can be translated to an inverse cumulative distribution function (CDF). This distribution can be described by a multiexponential function, from which the fractions of particles and their corresponding diffusion coefficients can be extracted (Fig. 3F).

Using the CDF all displacements of all tracks are pooled together; therefore, it is not possible to distinguish whether the obtained fractions are caused by individual proteins behaving differently or whether proteins are switching between different diffusing states. It could be that just a fraction of the proteins is immobile or that all proteins are transiently immobile. When longer tracks are available an MSD analysis of the single tracks can be used to study the dynamic behavior of the single proteins. The MSD of a single track can be calculated at different time steps (Fig. 3G). From the slope of a fitted linear function to the first few time the diffusion coefficient can be estimated:

$$\langle \text{MSD} \rangle = 4Dt$$

For all tracks in a cell this provides a distribution of diffusion coefficients of the individual proteins in the cells. This type of analysis can be very informative if populations of proteins with different diffusion rates are expected. When proteins rapidly switch between different dynamics states, also within

single tracks this information is lost by averaging; in those situations using the inverse CDF will be more reliable.



## 4. RELATIVE POSITION OF PROTEINS IN DSB FOCI

### 4.1 Super-Resolution Microscopy

For fluorescence microscopy using wavelengths in the visible spectrum spatial resolution is limited at about 200–250 nm and structural details below that resolution can in principle not be resolved. Super-resolution microscopy methods circumvent the resolution limit by spatially controlling the excitation and emission of the fluorescent molecule in the sample. This allows extra information to be obtained on the positioning of the fluorophores in the sample, hence a better resolution. Two of those techniques, structured illumination microscopy (SIM) and stimulated emission depletion microscopy (STED), require advanced microscope setups. SIM allows relative easy acquisition, recording of 3D stacks, and use of standard fluorophores. The total resolution increase can be twofold in all three spatial dimensions, with a lateral resolution of about 120 nm. SIM has been used to determine the differential localization of DSB factors 53BP1 and BRCA1 in DSB foci, showing the exclusion of 53BP1 from the core of the focus when BRCA1 is present and to determine spatial organization of  $\gamma$ H2AX at the chromatin around DSBs (Chapman, Sossick, Boulton, & Jackson, 2012; Natale et al., 2017). STED has a different approach by using a laser scanning microscope whereby a doughnut-shaped depletion beam is applied to detect the fluorescence from only a volume smaller than the resolution limit. The obtained lateral resolution can be about 40 nm.

Finally, SMLM refers to a group of different super-resolution microscopy techniques that use the localization of individual molecules to obtain a super-resolution image. The emission of individual molecules is separated in time and hence allows positions of single molecules in a densely labeled sample to be determined (Fig. 4A). There are different approaches to achieve the on- and off-switching of the molecules. PAINT is one way by using dyes which are transiently fluorescent by binding and dissociating from their target. Alternatively, the fluorescence of individual molecules can be controlled using photoactivatable dyes or proteins, in an approach called PALM. Most commonly stochastic on-/off-switching of organic dyes is used. This switching can be induced using intense laser power in combination with a buffer to control the chemical properties of the dyes, this is named GSDIM or dSTORM.

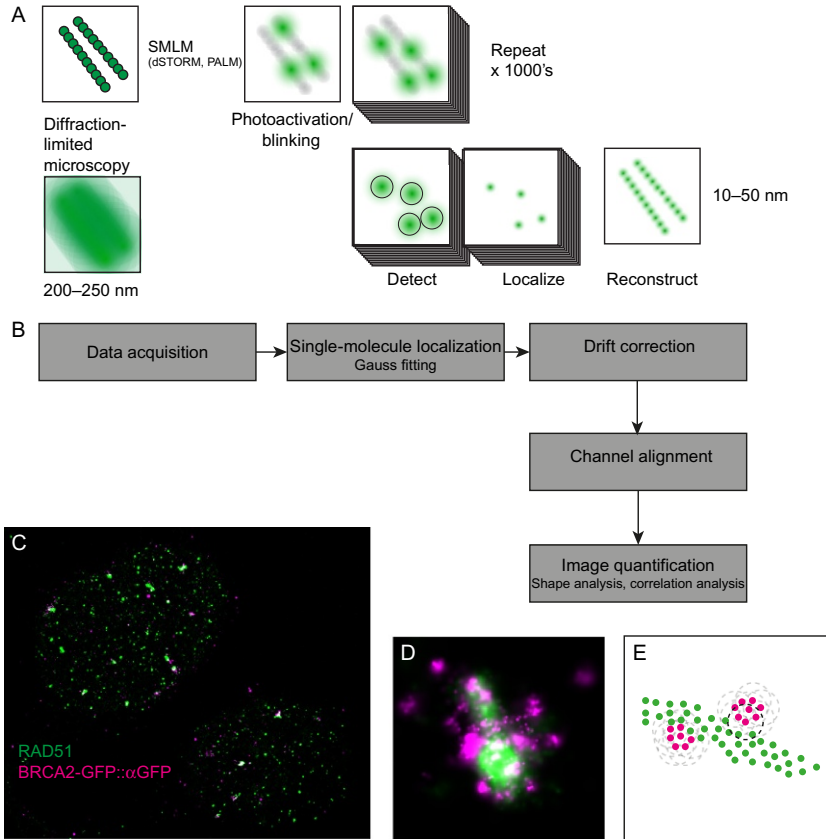


**Fig. 4** Single-molecule localization microscopy (SMLM) to study the organization of DNA repair proteins. (A) SMLM is based on the principle of localizing single molecules in densely labeled samples. By controlling the fluorescence of individual molecules, only a few molecules are fluorescent in a single image frame. Recording thousands of images every time with different fluorescent molecules, detection and localization by Gaussian fitting of the single molecules results in a high-resolution map with a spatial resolution up to 10 nm, while the resolution limit of conventional fluorescence microscopy is about 200 nm. (B) Workflow for SMLM; after acquisition of the data, single-molecule localization is applied to extract the positions of the molecules. This is followed by correction of drift during acquisition of the image using fiducial markers. When acquiring multiple channels, these channels need to be properly aligned; again this can be done using fiducial markers. The obtained images can then be used for image quantification. (C) A dual-color SMLM image of RAD51 (anti-RAD51 antibody) and BRCA2-GFP stained using anti-GFP nanobodies labeled with Alexa647 in BRCA2<sup>GFP/GFP</sup> mouse ES cells. (D) Example of a DSB focus showing RAD51 (green) and BRCA2-GFP (magenta). (E) Cartoon to clarify how overlap between two proteins can be analyzed using SMLM. By quantifying the number of localizations in the second channel that are within a certain radius of the first protein, the overlap between the localization of the proteins can be studied.

SMLM enables the analysis of protein localizations in unique ways. Instead of providing an image we obtain a map with the positions of the individual molecules, which can be used to analyze the distribution of the proteins with a localization accuracy below 25 nm. The accuracy depends on the brightness of individual fluorophores; the more photons collected, the better the localization accuracy (Thompson, Larson, & Webb, 2002). Additionally, the distance between the protein and the label affects the localization accuracy. Like numerous laboratories, we have frequently used primary antibodies together with fluorescently labeled secondary antibodies for our super-resolution studies. Using labeled secondary antibodies one introduces about 20 nm additional uncertainty to the actual localization of the protein recognized by the antibodies (Mikhaylova et al., 2015). This uncertainty can be reduced by using labeled primary antibodies and even further improved to use smaller antibody fragments such as single chain antibodies and nanobodies. Another attractive alternative is the use of SNAP-tag or HaloTag to directly perform super-resolution imaging using dyes bound to the tag (Grimm et al., 2015; Lukinavičius et al., 2013).

Although single-molecule localization is able to localize individual molecules, SMLM is generally not a quantitative technique, because the same molecule can be detected multiple times throughout the image recording due to blinking of the detected fluorophore. Additionally, the use of secondary antibodies obscures the exact number of proteins present in complexes. Several attempts have been made to extract information on the numbers of molecules in protein complexes, for example, by titrating the concentration of antibody in the sample (Ehmann et al., 2014) or by carefully analyzing blinking kinetics of the dyes (Nieuwenhuizen et al., 2015). Other approaches are needed to determine the number of molecules in complexes. By quantifying the total concentration in the cell nucleus using FCS, the number of molecules of RAD54 in DSB foci was estimated to be a few hundred (Agarwal et al., 2011). For BRCA2 we were able to establish that about three BRCA2 molecules were present per oligomeric complex using a step-bleaching approach after mild fixation (Reuter et al., 2014). Bleach step-fitting can be used for quantification of small numbers of proteins; however, when more than dozens of molecules are present, it is difficult to precisely detect all the bleaching steps.

## 4.2 Protocol: Dual-Color Super-Resolution Imaging of Nuclear Proteins

### 4.2.1 Reagents

- PBS
- Paraformaldehyde (Sigma) (prepare 2% (w/v) formaldehyde in PBS, heat up to 55°C add a few drops of 1 M NaOH until PFA is dissolved, adjust pH to 7.4, and store at -20°C for up to several months)
- Triton X-100 (Sigma)
- BSA (Sigma)
- Glycine (Sigma)
- Primary antibodies
- Secondary antibodies
  - For dSTORM it is important the use organic dyes that have nice blinking behavior. Alexa647 (Thermo Scientific) works best in our buffer and can be combined preferably with CF568 (Biotium) or alternatively with Atto488 (Rockland)
- PBS+ (100 mL PBS + 0.5 g BSA + 0.15 g glycine)
- 5 × Glucose Tris-HCl solution: 50% glucose (w/v), 250 mM Tris-HCl pH 8.0, 50 mM NaCl (can be stored in aliquots at -20°C)
- 100 × Glucose oxidase/catalase: 56 mg/mL glucose oxidase (Sigma), 3.4 mg/mL catalase in 50 mM Tris-HCl pH 8.0, 10 mM NaCl (can be stored in aliquots at -20°C)
- 1 M MEA in 50 mM Tris-HCl pH 8.0, 10 mM NaCl (can be stored in aliquots at -80°C)
- TetraSpeck Microspheres, 0.1 μm (ThermoFisher Scientific, T729)

### 4.2.2 Sample Preparation

1. Wash the cells with PBS.
2. Fix the cells for 20 min with 2% formaldehyde.
3. Permeabilize the cells using PBS+ 0.1% Triton X-100 wash three times, followed by incubation for two times 10 min.
4. Wash 20 min with PBS+.
5. Dilute primary antibody in PBS+ (leave for 2 h in humidified box).
6. Permeabilize the cells using PBS+ 0.1% Triton X-100 wash three times, followed by incubation for two times 10 min.
7. Wash with PBS+.
8. Dilute secondary antibody in PBS+ (leave for 1 h in humidified box).
9. Permeabilize the cells using PBS+ 0.1% Triton X-100 wash three times, followed by incubation for two times 10 min.

10. Wash with PBS.
11. Do a postlabeling fixation to cross-link the antibodies to their epitopes, this is done to avoid dissociation of the antibodies during imaging. Fix the cells for 20 min with 2% formaldehyde.
12. Samples can be stored in PBS at 4°C until the experiment.

#### 4.2.3 Image Acquisition—dSTORM Imaging

- Several hours before imaging add TetraSpeck beads dissolved in PBS to the sample. In our situation 3  $\mu\text{L}$  in 10 mL PBS gave a proper amount of beads per field of view. This can be adjusted to have between 3 and 10 beads per field of view while being at the correct focus level.
- Mount the coverslip in the microscope ring and add PBS.
- Briefly check the immunostaining under the microscope.
- Prepare dSTORM buffer right before imaging.
  1. Spin glucose oxidase/catalase solution to remove precipitation.
  2. For 1 mL of buffer for dual-color dSTORM (25 mM MEA, 50 mM Tris-HCl pH 8.0, 10 mM NaCl):
    - 200  $\mu\text{L}$  Glucose solution
    - 10  $\mu\text{L}$  Glucose oxidase/catalase
    - 25  $\mu\text{L}$  MEA
    - 765  $\mu\text{L}$  MQ
- Replace PBS with dSTORM buffer.
- Set camera to  $256 \times 256$  pixels and make sure a single-cell nucleus fits inside the image. When available use an option to focus the laser light to a smaller area of the camera chip. Make sure the image is homogeneously illuminated by adjusting the incidence (TIRF) angle of the laser.
- Select a cell and make sure sufficient TetraSpeck beads are visible in the image. Start image acquisition with the channel with the longest wavelength. Take a snapshot of the cell in widefield modus.
- Increase the laser power to induce blinking of the molecules.
- As soon as only individual blinking molecules are visible start acquisition, record 10,000–50,000 frames and use a fast frame acquisition time; we normally use 30 ms.
- Use 405 nm light to control the number of molecules visible per frame. During the acquisition the 405 nm laser power can be slowly increased to have a constant number of localizations per image frame.
- Change the laser and filter settings and record the image in the second channel, avoid movement of the stage and objective to allow proper alignment of the channels afterwards.

### 4.3 Data Analysis: Dual-Color SMLM

For analysis of dSTORM data dedicated software is required. Commercial super-resolution systems (Zeiss, Nikon, or Leica) are often packaged with software to create reconstructions from the raw data. Alternatively, a large number of open-source software analysis packages are available; for a benchmark and overview of these package, see [Sage et al. \(2015\)](#). One of these packages is ThunderSTORM which runs within ImageJ/Fiji ([Ovesný, Křížek, Borkovec, Švindrych, & Hagen, 2014](#)). The exact steps of the analysis depend on the package that is used. However, the following analysis steps have to be performed. For these steps we list some important considerations.

#### 4.3.1 Detection and Localization of the Single Molecules

It is important to define a proper threshold above which signals will be selected. Instead of using an absolute intensity threshold it is often useful to use a threshold that detects the peaks that are a number of times above the variance of the background signal. This avoids problems when the background signal is not entirely homogeneous. After identification of potential single molecules detections are processed by a Gaussian fitting procedure to determine their exact position of the molecule ([Fig. 4B](#)).

#### 4.3.2 Drift Correction

Because dSTORM involves collecting multiple images of the same sample over time, image frame registration is needed to reconstruct the accurate relative position of the detected molecules. There are two common procedures, the most precise way to correct for lateral sample drift is to use fiducial markers, which are present throughout the entire recording. However, when no fiducial markers are present, drift can also be corrected by dividing the localization data set in a number of segments. After reconstruction of these fragments the cross-correlation between the images can be used to determine the drift. The determined drift across the frames can be subsequently corrected on the coordinates of the localizations.

#### 4.3.3 Grouping

The same molecules are often localized in subsequent frames, linking those together increases their localization precision and at the same time enhances the image quality by reducing the overrepresentation of the same molecules. Grouping is done by linking localizations that are within a

defined distance from each other within the next frame. Often a single frame gap is tolerated to take blinking into account.

#### **4.3.4 Filtering**

The table of single-molecule localizations contains additional statistics about the localizations, such as the estimated localization precision, the standard deviation of the fitted PSF, and the number of photons collected for that localization. These statistics can be used to remove poorly localized molecules, which otherwise reduce the quality of the data. It is useful to make histograms of these statistics to determine which values can be used to filter the data. Normally we filter out the localizations that have a localization precision above 50 nm and that have a Gaussian fit outside the expected range. For this we use a range of  $\pm 50$  nm from the expected standard deviation from the PSF.

#### **4.3.5 Channel Alignment**

If the microscope system is very stable, without drift, in principle the channel registration can be done using a sample with multicolor fluorescent beads (fiducials) and a nonrigid registration algorithm can be used to register the channels. This registration can subsequently be applied to one of the channels of the localization data. We prefer to use fiducial markers inside the individual acquired images. These fiducials can then be used to correct for the chromatic aberrations and possible drift between the subsequent recorded frames. This makes sure every image is aligned properly and avoids variation in the alignment of different images.

### **4.4 Single-Molecule Colocalization Analysis**

In single-molecule localization microscopy, protein colocalization quantification differs from that determined with conventional microscopy. Colocalization in the traditional way is defined as the overlap in fluorescence signals of two different proteins, for example, proteins colocalizing in DSB foci. At higher resolution this definition becomes obsolete since molecules are never physically overlapping. With single-molecule localization microscopy it is possible to more precisely determine if proteins are found close together or what the distances between them are. Defining changes in these parameters that reflect protein function is a very powerful application. As already mentioned, single-molecule localization data can be seen as coordinate data and therefore different types of analysis can be applied. To study

the colocalization of coclustering of proteins throughout a cell it is possible to use nearest-neighbor methods, which provide a distribution of distances at which the nearest molecule is found. Alternatively, spatial descriptive methods such as Ripley-K functions can be used to define if molecules are, more than randomly expected, found close together and at what distance from each other the proteins are localized.

These methods work best when applied on larger areas in the cell and assume that proteins are spread equally throughout the area. DSB foci occupy only a small area of the image, and therefore, it is more insightful to study the distribution nearby within individual foci. To study the organization of proteins in DSB foci, we select the DSB foci from the entire super-resolution image. Selection of foci can be done manually, and we regularly use images of RAD51 immunostaining to select the foci; since these foci are easy to recognize, while BRCA2 foci are much more diffuse at high resolution. Foci can also be detected automatically, using localization-based clustering algorithms. RAD51 foci are relatively easy to detect using the DBSCAN clustering algorithm. Subsequently, a defined fixed radius can be used to quantify the amount of proteins within this radius (Fig. 4C–E). It should be kept in mind that the radius that is used might influence the outcome of the analysis; a small radius of, for example, 50 nm will give information at close interactions between proteins, while a larger radius reveal coclustering at longer distances (Georgieva et al., 2016).



---

## 5. CONCLUSION/PERSPECTIVE

The progress made in the development of gene-editing techniques, in particular CRISPR–Cas9, greatly enhances the possibilities to introduce (fluorescent) tags at endogenous gene loci to study the authentic behavior of proteins in living cells. The combination with bright fluorescent molecules to label and follow proteins inside living cells makes it now possible to study the dynamics and organization of even low-expressing and large proteins, such as BRCA2. Quantitative analysis of the mobility and the observed changes upon DNA damage reveal how protein dynamic behavior contributes to the local accumulation at sites of damage. Single-molecule tracking provides the possibility to understand how individual protein molecules behave in that context. In combination with experiments in fixed cells to study the nanoscale organization (and composition) of DNA repair

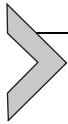
proteins at the sites of DNA damage, this provides the opportunity to bridge our knowledge from the biochemically well-characterized DNA repair reactions to understanding how DNA damage (e.g., DSBs) is detected and resolved in living cells.

## REFERENCES

- Agarwal, S., van Cappellen, W. A., Guenole, A., Eppink, B., Linsen, S. E. V., Meijering, E., et al. (2011). ATP-dependent and independent functions of Rad54 in genome maintenance. *The Journal of Cell Biology*, *192*, 735–750.
- Chapman, J. R., Sossick, A. J., Boulton, S. J., & Jackson, S. P. (2012). BRCA1-associated exclusion of 53BP1 from DNA damage sites underlies temporal control of DNA repair. *Journal of Cell Science*, *125*, 3529–3534.
- Cranfill, P. J., Sell, B. R., Baird, M. A., Allen, J. R., Lavagnino, Z., de Gruiter, H. M., et al. (2016). Quantitative assessment of fluorescent proteins. *Nature Methods*, *13*(7), 1–7.
- Doudna, J. A., & Charpentier, E. (2014). Genome editing. The new frontier of genome engineering with CRISPR–Cas9. *Science (New York, NY)*, *346*, 1258096.
- Ehmann, N., van de Linde, S., Alon, A., Ljaschenko, D., Keung, X. Z., Holm, T., et al. (2014). Quantitative super-resolution imaging of Bruchpilot distinguishes active zone states. *Nature Communications*, *5*, 1–12.
- Essers, J., Houtsmuller, A. B., & Kanaar, R. (2006). Analysis of DNA recombination and repair proteins in living cells by photobleaching microscopy. *Methods in Enzymology*, *408*, 463–485.
- Essers, J., Houtsmuller, A. B., Veelen, L. v., Paulusma, C., Nigg, A. L., Pastink, A., et al. (2002). Nuclear dynamics of RAD52 group homologous recombination proteins in response to DNA damage. *The EMBO Journal*, *21*, 2030–2037.
- Georgieva, M., Cattoni, D. I., Fiche, J.-B., Mutin, T., Chamousset, D., & Nollmann, M. (2016). Nanometer resolved single-molecule colocalization of nuclear factors by two-color super resolution microscopy imaging. *Methods*, *105*, 44–55.
- Geverts, B., van Royen, M. E., & Houtsmuller, A. B. (2015). Analysis of biomolecular dynamics by FRAP and computer simulation. In P. J. Verveer (Ed.), *Advanced fluorescence microscopy: Methods and protocols* (pp. 109–133). Springer New York: New York, NY.
- Gibson, D. G., Young, L., Chuang, R.-Y., Venter, J. C., Hutchison, C. A., & Smith, H. O. (2009). Enzymatic assembly of DNA molecules up to several hundred kilobases. *Nature Methods*, *6*, 343–345.
- Grimm, J. B., English, B. P., Chen, J., Slaughter, J. P., Zhang, Z., Revyakin, A., et al. (2015). A general method to improve fluorophores for live-cell and single-molecule microscopy. *Nature Methods*, *12*, 244–250.
- Hansen, A. S., Pustova, I., Cattoglio, C., Tjian, R., & Darzacq, X. (2017). CTCF and cohesin regulate chromatin loop stability with distinct dynamics. *eLife*, *6*, e25776.
- Haupts, U., Maiti, S., Schwille, P., & Webb, W. W. (1998). Dynamics of fluorescence fluctuations in green fluorescent protein observed by fluorescence correlation spectroscopy. *Proceedings of the National Academy of Sciences of the United States of America*, *95*, 13573–13578.
- Kepler, A., Pick, H., Arrivoli, C., Vogel, H., & Johnsson, K. (2004). Labeling of fusion proteins with synthetic fluorophores in live cells. *Proceedings of the National Academy of Sciences of the United States of America*, *101*, 9955–9959.
- Liu, Z., Legant, W. R., Chen, B.-C., Li, L., Grimm, J. B., Lavis, L. D., et al. (2014). 3D imaging of Sox2 enhancer clusters in embryonic stem cells. *eLife*, *3*, e04236.

- Los, G. V., Encell, L. P., McDougall, M. G., Hartzell, D. D., Karassina, N., Zimprich, C., et al. (2008). HaloTag: A novel protein labeling technology for cell imaging and protein analysis. *ACS Chemical Biology*, *3*, 373–382.
- Lukinavičius, G., Umezawa, K., Olivier, N., Honigsmann, A., Yang, G., Plass, T., et al. (2013). A near-infrared fluorophore for live-cell super-resolution microscopy of cellular proteins. *Nature Chemistry*, *5*, 132–139.
- Manley, S., Gillette, J. M., Patterson, G. H., Shroff, H., Hess, H. F., Betzig, E., et al. (2008). High-density mapping of single-molecule trajectories with photoactivated localization microscopy. *Nature Methods*, *5*, 155–157.
- Mikhaylova, M., Cloin, B. M. C., Finan, K., van den Berg, R., Teeuw, J., Kijanka, M. M., et al. (2015). Resolving bundled microtubules using anti-tubulin nanobodies. *Nature Communications*, *6*, 7933.
- Natale, F., Rapp, A., Yu, W., Maiser, A., Harz, H., Scholl, A., et al. (2017). Identification of the elementary structural units of the DNA damage response. *Nature Communications*, *8*, 15760.
- Natsume, T., Kiyomitsu, T., Saga, Y., & Kanemaki, M. T. (2016). Rapid protein depletion in human cells by auxin-inducible degron tagging with short homology donors. *Cell Reports*, *15*, 210–218.
- Nieuwenhuizen, R. P. J., Bates, M., Szyborska, A., Lidke, K. A., Rieger, B., & Stallinga, S. (2015). Quantitative localization microscopy: Effects of photophysics and labeling stoichiometry. *PLoS One*, *10*. e0127989.
- Ovesný, M., Křížek, P., Borkovec, J., Švindrych, Z., & Hagen, G. M. (2014). Thunder-STORM: A comprehensive ImageJ plug-in for PALM and STORM data analysis and super-resolution imaging. *Bioinformatics*, *30*, 2389–2390.
- Philip, S., Swaminathan, S., Kuznetsov, S. G., Kanugula, S., Biswas, K., Chang, S., et al. (2008). Degradation of BRCA2 in alkyltransferase-mediated DNA repair and its clinical implications. *Cancer Research*, *68*, 9973–9981.
- Pliatsika, V., & Rigoutsos, I. (2015). “Off-Spotter”: Very fast and exhaustive enumeration of genomic lookalikes for designing CRISPR/Cas guide RNAs. *Biology Direct*, *10*, 4.
- Prakash, R., Zhang, Y., Feng, W., & Jasin, M. (2015). Homologous recombination and human health: The roles of BRCA1, BRCA2, and associated proteins. *Cold Spring Harbor Perspectives in Biology*, *7*. a016600.
- Ran, F. A., Hsu, P. D., Wright, J., Agarwala, V., Scott, D. A., & Zhang, F. (2013). Genome engineering using the CRISPR–Cas9 system. *Nature Protocols*, *8*, 2281–2308.
- Reuter, M., Zelensky, A., Smal, I., Meijering, E., van Cappellen, W. A., de Gruiter, H. M., et al. (2014). BRCA2 diffuses as oligomeric clusters with RAD51 and changes mobility after DNA damage in live cells. *The Journal of Cell Biology*, *207*, 599–613.
- Sage, D., Kirshner, H., Pengo, T., Stuurman, N., Min, J., Manley, S., et al. (2015). Quantitative evaluation of software packages for single-molecule localization microscopy. *Nature Methods*, *12*, 717–724.
- Sánchez, H., Paul, M. W., Grosbart, M., Rossum-Fikkert, v., Sarah, E., Lebbink, J. H. G., et al. (2017). Architectural plasticity of human BRCA2–RAD51 complexes in DNA break repair. *Nucleic Acids Research*, *45*, 4507–4518.
- Schlacher, K., Christ, N., Siaud, N., Egashira, A., Wu, H., & Jasin, M. (2011). Double-strand break repair-independent role for BRCA2 in blocking stalled replication fork degradation by MRE11. *Cell*, *145*, 529–542.
- Stracy, M., Uphoff, S., Garza de Leon, F., & Kapanidis, A. N. (2014). In vivo single-molecule imaging of bacterial DNA replication, transcription, and repair. *FEBS Letters*, *588*, 3585–3594.
- Szymczak, A. L., Workman, C. J., Wang, Y., Vignali, K. M., Dilioglou, S., Vanin, E. F., et al. (2004). Correction of multi-gene deficiency in vivo using a single ‘self-cleaving’ 2A peptide-based retroviral vector. *Nature Biotechnology*, *22*, 589–594.

- Thompson, R. E., Larson, D. R., & Webb, W. W. (2002). Precise nanometer localization analysis for individual fluorescent probes. *Biophysical Journal*, *82*, 2775–2783.
- Tokunaga, M., Imamoto, N., & Sakata-Sogawa, K. (2008). Highly inclined thin illumination enables clear single-molecule imaging in cells. *Nature Methods*, *5*, 159–161.
- Van Royen, M. E., van Cappellen, W. A., Geverts, B., Schmidt, T., Houtsmuller, A. B., & Schaaf, M. J. M. (2014). Androgen receptor complexes probe DNA for recognition sequences by short random interactions. *Journal of Cell Science*, *127*, 1406–1416.
- Wang, S., Moffitt, J. R., Dempsey, G. T., Xie, X. S., & Zhuang, X. (2014). Characterization and development of photoactivatable fluorescent proteins for single-molecule-based superresolution imaging. *Proceedings of the National Academy of Sciences of the United States of America*, *111*, 8452–8457.
- Wright, A. V., Nunez, J. K., & Doudna, J. A. (2016). Biology and applications of CRISPR systems: Harnessing nature's toolbox for genome engineering. *Cell*, *164*, 29–44.
- Zhen, C. Y., Tatavosian, R., Huynh, T. N., Duc, H. N., Das, R., Kokotovic, M., et al. (2016). Live-cell single-molecule tracking reveals co-recognition of H3K27me3 and DNA targets polycomb Cbx7-PRC1 to chromatin. *eLife*, *5*, 1–36.



# Single-Stranded DNA Curtains for Studying the Srs2 Helicase Using Total Internal Reflection Fluorescence Microscopy

Luisina De Tullio<sup>2</sup>, Kyle Kaniecki<sup>2</sup>, Eric C. Greene<sup>1</sup>

Columbia University, New York, NY, United States

<sup>1</sup>Corresponding author: e-mail address: ecg2108@cumc.columbia.edu

## Contents

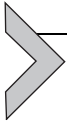
|  |     |
|--|-----|
| 1. Introduction  | 408 |
| 1.1 Homologous Recombination   | 408 |
| 1.2 Srs2 Functions and Activities During HR                            | 408 |
| 1.3 Single-Molecule Studies of Helicase Activities                     | 411 |
| 2. Methods   | 412 |
| 2.1 Overview of ssDNA Curtains for Studying Protein–ssDNA Interactions | 412 |
| 2.2 Protein and ssDNA Preparation                                      | 414 |
| 2.3 Procedures for ssDNA Curtain Assembly                              | 419 |
| 2.4 Visualizing Srs2 Translocation Activity Using ssDNA Curtains       | 424 |
| 2.5 Data Analysis  | 429 |
| 3. Conclusions and Future Directions                                   | 433 |
| Acknowledgments  | 433 |
| References   | 434 |

## Abstract

Helicases are crucial participants in many types of DNA repair reactions, including homologous recombination. The properties of these enzymes can be assayed by traditional bulk biochemical analysis; however, these types of assays cannot directly access some types of information. In particular, bulk biochemical assays cannot readily access information that may be obscured in population averages. Single-molecule assays offer the potential advantage of being able to visualize the molecules in question in real time, thus providing direct access to questions relating to translocation velocity, processivity, and insights into how helicases may behave on different types of substrates. Here, we describe the use of single-stranded DNA (ssDNA) curtains as an assay for directly

<sup>2</sup> Equal contribution.

viewing the behavior of the *Saccharomyces cerevisiae* Srs2 helicase on single molecules of ssDNA. When used with total internal reflection fluorescence microscopy, these methods can be used to track the binding and movements of individual helicase complexes, and allow new insights into helicase behaviors at the single-molecule level.



## 1. INTRODUCTION

### 1.1 Homologous Recombination

Homologous recombination (HR) is essential for maintaining genome integrity, and HR defects are directly linked to human cancers and cancer-prone syndromes (Kass, Moynahan, & Jasin, 2016; Malkova & Haber, 2012; Moynahan & Jasin, 2010; Prakash, Zhang, Feng, & Jasin, 2015). HR allows for the repair of double-stranded DNA breaks (DSBs) and is also necessary for the recovery of stalled or collapsed replication forks (Heyer, 2015; Jasin & Rothstein, 2013; Mazon, Mimitou, & Symington, 2010; Paques & Haber, 1999; Symington, Rothstein, & Lisby, 2014).

HR is promoted by the *RAD52* epistasis group of genes, which were originally identified in *Saccharomyces cerevisiae* as mutants defective in DNA repair (Paques & Haber, 1999; Symington et al., 2014). During HR, single-stranded DNA (ssDNA), derived from the nucleolytic processing of a DSB or collapsed replication fork, is quickly bound by RPA (replication protein A), which is a conserved heterotrimeric eukaryotic protein complex that removes ssDNA secondary structure, protects ssDNA from nucleolytic degradation, and serves as a platform from DNA damage signaling (Chen & Wold, 2014). With the aid of Rad52, RPA is replaced by the ATP-dependent DNA-binding protein Rad51, which forms an extended right-handed helical filament on ssDNA, and the resulting nucleoprotein filament is referred to as the presynaptic complex (Kowalczykowski, 2015). Pairing of the presynaptic complex with a homologous dsDNA template results in displacement of the noncomplementary strand from the duplex to generate a D-loop (Kowalczykowski, 2015). The resulting intermediate can be processed via one of several alternative pathways, all of which can allow for the repair of the DSB using information derived from the donor template (Paques & Haber, 1999; Symington et al., 2014) (Fig. 1).

### 1.2 Srs2 Functions and Activities During HR

There are approximately 95 helicases encoded within the human genome, and these proteins participate in nearly all aspects of nucleic acid metabolism,

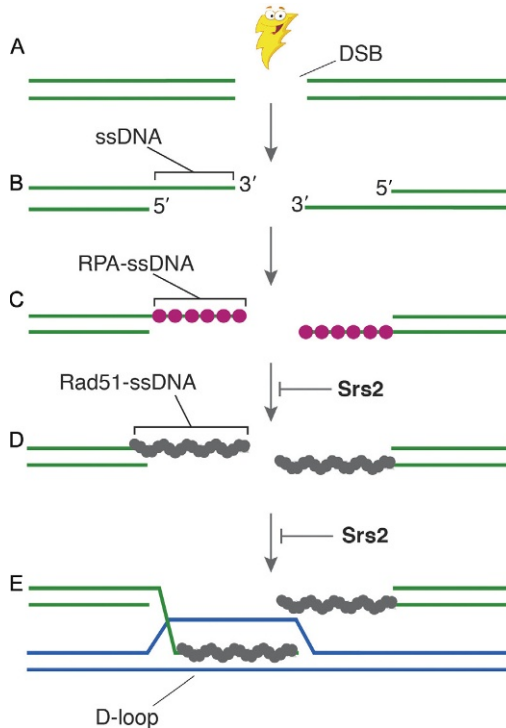


**Fig. 1** The role of Srs2 in HR. Here, we show a highly simplified overview of the early stages of HR and indicate the steps at which Srs2 has been implicated to act upon recombination intermediates. (A) In this simplified schematic, HR begins with the formation of a double-stranded break (DSB). (B) The break is then processed by 5' → 3' resection, resulting in the formation of long 3' ssDNA overhangs. (C) These ssDNA overhangs serve as a binding platform for replication protein A (RPA), which is necessary to protect the ssDNA against degradation and is also required for the removal of secondary structure to enable efficient assembly of the Rad51 filaments. (D) The RPA is then replaced by the Rad51 to yield Rad51-ssDNA filaments, which are also referred to as presynaptic complexes. (E) The presynaptic complex then performs the homology search to locate a double-stranded DNA molecule with sequence complementarity to the ssDNA that is bound by Rad51. Once homology has been identified, Rad51 catalyzes a strand invasion reaction to generate a D-loop intermediate in which the presynaptic ssDNA is paired with its complement, and the noncomplementary is displaced. The 3' terminus of the invading ssDNA within the D-loop can now serve as a primer for the DNA synthesis reactions that are required for downstream steps in the HR pathway. As highlighted in the figure, Srs2 has been reported to act at two key stages of this pathway, by either dismantling the Rad51 filaments (Krejci et al., 2003; Veaute et al., 2003), or by disrupting early strand invasion intermediates (Liu et al., 2017).

including the DNA repair pathways that are necessary for maintenance of genome stability (Bernstein, Gangloff, & Rothstein, 2010; Branzei & Szakal, 2017; Brosh, 2013; Croteau, Popuri, Opreko, & Bohr, 2014; Niu & Klein, 2017). For instance, HR is held in check by many regulatory mechanisms, including those mediated through the action of DNA helicases. Indeed, several helicases promote genome stability and accurate recombination by functioning as antirecombinases that prevent aberrant HR by dismantling inappropriate or toxic recombination intermediates (Bernstein et al., 2010; Branzei & Szakal, 2017; Brosh, 2013; Croteau et al., 2014; Niu & Klein, 2017). It is now thought that in many instances the normal behavior of these HR-related helicases is to disrupt recombination intermediates, rather than to simply separate duplex nucleic acids (Bernstein et al., 2010; Branzei & Szakal, 2017; Brosh, 2013; Croteau et al., 2014; Niu & Klein, 2017). The importance of these enzymes is underscored by helicase mutations that give rise to human diseases such as Rothmund–Thomson syndrome and Fanconi anemia, which are both characterized by genome instability and increased incidence of cancer (Bernstein et al., 2010; Brosh, 2013; Croteau et al., 2014).

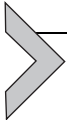
The *S. cerevisiae* protein Srs2 is a superfamily 1 (SF1) helicase and antirecombinase that is required for genome integrity, and deletion of the *SRS2* gene results in an increase in recombination frequency (Niu & Klein, 2017). Srs2 is considered a prototypical antirecombinase due to its well-characterized ability to remove Rad51 filaments from ssDNA (Fig. 1) (Antony et al., 2009; Krejci et al., 2003; Marini & Krejci, 2010; Niu & Klein, 2017; Qiu et al., 2013; Sasanuma, Furihata, Shinohara, & Shinohara, 2013; Vasianovich et al., 2017; Veaute et al., 2003). The importance of Srs2 for genome integrity was revealed in genetic studies showing that  $\Delta srs2 \Delta sgs1$  and  $\Delta srs2 \Delta Rad54$  double mutants, which are synthetic lethal, presumably due the accumulation of toxic recombination intermediates (Ira, Malkova, Liberi, Foiani, & Haber, 2003; Klein, 2001). Srs2 is homologous to the bacterial UvrD, PcrA, and Rep helicases, which are also thought to promote the removal of RecA from ssDNA (Marini & Krejci, 2010; Niu & Klein, 2017; Park et al., 2010; Petrova et al., 2015). Although Srs2 homologs have not yet been identified in humans, the mammalian protein FBH1 is a potential candidate, and FBH1 can also remove Rad51 from ssDNA (Simandlova et al., 2013). A growing body of evidence suggests similar antirecombinase regulatory roles might be filled by other helicases, including RECQ1, RECQ5, BLM (Sgs1 in yeast), FANCM (Mph1 in yeast), FANCI, and RTEL1 (Bernstein et al., 2010; Branzei & Szakal, 2017; Brosh, 2013; Heyer, Ehmsen, & Liu, 2010).

Thus, these types of helicases play crucial regulatory roles as anti-recombinases in many different organisms.

### 1.3 Single-Molecule Studies of Helicase Activities

Much of our knowledge of the helicases involved in HR comes from a combination of genetic and bulk biochemical studies. Indeed, Srs2 was originally identified in yeast as a suppressor of radiation-sensitive mutations in the error-prone repair pathway, and its deletion leads to a hyperrecombination phenotype (Niu & Klein, 2017; Palladino & Klein, 1992; Rong, Palladino, Aguilera, & Klein, 1991). Comparison of the Srs2 amino acid sequence revealed that the gene was highly homologous to the bacterial DNA helicases UvrD and Rep, and subsequent biochemical studies demonstrated that the protein has robust DNA-dependent ATP hydrolysis activity and helicase activity (Rong & Klein, 1993). Biochemical studies revealed the remarkable finding that Srs2 could strip Rad51 from ssDNA, providing detailed mechanistic insights into its antirecombinase activity (Krejci et al., 2003; Veaute et al., 2003). Further genetic analysis indicated that Srs2 suppressed crossovers, suggesting that it was capable of disrupting strand invasion intermediates (Ira et al., 2003), which was recently substantiated by in vitro biochemical analysis (Liu et al., 2017). Together, these studies illustrate the importance of genetics and biochemistry for defining protein functions in HR.

Single-molecule (SM) studies have the potential to further our understanding of HR by providing even more detailed insights into reaction mechanisms, and these methods are particularly beneficial for reactions that involve heterogeneous populations, transient intermediates, or both, as is often the case with reactions involving helicases. Indeed, SM methods have proven deeply insightful for understanding helicases, and some examples include SM studies of the RecBCD complex (Bianco et al., 2001; Spies et al., 2003), which is involved in DNA end processing in *Escherichia coli*, the bacterial Rep, UvrD, and PcrA helicases (Comstock et al., 2015; Myong, Rasnik, Joo, Lohman, & Ha, 2005; Park et al., 2010), the archaeal helicase XPD (Honda, Park, Pugh, Ha, & Spies, 2009), and the eukaryotic helicases Srs2 and Pif1 (Qiu et al., 2013; Sokoloski, Kozlov, Galletto, & Lohman, 2016). Studies of RecBCD relied primarily upon wide-field epi-illumination of bead-trapped DNA molecules, whereas most of the other helicases have been studied by smFRET. To help expand this toolbox of methods available for SM studies of helicases involved in HR, we have recently applied ssDNA curtain assays to study Srs2 activities at the SM level (De Tullio et al., 2017; Kaniecki et al., 2017).



## 2. METHODS

### 2.1 Overview of ssDNA Curtains for Studying Protein–ssDNA Interactions

We have developed DNA curtains as a tool for real-time visualization of protein–nucleic acid interactions at the SM level using total internal reflection fluorescence microscopy (TIRFM) (Fig. 2A) (Fazio, Visnapuu,

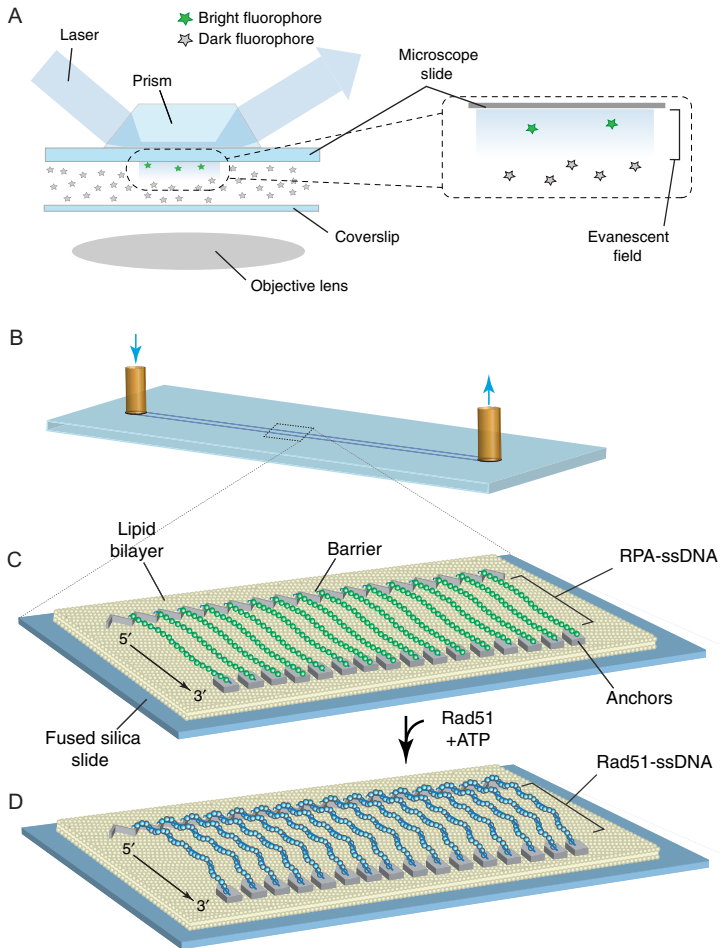


**Fig. 2** Schematic overviews of TIRFM and ssDNA curtains. (A) This illustration shows a simplified depiction of a typical prism-type TIRFM (Axelrod, 1989). Note: We use prism-type TIRFM setups because they allow for observation of reactions anchored to the

Wind, & Greene, 2008; Gorman, Fazio, Wang, Wind, & Greene, 2010; Graneli, Yeykal, Prasad, & Greene, 2006). In brief, DNA curtains are prepared by first depositing metal barriers and anchors on the surface of a fused silica microscope slide by electron-beam lithography. The slide is then coated with a fluid lipid bilayer, which prevents nonspecific surface adsorption and provides a mobile platform for anchoring DNA molecules through a biotin–streptavidin linkage. Buffer flow is used to push the DNA molecules into the barriers where they all align with one another (Fazio et al., 2008; Graneli et al., 2006). If desired, the second DNA end can be attached to a downstream anchor point (Fig. 2B–D) (Gorman, Fazio, et al., 2010). This approach can be used with dsDNA or ssDNA and allows for the direct visualization of hundreds of individual DNA molecules by TIRFM, thus offering a flexible experimental platform that can be adapted to the study of many types of protein–DNA interactions (Duzdevich et al., 2015; Gorman et al., 2012; Gorman, Plys, Visnapuu, Alani, & Greene, 2010; Lee, Finkelstein, Arciszewska, Sherratt, & Greene, 2014; Lee et al., 2015; Qi et al., 2015; Redding et al., 2015; Silverstein, Gibb, & Greene, 2014; Sternberg, Redding, Jinek, Greene, & Doudna, 2014; Wang et al., 2013). We have recently provided detailed descriptions of the TIRFM instrumentation used for these assays, the nanofabrication methods for

---

microscope slide glass, as opposed to the coverslip, which is visualized in objective-type TIRFM. The benefit of prism-type TIRFM is that the thicker microscope slides are more robust and can be easily modified by electron-beam lithography, and then repeated cleaned and reused (Greene et al., 2010; Ma et al., 2017). (B) Schematic illustration of a flow cell used for sample analysis by TIRFM. (C) Schematic showing a double-tethered ssDNA curtain. In this example, the surface is coated with a lipid bilayer, which is disrupted at defined locations by metallic patterns that have been deposited by electron-beam lithography (Greene et al., 2010; Ma et al., 2017). The zigzag-shaped upstream pattern is used for alignment of the ssDNA, and the pentagonal anchor points allow for nonspecific adsorption of the downstream ends of the RPA-ssDNA molecules. In this configuration, the RPA-ssDNA can be viewed even in the absence of buffer flow. Similar patterns, but omitting the anchor points, can be used to set up single-tethered ssDNA curtains, in which case constant buffer flow is necessary to keep the molecules within the evanescent field for visualization. (D) Rad51-ssDNA filaments can be assembled by injecting Rad51 into the sample chamber in the presence of ATP, and assembly of these filaments coincides with the loss of GFP signal due to dissociation of the GFP-tagged RPA (Qi et al., 2015). *Panels (B)–(D) were reproduced with permission from Qi, Z., Redding, S., Lee, J. Y., Gibb, B., Kwon, Y., Niu, H., et al. (2015). DNA sequence alignment by microhomology sampling during homologous recombination. Cell, 160, 856–869. doi: <https://doi.org/10.1016/j.cell.2015.01.029>.*

making patterned slide surfaces with electron-beam lithography, and the procedures for preparing microfluidic flow cells (Greene, Wind, Fazio, Gorman, & Visnapuu, 2010; Ma, Steinfeld, & Greene, 2017; Qi & Greene, 2016). Here, we describe methods for how ssDNA curtains can be used to study the *S. cerevisiae* helicase Srs2 as it acts upon ssDNA substrates bound by either Rad51 or RPA. Included in this information are details on fluorescent protein purification, ssDNA substrate preparation, and further details on bilayer deposition and ssDNA curtain preparation. We then provide a detailed overview on experiments using fluorescently tagged or unlabeled Srs2, and analysis of the resulting data.

## 2.2 Protein and ssDNA Preparation

A key aspect of using ssDNA curtains for studying the activities of Srs2 and other HR-related proteins is the need to prepare and purify fluorescently tagged proteins. For much of our work on HR we rely upon either unlabeled proteins, or proteins that are labeled with GFP or mCherry. Although GFP and mCherry are perhaps not as bright and photostable as many organic fluorophores, they offer the advantage of providing a homogeneous protein preparation where all of the proteins are labeled. Moreover, GFP-tagged versions of many HR proteins have already been evaluated in *in vivo* studies, including GFP-Srs2 and GFP-RPA, thus validating their biological functions (Burgess et al., 2009; Lisby, Barlow, Burgess, & Rothstein, 2004; Lisby & Rothstein, 2015). For GFP-labeled proteins that have not yet been tested, genetic assays are readily available to validate biological activities. Here, we will describe the procedures for producing GFP- or mCherry-labeled Srs2 and RPA; note that similar procedures also work for the unlabeled version of these proteins. For ssDNA curtains using Rad51, we rely upon unlabeled version of the protein, as GFP-tagged Rad51 is not functional *in vivo* (Lisby et al., 2004); procedures for purifying unlabeled *S. cerevisiae* Rad51 have been described elsewhere (Sung & Stratton, 1996).

### 2.2.1 Purification of GFP-Tagged Srs2

GFP- or mCherry-tagged Srs2 is expressed from a pET15b vector in *E. coli* Rosetta2 (DE3) cells (Novagen). In this instance, the N-terminus of the protein bears the GFP or mCherry fusion and also has a 9xHis tag that is used for purification. The GFP gene contains the A206K mutation to prevent GFP dimerization (Zacharias, Violin, Newton, & Tsien, 2002), and we typically work with Srs2<sup>898</sup>, which retains antirecombinase activity *in vitro*, but is less

prone to aggregation compared to the full-length construct (Antony et al., 2009). Unlabeled Srs2<sup>898</sup> is expressed from the pET11c vector.

1. Bacteria are freshly transformed, and then single colonies grown on LB-agar plates (supplemented with 100 µg/mL carbenicillin and 40 µg/mL chloramphenicol) are selected and grown in 25 mL culture for ~3–5 h. Then 1 mL of this culture is used to inoculate 1 L of LB medium supplemented with 100 µg/mL carbenicillin and 40 µg/mL chloramphenicol, and cultures are grown at 37°C with continuous shaking until reaching an OD<sub>600</sub> of ~1.0. The temperature is then reduced to 16°C before initiating protein expression by the addition of 0.1–0.5 mM isopropyl-β-D-thiogalactopyranoside (IPTG).
2. Cells are grown for an additional 20 h at 16°C with slow shaking (80 RPM). Cells are then harvested by centrifugation, and the cell pellet is frozen at –80°C.
3. The frozen cell pellet is thawed at 37°C and resuspended in cell breakage buffer containing 40 mM NaHPO<sub>4</sub> (pH 7.5), 600 mM KCl, 5% glycerol, 10 mM imidazole (pH 7.8), 0.1 mM TCEP (Tris(2-carboxyethyl)phosphine hydrochloride; Sigma, Cat. No. C4706), 0.05% Tween-20, 10 µM E-64 (Sigma-Aldrich, Cat. No. E3132), 100 µM AEBSF (4-(2-aminoethyl)benzenesulfonyl fluoride hydrochloride; Sigma-Aldrich, Cat. No. A8456), 1 mM benzamidine, and 1 mM PMSF (phenylmethanesulfonyl fluoride; Sigma-Aldrich, Cat. No. P7626). The cells are then lysed by sonication on ice, and the lysate was clarified by ultracentrifugation at 25,000 rpm for 30 min.
4. The clarified lysate (~30–40 mL) is then incubated for 30 min with a Talon metal affinity resin (5 mL bed volume per liter of culture; Clontech, Cat. No. 635503) equilibrated with Buffer Nickel A (40 mM NaHPO<sub>4</sub> [pH 7.5], 300 mM KCl, 5% glycerol, 15 mM imidazole, 0.02% Tween-20, 1 mM benzamidine, 1 mM PMSF, 0.125% myoinositol). Before elution, the column is washed extensively with Buffer Nickel A.
5. Proteins are eluted from the Talon metal affinity column with a step of Buffer Nickel A containing 400 mM imidazole (pH 7.8). Immediately after elution, the sample is adjusted to 5 mM EDTA (pH 8) and 1 mM TCEP.
6. The eluate is then dialyzed in SnakeSkin Dialysis Tubing (10,000 MWCO; Thermo Scientific, Cat. No. 68100) against 1 L of Heparin Buffer (20 mM NaHPO<sub>4</sub> [pH 7.5], 100 mM KCl, 5% glycerol, 0.01% Tween-20, 1 mM TCEP, 2 mM EDTA, 0.125% myoinositol) for 1.5 h, with 1 L buffer changes every 30 min.

7. The dialyzed eluate is then loaded onto a 5 mL HiTrap Heparin column (GE Lifesciences, Cat. No. 17-0406-01) equilibrated with Heparin Buffer, and proteins are eluted with a single step of Heparin Buffer containing 500 mM KCl.
8. The HiTrap Heparin-purified fraction (~4 mL) is then dialyzed in SnakeSkin Tubing (10,000 MWCO) against Storage buffer (40 mM NaHPO<sub>4</sub> [pH 7.5], 300 mM KCl, 10% glycerol, 0.01% Tween-20, 1 mM TCEP, 0.5 mM EDTA, 0.125% myoinositol) for 2 h at 4°C.
9. The sample is then applied to a Superdex 200 size exclusion column previously equilibrated with Storage buffer.
10. Peak fractions from the Superdex 200 corresponding to monomeric Srs2 are then pooled, flash frozen in liquid nitrogen, and stored in small aliquots at -80°C. The frozen aliquots should be small enough that each can be used for a single set of experiments to avoid multiple freeze-thaw cycles.

### 2.2.2 Purification of GFP-Tagged RPA

We use a GFP- or mCherry-tagged RPA to remove secondary structure from the ssDNA so that the molecules can be easily extended by buffer flow, and the fluorescent proteins also allow us to visualize the ssDNA with no need for any additional DNA-labeling dyes (Gibb, Silverstein, Finkelstein, & Greene, 2012). In addition, RPA-ssDNA is the physiological substrate for the early stages of HR in eukaryotes (Bianco, Tracy, & Kowalczykowski, 1998; Wold, 1997). *S. cerevisiae* RPA is a heterotrimeric protein complex comprised of Rfa1, Rfa2, and Rfa3 subunits, and we used a tagged version of RPA which bears the GFP or mCherry fusion on the C-terminus of the Rfa1 separated by a 7-alanine linker; note that this GFP-tagged version of RPA retains biological function in vivo (Lisby et al., 2004).

1. 6xHis-tagged *S. cerevisiae* RPA-eGFP and RPA-mCherry encoded in pET11d plasmid are expressed in *E. coli* Rosetta2 (DE3) cells (Novagen). The cells are grown in LB supplemented with 100 µg/mL carbenicillin and 40 µg/mL chloramphenicol at 37°C to an OD600 of ~1. The growth temperature is then reduced to 16°C and protein expression is induced by the addition of 0.5 mM IPTG, and the culture is grown for an additional 10–15 h at 16°C.
2. Cells are harvested by centrifugation, and the cell pellet is frozen at -80°C.

3. The cell pellet is then thawed and resuspended in cell lysis buffer (50 mM NaHPO<sub>4</sub>, 250 mM KCl, 5 mM imidazole [pH 7.9], 5% glycerol, 0.1 mM TCEP, 0.02% Tween-20, 10 μM E-64, 100 μM AEBSF, 1 mM benzamidine, 1 mM PMSF, and myoinositol 0.25%), and lysed by sonication. The lysate is clarified by ultracentrifugation at 25,000 rpm for 30 min.
4. The clarified lysate is then applied in batch to a Talon metal affinity resin (5 mL volume bed per liter of culture; Clontech, Cat. No. 635503) previously washed with Buffer A (30 mM NaHPO<sub>4</sub> [pH 7.5], 250 mM KCl, 5% glycerol, 10 mM imidazole, 0.02% Tween-20, 0.1 mM TCEP, 1 mM benzamidine, 1 mM PMSF, 0.125% myoinositol), and incubated with rotation for 30 min at 4°C.
5. The column is extensively washed with ~200 mL of Buffer A, and the bound RPA is then eluted with Buffer A containing 400 mM imidazole (pH 7.8).
6. The eluted protein is then dialyzed against buffer Superdex (30 mM NaHPO<sub>4</sub> [pH 7.5], 250 mM KCl, 10% glycerol, 0.02% Tween-20, 1 mM TCEP, 0.5 mM EDTA, 0.25% myoinositol) using a Float-A-Lyzer dialysis device (MWCO 3.5 kDa; Spectrum Labs, Cat. No. G235065).
7. The dialyzed fraction is concentrated to a final volume of ~4 mL using centrifugation (Vivaspin 6, 5000 MWCO; GE Healthcare, Cat. No. 28-9322-94), and is injected onto a Superdex 200 column. The peak containing trimeric RPA is pooled and concentrated using centrifugation (Vivaspin 6; GE Healthcare).
8. The final RPA-eGFP or RPA-mCherry concentrations can be determined from the absorbance of the eGFP or mCherry chromophores at 488 nm ( $\epsilon_{488\text{ nm}} = 55,000\text{ cm}^{-1}\text{ M}^{-1}$ ) or 587 nm ( $\epsilon_{587\text{ nm}} = 72,000\text{ cm}^{-1}\text{ M}^{-1}$ ), respectively. The presence of the three subunits of RPA can be verified by analysis using SDS/PAGE 4%–20% gradient gels (Invitrogen, Cat. No. XP00122BOX) with Coomassie staining.
9. The final protein concentration should be ~10–20 μM. The purified protein is then flash frozen in liquid nitrogen and stored at –80°C in small aliquots to avoid freeze–thaw cycles.

### 2.2.3 Preparation of ssDNA

An important benefit of ssDNA curtain assays is that they allow the use of long ssDNA substrates, on the order of  $\geq 40,000$  nucleotides in length. Use of this long ssDNA is important because TIRFM imaging allows one to visualize along the entire contour lengths of the molecules and thus obtain

spatial and temporal information from many different regions at once. These ssDNA substrates are prepared by rolling circle replication (RCR) using a circular ssDNA template and a biotinylated primer (Fig. 3A) (Gibb et al., 2012; Ma et al., 2017), as described below.

1. The biotinylated primer is annealed to a circular M13 DNA template in a 100  $\mu\text{L}$  reaction containing: 10 mM Tris-HCl (pH 8.0), 50 mM NaCl, 10 mM  $\text{MgCl}_2$ , 10  $\mu\text{g}$  (89.4 nM) of M13mp18 (New England

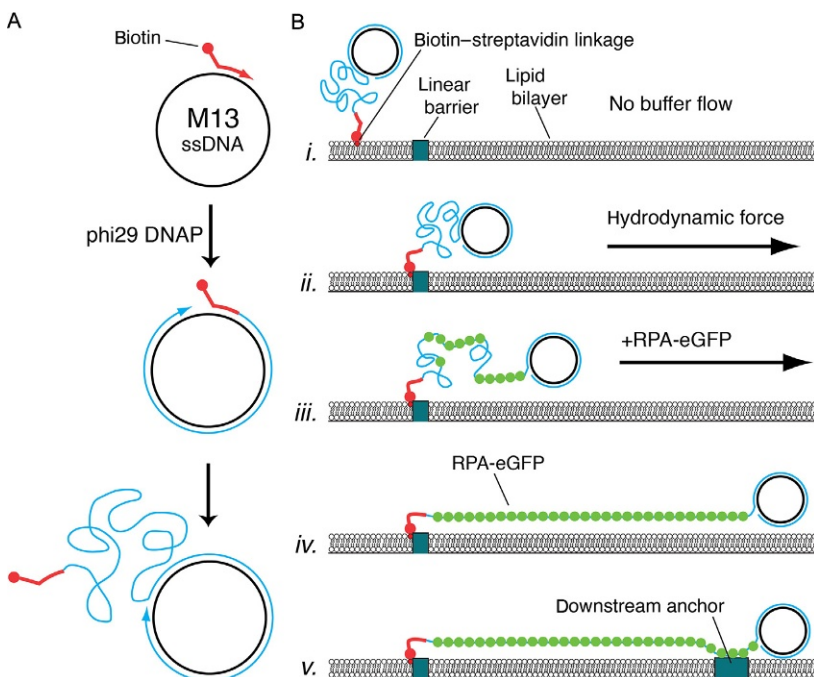


**Fig. 3** Schematic of ssDNA preparation and anchoring procedures. (A) The biotinylated ssDNA substrate is generated by rolling circle replication (RCR) using a biotinylated input primer, a circular ssDNA template such as M13mp18, and phi29 DNA polymerase (DNAP) (Gibb et al., 2012; Ma et al., 2017). (B) For single-tethered ssDNA curtains, the biotinylated ssDNA is first anchored to the bilayer, and the ssDNA is then aligned at the nanofabricated barriers through the application of buffer flow. RPA-GFP is then introduced into the flow cell to label the ssDNA and remove secondary structure. As RPA-GFP enters the sample chamber, the ssDNA becomes visible and gradually unfolds and extends parallel to the bilayer (Gibb et al., 2012; Ma et al., 2017). For double-tethered curtains, the RPA-ssDNA is nonspecifically adsorbed to exposed anchor points downstream from barriers (Gibb et al., 2012; Ma et al., 2017). Panels (A) and (B) were adapted with permission from Gibb, B., Silverstein, T. D., Finkelstein, I. J., & Greene, E. C. (2012). Single-stranded DNA curtains for real-time single-molecule visualization of protein-nucleic acid interactions. *Analytical Chemistry*, 84, 7607–7612. Copyright (2012) American Chemical Society.

Biolabs, Cat. No. N4040S), and 20 nM primer (5'—BIOTEG—TTT TTT TTT TTT TTT TTT TTT TTT TTT GTA AAA CGA CGG CCA GT). The annealing mix is placed in a  $\sim 95^{\circ}\text{C}$  water bath for  $\sim 5$  min, and the water bath is then placed on a benchtop and allowed to cool slowly to room temperature. Alternatively, the annealing mix can be placed in a thermocycler and slowly cooled from  $95^{\circ}\text{C}$  to  $4^{\circ}\text{C}$ , over 30 min. The annealing reactions are then diluted with buffer containing 10 mM Tris–HCl (pH 8.0), 50 mM NaCl, and 5 mM  $\text{MgCl}_2$  to a total volume of 300  $\mu\text{L}$  and can be stored at  $-20^{\circ}\text{C}$  until use.

2. We typically make a fresh preparation of ssDNA for each ssDNA curtain experiment using RCR. RCR reactions are prepared using 10  $\mu\text{L}$  of  $5\times$  reaction buffer (250 mM Tris–HCl [pH 7.5], 20 mM DTT, 50 mM ammonium sulfate, and 50 mM  $\text{MgCl}_2$ ), 1  $\mu\text{L}$  annealed M13 template (see above), 2  $\mu\text{L}$  of 10 mM dNTP mix, 1  $\mu\text{L}$  purified  $\phi 29$  polymerase (10  $\mu\text{M}$  stock) (Gibb et al., 2012), and 36  $\mu\text{L}$  water for a final sample volume of 50  $\mu\text{L}$ . Samples are mixed by gentle pipetting to avoid shearing the DNA.
3. RCR reactions are then incubated at  $30^{\circ}\text{C}$  for 25 min, and used immediately after preparation. Alternatively, we have also prepared RCR reactions in a final volume of 500  $\mu\text{L}$ . These larger reactions can then be divided into smaller aliquots, flash frozen on liquid nitrogen stored at  $-80^{\circ}\text{C}$ .

## 2.3 Procedures for ssDNA Curtain Assembly

An important aspect of DNA curtain experiments is the requirement for a supported lipid bilayer, which is deposited onto the nanopatterned surface of the sample chamber; detailed descriptions of nanofabrication and flow cell assembly procedures have been described elsewhere (Greene et al., 2010; Ma et al., 2017). The bilayer passivates the surface to minimize nonspecific adsorption of proteins, and the bilayer also serves as a mobile anchor point for tethering the 5' ends of the ssDNA substrates. Tethering is achieved by spiking the bilayer with a small fraction of biotinylated lipids to which the biotinylated ssDNA molecules are anchored through a biotin–streptavidin linkage (Fig. 3B).

### 2.3.1 Liposome Stock Solutions

A liposome stock solution is required to deposit the lipid bilayer onto the sample surface, and here we describe basic procedures for preparation of the liposome stock. It should be noted that if the lipid bilayer is not fluid,

then the tethered DNA molecules cannot be aligned into DNA curtains. Therefore, we encourage persons making lipid bilayers for the first time to prepare a control bilayer that is spiked with a small fraction ( $\leq 1\%$ ) of fluorescently tagged lipids (e.g., rhodamine-PE; L- $\alpha$ -phosphatidylethanolamine-*N*-(lissamine rhodamine B sulfonyl) (ammonium salt), Avanti Polar Lipids Inc., Cat. No. 810146C), and a simple FRAP (fluorescence recovery after photo-bleaching) measurement can be used to determine whether the lipids within the bilayer are mobile (Graneli et al., 2006).

1. Steps described that require the use of chloroform should be performed in an approved fume hood by laboratory personnel trained in the proper use of organic solvents.
2. Lipid stocks are prepared by dissolving the following components in 10 mL of chloroform: 1 g DOPC (1,2-dioleoyl-*sn*-glycero-3-phosphocholine) (Avanti Polar Lipids, Inc., Cat. No. 850375P), 100 mg PEG-2000 DOPE (18:1 PEG2000:1,2-dioleoyl-*sn*-glycero-3-phosphoethanolamine-*N*-[methoxy(polyethylene glycol)-2000] (ammonium salt)) (Avanti Polar Lipids, Inc., Cat. No. 880130P), and 5 mg biotinylated DOPE (1,2-dioleoyl-*sn*-glycero-3-phosphoethanolamine-*N*-(cap biotiny) (sodium salt)) (Avanti Polar Lipids, Inc., Cat. No. 870273P). The dissolved lipid mixtures can then be stored at  $-20^{\circ}\text{C}$ .
3. Clean an organic solvent-compatible syringe (e.g., Hamilton, Cat. No. 91022) by flushing the syringe with chloroform. Then use the syringe to transfer 200  $\mu\text{L}$  of the lipid stock to a 2-mL glass vial (National Scientific, Cat. No. C4015).
4. Apply a gentle stream of nitrogen gas to the sample to slowly evaporate the chloroform from the lipid stock; this step should take several minutes. The pressure of the nitrogen stream can be increased once the chloroform has visibly evaporated to help ensure speed evaporation of the chloroform. The uncapped glass vial can then be placed under vacuum overnight to ensure complete removal of all traces of chloroform. When complete, the lipid stock should appear as a solid residue visible on the side of the glass vial.
5. 2 mL of lipid buffer (10 mM Tris-HCl [pH 8.0], 100 mM NaCl) is then added to the dried lipid residue. The dry lipids are resuspended into the buffer with the help of an automatic pipette. The sample should be incubated at room temperature for approximately 1 h to help hydrate the lipids. Following this incubation, the sample is then vortexed until all the dried lipids are suspended into solution as judged by visual inspection. At this stage, the solution will appear turbid.

6. The dissolved lipid mixture is then transferred to a 5-mL polypropylene culture tube (Falcon, Cat. No. 35-2058) and sonicated in an ice bath using a microtip sonicator (Misonix S-4000). Sonication is performed in 5–10 s bursts, with 1-min intervals between bursts. Sonicate until the turbid lipid solution becomes clear—this typically takes ~3–5 min of total sonication time.
7. After sonication, the resulting liposomes should be filtered through a 0.22- $\mu\text{m}$  nylon syringe filter (Fisherbrand, Cat. No. 09-720-3). This liposome stock solution is ready for use and can be stored for approximately 30 days at 4°C.

### 2.3.2 Lipid Bilayers and ssDNA Substrate Attachment

Here, we describe how the bilayer is deposited onto the flow cell surface and how the ssDNA is attached to the bilayer. Note that if air bubbles pass through the sample chambers, they will destroy the lipid bilayer; in our experience, disruption of the bilayer due to passage of an air bubble through the sample chamber is a common failure point. Therefore, extreme care should always be taken to prevent any air from entering the flow cell, and drop-to-drop connections must be used for all tubing and syringe attachments. Degassing buffers prior to use can help minimize bubble accumulation and are highly recommended.

1. Make two pieces of tubing to connect the syringes to the flow cell ports (Greene et al., 2010; Ma et al., 2017). For this, cut ~8 cm of tubing (IDEX, Cat. No. 1907L), and attach a connector (IDEX, Cat. No. F-333NX) to the end of one piece of tubing—this end will be connected to the flow cell. On the other end of the tubing, place first one connector (IDEX, Cat. No. F-300X) and then attach a female-to-female Luer peek (IDEX, Cat. No. P-659)—this end will be attached to the syringe.
2. Fill two 3-mL plastic syringes (BD, Cat. No. 309657) with degassed MilliQ water. Remove all air bubbles from the syringe, and then connect the tubing to the syringe. Push some water into the tubing removing all the bubbles, and then connect one tubing with its attached syringe to the inlet port of the flow cell. Next, connect the second tubing with its attached syringe to the outlet port of the flow cell.
3. Once both syringes are connected, gently push 1 mL of water through the flow cell by hand and use the two syringes to gently flush the water back and forth through the sample chamber. This procedure helps remove any air bubbles from the sample chamber prior to bilayer deposition.

4. Next, fill two 10-mL plastic syringes (BD, Cat. No. 309604) with 5 mL of lipid buffer (10 mM Tris-HCl [pH 8], 100 mM NaCl). Disconnect one of the 3-mL syringes from the flow cell, gently push water from the remaining 3-mL syringe through the sample chamber, and then make a drop-to-drop connection with one of the 10-mL syringes. Next, disconnect the remaining 3-mL syringe, and replace it with the second 10-mL syringe, again being sure to make drop-to-drop connections. Then slowly flush the buffer back and forth several times until no bubbles are present in the flow cell.
5. Mix 40  $\mu\text{L}$  of the liposome stock solution with 960  $\mu\text{L}$  of lipid buffer (10 mM Tris-HCl [pH 8.0], 100 mM NaCl). Fill a 1-mL plastic syringe (BDH, Cat. No. 309659) with the lipid solution. Next, replace one of the 10-mL syringes with this 1-mL syringe using drop-to-drop connections. Gently push  $\sim 200$   $\mu\text{L}$  of the mixture into the flow cell, and then repeat this process every 5–8 min until all of the liposome mixture is used. After the final injection, wait 5–8 min more, and wash the flow cell with 3 mL of lipid buffer. Then incubate the flow cell for  $\sim 20$  min at room temperature to allow formation of the bilayer.
6. Any areas of the flow cell surface that remain exposed after bilayer deposition are then blocked by gently flushing 3 mL of HR buffer (30 mM Tris-Ac [pH 7.5], 50 mM KCl, 5 mM MgAc, 1 mM DTT, 0.3 mg/mL BSA) through the chamber and the flow cell is incubated for an additional  $\sim 5$  min at room temperature.
7. The biotinylated lipids must now be saturated with streptavidin to provide anchor points for the biotinylated ssDNA (see [Section 2.2.3](#)). For this, mix 980  $\mu\text{L}$  of HR buffer with 25  $\mu\text{L}$  of streptavidin stock mix (1 mg/mL; Sigma-Aldrich, Cat. No. S0677) and slowly flush the solution through the sample chamber in one step.
8. Carefully flush the sample chamber with 3 mL of HR buffer to remove all traces of free streptavidin. This step is crucial because it may not be possible to attach the biotinylated ssDNA to the surface if any free streptavidin remains in solution.
9. The sample chamber is now ready for addition of the ssDNA sample. Dilute the RCR reaction (30–50  $\mu\text{L}$ ) by the addition of 1 mL of HR buffer and then slowly push  $\sim 200$   $\mu\text{L}$  of the diluted ssDNA sample through the flow cell. Note: This injection should be in the direction that pushes the ssDNA into the barriers (e.g., from left to right in [Fig. 3B](#)). Repeat this process every 5 min until all of the solution is used.

Following the final ssDNA injection, replace the 1-mL syringe with a new 3-mL syringe containing HR buffer.

10. Once complete, the flow cell can be mounted onto the microscope stage and connected to a sample injection system; our group uses a simple injection system comprised of a syringe pump (KD Scientific KDS-201) and a high-pressure switch valve, which can be used for sample injections (IDEX Health & Science, MXP9900-000) (Greene et al., 2010; Ma et al., 2017). While attaching the flow cell to the injection system, it is again absolutely essential to use drop-to-drop connections to avoid inadvertently injecting air bubbles through the sample chamber. The first step in the connection process is to disconnect the inlet syringe from tubing and connect the tubing to a union body (IDEX, Cat. No. P-760-01). Make a drop-to-drop connection with the sample delivery system (0.2 mL/min). After that, disconnect the outlet syringe and close the system. Flush the flow cell with HR buffer at 0.5 mL/min for 5 min to push the ssDNA molecules into the barriers. Stop the flow, and then incubate for 10 min to help ensure that the ssDNA is evenly distributed along the barriers. After this incubation period the flow cell is ready for injection of RPA (see Section 2.3.3).

### 2.3.3 Using RPA-GFP to Visualize ssDNA

We use GFP- or mCherry-tagged RPA to both fluorescently label the tethered ssDNA molecules and to help remove the ssDNA secondary structure prior to testing the activities of other HR proteins (Gibb et al., 2012). The use of GFP-RPA offers the additional benefit that RPA-ssDNA is the physiological relevant substrate for early steps in HR (Chen & Wold, 2014; Wold, 1997). Here, we outline a typical procedure for labeling and extending double-tethered ssDNA curtains with RPA-GFP or RPA-mCherry. It should be noted that the same procedures can be used with unlabeled RPA, but the ssDNA will not be visible by TIRFM until another fluorescently tagged ssDNA binding protein, such as the mediator protein Rad52, is injected into the sample chamber (Gibb et al., 2014).

1. The stock solution of *S. cerevisiae* RPA-GFP taken from the  $-80^{\circ}\text{C}$  freezer is directly diluted into 30 mL of HR buffer at room temperature. RPA has a nanomolar binding affinity for ssDNA (Wold, 1997), so a final concentration of 0.1 nM RPA-GFP is typically sufficient to label and extend the tethered ssDNA molecules.

2. The RPA-GFP sample is then flushed through the sample chamber containing tethered ssDNA molecules at a rate of 0.8 mL/min for approximately 5–10 min. The unbound ssDNA is not visible, but will become labeled almost immediately upon injecting RPA-GFP. The ssDNA will initially appear as highly compacted fluorescent foci due to the presence of extensive secondary structure, but the molecules will extend over the course of the RPA injection as this secondary structure is disrupted (Fig. 3B).
3. Shortly after beginning the RPA buffer flow, a 500  $\mu$ L pulse of 6 M urea is flushed through the sample chamber at a flow rate of 0.8 mL/min. This pulse of 6 M urea does not affect the lipid bilayer or disrupt the biotin–streptavidin linkages, and is used to help remove any residual ssDNA secondary structure,  $\phi$ 29 DNA polymerase, or M13 circular ssDNA template. The urea is then flushed out of the sample chamber by continuous buffer flow at a flow rate of 0.8 mL/min—this high flow rate helps ensure that the RPA–ssDNA molecules will adhere to the downstream anchor points (see Figs. 2C and 3B).
4. The location and the quality of the RPA-bound ssDNA curtains can now be verified by visual inspection using TIRFM, and once their locations have been determined, the RPA–ssDNA molecules are ready for subsequent experimental analysis.

## 2.4 Visualizing Srs2 Translocation Activity Using ssDNA Curtains

Here, we provide detailed examples of experimental methods for visualizing the behavior of either unlabeled or GFP-tagged Srs2 as it acts upon Rad51-bound ssDNA, and we also provide methods for visualizing the behavior of GFP- or mCherry-tagged Srs2 as it acts upon ssDNA bound by fluorescent RPA. The experiments described below utilize a prism-type total TIRFM microscope (Nikon) equipped with a 488-nm laser (Coherent Sapphire, 200 mW) and a 561-nm laser (Coherent Sapphire, 200 mW), which can be used to excite GFP and mCherry fluorescent proteins, respectively.

### 2.4.1 Visualizing Srs2 as It Acts Upon Rad51-ssDNA

The following procedure describes how to prepare Rad51 filaments and visualize Srs2 translocation beginning with double-tethered ssDNA curtains bound by RPA-GFP (see Section 2.3.3). These assays can be used with unlabeled Srs2, and in this case, the movement of Srs2 along the Rad51–ssDNA can be revealed by the rebinding of fluorescent RPA (Fig. 4A).

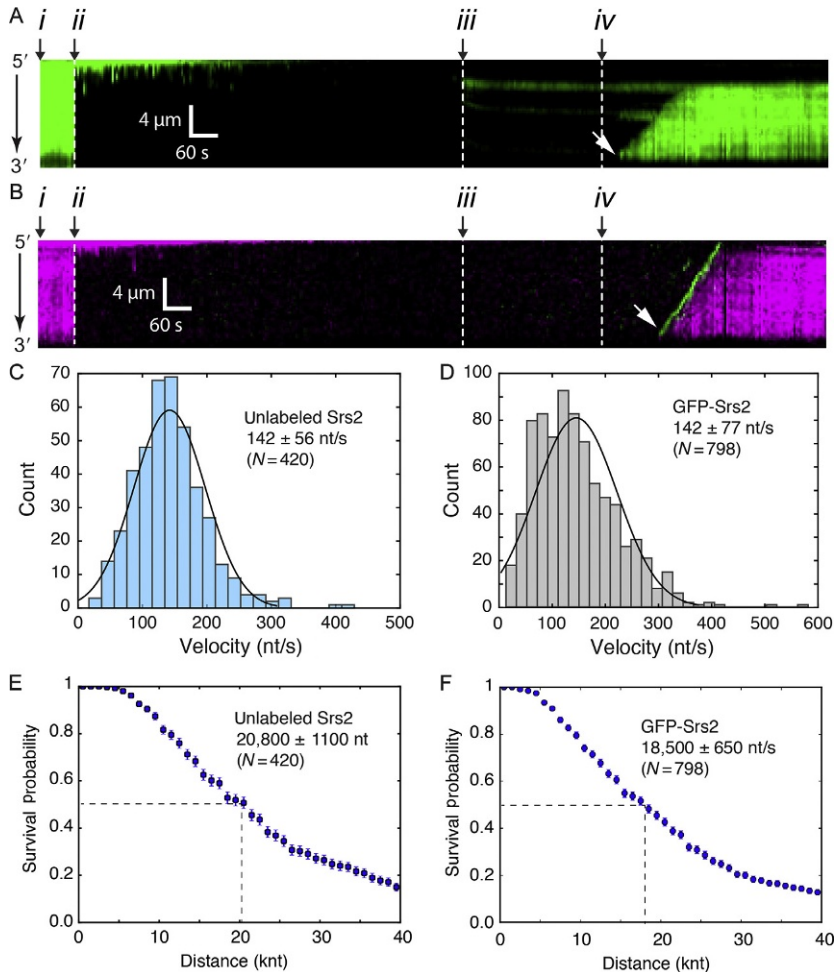


**Fig. 4** Examples of Srs2 translocation on single Rad51-ssDNA molecules. (A) Examples of kymographs for double-tethered ssDNA curtain assays for Srs2<sup>898</sup> and GFP-RPA. (B) Examples of kymographs for double-tethered ssDNA curtain assays for GFP-Srs2<sup>898</sup> and mCherry-RPA. In (A) and (B): (i) corresponds to the start of the experiment, in which the ssDNA is coated with fluorescent RPA; (ii) indicates assembly of the Rad51 filaments upon injection of Rad51 and ATP; (iii) free Rad51 is then flushed from the sample chamber; and (iv) Srs2 is injected into the sample chamber; and (v) the white arrowheads highlight the beginning of Srs2 translocation events. (C) Velocity distributions for unlabeled Srs2<sup>898</sup> acting upon Rad51-ssDNA in the presence of RPA-GFP. (D) Velocity distributions for GFP-Srs2<sup>898</sup> acting upon Rad51-ssDNA in the presence of RPA-mCherry. Survival probability of (E) unlabeled Srs2<sup>898</sup> and (F) GFP-Srs2<sup>898</sup> acting on Rad51-ssDNA. Dashed lines in (E) and (F) highlight the values at which half of the complexes stop translocating. Error bars in the survival probability plots represent s.d. calculated from bootstrap analysis. Panels reproduced with permission from Kaniecki, K., De Tullio, L., Gibb, B., Kwon, Y.-H., Sung, P., & Greene, E. C. (2017). Dissociation of Rad51 presynaptic complexes and heteroduplex DNA joints by tandem assemblies of Srs2. *Cell Reports*, 21(11), 3166–3177.

Alternatively, fluorescently tagged Srs2 can be visualized as fluorescent molecules that bind to and translocate along the Rad51-ssDNA, while the tracts of Rad51 that are removed from the DNA can be concurrently visualized by the reappearance of fluorescent RPA (Fig. 4B).

1. Rad51 filament assembly is initiated by injecting 1–2  $\mu\text{M}$  *S. cerevisiae* Rad51 in HR buffer containing 2 mM ATP in the absence of RPA. Rad51 filament formation can proceed in the presence of RPA, but is inhibited with increasing concentrations of RPA in solution.
2. The sample is then incubated in the absence of flow for 10–15 min at 32°C to allow for Rad51 filament assembly. If using fluorescent RPA, the Rad51 assembly reaction can be monitored by visual inspection of the RPA-GFP, which will be displaced from the ssDNA upon Rad51 binding.
3. Buffer flow is then resumed with HR buffer containing 2 mM ATP and 100 pM RPA-GFP at 0.2 mL/min for 3 min to flush away any remaining free Rad51. The Rad51 filaments will remain stable so long as ATP is present in the buffer, so the RPA-GFP present in the buffer should not bind to the ssDNA, but rather serves to verify that the Rad51 filaments remain intact.
4. A 150  $\mu\text{L}$  inline loop containing a sample of Srs2 (unlabeled, GFP- or mCherry-tagged, as desired; typically, at a concentration of 100 pM) diluted in the same HR buffer flowing through the sample chamber is opened, and the ssDNA molecules are observed by TIRFM while continuously flushing with HR buffer. This procedure results in a short pulse of Srs2 activity, coinciding with the 150  $\mu\text{L}$  injection, and free Srs2 will quickly be flushed from the sample chamber by the continuous buffer flow. This procedure restricts the number of Srs2 molecules that bind to the ssDNA during the initial injection, thus facilitating data analysis (see Section 2.5) by helping to ensure that a relatively small number of translocation trajectories will occur on any given ssDNA molecule.
5. Note that for experiments using the combination of GFP and mCherry, we use a two-color prism-type TIRFM system (Nikon) equipped with a 488-nm laser (Coherent Sapphire, 200 mW) for detecting GFP and a 561-nm laser (Coherent Sapphire, 200 mW) for detecting mCherry. For visualizing RPA-GFP, we typically use  $\sim 20\%$  ( $\sim 40$  mW) of the laser power (488 nm) for sample illumination. To detect single translocating mCherry-Srs2 complexes, we typically employ between 50% and 75% ( $\sim 100$ – $150$  mW) of the laser power (561 nm). To avoid the bleed-through from the green into the red channel during image acquisition,

we use a custom-built shuttering system in which the image from the green (GFP) and the red (mCherry) channels are recorded independently, and the green and red images are offset separating the acquisition of each other by 100 ms. With this shutter system, when one camera records the red channel image, the green laser is shuttered off, and vice versa.

6. For some experiments, it may be desirable to utilize dark RPA and dark Rad51. In these situations, the ssDNA will not be visible until bound by fluorescent Srs2, so researchers must rely upon control experiments previously performed using the fluorescent RPA to verify that all of the above procedure work as expected. It is also helpful in these cases to use ssDNA prepared from a larger RCR reaction that has been aliquoted and flash frozen and stored at  $-80^{\circ}\text{C}$  (see [Section 2.2.3](#)). Use of the frozen stock helps to avoid any batch-to-batch variability in the RCR ssDNA preparation, thereby ensuring that more reliable amounts of ssDNA are present on the flow cell surface.

#### **2.4.2 Visualizing Srs2 Binding and Translocation on RPA-ssDNA**

The following procedure describes how to visualize Srs2 translocation on double-tethered ssDNA curtains bound by RPA-GFP (i.e., in the absence of Rad51). Again, this procedure begins with the RPA-ssDNA curtains that are described in [Section 2.3.3](#). With this procedure, fluorescently tagged Srs2 can be visualized as fluorescent molecules that bind to and translocate along the fluorescent RPA-ssDNA ([Fig. 5A](#)). Srs2 removes RPA from the ssDNA, and the displaced RPA is continuously replenished by the free RPA in the sample buffer. However, as noted below, the experiment can also be modified to monitor the removal of fluorescent RPA from the ssDNA ([Fig. 5B](#)).

1. Experiments for mCherry-Srs2 translocation on RPA-GFP-bound ssDNA are performed in HR buffer (30 mM Tris-Ac [pH 7.5], 50 mM KCl, 5 mM MgAc, 1 mM DTT, 0.3 mg/mL BSA, and 2 mM ATP), and reactions are performed in flow cells maintained at  $32^{\circ}\text{C}$ , as described ([Ma et al., 2017](#)). Note that in this particular protocol, RPA-GFP is maintained in the buffer at a concentration of 100 pM, which ensures that the ssDNA is visible throughout the experiment.
2. For experiments using the combination of GFP and mCherry, we use the two-color prism-type TIRFM system (Nikon) equipped with a 488-nm laser (Coherent Sapphire, 200 mW) for detecting GFP, a 561-nm laser (Coherent Sapphire, 200 mW) for detecting mCherry,

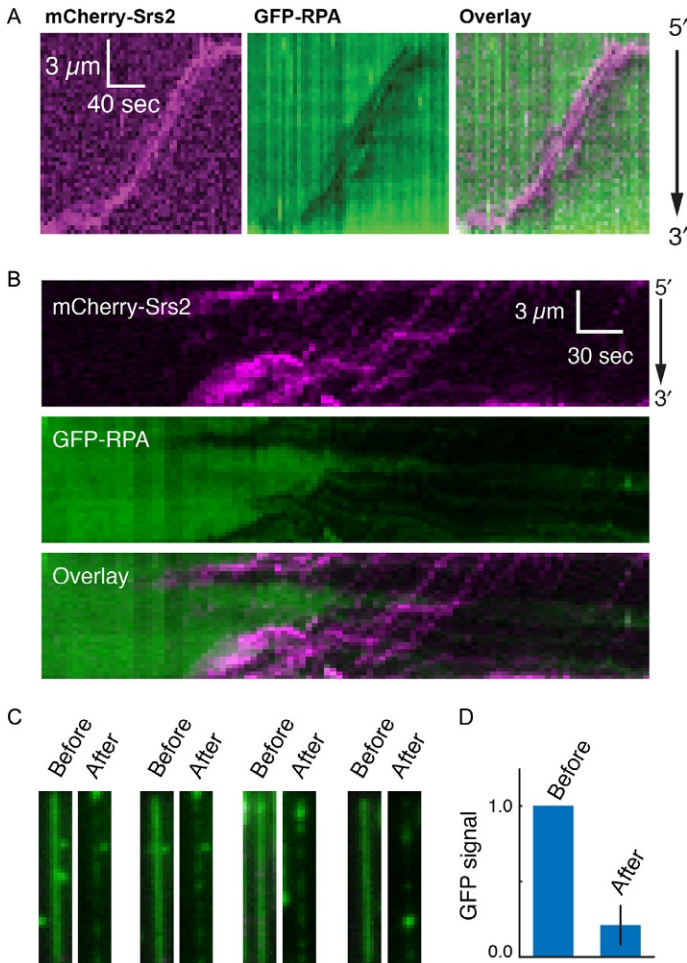


**Fig. 5** Examples of Srs2 translocation on single molecules of RPA-ssDNA. (A) Kymographs demonstrating the 3' → 5' movement of mCherry-Srs2 (magenta) along GFP-RPA-bound ssDNA (green). The orientation of the ssDNA is indicated, and the images show the mCherry-Srs2 fluorescence signal, the GFP-RPA fluorescence signal, and the overlaid fluorescence signals, as indicated. (B) mCherry-Srs2 translocation on GFP-RPA-bound ssDNA when free GFP-RPA is absent from solution. The three kymographs show the mCherry-Srs2 fluorescence signal (top), the GFP-RPA signal (middle), and the overlaid images (bottom), as indicated. (C) Images of GFP-RPA-bound ssDNA before and after injection of mCherry-Srs2. (D) Fractional loss of normalized GFP-RPA signal (integrated over entire ssDNA molecules;  $N = 20$ ) due to the action of Srs2. Panels reproduced with permission from De Tullio, L., Kaniecki, K., Kwon, Y.-H., Crickard, J. B., Sung, P., & Greene, E. C. (2017). Yeast Srs2 helicase promotes redistribution of single-stranded DNA-bound RPA and Rad52 in homologous recombination regulation. *Cell Reports*, 21(3), 570–577.

and the custom-built shuttering system to eliminate signal bleed-through (see [Section 2.4.1](#)).

3. To visualize mCherry-Srs2 binding and translocation, inject a 150  $\mu\text{L}$  aliquot of mCherry-Srs2 (typically 100  $\mu\text{M}$ ) in HR buffer while maintaining a constant flow rate of 0.2 mL/min. This procedure results in a 45-s injection window during which mCherry-Srs2 can bind to the RPA-ssDNA molecules; after this time period the HR buffer behind the injection loop *does not* contain any Srs2. Therefore, any unbound mCherry-Srs2 will be flushed from the sample chamber. This procedure helps minimize the number of mCherry-Srs2 binding events, which makes interpretation of the resulting data much easier (see [Section 2.5](#)).
4. Begin recording data  $\sim 2$  min before mCherry-Srs2 enters the sample chamber, and continue data collection for a total of 20 min (300 frames total). For a typical experiment, data can be collected at a rate of 1 frame per 4 s with 100 ms integration time, and the laser should be shuttered between each acquired image to minimize photobleaching. These acquisition rates can be adjusted as deemed necessary by the user.
5. As an alternative to the procedure described above, one can also assay the ability of mCherry-Srs2 to remove RPA-GFP from the ssDNA ([Fig. 5B–D](#)). For this, RPA-GFP is simply omitted from the HR buffer that is flushed through the sample chamber following the 150  $\mu\text{L}$  injection of mCherry-Srs2. It should however be noted that the ssDNA can readily break when RPA is absent, making these types measurements more challenging.

## 2.5 Data Analysis

In the following sections, we describe general procedures for analyzing Srs2 data from ssDNA curtain experiments using measurements of GFP-Srs2 translocating on Rad51-ssDNA in the presence of free RPA-mCherry as an example (see [Fig. 4B](#)). Similar procedures can be used to analyze the behavior of dark Srs2 on Rad51-ssDNA in the presence of RPA-GFP (see [Fig. 4A](#)), or mCherry-Srs2 on RPA-ssDNA (see [Fig. 5](#)), and pertinent details of these procedures are also highlighted below. The general workflow for these analysis procedures is shown in [Fig. 6](#).

### 2.5.1 Generating Kymographs From Wide-Field Images

All TIRFM data are collected as raw TIFF files using Nikon NIS Elements software, and then these raw TIFF files are converted into kymographs for data analysis ([Fig. 6A–D](#)).

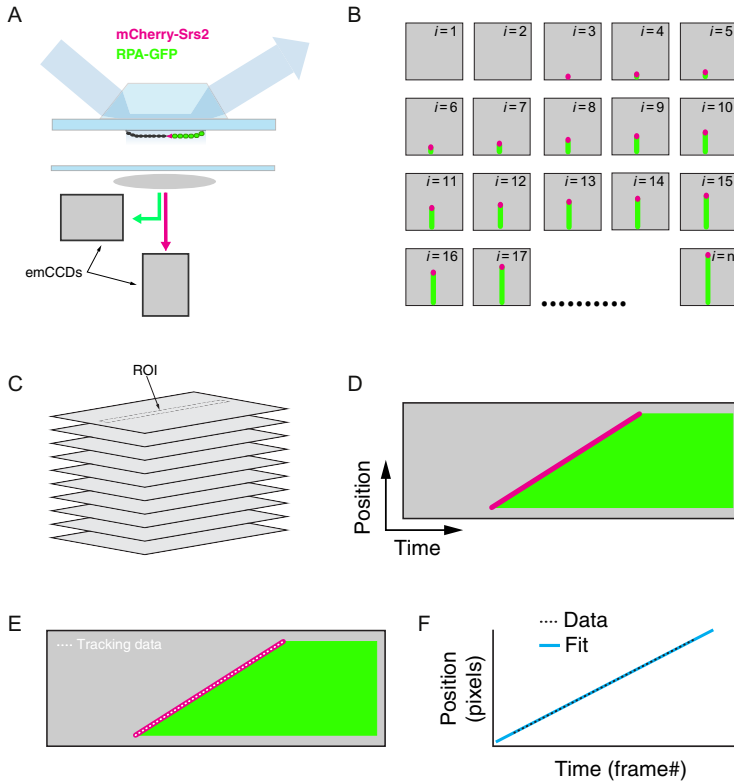


**Fig. 6** Work flow for data analysis procedures for two-color analysis of Srs2 trajectories. (A) Schematic illustration of the TIRFM system for analysis of Srs2-mCherry (shown in *magenta*) translocation on dark Rad51-ssDNA filaments (shown in *black*) in the presence of RPA-GFP (shown in *green*); color coding for mCherry-Srs2 (*magenta*) and RPA-GFP (*green*) is the same throughout the figure. (B) Cartoon illustration of a hypothetical set of raw TIFF files representing the initial binding of Srs2-mCherry to the Rad51-ssDNA (beginning in frame  $i = 1$ ) and following its movement along the ssDNA over the course of an entire experiment (ending in frame  $i = n$ ). (C) The raw TIFF files are then used to generate a tiff stack (i.e., a movie). (D) Two-color kymographs are then extracted from these movies with NIH ImageJ based upon user-defined ROIs (regions of interest), which represent 1-pixel-wide areas encompassing individual ssDNA molecules from within the ssDNA curtain. (E) The NeuronJ plugin in NIH ImageJ is then used to track the movement of Srs2 along the ssDNA. (F) The resulting  $x,y$  values in pixels are converted into nucleotides and time, respectively, and linear fits to the data are used to determine translocation velocities. For each movie, steps (D–F) are repeated until all of the Srs2 trajectories have been analyzed.

1. First, the raw TIFF files are used to create a tiff stack (i.e., movie) showing the entire field of view using Fiji software (ImageJ 1.48b, Wayne Rasband; National Institutes of Health, USA) (Fig. 6B and C).
2. The resulting tiff stack is then used to generate kymographs that illustrate the events which take place on individual ssDNA molecules during

the experimental observation period (Fig. 6D). Kymographs are generated using the “Reslice” function in Fiji. For this, a 1-pixel-wide region of interest (ROI) is superimposed on a selected ssDNA molecule from within the tiff stack, and the corresponding information for every image within the entire tiff stack is compiled as single kymograph (e.g., Figs. 4A, B, 5A, B, and 6D). Within each kymograph, the  $y$ -axis reflects the spatial information along the length of the ssDNA, and  $x$ -axis represents time.

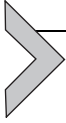
3. The resulting kymographs can then be used to determine the sites at which Srs2 initiates translocation, translocation velocities (Fig. 4C and D), and the processivity of each translocating protein (Fig. 4E and F).

### 2.5.2 Analysis of Srs2 Translocation Trajectories

All analyses of Srs2 translocation are performed from the kymographs that are generated as described above.

1. Individual dark Srs2 trajectories were manually analyzed by selecting the starting and ending point of a “wedge” of fluorescent RPA (e.g., see Fig. 4A). These wedges are evaluated as linear traces to estimate velocity, whereas fluorescent Srs2 trajectories are tracked in NIH ImageJ, as described below.
2. To analyze fluorescently tagged Srs2 trajectories (e.g., Fig. 4B), we use the NIH ImageJ plugin NeuronJ (Meijering et al., 2004). NeuronJ is a semiautomated algorithm that can be used to define and track contiguous changes in signal intensity, also called “ridges” or “ridge pixels,” in a two-dimensional image. In the case of GFP- or mCherry-tagged Srs2, the ridges are the bright fluorescence signals observed for the moving molecules of Srs2 (e.g., see Figs. 4B and 6E).
3. NeuronJ processes 8-bit-type images. So before starting, the kymographs are transformed from 16-bit to 8-bit images. The user defines a starting and end points within the image, and then the program defines and tracks the ridge pixels, and records the  $x,y$ -coordinates of each trajectory (Fig. 6F). For our analysis, we define the end points as either when the Srs2 signal disappears (i.e., dissociation) or when the slope of the Srs2 trajectory reaches a plateau (i.e., Srs2 stalls). In the case of Srs2 kymographs, the output for the  $y$ -axis represents distance in pixels. The output for the  $x$ -coordinate is in pixels, and each pixel represents a single frame from the original tiff stack from which the kymograph was constructed.
4. The  $x$ -coordinate values are readily converted from pixel values to units of time. For instance, assuming that data are collected using 5 s shuttering, then a kymograph that started at  $x = 10$  (where  $x$  corresponds

- to the  $x$ -axis pixel value) and ending when  $x = 20$  would have activity that occurred over a 50-s time period.
5. The  $y$ -coordinate pixel values are converted into nucleotide values based upon the estimated lengths of the protein-bound ssDNA substrates. These calculated estimates will differ for Rad51-ssDNA and RPA-ssDNA, which are anticipated to be extended to differing lengths (Qi et al., 2015). For Rad51-ssDNA, this corresponds to  $\sim 725$  nucleotides (nt) of Rad51-ssDNA per pixel. This calculation was made based upon the observation that dsDNA with homology to a single location within a single repetition of M13mp18 ssDNA displayed peak-to-peak distances of  $2.7 \mu\text{m}$ . A single repetition of M13mp18 ssDNA is 7249 nt and each pixel within our  $60 \times$  objective is  $0.27 \mu\text{m}$ . Thus, there are 7249 nt of Rad51-ssDNA within 10 pixels. For RPA-ssDNA, we assumed that 1 pixel corresponds to  $\sim 1087$  nucleotides of ssDNA-RPA filament. This value is based on the observation that the length of ssDNA is  $1.5 \times$  times shorter when is bound by RPA than when it is bound to Rad51 (Gibb et al., 2014). Therefore, it must be emphasized that the apparent velocities when converted from pixels/s to nt/s values will depend upon these assumed contour lengths of the extended Rad51-ssDNA and RPA-ssDNA complexes within the ssDNA curtains.
  6. Once these conversions are completed, translocation velocity (in nt/s) can be calculated from the kymographs based on the slope of each Srs2 trajectory (Fig. 6F), which is readily obtained by fitting the tracking data to a linear equation. The resulting data can be presented as distribution histograms to obtain the mean and standard deviation for the Srs2 translocation velocities under any given experimental condition (e.g., Fig. 4C and D).
  7. Srs2 processivity can also be defined from the same analysis of the kymographs (e.g., Fig. 4E and F). The distance of each translocation event is defined as the total length in nucleotides from each initial Srs2 binding position to the end of the translocation trajectory and defined by the location where Srs2 either dissociated from the ssDNA, photobleached, or stopped moving. The resulting values are used to generate survival probability plots, where the apparent processivity values reflect the distance at which 50% of the Srs2 complexes dissociate, photobleach, or stop moving. Note that the reported error bars for the survival probability correspond to standard deviation calculated by bootstrap analysis using a custom Python script that has been reported elsewhere (Qi & Greene, 2016).



### 3. CONCLUSIONS AND FUTURE DIRECTIONS

Helicases play crucial roles in all aspects of nucleic acid metabolism, and mutations in these important motor proteins can give rise to severe genetic disorders and cancer-prone syndromes (Bernstein et al., 2010; Branzei & Szakal, 2017; Brosh, 2013). Here, we have described assays that can be used to visualize the behaviors of the *S. cerevisiae* helicase and antirecombinase Srs2 as it acts upon long ssDNA substrates bound by either Rad51 or RPA. We anticipate that relatively simple modifications of the procedures described here will allow these protocols to be applied to many other types of helicases and motor proteins that act upon ssDNA. We can also envision some technical improvements that may increase the utility of this approach. In particular, the long ssDNA molecules used in these assays are inherently more challenging to work with than dsDNA, which is a relatively stiff molecule that is well behaved in flow. Therefore, although we can directly measure distances in micron or pixels, we can only estimate the lengths (in nucleotides) of the ssDNA molecules under observation. One way to overcome this problem may be to include fluorescent fiduciary markers at known locations along the ssDNA, which would allow for more accurately measure the lengths of Rad51-ssDNA and RPA-ssDNA rather than relying upon length estimates. In addition, the methodologies described here for tracking Srs2 movement rely upon relatively simple tracking procedure found in the NIH ImageJ plugin NeuronJ. This approach is fast and relatively simple, so it is very suitable for many types of investigations. However, it cannot be used to decipher high-resolution features of the trajectories—for instance, we can clearly see examples of pauses and changes in velocity in the Srs2 kymographs. Analysis of these detailed features would require implementation of a more intensive particle tracking algorithm that could be utilized for tracking the progress of GFP- or mCherry-tagged Srs2.

### ACKNOWLEDGMENTS

We thank J. Brooks Crickard and Upasana Roy for comments on the manuscript. This research was funded by an NIH grant R35GM118026 (E.C.G.). L.D.T. was funded by a PEW Latin American postdoctoral fellowship, the Williams Foundation, and by a program for Assistant Researchers, CONICET, Argentina.

## REFERENCES

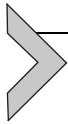
- Antony, E., Tomko, E. J., Xiao, Q., Krejci, L., Lohman, T. M., & Ellenberger, T. (2009). Srs2 disassembles Rad51 filaments by a protein-protein interaction triggering ATP turnover and dissociation of Rad51 from DNA. *Molecular Cell*, *35*, 105–115.
- Axelrod, D. (1989). Total internal reflection fluorescence microscopy. *Methods in Cell Biology*, *30*, 245–270.
- Bernstein, K. A., Gangloff, S., & Rothstein, R. (2010). The RecQ DNA helicases in DNA repair. *Annual Review of Genetics*, *44*, 393–417.
- Bianco, P. R., Brewer, L. R., Corzett, M., Balhorn, R., Yeh, Y., Kowalczykowski, S. C., et al. (2001). Processive translocation and DNA unwinding by individual RecBCD enzyme molecules. *Nature*, *409*, 374–378.
- Bianco, P. R., Tracy, R. B., & Kowalczykowski, S. C. (1998). DNA strand exchange proteins: A biochemical and physical comparison. *Frontiers in Bioscience*, *3*, D570–D603.
- Branzei, D., & Szakal, B. (2017). Building up and breaking down: Mechanisms controlling recombination during replication. *Critical Reviews in Biochemistry and Molecular Biology*, *52*, 381–394.
- Brosh, R. M., Jr. (2013). DNA helicases involved in DNA repair and their roles in cancer. *Nature Reviews. Cancer*, *13*, 542–558.
- Burgess, R. C., Lisby, M., Altmanova, V., Krejci, L., Sung, P., & Rothstein, R. (2009). Localization of recombination proteins and Srs2 reveals anti-recombinase function in vivo. *The Journal of Cell Biology*, *185*, 969–981.
- Chen, R., & Wold, M. S. (2014). Replication protein A: Single-stranded DNA's first responder: Dynamic DNA-interactions allow replication protein A to direct single-strand DNA intermediates into different pathways for synthesis or repair. *Bioessays*, *36*, 1156–1161.
- Comstock, M. J., Whitley, K. D., Jia, H., Sokoloski, J., Lohman, T. M., Ha, T., et al. (2015). Protein structure. Direct observation of structure-function relationship in a nucleic acid-processing enzyme. *Science*, *348*, 352–354.
- Croteau, D. L., Popuri, V., Opresko, P. L., & Bohr, V. A. (2014). Human RecQ helicases in DNA repair, recombination, and replication. *Annual Review of Biochemistry*, *83*, 519–552.
- De Tullio, L., Kaniecki, K., Kwon, Y.-H., Crickard, J. B., Sung, P., & Greene, E. C. (2017). Yeast Srs2 helicase promotes redistribution of single-stranded DNA-bound RPA and Rad52 in homologous recombination regulation. *Cell Reports*, *21*, 570–577.
- Duzdevich, D., Warner, M. D., Ticau, S., Ivica, N. A., Bell, S. P., & Greene, E. C. (2015). The dynamics of eukaryotic replication initiation: Origin specificity, licensing, and firing at the single-molecule level. *Molecular Cell*, *58*, 483–494.
- Fazio, T., Visnapuu, M. L., Wind, S., & Greene, E. C. (2008). DNA curtains and nanoscale curtain rods: High-throughput tools for single molecule imaging. *Langmuir*, *24*, 10524–10531.
- Gibb, B., Silverstein, T. D., Finkelstein, I. J., & Greene, E. C. (2012). Single-stranded DNA curtains for real-time single-molecule visualization of protein-nucleic acid interactions. *Analytical Chemistry*, *84*, 7607–7612.
- Gibb, B., Ye, L. F., Kwon, Y., Niu, H., Sung, P., & Greene, E. C. (2014). Protein dynamics during presynaptic-complex assembly on individual single-stranded DNA molecules. *Nature Structural & Molecular Biology*, *21*, 893–900.
- Gorman, J., Fazio, T., Wang, F., Wind, S., & Greene, E. C. (2010). Nanofabricated racks of aligned and anchored DNA substrates for single-molecule imaging. *Langmuir*, *26*, 1372–1379.
- Gorman, J., Plys, A. J., Visnapuu, M. L., Alani, E., & Greene, E. C. (2010). Visualizing one-dimensional diffusion of eukaryotic DNA repair factors along a chromatin lattice. *Nature Structural & Molecular Biology*, *17*, 932–938.

- Gorman, J., Wang, F., Redding, S., Plys, A. J., Fazio, T., Wind, S., et al. (2012). Single-molecule imaging reveals target-search mechanisms during DNA mismatch repair. *Proceedings of the National Academy of Sciences of the United States of America*, *109*, E3074–E3083.
- Graneli, A., Yeykal, C. C., Prasad, T. K., & Greene, E. C. (2006). Organized arrays of individual DNA molecules tethered to supported lipid bilayers. *Langmuir*, *22*, 292–299.
- Greene, E. C., Wind, S., Fazio, T., Gorman, J., & Visnapuu, M. L. (2010). DNA curtains for high-throughput single-molecule optical imaging. *Methods in Enzymology*, *472*, 293–315.
- Heyer, W. D. (2015). Regulation of recombination and genomic maintenance. *Cold Spring Harbor Perspectives in Biology*, *7*, a016501.
- Heyer, W. D., Ehmsen, K. T., & Liu, J. (2010). Regulation of homologous recombination in eukaryotes. *Annual Review of Genetics*, *44*, 113–139.
- Honda, M., Park, J., Pugh, R. A., Ha, T., & Spies, M. (2009). Single-molecule analysis reveals differential effect of ssDNA-binding proteins on DNA translocation by XPD helicase. *Molecular Cell*, *35*, 694–703.
- Ira, G., Malkova, A., Liberi, G., Foiani, M., & Haber, J. E. (2003). Srs2 and Sgs1-Top3 suppress crossovers during double-strand break repair in yeast. *Cell*, *115*, 401–411.
- Jasin, M., & Rothstein, R. (2013). Repair of strand breaks by homologous recombination. *Cold Spring Harbor Perspectives in Biology*, *5*, a012740.
- Kaniecki, K., De Tullio, L., Gibb, B., Kwon, Y.-H., Sung, P., & Greene, E. C. (2017). Dissociation of Rad51 presynaptic complexes and heteroduplex DNA joints by tandem assemblies of Srs2. *Cell Reports*, *21*, 3166–3177.
- Kass, E. M., Moynahan, M. E., & Jasin, M. (2016). When genome maintenance goes badly awry. *Molecular Cell*, *62*, 777–787.
- Klein, H. L. (2001). Mutations in recombinational repair and in checkpoint control genes suppress the lethal combination of srs2Delta with other DNA repair genes in *Saccharomyces cerevisiae*. *Genetics*, *157*, 557–565.
- Kowalczykowski, S. C. (2015). An overview of the molecular mechanisms of recombinational DNA repair. *Cold Spring Harbor Perspectives in Biology*, *7*, a016410.
- Krejci, L., Van Komen, S., Li, Y., Villemain, J., Reddy, M. S., Klein, H., et al. (2003). DNA helicase Srs2 disrupts the Rad51 presynaptic filament. *Nature*, *423*, 305–309.
- Lee, J. Y., Finkelstein, I. J., Arciszewska, L. K., Sherratt, D. J., & Greene, E. C. (2014). Single-molecule imaging of FtsK translocation reveals mechanistic features of protein-protein collisions on DNA. *Molecular Cell*, *54*, 832–843.
- Lee, J. Y., Terakawa, T., Qi, Z., Steinfeld, J. B., Redding, S., Kwon, Y., et al. (2015). DNA recombination. Base triplet stepping by the Rad51/RecA family of recombinases. *Science*, *349*, 977–981.
- Lisby, M., Barlow, J. H., Burgess, R. C., & Rothstein, R. (2004). Choreography of the DNA damage response: Spatiotemporal relationships among checkpoint and repair proteins. *Cell*, *118*, 699–713.
- Lisby, M., & Rothstein, R. (2015). Cell biology of mitotic recombination. *Cold Spring Harbor Perspectives in Biology*, *7*, a016535.
- Liu, J., Ede, C., Wright, W. D., Gore, S. K., Jenkins, S. S., Freudenthal, B. D., et al. (2017). Srs2 promotes synthesis-dependent strand annealing by disrupting DNA polymerase delta-extending D-loops. *eLife*, *6*, e22195.
- Ma, C. J., Steinfeld, J. B., & Greene, E. C. (2017). Single-stranded DNA curtains for studying homologous recombination. *Methods in Enzymology*, *582*, 193–219.
- Malkova, A., & Haber, J. E. (2012). Mutations arising during repair of chromosome breaks. *Annual Review of Genetics*, *46*, 455–473.
- Marini, V., & Krejci, L. (2010). Srs2: The “Odd-Job Man” in DNA repair. *DNA Repair*, *9*, 268–275.

- Mazon, G., Mimitou, E. P., & Symington, L. S. (2010). SnapShot: Homologous recombination in DNA double-strand break repair. *Cell*, *142*, 646.
- Meijering, E., Jacob, M., Sarria, J. C., Steiner, P., Hirling, H., & Unser, M. (2004). Design and validation of a tool for neurite tracing and analysis in fluorescence microscopy images. *Cytometry. Part A*, *58*, 167–176.
- Moynahan, M. E., & Jasin, M. (2010). Mitotic homologous recombination maintains genomic stability and suppresses tumorigenesis. *Nature Reviews Molecular Cell Biology*, *11*, 196–207.
- Myong, S., Rasnik, I., Joo, C., Lohman, T. M., & Ha, T. (2005). Repetitive shuttling of a motor protein on DNA. *Nature*, *437*, 1321–1325.
- Niu, H., & Klein, H. L. (2017). Multifunctional roles of *Saccharomyces cerevisiae* Srs2 protein in replication, recombination and repair. *FEMS Yeast Research*, *17*, fow111.
- Palladino, F., & Klein, H. L. (1992). Analysis of mitotic and meiotic defects in *Saccharomyces cerevisiae* SRS2 DNA helicase mutants. *Genetics*, *132*, 23–37.
- Paques, F., & Haber, J. E. (1999). Multiple pathways of recombination induced by double-strand breaks in *Saccharomyces cerevisiae*. *Microbiology and Molecular Biology Reviews*, *63*, 349–404.
- Park, J., Myong, S., Niedziela-Majka, A., Lee, K. S., Yu, J., Lohman, T. M., et al. (2010). PcrA helicase dismantles RecA filaments by reeling in DNA in uniform steps. *Cell*, *142*, 544–555.
- Petrova, V., Chen, S. H., Molzberger, E. T., Tomko, E., Chitteni-Pattu, S., Jia, H., et al. (2015). Active displacement of RecA filaments by UvrD translocase activity. *Nucleic Acids Research*, *43*, 4133–4149.
- Prakash, R., Zhang, Y., Feng, W., & Jasin, M. (2015). Homologous recombination and human health: The roles of BRCA1, BRCA2, and associated proteins. *Cold Spring Harbor Perspectives in Biology*, *7*, a016600.
- Qi, Z., & Greene, E. C. (2016). Visualizing recombination intermediates with single-stranded DNA curtains. *Methods*, *105*, 62–74.
- Qi, Z., Redding, S., Lee, J. Y., Gibb, B., Kwon, Y., Niu, H., et al. (2015). DNA sequence alignment by microhomology sampling during homologous recombination. *Cell*, *160*, 856–869.
- Qiu, Y., Antony, E., Doganay, S., Koh, H. R., Lohman, T. M., & Myong, S. (2013). Srs2 prevents Rad51 filament formation by repetitive motion on DNA. *Nature Communications*, *4*, 2281.
- Redding, S., Sternberg, S. H., Marshall, M., Gibb, B., Bhat, P., Guegler, C. K., et al. (2015). Surveillance and processing of foreign DNA by the *Escherichia coli* CRISPR-Cas system. *Cell*, *163*, 854–865.
- Rong, L., & Klein, H. L. (1993). Purification and characterization of the SRS2 DNA helicase of the yeast *Saccharomyces cerevisiae*. *The Journal of Biological Chemistry*, *268*, 1252–1259.
- Rong, L., Palladino, F., Aguilera, A., & Klein, H. L. (1991). The hyper-gene conversion *hpr5-1* mutation of *Saccharomyces cerevisiae* is an allele of the SRS2/RADH gene. *Genetics*, *127*, 75–85.
- Sasanuma, H., Furihata, Y., Shinohara, M., & Shinohara, A. (2013). Remodeling of the Rad51 DNA strand-exchange protein by the Srs2 helicase. *Genetics*, *194*, 859–872.
- Silverstein, T. D., Gibb, B., & Greene, E. C. (2014). Visualizing protein movement on DNA at the single-molecule level using DNA curtains. *DNA Repair (Amst)*, *20*, 94–109.
- Simandlova, J., Zagebaum, J., Payne, M. J., Chu, W. K., Shevelev, I., Hanada, K., et al. (2013). FBH1 helicase disrupts RAD51 filaments in vitro and modulates homologous recombination in mammalian cells. *The Journal of Biological Chemistry*, *288*, 34168–34180.
- Sokoloski, J. E., Kozlov, A. G., Galletto, R., & Lohman, T. M. (2016). Chemo-mechanical pushing of proteins along single-stranded DNA. *Proceedings of the National Academy of Sciences of the United States of America*, *113*, 6194–6199.

- Spies, M., Bianco, P. R., Dillingham, M. S., Handa, N., Baskin, R. J., & Kowalczykowski, S. C. (2003). A molecular throttle: The recombination hotspot chi controls DNA translocation by the RecBCD helicase. *Cell*, *114*, 647–654.
- Sternberg, S. H., Redding, S., Jinek, M., Greene, E. C., & Doudna, J. A. (2014). DNA interrogation by the CRISPR RNA-guided endonuclease Cas9. *Nature*, *507*, 62–67.
- Sung, P., & Stratton, S. A. (1996). Yeast Rad51 recombinase mediates polar DNA strand exchange in the absence of ATP hydrolysis. *The Journal of Biological Chemistry*, *271*, 27983–27986.
- Symington, L. S., Rothstein, R., & Lisby, M. (2014). Mechanisms and regulation of mitotic recombination in *Saccharomyces cerevisiae*. *Genetics*, *198*, 795–835.
- Vasianovich, Y., Altmannova, V., Kotenko, O., Newton, M. D., Krejci, L., & Makovets, S. (2017). Unloading of homologous recombination factors is required for restoring double-stranded DNA at damage repair loci. *The EMBO Journal*, *36*, 213–231.
- Veaute, X., Jeusset, J., Soustelle, C., Kowalczykowski, S. C., Le Cam, E., & Fabre, F. (2003). The Srs2 helicase prevents recombination by disrupting Rad51 nucleoprotein filaments. *Nature*, *423*, 309–312.
- Wang, F., Redding, S., Finkelstein, I. J., Gorman, J., Reichman, D. R., & Greene, E. C. (2013). The promoter-search mechanism of *Escherichia coli* RNA polymerase is dominated by three-dimensional diffusion. *Nature Structural & Molecular Biology*, *20*, 174–181.
- Wold, M. S. (1997). Replication protein A: A heterotrimeric, single-stranded DNA-binding protein required for eukaryotic DNA metabolism. *Annual Review of Biochemistry*, *66*, 61–92.
- Zacharias, D. A., Violin, J. D., Newton, A. C., & Tsien, R. Y. (2002). Partitioning of lipid-modified monomeric GFPs into membrane microdomains of live cells. *Science*, *296*, 913–916.

This page intentionally left blank



# Single-Molecule Analysis of Replication Protein A–DNA Interactions

Fletcher E. Bain\*, Laura A. Fischer\*, Ran Chen<sup>†</sup>, Marc S. Wold\*,<sup>1</sup>

\*University of Iowa Carver College of Medicine, Iowa City, IA, United States

<sup>†</sup>Washington University, St. Louis, MO, United States

<sup>1</sup>Corresponding author: e-mail address: marc-wold@uiowa.edu

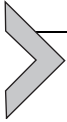
## Contents

|   |     |
|---|-----|
| 1. Expression and Purification of RPA   | 440 |
| 1.1 Overview  | 440 |
| 1.2 Purification Buffers and Materials  | 440 |
| 1.3 Transformation, Expression, and Preparation of Cell Extracts                              | 441 |
| 1.4 Purification and Storage  | 442 |
| 2. Labeling of RPA  | 444 |
| 2.1 Biotin Labeling of RPA  | 444 |
| 2.2 Fluorescent Labeling of RPA   | 444 |
| 3. Single-Molecule Analysis of RPA–DNA Interactions: How to Do It                             | 446 |
| 3.1 Experimental Considerations—Protein vs DNA Tethering                                      | 446 |
| 3.2 Setup: Preparation of Slides and Assembly of Chamber for Single-Molecule TIRF Experiments | 448 |
| 3.3 Single-Molecule Analysis of RPA–DNA Interactions  | 451 |
| 3.4 Experimental Procedure—Surface-Tethered DNA   | 452 |
| 3.5 Experimental Procedure—Surface-Tethered RPA   | 453 |
| 3.6 Generating a Mapping File for Single-Molecule Analysis                                    | 453 |
| 3.7 Analysis of Single-Molecule Trajectories  | 454 |
| Acknowledgments   | 460 |
| References  | 460 |

## Abstract

Replication protein A (RPA) is a highly conserved, eukaryotic ssDNA-binding protein essential for genome stability. RPA interacts with ssDNA and with protein partners to coordinate DNA replication, repair, and recombination. Single-molecule analysis of RPA–DNA interactions is leading to a better understanding of the molecular interactions and dynamics responsible for RPA function in cells. Here, we first describe how to express, purify, and label RPA. We then describe how to prepare materials and carry

out single-molecule experiments examining RPA–DNA interactions using total internal reflection fluorescence microscopy (TIRFM). Finally, the last section describes how to analyze TIRFM data. This chapter will focus on human RPA. However, these methods can be applied to RPA homologs from other species.



## 1. EXPRESSION AND PURIFICATION OF RPA

### 1.1 Overview

Human replication protein A (RPA) is a heterotrimeric complex containing three subunits of 70, 32, and 14 kDa. The RPA complex is very stable and thought to form as the subunits are translated. Recombinant RPA is made by coexpressing the three subunits in *Escherichia coli*. Expression of RPA genes is toxic to *E. coli* (Henricksen, Umbricht, & Wold, 1994), so expression is directed using plasmids with the T7 promoter (Studier, Rosenberg, Dunn, & Dubendorff, 1990). For maximal expression, it is important to minimize the number of generations of growth of an expression strain carrying RPA expression plasmid(s). A freshly transformed expression strain should be prepared for each induction and cultures should be induced without using a starter culture or passing through stationary phase. The purification of RPA described later is based on previously published descriptions (Binz, Dickson, Haring, & Wold, 2006; Henricksen et al., 1994).

### 1.2 Purification Buffers and Materials

#### 1.2.1 Buffers

L-broth (LB): 10.0 g Bacto-tryptone, 5.0 g yeast extract, 5.0 g NaCl. Bring to 1 L with H<sub>2</sub>O and autoclave to sterilize.

HI-0 buffer: 30 mM HEPES (diluted from 1 M HEPES, pH 7.8), 0.5% inositol, 0.25 mM EDTA, 0.01% NP-40, 1 mM DTT (added fresh). HI buffers used during purification also have the indicated concentration of the specified salt added. HI buffers containing phosphate are made by making up one buffer containing the indicated concentration of mono-basic salt and a second buffer containing the di-basic salt. The mono-basic buffer is then added to the di-basic buffer until pH 7.6.

Resuspension buffer: HI buffer containing 50 mM KCl. In addition, 1 mM phenylmethylsulfonyl fluoride (PMSF), 1 mM dithiothreitol (DTT), and 2 μL/mL bacterial protease inhibitor cocktail (Sigma, P8465) are added immediately before use.

### 1.2.2 Plasmids

RPA is generated through coexpression of the three subunits in *E. coli*. The three RPA subunit genes can be contained in one plasmid (pET11d-tRPA which has all three genes arranged as a synthetic operon; [Henricksen et al., 1994](#)) or two compatible plasmids (e.g., pET11d-RPA1-RPA3 and pRSF-DUET-RPA2; [Mason et al., 2009](#)). (Plasmids are available upon request from the corresponding author; p11d-tRPA is available from Addgene (#102613).) Both methods show similar expression of RPA. In all cases, the RPA genes are under the control of an inducible T7 promoter and have a Shine-Dalgarno sequence upstream of each ATG initiation site.

## 1.3 Transformation, Expression, and Preparation of Cell Extracts

Expression plasmids are introduced into competent expression cells (can be either commercial or in-house prepared chemically competent cells). Good expression has been obtained using a variety of T7 RNA polymerase-based expression strains including BL21(DE3), BL21(DE3)pLysS, or Rosetta cells. To minimize the number of generations prior to induction, individual colonies from freshly transformed cells are used to directly inoculate individual 1 L cultures. Preparations are scaled up by inducing multiple 1 L cultures.

### 1.3.1 Transformation

Approximately 50  $\mu\text{L}$  of chemically competent expression cells are incubated with  $\sim 10$ – $100$  ng of each plasmid DNA on ice for 20 min. The sample is incubated in a 37°C water bath for 1 min and then placed on ice for 2 min. This heat shock causes plasmid uptake. One milliliter of LB is added and the sample is incubated at 37°C for 45–60 min to allow for the expression of antibiotic resistance genes. After incubation, 100  $\mu\text{L}$  is transferred to a 10-cm LB-agar plate (LB media containing 1.5% agar) containing the appropriate antibiotic(s). The sample is spread evenly by shaking with 5–15 sterile glass beads and is incubated at 37°C for 12–18 h or until colonies form. Plates can be stored at 4°C for up to 5 days before growth and induction.

### 1.3.2 Induction

Individual 1 L cultures of LB (containing appropriate antibiotic(s)) are inoculated with a single colony late in the day. The cultures are then incubated overnight at 37°C without shaking (this limits maximum cell density to 0.3–0.5). The following morning, the cultures are shaken at  $\sim 250$  rpm until  $OD_{600} = 0.6$ – $0.8$ . It usually takes 1–2 h for cultures to return to exponential

growth. Protein expression is induced with isopropylthiogalactoside (IPTG) at a final concentration of 0.3 mM (3 mL of 100 mM IPTG). The cultures are then incubated at 37°C with shaking for 2 h to allow protein expression. Cells are then pelleted by centrifugation at 3–4000 × *g* at 4°C for 30 min. Supernatant is removed and cells are resuspended in 15 mL resuspension buffer.

1 L cultures inoculated with a single colony can also be induced using autoinduction protocols (Studier, 2005).

### 1.3.3 Cell Lysis

Cells can be lysed using multiple methods, including Emulsiflex cell breakers, sonication, or French press. This description is for sonication using a Fisher Sonicator (Model FB50). Resuspended cells are subjected to multiple short pulses of sonication with cooling on ice to prevent overheating and protein denaturation. For example, cells are sonicated at 40% power for 15 s and then chilled on ice for 30 s. This cycle is repeated a total of three to five times. (Solution viscosity will initially increase as chromosomal DNA is released, and then decrease as the chromosomal DNA is sheared. Optimal lysis usually occurs as the viscosity is decreasing.) Avoid excess sonication as it can denature proteins.

The sample is then centrifuged at 20–25,000 × *g* at 4°C for 35 min to remove cell debris. The supernatant contains the protein lysate. Bradford Protein Assay with BSA used as a standard (Bio-Rad; Bradford, 1976) is used to measure the protein concentration of the cell lysate. Lysate can be stored at –80°C.

## 1.4 Purification and Storage

RPA is purified over three columns: Affi-Gel Blue (affinity chromatography—purification), Hydroxylapatite (adsorption chromatography—additional purification and desalting), and Mono Q (ion exchange chromatography—polishing). All columns are run at 4°C and the best yields are obtained when all three columns are run sequentially. RPA fractions after Hydroxylapatite are ~90% pure and can be used for DNA-binding assays, but small amounts of impurities make HAP fractions problematic for most other functional assays. Mono Q fractions are usually ~95+% pure.

### 1.4.1 Affi-Gel Blue

The cell lysate is first purified using an Affi-Gel Blue (Bio-Rad, 100–200 mesh) affinity column (loading 10 mg total protein per mL of column). The column is equilibrated with 3 column volumes (CV) of HI-50 mM

KCl buffer. Protein is loaded onto the column and washed with an additional 3 CV of HI-50 mM KCl buffer. Weakly binding proteins are eluted using 3 CV of HI-50 mM KCl + 500 mM NaSCN. Strongly binding proteins, predominantly RPA, are eluted using 3 CV of HI-50 mM KCl + 1.5 M NaSCN. The column is then rinsed with 1 CV of HI-50 mM KCl to elute the remaining high-salt buffer. On automated chromatography systems (e.g., FPLC), washes are generated by combining different proportions of HI-50 mM KCl and HI-50 mM KCl + 2 M NaSCN. The protein concentration of each fraction is determined using a Bradford Assay with BSA used as a standard (Bio-Rad; Bradford, 1976). The peak protein fractions within the 1.5 M NaSCN wash should contain RPA.

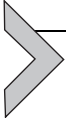
#### **1.4.2 Hydroxylapatite**

The RPA-containing fractions from the Affi-Gel Blue column are loaded onto a Hydroxylapatite column (EMD Millipore, Fast Flow, catalog no. 391947) at 7 mg total protein per mL of column. The column is equilibrated with HI-50 mM KCl buffer. The column is washed with 3 CV of HI-50 mM KCl buffer, 5 CV of HI-100 mM phosphate buffer, and then 5 CV of HI-300 mM phosphate buffer. Protein concentrations of each fraction are determined. The column may be washed with additional HI-300 mM phosphate if necessary. Typically, 40% of the RPA will elute in the 100 mM phosphate peak and 60% in the 300 mM phosphate peak. Because many low molecular weight proteins elute in the second peak, only the first peak is used in subsequent steps.

#### **1.4.3 Mono Q**

The peak fractions from the HI-100 mM phosphate peak (which has conductivity equivalent to ~200 mM KCl) are diluted 1:4 in HI-0 to reduce the ionic strength to the equivalent of ~50 mM. The protein sample (up to 5–7 mg protein per mL of column) is loaded onto a Mono Q anion exchange column (GE Biosciences) equilibrated in HI-50 mM KCl. The column is washed with 3 CV of HI-50 mM KCl and then 3 CV of HI-200 mM KCl. A gradient wash of 12 CV spanning HI-200 mM to HI-400 mM KCl is run to elute RPA. Finally, the column is cleaned with 3 CV of HI-2 M KCl, followed by reequilibration with 3 CV of HI-50 mM KCl. RPA elutes between 250 and 300 mM KCl.

Purified Mono Q fractions should be aliquoted and stored at  $-80^{\circ}\text{C}$ . Purified RPA can be stored for long periods at  $-80^{\circ}\text{C}$  and is generally stable through several freeze/thaw cycles.



## 2. LABELING OF RPA

### 2.1 Biotin Labeling of RPA

Biotinylation is a convenient method for tethering RPA in single-molecule experiments. RPA is biotin labeled using endogenous *E. coli* biotin holoenzyme synthetase (BirA). BirA recognizes the minimal target sequence (GLNDIFEAQKIEWHE) and links biotin to the central lysine residue (Beckett, Kovaleva, & Schatz, 1999). Addition of the BirA target sequence to one of the subunits of RPA allows efficient biotin labeling concurrent with expression in *E. coli*. The N-terminus of each of the RPA subunits is amenable to protein/peptide labeling (for example, Haring, Mason, Binz, & Wold, 2008). Previous single-molecule analysis used RPA with His- and biotin-tags on RPA3. A synthetic gene was constructed containing an N-terminal His-tag, a factor Xa site, and the BirA recognition site followed by the RPA3-coding sequence (p11d-tRPA•biotinRPA3 (Chen, Subramanyam, Elcock, Spies, & Wold, 2016), available upon request from the corresponding author).

Biotinylated RPA is made by inducing RPA expression with one of the genes containing the BirA recognition site (e.g., p11d-tRPA•biotinRPA3; Chen et al., 2016) as described earlier. The only change is that 100  $\mu$ M biotin is added to the LB media concomitant with the induction of 0.3 mM IPTG. Using this procedure, a majority of the RPA purified is biotinylated.

### 2.2 Fluorescent Labeling of RPA

Fluorescent labeling of RPA with Cy3 or Cy5 is carried out by chemically modifying purified RPA. N-termini can be labeled with Cy5 Mono NHS ester (Galletto, Amitani, Baskin, & Kowalczykowski, 2006; Nguyen et al., 2014). While this method has been used successfully to make fluorescent RPA for TIRFM studies (Nguyen et al., 2014), it results in up to all three subunits being labeled. Therefore, this chapter will focus on specific labeling using formylglycine-generating enzyme (FGE; Ghoneim & Spies, 2014; Rabuka, Rush, Dehart, Wu, & Bertozzi, 2012; Shi et al., 2012). FGE is an enzyme from *Mycobacterium tuberculosis* that recognizes the six amino acid sequence LCTPSR, and converts the cysteine into a formylglycine in vivo. The aldehyde group can then be reacted with fluorescent dye hydrazine compounds to specifically label a single location on RPA. This method can be used to selectively label individual domains of a

single subunit of RPA or to position the label close to a specific site of interest for FRET-based studies.

### **2.2.1 Purification of Aldehyde-Tagged RPA**

FGE labeling requires an inducible plasmid carrying the FGE gene: for example, pBAD/myc-hisA Rv0712 (FGE) (Addgene (#16132); Carrico, Carlson, & Bertozzi, 2007) contains the FGE gene under the control of the arabinose operon. For labeling of RPA, the promoter and FGE gene were subcloned into pRSF to generate a kanamycin-resistant plasmid that is compatible with pET-RPA expression plasmids (pRSF-FGE; Addgene (#102615)).

The six amino acid FGE recognition signal LCTPSR can be inserted into a surface loop near the desired site of labeling in RPA. Cells are then transformed with both pRSF-FGE and p11d-tRPA variant containing the FGE recognition site. Cell cultures are grown and induced as described earlier, except that 0.2% arabinose (Sigma) is added 30 min before adding IPTG to induce expression of FGE. Reduced levels of RPA are made under these conditions and the level of expression can vary with the labeling site.

### **2.2.2 Labeling Aldehyde-Tagged RPA**

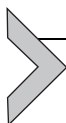
The following example describes labeling RPA with Cy3 dye. Other dyes attached to hydrazine can also be used.

The purified aldehyde-tagged RPA is concentrated to 20–40  $\mu\text{M}$  and exchanged into the labeling buffer (250 mM potassium phosphate (pH 7), 500 mM KCl, 5 mM DTT) using Amicon Ultra (0.5 mL) Centrifugal Filter 10K (usually four concentration–dilution cycles following manufacturer's instructions). Final volume of concentrated protein should be no less than 20–25  $\mu\text{L}$ .

Small aliquots of 0.1 mg Cy3 hydrazide (GE Healthcare, PA15120) are prepared for individual labeling reactions. Mix 1 mg Cy3 hydrazide with 100  $\mu\text{L}$  ultra-pure methanol. Mix by vortexing and pipetting followed by brief centrifugation to concentrate in the bottom of the tube ( $15,000 \times g$  for 30 s). Place 10  $\mu\text{L}$  in individual 1.5 mL tubes, centrifuge briefly, and then evaporate methanol using a SpeedVac (15–20 min at  $\sim 50^\circ\text{C}$ ).

Depending on amount of labeled RPA desired, a few or all of the tubes are then used for labeling reactions. Each labeling reaction is set up by adding 3  $\mu\text{L}$  of concentrated RPA to a tube with 0.1 mg of Cy3 hydrazide. Gently mix and then centrifuge ( $1000 \times g$  for 1 min) and repeat. Wrap each tube in aluminum foil and incubate in darkness at  $4^\circ\text{C}$  for 24 h with gentle rotation.

Pool labeling reactions and then exchange buffer and remove free dye using a Bio-Spin 6 (Bio-Rad) column. The column is equilibrated in storage buffer (HI-300 mM KCl). Labeling efficiency is measured by comparing UV and visible spectra. The absorption of protein and Cy3 is measured at 280 and 532 nm, respectively. Labeled protein should be aliquoted and stored at  $-80^{\circ}\text{C}$ . Labeled RPA is less stable than unlabeled RPA, so aliquots should not be refrozen after thawing.



### 3. SINGLE-MOLECULE ANALYSIS OF RPA–DNA INTERACTIONS: HOW TO DO IT

The following sections describe the setup, data collection, and data analysis of single-molecule RPA–DNA-binding studies. The data is collected with a fluorescent TIRF microscope with a high-resolution EMCCD camera. Setup and configuration of such a microscope have been described previously (Bain, Wu, & Spies, 2016; Joo & Ha, 2008).

For the RPA experiments, we chose to use Cy3 and Cy5 fluorophores to visualize DNA–protein interactions. These dyes have sufficient quantum yield for detection at the single-dye per molecule level of the experiments. Additionally, these dyes form a FRET pair, which is useful for mechanistic insights in protein–nucleic acid interactions. Direct excitation of Cy3 requires a 532 nm laser, and emission filters that allow a narrow band around 560 nm to pass. Direct excitation of Cy5 requires the use of a 640 nm laser, and emission filters that allow a narrow band around 670 nm to pass. Other high quantum yield dyes can be used with this methodology but may require different excitation sources and appropriate filter sets.

#### 3.1 Experimental Considerations—Protein vs DNA Tethering

In total internal reflection fluorescence microscopy (TIRFM), laser light is used to create an evanescent field on the surface of a slide. Dye molecules that enter the field, which only extends  $\sim 100\text{ nm}$  from the slide surface, are excited and fluoresce. This dramatically lowers the background signal from free molecules in solution and allows visualization of single-labeled molecules at the surface of the slide. Using this methodology, one ligand is attached to the slide and the other freely diffuses in solution. The tethered or free molecules may be fluorescently labeled, meaning that there are two general approaches for examining binding interactions between RPA and DNA at the single-molecule level. The experimentalist can either tether biotinylated DNA to the slide surface and use fluorescently labeled RPA

or tether RPA to the slide surface and use fluorescently labeled DNA. Depending on the experimental question being asked, one of the two approaches may be preferred. The following briefly discusses the considerations when selecting which approach to use.

In general, it is easiest to use biotinylated protein and fluorescently labeled DNA. Commercial DNA synthesis makes it simple to obtain oligonucleotides that are fluorescently labeled (or biotinylated, or that contain multiple labels). Any sequence can be synthesized and multiple oligonucleotides can be annealed to form partially duplex structures similar to intermediates found in cells (for example, [Bain et al., 2016](#)). Commercial labeling is also very efficient (~100%) and generally does not affect the properties of the oligonucleotide. In contrast, it is difficult to label proteins with 100% efficiency. It is possible to correct for inefficient fluorescent labeling during data analysis ([Boehm, Subramanyam, Ghoneim, Washington, & Spies, 2016](#)); however, it is simplest if this issue can be bypassed completely.

Biotin is used to attach ligand to the slide. Since only biotinylated molecules are attached to the slide surface (with unlabeled molecules being washed away before the start of the experiment), the efficiency of labeling is generally not an issue for biotinylation. This makes it advantageous to biotinylate the protein. As with any protein modification, it is possible that biotinylation can cause loss of activity, restriction of domain movements, or affect protein folding during expression. So, it is always necessary to do control experiments to test whether the modified protein retains full activity. (This is also a concern when fluorescently labeling a protein.) Often, loss of activity can be overcome by testing labeling at multiple sites on the protein. In cases where biotinylation affects protein activity, it is also possible to tether the protein using antibody interaction with biotinylated antibodies ([Jain et al., 2011](#)).

Another consideration is the functional unit of the protein. Single-molecule studies require sparse attachment of individual proteins to the surface. This works well if the protein functions as a monomer (or, like RPA, as a very stable multimer). If the protein functions as an oligomer, surface tethering of the protein will prove ineffective because only one polypeptide chain is attached to the slide.

Fortunately, in the case of RPA, either method can be used. Biotinylation of the N-terminus of RPA3 appears to have no effect on RPA activity and biotinylated RPA can be purified in high quantities ([Chen et al., 2016](#)). Fluorescently labeled RPA has also been used effectively to look at interactions with tethered DNA ([Nguyen et al., 2014](#)). The

functional unit of RPA is a very stable heterotrimer that remains active over the timescale needed for single-molecule DNA-binding studies. However, it has been shown that binding of multiple molecules of RPA is needed to destabilize partially duplex DNA structures. Tethered-DNA experiments would be needed to analyze this activity (Chen et al., 2016).

### 3.2 Setup: Preparation of Slides and Assembly of Chamber for Single-Molecule TIRF Experiments

The first step in performing single-molecule TIRFM experiments is preparation of the quartz slide and coverslip. This requires carefully cleaning and then preparing the surface of the slide to prevent nonspecific binding of proteins or DNA (passivation). A sample chamber is made with the slide and coverslip to allow binding reactions in a deoxygenated aqueous environment that ensures dye photostability. Holes are drilled in the slide to allow the introduction of buffers and samples. Because of the time involved, groups of slides (5–10) are prepared and then used individually for experiments.

#### 3.2.1 Cleaning

Start with quartz slides (Chemglass, CGQ-0640-01) and cover glasses (Azer Scientific, ES0107242). Other materials needed include tweezers, a bath sonicator, and glass staining dishes (Fisher Scientific, 08-817), which are used for all sonication steps. Slides are prepared for use by aminosilanization and PEGylation as follows. Slides are typically prepared in groups of five or more and can be stored for use at  $-20^{\circ}\text{C}$  for no more than 2 months. Six holes are drilled in the experimental slide using a 0.75-mm diamond drill bit (Lasco, WD\_0-75) (see Fig. 1A). At this time, etch one side to indicate the “top” of slide, or the passivated surface at the end of the preparation process. The slide is then subjected to sonication in 10% Alconox for 20 min. Rinse slides, in glass staining dish, in MilliQ water until all the Alconox is removed. Rinse at least five times by filling the glass staining dish with the slides with MilliQ water. Rinse until no bubbles, from the detergent, form. Sonicate slides in MilliQ water for 5 min and rinse three times with MilliQ water. Next, sonicate the slides in Optima acetone (Fisher Scientific, MFCD00008765) for 30 min and then rinse three times with MilliQ water. Next the slides and cover glasses, as well as a flask used for mixing the aminosilanization solution, are sonicated in 1 M KOH for 40 min. (Prepare # Slides + 4 cover glasses, due to breakage during passivation). Rinse the slides, cover glasses, and aminosilanizing flask with MilliQ water

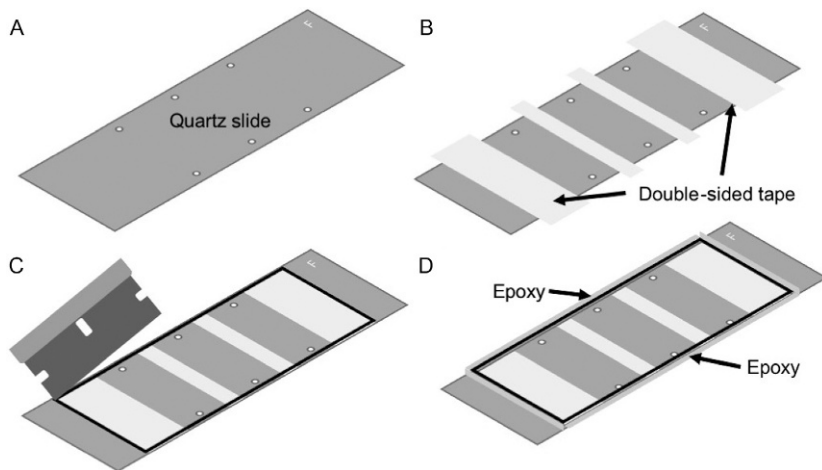


**Fig. 1** Drill six 0.75 mm holes and scratch the upper corner of the slide to denote the passivated surface (A). When assembling the slide, place slide in the orientation with passivated side up. Make three equivalent chambers using double-sided tape (B) and then place the cover glass, passivated side down, over the double-sided tape. Make sure that the tape is well adhered and trim excess with a razor blade (C). Seal around all four sides of the cover glass with 5-min epoxy (D). After removing excess epoxy slide is ready for use.

five times. Next, the slides and cover glasses are burned using an open flame. Make sure to use a blue flame to ensure that no carbon deposits are left on the cleaned slide. Burn each side of the slide for 90 s. Reduce the flame and burn each cover glass for 60 s on each side. Make quick passes with the cover glass, as overheating will cause the cover glass to shatter. As each slide/cover glass burning is completed, transfer it to a separate clean, dry glass staining dish that is only used for the aminosilanization step.

### 3.2.2 Surface Passivation

After thorough cleaning of the slide, one surface will be passivated using aminosilane. Equilibrate the aminosilane stock to room temperature prior to use. Aminosilane solution is prepared just prior to use by mixing 150 mL Optima methanol, 7.5 mL glacial acetic acid, and 1.5 mL aminosilane (UCT Inc., A0700). When working with the aminosilane stock, make certain to use a glass pipette. Pour the aminosilane solution into the containers with the slides and cover glasses. Incubate in darkness for 10 min. Sonicate the slides and cover glass for 1 min in the aminosilane solution and then incubate, in darkness, for an additional 10 min. Rinse slides and cover glasses with

Optima methanol three times and then use dry compressed nitrogen gas to dry the slides and cover glasses while still in the aminosilanization containers.

PEGylation is the final passivation step in preparing the slide surface. For surface tethering, our lab utilizes Biotin-PEG-SVA mw 5000 (Laysan Bio Inc., Biotin-PEG-SVA-5000) in a mixture with mPEG-SVA (mw: 5000) (Laysan Bio Inc., mPEG-SVA-5000) in a ratio of 1:25 (biotin:mPEG). Measure 16 mg of biotin-PEG and 400 mg of mPEG. Solubilize the mPEG in 800  $\mu\text{L}$  of freshly made 8.4 mg/mL sodium bicarbonate and invert to mix. It is important not to introduce bubbles while mixing. Centrifuge the PEG mixture at  $7200 \times g$  for 1 min at  $4^\circ\text{C}$ . Dispense 70  $\mu\text{L}$  of the PEG mixture onto the slide surface that was etched as the slide top at the start of the process. Sandwich on a cover glass, ensuring that the PEG solution completely covers the surface between the slide and cover glass. If bubbles are present, slide the cover glass around, moving the bubbles toward the slide edge or the predrilled holes to remove them. Slides are incubated in an empty 200  $\mu\text{L}$  pipette tip box (containing several tips spaced to support the slides), with 10 mL of water in the bottom, overnight in the dark. The water ensures that the water/PEG solution does not evaporate during overnight incubation. The next day, label the top, uncoated side of the cover glass with a permanent marker and then thoroughly rinse the cover glass and slide with sterile water from a squeeze bottle. After rinsing, use dry compressed nitrogen gas to completely dry the individual slides/cover glass. Store the slide and corresponding cover glass in a 50-mL plastic screw-top tube, with the uncoated sides sandwiched together. Individually vacuum seal the 50 mL tubes using a food saver system and store at  $-20^\circ\text{C}$  in the dark until used. Slides are stable for up to 2 months at  $-20^\circ\text{C}$ .

### **3.2.3 Assembly of Single-Molecule Chamber**

It takes multiple hours to set up one slide and collect single-molecule data sets. In addition, the proteins, dyes, and single-molecule (SM) buffer all are labile, so slides are used individually. Each slide is set up with three reaction chambers. Generally, one is used as a control and the others for different experimental conditions.

The single-molecule chambers are assembled using a 3M double-sided scotch tape and 5-min epoxy. Remove the slide from  $-20^\circ\text{C}$  storage, and equilibrate to room temperature, in the dark, while still sealed in the food saver bag. Remove the slide and place it passivated side up (Fig. 1A). Tear off a piece of double-sided tape that is approximately 2 in. long, cut it in half lengthwise using a razor blade, and place each half roughly 5 mm from

the outermost holes of the slide (Fig. 1B). Tear off a second 2-in. piece of double-sided tape and cut lengthwise into three pieces. Take one piece and place it halfway between the first and second hole set, and another piece of tape between the second and third (Fig. 1B). Carefully lay the cover glass, passivated side down, over the tape such that three individual chambers are formed (Fig. 1C). Use a pipette tip to press the cover glass into the double-sided tape. This ensures that no liquid will leak between the chambers. Use a razor blade to trim any excess tape. Next, place a thin layer of epoxy around all edges of the cover glass. This seals the chamber, ensuring no leaks during experimentation (Fig. 1D). Allow the epoxy to harden for 3 min in the dark. Remove any excess epoxy by trimming with a razor blade. Allow the epoxy to harden for another 20 min, again in the dark, and wipe the surface of the cover glass with a kimwipe and acetone to remove any remaining epoxy residue. Flow 100  $\mu$ L T50 buffer (20 mM Tris–HCl pH 7.4, 50 mM NaCl) into each chamber until no air remains. Pockets of air in the chamber will lead to an increased photobleaching rate during experiments; therefore, it is necessary to ensure that no bubbles are in the experimental chambers.

Just prior to performing the experiment, flow 100  $\mu$ L of 0.2 mg/mL neutravidin into each slide chamber and incubate for 3 min. Biotin–neutravidin interactions are extremely strong, and this methodology ensures that biotinylated substrates or proteins remain in a single location during experiments. Wash the slide chambers three times with 100  $\mu$ L T50 buffer to remove any excess neutravidin. The slide chamber is now ready to be treated with biotinylated molecules, and used in an experiment.

### 3.3 Single-Molecule Analysis of RPA–DNA Interactions

#### 3.3.1 General Methodology

Regardless of the tethered molecule, most of the experimental conditions remain unchanged. The standard buffer for single-molecule experimentation, SM buffer, contains 50 mM Tris–HCl (pH 7.5), 100 mM NaCl, 5 mM MgCl<sub>2</sub>, 100 mg/mL BSA, 1 mg/mL glucose oxidase (Sigma-Aldrich), 0.4% D-glucose, and 0.04 mg/mL catalase (Calbiochem). As a substitute for water, this buffer is made in 6 mg/mL TROLOX (6-hydroxy-2,5,7,8-tetramethylchroman-2-carboxylic acid; Sigma-Aldrich). TROLOX is used as a water substitute in order to stabilize the fluorescent properties of the attached dyes, specifically reducing blinking, or nonradiative relaxation, of the dyes. Prepare TROLOX by adding 60 mg of TROLOX powder to 10 mL of MilliQ water. Add 60  $\mu$ L of 2 M NaOH, and invert several times to mix. Attach the mixture to a rotating shaker and incubate at room

temperature for 3 days. The shaker should be illuminated 24 h a day during incubation using a fluorescent bulb to activate the TROLOX. In our experience, a 3500K color, 835 phosphor bulb yields the best results. TROLOX can be stored for 1 month in the dark at 4°C. Glucose oxidase and catalase mix (gloxy) is prepared by first making a 40 mg/mL stock of catalase in T50 buffer. Next, add 10 mg glucose oxidase to 90  $\mu$ L T50 and add 10  $\mu$ L of the catalase mix. Mix solutions gently to avoid bubbles. Centrifuge 1 min at 1000  $\times$  *g* and collect supernatant in a new tube. Stock concentration of gloxy is 100 mg/mL glucose oxidase and 4 mg/mL catalase. This solution can be stored for 1 month in the dark at 4°C. Gloxy, in conjunction with glucose, removes molecular oxygen from the system, protecting dyes from oxidization and enhancing the lifetime of fluorescence. As D-glucose is consumed in this reaction, it is important to add the gloxy to buffers just prior to recording experimental movies. Finally, when recording movies, several settings remain unchanged. All movies are recorded at 100 ms exposure and with a gain of 290. Gain can be adjusted to enhance signal; however, once the gain is set, it should be held constant for all movies in a data set. Likewise, exposure time can be altered. If the kinetic events are very fast, it may be necessary to shorten the exposure time. However, as with gain, once an exposure has been selected, all films in a data set should use the same setting. Movies are recorded for 3–6 min.

### 3.4 Experimental Procedure—Surface-Tethered DNA

RPA has an occluded binding site of  $\sim$ 30 nucleotides and can bind oligonucleotides as short as 15 nucleotides with high affinity (Chen et al., 2016). Therefore, substrates for experiments with surface-tethered DNA should use at least a 35 nucleotide single-strand site to ensure binding (and prevent surface effects). Partially duplex DNA structures can be assembled and attached to the slide (Bain et al., 2016; Nguyen et al., 2014). The DNA must be biotinylated at one end to tether it to the slide surface. To begin the experiment, flow 100  $\mu$ L of SM buffer containing 50 pM of biotin-labeled DNA into the experimental chamber. Incubate for 3 min and then wash with 100  $\mu$ L SM buffer to remove any free DNA that did not bind. Next flow Cy5-RPA into the chamber, focus and begin recording movies. You should be able to see binding events as flashing spots with the recording software. Record at least three movies, each at a different spot within the chamber. To determine the on-rate of binding, it is necessary to perform the single-molecule experiment at three different concentrations of RPA, as this process is concentration dependent.

### 3.5 Experimental Procedure—Surface-Tethered RPA

Surface tethering of RPA requires the use of biotinylated protein. Flow 100  $\mu\text{L}$  of 100 pM biotin-tagged RPA in SM buffer into the experimental chamber and incubate for 3 min to ensure protein binding to the neutravidinated chamber. Wash the chamber with 100  $\mu\text{L}$  of SM buffer to remove any unbound RPA and then flow in 100  $\mu\text{L}$  of 50 pM Cy3- or Cy5-ssDNA in imaging buffer. Again, record movies at three different spots in the chamber, and at three different concentrations.

### 3.6 Generating a Mapping File for Single-Molecule Analysis

Extraction of single-molecule movies requires the use of a mapping file. The mapping file is used to align the split Cy3 and Cy5 channels, to ensure that the same spot is analyzed in both channels. In single-color experiments the colocalization of spots is unnecessary; nevertheless, because the same software is used to extract individual traces from the experimental movie, a mapping file is needed. This file is generated using a slide that has been treated with fluorescent beads that fluoresce in both channels of the microscope.

A new mapping file should be generated each week and used to analyze all the data collected during the week. (There can be slow changes in instrument alignment and it is necessary to have an accurate mapping file to extract the data.)

#### 3.6.1 Preparation of the Single-Molecule Bead Slide

With acetone, clean a glass slide and a cover glass. Using scotch 3M double-sided tape, tape the cover glass to the slide by placing the tape lengthwise on the slide and then carefully laying the cover glass over the tape. Use a pipette tip to press the cover glass tightly to the slide and tape, ensuring proper sealing of the long edges. Remove the excess tape with a razor blade. Next dilute 0.2  $\mu\text{L}$  of FluoSpheres Carboxylate-Modified Microspheres, crimson fluorescent (Thermo Fisher, F-8806) into 1 mL of Tris–HCl pH 8.0. Sonicate the mixture in a bath sonicator for 5 min. Immediately following sonication, flow 60  $\mu\text{L}$  of the bead solution into the slide chamber using a pipette. Be sure to remove all air bubbles in the flow chamber as this can lead to pH changes and breakdown of the beads. Seal the ends of the chamber using 5-min epoxy. Make sure to remove any excess epoxy, as this will cause the slide to sit unevenly on the microscope, making the TIRFM

signal:noise very low. The bead slide should be stored at ambient temperature in the dark and can be used until it starts drying out (air bubbles appear).

### **3.6.2 Recording of the Single-Molecule Mapping File**

Mount the bead slide on the microscope and turn on green laser (532 nm) to obtain TIR fluorescence. Set the gain to the minimum setting on the camera. The fluorescent beads are significantly brighter than the experimental dyes, and they will oversaturate the detector at the experimental gain. In addition, adjust the laser intensity mechanically through the use of the wave plate, or by defocusing the beam, to ensure that the spots seen in the camera are similar in color to those seen when recording the experiment. Blue spots are a lower intensity, while white spots have saturated the detector. Select the autoscale function in the single recording software. This will automatically, and on the fly, adjust the background and data scaler while recording. Record a movie at 100 ms exposure for 10 s. Rename the movie file (.pma extension) and log file (.log) to “rough.” This will make the mapping file ready for software analysis in the following steps.

## **3.7 Analysis of Single-Molecule Trajectories**

The following describes the conversion of raw movies of the binding experiment, observed by TIRFM, into trajectories of the binding events of a single molecule. This is done by (i) identifying spots on the slide at which binding events are occurring, (ii) determining the fluorescent intensity observed over time at these positions, and (iii) idealizing (fitting) the resulting traces to obtain the observed population of binding events (on-times) and periods where there is no binding (off-times; Fig. 2A). The distributions of the on-times and off-times depend on the dissociation constant and the product of the association constant times the ligand concentration, respectively. Fitting of the histograms of these distributions defines the kinetic parameters for the interaction.

### **3.7.1 Preprocessing of Single-Molecule Movies**

Prior to examining single-molecule traces, the experimental movie must be extracted. The extraction process takes the raw movie file and outputs the fluorescent intensity over time of each individual fluorescent spot that is found in the movie. Single-molecule movies are extracted using IDL scripts provided by the University of Illinois Center for the Physics of Living Cells (<https://cplc.illinois.edu/software/>).

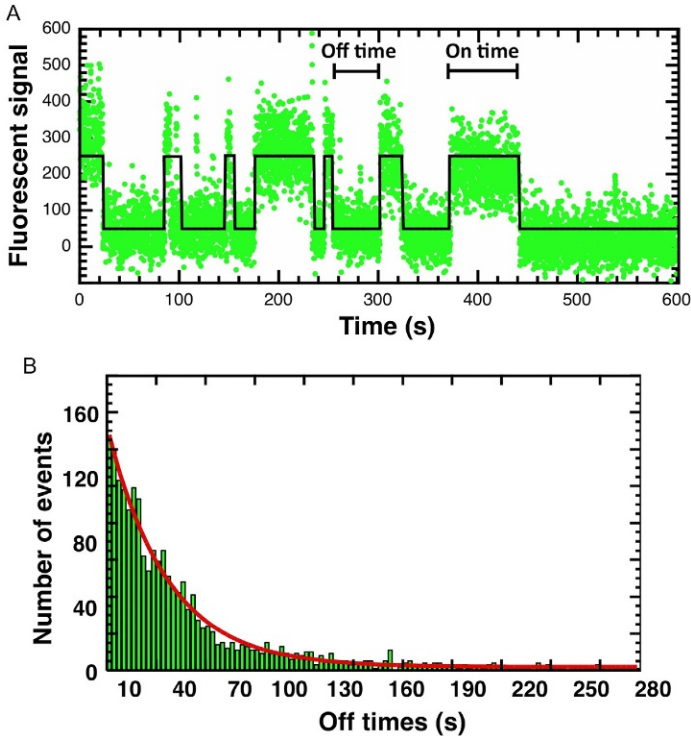


**Fig. 2** (A) A representative trajectory one RPA molecule monitored in the presence of 100 nM Cy3-labeled dT20 for 600 s. Each *dot* represents a fluorescence reading and the *black line* represents the two-state model determined by QuB. The time of each binding event is an “on-time,” and the time between binding events is counted as an “off-time.” (B) Histogram of the distribution of “off-times” for RPA binding to 100 nM dT20. *Curve* represents the best fit of the data to a single exponential (Eq. 1).

The first step of extraction is using the IDL script **maketiff** to create a tiff image of the recorded mapping file. This creates an image of the first 10 frames of the mapping movie as a reference for ensuring the donor (Cy3) and acceptor (Cy5) channels will be mapped such that fluorescent intensities of each channel correspond to the same geographic location. The next IDL script, **calc\_mapping2**, is run and a unique spot is selected in the Cy3 channel. IDL then selects the corresponding location in the Cy5 channel. The spot in the Cy3 channel and the corresponding spot in the Cy5 channel are outlined with a circle. If the spots are not centered in the outlining circles, one or both are manually adjusted to ensure the best possible map. This is repeated two times, for a total of three selected spots. When selecting the three spots for alignment, it is important to select from different

areas of the image. Typically, a spot in the upper left, center, and lower right of the image is selected. Next, run **nxgn1\_cm** in IDL to map all of the spots based upon the coordinates determined by the previous step. Spots that were aligned from both channels will be circled in white, whereas spots that were not found in both channels will be circled in red. It is important to have at least 100 matched spots to properly extract traces from experimental movies. Next run **ana\_all**, this script takes the mapping file and uses the identified coordinates to map the Cy3 and Cy5 channels of the experimental movie and then saves all of the spots found in a movie in a .traces file. This file contains all the spots from a movie and the red and green intensities of each spot for the duration of the experimental movie. As previously noted, when performing single-color experiments, the use of the mapping file is only necessary due to software restrictions, and the traces in both fluorescent channels will be extracted regardless of the presence of only a single color.

### **3.7.2 Selection of Individual Single-Molecule Traces**

Matlab scripts are used to extract the .traces file into single-molecule trajectories. All Matlab scripts used in this process are available upon request, from the corresponding author. Background correction is necessary prior to selection of the individual traces. **Trace\_Viewer\_Background** is used to determine the background values of a movie. When running this script, it is important to select the background values from the region of the trace that has a consistent minimum signal. When using a tethered fluorescent molecule, this is easily accomplished by looking for a single frame loss of signal with no increases in fluorescent intensity following the decrease. This indicates photobleaching of the dye and therefore ensures that the only signal present is due to background noise. When using free fluorescently labeled molecules, this can be more difficult as photobleaching is less likely to be seen. Collect the background value from at least 20 traces within the movie to ensure that a proper average background value can be calculated. The output from the script will be a number for the background correction value. Note this value, as it will be needed when running the next script. Next, run **Trace\_Viewer\_Regular** in Matlab. Enter the background values that were obtained in the previous step when running this script. Select traces on the following criteria: An increase in fluorescence must be two standard deviations above the noise to be considered a binding event. Bound events must start and end during the movie, and the trace will, ideally, have at least two binding events. Traces are trimmed

to remove bound events that start prior to the movie and that persist beyond the end of the movie. Traces are saved as a comma separated text file in the format of Time, Donor Intensity, Acceptor Intensity.

### 3.7.3 Idealization of Traces

Traces must be binned as either bound or unbound events in order to determine the kinetic rates of the protein–nucleic acid interactions. It would be extremely tedious to attempt to determine the duration of bound and unbound events by hand, and therefore hidden Markov modeling software can be used to idealize a fit to these traces to represent all of the bound and unbound events, as well as quantifying the durations of each event. Traces selected using Matlab **Trace\_Viewer\_Regular** are now idealized using the hidden Markov modeling tools of QuB (freeware developed in the Sachs lab at the University of Buffalo (Milescu et al., 2000–2017; Nicolai & Sachs, 2013), available from the corresponding author upon request). The first step of idealizing traces using QuB is to create a model that represents the number of kinetic events that the trace should be fit to. In the case of RPA, a two-state model most accurately described the kinetic states, and therefore this method will describe the process of analyzing the data with this model. The same process could be used to analyze data with a three- or four-state model by adding these states to the initial model.

First, open QuB and select the model view from the view drop down. In the model window, create a two-state model by left-clicking in the window. This will create a black box labeled “1” to create the free state (state 1). Click a second time create a second state labeled “2” to create the bound state (bound state 2). Double-click on the second state to change the color of the second state. This informs QuB to recognize the two events as independent states. Right-click and hold on state one and drag a line from state one to state two linking the two events. Set  $k_1$  by double-clicking on the 1000 above the line and change  $k_0$  to 0.1. Change  $k_{-1}$  to 0.01 by clicking the 1000 below the line and changing  $k_0$ . These values will give QuB an initial value when determining the bound and unbound events. For the RPA experiments described, these values were found to give the best overall results. (However, it is recommended that a range of initial values be tested in preliminary experiments because initial values that are too large or too small can cause QuB to underrepresent the states or overfit the data, respectively.) Open traces saved from Matlab by clicking open a data file. Multiple files can be opened from the pop-up window by ctrl+clicking multiple files. In the new pop-up window, several options are chosen. These options

instruct QuB how to handle the raw trace data for analysis. **A/D Channel count** is set to 2, **A/D Data size** is 2 bytes, **Time column** and **Segmented** are checked, and the sequence **A1, A2...B1, B2** is checked. Once these settings have been selected, they will be saved for future files opened. Click **Est. Scaling** for each file and then **OK** to open the file. Once all files have been opened, double-click on the trace in the **Data** window. This opens a larger view of the trace which can be more easily manipulated. The black trace represents the Cy3 channel, while the orange trace represents the Cy5 channel. Double-click and drag a region of the enlarged trace, which has no binding events present, to select, and then right-click and select **set baseline**. In the **Actions** menu select **Modeling** → **Amps** and input the following values in the pop-up window. **Data source** is Whole file, **Preprocess data** is None—use original data, and **Dead time** is set to three frames. Setting the dead-time eliminates short events that are not binding events, but rather diffusion of molecules through the spot of the trace during recording of the experimental movie. The remaining options in this window are left default, click **Run**. This action determines the average values for a low fluorescent intensity unbound state and high fluorescent intensity bound state.

Next, select the **Actions** menu and **Modeling** → **Idealize**. In the new pop-up window select the following options. Check **Clear existing idealization**, **Data source** and **Preprocess data** are selected as in **Amps** action, **SKM** is checked, **LL conv** is 0.01, **Max iter.** is 1000, check **Drop first/last event**, **Reestimate**, **Apply dead-time to statistics**, and **Apply dead-time to idealization**. Click **Run** and QuB will fit bound and unbound events using the amplitude data from the previous step. The events will be fit if they are within one standard deviation of the low- and high-intensity states determined by the Amps action. An idealized fit will be overlaid on the raw trace in the Data window (Fig. 2A). Each trace must then be examined individually by eye. If the data is noisy, it is possible that QuB over/under fit the trace. Events that have been missed, or created, by the idealization need to be removed manually. To do so, check **Sel** under **Data source**. This ensures only the selected region of the trace will be altered. Double-click and drag the region of the enlarged trace that is to be modified and click **Edit Idl**. In the new pop-up window, several options can be selected. If the idealization has fit a bound event (state 2), check box **Change class** and enter 1 to change events to state 1 (unbound event). Do the inverse if the idealization incorrectly classifies an unbound event (state 1) as bound (state 2). In the **File** menu select **Idealized data** → **Save idealized data**.

This creates a comma separated file in the format .dwt. At this time, QuB will now save all unbound events (state 1) as a “0” in the raw .dwt file, and all bound states (state 2) as a “1” in the raw file. Sort traces into bound (0) and unbound (1) events, with corresponding durations. Combine the data from all the idealized trajectories and bin them to create a histogram of the durations of the on (bound) and off (unbound) states following the guidelines from [Boehm et al. \(2016\)](#).

### 3.7.4 Determination of Binding Kinetics

Histograms of bound and unbound states (on-times and off-times, respectively) are analyzed to determine interaction parameters ([Fig. 2B](#)). Simple bimolecular interactions should be fit to a single exponential and the  $K_D$  determined from the resulting on-rate ( $k_1$ ) and off-rate ( $k_{-1}$ ).  $k_1$  is determined by fitting a single-phase exponential decay (Eq. 1) to the histogram of the unbound events (off-times; [Fig. 2B](#)). This process is concentration dependent and therefore must be determined for multiple concentrations of protein

$$Y = a * e^{-\nu_1 t} \quad (1)$$

The resultant  $\nu_1$  is plotted vs protein concentration and fit to a line. The slope determines the  $k_1$  of the protein–substrate interaction. Likewise, fit the histogram of the bound events (Eq. 2) to a one-phase exponential decay to determine  $k_{-1}$ , which is a concentration-independent process

$$Y = a * e^{-k_{-1} t} \quad (2)$$

In the case of RPA binding to oligonucleotides 20 nt or longer, it has been found that association of RPA was a single exponential (Eq. 1) and that dissociation was best described by a two-term exponential ([Chen et al., 2016](#)). This indicated that there are at least two kinetic steps during dissociation. In this scenario, the bound event frequency distribution is fit to a two-phase exponential decay (Eq. 3).

$$Y = a_1 * e^{-k_{-1} t} + a_2 * e^{-k_{-2} t} \quad (3)$$

Fitting determines  $k_{-1}$  and  $k_{-2}$  (and the proportion of each). Similarly, two-phase association kinetics can be determined by substituting  $\nu_1$  and  $\nu_2$  in Eq. (3) and then plotting each  $\nu$  vs protein concentration to determine  $k_1$  and  $k_2$ . Regardless of the kinetic process, the rate

constants can be used to determine the equilibrium dissociation constant,  $K_D$ , from the ratio of  $k_{-1}$  to  $k_1$  (Eq. 4).

$$K_D = \frac{k_{-1}}{k_1} \quad (4)$$

When fitting single-molecule data, it is critical to include the labeling efficiency in the determination of the kinetic rates. This is because unlabeled molecules act as competitive inhibitors to the binding of the fluorescently labeled substrate. A detailed method to correct for inefficient labeling is described in section 3.3 in [Boehm et al. \(2016\)](#). This correction can be ignored when labeling is efficient. For example, commercially fluorescent DNA substrates are usually shipped with 100% labeled product. In contrast, aldehyde labeling of proteins can range from 10% to 50% efficiency.

## ACKNOWLEDGMENTS

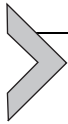
We thank Dr. Maria Spies and the members of her lab for their advice and many of the basic protocols used for analyzing single-molecule studies of RPA–DNA interactions. We also thank the single-molecule community for developing the methods and software tools used for collecting and analyzing single-molecule data. Support for F.E.B. from NIH P30-CA086862 from the University of Iowa Holden Cancer Center and a training fellowship from the University of Iowa Center for Biocatalysis and Bioprocessing and of the NIH-sponsored Predoctoral Training Program in Biotechnology (2 T32 GM008365).

## REFERENCES

- Bain, F. E., Wu, C. G., & Spies, M. (2016). Single-molecule sorting of DNA helicases. *Methods*, 108, 14–23.
- Beckett, D., Kovaleva, E., & Schatz, P. J. (1999). A minimal peptide substrate in biotin holo-enzyme synthetase-catalyzed biotinylation. *Protein Science*, 8(4), 921–929.
- Binz, S. K., Dickson, A. M., Haring, S. J., & Wold, M. S. (2006). Functional assays for replication protein A (RPA). *Methods in Enzymology*, 409, 11–38.
- Boehm, E. M., Subramanyam, S., Ghoneim, M., Washington, M. T., & Spies, M. (2016). Quantifying the assembly of multicomponent molecular machines by single-molecule total internal reflection fluorescence microscopy. *Methods in Enzymology*, 581, 105–145.
- Bradford, M. M. (1976). A rapid and sensitive method for the quantitation of microgram quantities of protein utilizing the principle of protein-dye binding. *Analytical Biochemistry*, 72, 248–254.
- Carrico, I. S., Carlson, B. L., & Bertozzi, C. R. (2007). Introducing genetically encoded aldehydes into proteins. *Nature Chemical Biology*, 3(6), 321–322.
- Chen, R., Subramanyam, S., Elcock, A. H., Spies, M., & Wold, M. S. (2016). Dynamic binding of replication protein a is required for DNA repair. *Nucleic Acids Research*, 44, 5758–5772.
- Galletto, R., Amitani, I., Baskin, R. J., & Kowalczykowski, S. C. (2006). Direct observation of individual RecA filaments assembling on single DNA molecules. *Nature*, 443(7113), 875–878.

- Ghoneim, M., & Spies, M. (2014). Direct correlation of DNA binding and single protein domain motion via dual illumination fluorescence microscopy. *Nano Letters*, *14*(10), 5920–5931.
- Haring, S. J., Mason, A. C., Binz, S. K., & Wold, M. S. (2008). Cellular functions of human RPA1. Multiple roles of domains in replication, repair, and checkpoints. *The Journal of Biological Chemistry*, *283*(27), 19095–19111.
- Henricksen, L. A., Umbricht, C. B., & Wold, M. S. (1994). Recombinant replication protein A: Expression, complex formation, and functional characterization. *The Journal of Biological Chemistry*, *269*, 11121–11132.
- Jain, A., Liu, R., Ramani, B., Arauz, E., Ishitsuka, Y., Ragunathan, K., et al. (2011). Probing cellular protein complexes using single-molecule pull-down. *Nature*, *473*(7348), 484–488.
- Joo, C., & Ha, J. (2008). Single-molecule FRET with total internal reflection microscopy. In P. R. Selvin & J. Ha (Eds.), *Single-molecule techniques: A laboratory manual* (pp. 3–36). Cold Spring Harbor, NY: Cold Spring Harbor Laboratory Press.
- Mason, A. C., Haring, S. J., Pryor, J. M., Staloch, C. A., Gan, T. F., & Wold, M. S. (2009). An alternative form of replication protein A prevents viral replication in vitro. *The Journal of Biological Chemistry*, *284*, 5324–5331.
- Milescu, L. S., Nicolai, C., & Bannen, J. (2000–2017). *QuB software*.
- Nguyen, B., Sokoloski, J., Galletto, R., Elson, E. L., Wold, M. S., & Lohman, T. M. (2014). Diffusion of human replication protein A along single stranded DNA. *Journal of Molecular Biology*, *21*(14), 3246–3261.
- Nicolai, C., & Sachs, F. (2013). Solving ion channel kinetics with the QuB software. *Biophysical Reviews and Letters*, *08*(03), 1–21.
- Rabuka, D., Rush, J. S., Dehart, G. W., Wu, P., & Bertozzi, C. R. (2012). Site-specific chemical protein conjugation using genetically encoded aldehyde tags. *Nature Protocols*, *7*(6), 1052–1067.
- Shi, X., Jung, Y., Lin, L. J., Liu, C., Wu, C., Cann, I. K., et al. (2012). Quantitative fluorescence labeling of aldehyde-tagged proteins for single-molecule imaging. *Nature Methods*, *9*, 499–503.
- Studier, F. W. (2005). Protein production by auto-induction in high density shaking cultures. *Protein Expression and Purification*, *41*(1), 207–234.
- Studier, F. W., Rosenberg, A. H., Dunn, J. J., & Dubendorff, J. W. (1990). Use of T7 RNA polymerase to direct expression of cloned genes. *Methods in Enzymology*, *185*, 60–89.

This page intentionally left blank



# Single-Molecule Studies of ssDNA-Binding Proteins Exchange

Olivia Yang\*, Taekjip Ha\*,†,‡,1

\*Johns Hopkins School of Medicine, Baltimore, MD, United States

†Howard Hughes Medical Institute, Baltimore, MD, United States

‡Johns Hopkins University, Baltimore, MD, United States

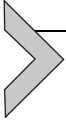
1Corresponding author: e-mail address: tjha@jhu.edu

## Contents

|  |     |
|--|-----|
| 1. Introduction  | 464 |
| 2. Single-Molecule FRET Experimental Strategies            | 465 |
| 2.1 Preparation and Assembly of Polyethylene Glycol Slides | 465 |
| 2.2 DNA Substrate Preparation                              | 466 |
| 2.3 Single-Molecule FRET With TIR Microscopy               | 468 |
| 2.4 SSB Replacement Assay                                  | 469 |
| 2.5 SSB Transfer Assay                                     | 472 |
| 3. Notes   | 474 |
| 4. Summary   | 476 |
| Acknowledgments  | 477 |
| References   | 477 |

## Abstract

Single-stranded DNA-binding protein (SSB) is important not only for the protection of single-stranded DNA (ssDNA) but also for the recruitment of other proteins for DNA replication, recombination, and repair. The interaction of SSB with ssDNA is highly dynamic as it exists as an intermediate during cellular processes that unwind dsDNA. It has been proposed that SSB redistributes itself among multiple ssDNA segments, but transient intermediates are difficult to observe in bulk experiments. We can use single-molecule FRET microscopy to observe intermediates of the transfer of a single *Escherichia coli* SSB from one ssDNA strand to another or exchange of one SSB for another on a single ssDNA in real time. This single-molecule approach can be further applicable to understand relative binding affinities and competitive dynamics for other SSBs and variants across various systems.



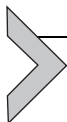
## 1. INTRODUCTION

In order to access and use genomic DNA for processes such as replication, recombination, and repair, single-stranded DNA (ssDNA) is generated as an intermediate. In this state, DNA is more susceptible to breakage, chemical mutagens, or nuclease digestion. ssDNA-binding protein (SSB) not only exists in most biological systems to prevent these damages but also plays an important role in recruitment of relevant proteins to regions of ssDNA to carry out their own functions. In order to efficiently distribute SSB among exposed ssDNA, it is likely that SSB is recycled and redistributed. SSB transfer between adjacent and distant DNA segments can allow rapid recycling and redistribution. Exchange of a bound SSB with another may make it possible to replace a set of proteins bound to the incumbent SSB with another set bound to the incoming SSB. Therefore, a detailed investigation of SSB transfer and exchange kinetics is expected to reveal functionally important properties. While a mechanism of interstrand exchange has been proposed, it is difficult to observe transient intermediates in most ensemble experiments (Kozlov & Lohman, 2002; Lee et al., 2014). To focus on the transfer of a single SSB to another DNA, or the exchange of one SSB for another at the single molecule level, we can use surface-tethered DNA substrates.

We have previously described detailed single molecule methods to observe transitions different binding modes of SSB and SSB diffusion along short ssDNA (Roy, Kozlov, Lohman, & Ha, 2007; Zhou & Ha, 2012). For *Escherichia coli* SSB, there are two major binding modes, (SSB)<sub>65</sub> and (SSB)<sub>35</sub>, which have well-defined ssDNA wrapping lengths. The numbers 65 and 35 refer to the number of nucleotides contacted by the SSB homotetramer in each mode (Roy et al., 2007). Here, we describe an assay of using a mutant SSB with a distinct binding behavior as compared to wild-type SSB (wtSSB) to observe exchange of a DNA-bound SSB for wtSSB in solution. We can also observe an exchange of a labeled SSB for an unlabeled SSB. Exchange kinetics has been measured in ensemble, and it was proposed that there must exist an intermediate of multiple SSB bound to a single ssDNA region (Kunzelmann, Morris, Chavda, Eccleston, & Webb, 2010). Using single-molecule fluorescence resonance energy transfer (smFRET), we can directly observe the real-time formation of a reaction intermediate with more than one SSB bound to the same DNA. We can also use the FRET difference between a DNA fully wrapped around SSB

and a free DNA to observe the transfer of SSB to a separate DNA strand. We can use these observations to dissect the exchange kinetics and mechanisms.

In this chapter, we describe protocols for studying replacement (bound SSB being exchanged for SSB in solution) and transfer (bound SSB transferred to free ssDNA in solution) mechanisms using *E. coli* SSB as a model.



## 2. SINGLE-MOLECULE FRET EXPERIMENTAL STRATEGIES

### 2.1 Preparation and Assembly of Polyethylene Glycol Slides

In order to perform single-molecule microscopy experiments using surface-tethered molecules, a clean and passivated surface is required. This minimizes the loss of sample protein and DNA through nonspecific adsorption, as well as potential artifacts caused by interaction with the surface. Generally, polyethylene glycol (PEG)-coated quartz slides and glass coverslips are used for single-molecule total internal reflection fluorescence (TIRF) experiments.

PEG slides and coverslips for TIRF microscopy purposes were obtained from Microscope Slides Core facility in Johns Hopkins University School of Medicine. Each slide has multiple channels and is suitable for multiple experiments.

#### 2.1.1 Materials

- PEGylated quartz slide and coverslip
- Double sided tape
- 5-min epoxy
- Tubing: WEICO ETT-28 (inner diameter = 0.015", outer wall = 0.016")
- Needle: BD (26 gauge, 3/8")
- 1-mL syringe
- 20–200- $\mu$ L pipette tips
- Vacuum sealable food saver bags

#### 2.1.2 Procedure

1. Slides are assembled with PEG surfaces of the slide and coverslip facing each other to create passivated channels. PEGylated surfaces can be distinguished from untreated surfaces by dropping water and observing the hydrophobicity of the surface; a treated surface will be more hydrophobic.

2. After testing, surfaces can be dried with house air or  $N_2(g)$ ; PEGylated surfaces should not be physically touched or the passivation will be disrupted.
3. Double-sided tape ( $\sim 100\ \mu\text{m}$  thick) is used as a spacer between the slide and coverslip, and to create the channels for multiple experiments (see Fig. 1). Tape is cut into thin strips on a clean surface with a clean razor blade. Do not move tape once it has been placed.
4. Place the coverslip on top of the slide and tape, PEG side down, and press with pipette tip to secure the adhesion and prevent leaks between channels.
5. Ends of the channel are sealed with 5-min epoxy as marked in yellow (see Fig. 1). Excessive epoxy used in this step may block the inlet holes drilled in the slide, so use sparingly.
6. For real-time flow experiments, additional setup is required (see Fig. 3; Section 3)
7. Slides are typically stored at  $-20^\circ\text{C}$  in 50-mL tubes, into vacuum sealed bags to avoid moisture. Slides with unused channels can be similarly stored for later use.

## 2.2 DNA Substrate Preparation

A DNA substrate similar to previously used for SSB-binding mode and dynamics studies is tethered to the surface for single-molecule experiments

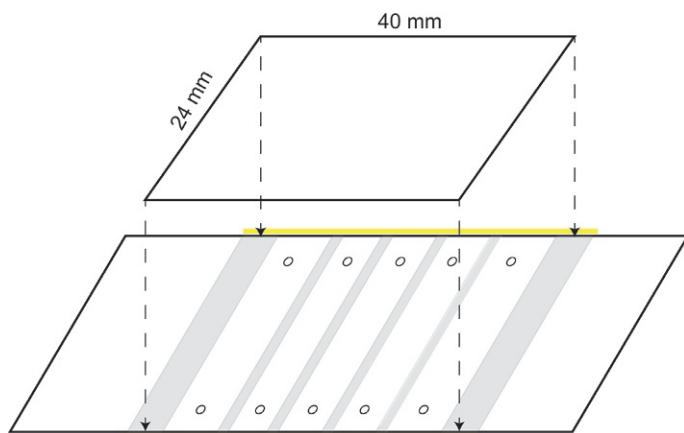


**Fig. 1** PEG slide assembly. Slides are assembled with PEG surfaces facing inward. Double-sided tape is placed as marked in *gray*, between holes drilled. The long edge of the coverslip and slide is sealed with 5-min epoxy (*yellow region*). One channel is the space between two tapes.

(Roy et al., 2007; Zhou et al., 2011). The partial duplex substrate is made of an 18 bp duplex with a polydeoxythymidine (poly-dT) overhang of varying lengths. The 18 bp duplex is used as a spacer to minimize potential surface effects. Poly dT is used for its lack of secondary structure and high binding affinity to SSB, although other sequences may also work (Lohman & Overman, 1985). The length of the ssDNA used is approximately 70 nt, enough to allow for a full wrapping of SSB ((SSB)<sub>65</sub> mode) or two partially wrapped SSB ((SSB)<sub>35</sub> mode).

The end of the duplex without the ssDNA overhang is biotinylated to specifically tether the DNA to the surface, while the other end of the duplex is Cy5 labeled. For smFRET experiments, cyanine dyes Cy3 and Cy5 are commonly used for donor and acceptor molecules, respectively, on DNA due to their high photostability under deoxygenated conditions and high brightness. A detailed labeling procedure is previously published (Joo & Ha, 2012). For experiments with labeled SSB, the substrate is labeled with Cy5 only. For unlabeled SSB, the far end of the ssDNA is additionally labeled in order to observe FRET changes upon SSB binding. SSB is labeled with an average of one Alexa 555, a small organic dye with excitation and emission spectra similar to Cy3, per SSB tetramer as previously described (Lee et al., 2014; Roy, Kozlov, Lohman, & Ha, 2009; Zhou et al., 2011).

The DNA oligonucleotides (oligos) used are listed below:

1. 5'-/Cy5/ GCC TCG CTG CCG TCG CCA -/biotin/-3'.
2. 5'-TGG CGA CGG CAG CGA GGC (T)<sub>m</sub>-/Cy3/-3' ( $m = 72$ ).
3. 5'-TGG CGA CGG CAG CGA GGC (T)<sub>m</sub>-3' ( $m = 70$ ).
4. 5'-(T)<sub>m</sub>-3' ( $m = 60$ ).

The DNA substrate for labeled SSB experiments was annealed by mixing oligos 1 and 3 at 10  $\mu$ M and 20  $\mu$ M, respectively, in 10 mM Tris-HCl (pH 8) and 50 mM NaCl, then slow cooling from 95°C to 4°C over  $\sim$ 4 h. The cooling can be done in a thermocycler at a rate of 1°C/min, or with a heat block taken off heat and allowed to cool to RT then stored at -20°C. The substrate for unlabeled SSB experiments was prepared similarly, but using oligos 1 and 2. Typical annealing uses an excess (1.2  $\times$  to 2  $\times$ ) of nonbiotinylated strands in order to ensure that surface-bound DNA contain both strands.

DNA substrates are stored at -20°C, covered in foil to prevent photobleaching. For single-molecule experiments, a substock of 5–10 nM DNA is prepared. At lower concentrations, DNA can be lost due to nonspecific adsorption to tube surfaces. 1% v/v BSA (20 mg/mL stock) in solution can act to passivate surfaces and prevent some loss.

## 2.3 Single-Molecule FRET With TIR Microscopy

A detailed explanation of the prism-type TIRF microscope setup used in these protocols can be found as previously published (Joo & Ha, 2012). Video recordings were processed to extract single molecule fluorescence intensities at each frame, and custom written scripts were used to calculate FRET efficiencies. Data acquisition and analysis software can be downloaded from <https://cplc.illinois.edu/software/>.

Alternating laser excitation (ALEX) is used to filter out molecules with donor only or acceptor only (Kapanidis et al., 2005). We require a minimum intensity cutoff during donor (green) or acceptor (red) excitation. If a fluorescence spot has a combined intensity from donor and acceptor channels less than the cutoff, then it is not counted. Stoichiometry parameter  $S$  can also be used to identify the donor and acceptor only spots. The stoichiometry  $S$  of each molecule is calculated as

$$S = \frac{I_A^G + I_D^G}{I_A^G + I_D^G + I_A^R}$$

Where  $I_A^G$  is the acceptor intensity during green excitation,  $I_D^G$  is the donor intensity during green excitation, and  $I_A^R$  is the acceptor intensity during red excitation. Molecules with low  $S$  values (0–0.2) correspond to acceptor only molecules, while molecules with high  $S$  values (0.8–1) correspond to donor only molecules. Molecules with both donor and acceptor have stoichiometry  $S \sim 0.5$ .

Our typical data acquisition sequence is an initial set of 10 frames of red laser excitation, followed by green laser excitation. FRET efficiency is calculated from green excitation periods. Long movies had an additional 10 frames of red excitation at the end to test if the acceptor has photobleached during data acquisition. A “snapshot” is defined as 20 frames taken at a single imaging area. “Long movies” are defined as enough frames to photobleach  $\sim 80\%$  of the molecules within the imaging area, usually around 2000–3000 frames. Leakage of donor signal to the acceptor channel and background signals of both channels were corrected similar to as previously described (Roy, Hohng, & Ha, 2008). Apparent FRET efficiency is calculated with the equation

$$E_{\text{FRET}} = \frac{I_A - \text{leakage} \times I_D}{I_A - \text{leakage} \times I_D + I_D}$$

where  $I_A$  is the acceptor intensity, leakage is the leakage factor from the donor to the acceptor detection channel, and  $I_D$  is the donor intensity. Leakage factor will vary depending on the microscope setup used. Background for long movies is corrected to make the intensities after donor photo-bleaching equal to zero. Histograms were made from at least 10 individual snapshots of a single sample, with approximately 200–300 molecules imaged per area for a total of 2000–3000 molecules used per histogram. The FRET efficiency of each molecule was calculated based on the average intensity of donor and acceptor over eight frames, avoiding the frames around when excitation is changing.

## 2.4 SSB Replacement Assay

In this chapter, we describe the use of *E. coli* SSB's well-characterized and controlled binding modes (Roy et al., 2007). The method of purification and labeling of SSB can be found as previously published (Lohman, Green, & Beyer, 1986; Roy et al., 2009). Because we want to observe primarily exchange of a single SSB ((SSB)<sub>65</sub>), we use NaCl concentrations greater than or equal to 100 mM; any lower NaCl concentration and there would be a significant population of two SSB molecules bound to 70-mer ssDNA ((SSB)<sub>35</sub> mode). Similarly, SSB concentration should be kept relatively low (<10 nM in 100 mM NaCl) to minimize binding in the (SSB)<sub>35</sub> mode. For an SSB variant with lower binding affinity, lower concentrations of wtSSB will be required for displacement. With only free DNA, 1 nM SSB is expected to bind almost fully within 1 min in high salt conditions.

### 2.4.1 Materials

- T50 buffer: 10 mM Tris–HCl (pH 8.0), 50 mM NaCl in ddH<sub>2</sub>O, filtered through 0.22- $\mu$ m membrane
- SSB imaging buffer (SSB IB 100 mM NaCl): 100 mM NaCl, 10 mM Tris–HCl (pH 8.0), 0.1 mg/mL BSA, 0.8% (w/v) dextrose, 165 U/mL glucose oxidase, 2170 U/mL catalase, 2–3 mM Trolox, and indicated amounts of SSB. See Section 3.
- Neutravidin: 0.2 mg/mL neutravidin diluted in T50 buffer
- Assembled PEG slide (see above)
- Prism-type TIRF microscope
- Labeled DNA substrate (oligomers 1 + 3, see above)
- Unlabeled DNA substrate (oligomers 1 + 2, see above)
- SSB stock: to be kept at –20°C, secondary stock can be made in SSB IB and kept on ice during the course of one set of experiments.

## 2.4.2 Procedure

### 2.4.2.1 Experiment Procedure

1. Confirm quality of slide (see [Section 3](#)).
2. Flow in  $\sim 20\ \mu\text{L}$  T50 buffer to each channel expected to be used for one experiment. The approximate channel volume is about  $20\ \mu\text{L}$ . For thorough flushing or between different buffer conditions, use at least  $30\ \mu\text{L}$  of solution.
3. Flow in  $\sim 20\ \mu\text{L}$  neutravidin to each channel. Incubate 1–2 min, then flush with T50.
4. Prepare 10–30 pM DNA substrate in T50 (“labeled” for labeled SSB displacement, “unlabeled” for mutant SSB displacement) and add to channel. Incubate for 1–2 min, then flush with SSB IB + “gloxy” to check the spot density. For “labeled” substrate, there should only be Cy5 signal, while “unlabeled” substrate should have both Cy3 and Cy5 signal. There should be 200–300 spots of a single dye within one imaging area. If the number of spots is too little, dilute more DNA and add to channel until desired density is reached.
5. Flush with SSB IB + gloxy. Take snapshots to generate DNA only histogram.
6. Add  $40\ \mu\text{L}$  of 1 nM SSB (labeled or mutant) in SSB IB 100 mM NaCl and incubate for at least 5 min ([Fig. 2A](#)).
7. Remove unbound SSB by flushing with SSB IB 100 mM NaCl + gloxy ([Fig. 2B](#)). Take snapshots to get initial time point.
8. Add wtSSB at desired concentration. To observe real-time exchange, a flow cell assembly must be used (see [Fig. 3](#); [Section 3](#)).
9. Take at least 10 snapshots at each given time point (0–30 min).

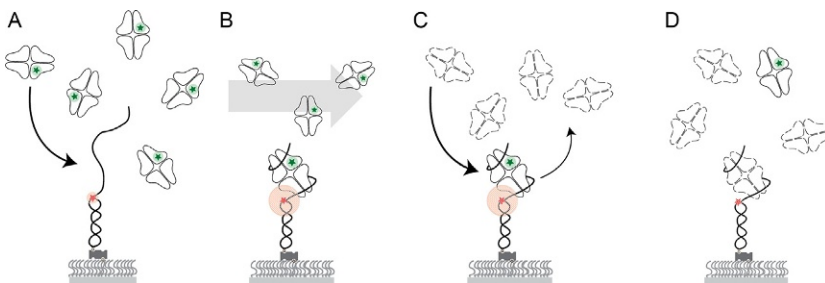


**Fig. 2** Scheme of SSB replacement assay. (A) Labeled SSB is added to ssDNA tethered to the PEG slide. (B) Unbound labeled SSB is flushed from sample chamber. (C) wtSSB (*dashed outline*) is added to sample chamber. (D) Labeled SSB is displaced from tethered DNA.

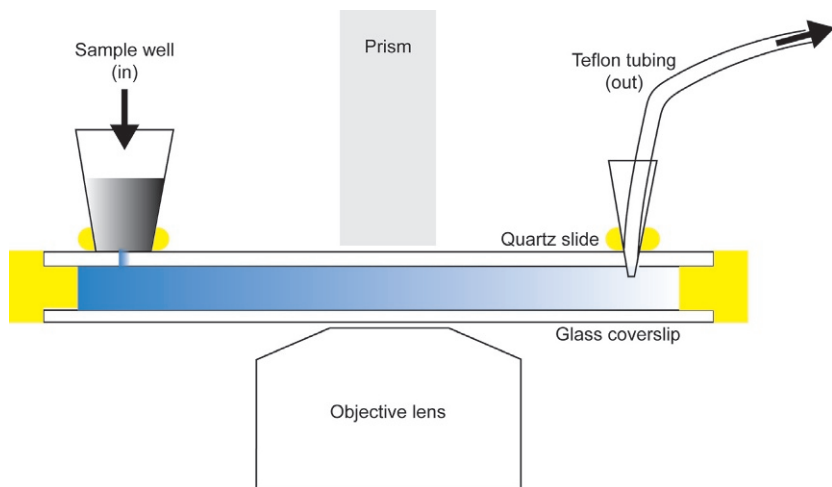


**Fig. 3** Real-time flow experiment setup—cross section of single channel. Pipette tip segments are stuck to the quartz slide with epoxy. “Sample well” holds the sample to flow in. Teflon tubing is stuck into pipette tip which has been adhered to hole with epoxy. Tubing is attached to a 1-mL syringe with 26-gauge needle.

#### 2.4.2.2 Data Analysis

For labeled SSB, replacement can be observed as the disappearance of fluorescent spots over time. Because the DNA substrate used is labeled with Cy5, we can use Alexa 555 as a label on SSB to distinguish it from unlabeled SSB and to observe FRET upon binding. We include in our analysis only those spots with both the acceptor (Cy5 on DNA) and donor (Alexa 555 labeled SSB) signals using ALEX. The two color colocalization allows us to reject SSB bound to the surface nonspecifically from analysis, and FRET provides an additionally stringent criterion for specific binding. Fluorescence spots with excessively high or low intensity are also rejected because they typically are not due to the molecules of interest.

Generally, spots will also disappear due to photobleaching, so it is important to use the condition with no wtSSB added to determine a photobleaching rate. It is important to keep the laser intensity constant to avoid changing this photobleaching rate too much between different experiment repeats. The number of spots is normalized to the initial time point, since for a given experiment the actual spot density at the beginning of experiment may vary. The displacement rate can be determined from a single exponential decay fit, then subtracting the photobleaching rate determined separately. Plotting the rate of spot disappearance against concentration of wtSSB added shows a linear relation.

For a mutant SSB with less than full wrapping properties, the exchange is observed through a shift in the FRET efficiency. As shown in Fig. 4, the mutant has a FRET efficiency centered around 0.5 (Fig. 4C, top panel), while wtSSB has a FRET efficiency about 0.7 (Fig. 4C, bottom panel). In order to confirm what FRET efficiencies each species corresponds with, controls should be done to see binding in the same buffer conditions at low [SSB]. The simplest way of determining exchange is imposing a FRET cut-off (0.6) to distinguish the mutant-bound DNA population vs the wtSSB-bound population. For variants with more overlapping FRET efficiencies, it would be more reasonable to fit the histogram with a Gaussian function for each population and use the area to calculate the population ratio. Using this ratio, we can plot the binding of wtSSB over time as it replaces the mutant. Similar to the labeled SSB assay, we can use this plot to obtain exchange rates at various concentrations of wtSSB.

Movies taken during real-time replacement assays will result in FRET traces as sketched in Fig. 4B. Three species are expected to exist in this experiment: the initial, mutant-bound SSB (0.5 FRET); the transient, 2 SSB-bound state with one mutant and one wild type (0.2 FRET, (SSB)<sub>35</sub>); and the final, wtSSB-bound species (0.7 FRET) (see Fig. 4A) (Roy et al., 2007). Through measuring dwell times of each FRET state on a single molecule trace, the rates of exchange between these three species can be determined. In this case, since we flood the system with wtSSB in a high salt buffer, we expect the reaction to be pushed toward the wtSSB-bound state. The  $E_{\text{FRET}}$  observed in the single molecule traces (Fig. 4B) should correspond with the centers of peaks as observed in histograms (Fig. 4C). Because the (SSB)<sub>35</sub> mode is not favored in these salt conditions, it does not exist long enough to be captured in histograms. However, it can be seen as an intermediate during real-time experiments.

## 2.5 SSB Transfer Assay

For this experiment, we use (dT)<sub>60</sub> because the expected binding site size for a single SSB is approximately 65 nt. Varying lengths or sequences of DNA oligomers can be tested for transfer activity with the same assay, though may require different concentration ranges. Sequences with secondary structures may also be inefficient in competing with the poly-dT substrate used.

### 2.5.1 Materials

The same materials as listed in the SSB displacement assay are used. Additional/alternative materials required are listed below.

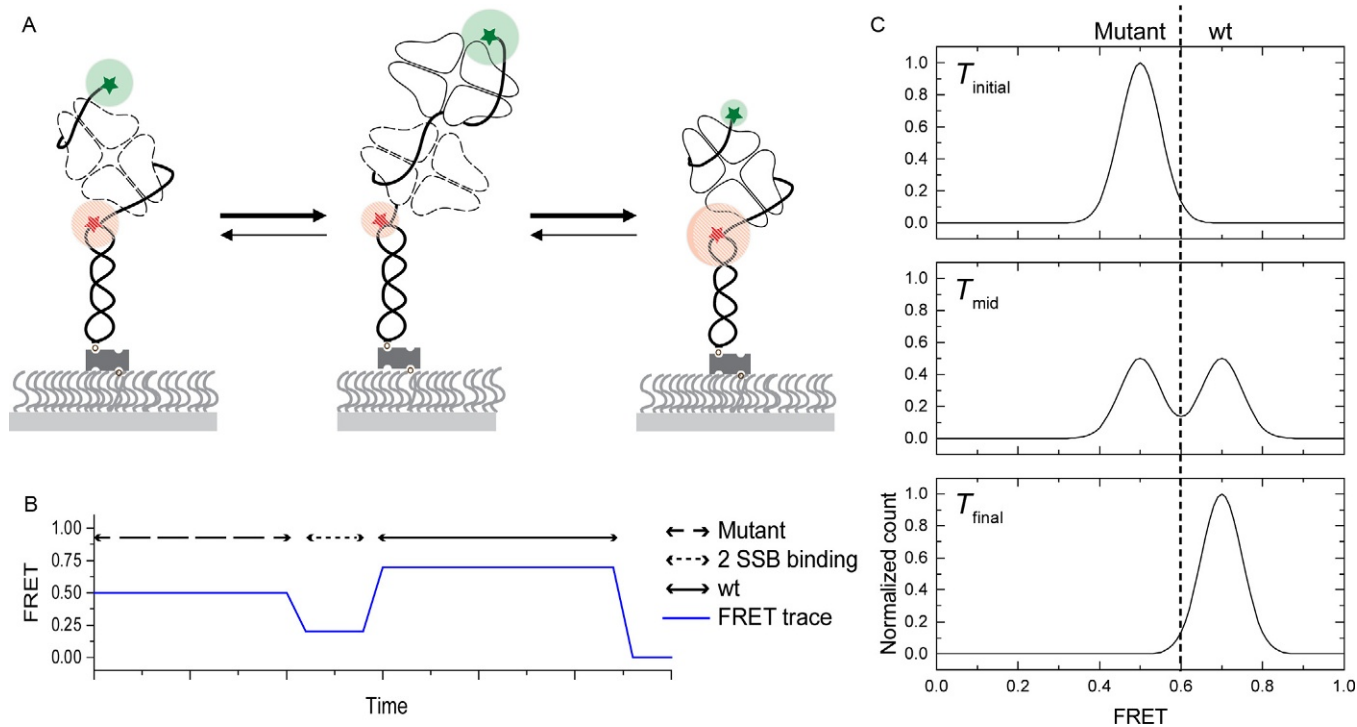


**Fig. 4** Results from mutant to wtSSB displacement (A) Scheme of displacement mechanism. (B) Ideal FRET trace of mutant to wtSSB in a “two-step” transition. (C) FRET histograms of populations observed during experiment.

- dT60 (oligomer 4): stock diluted in T50, stored at  $-20^{\circ}\text{C}$
- SSB imaging buffer (SSB IB 500mM NaCl): 500mM NaCl, 10mM Tris-HCl (pH 8.0), 0.1 mg/mL BSA, 0.8% (w/v) dextrose, 165 U/mL glucose oxidase, 2170 U/mL catalase, 2–3mM Trolox, and indicated amounts of SSB.

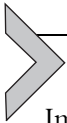
## 2.5.2 Procedure

### 2.5.2.1 Experiment Procedure

The same procedure for SSB replacement is followed for SSB transfer, but rather than SSB added at step 6, dT60 at varying concentrations is used in a SSB IB 500mM NaCl buffer, and throughout the experiment SSB IB 500mM NaCl is used in place of SSB IB 100mM NaCl.

### 2.5.2.2 Data Analysis

The initial state of the tethered substrate is bound by a single SSB, so shows a  $E_{\text{FRET}} \sim 0.7$ . The  $E_{\text{FRET}}$  of unbound ssDNA of a dT70 construct in 500mM NaCl is  $\sim 0.15$ . The exact value will vary slightly based on NaCl or other salt concentrations. Since the difference in  $E_{\text{FRET}}$  is large, a cutoff can be used to determine the bound and unbound DNA substrate populations.



## 3. NOTES

Imaging buffer is generally prepared as follows:

1. Trolox + dextrose solution: 10 mg Trolox (( $\pm$ )-6-Hydroxy-2,5,7,8-tetramethylchromane-2-carboxylic acid, Sigma-Aldrich) and 80 mg dextrose (Sigma-Aldrich) is dissolved in 10 mL ddH<sub>2</sub>O and 10  $\mu\text{L}$  5 M NaOH. Mixture is rotated for at least 4 h, RT, covered in foil. Solution is filtered through 0.22- $\mu\text{m}$  membrane and stored at  $4^{\circ}\text{C}$ . This solution can be used for 2–3 weeks when stored at  $4^{\circ}\text{C}$ , or longer if stored frozen.
2. SSB IB: NaCl, Tris-HCl (pH 8.0), and BSA are added to Trolox + dextrose solution to the final concentrations listed above to make a flush buffer for removing free protein from channel. NaCl, Tris-HCl, and BSA are added with SSB to Trolox + dextrose solution to final concentrations as needed for steps adding SSB to channel.
3. “Gloxy”: 10 mg glucose oxidase (G2133, Sigma-Aldrich) and 20  $\mu\text{L}$  bovine liver catalase (C30, Sigma-Aldrich) is dissolved in 100  $\mu\text{L}$  T50 buffer. Mixture is spun down for 2 min at  $10,000 \times g$ . The top 100  $\mu\text{L}$  of the solution is transferred and stored at  $4^{\circ}\text{C}$ , and can be used for

~2–4 weeks. This solution is  $100\times$  concentrated, and is typically not added until right before samples are added to the slide. Upon mixing with IB, the solution will continually become more acidic upon reacting with atmospheric oxygen (Joo & Ha, 2012).

Slides should always be checked for cleanliness and passivation before use, as follows:

1. Cleanliness: With just T50 in the channel, there should be fewer than 10 observable fluorescent spots per imaging area.
2. Passivation: After flowing in 1 nM labeled DNA or protein, there should be less than 30 observable spots stuck to the surface. After flushing with T50, there should be significantly less spots compared to earlier. Protein is generally stickier than DNA and is expected to have slightly more nonspecific binding.
3. Only after the channel has passed these checks should the user proceed with the experiment.

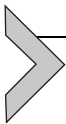
Real-time flow experiments have other considerations:

1. 20–200- $\mu$ L pipette tips are used in this setup. The sample well is made from the wider portion of the tip, while the outlet side is the sharper portion of the tip. Both are adhered to the slide with epoxy. Fig. 3 shows the cross section of a channel assembled for a real-time flow experiment.
2. It is not necessary to epoxy the tubing to the tip, though it helps make the assembly more secure. Care should be taken to avoid clogging the drilled holes with epoxy.
3. A minimum of 40  $\mu$ L of sample must be added to the sample well to avoid drawing bubbles through the channel.
4. Sample is drawn through by pulling with a syringe. This can be done manually, or in a more controlled way with a syringe pump. With a syringe pump, the exact flow time and rate can also be controlled. At no point should the sample be pushed back through the channel.
5. All solutions added to this channel will be drawn through by adding the solution to the sample well and pulling through with the syringe.
6. Because a sample is being pulled through during the recording of a movie, care must be taken that the pulling action does not perturb the sample stage or any part of the microscope. Slight motions of the slide or sample will affect the focus and the quality of the movie.

7. After the initial movie is taken, further long movies or snapshots can be taken of the same channel.
8. Tubing and syringes can be reused, but fresh pipette tips should be used for adhering to the slide.

Other general notes:

1. During imaging, general exposure time used is 50–100 ms. Highest time resolution for the camera used in these experiments (Andor DU-897E-CSO-#BV) is 30 ms for  $512 \times 512$  pixels, though the imaging area can be decreased to increase time resolution. To avoid photobleaching, a longer exposure time should be used to minimize laser intensity. To observe faster dynamics, shorter exposure times should be used, but higher laser intensities will be required to increase signal to noise ratios.
2. Slides can be reused. By soaking in methanol, epoxy is weakened and the coverslip and double sided tape can also be removed and disposed of. Then, slides should be boiled in water and any visible junk can be washed off before proceeding with usual treatment (Roy et al., 2008).
3. All concentrations of SSB in this text refer to concentration of SSB tetramer.
4. DNA substrate concentration refers to the concentration of the biotinylated strand. Nonbiotinylated strand is used in excess in order to maximize the amount of annealed DNA that gets specifically tethered to the slide. Nonbiotinylated strand will get flushed from the channel and should not interfere with experiments.
5. High concentrations of DTT cannot be used in imaging buffers for single-molecule experiments, as blinking will be observed.



---

## 4. SUMMARY

smFRET and single molecule experiments are especially useful for understanding more detailed dynamics of SSB, especially on a small length scale. These details may be helpful to explain steps in protein recruitment processes during replication, recombination, and repair related to ssDNA processing. Though *E. coli* SSB was used throughout these experiments, similar single molecule studies regarding transfer and replacement mechanisms can be done with the same method for other relevant SSB variants to further understand the differences between SSBs from different organisms. However, the binding of each new variant needs to be well

characterized for a given substrate before observing exchange in order to properly attribute a given FRET efficiency to a specific variant. Using single-molecule methods can be useful for observing and confirming intermediates as proposed by other ensemble scale SSB experiments.

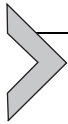
## ACKNOWLEDGMENTS

The authors would like to thank Dr. Jichuan Zhang for his guidance and advice throughout this project, and Prof. I-Ren Lee for his helpful ideas. Research in this chapter was funded by NIH Grant R35 GM 122569.

## REFERENCES

- Joo, C., & Ha, T. (2012). Single-molecule FRET with total internal reflection microscopy. *Cold Spring Harbor Protocols*, 2012(12), 1223–1237. <https://doi.org/10.1101/pdb.top072058>. [pdb.top072058](https://doi.org/10.1101/pdb.top072058).
- Kapanidis, A. N., Laurence, T. A., Nam, K. L., Margeat, E., Kong, X., & Weiss, S. (2005). Alternating-laser excitation of single molecules. *Accounts of Chemical Research*, 38(7), 523–533. <https://doi.org/10.1021/ar0401348>.
- Kozlov, A. G., & Lohman, T. M. (2002). Kinetic mechanism of direct transfer of Escherichia coli SSB tetramers between single-stranded DNA molecules. *Biochemistry*, 41(39), 11611–11627. <https://doi.org/10.1021/BI020361M>.
- Kunzelmann, S., Morris, C., Chavda, A. P., Eccleston, J. F., & Webb, M. R. (2010). Mechanism of interaction between single-stranded DNA binding protein and DNA. *Biochemistry*, 49, 843–852. <https://doi.org/10.1021/bi901743k>.
- Lee, K. S., Marciel, A. B., Kozlov, A. G., Schroeder, C. M., Lohman, T. M., & Ha, T. (2014). Ultrafast redistribution of E. coli SSB along long single-stranded DNA via inter-segment transfer. *Journal of Molecular Biology*, 426(13), 2413–2421. <https://doi.org/10.1016/j.jmb.2014.04.023>.
- Lohman, T. M., Green, J. M., & Beyer, R. S. (1986). Large-scale overproduction and rapid purification of the Escherichia coli ssb gene product. Expression of the ssb gene under lambda PL control. *Biochemistry*, 25(1), 21–25. <https://doi.org/10.1021/bi00349a004>.
- Lohman, T. M., & Overman, L. B. (1985). Two binding modes in Escherichia coli single strand binding protein–single stranded DNA complexes: Modulation by NaCl concentration. *The Journal of Biological Chemistry*, 260(6), 3594–3603. Retrieved from <http://www.jbc.org/content/260/6/3594.full.pdf>.
- Roy, R., Hohng, S., & Ha, T. (2008). A practical guide to single-molecule FRET. *Nature Methods*, 5(6), 507–516. <https://doi.org/10.1038/nmeth.1208>.
- Roy, R., Kozlov, A. G., Lohman, T. M., & Ha, T. (2007). Dynamic structural rearrangements between DNA binding modes of E. coli SSB protein. *Journal of Molecular Biology*, 369(5), 1244–1257. <https://doi.org/10.1016/j.jmb.2007.03.079>.
- Roy, R., Kozlov, A. G., Lohman, T. M., & Ha, T. (2009). SSB protein diffusion on single-stranded DNA stimulates RecA filament formation. *Nature*, 461, 1092–1097. <https://doi.org/10.1038/nature08442>.
- Zhou, R., & Ha, T. (2012). Single-molecule analysis of SSB dynamics on single-stranded DNA. In *Single-stranded DNA binding proteins* (pp. 85–100). Totowa, NJ: Humana Press. [https://doi.org/10.1007/978-1-62703-032-8\\_5](https://doi.org/10.1007/978-1-62703-032-8_5).
- Zhou, R., Kozlov, A. G., Roy, R., Zhang, J., Korolev, S., Lohman, T. M., et al. (2011). SSB functions as a sliding platform that migrates on DNA via reptation. *Cell*, 146(2), 222–232. <https://doi.org/10.1016/j.cell.2011.06.036>.

This page intentionally left blank



# Dissecting the Recombination Mediator Activity of BRCA2 Using Biochemical Methods

Catharina von Nicolai<sup>\*,†</sup>, Åsa Ehlén<sup>\*,†</sup>, Juan S. Martinez<sup>\*,†</sup>,  
Aura Carreira<sup>\*,†,1</sup>

<sup>\*</sup>Institut Curie, PSL Research University, CNRS, UMR3348, Orsay, France

<sup>†</sup>Paris Sud University, Paris-Saclay University, CNRS, UMR3348, Orsay, France

<sup>1</sup>Corresponding author: e-mail address: [aura.carreira@curie.fr](mailto:aura.carreira@curie.fr)

## Contents

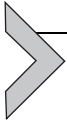
|   |     |
|---|-----|
| 1. Introduction   | 480 |
| 2. Biochemical Assays to Study the Mediator Function of BRCA2 | 481 |
| 2.1 BRCA2 Protein and Fragments Purification                  | 482 |
| 2.2 Pull-Down With Purified Proteins                          | 490 |
| 2.3 ATPase Activity Assay by Thin-Layer Chromatography        | 493 |
| 2.4 DNA Binding Assay   | 497 |
| 2.5 Oligonucleotide-Based EMSA                                | 498 |
| 2.6 Joint Molecule (D-Loop) Assay                             | 501 |
| 2.7 DNA Strand Exchange Assay                                 | 503 |
| 3. Conclusions and Future Directions                          | 509 |
| References  | 510 |

## Abstract

Homologous recombination (HR) is an essential pathway to restart stalled replication forks, repair spontaneous DNA double-strand breaks, and generate genetic diversity. Together with genetic studies in model organisms, the development of purification protocols and biochemical assays has allowed investigators to begin to understand how the complex machinery of HR functions.

At the core of the HR process is the recombination enzyme RecA in bacteria or RAD51 and DMC1 in eukaryotes. The main steps of HR can be reconstituted *in vitro* and involve: (1) The formation of a ssDNA-RAD51 complex into a helical structure termed the nucleoprotein filament after one DNA strand has been resected at the site of the break. (2) The homologous DNA pairing with an intact copy of the damaged chromatid to form a joint molecule also called displacement loop (D-loop). (3) The exchange of DNA strands and *de novo* DNA synthesis to restore the damaged/lost DNA. (4) The resolution of joint molecules by nucleolytic cleavage.

The human tumor suppressor BRCA2 is a mediator of HR as it actively facilitates the DNA transactions of the recombination proteins RAD51 and DMC1 in a variety of ways: It stabilizes ssDNA-RAD51/DMC1 nucleoprotein filaments. It limits the assembly of RAD51 on dsDNA. It facilitates the replacement of replication protein A by RAD51. The result of these activities is a net increase of DNA strand exchange products as observed *in vitro*. Here, we describe some of the biochemical assays used to dissect the mediator activities of BRCA2.

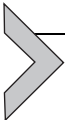


## 1. INTRODUCTION

DNA double-strand breaks (DSBs) arising from exogenous sources such as radiation exposure or endogenous sources such as byproducts of replication represent a major threat to genome integrity. Failure to process these lesions can lead to chromosomal aberrations, cell death, or tumorigenesis. All organisms have evolved pathways to deal with DSBs, and one of the most accurate means to repair them is the homologous recombination (HR) pathway. Several factors are implicated in this pathway, the central player being the bacterial RecA homolog RAD51 in somatic cells or DMC1 and RAD51 in meiotic cells. The mechanism of HR involves several DNA transactions, most of which depend on the energy provided by ATP hydrolysis (Bianco, Tracy, & Kowalczykowski, 1998; Chi, Van Komen, Sehorn, Sigurdsson, & Sung, 2006). These steps include the formation of a helical nucleoprotein filament on ssDNA generated after nucleolytic resection, the search for homology in the sister chromatid (or homologous chromosome in meiosis), the invasion of the latter to form a DNA displacement loop (D-loop), and the strand exchange and DNA synthesis necessary to replace the DNA eliminated during resection of the DSB. The final steps of the HR pathway include the resolution of the recombination intermediates (Kowalczykowski, 2015). Mediator proteins such as BRCA2, RAD54, or the RAD51 paralogs play a very important role in this process by facilitating and regulating the extent of these DNA transactions (Sung & Klein, 2006).

Human BRCA2 contains several functional domains (Martinez, Baldeyron, & Carreira, 2014). The N-terminal region harbors interaction sites for PALB2 and a transactivation domain. Recently, we found that this region contains a DNA binding domain (NTD) that can promote the HR activity of RAD51 (von Nicolai, Ehlen, Martin, Zhang, & Carreira, 2016).

Located in the central portion of the protein are eight BRC repeats, each about 35 amino acids in length. BRCA2 binds RAD51 primarily through these conserved motifs, an interaction required for the formation of RAD51 foci at DNA breaks in vivo (Carreira et al., 2009; Carreira & Kowalczykowski, 2011; Galkin et al., 2005). Recently, we found that the BRC repeats also bind to DMC1, the meiotic counterpart of RAD51 (Martinez et al., 2016). Downstream of the BRC repeats, there is another binding site for DMC1 (Thorslund, Esashi, & West, 2007). In addition to the BRC repeats, there is an unrelated RAD51 binding sequence at the C-terminus of BRCA2 (Davies & Pellegrini, 2007; Esashi, Galkin, Yu, Egelman, & West, 2007) that is not required for DSB repair but is essential for the replication protection function of BRCA2 (Schlachter et al., 2011). The C-terminal region of BRCA2 also contains a conserved DNA binding domain (CTD) (Yang et al., 2002) and a binding site for DSS1 protein, a small acidic protein that cooperates with BRCA2 to displace RPA from ssDNA (Zhao et al., 2015). At the extreme C-terminus, there are two nuclear localization signals (Spain, Larson, Shihabuddin, Gage, & Verma, 1999).



## 2. BIOCHEMICAL ASSAYS TO STUDY THE MEDIATOR FUNCTION OF BRCA2

At 3418 amino acids, BRCA2 is one of the largest proteins in the human proteome. Because of this, most of the biochemical activities we know about BRCA2 come from studies with fragments of the protein (Buisson et al., 2010; Carreira et al., 2009; Galkin et al., 2005; Rajendra & Venkitaraman, 2010; San Filippo et al., 2006; Siaud et al., 2011; von Nicolai et al., 2016) or with smaller homologs of the protein in other organisms such as *Ustilago maydis* Brh2 (Yang, Li, Fan, Holloman, & Pavletich, 2005). The purification of the full-length protein provided the means to validate and extend the physiological relevance of these discoveries (Jensen, Carreira, & Kowalczykowski, 2010; Liu, Doty, Gibson, & Heyer, 2010; Thorslund et al., 2010). Nevertheless, the study of fragments of BRCA2 has provided important clues about the versatility and specificities of BRCA2 that would not have been revealed with the full-length protein mainly because of the presence of interaction sites for DNA and RAD51/DMC1 that appear redundant in the protein.

The mediator activity of BRCA2 essentially entails: (1) Modulating the DNA binding selectivity of RAD51 for ssDNA over dsDNA. (2) Stabilizing

the RAD51-ssDNA nucleoprotein filament by locally inhibiting its ATPase activity. (3) Facilitating the displacement of the ssDNA binding protein RPA. In this chapter, we will describe how these biochemical properties can be studied *in vitro*.

## 2.1 BRCA2 Protein and Fragments Purification

The purification of BRCA2 full-length protein in sufficient quantity and purity to study its biochemical properties was first achieved in 2010 (Jensen et al., 2010). Here, we describe a modified version of the described protocol. It can be used to purify either fragments of the protein or full-length BRCA2 from human cells. We also describe the protocol of purification of the BRC repeats (Carreira & Kowalczykowski, 2011) and the human C-terminal DNA binding domain (CTD) (von Nicolai et al., 2016) from bacteria.

All plasmids for protein or BRCA2 fragment purification mentioned below are available upon request from the corresponding author except for phCMV1 2XMBP-BRCA2 that is available from Prof. Kowalczykowski's lab.

### 2.1.1 Purification of Full-Length BRCA2 From Human Cells

#### 2.1.1.1 Equipment

- Expression vector: EGFP-MBP-BRCA2 in phCMV1 (Genlantis) mammalian expression vector derived by subcloning from phCMV1 2XMBP-BRCA2 (Jensen et al., 2010)
- Cell line: Human HEK293T
- Biosafety level 2 cell culture laboratory
- CO<sub>2</sub> incubator (37°C, 5% CO<sub>2</sub>)
- Sorvall Evolution RC Superspeed Centrifuge, SS-34 fixed angle rotor
- Amylose Resin (NEB)
- Bio-Rex 70 Cation Exchange Resin (Bio-Rad)
- pH-indicator strips pH 0–14 Universal indicator (Merck Millipore)
- Tube rotator for 50- and 15-mL tubes
- Disposable 5 mL polypropylene gravity flow columns (Thermo Scientific)
- Microtubes, MAXYMum Recovery, 1.7 mL (Axygen Scientific)
- 7.5% Stain-free SDS-PAGE gel (Bio-Rad)
- ChemiDoc XRS+ System with Image Lab 5.2.1 Software (Bio-Rad)
- NanoOrange Protein Quantitation Kit (Invitrogen)

#### 2.1.1.2 Buffers and Reagents

- Antibiotics: Kanamycin 50 µg/mL
- Cell culture media: DMEM supplemented with 10% fetal bovine serum and 2 mM L-glutamine

- PBS (140 mM NaCl, 2.7 mM KCl, 10 mM Na<sub>2</sub>HPO<sub>4</sub>, and 1.8 mM KH<sub>2</sub>PO<sub>4</sub>, pH 7.3)
- Trypsin (EuroBio)
- Transfection reagent: TurboFect (Thermo Fisher Scientific)
- Lysis buffer: 50 mM HEPES (pH 7.5), 250 mM NaCl, 1% NP-40, 5 mM EDTA, EDTA-free Protease Inhibitor Cocktail (Roche), 1 mM DTT, 1 mM PMSF freshly prepared
- Maltose elution buffer: Lysis buffer with 10 mM maltose
- No-salt buffer: 50 mM HEPES (pH 7.5), 0.5 mM EDTA, 10% glycerol, 1 mM DTT, 1 mM PMSF freshly prepared
- Bio-Rex equilibration buffer: 50 mM HEPES (pH 7.5), 100 mM NaCl, 0.5 mM EDTA, 10% glycerol, 1 mM DTT, 1 mM PMSF freshly prepared
- Bio-Rex elution buffer: 50 mM HEPES (pH 7.5), 250/450/1000 mM NaCl, 0.5 mM EDTA, 10% glycerol, 1 mM DTT, 1 mM PMSF freshly prepared

### 2.1.1.3 Procedure

#### *Day 1: Seeding of the cells*

1. Seed HEK293T cells in twenty 15-cm plates,  $6 \times 10^6$  cells/plate.

#### *Day 2: Transient transfection*

Transfect the cells at 70% confluence with the phCMV1-GFP-MBP-BRCA2 plasmid:

2. Dilute 400  $\mu$ g DNA in 20 mL serum-free culture media, vortex.
3. Add 800  $\mu$ L TurboFect to the diluted DNA, mix immediately, and incubate 20 min at room temperature.
4. Add 1 mL of the DNA/TurboFect mixture dropwise to each plate.
5. Incubate the cells for 30 h at 37°C, 5% CO<sub>2</sub>.

#### *Day 3: Harvesting of the cells by trypsin treatment*

6. Rinse the cells twice in 1  $\times$  PBS, add 3 mL 1  $\times$  trypsin to each plate, and incubate for 5 min at 37°C.
7. Collect the detached cells with medium, centrifuge at  $300 \times g$  at 4°C for 5 min.
8. Resuspend the cells in cold 1  $\times$  PBS, centrifuge at  $300 \times g$  at 4°C for 5 min.
9. Remove the supernatant and store the cell pellet at  $-80^\circ\text{C}$ .

#### *Day 4: Equilibration of Bio-Rex resin; Lysis and purification (perform preferably steps 10–30 the same day)*

Equilibrate the Bio-Rex 70 cation exchange resin as follows—the equilibration of the resin is critical; if possible, perform the equilibration procedure the day before the purification.

- Place 2g Bio-Rex 70 resin in a beaker with excess volume of the Bio-Rex equilibration buffer.
  - Equilibrate the resin for at least 30 min. Adjust the pH to 7.5 and reequilibrate. Repeat until the pH is stable.
  - Remove the buffer and add fresh Bio-Rex equilibration buffer and repeat step 2.
  - Repeat steps 2–3 until the pH does not change when adding fresh buffer.
  - Store the equilibrated resin in Bio-Rex equilibration buffer at 4°C.
  - Control the pH before use.
10. Resuspend the cell pellet in 80 mL cold lysis buffer and divide in two 50-mL Falcon tubes, rotate the tubes for 30 min at 4°C.
  11. Centrifuge at  $10,000 \times g$  for 15 min at 4°C (Sorvall Evolution RC Superspeed Centrifuge, SS-34 fixed angle rotor).
  12. During centrifugation, wash 8 mL of amylose bead slurry three times with large volumes of cold lysis buffer, centrifuge at  $2000 \times g$  for 2 min at 4°C.
  13. Collect the supernatant and add the washed amylose beads, rotate the tubes for 3 h at 4°C.
  14. Centrifuge at  $2000 \times g$  for 2 min at 4°C.
  15. Wash the beads three times with 20 mL cold lysis buffer, centrifuge at  $2000 \times g$  for 2 min at 4°C.
  16. Resuspend the beads in 4 mL cold maltose elution buffer; rotate the tubes for 1 h at 4°C.
  17. Centrifuge the samples at  $2000 \times g$  for 2 min at 4°C.
  18. Collect the supernatant and dilute to 100 mM NaCl by adding 6 mL of no-salt buffer.
  19. Transfer the equilibrated Bio-Rex resin (see equilibration procedure in Day 4) to a 15-mL tube, let the bead sediment to the bottom before removing the buffer, the bead volume should be 0.6 mL. Add the diluted eluate from step 18 to the beads. Rotate the tubes for 1 h at 4°C.
  20. During incubation: Rinse a disposable 5 mL polypropylene column with one column volume of cold H<sub>2</sub>O followed with one volume of cold Bio-Rex equilibration buffer.

*Note:* Perform steps 21–30 preferably in a cold room. Collect all eluates in MAXYMum Recovery microtubes.
  21. Transfer the sample from step 19 to the column. Let the resin sediment to the bottom of the column before collecting the flow through.

22. Rinse the column with one column volume of cold Bio-Rex equilibration buffer. Discard the flow through.
23. Add 600  $\mu\text{L}$  of cold 250 mM NaCl Bio-Rex elution buffer to the column. Let the resin sediment to the bottom of the column. Collect the eluate.
24. Transfer the eluate from step 23 back into the column and repeat step 23.
25. Add 600  $\mu\text{L}$  of cold 450 mM NaCl Bio-Rex elution buffer to the column. Let the resin sediment and set to the bottom of the gravity flow column. Collect the eluate.
26. Transfer the eluate from step 25 back into the column and repeat step 25.
27. Add 600  $\mu\text{L}$  of cold 1 M NaCl Bio-Rex elution buffer to the column. Let the resin sediment to the bottom of the column. Collect the eluate.
28. Transfer the eluate from step 27 back into the column and repeat step 27.
29. Snap-freeze immediately small aliquots of the eluate in liquid nitrogen. Store at  $-80^{\circ}\text{C}$ .
30. Determine the protein concentration using NanoOrange Protein Quantitation Kit following manufacturer's specifications. Adjust the protein concentration by density determination of the nuclease-free fractions in 7.5% stain-free SDS-PAGE gel, subtracting the contributions from contaminants or truncated BRCA2 polypeptides and using BSA as a standard.

A typical yield of purified BRCA2 protein is 10–20  $\mu\text{g}$  from twenty 15-cm plates of HEK293T.

An example of the purification procedure can be seen in [Fig. 1](#).

## **2.1.2 Purification of the BRC Peptides From Bacteria**

### **2.1.2.1 Equipment**

- Expression vector: BRC motif sequence(s) subcloned in pGEX-6-1 bacterial expression vector (GE Healthcare) ([Carreira & Kowalczykowski, 2011](#))
- Bacterial strain: *E. coli*, BL21 (DE3) pLysS
- 37°C shaking incubator
- UV spectrometer
- Plastic cuvettes
- Quartz cuvette

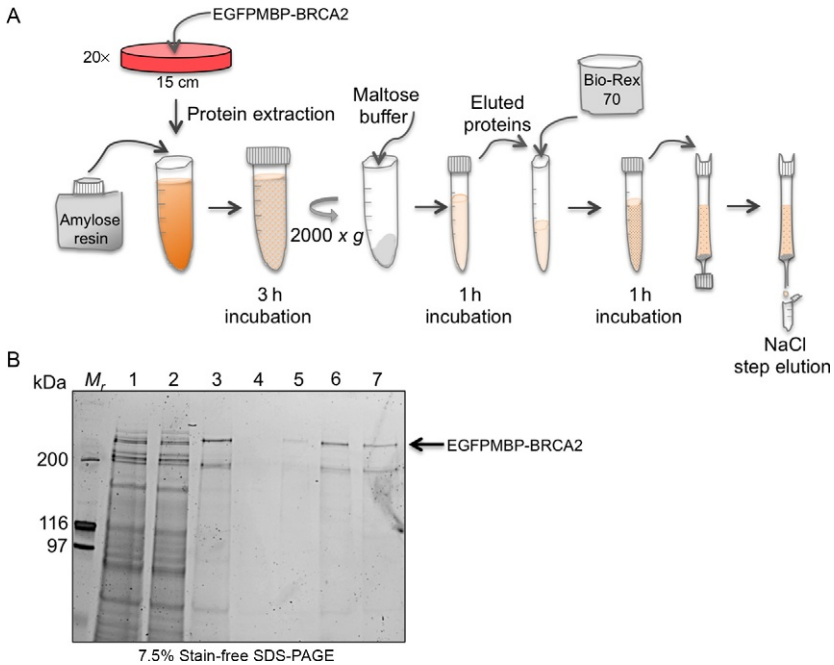


**Fig. 1** Purification of full-length BRCA2 from human cells. (A) Schematic overview of the purification procedure. (B) Stain-free 7.5% SDS-PAGE. Lanes 1: HEK293T cell lysate—input amylose beads, 2: Unbound proteins (amylose beads), 3: Amylose eluate—input Bio-Rex 70, 4: Flow through (Bio-Rex 70), 5: 250 mM NaCl Bio-Rex 70 eluate, 6: 450 mM NaCl Bio-Rex 70 eluate, 7: 1 M NaCl Bio-Rex 70 eluate.  $M_r$ , molecular size markers.

- Ultracentrifuge
- JLA 8.1000 and 45 Ti rotors
- French press
- GST trap column (5 mL) (GE Healthcare)
- Resource Q column (1 mL) (GE Healthcare)
- Spectra/Por dialysis tubing MWCO: 3 kDa (Spectrum Laboratories)
- ÄKTAprius plus chromatography system (GE LifeSciences)
- SDS-PAGE system
- Bio-Rad protein assay

#### 2.1.2.2 Culture Medium, Buffer, and Reagents

- Bacterial culture medium: LB autoclaved
- Antibiotics: Ampicillin 50  $\mu\text{g}/\text{mL}$ , chloramphenicol 34  $\mu\text{g}/\text{mL}$
- IPTG (isopropyl  $\beta$ -D-1-thiogalactopyranoside)

- GST binding buffer:  $1 \times$  PBS (140 mM NaCl, 2.7 mM KCl, 10 mM  $\text{Na}_2\text{HPO}_4$ , 1.8 mM  $\text{KH}_2\text{PO}_4$  pH 7.3), 1 mM PMSF freshly prepared
- GST elution buffer: 50 mM Tris-HCl pH 8.0, 10 mM reduced glutathione
- Resource Q binding buffer: 20 mM Tris-HCl pH 7.5, 10% glycerol, 1 mM EDTA, 1 mM DTT, 1 mM PMSF freshly prepared
- Resource Q elution buffer: 20 mM Tris-HCl pH 7.5, 10% glycerol, 1 M KCl, 1 mM EDTA, 1 mM DTT, 1 mM PMSF freshly prepared
- Storage buffer: 50 mM Tris-HCl, 10% glycerol, 0.2 M KCl, 1 mM EDTA, 1 mM DTT

### 2.1.2.3 Procedure

#### **Expression procedure**

1. Inoculate two flasks of 1.5 L of LB + antibiotics using a 50 mL overnight culture of one clone shaking at 300 rpm at 37°C.
2. Read the  $\text{OD}_{600}$  every hour until it reaches  $\text{OD} = 1$ .
3. At  $\text{OD} = 1$ , induce with 1 mM IPTG and let grow for 3 h.
4. Harvest the cells by centrifugation at  $5000 \times g$  at 4°C for 15 min in JLA rotor.
5. Immediately remove the supernatant and resuspend the cells in 40 mL of binding buffer.
6. Transfer the cells into a 50-mL Falcon tube and centrifuge at  $9000 \times g$  at 4°C for 10 min.
7. Store the pellet at  $-80^\circ\text{C}$  or continue to purification.

#### **Purification procedure (work on ice)**

8. Resuspend the cell pellet in binding buffer (use  $\sim 50$  mL of buffer per 10 g of pellet).
9. Apply the cells to the French Press five times.
10. Centrifuge at  $142,032 \times g$  in a 45 Ti rotor in the ultracentrifuge for 1 h at 4°C.
11. Wash the GST-trap column in an ÄKTAprime chromatography system with water and equilibrate with 5 volumes of GST binding buffer.
12. Load the supernatant from step 10 onto the GST-trap column.
13. Wash the column with 5–10 volumes of GST binding buffer or until the absorbance is at  $\sim 0$ .
14. Elute the GST-tagged protein with GST elution buffer.
15. Analyze the fractions on a 12% SDS-PAGE gel.

16. Pool and dialyze the purest fractions against a large volume of Resource Q binding buffer overnight at 4°C. Change the buffer at least once the next day.
17. Equilibrate Resource Q column with 5 volumes of Resource Q binding buffer.
18. Load the dialyzed fractions onto the Resource Q column.
19. Wash the column with 5–10 volumes Resource Q binding buffer or until the absorbance reaches  $\sim 0$ .
20. Elute the protein using a continuous KCl gradient (0%–40% Resource Q elution buffer).
21. Load the 280 nm absorbance peak fractions on a 12% SDS-PAGE gel. Pool and dialyze the purest fractions against storage buffer overnight at 4°C. Change the buffer once the next day.
22. Snap-freeze in liquid nitrogen and store the protein immediately at  $-80^{\circ}\text{C}$  in small aliquots.
23. Determine the protein concentration using an extinction coefficient at 280 nm of  $40,920 \text{ M}^{-1} \text{ cm}^{-1}$ .

### 2.1.3 Purification of Human BRCA2 CTD

#### 2.1.3.1 Equipment

- Expression vector for BRCA2<sub>CTD</sub>: BRCA2 aa 2474–3190 subcloned into pET28 bacterial expression vector downstream 6 × His-tag and SUMO protease sequence (von Nicolai et al., 2016)
- Expression vector for DSS1: Human DSS1 subcloned by HIFI Gibson Assembly (NEB) in pCDFDuet bacterial expression vector (von Nicolai et al., 2016)
- Bacterial strain: *E. coli*, BL21 DE3 pISO Dscb
- 37°C shaking incubator
- Fermenter
- UV spectrometer and plastic cuvettes for OD measurement
- Ultracentrifuge to  $75,000 \times g$
- JLA 8.1000 rotor
- 45 Ti rotor
- Desintegrator (Constant System (CellD))
- Protino<sup>®</sup> Ni-NTA agarose (Macherey Nagel)
- Spectra/Por dialysis tubing MWCO: 3 kDa (Spectrum Labs)
- 5 mL HiTrap Heparin HP column (GE Healthcare)
- ÄKTAprime plus chromatograph (GE LifeSciences)
- SDS-PAGE apparatus
- Bio-Rad protein assay

### 2.1.3.2 Culture Medium, Buffer, and Reagents

- Bacterial culture medium: Yeast extract 24 g/L, peptone 12 g/L, glycerol 10%,  $K_2HPO_4$  9.4 g/L,  $KH_2PO_4$  2.2 g/L
- Antibiotics: Kanamycin 50  $\mu$ g/mL, chloramphenicol 34  $\mu$ g/mL, spectinomycin 50  $\mu$ g/mL
- L-(+)-Arabinose
- IPTG (isopropyl  $\beta$ -D-1-thiogalactopyranoside)
- Lysis buffer: 300 mM NaCl, 20 mM Tris-HCl pH 8.0, 10% 5 mM  $\beta$ -mercaptoethanol (freshly added), 0.5 mM EDTA. Adjust pH to 8.0, filter. Add fresh: Protease Inhibitor Cocktail 1 $\times$  (Roche), 10 mM  $MgCl_2$ , 1 $\times$  DNase, lysozyme
- Equilibration buffer NiNTA: 300 mM NaCl, 20 mM Tris-HCl pH 8.0, 5 mM  $\beta$ -mercaptoethanol, 0.5 mM EDTA, 10% glycerol, and 10 mM imidazole
- Wash buffer NiNTA: 300 mM NaCl, 20 mM Tris-HCl pH 8.0, 5 mM  $\beta$ -mercaptoethanol, 0.5 mM EDTA, 10% glycerol, and 20 mM imidazole
- Elution buffer NiNTA: 300 mM NaCl, 20 mM Tris-HCl pH 8.0, 5 mM  $\beta$ -mercaptoethanol, 0.5 mM EDTA, 10% glycerol, and 200 mM imidazole
- Dialysis buffer NiNTA: 20 mM Tris-HCl pH 8.0, 100 mM NaCl, 10% glycerol, 0.5 mM EDTA, 5 mM  $\beta$ -mercaptoethanol
- HiTrap column equilibration buffer: 20 mM Tris-HCl pH 8.0, 100 mM NaCl, 5 mM  $\beta$ -mercaptoethanol, 0.5 mM EDTA, 10% glycerol
- HiTrap NaCl gradient elution buffer: 20 mM Tris-HCl pH 8.0, 1 M NaCl, 10% glycerol, 0.5 mM EDTA, 5 mM  $\beta$ -mercaptoethanol
- HiTrap dialysis buffer: 20 mM Tris-HCl pH 8.0, 150 mM NaCl, 10% glycerol, 0.5 mM EDTA, 5 mM  $\beta$ -mercaptoethanol
- 6 $\times$  SDS loading buffer

### 2.1.3.3 Procedure

#### Expression procedure

1. *E. coli* BL21 DE3 pISO Dscb cells are cotransformed with BRCA2<sub>CTD</sub> plasmid and DSS1 plasmid (DSS1 is coexpressed with the CTD to ensure CTD peptide stability).
2. First day: Grow 5 mL of bacterial culture with antibiotics during the day at 37°C, 600 rpm.
3. In the evening, inoculate a second culture of 200 mL with antibiotics and grow overnight at 37°C, 600 rpm.
4. Second day: Dilute overnight culture to  $OD_{600} = 0.1$  and grow 7 L in a fermenter ( $PO_2$ : 20%; pH 6.9).

5. Grow bacteria at 37°C 600 rpm in culture medium until OD=2; reduce the temperature to 20°C.
6. Add 0.5% arabinose 30 min before induction with 1 mM IPTG and grow culture overnight at 700 rpm at 20°C.
7. Collect the cells at  $4000 \times g$  for 10 min at 4°C in JLA rotor.
8. Resuspend half of the cell pellet (ca. 80 g) in lysis buffer by rotation at 4°C and lyse by disintegration at 1.7 kbar.
9. Centrifuge lysate at  $70,000 \times g$  in 45 Ti rotor for 30 min at 4°C, collect supernatant, and discard cell debris.

#### **Purification procedure (work on ice)**

10. Preequilibrate Protino Ni-NTA agarose with equilibration buffer.
11. Incubate lysate with Protino Ni-NTA agarose at 4°C for 1 h in a rotator.
12. Wash the resin extensively (at least three times for 10 min rotating at 4°C) in Ni-NTA wash buffer and centrifuge at  $500 \times g$  for 5 min each time at 4°C.
13. Elute the protein with 150 mL Ni-NTA elution buffer.
14. Dialyze overnight against Ni-NTA dialysis buffer at 4°C using dialysis tubing. Change the buffer at least once the next day.
15. Equilibrate a HiTrap Heparin HP column in an ÄKTAprime chromatography system with HiTrap column equilibration buffer.
16. Load the dialyzed eluate on the column and monitor protein binding.
17. Wash the column extensively with HiTrap column equilibration buffer.
18. Elute the protein using a continuous NaCl gradient (0.1–1 M NaCl) with HiTrap NaCl gradient elution buffer.
19. Load the fractions on a 7.5% SDS gel.
20. Pool the purest fractions against HiTrap dialysis buffer overnight at 4°C. Change the buffer at least once the next day.
21. Load the pooled fractions on a 7.5% SDS gel and determine protein concentration by using Bio-Rad protein assay.
22. Snap-freeze in liquid nitrogen and store the protein immediately at –80°C in small aliquots.

A typical yield for half of a fermenter (~80 g of bacterial cell pellet) is: 8–10 mg of CTD.

## **2.2 Pull-Down With Purified Proteins**

The first evidence for the homologous recombination function of BRCA2 comes from studies that showed the interaction of BRCA2 and RAD51

through the BRC repeats (Wong, Pero, Ormonde, Tavtigian, & Bartel, 1997). By linking RAD51 to a BRC peptide to generate a high-resolution crystal structure, Pellegrini and coworkers revealed that the interaction between the BRC repeats and RAD51 mimic the oligomeric interface of RAD51 (Pellegrini et al., 2002).

Unlike the pull-down assay with cell lysates, the pull-down assay with purified proteins reveals whether a protein–protein interaction is direct; moreover, this assay can be used to determine the affinity and stoichiometry of the interaction. We have used this method to determine the affinity of the individual BRC peptides and RAD51 (Carreira & Kowalczykowski, 2011) and to reveal that the BRC peptides are also the site of interaction for DMC1 (Martinez et al., 2016). We describe here the protocol used for the pull-down assay.

### 2.2.1 Equipment

- Glutathione Sepharose 4B beads (GE)
- Hoefer gel casting system (Dutscher)
- Hoefer Protein vertical electrophoresis system Mighty Small II SE 250 (Dutscher)
- Typhoon PhosphorImager (Amersham Biosciences)
- ImageQuant TL software (GE Healthcare)
- GraphPad Prism software

### 2.2.2 Buffers and Reagents

- GST binding buffer: 20 mM Tris–HCl (pH 7.5), 100 mM NaCl, 1 mM EDTA, 1 mM DTT, 10% glycerol, 0.01% NP-40
- GST wash buffer: 20 mM Tris–HCl (pH 7.5), 100 mM NaCl, 1 mM EDTA, 1 mM DTT, 10% glycerol, 0.1% NP-40
- Purified proteins (GST-tagged BRC peptides and RAD51) in respective storage buffer
- 1 × Protein sample buffer
- 12% SDS-PAGE gels
- SYPRO Orange stain (Invitrogen)

### 2.2.3 Procedure

1. Preequilibrate glutathione beads in GST binding buffer.
2. Mix GST-BRC<sub>x</sub> (0.5 μg) with 0.4–2.4 μg of RAD51 in GST binding buffer and incubate for 15 min at 37°C.

3. Add 30  $\mu\text{L}$  of equilibrated glutathione beads to each reaction and batch bind for 30 min at 37°C rotating.
4. As controls for nonspecific binding to the glutathione beads, incubate the maximum amount of RAD51 used in the reaction (2.4  $\mu\text{g}$ ) with glutathione beads in the absence of GST-BRC peptide (Fig. 2, lane 6). Use also the maximum amount of GST-BRC peptide alone (0.5  $\mu\text{g}$ ) with the beads in the absence of RAD51 (Fig. 2, lane 7).
5. Wash beads extensively with GST wash buffer.
6. For a standard curve, load known concentrations of RAD51 (Fig. 2, lanes 1–4) and GST-BRC<sub>x</sub> (Fig. 2, lanes 12–15) on the same gel.
7. Resuspend the beads in protein sample buffer, heat to 95°C for 4 min, and load the supernatant on a 12% SDS-polyacrylamide gel.
8. Run gel for 1.5 h at 130 V, stain for 30 min in SYPRO Orange protein stain, and rinse briefly with acetic acid (7.5%).
9. Scan the gel with a Typhoon PhosphorImager and quantify the bands corresponding to GST-BRC and DMC1 in all lanes.
10. Determine the amount of pulled-down RAD51/DMC1 by using standard curves generated from known concentrations of RAD51/DMC1 and GST-BRC peptides from lanes 1–4 and 12–15 in the same gel.
11. Subtract RAD51 that binds nonspecifically to the beads (lane 6).

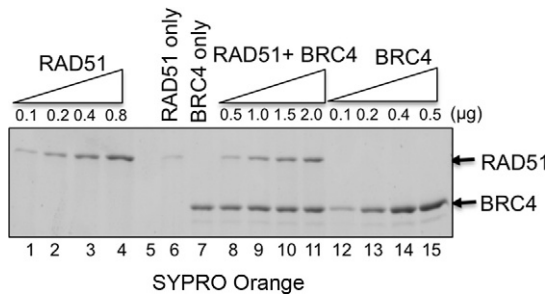


**Fig. 2** Affinity pull-down assay. Example of a pull-down assay with purified RAD51 and GST-tagged BRC4. The GST-tagged BRC peptide is tested for binding to RAD51 in a GST pull-down assay: RAD51 is incubated with GST-BRC4, captured using glutathione beads, washed extensively to remove unbound proteins, analyzed by SDS/PAGE, and stained with SYPRO ORANGE. Lanes 1–4 contain increasing amounts of RAD51 (0.1, 0.2, 0.4, and 0.8  $\mu\text{g}$ ) to generate a standard curve. Lane 6 is a control that contains the highest concentration of RAD51 used in the pull-down (2.4  $\mu\text{g}$ ). Lane 7 is a control showing the BRC4 peptide, “BRC4 only” (0.5  $\mu\text{g}$ ) used in the pull-down experiment in the absence of RAD51. Lanes 8–11 show increasing amounts of RAD51 incubated with each BRC peptide. Lanes 12–15 contain increasing amounts of each BRC peptide (0.1, 0.2, 0.4, and 0.5  $\mu\text{g}$ ) to generate a standard curve for the BRC peptide.

12. The molar input concentration of each GST-BRC peptide in the pull-down reaction is  $2.3\ \mu\text{M}$ . The input concentration of RAD51 is  $1.6\text{--}9.6\ \mu\text{M}$ .
13. To calculate the binding affinity, plot the signal from RAD51 bound per BRC peptide in the  $y$ -axis against the total amount of RAD51/DMC1 in the  $x$ -axis and fit the data to a hyperbola.

## 2.3 ATPase Activity Assay by Thin-Layer Chromatography

### 2.3.1 ATP Hydrolysis Assay

The formation of the nucleoprotein filament by the recombination proteins requires the presence of ATP (Bianco et al., 1998). On the other hand, the ATP hydrolysis activity of RAD51 (DMC1) leads to the disassembly of RAD51 from the DNA; thus, the filament needs to be stabilized to form a continuous filament away from the DSB. BRCA2 and, in particular, BRC repeats 1–4 stabilize the RAD51-ssDNA complex by two reinforcing activities: (1) Reducing the ssDNA-dependent ATPase activity of RAD51. (2) Enhancing the stability of the RAD51-ADP-bound form which allows the ADP to ATP exchange of RAD51 filament, resulting in a net accumulation of the active ATP-bound form of the RAD51-ssDNA complex (Carreira et al., 2009; Carreira & Kowalczykowski, 2011; Jensen et al., 2010). This ATPase inhibition first observed in the *C. elegans* homolog of BRCA2, CeBRC2 (Petalcorin, Galkin, Yu, Egelman, & Boulton, 2007), was further confirmed using the full-length BRCA2 protein (Jensen et al., 2010).

Using the ATP hydrolysis assay, we can determine the ATPase activity of RAD51/DMC1, examine the activation of the rate of hydrolysis by different DNA substrates, and measure the effect of BRCA2 or fragments of BRCA2 (BRC peptides) on this activity. There are several means to measure the ATP hydrolysis rate: A spectrophotometric assay that monitors the coupled oxidation of NADH to the hydrolysis of ATP. This assay is very useful to determine the kinetics of ATP hydrolysis as it has been described (Lindsley, 2001). Another method, on which we will focus here, is the thin-layer chromatography (TLC)-based assay (Rajagopal & Lorsch, 2012) that we have used to study the effect of BRCA2 or the BRC repeats on the ATPase activity of RAD51/DMC1 (Carreira et al., 2009; Carreira & Kowalczykowski, 2011; Jensen et al., 2010; Martinez et al., 2016).

In this assay, BRCA2 or the BRC peptides are preincubated with RAD51/DMC1-purified proteins prior to the addition of ssDNA in a reaction buffer consisting of a mixture of nonradiolabeled ATP and [ $\gamma$ - $^{32}\text{P}$ ] ATP.

The ATP species are separated by TLC whereby the free  $^{32}\text{P}_i$  and  $[\gamma\text{-}^{32}\text{P}]$  ATP can be visualized and quantified by autoradiography. A variation of this protocol can be used to determine the nucleotide composition of the nucleoprotein filament of RAD51 (DMC1) (see Section 2.3.2).

### 2.3.1.1 Equipment

- Polyethyleneimine (PEI) thin-layer chromatography plate (EMD chemicals)
- Storage phosphor screen (GE Healthcare)
- Typhoon PhosphorImager (Amersham Biosciences)
- ImageQuant TL software (GE Healthcare)
- GraphPad Prism software

### 2.3.1.2 Buffers and Reagents

- Reaction buffer: 25 mM Tris–acetate pH 7.5, 0.1 mg/mL BSA, 1 mM  $\text{MgCl}_2$ , 1 mM DTT, 2 mM ATP, 20  $\mu\text{Ci/mL}$   $[\gamma\text{-}^{32}\text{P}]$  ATP
- Developing buffer: 1 M formic acid and 0.5 M LiCl
- Purified proteins in respective storage buffer
- ssDNA (90mer, oAC203) HPLC purified:  
5-CGGGTGTCGGGGCTGGCTTA ACTATGCGGCATCAGA  
GCAGATTGTACTGAGAGTGCACCATATGCGGTGTGAAA  
TACCGCACAGATGCGT-3
- ATP  $[\gamma\text{-}^{32}\text{P}]$ - 3000 Ci/mmol 10 mCi/mL EasyTide (Perkin Elmer)

### 2.3.1.3 Procedure

1. RAD51 (DMC1) (3  $\mu\text{M}$ ) is preincubated with increasing concentrations of BRCA2 or BRC peptides for 15 min at 37°C.  
*Note:* To mimic the conditions in vivo, RPA can be preincubated with the ssDNA prior the addition of RAD51.
2. ssDNA 90mer (oAC203), dT<sub>40</sub>, or other ssDNA substrate (9  $\mu\text{M}$  nucleotides, nt) is added in a total volume of 10  $\mu\text{L}$  and the sample is further incubated for 1 h at 37°C.
3. Cut a PEI thin-layer chromatography sheet in 20 × 6 cm slices. Using a ruler and a pencil, draw a line at ~0.6 cm from the bottom and mark a dot along the line for each sample at ~1-cm intervals to avoid overlapping. Spot 1  $\mu\text{L}$  of each reaction on each dot and air-dry.
4. Dip the TLC plate in a small plastic or glass tank a thin layer of 1 M formic acid and 0.5 M LiCl. Allow the solvent front to reach ~0.5 cm of the top of the sheet.

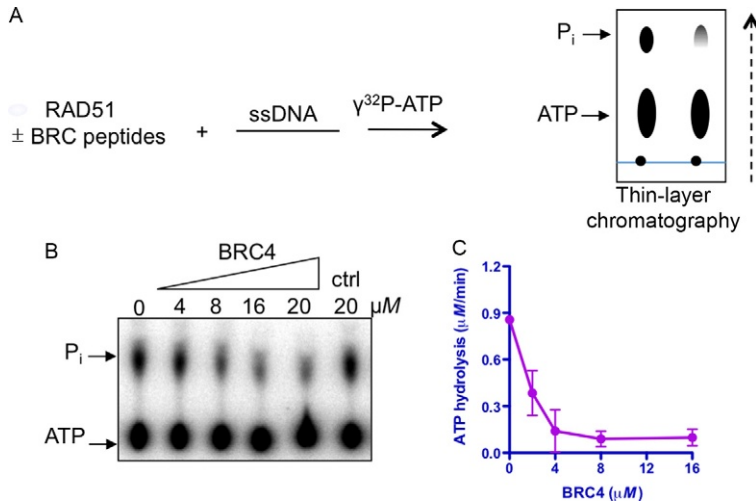


**Fig. 3** ATPase assay. (A) Scheme of the DNA-dependent ATP hydrolysis reaction. (B) Representative example of an ATPase assay using dT<sub>40</sub> homopolymer as DNA substrate, RAD51, and increasing concentrations of BRC4 peptide. Ctrl is the same reaction using a BRC4-mutated peptide that cannot bind RAD51. (C) Quantification of the rate of ATP hydrolysis as a function of BRC4 peptide concentration.

*Note:* It is important to use fresh running solution; an old one may result in smearing.

- Remove the TLC plate from the tank and allow it to air-dry placing it horizontally on the bench. Wrap the plate in plastic foil and expose it on a storage phosphor screen for 1 h or overnight.
- The storage phosphor screen is scanned using a Typhoon PhosphorImager and the amount of free <sup>32</sup>P<sub>i</sub> (farther from the origin of spotting) and of [ $\gamma$ -<sup>32</sup>P] ATP (closer to the spots) (Fig. 3A) is quantified using ImageQuant.
- ATP hydrolysis rate of RAD51 or DMC1 (%) is determined calculating the ratio between ATP [ $\gamma$ -<sup>32</sup>P] and free <sup>32</sup>P<sub>i</sub> as a function of BRCA2 or BRC peptide concentration with respect to the total amount of ATP added to the reaction and plotted using GraphPad Prism (Fig. 3B and C).

### 2.3.2 Nucleotide Composition of the RAD51 Nucleoprotein Filament

We can use a variation of the TLC-based ATP hydrolysis assay to determine the amount of total nucleotide (ATP + ADP) bound to RAD51 (DMC1)-DNA complex as described previously (Bugreev & Mazin, 2004). We have used a modified version of this protocol to measure the nucleotide

composition of RAD51-ssDNA complex as a function of BRCA2 (BRC peptide) concentration. In this assay, [ $\alpha^{32}\text{P}$ ] ATP is used instead of [ $\gamma^{32}\text{P}$ ] ATP. The ADP will migrate farther from the origin of spotting of the samples compared to the ATP.

### 2.3.2.1 Equipment

- Polyethyleneimine (PEI) thin-layer chromatography plate (EMD chemicals)
- P30 column (Bio-Rad)
- Storage phosphor screen (GE Healthcare)
- Typhoon PhosphorImager (Amersham Biosciences)
- ImageQuant TL software (GE Healthcare)
- GraphPad Prism software

### 2.3.2.2 Buffers and Reagents

- Reaction buffer: 20 mM Tris-HCl (pH 7.5), 4 mM  $\text{MgCl}_2$ , 1 mM DTT, 0.5 mM ATP, and 6  $\mu\text{Ci}$  [ $\alpha^{32}\text{P}$ ] ATP
- Developing buffer: 1 M formic acid and 0.5 M LiCl
- Purified proteins in respective storage buffer
- ssDNA: dT<sub>40</sub> homopolymer HPLC purified or linear  $\phi\text{X174}$  ssDNA (viral (+) strand) (NEB).
- ATP [ $\alpha^{32}\text{P}$ ]- 3000 Ci/mmol 10 mCi/mL EasyTide (Perkin Elmer)

### Preparation of linear $\phi\text{X174}$ ssDNA

- Anneal an oligonucleotide (80mer) complementary to the *AluI* restriction site contained within the sequence (5207–5286) of  $\phi\text{X174}$  ssDNA.
- Digest with *AluI* restriction enzyme
- Purify the DNA using a MicroSpin S-400 HR column (Amersham)

### 2.3.2.3 Procedure

1. RAD51 (3  $\mu\text{M}$ ) is preincubated with increasing concentrations of BRC4 peptide for 15 min at 37°C.
2. ssDNA: dT<sub>40</sub> or linear  $\phi\text{X174}$  ssDNA (9  $\mu\text{M}$  nucleotides, nt) is added to the reaction in 20  $\mu\text{L}$  total volume and is further incubated for 1 h at 37°C.
3. Spot 1  $\mu\text{L}$  onto a TLC plate to determine the rate of hydrolysis as control. Immediately load 19  $\mu\text{L}$  into a TE (10 mM Tris-HCl, pH 7.5, 1 mM EDTA) preequilibrated P30 column.
4. Spot 10  $\mu\text{L}$  of the eluate onto a different TLC plate (this plate will need more exposure than the previous one) and air-dry.

5. Develop the TLC plates, air-dry, and expose on a storage phosphor screen as explained above.
6. Scan the phosphor screen using a Typhoon PhosphorImager and calculate the amount of [ $\alpha$ - $^{32}$ P] ADP and of [ $\alpha$ - $^{32}$ P] ATP using ImageQuant.
7. The amount of nucleotide bound to the isolated protein–DNA complexes is calculated from the [ $\alpha$ - $^{32}$ P] ATP + [ $\alpha$ - $^{32}$ P] ADP content of each lane and expressed relative to the amount of [ $\alpha$ - $^{32}$ P] ATP + [ $\alpha$ - $^{32}$ P] ADP bound when the BRC peptide is absent. The ATP and ADP bound to DNA-free RAD51 is determined in parallel by doing the same experiment in the absence of DNA and is subtracted from each lane of the experiment done in the presence of DNA.

## 2.4 DNA Binding Assay

The electrophoretic mobility shift assay (EMSA) is a common technique to study protein–DNA interactions (Fried & Crothers, 1981). The principle being that a nucleic acid with protein bound has less mobility through a native gel matrix than a free nucleic acid. Generally, either a radio- or fluorescent-labeled DNA is used for this type of assays.

BRCA2 has been shown to bind various DNA substrates via two distinct DNA binding sites located at the N-terminus and the C-terminus. In addition, BRCA2 through the BRC repeats also stimulates the formation of DMC1- and RAD51–ssDNA nucleoprotein filaments. All of these findings were made using EMSA reactions with recombinant wild-type protein or fragments of BRCA2 and various radiolabeled DNA substrates (Carreira et al., 2009; Carreira & Kowalczykowski, 2011; Jensen et al., 2010; Martinez et al., 2016; von Nicolai et al., 2016; Yang et al., 2002). EMSA experiments can be complemented with single-molecule studies where we can follow the nucleation and growth of recombination proteins in real time, and the effect of proteins or fragments on these activities. We have used such an approach to reveal the inhibitory effect of RAD51 nucleation on dsDNA. This technique has been described in detail before (Amitani, Liu, Dombrowski, Baskin, & Kowalczykowski, 2010; Hilario & Kowalczykowski, 2010).

Here, we describe the assays used to determine the DNA substrate specificity of BRCA2 (or its DNA binding domains) as well as the protocol to determine the effect of the BRC peptides on RAD51/DMC1 DNA binding selectivity.

## 2.5 Oligonucleotide-Based EMSA

### 2.5.1 Equipment

- NanoDrop 2000 (Thermo Scientific)
- Illustra MicroSpin G-25 columns (GE Healthcare)
- Hoefer gel casting system (Dutscher)
- Hoefer Protein vertical electrophoresis system Mighty Small II SE 250 (Dutscher)
- Whatman paper 3MM
- Whatman DE81 grade paper (GE Healthcare)
- Gel dryer
- Storage phosphor screen (GE Healthcare)
- Typhoon PhosphorImager FLA7000 (Amersham Biosciences)
- ImageQuant TL software (GE Healthcare)
- GraphPad Prism

### 2.5.2 Buffers and Reagents

- T4 Polynucleotide Kinase (NEB) kit
- ATP [ $\gamma$ - $^{32}\text{P}$ ]- 3000 Ci/mmol 10 mCi/mL EasyTide (Perkin Elmer)
- 1  $\times$  STE buffer: 100 mM NaCl, 10 mM Tris-Cl, pH 8.0, 1 mM EDTA
- Purified proteins in storage buffer
- 6  $\times$  DNA loading buffer: 0.25% xylene cyanol solution (1%), 0.25% bromophenol blue 1% solution (0.25%), 30% glycerol
- 1  $\times$  TAE buffer: 40 mM Tris-acetate, 0.5 mM EDTA
- 6% PAGE gel (native)
- EMSA reaction buffer A: 25 mM Tris-acetate pH 7.5, 1 mM DTT, 1 mM MgCl<sub>2</sub>, 2 mM CaCl<sub>2</sub>

#### *DNA labeling*

- All DNA substrates are labeled at the 5'-end using T4 Polynucleotide Kinase according to the manufacturer's instructions. Before labeling, measure the exact DNA concentration using a NanoDrop 2000
- DNA substrates are purified using Illustra MicroSpin columns following manufacturer's specifications
- ssDNA substrates are purchased PAGE-purified:
  - oAC423 (167mer): 5'-CTGCTTTATCAAGATAATTTTTTCGA CTCATCAGAAATATCCGTTTCCTATA TTTATTCCTAT TATGTTTTATTTCATTTACTTATTCTTTATGTTTCATTT-TTTATAT CCTTTACTTTATTTTCTCTGTTTATTCATTT ACTTATTTTGTATTATCCTTATC TTATTTA-3'

- oAC403 (42mer): 5'-CGGATATTTCTGATGAGTCGAAAA TTATCTTGATAAAGCAG-3'
- oAC490 (42mer): 5'-TAAATAAGATAAGGATAATACAAAAT AAGTAAATGAATAAAC-3'
- oAC405 (40mer): 5'-TAA TAC AAA ATA AGT AAA TGA ATA AAC AGA GAA AAT AAA G-3'
- oAC406 (40mer): 5'-CTTTATTTTCTCTGTTTATTCATTT ACTTATTTTGTATTA-3'
- oAC203 (90mer): 5'-CGGGTGTCTGGGGCTGGCTTAACTAT GCGGCATCAGAGCAGATTGTACTGAGAGTGCACCAT ATGCGGTGTGAAATACCGCACAGATGCGT-3'
- dT<sub>40</sub> homopolymer
- dA<sub>40</sub> homopolymer

*Generation of duplex DNA-containing substrates by annealing reaction*

- dsDNA 40mer and dA<sub>40</sub>·dT<sub>40</sub>: 5'-end <sup>32</sup>P-labeled oAC405 and oAC406 or the dT<sub>40</sub> and dA<sub>40</sub> homopolymers are mixed in a 1:1 ratio in 1 × STE buffer and heated to 95°C, then slowly cooled down placing the samples at room temperature overnight
- 3' and 5' overhang substrates are produced by annealing 5'-end <sup>32</sup>P-labeled oAC490 (42mer -3') to oAC423 (167mer) or oAC403 (42mer -5') to oAC423 in a 1:1 *M* ratio, respectively, as described above
- 5'-end <sup>32</sup>P-labeled oAC423, oAC403, and oAC490 are annealed in a 1:1:1 ratio to produce the gapped DNA substrate

### 2.5.3 Procedure

#### A. DNA binding specificity of BRCA2 or BRCA2 NTD

1. BRCA2 or BRCA2 NTD is mixed in the desired concentration in a 10 μL reaction in EMSA reaction buffer A.
2. 0.2 μM nucleotides 5'-end <sup>32</sup>P-labeled DNA substrates are added and the reaction is incubated for 1 h at 37°C.
3. The protein–DNA complexes are mixed with 6 × DNA loading buffer and resolved on a 6% PAGE gel in 1 × TAE buffer for 75 min at 70 V.
4. The gel is dried onto DE81 paper in a gel dryer and exposed on a phosphor screen overnight.
5. The next day, gels are scanned using a Typhoon PhosphorImager and quantified with ImageQuant software. The ratio of DNA–protein complexes formed is calculated as the percentage of bound DNA relative to free DNA.

An example of an EMSA experiment can be seen in Fig. 4.

**B.** Effect of the BRC peptides on the DNA binding specificity of RAD51/DMC1

1. RAD51 (3  $\mu\text{M}$ ) is preincubated with the BRC peptide for 15 min at 37°C in 10  $\mu\text{L}$  EMSA reaction buffer B (20 mM Tris-HCl (pH 7.5), 10 mM Mg(OAc)<sub>2</sub>, 2 mM CaCl<sub>2</sub>, 2 mM ATP).

*Note:* The concentration of DMC1 used to determine the effect of the BRC peptides on DMC1-DNA complex formation is: 25 nM for ssDNA, 0.3 or 0.6  $\mu\text{M}$  for dsDNA.

2. 0.3  $\mu\text{M}$  nt 5'-end 32P-labeled ssDNA (oAC203 90mer or dT40) or 0.3  $\mu\text{M}$  base pairs 5'-end 32P-labeled dsDNA (dA40·dT40) are added and the reaction is incubated for 1 h at 37°C.

*Note:* The concentration of DNA used to determine the effect of the BRC peptides on DMC1-DNA complex formation is: 0.2  $\mu\text{M}$  nt ssDNA 90mer, 3  $\mu\text{M}$  bp <sup>32</sup>P-labeled dsDNA (dA<sub>40</sub>·dT<sub>40</sub>).

3. The protein-DNA complexes are mixed with 6  $\times$  DNA loading buffer and resolved on a 6% PAGE gel in 1  $\times$  TAE buffer for 75 min at 70 V.
4. The gel is dried onto DE81 paper in a gel dryer and exposed on a phosphor screen overnight.
5. Gels are scanned with a Typhoon PhosphorImager and quantified with ImageQuant. The ratio of DNA-protein complexes formed is calculated as the free radiolabeled DNA relative to the protein-free lane which defines the value of 0% complex formation.

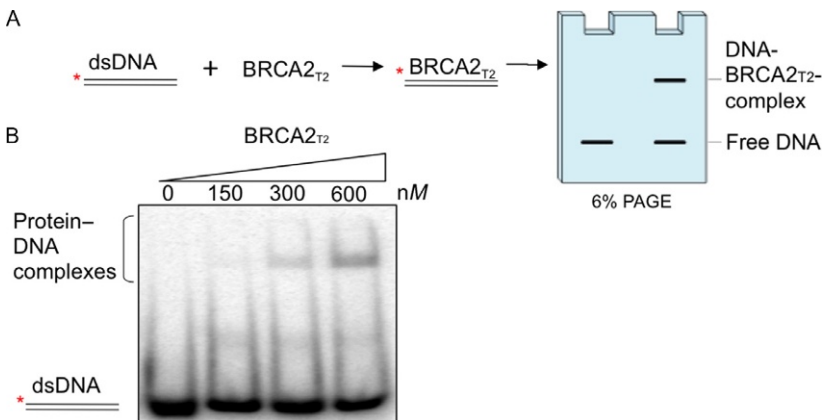


**Fig. 4** DNA binding (EMSA) experiment: (A) Reaction scheme: Radiolabeled dsDNA is incubated with BRCA2<sub>T2</sub> for 1 h at 37°C and loaded on a 6% PAGE gel to separate the DNA-protein products from free dsDNA. (B) EMSA with BRCA2<sub>T2</sub> and dsDNA using the indicated concentrations of protein.

*Note:* We have used a variation of this assay to study the effect of the BRC peptides on the stability of the RAD51-ssDNA complex in the presence of ADP. The DNA-RAD51 complex is formed using the same procedure only adding up to 1 M NaCl concentration in the presence of a fix amount of BRC4. By examining the amount of free DNA under both conditions we could show that BRC4 enhances the stability of the ADP-bound RAD51-ssDNA complex (Carreira et al., 2009). The same reaction can be performed with larger DNA substrates in which case the samples are run on an agarose gel.

## 2.6 Joint Molecule (D-Loop) Assay

After the RAD51/DMC1 nucleoprotein filament is assembled (as detected by EMSA in Section 2.4), it conducts the search for a homologous sequence in the sister chromatid/homologous chromosome. At this point, the recombination protein invades the latter to form a DNA displacement loop (D-loop). Then the D-loop would be extended by strand exchange (Section 2.7) and by de novo DNA synthesis. We describe here the biochemical reaction that recapitulates the D-loop formation step in vitro and the effect of BRCA2/BRC peptides in the D-loop formed by a DMC1 nucleoprotein filament (Martinez et al., 2016). In the D-loop formation assay, supercoiled dsDNA serves as the homologous template. The use of detergent lysis preparation of the supercoiled DNA is critical to minimize experimental artifacts coming from nicks in the DNA.

### 2.6.1 Equipment

- NanoDrop 2000 (Thermo Scientific)
- Illustra MicroSpin G-25 columns (GE Healthcare)
- Agarose gel electrophoresis Sub-Cell GT system with 15 × 25 cm tray (Bio-Rad)
- PowerPac HC Power Supply (Bio-Rad)
- Whatman paper 3MM
- Whatman DE81 grade paper (GE Healthcare)
- Gel dryer
- Storage phosphor screen (GE Healthcare)
- Typhoon PhosphorImager FLA7000 (Amersham Biosciences)
- ImageQuant software (GE Healthcare)

### 2.6.2 Buffers and Reagents

- DNA substrate (PAGE-purified) oAC203 (90mer):  
5'-CGGGTGTCTGGGGCTGGCTTAACTATGCGGCATCAG  
AGCAGATTGTACTGAG AGTGCACCATATGCGGTGTGAAA  
TACCGCACAGATGCGT-3'
- [ $\gamma$ - $^{32}\text{P}$ ] ATP- 3000 Ci/mmol 10 mCi/mL EasyTide (Perkin Elmer)
- T4 Polynucleotide Kinase (NEB) kit
- Purified proteins in respective storage buffer
- $^{32}\text{P}$ -radiolabeled ssDNA (oAC203, see below)
- Covalently closed supercoiled plasmid DNA (pUC19) purified from *E. coli* DH5 $\alpha$  cells by detergent lysis followed by equilibrium centrifugation in a CsCl–ethidium bromide gradient (Liu, Sneed, & Heyer, 2010)
- 1% Agarose gel
- Reaction buffer: 25 mM Tris–acetate pH 7.5, 1 mM DTT, 2 mM ATP, 1 mM MgCl<sub>2</sub>, 2 mM CaCl<sub>2</sub>, 0.1 mg/mL BSA
- Stop solution: 0.25% SDS and 0.5 mg/mL proteinase K
- 6 × DNA loading buffer: 0.25% xylene cyanol solution (1%), 0.25% bromophenol blue 1% solution (0.25%), 30% glycerol
- 1 × TAE buffer: 40 mM Tris–acetate, 0.5 mM EDTA

### 2.6.3 Procedure

#### *DNA substrate preparation*

1. Prior to labeling, the exact DNA concentration is measured using a NanoDrop 2000.
2. The DNA substrate (oAC203) is labeled with [ $\gamma$ - $^{32}\text{P}$ ] ATP at the 5'-end using T4 Polynucleotide Kinase (NEB) according to the manufacturer's instructions for 30 min at 37°C and subsequently purified using Illustra MicroSpin columns.

#### *D-loop reaction*

3. DMC1 protein (75 nM) is mixed with the labeled oAC203 at a saturating concentration of 2.5 nM molecules (225 nM nt) (3:1 ssDNA:DMC1 ratio) in reaction buffer.
4. BRC peptide (0.25–2.5  $\mu\text{M}$ ) or BRCA2 (0.8–10 nM) is added to the reaction and the mixture is incubated for 10 min at 37°C.
5. Joint molecule (D-loop) formation is initiated by addition of supercoiled pUC19 dsDNA (scDNA) at 0.8 nM molecules and further incubated for 30 min at 37°C.

6. The reactions are terminated by adding the stop solution and incubating for 10 min at 37°C.
7. After adding 6 × loading buffer, the samples are run by electrophoresis on a 1% agarose gel in 1 × TAE buffer run at 120 V for 1.5 h.
8. The gel is then dried onto DE81 paper with a backing of several sheets of Whatman paper in a gel dryer and exposed overnight on a storage phosphor screen.
9. The extent of joint molecule formation is determined by scanning the screen in a Typhoon PhosphorImager and quantification is done using ImageQuant.
10. Joint molecule yield is expressed as a percentage of the total label concentration and multiplied by 3 to get the yield with respect to the limiting ssDNA.

An example of a D-loop reaction can be seen in [Fig. 5](#).

## 2.7 DNA Strand Exchange Assay

Upon a DSB, the ssDNA binding protein replication protein A (RPA) coats the ssDNA generated upon nucleolytic resection, which is required to

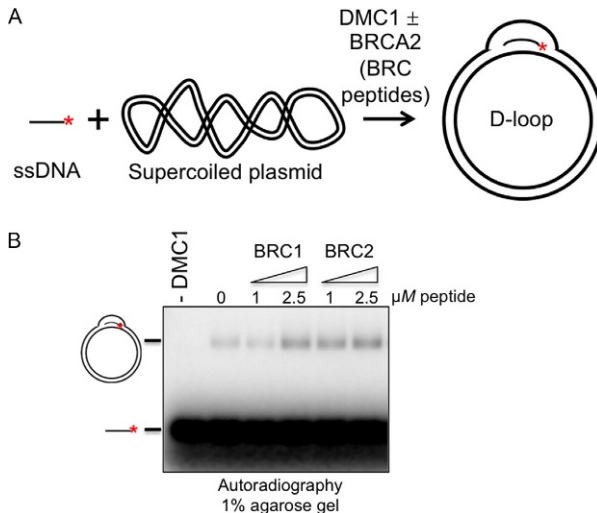


**Fig. 5** Joint molecule (D-loop) reaction. (A) Diagram of the D-loop assay. Radiolabeled ssDNA is incubated with supercoiled plasmid (pUC19), DMC1, and the protein (or peptide) of interest (e.g., BRCA2 or BRC peptide). The reaction is deproteinized and loaded on a 1% agarose gel. The joint molecules (D-loops) migrate slower than the free ssDNA. (B) Representative example of a D-loop assay testing the effect exerted by different BRC peptides (as marked) on the DMC1-dependent D-loop formation activity.

remove the secondary structure that would preclude strand exchange. However, because RPA is tightly bound to the ssDNA, it also inhibits RAD51 binding. Mediator proteins such as BRCA2 facilitate the displacement of RPA by RAD51 that result in a nucleoprotein filament, the active species for homology pairing and strand exchange.

The mediator activity of BRCA2 in homologous recombination has been demonstrated in several studies by recapitulating the DNA strand exchange reaction *in vitro* using recombinant purified BRCA2 or BRCA2 peptides, RAD51 (DMC1) and RPA, and different DNA substrates that mimic the *in vivo* DNA context (Carreira et al., 2009; Carreira & Kowalczykowski, 2011; Chatterjee, Jimenez-Sainz, Presti, Nguyen, & Jensen, 2016; Jensen et al., 2010; Liu, Doty, et al., 2010; Martinez et al., 2016; San Filippo et al., 2006; Thorslund et al., 2010; von Nicolai et al., 2016; Zhao et al., 2015).

### **2.7.1 Plasmid-Based DNA Strand Exchange Assay**

The *in vitro* plasmid-based DNA strand exchange assay has been used extensively to characterize the recombination activity of RAD51, RecA, and define the function of mediator or accessory factors such as RPA, BRCA2, and RAD54. In this reaction, the DNA substrates typically used are the  $\phi$ X174 circular ssDNA [viral (+) strand] and a linear duplex template with 3–4 bases overhang containing a homologous strand ( $\phi$ X174 dsDNA linearized by restriction enzyme digestion). The DNA strand exchange products consist of plectonemic joint molecules (stable after protease treatment) and nicked circular DNA. The following protocol is a modified version of the one described in Bugreev and Mazin (2004) that has been used to study the effect of the BRC peptides of BRCA2 on the recombination activity of RAD51 (Carreira et al., 2009; Carreira & Kowalczykowski, 2011).

#### **2.7.1.1 Equipment**

- NanoDrop 2000 (Thermo Scientific)
- Illustra MicroSpin G-25 columns (GE Healthcare)
- Agarose gel electrophoresis Sub-Cell GT system with 15 × 25 cm tray (Bio-Rad)
- PowerPac HC Power Supply (Bio-Rad)
- Whatman paper 3MM
- Whatman DE81 grade paper (GE Healthcare)
- Gel dryer
- Storage phosphor screen (GE Healthcare)

- Typhoon PhosphorImager FLA7000 (Amersham Biosciences)
- ImageQuant software (GE Healthcare)
- GraphPad Prism

### 2.7.1.2 Buffers and Reagents

- [ $\gamma$ - $^{32}\text{P}$ ] ATP- 3000 Ci/mmol 10 mCi/mL EasyTide (Perkin Elmer)
- T4 Polynucleotide Kinase (NEB)
- Antarctic Phosphatase (NEB)
- *Xho*I restriction enzyme (NEB)
- Purified proteins in respective storage buffer
- 5'-labeled  $^{32}\text{P}$  linear dsDNA  $\phi$ X174 RFI (see below)
- $\phi$ X174 circular ssDNA [viral (+) strand]
- 1% Agarose gel
- Reaction buffer: 25 mM Tris-acetate pH 7.5, 250 mM NaCl, 1 mM DTT, 2 mM ATP, 1 mM  $\text{MgCl}_2$ , 2 mM  $\text{CaCl}_2$
- Stop solution: 4.8% SDS, 7 mg/mL proteinase K (Roche)
- 6 $\times$  DNA loading buffer: 0.25% xylene cyanol solution (1%), 0.25% bromophenol blue 1% solution (0.25%), 30% glycerol
- 1 $\times$  TAE buffer: 40 mM Tris-acetate, 0.5 mM EDTA

#### *Linear dsDNA preparation and labeling*

- Digest 20  $\mu\text{g}$  of  $\phi$ X174 (1 mg/mL) NEB with *Xho*I restriction enzyme in 30  $\mu\text{L}$
- Take 2/3 (20  $\mu\text{L}$ ) and precipitate it using a standard ethanol precipitation protocol and resuspend it in 10  $\mu\text{L}$  of TE
- Dephosphorylate the rest of the sample (10  $\mu\text{L}$ , 6.6  $\mu\text{g}$ ) with Antarctic Phosphatase following manufacturer's specifications
- Label the dephosphorylated DNA in a 30  $\mu\text{L}$  reaction using 5  $\mu\text{L}$  of  $^{32}\text{P}$ - $\gamma$  ATP and 2  $\mu\text{L}$  of T4 PNK for 30 min and remove the unincorporated label applying the sample to a G25 column

Either labeled-only or a mixture of labeled and nonlabeled duplex DNA is used in the reaction; this needs to be tested for each experimental condition.

### 2.7.1.3 Procedure

To determine the optimal amounts of RAD51 and RPA, it is recommended to titrate the proteins and DNA taking into account that one molecule of RAD51 binds  $\sim$ 3–4 nt or base pairs (bp) of DNA (Bianco et al., 1998) and one molecule of RPA coats  $\sim$ 30 nt (Henricksen, Umbrecht, & Wold, 1994). Although the standard reaction involves saturating concentrations of RAD51, the stimulatory effect of the BRC peptides is only observed

under conditions of excess RAD51 in which the self-inhibitory action of RAD51 binding to the nonproductive substrate dsDNA is at play.

#### *Reaction*

1. RAD51 (3.75  $\mu\text{M}$  or excess [7.5  $\mu\text{M}$ ])  $\pm$  BRC peptide (0–24  $\mu\text{M}$ ) are preincubated with the ssDNA (15  $\mu\text{M}$  nt) for 5 min at 37°C.
2. RPA (1  $\mu\text{M}$ ) is added to the reaction and further incubated for 5 min at 37°C.
3. To start the reaction, the linear dsDNA (15  $\mu\text{M}$  nt) is added in a total volume of 20  $\mu\text{L}$  and the samples are further incubated for 2 h at 37°C.
4. The reaction is stopped by adding 6  $\mu\text{L}$  of stop solution for 15 min at 37°C.
5. Samples are mixed with 6  $\times$  DNA loading buffer and loaded on a 1% agarose gel and the products are resolved by electrophoresis on a 1% agarose gel (1  $\times$  TAE) at 40 V overnight ( $\sim$ 13 h).
6. The gel is then dried onto DE81 paper in a gel dryer and exposed overnight on a storage phosphor screen.
7. The screen is scanned using a Typhoon PhosphorImager and quantified using ImageQuant.
8. The amount of DNA strand exchange product at each BRC peptide concentration is calculated as a percentage of the joint molecules (JM) or nicked circular DNA (NC) products relative to the total amount of DNA in the same lane.

An example of the DNA strand exchange assay can be seen in [Fig. 6A](#).

### **2.7.2 Oligonucleotide-Based DNA Strand Exchange Assay**

The oligonucleotide-based DNA strand exchange assay is convenient when using the full-length BRCA2 protein or fragments that are obtained at limited concentrations (nanomolar range). In addition, this assay requires less time than the plasmid-based assay. In this reaction, a 3' overhang ssDNA substrate that mimics the 3' DNA tail generated upon resection is incubated with RAD51 in the presence or absence of RPA and increasing amounts of BRCA2. After incubation, a radiolabeled dsDNA substrate, complementary to the ssDNA portion of the tailed DNA, is added and RAD51 will exchange the homologous strands between the two substrates. The product of this reaction is a displaced ssDNA and a radiolabeled dsDNA composed of one strand from the template and one strand from the 3'-tailed substrate and can be distinguished from the free-labeled dsDNA as it migrates slower during gel electrophoresis. In the absence of BRCA2, the ability to displace RPA is reduced and little product is formed. When BRCA2 is added to

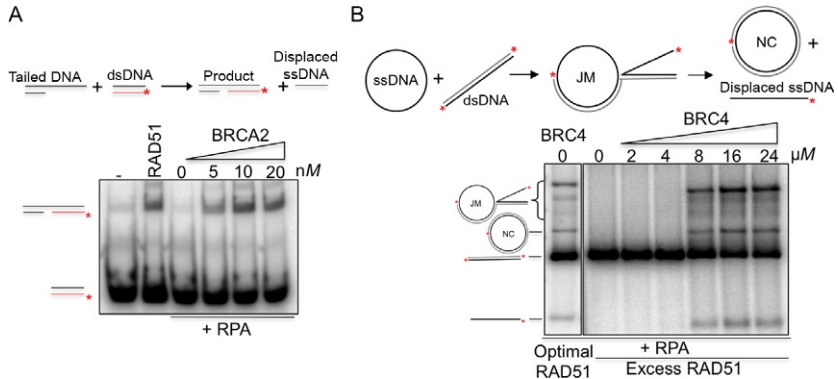


**Fig. 6** DNA strand exchange assay. (A). Example of oligonucleotide-based DNA strand exchange. *Top*: Reaction scheme. *Bottom*: DNA strand exchange assay using RAD51, RPA, and BRCA2 at the indicated concentrations and tailed DNA and short duplex DNA as substrates. (B) Plasmid-based DNA strand exchange assay. *Top*: Reaction scheme. *Bottom*: DNA strand exchange assay using RAD51, RPA, and BRC4 at the indicated concentrations and  $\phi$ x174-based linear duplex DNA and circular ssDNA as substrates. *JM*, joint molecules; *NC*, nicked circular DNA.

the reaction, it limits RAD51 assembly on dsDNA and alleviates the suppressive effect of RPA resulting in a net increased amount of DNA strand exchange product.

### 2.7.2.1 Equipment

- NanoDrop 2000 (Thermo Scientific)
- Illustra MicroSpin G-25 columns (GE Healthcare)
- Hoefer gel casting system (Dutscher)
- Hoefer Protein vertical electrophoresis system Mighty Small II SE 250 (Dutscher)
- Whatman paper 3MM
- Whatman DE81 grade paper (GE Healthcare)
- Gel dryer
- Storage phosphor screen (GE Healthcare)
- Typhoon PhosphorImager FLA7000 (Amersham Biosciences)
- ImageQuant software (GE Healthcare)
- GraphPad Prism

### 2.7.2.2 Buffers and Reagents

- [ $\gamma$ - $^{32}$ P] ATP- 3000 Ci/mmol 10 mCi/mL EasyTide (Perkin Elmer)
- T4 Polynucleotide Kinase (NEB) kit

- 1 × STE buffer: 100 mM NaCl, 10 mM Tris–Cl, pH 8.0, 1 mM EDTA
- Purified proteins in respective storage buffer
- <sup>32</sup>P-radiolabeled dsDNA 3' overhang substrate oAC423 and oAC490 (see below)
- <sup>32</sup>P-radiolabeled dsDNA (oAC405 and oAC406, see below)
- 6% PAGE gel
- Reaction buffer: 25 mM Tris–acetate pH 8.0, 1 mM DTT, 2 mM ATP, 1 mM MgCl<sub>2</sub>, 2 mM CaCl<sub>2</sub>, 0.1 mg/mL BSA
- Stop solution: 0.25% SDS and 0.5 mg/mL proteinase K
- 6 × DNA loading buffer: 0.25% xylene cyanol solution (1%), 0.25% bromophenol blue 1% solution (0.25%), 30% glycerol
- 1 × TAE buffer: 40 mM Tris–acetate, 0.5 mM EDTA

#### *DNA substrates PAGE-purified*

oAC423(167mer): 5'-CTGCTTTATCAAGATAATTTTTTCGACTC  
ATCAGAAATATCCGTTTCTATA TTTATTCCTATTATGTT  
TTATTCATTTACTTATTCTTTATGTTTATTTTTTATAT  
CCTTTACTTTATTTTTCTCTGTTTATTCATTTACTTATTTT  
GTATTATCCTTATCTTATTTA-3'

oAC405 (40mer): 5'-TAATAC AAA ATA AGT AAA TGA ATA AAC  
AGA GAA AATAAA G-3'

oAC406 (40mer): 5'-CTTTATTTTCTCTGTTTATTCATTTACT  
TATTTTGTATTA-3'

oAC490 (42mer): 5'-TAAATAAGATAAGGATAATACAAAATAA  
GTAAATGAATAAAC-3'

#### *DNA labeling*

- Prior to labeling, the exact DNA concentration is measured using a NanoDrop 2000.
- All DNA substrates are labeled at the 5'-end using T4 Polynucleotide Kinase according to the manufacturer's manual for 30 min at 37°C and purified using Illustra MicroSpin columns.

#### *DNA substrate preparation*

- DsDNA: <sup>32</sup>P-labeled oAC405 and oAC406 are mixed in a 1:1 ratio in 10 μL 1 × STE buffer and heated at 95°C for 5 min, then slowly cooled down by placing the samples at room temperature overnight.
- 3' ssDNA is produced by annealing <sup>32</sup>P-labeled oAC490 (42mer -3') to oAC423 (167mer) a 1:1 M ratio as described for dsDNA.

### 2.7.2.3 Procedure

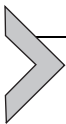
To determine the optimal amounts of RAD51 and RPA, it is recommended to titrate the proteins and DNA taking into account that one molecule of

RAD51 binds ~3 nt or base pairs (bp) of DNA (Bianco et al., 1998) and one molecule of RPA coats ~30 nt (Henricksen et al., 1994).

### Reaction

1. When required, RPA is preincubated for 5 min at 37°C with the 3'-tailed DNA (4 nM molecules).
2. RAD51 ± BRCA2 (or BRC peptides) are added to the reaction and incubated 5 min at 37°C.
3. To start the reaction, the dsDNA (4 nM molecules, oAC405 and oAC406 1:1) is added in a total volume of 10 µL and the samples are further incubated for 30 min at 37°C.
4. The reaction is deproteinized by adding 1 µL of stop solution for 10 min at 37°C.
5. Samples are mixed with 6 × DNA loading buffer and loaded on a 6% PAGE gel and electrophoresis is ran for 75 min at 70 V.
6. The gel is then dried onto DE81 paper in a gel dryer and exposed overnight on a storage phosphor screen.
7. The screen is scanned with a Typhoon PhosphorImager and quantified using ImageQuant.
8. The percentage of DNA strand exchange product is calculated as the radiolabeled product relative to the total radiolabeled input DNA in each lane.

An example of the oligonucleotide-based strand exchange assay can be seen in Fig. 6B.



---

## 3. CONCLUSIONS AND FUTURE DIRECTIONS

BRCA2 is involved in the maintenance of genome integrity throughout the cell cycle including DNA repair, protection of stalled replication forks, proper chromosome segregation, and cytokinesis. In this chapter, we have focused on the methods utilized to purify and analyze BRCA2 main activities in DNA repair by promoting homologous recombination. We have also given an overview of functional assays that are used to dissect BRCA2 activities and provided evidence that the use of a combination of fragments and the full-length protein has allowed us to gain insight on the complex mechanism of BRCA2 mediator function in DNA repair in mitotic and meiotic cells.

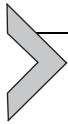
We envision that these tools may be useful to further shed light on the mechanism of HR but also will help decipher other functions of BRCA2 beyond DNA repair essential for its tumor suppressor activity and the maintenance of chromosome stability.

## REFERENCES

- Amitani, I., Liu, B., Dombrowski, C. C., Baskin, R. J., & Kowalczykowski, S. C. (2010). Watching individual proteins acting on single molecules of DNA. *Methods in Enzymology*, *472*, 261–291.
- Bianco, P. R., Tracy, R. B., & Kowalczykowski, S. C. (1998). DNA strand exchange proteins: A biochemical and physical comparison. *Frontiers in Bioscience*, *3*, D570–D603.
- Bugreev, D. V., & Mazin, A. V. (2004). Ca<sup>2+</sup> activates human homologous recombination protein Rad51 by modulating its ATPase activity. *Proceedings of the National Academy of Sciences of the United States of America*, *101*, 9988–9993.
- Buisson, R., Dion-Côté, A.-M., Coulombe, Y., Launay, H., Cai, H., Stasiak, A. Z., et al. (2010). Cooperation of breast cancer proteins PALB2 and piccolo BRCA2 in stimulating homologous recombination. *Nature Structural & Molecular Biology*, *17*, 1247–1254.
- Carreira, A., Hilario, J., Amitani, I., Baskin, R. J., Shivji, M. K. K., Venkitaraman, A. R., et al. (2009). The BRC repeats of BRCA2 modulate the DNA-binding selectivity of RAD51. *Cell*, *136*, 1032–1043.
- Carreira, A., & Kowalczykowski, S. C. (2011). Two classes of BRC repeats in BRCA2 promote RAD51 nucleoprotein filament function by distinct mechanisms. *Proceedings of the National Academy of Sciences of the United States of America*, *108*, 10448–10453.
- Chatterjee, G., Jimenez-Sainz, J., Presti, T., Nguyen, T., & Jensen, R. B. (2016). Distinct binding of BRCA2 BRC repeats to RAD51 generates differential DNA damage sensitivity. *Nucleic Acids Research*, *44*, 5256–5270.
- Chi, P., Van Komen, S., Sehorn, M. G., Sigurdsson, S., & Sung, P. (2006). Roles of ATP binding and ATP hydrolysis in human Rad51 recombinase function. *DNA Repair*, *5*, 381–391.
- Davies, O. R., & Pellegrini, L. (2007). Interaction with the BRCA2 C terminus protects RAD51-DNA filaments from disassembly by BRC repeats. *Nature Structural & Molecular Biology*, *14*, 475–483.
- Esashi, F., Galkin, V. E., Yu, X., Egelman, E. H., & West, S. C. (2007). Stabilization of RAD51 nucleoprotein filaments by the C-terminal region of BRCA2. *Nature Structural & Molecular Biology*, *14*, 468–474.
- Fried, M., & Crothers, D. M. (1981). Equilibria and kinetics of lac repressor-operator interactions by polyacrylamide gel electrophoresis. *Nucleic Acids Research*, *9*(23), 6505–6525.
- Galkin, V. E., Esashi, F., Yu, X., Yang, S., West, S. C., & Egelman, E. H. (2005). BRCA2 BRC motifs bind RAD51-DNA filaments. *Proceedings of the National Academy of Sciences of the United States of America*, *102*, 8537–8542.
- Henricksen, L. A., Umbricht, C. B., & Wold, M. S. (1994). Recombinant replication protein A: Expression, complex formation, and functional characterization. *The Journal of Biological Chemistry*, *269*, 11121–11132.
- Hilario, J., & Kowalczykowski, S. C. (2010). Visualizing protein-DNA interactions at the single-molecule level. *Current Opinion in Chemical Biology*, *14*, 15–22.
- Jensen, R. B., Carreira, A., & Kowalczykowski, S. C. (2010). Purified human BRCA2 stimulates RAD51-mediated recombination. *Nature*, *467*, 678–683.
- Kowalczykowski, S. C. (2015). An overview of the molecular mechanisms of recombinational DNA repair. *Cold Spring Harbor Perspectives in Biology*, *7*, a016410.
- Lindsley, J. E. (2001). Use of a real-time, coupled assay to measure the ATPase activity of DNA topoisomerase II. *Methods in Molecular Biology*, *95*, 57–64.
- Liu, J., Doty, T., Gibson, B., & Heyer, W.-D. (2010). Human BRCA2 protein promotes RAD51 filament formation on RPA-covered single-stranded DNA. *Nature Structural & Molecular Biology*, *17*, 1260–1262.
- Liu, J., Sneed, J., & Heyer, W.-D. (2010). In vitro assays for DNA pairing and recombination-associated DNA synthesis. *Methods in Molecular Biology*, *745*, 363–383.

- Martinez, J. S., Baldeyron, C., & Carreira, A. (2014). Molding BRCA2 function through its interacting partners. *Cell Cycle*, *14*, 3389–3395.
- Martinez, J. S., Nicolai von, C., Kim, T., Ehlen, A., Mazin, A. V., Kowalczykowski, S. C., et al. (2016). BRCA2 regulates DMC1-mediated recombination through the BRC repeats. *Proceedings of the National Academy of Sciences of the United States of America*, *113*, 3515–3520.
- Pellegrini, L., Yu, D. S., Lo, T., Anand, S., Lee, M., Blundell, T. L., et al. (2002). Insights into DNA recombination from the structure of a RAD51–BRCA2 complex. *Nature*, *420*, 287–293.
- Petalcorin, M. I. R., Galkin, V. E., Yu, X., Egelman, E. H., & Boulton, S. J. (2007). Stabilization of RAD-51-DNA filaments via an interaction domain in *Caenorhabditis elegans* BRCA2. *Proceedings of the National Academy of Sciences of the United States of America*, *104*, 8299–8304.
- Rajagopal, V., & Lorsch, J. R. (2012). ATP and GTP hydrolysis assays (TLC)—Chapter twenty-five. *Methods in Enzymology*, *533*, 325–334.
- Rajendra, E., & Venkitaraman, A. R. (2010). Two modules in the BRC repeats of BRCA2 mediate structural and functional interactions with the RAD51 recombinase. *Nucleic Acids Research*, *38*, 82–96.
- San Filippo, J., Chi, P., Sehorn, M. G., Etchin, J., Krejci, L., & Sung, P. (2006). Recombination mediator and Rad51 targeting activities of a human BRCA2 polypeptide. *The Journal of Biological Chemistry*, *281*, 11649–11657.
- Schlacher, K., Christ, N., Siaud, N., Egashira, A., Wu, H., & Jasin, M. (2011). Double-strand break repair-independent role for BRCA2 in blocking stalled replication fork degradation by MRE11. *Cell*, *145*, 529–542.
- Siaud, N., Barbera, M. A., Egashira, A., Lam, I., Christ, N., Schlacher, K., et al. (2011). Plasticity of BRCA2 function in homologous recombination: Genetic interactions of the PALB2 and DNA binding domains. *PLoS Genetics*, *7*, e1002409.
- Spain, B. H., Larson, C. J., Shihabuddin, L. S., Gage, F. H., & Verma, I. M. (1999). Truncated BRCA2 is cytoplasmic: Implications for cancer-linked mutations. *Proceedings of the National Academy of Sciences of the United States of America*, *96*, 13920–13925.
- Sung, P., & Klein, H. L. (2006). Mechanism of homologous recombination: Mediators and helicases take on regulatory functions. *Nature Reviews. Molecular Cell Biology*, *7*, 739–750.
- Thorslund, T., Esashi, F., & West, S. C. (2007). Interactions between human BRCA2 protein and the meiosis-specific recombinase DMC1. *The EMBO Journal*, *26*, 2915–2922.
- Thorslund, T., McIlwraith, M. J., Compton, S. A., Lekomtsev, S., Petronczki, M., Griffith, J. D., et al. (2010). The breast cancer tumor suppressor BRCA2 promotes the specific targeting of RAD51 to single-stranded DNA. *Nature Structural & Molecular Biology*, *17*, 1263–1265.
- Nicolai von, C., Ehlen, A., Martin, C., Zhang, X., & Carreira, A. (2016). A second DNA binding site in human BRCA2 promotes homologous recombination. *Nature Communications*, *7*, 12813.
- Wong, A. K., Pero, R., Ormonde, P. A., Tavtigian, S. V., & Bartel, P. L. (1997). RAD51 interacts with the evolutionarily conserved BRC motifs in the human breast cancer susceptibility gene *brca2*. *The Journal of Biological Chemistry*, *272*, 31941–31944.
- Yang, H., Jeffrey, P. D., Miller, J., Kinnucan, E., Sun, Y., Thoma, N. H., et al. (2002). BRCA2 function in DNA binding and recombination from a BRCA2-DSS1-ssDNA structure. *Science*, *297*, 1837–1848.
- Yang, H., Li, Q., Fan, J., Holloman, W. K., & Pavletich, N. P. (2005). The BRCA2 homologue Brh2 nucleates RAD51 filament formation at a dsDNA-ssDNA junction. *Nature*, *433*, 653–657.
- Zhao, W., Vaithiyalingam, S., San Filippo, J., Maranon, D. G., Jimenez-Sainz, J., Fontenay, G. V., et al. (2015). Promotion of BRCA2-dependent homologous recombination by DSS1 via RPA targeting and DNA mimicry. *Molecular Cell*, *59*, 176–187.

This page intentionally left blank



# Approaches to Understanding the Mediator Function of Brh2 in *Ustilago maydis*

Qingwen Zhou, William K. Holloman<sup>1</sup>, Milorad Kojic<sup>2</sup>

Weill Cornell Medical College, New York, NY, United States

<sup>1</sup>Corresponding author: e-mail address: wkhollo@med.cornell.edu

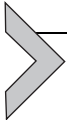
## Contents

|   |     |
|---|-----|
| 1. Introduction   | 514 |
| 2. Biochemical Methods  | 516 |
| 2.1 Brh2/Dss1 Complex Purification  | 516 |
| 2.2 Rad51 Purification  | 517 |
| 2.3 Dss1 Purification   | 518 |
| 3. Genetic Methods  | 519 |
| 3.1 Construction of a Vector That Enables Screening for In-Frame Insertions | 520 |
| 3.2 Scanning Mutagenesis and Mapping Mutations                              | 521 |
| 3.3 Rapid Construction of Internal In-Frame Deletion Mutants                | 523 |
| Acknowledgments   | 523 |
| References  | 523 |

## Abstract

Primary components of the homologous recombination pathway in eukaryotes include Rad51 whose function is to search for DNA sequence homology and promote strand exchange, its mediator BRCA2, and Dss1, a key regulator of BRCA2. We seek to understand the role of BRCA2 in governing the activity of Rad51 and to learn how BRCA2 function is regulated by Dss1. We use the microbe *Ustilago maydis* as a model system for experimentation because it has a well-conserved BRCA2-homolog, Brh2, and is amenable to biochemical and molecular genetic manipulations and analysis. The powerful attributes of this system open the way for gaining insight into BRCA2's molecular mechanism through avenues not immediately approachable in the vertebrate systems. Here we provide protocols for preparing Brh2, Dss1, and Rad51 as reagents for use in biochemical assays to monitor function and present methods for transposon-based mutational analysis of Brh2 for use in genetic dissection of function.

<sup>2</sup> Present address: Institute of Molecular Genetics and Genetic Engineering, University of Belgrade, Belgrade, Serbia.



## 1. INTRODUCTION

A driving force behind tumorigenic transformation is genomic instability that can result from a defective homologous recombination (HR) system (Bartek, Bartkova, & Lukas, 2007; Halazonetis, Gorgoulis, & Bartek, 2008; Helleday, 2010; Venkitaraman, 2014). Mutation of BRCA2, a central component of HR, predisposes individuals to development of breast, ovarian, and other types of tumors (Stratton & Rahman, 2008). Cells defective in BRCA2 are characterized by severe chromosome breakage, translocations, rearrangements, and other abnormalities. Accordingly, germline mutations in BRCA2 are associated with a highly penetrant incidence of breast, ovarian, and other types of cancers (Moynahan & Jasin, 2010; Rahman & Stratton, 1998; Shivji & Venkitaraman, 2004). At the cellular level loss of BRCA2 function results in loss of resistance to radiation and to genotoxins such as DNA cross-linking agents, decreased HR, and defects in replication (Moynahan & Jasin, 2010; Moynahan, Pierce, & Jasin, 2001; Patel et al., 1998; Yu et al., 2000). BRCA2 is required for formation of Rad51 foci, considered to be sites of recombinational repair, after DNA damage (Tarsounas, Davies, & West, 2003). Rad51 has a central role in HR assembling onto single-stranded DNA (ssDNA) as a nucleoprotein filament and catalyzing the invasion and exchange of homologous DNA sequences (Jasin & Rothstein, 2013; San Filippo, Sung, & Klein, 2008).

Human BRCA2 is the founding member of a family of proteins found throughout the eukaryotic domain of life. The human protein is unusually large, but there is a great deal of size variation among orthologs in different taxa. Regardless of divergence in size and sequence of BRCA2 family members, two defining features prevail. These are the BRC repeats (Bignell, Micklem, Stratton, Ashworth, & Wooster, 1997) that bind Rad51 (Pellegrini et al., 2002; Wong, Pero, Ormonde, Tavtigian, & Bartel, 1997) and the Dss1/DNA-binding domain (DBD), which is composed of a helix-rich region and a tandem array of oligonucleotide/oligosaccharide-binding (OB) folds, the latter being modules with the potential for binding ssDNA (Yang et al., 2002). The number of BRC repeats is variable depending on the species and can range from one in the case of Brh2 protein—the BRCA2 ortholog of the fungus *Ustilago maydis* that is the subject of this proposal, to 4 in higher plants, 8 in vertebrates, and up to 15 in certain protozoans (Lo, Pellegrini, Venkitaraman, & Blundell, 2003). There is also interspecies variation in the number of OB folds, from one in the

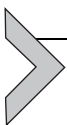
worm *Caenorhabditis elegans*, two in *U. maydis* Brh2, and three in higher plants and animals. The helix-rich region and adjacent OB1 module of the DBD is bound tightly by Dss1, a small intrinsically unstructured protein (Yang et al., 2002), which appears to act as both a positive and negative regulator of BRCA2 and is essential for its function (Gudmundsdottir, Lord, Witt, Tutt, & Ashworth, 2004; Jeyasekharan et al., 2013; Kojic, Zhou, Lisby, & Holloman, 2005; Li et al., 2006; Zhou et al., 2007). The residues forming the Dss1-interacting interface comprise the most highly conserved region of the BRCA2 sequence.

As first demonstrated with *U. maydis* Brh2 protein (Yang, Li, Fan, Holloman, & Pavletich, 2005), the BRCA2 class of proteins acts to stimulate the activity of Rad51 in DNA strand exchange, a key step in the process of repairing DNA directed by the HR system (Jensen, Carreira, & Kowalczykowski, 2010; Liu, Doty, Gibson, & Heyer, 2010; San Filippo et al., 2008; Thorslund et al., 2010). Physical interaction between Rad51 and BRCA2's BRC elements and an unrelated region at its carboxy-terminus contribute to Rad51 stimulation (Carreira & Kowalczykowski, 2011; Esashi, Galkin, Yu, Egelman, & West, 2007). Rad51 must bind to ssDNA to form a polymerized nucleoprotein filament, the active form for strand invasion, but in vivo is prevented from doing so due to competition from RPA, the abundant single-strand-specific DNA-binding protein that binds tightly to protect it. BRCA2 serves as a mediator enabling Rad51 to gain access to ssDNA coated with RPA and ultimately to displace it (Jensen et al., 2010; San Filippo et al., 2008), as shown first with *U. maydis* Brh2 (Yang et al., 2005). The molecular mechanism of how BRCA2 promotes this process is not clear, but based on the structural features of the BRC and DBD, it would seem logical to suppose that the mechanism involves coupling the inherent Rad51-binding activity with the DNA-binding activity (San Filippo et al., 2008; Shivji et al., 2006; Yang et al., 2005). Recent observations suggest, however, that this notion could be too simplistic. New evidence indicates that Dss1 plays a direct role in helping BRCA2 associate with RPA to exchange it for Rad51 (Zhao et al., 2015). In addition, current findings from our laboratory on Brh2 support a model in which Dss1 mediates multifaceted interactions between Rad51 and Brh2's BRC and C-terminal Rad51 interaction region through coordinated interplay of two different DNA-binding domains (Zhou & Holloman, 2017).

In addition to the canonical DNA-binding domain located in the C-terminal domain (CTD) (Zhou, Mazloum, Mao, Kojic, & Holloman, 2009) of Brh2, there is another DNA-binding region present in the

N-terminal region of the protein (termed NBD) (Zhou, Kojic, & Holloman, 2009). The Brh2 NBD is capable of working in concert with the BRC motif to promote biological function in DNA repair (Kojic et al., 2005). It was localized by deletion mapping to a stretch of 144 residues between the BRC element and the canonical CTD, but that sequence stretch is poorly conserved and has no hallmark indicative of a DNA-binding motif (Zhou, Kojic, et al., 2009). However, the binding activity is robust, and a side-by-side comparison of polypeptides Brh2<sup>106–551</sup> and Brh2<sup>551–1075</sup>, denoted as Brh2<sup>N<sup>T</sup></sup> and Brh2<sup>C<sup>T</sup></sup>, containing NBD or CTD, respectively, revealed that the two different DNA-binding regions display remarkable similarities but differ sharply in response to Dss1 (Zhou & Holloman, 2014). DNA-binding activity of the CTD is tightly regulated by Dss1, while the activity of NBD is independent of Dss1 (Zhou, Kojic, & Holloman, 2012). When the CTD is associated with Dss1, it has no apparent DNA-binding activity, but when freed of Dss1 it binds DNA as tightly as the NBD. It seems clear from these findings that Dss1 plays an important role in mediating cooperation between the two different DNA-binding regions of Brh2 (Zhou, Kojic, et al., 2009; Zhou et al., 2012). We note that a second DNA-binding region outside of the canonical DNA-binding domain has also been recognized in human BRCA2, suggesting parallels in functional activity (Chatterjee, Jimenez-Sainz, Presti, Nguyen, & Jensen, 2016).

Analysis of the function of Brh2, its interaction with Rad51, and regulation by Dss1 requires both biochemical and molecular genetic approaches. For biochemical studies of intermolecular interactions, it is of great benefit to have proteins available with affinity tags for selective precipitations. Here we present procedures for obtaining suitable quantities of the relevant proteins for analysis. Furthermore, we present procedures for generating mutations in Brh2 as an approach to mapping domains in a protein of unknown function.



## 2. BIOCHEMICAL METHODS

### 2.1 Brh2/Dss1 Complex Purification

Brh2 is purified as an MBP-fusion protein in a complex with His-tagged Dss1 protein. The Brh2/Dss1 complex is referred to as Brh2 for simplicity unless otherwise noted. The Brh2 cDNA was cloned into pMAL-C2 (New England Biolabs) such that the fusion begins at Brh2 residue 106. The Dss1 cDNA was cloned into pACYC Duet vector (Novagen) for expression with an N-terminal hexahistidine affinity tag. The Brh2 and Dss1 fusion

constructs are completely functional in complementing the radiation sensitivity of the *U. maydis brh2* $\Delta$  and *dss1* $\Delta$  mutants, respectively. The plasmids are sequentially transformed into *Escherichia coli* BL21 (DE3) cells and cultures grown in LB medium containing ampicillin and chloramphenicol. Cell cultures (3 L) are grown at 37° to  $A_{600}$  of 0.6, induced by addition of isopropyl  $\beta$ -D-1-thiogalactopyranoside (IPTG) to 0.1 mM, but maintained at 18° after induction for 10 h. After harvesting, cells are resuspended in 50 mL BA buffer (25 mM Tris-HCl, pH 7.5, 200 mM KCl, 1 mM dithiothreitol (DTT), 10% glycerol, 0.1% NP40) + 20 mM imidazole, crushed by two passes through a French pressure cell at 20,000 p.s.i., and centrifuged at 16,000 rpm in a Sorvall SS34 rotor for 30 min. The supernatant is recovered and centrifuged at 27,000 rpm for 1 h in a Beckman SW28 rotor. Subsequent procedures are all performed at 0–4°. The supernatant is passed onto a column (6 mL bed volume) of NTA-agarose (Novagen) charged with Ni<sup>2+</sup> and equilibrated in the same buffer. The column is washed with 40 mL of buffer and protein eluted with 25 mL BA buffer + 200 mM imidazole. The eluate is loaded on a 5-mL column of cross-linked amylose resin (New England Biolabs) which is washed with 40 mL of BA buffer followed by 25 mL BA buffer + 10 mM maltose. The fractions containing Brh2 protein are pooled, diluted to 100 mM KCl, and applied to a 1-mL MonoQ column (GE Healthcare) equilibrated in buffer BB (25 mM Tris-HCl, pH 7.5, 100 mM KCl, 1 mM DTT, 10% glycerol). After washing with 5 mL of buffer, the protein is eluted with a linear gradient (20 mL) from 0.1 to 0.6 M KCl using an AKTA Explorer FPLC (GE Healthcare). Peak fractions are pooled and dialyzed against buffer BB and stored frozen at –80°.

## 2.2 Rad51 Purification

For production of Rad51 in *E. coli* BL21 (DE3) the *U. maydis* cDNA encoding Rad51 was cloned in pET3a vector derivative (Novagen) under control of the T7 promoter so as not to include any affinity tag. Cultures (6 L) are grown at 37°, induced as above and cells harvested 5 h later after continued incubation at 37°. Cells are resuspended in ice cold 50 mL buffer A (25 mM Tris-HCl, pH 7.5, 1 mM DTT, 1 mM EDTA, 10% glycerol, and 0.1% NP40) + 0.5 M KCl, crushed and centrifuged as above. Subsequent procedures are all performed at 0–4°. The high speed supernatant is diluted with buffer RA (25 mM Tris-HCl, pH 7.5, 1 mM DTT, 1 mM EDTA, 10% glycerol), to a conductivity equivalent to

100 mM KCl, mixed with 200 mL gravity-settled DEAE-cellulose slurry (Whatman DE52), stirred for 45 min, then passed onto a Buchner funnel with sintered glass filter. The resin is washed batchwise on the funnel under gentle vacuum with 2 L buffer RA + 100 mM KCl, followed by a wash of 200 mL with buffer A + 2 M KCl. The 2 M eluate is diluted fourfold then loaded onto a column (20 mL bed volume) of Affi-Gel Blue (BioRad Laboratories) equilibrated in buffer RA + 0.2 M KCl. The column is eluted with a linear salt gradient (200 mL) from 0.2 to 1.5 M KCl, peak fractions pooled after identification of those containing Rad51 by SDS gel electrophoresis and passed over a column (20 mL bed volume) of Bio-Gel HTP hydroxyapatite (BioRad Laboratories) equilibrated with buffer RB (25 mM potassium phosphate, pH 7.5, 500 mM KCl, 1 mM DTT, 10% glycerol) which is then eluted with a linear gradient (200 mL) from 25 mM to 0.8 M of potassium phosphate. Peak fractions are pooled and dialyzed against buffer RC (25 mM Tris-HCl, pH 7.5, 100 mM KCl, 1 mM DTT, 10% glycerol), then applied to a 1-mL MonoQ column, washed with 10 mL of RC buffer, and eluted with a linear gradient (20 mL) from 0.1 to 1 M KCl. Peak fractions that appear >95% homogeneous are pooled and dialyzed against buffer RD, 25 mM Tris-HCl, pH 7.5, 0.5 M KCl, 1 mM DTT, 0.1 mM EDTA, 20% glycerol, snap-frozen in liquid nitrogen, and stored at  $-80^{\circ}$ .

### 2.3 Dss1 Purification

Brh2/Dss1 complex (10 mg) purified from 3 L of cell culture as above is resuspended in 20 mL DA buffer (25 mM Tris-HCl, pH 7.5, 100 mM KCl, 1 mM DTT, 10% glycerol) containing 20 mM  $MgCl_2$  and incubated at  $37^{\circ}$  for 1 h. Mixture is then loaded onto a 5-mL HiTrap Heparin HP column (GE Healthcare), and the column is washed with 5 mL of DA buffer. The flow through and wash are pooled and adjusted to 20 mM imidazole, then loaded onto an  $Ni^{2+}$ -NTA-agarose (8 mL) equilibrated in the same buffer. The column is washed with 40 mL of buffer and protein eluted with 25 mL DA buffer + 300 mM imidazole. Fractions containing Dss1 are pooled, diluted with DA buffer to 100 mM imidazole, and loaded onto a 1-mL MonoQ column. After washing with 5 mL of buffer, the protein is eluted with a linear gradient (20 mL) from 0.1 to 0.6 M KCl using an AKTA Explorer FPLC. Peak fractions are pooled and dialyzed against buffer BB, and stored frozen at  $-80^{\circ}$ .

Proteins purified by the above procedures are shown in [Fig. 1](#).

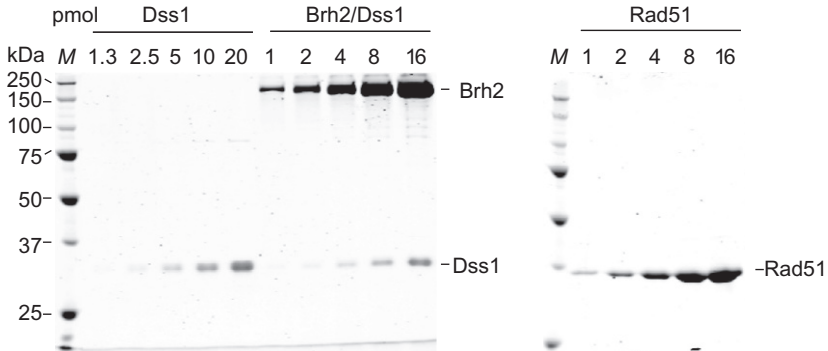


**Fig. 1** Purified proteins. Brh2/Dss1, Dss1, and Rad51 purified as described were analyzed by SDS-polyacrylamide gel electrophoresis. Increasing amounts of proteins are shown.

### 3. GENETIC METHODS

We present a strategy to identify and analyze functional domains and interdomain regions of Brh2 (Kojic, Zhou, Fan, & Holloman, 2011), which can be generalized and applied to any protein of interest. The approach was to generate random pool of *Brh2* mutants using a transposon-based linker insertion mutagenesis screen. Linker insertion scanning was performed using the GPS-LS system (New England Biolabs), which employs a Tn7-derived minitransposon harboring a selectable marker and ends modified to encode for *PmeI* restriction sites (5'...GTTTAAAC...3'). In vitro DNA transposition is achieved in a reaction mixture containing a transposon donor plasmid, a target DNA, and the TnsABC\* transposase. As the transposase excises the transposon from the donor and inserts it into the target DNA 5 base pairs (bp) of the target sequence become duplicated so that one copy is present at each side of the insertion. The reaction mixture is transformed into an *E. coli* strain nonpermissive for donor plasmid replication and exclusive recovery of the targets with transposon insertions is achieved by selection for the antibiotic marker in the transposon. When target derivatives, each harboring a transposon insertion, are subsequently digested with *PmeI* restriction enzyme nearly the entire transposon gets excised, leaving at the site of transposition 15 bp of which 10 bp that include a unique *PmeI* site are donated by the residual transposon itself, and 5 bp contributed by the duplication of the target site sequence (Biery, Stewart, Stellwagen, Raleigh, & Craig, 2000). These 15 bp are translated to five new amino acids if inserted

into a coding sequence. However, since the *PmeI* site has TAA sequence in a subset of insertions, i.e., in one of three reading frames, the insertion of the linker brings a translation termination (stop) codon that generates truncations in the protein.

### 3.1 Construction of a Vector That Enables Screening for In-Frame Insertions

To facilitate the generation of a collection of in-frame insertions, we have developed a simple frame-checking procedure that eliminates mutants containing stop codons. Since we wanted to include a majority of the *Brh2* sequence, we first tested whether 2646 bp *MluI*–*NsiI* fragment of the *Brh2*-coding sequence when inserted in frame into the  $\alpha$ -complementing domain of *E. coli*  $\beta$ -galactosidase (*LacZ* $\alpha$ -donor) (for example, into pUC19 polylinker) would affect the  $\alpha$ -complementation. The *MluI*/*NsiI* linker, specifically designed to accept *MluI*–*NsiI* *Brh2* fragment in frame with *LacZ* $\alpha$ -donor, was ligated to *HindIII*–*EcoRI* digested but not dephosphorylated pUC19 plasmid DNA. The *MluI*/*NsiI* forward oligonucleotide (5'-AGCTTGAACGCGTAAGATGCATCG-3') and the *NsiI*/*MluI* reverse oligonucleotide (5'-AATTCGATGCATCTTACGCGTTCA-3') were annealed by heating an equal volume of 20  $\mu$ M oligonucleotides for 5 min at 90°C in 10 mM Tris–HCl, pH 7.5, 1 mM EDTA, 0.2 M NaCl buffer followed by a slowly cooling to room temperature over 30 min resulting in 50  $\mu$ M *NsiI*/*MluI* linker. The annealed product is a double-stranded linker of which one end has a protruding 5' *HindIII* overhang, while the other has a 5'–*EcoRI* overhang enabling ligation to *HindIII*–*EcoRI*-opened pUC19. The linker also contained a TAA stop codon in order to easily detect its proper insertion into the pUC19 polylinker, that is into *lacZ* $\alpha$  reading frame resulting in the premature termination of translation of its messenger RNA. To eliminate the formation of linker dimers during the ligation we used unphosphorylated oligonucleotides. Following ligation, the mixture was transformed into chemically competent *E. coli* NM522 cells expressing *LacZ* $\alpha$ -acceptor ( $\Delta$ *LacZ*M15). The cells were plated onto LB agar supplemented with 100  $\mu$ g/mL ampicillin, 40  $\mu$ g/mL 5-bromo-4-chloro-3-indolyl- $\beta$ -D-galactopyranoside (X-gal), and 1 mM IPTG and screened for the relatively abundant white colonies. The proper insertion of the linker was confirmed by restriction enzyme analyzes of the plasmid DNA isolated from the individual white colonies. The plasmid was designated as pUCMN.

In the next step we inserted the 2646 bp *MluI*–*NsiI* *Brh2* fragment into *LacZ* $\alpha$ -donor sequence by its ligation to *MluI*/*NsiI* opened pUCMN. The

ligation mixture was introduced into *E. coli* NM522 cells. The ability of Brh2-LacZ $\alpha$  hybrid to restore (by  $\alpha$ -complementation)  $\beta$ -galactosidase activity of the *E. coli* NM522 cells was tested by plating the transformed cells onto LB agar containing 100  $\mu\text{g}/\text{mL}$  ampicillin; 40, 60, or 80  $\mu\text{g}/\text{mL}$  X-gal; and 1 mM IPTG and incubating them overnight at 37°C. We found that the colonies of *E. coli* NM522 with plasmids carrying Brh2-LacZ $\alpha$  fusion could readily be identified by their blue color on LB agar supplemented with 80  $\mu\text{g}/\text{mL}$  X-gal making it possible to use this chromogenic system to eliminate stop codon-producing Tn7 insertions.

### 3.2 Scanning Mutagenesis and Mapping Mutations

Mutagenesis was performed with the GPS-LS linker scanning system (New England Biolabs) essentially according to the manufacturer's instructions. The transposon donor plasmid (pGPS5, 0.05  $\mu\text{g}$ ) was mixed with TnsABC (1  $\mu\text{L}$ ) and the target Brh2 plasmid (pUCMN-*Brh2*, 0.15  $\mu\text{g}$ ) and incubated for 10 min at 37°C. After start solution was added, the mixture was incubated for 1 h at 37°C and heated at 75°C for 10 min. Following transposition, the DNA mixture was transformed into *E. coli* NM522 strain. The transformants were plated onto LB agar containing 50  $\mu\text{g}/\text{mL}$  kanamycin (to select for transposition), 100  $\mu\text{g}/\text{mL}$  ampicillin (to eliminate transposon insertions within  $\beta$ -lactamase gene) and incubated overnight at 37°C. The transformants were subsequently washed off the plates inoculated in fresh LB broth containing 50  $\mu\text{g}/\text{mL}$  kanamycin for 2 h at 37°C. The plasmid DNA from the pool was harvested and digested with *PmeI* restriction enzyme, to remove the bulk of the transposon. Recircularized plasmids were transformed into *E. coli* (NM522) strain and selected on LB agar containing 100  $\mu\text{g}/\text{mL}$  ampicillin, 80  $\mu\text{g}/\text{mL}$  X-gal, and 1 mM IPTG. Plasmid DNA was recovered only from blue colonies, and the positions of the insertions were mapped by *EcoRI PmeI* restriction analysis. 216 unique *Brh2* linker insertion mutants were analyzed by *EcoRI PmeI* digestion and those judged to have the insertion within the *Brh2* fragment were sequenced by using standard M13 forward and reverse primers to verify the position of each insertion. Representatives along the gene can be chosen for further analysis by expression in various *U. maydis* mutants (i.e., *brh2* $\Delta$ , *brh2* $\Delta$  *rad52* $\Delta$ , etc.) using a suitable expression vector and tested for activity in complementation (or suppression) of DNA repair deficiency by means of survival after DNA damage.

The flowchart in Fig. 2 illustrates the steps to obtain a library of random five-codon inserts in frame within the Brh2 coding sequence.

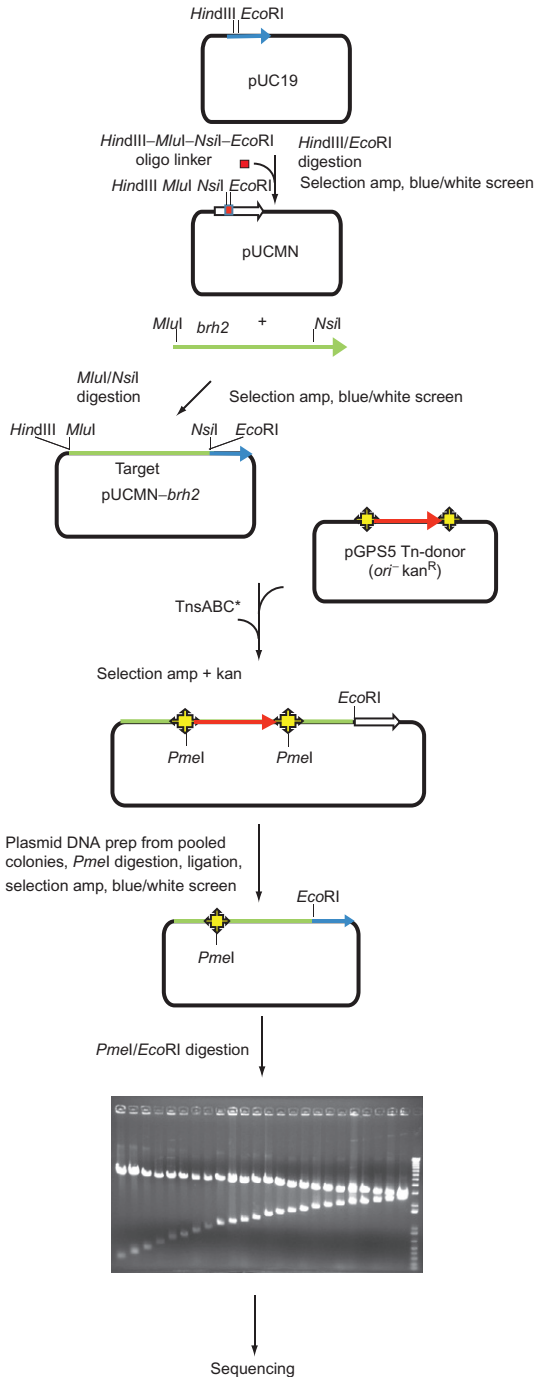


**Fig. 2** Transposon mutagenesis flow chart. After inserting linker, the *Brh2* target sequence is inserted, followed by in vitro transposition and processing to remove the minitransposon. *LacZ* $\alpha$  fragment activity in  $\alpha$  complementation is indicated by the blue or white arrows. Yellow-centered diamonds indicate 15 bp transposition footprints. Candidate plasmids from a mutagenesis procedure were mapped by digestion with *PmeI* and *EcoRI* and analyzed by agarose gel electrophoresis. A DNA ladder is shown on the right.

### 3.3 Rapid Construction of Internal In-Frame Deletion Mutants

One of the advantages that comes from a collection of the random transposon-introduced in-frame linker insertions constructed as above is the ability to make internal in-frame deletions without a laborious cloning procedure. This is facilitated by the presence of the introduced *PmeI* sites, which are on average located in every other instance within the same open reading frame. Accordingly, use of the *PmeI* sites provides great versatility in construction of internal in-frame deletions of the desired location and size. Brh2 mutants deleted of various domain can be constructed in this way by taking advantage of the unique *PmeI* sites introduced by transposon linker scanning mutagenesis method described. In general, to generate a set of in-frame deletion constructs we use three-way ligation methodology. Since *MluI* and *NsiI* restriction sites are unique in *brh2* sequence as well as in an expression vector harboring *brh2* gene under a heterologous promoter, we digest the vector with *MluI* and *NsiI*. The 5'-*brh2* fragments are prepared by *MluI*-*PmeI* digestion of DNA from mutants that have in-frame linker insertion located at the starting point of the desired deletions. The 3'-*brh2* fragments are excised by *PmeI*-*NsiI* digestion from mutants having the linker insertions at the end point of the desired deletions. For these three-way ligations a 1:1 *M* ratio of the 5'- and 3'-*Brh2* fragments and a 3:1 insert vector ratio are used. To verify the size of the deletions the plasmid DNA of the constructs are digested by *MluI* and *NsiI*, and the deletions are further confirmed by sequencing.

In summary, the frame-checking procedure we described here can bring increased convenience to constructing in-frame mutations. The method is not only limited to the linker insertions but also extends to the internal deletions of the coding DNA sequence of variable lengths. This generally applicable procedure requires the minimal screening to derive positive clones and helps construction of in-frame deletions without a laborious cloning route.

### ACKNOWLEDGMENTS

Work in the Holloman laboratory was supported by Grant GM079859 from the National Institutes of Health. Work in the Kojic laboratory is supported by Grant 173005 from Ministry of Education, Science and Technology, Republic of Serbia.

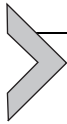
### REFERENCES

- Bartek, J., Bartkova, J., & Lukas, J. (2007). DNA damage signalling guards against activated oncogenes and tumour progression. *Oncogene*, 26, 7773–7779.
- Biery, M. C., Stewart, F. J., Stellwagen, A. E., Raleigh, E. A., & Craig, N. L. (2000). A simple in vitro Tn7-based transposition system with low target site selectivity for genome and gene analysis. *Nucleic Acids Research*, 28, 1067–1077.

- Bignell, G., Micklem, G., Stratton, M. R., Ashworth, A., & Wooster, R. (1997). The BRC repeats are conserved in mammalian BRCA2 proteins. *Human Molecular Genetics*, *6*, 53–58.
- Carreira, A., & Kowalczykowski, S. C. (2011). Two classes of BRC repeats in BRCA2 promote RAD51 nucleoprotein filament function by distinct mechanisms. *Proceedings of the National Academy of Sciences of the United States of America*, *108*, 10448–10453.
- Chatterjee, G., Jimenez-Sainz, J., Presti, T., Nguyen, T., & Jensen, R. B. (2016). Distinct binding of BRCA2 BRC repeats to RAD51 generates differential DNA damage sensitivity. *Nucleic Acids Research*, *44*, 5256–5270.
- Esashi, F., Galkin, V. E., Yu, X., Egelman, E. H., & West, S. C. (2007). Stabilization of RAD51 nucleoprotein filaments by the C-terminal region of BRCA2. *Nature Structural & Molecular Biology*, *14*, 468–474.
- Gudmundsdottir, K., Lord, C. J., Witt, E., Tutt, A. N., & Ashworth, A. (2004). DSS1 is required for RAD51 focus formation and genomic stability in mammalian cells. *EMBO Reports*, *5*, 989–993.
- Halazonetis, T. D., Gorgoulis, V. G., & Bartek, J. (2008). An oncogene-induced DNA damage model for cancer development. *Science*, *319*, 1352–1355.
- Helleday, T. (2010). Homologous recombination in cancer development, treatment and development of drug resistance. *Carcinogenesis*, *31*, 955–960.
- Jasin, M., & Rothstein, R. (2013). Repair of strand breaks by homologous recombination. *Cold Spring Harbor Perspectives in Biology*, *5*, a012740.
- Jensen, R. B., Carreira, A., & Kowalczykowski, S. C. (2010). Purified human BRCA2 stimulates RAD51-mediated recombination. *Nature*, *467*, 678–683.
- Jeyasekharan, A. D., Liu, Y., Hattori, H., Pisupati, V., Jonsdottir, A. B., Rajendra, E., et al. (2013). A cancer-associated BRCA2 mutation reveals masked nuclear export signals controlling localization. *Nature Structural & Molecular Biology*, *20*, 1191–1198.
- Kojic, M., Zhou, Q., Fan, J., & Holloman, W. K. (2011). Mutational analysis of Brh2 reveals requirements for compensating mediator functions. *Molecular Microbiology*, *79*, 180–191.
- Kojic, M., Zhou, Q., Lisby, M., & Holloman, W. K. (2005). Brh2-Dss1 interplay enables properly controlled recombination in *Ustilago maydis*. *Molecular and Cellular Biology*, *25*, 2547–2557.
- Li, J., Zou, C., Bai, Y., Wazer, D. E., Band, V., & Gao, Q. (2006). DSS1 is required for the stability of BRCA2. *Oncogene*, *25*, 1186–1194.
- Liu, J., Doty, T., Gibson, B., & Heyer, W. D. (2010). Human BRCA2 protein promotes RAD51 filament formation on RPA-covered single-stranded DNA. *Nature Structural & Molecular Biology*, *17*, 1260–1262.
- Lo, T., Pellegrini, L., Venkitaraman, A. R., & Blundell, T. L. (2003). Sequence fingerprints in BRCA2 and RAD51: Implications for DNA repair and cancer. *DNA Repair (Amst)*, *2*, 1015–1028.
- Moynahan, M. E., & Jasin, M. (2010). Mitotic homologous recombination maintains genomic stability and suppresses tumorigenesis. *Nature Reviews. Molecular Cell Biology*, *11*, 196–207.
- Moynahan, M. E., Pierce, A. J., & Jasin, M. (2001). BRCA2 is required for homology-directed repair of chromosomal breaks. *Molecular Cell*, *7*, 263–272.
- Patel, K. J., VP, Y., Lee, H., Corcoran, A., Thistlethwaite, F. C., Evans, M. J., et al. (1998). Involvement of Brca2 in DNA repair. *Molecular Cell*, *1*, 347–357.
- Pellegrini, L., DS, Y., Lo, T., Anand, S., Lee, M., Blundell, T. L., et al. (2002). Insights into DNA recombination from the structure of a RAD51-BRCA2 complex. *Nature*, *420*, 287–293.
- Rahman, N., & Stratton, M. R. (1998). The genetics of breast cancer susceptibility. *Annual Review of Genetics*, *32*, 95–121.

- San Filippo, J., Sung, P., & Klein, H. (2008). Mechanism of eukaryotic homologous recombination. *Annual Review of Biochemistry*, 77, 229–257.
- Shivji, M. K., Davies, O. R., Savill, J. M., Bates, D. L., Pellegrini, L., & Venkitaraman, A. R. (2006). A region of human BRCA2 containing multiple BRC repeats promotes RAD51-mediated strand exchange. *Nucleic Acids Research*, 34, 4000–4011.
- Shivji, M. K., & Venkitaraman, A. R. (2004). DNA recombination, chromosomal stability and carcinogenesis: Insights into the role of BRCA2. *DNA Repair (Amst)*, 3, 835–843.
- Stratton, M. R., & Rahman, N. (2008). The emerging landscape of breast cancer susceptibility. *Nature Genetics*, 40, 17–22.
- Tarsounas, M., Davies, D., & West, S. C. (2003). BRCA2-dependent and independent formation of RAD51 nuclear foci. *Oncogene*, 22, 1115–1123.
- Thorslund, T., McIlwraith, M. J., Compton, S. A., Lekomtsev, S., Petronczki, M., Griffith, J. D., et al. (2010). The breast cancer tumor suppressor BRCA2 promotes the specific targeting of RAD51 to single-stranded DNA. *Nature Structural & Molecular Biology*, 17, 1263–1265.
- Venkitaraman, A. R. (2014). Cancer suppression by the chromosome custodians, BRCA1 and BRCA2. *Science*, 343, 1470–1475.
- Wong, A. K., Pero, R., Ormonde, P. A., Tavtigian, S. V., & Bartel, P. L. (1997). RAD51 interacts with the evolutionarily conserved BRC motifs in the human breast cancer susceptibility gene *brca2*. *The Journal of Biological Chemistry*, 272, 31941–31944.
- Yang, H., Jeffrey, P. D., Miller, J., Kinnucan, E., Sun, Y., Thoma, N. H., et al. (2002). BRCA2 function in DNA binding and recombination from a BRCA2-DSS1-ssDNA structure. *Science*, 297, 1837–1848.
- Yang, H., Li, Q., Fan, J., Holloman, W. K., & Pavletich, N. P. (2005). The BRCA2 homologue Brh2 nucleates RAD51 filament formation at a dsDNA-ssDNA junction. *Nature*, 433, 653–657.
- Yu, V. P., Koehler, M., Steinlein, C., Schmid, M., Hanakahi, L. A., van Gool, A. J., et al. (2000). Gross chromosomal rearrangements and genetic exchange between non-homologous chromosomes following BRCA2 inactivation. *Genes & Development*, 14, 1400–1406.
- Zhao, W., Vaithiyalingam, S., San Filippo, J., Maranon, D. G., Jimenez-Sainz, J., Fontenay, G. V., et al. (2015). Promotion of BRCA2-dependent homologous recombination by DSS1 via RPA targeting and DNA mimicry. *Molecular Cell*, 59, 176–187.
- Zhou, Q., & Holloman, W. K. (2014). Dual DNA-binding domains shape the interaction of Brh2 with DNA. *DNA Repair (Amst)*, 22, 104–111.
- Zhou, Q., & Holloman, W. K. (2017). Dss1 regulates association of Brh2 with Rad51. *Biochemistry*, 56, 3318–3327.
- Zhou, Q., Kojic, M., Cao, Z., Lisby, M., Mazloun, N. A., & Holloman, W. K. (2007). Dss1 interaction with Brh2 as a regulatory mechanism for recombinational repair. *Molecular and Cellular Biology*, 27, 2512–2526.
- Zhou, Q., Kojic, M., & Holloman, W. K. (2009). DNA-binding domain within the Brh2 N terminus is the primary interaction site for association with DNA. *The Journal of Biological Chemistry*, 284, 8265–8273.
- Zhou, Q., Kojic, M., & Holloman, W. K. (2012). Dss1 release activates DNA binding potential in Brh2. *Biochemistry*, 51, 9137–9146.
- Zhou, Q., Mazloun, N., Mao, N., Kojic, M., & Holloman, W. K. (2009). Dss1 regulates interaction of Brh2 with DNA. *Biochemistry*, 48, 11929–11938.

This page intentionally left blank



# GEN1 Endonuclease: Purification and Nuclease Assays

Ying Wai Chan, Stephen C. West<sup>1</sup>

The Francis Crick Institute, London, United Kingdom

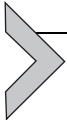
<sup>1</sup>Corresponding author: e-mail address: stephen.west@crick.ac.uk

## Contents

|   |     |
|---|-----|
| 1. Introduction   | 528 |
| 2. Purification of GEN1                                   | 529 |
| 2.1 Protein Expression                                    | 529 |
| 2.2 Protein Purification                                  | 532 |
| 3. Cleavage of Synthetic DNA Substrates                   | 533 |
| 3.1 Oligonucleotide Purification                          | 535 |
| 3.2 Preparation of <sup>32</sup> P-Labeled DNA Substrates | 536 |
| 3.3 DNA Cleavage Assays                                   | 537 |
| 4. Cleavage of Cruciform-Containing Plasmids by GEN1      | 538 |
| 4.1 Plasmid Cleavage Assays                               | 538 |
| 5. Summary  | 540 |
| Acknowledgments   | 540 |
| References  | 541 |

## Abstract

Successful chromosome segregation depends on the timely removal of DNA recombination and replication intermediates that interlink sister chromatids. These intermediates are acted upon by structure-selective endonucleases that promote incisions close to the junction point. GEN1, a member of the Rad2/XPG endonuclease family, was identified on the basis of its ability to cleave Holliday junction recombination intermediates. Resolution occurs by a nick and counter-nick mechanism in strands that are symmetrically related across the junction point, leading to the formation of ligatable nicked duplex products. The actions of GEN1 are, however, not restricted to HJs, as 5'-flaps and replication fork structures also serve as excellent *in vitro* substrates for the nuclease. In the cellular context, GEN1 activity is observed late in the cell cycle, as most of the protein is excluded from the nucleus, such that it gains access to DNA intermediates after the breakdown of nuclear envelope. Nuclear exclusion ensures the protection of replication forks and other DNA secondary structures important for normal metabolic processes. In this chapter, we describe the purification of recombinant GEN1 and detail biochemical assays involving the use of synthetic DNA substrates and cruciform-containing plasmids.



## 1. INTRODUCTION

Structure-selective endonucleases that process recombination intermediates, such as Holliday junctions (HJs) have been identified from various organisms, including bacteriophage (T4 endonuclease VII, T7 endonuclease I) (de Massy, Weisberg, & Studier, 1987; Mizuuchi, Kemper, Hays, & Weisberg, 1982), bacteria (*Escherichia coli* RuvC) (Connolly et al., 1991; Dunderdale et al., 1991; Iwasaki, Takahagi, Shiba, Nakata, & Shinagawa, 1991), yeast (mitochondrial resolvase Cce1, nuclear resolvase Yen1) (Fogg, Schofield, Declais, & Lilley, 2000; Ip et al., 2008; Kleff, Kemper, & Sternglanz, 1992), plants (*Arabidopsis thaliana* AtGEN1 and AtSEND1, chloroplast resolvase AtMOC1) (Bauknecht & Kobbe, 2014; Kobayashi et al., 2017), archaea (*Pyrococcus furiosus* Hjc) (Komori, Sakae, Shinagawa, Morikawa, & Ishino, 1999), fungi (*Chaetomium thermophilum* CtGEN1) (Freeman, Liu, Declais, Gartner, & Lilley, 2014), and humans (GEN1) (Ip et al., 2008).

Although the resolvases share very little sequence homology, they do share a common mechanism of HJ resolution (Wyatt & West, 2014). For example, (i) their active sites contain three or four negatively charged amino acids that are required for metal binding and catalysis, (ii) catalytic activity requires a divalent metal ion, usually  $Mg^{2+}$ , (iii) all resolvases are homodimers that bind specifically to junctions, and (iv) the two active sites introduce a pair of symmetrically related nicks in the strands that lie diametrically opposed across the junction point. Importantly, all Holliday junction resolvases mediate bilateral cleavage within the lifetime of the protein–HJ complex.

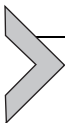
Previously, we identified GEN1, a member of the Rad2/XPG nuclease family, as a human HJ resolvase (Ip et al., 2008). GEN1 orthologs are present in most higher eukaryotes, including rice (*Oryza sativa* OsSEND-1) (Furukawa et al., 2003), worms (*Caenorhabditis elegans* GEN1) (Bailly et al., 2010), and flies (*Drosophila melanogaster* DmGEN1/mus309) (Andersen, Kuo, Savukoski, Brodsky, & Sekelsky, 2011; Ishikawa et al., 2004). Although budding yeast *Saccharomyces cerevisiae* has a GEN1 ortholog (Yen1) (Ip et al., 2008), the fission yeast *Schizosaccharomyces pombe* does not.

The domain architecture of human GEN1 contains three characteristic motifs: the N-terminal (N) and internal (I) XPG nuclease domains, and a helix-hairpin-helix (HhH) domain that is important for DNA binding (Ip et al., 2008; Rass et al., 2010). While the core of the protein is structurally similar to that found in other Rad2/XPG nucleases (Williams & Kunkel, 2011), GEN1 contains a chromodomain as an additional DNA interaction site

(Lee et al., 2015; Liu et al., 2015). The large C-terminal tail appears to be disordered and has no known function (Ip et al., 2008; Rass et al., 2010). In contrast to other resolvases which are constitutive homodimers, GEN1 is monomeric in solution and dimerizes upon binding to the HJ (Chan & West, 2015; Liu et al., 2015; Rass et al., 2010).

GEN1 promotes HJ resolution in a manner that resembles RuvC-mediated junction cleavage: it introduces a pair of symmetrically related nicks across the junction within the lifetime of the enzyme–HJ complex to produce ligatable nicked linear duplex products (Chan & West, 2015; Ip et al., 2008; Rass et al., 2010). Cleavage involves relaxation of the junction, such that second strand cleavage is accelerated by introduction of the first nick to ensure a productive resolution event (Liu et al., 2015). In addition to its structure specificity, GEN1 exhibits a weak sequence preference (Shah Punatar, Martin, Wyatt, Chan, & West, 2017). In addition to the resolution of HJs, GEN1 promotes the cleavage of 5'-flaps and replication fork (RF) structures in vitro, but is inactive on 3'-flaps, splayed-arm structures, or duplex DNA. Cleavage reactions with flap/fork DNAs are likely to be mediated by the monomeric form of GEN1 (Bellendir et al., 2017).

Here, we describe protocols for the purification and characterization of GEN1 protein. We detail: (i) the purification of recombinant human GEN1 following expression in yeast cells; (ii) the generation and use of synthetic DNA substrates to analyze GEN1's substrate specificity; and (iii) the use of cruciform plasmid DNAs to demonstrate the coordinated dual incisions mediated by GEN1.



---

## 2. PURIFICATION OF GEN1

### 2.1 Protein Expression

To express full-length GEN1, we employed the yeast *GAL1* expression system. The coding sequence of GEN1 with a C-terminal FLAG tag (AGDYKDDDDK) was first shuttled into a pDONOR221 vector using a BP Gateway recombination reaction (Thermo Fisher Scientific). Note that it is important not to use N-terminal affinity tags as these inactivate the nuclease activity of GEN1. GEN1-FLAG was then shuttled into the pYES-DEST52 yeast expression vector using a LR Gateway recombination reaction (Thermo Fisher Scientific). The Gateway recombination steps were performed according to Thermo Fisher's protocol. The pYES-DEST52 plasmid contains: (i) a *GAL1* promoter for high-level, galactose-inducible protein expression in *S. cerevisiae*; (ii) a *URA3* auxotrophic marker for selecting yeast transformants; and (iii) V5 epitope and 6 × His affinity tags.

The final plasmid expresses GEN1-FLAG-V5-6 × His and is available on request from S. West. The yeast cells are cultured in synthetic complete (SC)-Ura/2% Raffinose medium before protein induction. The advantage of using raffinose as the carbon source is that it does not inhibit transcription from the *GAL* promoter. Therefore, transcription of GEN1 can be induced directly by adding galactose to the growth medium (Fig. 1A).

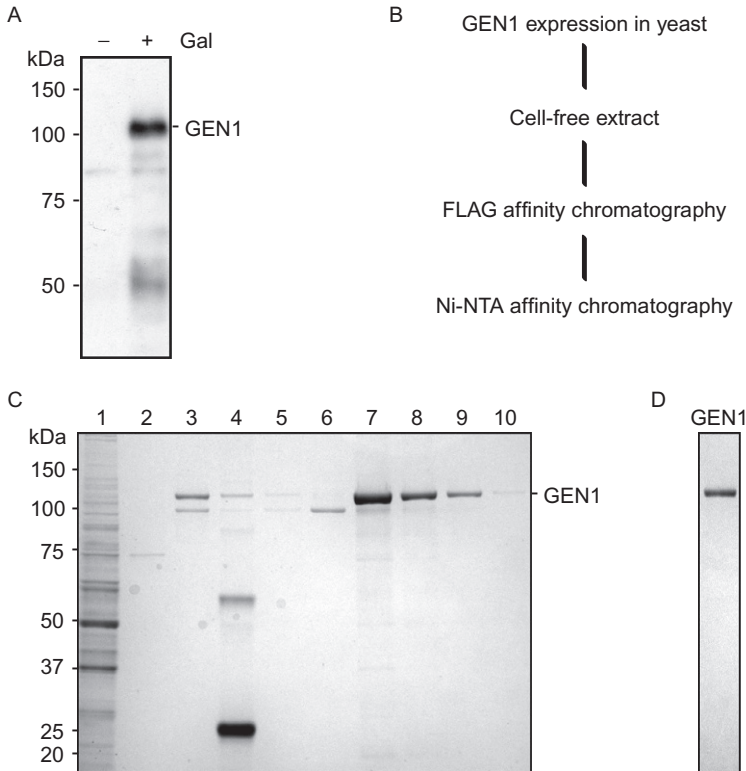


**Fig. 1** Purification of recombinant GEN1 following expression in yeast. (A) Yeast cells transformed with the GEN1 plasmid were grown in media with or without 2% galactose (Gal) for 16 h. Extracts were prepared and analyzed for GEN1 by Western blotting. (B) Overview of the purification scheme. (C) Purification of GEN1. Lane 1: Whole cell extract prepared from yeast cells expressing GEN1; lane 2: flow through following the ATP wash; lane 3: FLAG elute from the M2 agarose after the ATP wash; lane 4: proteins remaining bound to the M2 agarose after FLAG elution; lane 5: Ni-NTA agarose flow through after application of the FLAG-eluted GEN1; lane 6: flow through of His wash buffer 2; lanes 7–10: the elutes from the Ni-NTA agarose. Samples were analyzed by SDS-PAGE and stained with InstantBlue. (D) Purified GEN1 was analyzed by SDS-PAGE and stained with InstantBlue.

### 2.1.1 Yeast Transformation

- *S. cerevisiae* W303 strain
- YPD broth (dissolve 20 g peptone, 10 g yeast extract, and 20 g glucose in 1 L water and sterilize by autoclaving).
- Yeast transformation solution: 1 M lithium acetate and 1 M sorbitol
- 50% (v/v) polyethylene glycol (PEG)
- Salmon sperm DNA solution (Thermo Fisher 15632011)
- Dimethylsulfoxide (DMSO)
- SC-Ura plates: To prepare 1 L, dissolve 44.9 g of SD agar/2% (w/v) glucose (Formedium CSM0105) and 0.77 g of CSM-Ura single drop-out (Formedium DCS0169) in water and sterilize by autoclaving. Fill sterile Petri dishes with ~25 mL of autoclaved medium

#### Protocol

1. Grow 50 mL of W303 yeast cells in YPD medium at 30°C overnight.
2. Dilute the culture with YPD broth to ~0.2 OD<sub>600</sub> and continue growth until OD<sub>600</sub> reaches ~0.7–1.0.
3. Centrifuge the cells at 2500 rpm and discard the medium.
4. Resuspend the cell pellet in 10 mL of yeast transformation solution and then spin down at 2500 rpm.
5. Remove most of the solution before resuspending the cells in the remaining liquid.
6. Mix the following reagents in a 1.5-mL Eppendorf tube: (i) 100 µL of yeast cells; (ii) 0.1 µg GEN1 plasmid DNA; (iii) 280 µL 50% (v/v) PEG; (iv) 15 µL salmon sperm DNA (the sperm DNA is first denatured by boiling for 10 min and then cooled on ice).
7. Incubate the transformation mixture at room temperature for 40 min, and then add 40 µL of DMSO. The mixture is then incubated at 42°C for 15 min.
8. Centrifuge the solution at 2000 rpm for 2 min and resuspend the pellet in ~150 µL of water.
9. Spread the yeast cells on a SC-Ura plate and incubate for 2–3 days at 30°C.
10. Pick a few colonies and streak on a new SC-Ura plate. Let the colonies grow for 2 days to enable the isolation of single colony.

### 2.1.2 Growth and Lysis of Yeast Cells

- SC-Ura/2% Raffinose medium: For 1 L, dissolve 26.9 g SD Broth/2% Raffinose (Formedium CSM0605) and 0.77 g of CSM-Ura single drop-out (Formedium DCS0169) in water and sterilize by filtration

- Galactose
- Lysis buffer: 40 mM Tris-HCl pH 7.5, 500 mM NaCl, 10% (v/v) glycerol, 2 mM EDTA, 0.1% (v/v) NP-40, 1 mM dithiothreitol. Add 1 tablet of Complete EDTA-free Protease Inhibitor Cocktail (Sigma 000000011873580001) per 20 mL of buffer

### Protocol

1. Pick a single colony from the SC-Ura plate and grow the cells in ~200 mL SC-Ura/2% Raffinose medium overnight. Next day, dilute the culture and scale up to 5 L.
2. Grow the cells to an  $OD_{600} \approx 1.0$ , and then add 2% (w/v) galactose to the culture for 16 h to induce expression of GEN1.
3. Harvest the cells and wash once with lysis buffer, and then resuspend the cell pellet in 2–3 volumes of lysis buffer.
4. Disrupt the yeast cells using a freezer mill (SPEX CertiPrep 6850).

## 2.2 Protein Purification

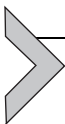
The purification of recombinant GEN1 was performed by a simple two-step affinity purification procedure using FLAG agarose and Ni-NTA agarose (Fig. 1B–D) The concentration of GEN1 was measured by Bradford protein assay (Bio-Rad).

### 2.2.1 Reagents

- Anti-FLAG M2 Affinity Agarose Gel (Sigma-Aldrich A2220)
- Lysis buffer (see Section 2.1.2)
- ATP wash buffer: 40 mM Tris-HCl pH 7.5, 500 mM NaCl, 10% (v/v) glycerol, 0.1% (v/v) NP-40, 1 mM dithiothreitol, 1 mM ATP, and 3 mM  $MgCl_2$
- FLAG elution buffer: lysis buffer without EDTA, supplemented with 0.5 mg/mL 3 × FLAG peptide and 10 mM imidazole
- Ni-NTA agarose (Qiagen 30210)
- His wash buffer 1: lysis buffer without EDTA, supplemented with 10 mM imidazole
- His wash buffer 2: lysis buffer without EDTA, supplemented with 25 mM imidazole
- His elution buffer: lysis buffer without EDTA, supplemented with 300 mM imidazole
- Dialysis buffer: 40 mM Tris-HCl pH 7.5, 250 mM NaCl, 10% (v/v) glycerol, 0.1 mM EDTA, 0.05% (v/v) NP-40, and 1 mM dithiothreitol
- InstantBlue Protein Stain (Expedeon ISB1L)

### 2.2.2 Protocol

1. Resuspend the cell powder from the freezer mill in  $\sim 200$  mL lysis buffer.
2. Clear the lysate by ultracentrifugation at 40,000 rpm for 40 min using Ti45 rotor (Beckman Coulter).
3. Add 0.4 mL anti-FLAG M2 affinity agarose gel to the cleared lysate and incubate the mixture in a rotator in the cold room for 1 h. Prior to addition to the cleared lysate, the M2 agarose needs to be washed twice in lysis buffer.
4. Transfer the lysate into 50-mL falcon tubes and spin at 1000 rpm for 1 min to recover the M2 agarose. The M2 agarose is then washed thoroughly  $2 \times$  with lysis buffer.
5. Resuspend the M2 agarose in  $\sim 5$  mL of lysis buffer and load it into a Poly-Prep chromatography column (Bio-Rad 7311550). Allow the buffer to flow through the column by gravity.
6. Wash the M2 agarose with 5 mL of ATP wash buffer and then wash again with 5 mL of lysis buffer. This ATP elution step helps to dissociate heat shock proteins and other contaminants.
7. Elute GEN1 with 0.5 mL of FLAG elution buffer twice.
8. Incubate the FLAG elute with 100  $\mu$ L Ni-NTA agarose. Prior to use, the Ni-NTA agarose needs to be washed  $2 \times$  in His wash buffer.
9. Load the mixture into a Bio-Spin chromatography column (Bio-Rad 7326008). Allow the solution to flow through by gravity.
10. Wash the Ni-NTA agarose with 2 mL of His wash buffer 1 followed by His wash buffer 2.
11. Elute the protein from the Ni-NTA agarose using four washes of 100  $\mu$ L of His elution buffer. The fractions are then analyzed by SDS-PAGE, and the gel is stained with InstantBlue.
12. Select the fractions that contain GEN1.
13. Transfer the protein to a Slide-A-Lyzer dialysis cassette G2 (Thermo Fisher 87729) and dialyze overnight against 2 L of dialysis buffer in the cold room.
14. Aliquot the protein and fast freeze in liquid nitrogen. The aliquots are then stored at  $-80^\circ\text{C}$ .



## 3. CLEAVAGE OF SYNTHETIC DNA SUBSTRATES

Small synthetic DNAs provide simple substrates for the analysis of nuclease activities. Synthetic Holliday junctions may be generated by annealing four partially complementary oligonucleotides. For the method

described here, we prepare immobile HJs in which all four arms are composed of heterologous sequences, such that the junction point is fixed and cannot branch migrate. To demonstrate the broad substrate specificity of GEN1, we made other DNA structures including RFs and 5'-flaps (shown schematically in Fig. 2A). Linear duplex and single-stranded DNA (ssDNA) serve as controls, as they are not cut by GEN1. The HJ is made from four oligonucleotides, X0-1, X0-2, X0-3, and X0-4 (each 60 nucleotides in length). The duplex DNA consists of X0-1 and X0-4; the RF consists of X0-1, the first half of X0-2 and X0-3 (named X0-2(1/2) and X0-3(1/2), respectively, each 30 nucleotides in length), and X0-4; the 5'-flap comprises X0-1, X0-2(1/2), and X0-4 (Table 1). The X0-1 oligo is common to all other substrates and should be 5'-<sup>32</sup>P-end-labeled prior to annealing. This allows the easy detection of the substrates and cleavage products.

Since commercially available oligonucleotides that are 60n in length also contain shortened species (e.g., 59n, 58n, etc.), it is important to purify X0-1 by denaturing PAGE before annealing it to the other oligonucleotides. After annealing, each DNA substrate is then purified by neutral PAGE to remove any incomplete DNA species formed during the annealing process.

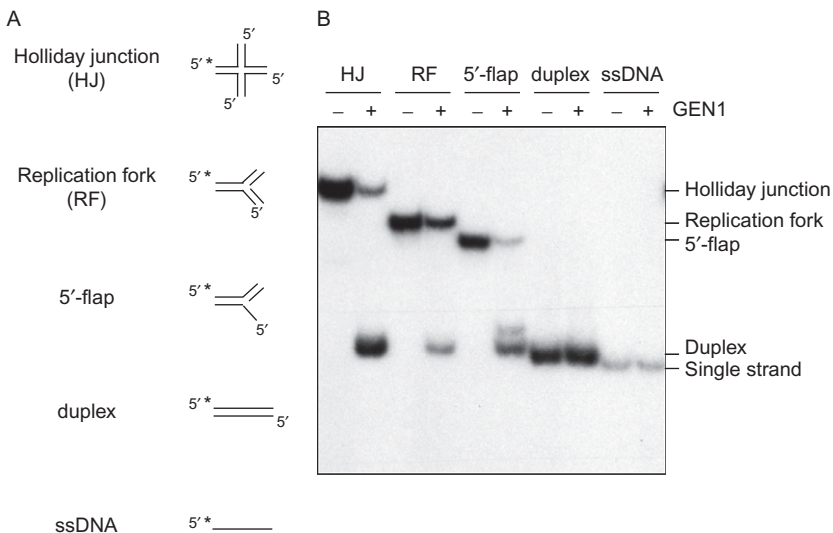


**Fig. 2** Cleavage of synthetic DNA substrates by GEN1. (A) Schematic diagrams indicating the synthetic DNA substrates, 5'-<sup>32</sup>P-end labels are indicated with *asterisks*. (B) The indicated DNA substrates (~1 nM) were incubated with or without GEN1 (10 nM) for 5 min. Products were analyzed by neutral PAGE and visualized by autoradiography.

**Table 1** Oligonucleotides Used to Prepare the Model DNA Substrates

| <i>Oligonucleotides</i> | <i>Sequence (5'–3')</i>  |
|-------------------------|--|
| X0-1                    | ACGCTGCCGAATTCTACCAGTGCCTTGCTAGGACA<br>TCTTTGCCACCTGCAGGTTACCC   |
| X0-2                    | GGGTGAACCTGCAGGTGGGCAAAGATGTCCATCTG<br>TTGTAATCGTCAAGCTTTATGCCGT |
| X0-3                    | ACGGCATAAAGCTTGACGATTACAACAGATCATG<br>GAGCTGTCTAGAGGATCCGACTATCG |
| X0-4                    | CGATAGTCGGATCCTCTAGACAGCTCCATGTAGCA<br>AGGCACTGGTAGAATTCGGCAGCGT |
| X0-2(1/2)               | GGGTGAACCTGCAGGTGGGCAAAGATGTCC                                   |
| X0-3(1/2)               | CATGGAGCTGTCTAGAGGATCCGACTATCG                                   |
| <i>Substrates</i>       | <i>Oligonucleotides used for each DNA substrate</i>              |
| ssDNA                   | X0-1   |
| Duplex                  | X0-1 + X0-4  |
| 5'-flap                 | X0-1 + X0-2(1/2) + X0-4  |
| RF                      | X0-1 + X0-2(1/2) + X0-3(1/2) + X0-4                              |
| HJ                      | X0-1 + X0-2 + X0-3 + X0-4  |

Once prepared, each labeled DNA substrate is incubated individually with purified GEN1 protein. GEN1 cleaves the RF, 5'-flap, and HJ as indicated by the appearance of faster-migrating products after neutral PAGE (Fig. 2B). This result shows that GEN1 cuts a variety of recombination/replication intermediates in preparation for chromosome segregation.

## 3.1 Oligonucleotide Purification

### 3.1.1 Reagents

- 10× TBE: 108 g Tris base, 55 g boric acid and 9.3 g EDTA in 1 L water
- 15% Urea–acrylamide gel: 75 mL of 7 M urea, 29.5 mL acrylamide (19:1, 40%, Bio-Rad), 7.5 mL 10× TBE, 450 μL 10% (w/v) ammonium persulfate (APS), 36 μL TEMED, and 15.5 mL water
- Loading buffer: 90% (w/v) formamide, 0.1% (w/v) bromophenol blue, and 0.1% (w/v) xylene cyanol in 1× TBE
- TE: 10 mM Tris–HCl pH 8.0, 1 mM EDTA

- “Stains-all” staining solution: 0.005% (w/v) Stains-All (Sigma E9379), 10% (v/v) formamide, 25% (v/v) isopropanol, 15 mM Tris-HCl pH 8.8, and 65% (v/v) water

### 3.1.2 Protocol

1. Set up a 15% urea-acrylamide gel using a Bio-Rad protean II xi cell system (20 cm gel length, 1.5 mm thick gel).
2. Prerun the gel at 400–450 V, 30 mA, 15 W, for ~1 h.
3. Dissolve oligonucleotide X0-1 in water at 200  $\mu$ M, and then mix 35  $\mu$ L of X0-1 with an equal volume of loading buffer.
4. Boil for 2 min and load the sample on a warm, prerun gel. Run the gel for 2–3 h at ~15 W.
5. Remove the gel and stain with “Stains-all” solution.
6. Cut out the upper half of the gel band (to avoid smaller species) and elute the oligonucleotide into 1 mL TE on a rotator at room temperature overnight.
7. Ethanol-precipitate the oligonucleotide.
8. Dissolve the pellet in 60  $\mu$ L TE, measure the concentration of the DNA by spectrophotometer (1 OD<sub>260</sub> = 33  $\mu$ g/mL), and adjust the volume to get a 10  $\mu$ M stock solution.

## 3.2 Preparation of <sup>32</sup>P-Labeled DNA Substrates

### 3.2.1 Reagents

- [ $\gamma$ -<sup>32</sup>P] ATP (10 mCi/mL, PerkinElmer NEG026250UC)
- T4 polynucleotide kinase (T4 PNK) and PNK 10  $\times$  buffer (NEB M0201)
- MicroSpin G-25 column (GE Healthcare 27-5325-01)
- Native gel loading buffer: 50% (v/v) glycerol, 0.1% (w/v) bromophenol blue, and 0.1% (w/v) xylene cyanol in 1  $\times$  TBE
- 12% Neutral acrylamide/bis-acrylamide (37.5:1) gel: 30 mL acrylamide (37.5:1, 30%, Bio-Rad), 7.5 mL 10  $\times$  TBE, 37.5 mL water, 900  $\mu$ L 10% APS, and 45  $\mu$ L TEMED. Stand gel in cold room
- Phosphorescent TrackerTape (GE Healthcare RPN2050)
- TMgN buffer: 10 mM Tris-HCl pH 8.0, 1 mM MgCl<sub>2</sub>, and 50 mM NaCl

### 3.2.2 Protocol

1. Label the 5' end of gel-purified X0-1 with <sup>32</sup>P using the following reaction mixture: 0.5  $\mu$ L of 10  $\mu$ M gel-purified X0-1, 1  $\mu$ L of 10  $\times$  T4 PNK

buffer, 2  $\mu\text{L}$  of T4 PNK, 3  $\mu\text{L}$  of [ $\gamma$ - $^{32}\text{P}$ ] ATP, 3.5  $\mu\text{L}$  water (total 10  $\mu\text{L}$ ). Incubate the mixture at 37°C water bath for 45 min.

2. Terminate the labeling reaction by addition of 60  $\mu\text{L}$  of  $1 \times$  T4 PNK buffer and 1  $\mu\text{L}$  0.5 M EDTA.
3. Remove unincorporated label using the MicroSpin G-25 column. To do this, load the terminated labeling mixture on top of the resin and spin at 3000 rpm for 2 min. The elute contains the 5'- $^{32}\text{P}$ -labeled X0-1 oligonucleotide.
4. Oligonucleotide X0-1 is then supplemented with a threefold excess of each of the other partner oligonucleotides (300 ng each, dissolve the oligonucleotides in water at 10  $\mu\text{M}$  and add 1.5  $\mu\text{L}$  each to the elute).
5. Heat the mixture in a boiling water bath. After 2 min, switch off the water bath and allow it to cool slowly overnight to room temperature.
6. Add 15  $\mu\text{L}$  of native gel loading buffer to the mixture and apply to a 12% neutral acrylamide/bis-acrylamide gel using a Bio-Rad protean II xi cell system (20 cm gel length, 1.5 mm gel thickness). Run for 4–5 h at 200 V at cold room in  $1 \times$  TBE.
7. After finishing the run, remove one gel plate and overlay the gel with plastic wrap. Mark a corner of the gel with phosphorescent TrackerTape and expose to Kodak BioMax MR film for 2 min. The TrackerTape helps with precise alignment of the gel on the film.
8. Excise the substrate bands using a sharp blade and transfer each gel slice to a screw-capped 1.5-mL Eppendorf.
9. Add 300  $\mu\text{L}$  of TMgN buffer and elute overnight with gentle shaking in the cold room. To facilitate the diffusion of the DNA to the buffer, the gel slices can be fragmented into smaller pieces using a small plastic rod. The concentration of the resulting substrate should be  $\sim 20 \text{ nM}$ .

### 3.3 DNA Cleavage Assays

#### 3.3.1 Reagents

- 10  $\times$  cleavage buffer: 500 mM Tris-HCl pH 7.5, 10 mM  $\text{MgCl}_2$ , and 10 mM dithiothreitol
- Stop buffer: 100 mM Tris-HCl pH 7.5, 50 mM EDTA, 2.5% (w/v) SDS, and 10 mg/mL proteinase K (Promega V3201)
- 10% Neutral acrylamide/bis-acrylamide (37.5:1) gel: 10 mL acrylamide (37.5:1, 30%, Bio-Rad), 3 mL 10  $\times$  TBE, 27 mL water, 105  $\mu\text{L}$  10% APS, and 25  $\mu\text{L}$  TEMED

### 3.3.2 Protocol

1. Set up a 10  $\mu$ L cleavage reaction containing  $\sim$ 1 nM DNA substrate in 1  $\times$  cleavage buffer. Start the reaction by addition of 10 nM GEN1.
2. Incubate 37°C for 5 min.
3. Add 2.5  $\mu$ L of stop buffer and incubate at 37°C for 30 min to deproteinize the DNA products.
4. Add 3  $\mu$ L of native loading buffer and load onto a 10% neutral acrylamide/bis-acrylamide gel (10 cm long, 0.5 mm thick gel). Run for 1.5–2 h at 120 V at room temperature in 1  $\times$  TBE.
5. Dry the gel and expose to a BioMax MR film with a BioMax MS intensifying screen (Sigma) for 1 h to overnight at  $-80^{\circ}\text{C}$ .



## 4. CLEAVAGE OF CRUCIFORM-CONTAINING PLASMIDS BY GEN1

HJ resolvases are generally homodimers that bind to the junction and mediate bilateral cleavage within the lifetime of the enzyme–HJ complex. This unique property of HJ resolution can be elegantly demonstrated using a plasmid that contains an inverted repeat sequence that extrudes to form a cruciform structure. The cruciform plasmid used here is pIRbke8<sup>mut</sup> (Rass et al., 2010), a derivative of pIRbke8 (Fogg & Lilley, 2000; Giraud-Panis & Lilley, 1997) (Fig. 3). The plasmid is available on request from the West lab. Coordinated bilateral cleavage of the cruciform by GEN1 generates a linear DNA product with hairpin termini (Figs. 3 and 4A). When reactions are carried out using a mixture of wild-type GEN1 and catalytically dead GEN1<sup>EEAA</sup> (GEN1<sup>EEAA</sup> was generated by mutating the two active site residues E134 and E136 to alanine) (Chan & West, 2015), the GEN1–GEN1<sup>EEAA</sup> heterodimer makes a single incision to generate nicked circular products (Figs. 3 and 4B). This assay therefore provides a good demonstration of the coordinated cleavage reaction that occurs during HJ resolution.

## 4.1 Plasmid Cleavage Assays

### 4.1.1 Reagents

- pIRbke8<sup>mut</sup> (3683 bp) is propagated in *E. coli* DH5-Alpha and isolated in supercoiled form using a Qiagen Plasmid Maxi Kit.
- The catalytic-dead version of GEN1, GEN1<sup>EEAA</sup> (Chan & West, 2015), is purified by a procedure similar to that described for GEN1.
- Cruciform extrusion buffer: 50 mM Tris–HCl pH 7.5, 50 mM NaCl, and 0.1 mM EDTA

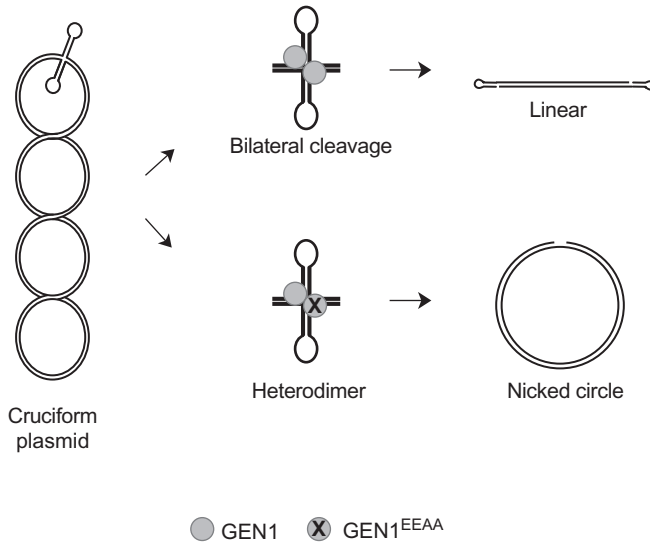


**Fig. 3** Schematic representation of the cruciform cleavage assay used to determine whether GEN1 dimerizes at the junction to introduce coordinated dual incisions within the lifetime of the protein–HJ complex. Bilateral cleavage at the junction point results in the formation of linear products that have hairpin termini. The presence of catalytically dead GEN1, GEN1<sup>E<sup>EAA</sup></sup>, leads to the formation of GEN1–GEN1<sup>E<sup>EAA</sup></sup> dimers that can only introduce a single nick at the junction point. The resolution product in this case is nicked plasmid DNA.

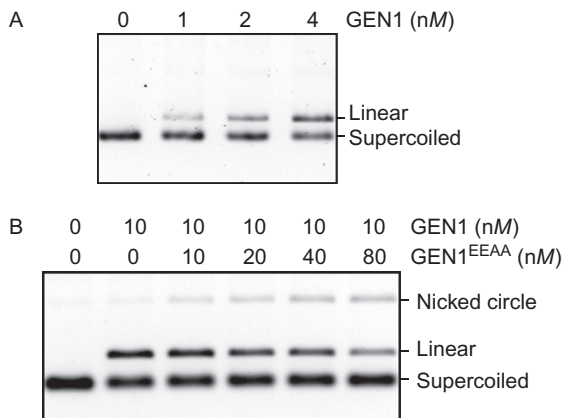
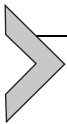


**Fig. 4** Cleavage of the cruciform plasmid by GEN1. (A) Plasmid pIRbke8<sup>mut</sup> (1 nM) was incubated with the indicated concentration of GEN1 for 20 min at 37°C. Products were analyzed by agarose gel electrophoresis. (B) Plasmid pIRbke8<sup>mut</sup> (1 nM) was incubated with the indicated concentrations of GEN1 and GEN1<sup>E<sup>EAA</sup></sup> for 5 min at 37°C. Products were analyzed by agarose gel electrophoresis.

- 0.8% Agarose gel: dissolve 0.8 g of UltraPure agarose (Thermo Fisher 16500100) in  $1 \times$  TBE
- SYBR Gold nucleic acid stain (Thermo Fisher S11494)
- $6 \times$  DNA loading dye (Thermo Fisher R0611)

#### 4.1.2 Protocol

1. To induce cruciform extrusion, pIRbke8<sup>mut</sup> plasmid DNA is incubated in extrusion buffer (at  $50 \text{ ng}/\mu\text{L}$ ,  $\sim 20 \text{ nM}$ ) for 90 min at  $37^\circ\text{C}$ .
2. Set up a  $10 \mu\text{L}$  cleavage reaction with GEN1 protein (wild type alone or together with GEN1<sup>EEAA</sup>) and  $1 \text{ nM}$  pIRbke8<sup>mut</sup> plasmid in cleavage buffer (see Section 3.3.2). Incubate for 5–20 min at  $37^\circ\text{C}$
3. Deproteinize the DNA products by addition of  $2.5 \mu\text{L}$  of stop buffer (see Section 3.3.2) and incubation at  $37^\circ\text{C}$  for 30 min
4. Add  $2.5 \mu\text{L}$   $6 \times$  DNA loading dye to the samples and load them onto a 0.8% agarose gel. Run at 90 V for 90 min in  $1 \times$  TBE using a Bio-Rad mini-Sub cell GT gel tank.
5. Stain the gel with SYBR Gold nucleic acid stain (1:10,000 in  $1 \times$  TBE) for 40 min, wash the gel with  $1 \times$  TBE, and image it with a Bio-Rad Gel Doc XR+ System.



## 5. SUMMARY

The yeast expression system with an inducible *GAL* promoter leads to good expression of GEN1, and the FLAG- and His-tags enable purification to homogeneity by a simple two-step procedure. The use of synthetic DNA substrates generated by annealing oligonucleotides is well established as a means to produce good quality substrates that model DNA recombination and replication intermediates. Although the DNAs used here are labeled with  $^{32}\text{P}$ , which provides the best method of analysis to date, it is also possible to use fluorescent tags in place of radioactive label (Matos & West, 2017). Cruciform containing plasmids also provide a quick and easy way to investigate mechanisms of cleavage, as true resolvases give rise to the characteristic signature of bilateral cleavage. The protocols described here can be adapted for the study of other cellular endonucleases.

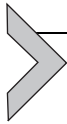
## ACKNOWLEDGMENTS

Work in the author's laboratory is supported by the Francis Crick Institute (FC10212), the European Research Council (ERC-ADG-66640), and the Louis-Jeantet Foundation. The Francis Crick Institute receives core funding from Cancer Research UK, the Medical Research Council, and the Wellcome Trust.

## REFERENCES

- Andersen, S. L., Kuo, H. K., Savukoski, D., Brodsky, M. H., & Sekelsky, J. (2011). Three structure-selective endonucleases are essential in the absence of BLM helicase in *Drosophila*. *PLoS Genetics*, *7*, e1002315.
- Bailly, A. P., Freeman, A., Hall, J., Declais, A. C., Alpi, A., Lilley, D. M. J., et al. (2010). The *Caenorhabditis elegans* homolog of Gen1/Yen1 resolves links DNA damage signaling to DNA double-strand break repair. *PLoS Genetics*, *6*, e1001025.
- Bauknecht, M., & Kobbe, D. (2014). AtGEN1 and AtSEND1, two paralogs in *Arabidopsis*, possess Holliday junction resolvase activity. *Plant Physiology*, *166*, 202–216.
- Bellendir, S. P., Rogstad, D. J., Morris, L. P., Zapotoczny, G., Walton, W. G., Redinbo, M. R., et al. (2017). Substrate preference of Gen endonucleases highlights the importance of branched structures as DNA damage repair intermediates. *Nucleic Acids Research*, *45*, 5333–5348.
- Chan, Y. W., & West, S. C. (2015). GEN1 promotes Holliday junction resolution by a coordinated nick and counter-nick mechanism. *Nucleic Acids Research*, *43*, 10882–10892.
- Connolly, B., Parsons, C. A., Benson, F. E., Dunderdale, H. J., Sharples, G. J., Lloyd, R. G., et al. (1991). Resolution of Holliday junctions *in vitro* requires the *Escherichia coli* *ruvC* gene product. *Proceedings of the National Academy of Sciences of the United States of America*, *88*, 6063–6067.
- de Massy, B., Weisberg, R. A., & Studier, F. W. (1987). Gene 3 endonuclease of bacteriophage T7 resolves conformationally branched structures in double-stranded DNA. *Journal of Molecular Biology*, *193*, 359–376.
- Dunderdale, H. J., Benson, F. E., Parsons, C. A., Sharples, G. J., Lloyd, R. G., & West, S. C. (1991). Formation and resolution of recombination intermediates by *E. coli* RecA and RuvC proteins. *Nature*, *354*, 506–510.
- Fogg, J. M., & Lilley, D. M. J. (2000). Ensuring productive resolution by the junction-resolving enzyme RuvC: Large enhancement of the second-strand cleavage rate. *Biochemistry*, *39*, 16125–16134.
- Fogg, J. M., Schofield, M. J., Declais, A. C., & Lilley, D. M. J. (2000). Yeast resolving enzyme CCE1 makes sequential cleavages in DNA junctions within the lifetime of the complex. *Biochemistry*, *39*, 4082–4089.
- Freeman, A. D. J., Liu, Y., Declais, A. C., Gartner, A., & Lilley, D. M. J. (2014). GEN1 from a thermophilic fungus is functionally closely similar to non-eukaryotic junction-resolving enzymes. *Journal of Molecular Biology*, *426*, 3946–3959.
- Furukawa, F., Kimura, M., Ishibashi, T., Mori, Y., Hashimoto, J., & Sakaguchi, K. (2003). OsSEND-1: A new RAD2 nuclease family member in higher plants. *Plant Molecular Biology*, *51*, 59–70.
- Giraud-Panis, M. J. E., & Lilley, D. M. J. (1997). Near simultaneous DNA cleavage by the subunits of the junction-resolving enzyme T4 endonuclease VII. *The EMBO Journal*, *16*, 2528–2534.
- Ip, S. C. Y., Rass, U., Blanco, M. G., Flynn, H. R., Skehel, J. M., & West, S. C. (2008). Identification of Holliday junction resolvases from humans and yeast. *Nature*, *456*, 357–361.
- Ishikawa, G., Kanai, Y., Takata, K., Takeuchi, R., Shimanouchi, K., Ruike, T., et al. (2004). DmGEN, a novel RAD2 family endo-exonuclease from *Drosophila melanogaster*. *Nucleic Acids Research*, *32*, 6251–6259.
- Iwasaki, H., Takahagi, M., Shiba, T., Nakata, A., & Shinagawa, H. (1991). *Escherichia coli* RuvC protein is an endonuclease that resolves the Holliday structure. *The EMBO Journal*, *10*, 4381–4389.
- Kleff, S., Kemper, B., & Sternglanz, R. (1992). Identification and characterization of yeast mutants and the gene for a cruciform cutting endonuclease. *The EMBO Journal*, *11*, 699–704.

- Kobayashi, Y., Misumi, O., Odahara, M., Ishibashi, K., Hirono, M., Hidaka, K., et al. (2017). Holliday junction resolvases mediate chloroplast nucleoid segregation. *Science*, *356*, 631–634.
- Komori, K., Sakae, S., Shinagawa, H., Morikawa, K., & Ishino, Y. (1999). A Holliday junction resolvase from *Pyrococcus furiosus*: Functional similarity to *Escherichia coli* RuvC provides evidence for conserved mechanism of homologous recombination in bacteria, eukarya, and archaea. *Proceedings of the National Academy of Sciences of the United States of America*, *96*, 8873–8878.
- Lee, S.-H., Princz, L. N., Klügel, M. F., Habermann, B., Pfänder, B., & Biertümpfel, C. (2015). Human Holliday junction resolvase GEN1 uses a chromodomain for efficient DNA recognition and cleavage. *eLife*, *4*, e12256.
- Liu, Y., Freeman, A. D. J., Déclais, A.-C., Wilson, T. J., Gartner, A., & Lilley, D. M. J. (2015). Crystal structure of a eukaryotic GEN1 resolving enzyme bound to DNA. *Cell Reports*, *13*, 2565–2575.
- Matos, J., & West, S. C. (2017). Analysis of structure-selective endonuclease activities from yeast and human extracts. In B. F. Eichman (Ed.), *Methods in enzymology: Vol. 591* (pp. 271–286). Burlington: Academic Press.
- Mizuuchi, K., Kemper, B., Hays, J., & Weisberg, R. A. (1982). T4 endonuclease VII cleaves Holliday structures. *Cell*, *29*, 357–365.
- Rass, U., Compton, S. A., Matos, J., Singleton, M. R., Ip, S. C. Y., Blanco, M. G., et al. (2010). Mechanism of Holliday junction resolution by the human GEN1 protein. *Genes & Development*, *24*, 1559–1569.
- Shah Punatar, R., Martin, M. J., Wyatt, H. D., Chan, Y. W., & West, S. C. (2017). Resolution of single and double Holliday junction recombination intermediates by GEN1. *Proceedings of the National Academy of Sciences of the United States of America*, *114*, 443–450.
- Williams, R. S., & Kunkel, T. A. (2011). FEN1 nucleases: Bind, bend, fray, cut. *Cell*, *145*, 171–172.
- Wyatt, H. D. M., & West, S. C. (2014). Holliday junction resolvases. *Cold Spring Harbor Perspectives in Biology*, *6*, a023192.



# Biochemical and Structural Properties of Fungal Holliday Junction-Resolving Enzymes

Yijin Liu, Alasdair Freeman, Anne-Cécile Déclais, Anton Gartner<sup>2</sup>,  
David M.J. Lilley<sup>1</sup>

Cancer Research UK Nucleic Acid Structure Research Group, The University of Dundee, Dundee, United Kingdom

<sup>1</sup>Corresponding author: e-mail address: d.m.j.lilley@dundee.ac.uk

## Contents

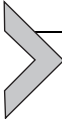
|   |     |
|---|-----|
| 1. Holliday Junctions and Their Resolution  | 544 |
| 2. The Resolution Process   | 544 |
| 3. A Mechanism Ensuring Productive Junction Resolution                                    | 546 |
| 4. Processing of Holliday Junctions in Eukaryotes   | 550 |
| 5. Genes for the FEN1/XPG1 Superfamily in Thermophilic Fungi                              | 551 |
| 6. Expression and Purification of GEN1 From <i>C. thermophilum</i>                        | 552 |
| 7. The Biochemical Properties of CtGEN1   | 553 |
| 7.1 The State of Oligomerization of CtGEN-1 in the Absence of DNA                         | 553 |
| 7.2 Binding of CtGEN1 to a Four-Way DNA Junction  | 553 |
| 7.3 CtGEN1 Binds to a Four-Way DNA Junction in Dimeric Form                               | 555 |
| 7.4 CtGEN1 Introduces Symmetrically Paired Cleavages Into a Four-Way DNA Junction         | 555 |
| 7.5 CtGEN1 Exhibits Second Strand Cleavage Acceleration                                   | 556 |
| 7.6 CtGEN1 Distorts the Structure of a Four-Way DNA Junction                              | 557 |
| 8. The Crystal Structure of a CtGEN1-Product Complex                                      | 560 |
| 9. The Interaction of CtGEN1 With Four-Way DNA Junctions Deduced From the Crystal Lattice | 562 |
| 10. Comparison With Other Junction-Resolving Enzymes                                      | 563 |
| Acknowledgments   | 564 |
| References  | 564 |

## Abstract

Four-way Holliday junctions in DNA are the central intermediates of genetic recombination and must be processed into regular duplex species. One mechanism for

<sup>2</sup> Centre for Gene Regulation and Expression, The University of Dundee

achieving this is called resolution, brought about by structure-selective nucleases. GEN1 is an important junction-resolving enzyme in eukaryotic cells, a member of the FEN1/EXO1 superfamily of nucleases. While human GEN1 is difficult to work with because of aggregation, orthologs from thermophilic fungi have been identified using bioinformatics and have proved to have excellent properties. Here, the expression and purification of this enzyme from *Chaetomium thermophilum* is described, together with the means of investigating its biochemical properties. The enzyme is quite similar to junction-resolving enzymes from lower organisms, binding to junctions in dimeric form, introducing symmetrical bilateral cleavages, the second of which is accelerated to promote productive resolution. Crystallization of *C. thermophilum* GEN1 is described, and the structure of a DNA-product complex. Juxtaposition of complexes in the crystal lattice suggests how the structure of a dimeric enzyme with an intact junction is organized.



---

## 1. HOLLIDAY JUNCTIONS AND THEIR RESOLUTION

Holliday junctions (Holliday, 1964) are four-way junctions in DNA formed by the mutual exchange of strand connectivity, and thus connected by the covalent continuity of each strand of the junction (Orr-Weaver, Szostak, & Rothstein, 1981; Potter & Dressler, 1976; Schwacha & Kleckner, 1995). They are the central intermediates of genetic recombination, formed in the repair of double-strand DNA breaks and by fork reversal at blocked replication forks. In the presence of metal ions the free four-way junction undergoes pairwise coaxial stacking of helical arms to form the right-handed stacked-X structure (Duckett et al., 1988; Eichman, Vargason, Mooers, & Ho, 2000; Murchie et al., 1989). This conformation exists in one of two alternative stacking conformers (Clegg et al., 1992) that interconvert in solution (Grainger, Murchie, & Lilley, 1998; McKinney, Declais, Lilley, & Ha, 2003).

Holliday junctions must be processed into duplex DNA species, and this can occur in two main ways. One is by the action of nucleases that are selective for branched DNA—the junction-resolving enzymes. Proteins with junction-resolution activity have been isolated from a wide range of organisms and their viruses or phages. The second way of processing junctions is called dissolution and is important in eukaryotes. In this process junctions are translocated toward each other by a helicase (Bloom's helicase in humans) until decatenated by a topoisomerase.



---

## 2. THE RESOLUTION PROCESS

Much of the analysis of the key defining properties of junction-resolving enzymes came from the study of relatively simple proteins from

bacteria, phage, yeast mitochondria, and archaea (Lilley & White, 2001; West, 2003). These are small proteins (typically around 150 amino acids, apart for the mitochondrial enzymes) that are basic, with pI between 8.8 and 9.8. Most of these enzymes group into one of two superfamilies (Lilley & White, 2000; Makarova, Aravind, & Koonin, 2000). Some of the techniques that were developed in the study of these enzymes (e.g., the supercoiled cruciform assay for analysis of bilateral cleavage and its kinetics; Fogg, Schofield, Déclais, & Lilley, 2000; Giraud-Panis & Lilley, 1997) have become standard tools that can be applied to new enzymes as they are found.

As a group, the junction-resolving enzymes exhibit a broadly similar set of properties that reflect their function in the productive resolution of Holliday junctions. We can draw a scheme for the resolution process (Fig. 1) and see how these properties relate to this.

In free solution the enzymes exist in a monomer–dimer equilibrium that varies widely in terms of the affinity and rate of association (Freeman, Liu, Déclais, Gartner, & Lilley, 2014; Parkinson & Lilley, 1997; Pöhler, Giraud-Panis, & Lilley, 1996; White & Lilley, 1996). However, the enzymes all bind to the junction in dimeric form (Giraud-Panis & Lilley, 1998; Parkinson & Lilley, 1997; Pöhler et al., 1996; White & Lilley, 1996, 1997a), consistent with the requirement for bilateral cleavage in order to achieve a resolution. Binding to junctions occurs in the low nM range (Giraud-Panis & Lilley, 1998; Pöhler et al., 1996; White & Lilley, 1997b, 1998), but importantly this is typically 1000-fold higher than the affinity of binding to duplex DNA of the same sequence (Pöhler et al., 1996). However, at the present time we know nothing about the searching mechanisms that allow the

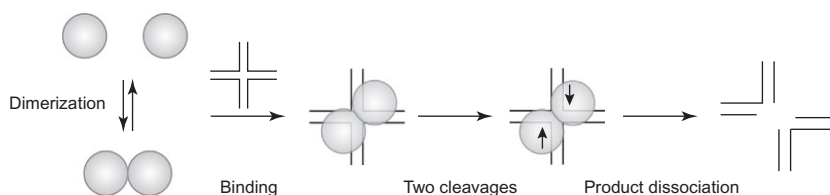
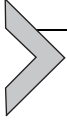


**Fig. 1** Scheme showing the steps involved in the resolution of a four-way junction by a Holliday junction-resolving enzyme. The resolving enzymes exist in a monomer–dimer equilibrium in solution, which can be biased toward monomer or dimer for different enzymes. The enzyme binds as a dimer, with the two active sites juxtaposed with the DNA to make two, symmetrically disposed hydrolytic cleavages. In general the second cleavage is accelerated relative to the first, so that bilateral cleavage has been achieved before dissociation of the protein from the resolved junction. The resolving enzyme should dissociate from the DNA leaving nicked duplexes that can be ligated.

proteins to find their targets in cellular DNA. In each case studied, the global structure of the DNA junction in the enzyme-bound complex is altered from that of the free junction (Bennett & West, 1995; Duckett, Giraud-Panis, & Lilley, 1995; Pöhler et al., 1996; White & Lilley, 1997b, 1998).



### 3. A MECHANISM ENSURING PRODUCTIVE JUNCTION RESOLUTION

Once the dimeric enzyme has bound to the junction then cleavage should proceed. The resolving enzymes hydrolyze single phosphodiester linkages in two arms of the junction, symmetrically disposed relative to the junction. These are typically one or two nucleotides either 3' or 5' to the junction; so long as it's the same on both sides for a given enzyme, a productive resolution is achieved. At the end of this process it will leave ligatable nicks in the resulting duplex DNA. It is, however, critical that the two cleavages are made within the lifetime of the enzyme-junction complex. Premature dissociation after unilateral cleavage would leave a nicked junction that is likely to be dangerous to the cell, and therefore a mechanism is required to avoid this.

The relative timing of cleavages has been studied using the cruciform cleavage assay (Fogg & Lilley, 2001; Fogg et al., 2000; Giraud-Panis & Lilley, 1997) (see later for an example). A cruciform can be formed at an inverted repeat in DNA by the extrusion of two opposed stem-loop structures (Lilley, 1980; Mizuuchi, Kemper, Hays, & Weisberg, 1982). The junction between the two stem-loops and the duplex DNA is a four-way junction and is a substrate for junction-resolving enzymes (Lilley & Kemper, 1984; Mizuuchi, Mizuuchi, & Gellert, 1982). Normally cruciform structures do not form in DNA, because they are less stable than the duplex by at least  $55 \text{ kJ mol}^{-1}$ . However, the cruciform can become stable in negatively supercoiled DNA because of the local negative twist change that occurs when it forms; this relaxes the superhelical stress and the free energy corresponding to that will be greater than the cost of extrusion above a critical level of negative supercoiling (Lilley & Hallam, 1984). Thus a cruciform with arms of 20 bp will be stable in a plasmid extracted from *Escherichia coli* (with a superhelix density— $\sigma \sim 0.06$ ), but if a nick is introduced anywhere within that circular DNA the supercoiling will be lost and consequently the cruciform reabsorbed. This is the basis of the assay for bilateral cleavage.

We use a plasmid containing an inverted repeat where the central region is an alternating (AT)<sub>n</sub> sequence. For the majority of sequences there is a

strong kinetic barrier to extrusion (Courey & Wang, 1983; Gellert, O'Dea, & Mizuuchi, 1983; Lilley, 1985), but for (AT)<sub>n</sub> there is none (Greaves, Patient, & Lilley, 1985; McClellan & Lilley, 1987; Murchie & Lilley, 1987); these can be extruded from DNA inside bacterial cells (McClellan, Boublikova, Palecek, & Lilley, 1990). Plasmid DNA is extracted from *E. coli* cells in exponential growth and purified by two rounds of isopycnic centrifugation to give >95% supercoiled circular DNA.

The assay can be stated in a very simple way. If the resolving enzyme introduces bilateral cleavages the product will be linear DNA. However, if the enzyme only makes a unilateral cleavage then the product is a nicked circle (Fig. 2). Moreover the reaction is inherently self-limiting. If the enzyme dissociates after making just a single cut in the DNA, the supercoiling is released and consequently the cruciform is reabsorbed so that there

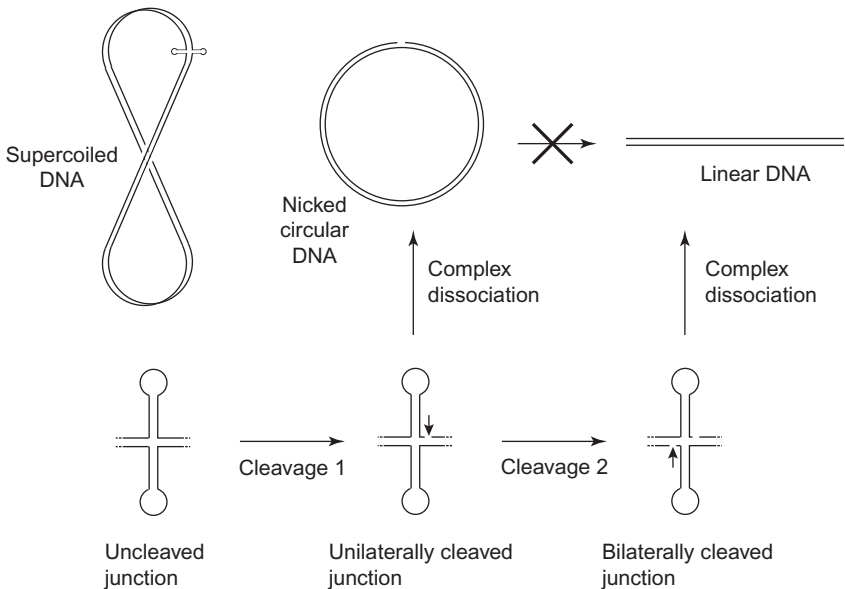


**Fig. 2** Scheme showing the principle of studying the unilateral and bilateral cleavage of a four-way junction using a cruciform extruded from an inverted repeat in supercoiled DNA. The cruciform structure is not stable in duplex DNA ( $\Delta G_{\text{formation}} \geq 50 \text{ kJ mol}^{-1}$ ) but is stabilized in negatively supercoiled DNA due to its local twist change. However, once a cleavage is introduced the cruciform is no longer stable and so absorbed into the body of the plasmid. Thus if the resolving enzyme dissociates after a unilateral cleavage, no further cleavage is possible because the substrate no longer exists and the product is a nicked circular DNA. By contrast, bilateral cleavage leads to the formation of a linear DNA product. Supercoiled, nicked, and linear DNA can be simply separated by agarose gel electrophoresis.

is no longer any substrate present to be resolved. Supercoiled, nicked, and linear DNA are readily separated and quantified because they migrate very differently from each other by electrophoresis in agarose, in the order nicked circle (slowest migration), linear (intermediate migration), and supercoiled DNA (fastest migration).

Formation of nicked circle shows that a unilateral cleavage has occurred. A linear product indicates bilateral cleavage, but the two cleavages could occur simultaneously or sequentially. In fact so long as both cleavages occur within the lifetime of the complex, then linear product could result. These schemes are shown in Fig. 2. It was found that a phage-derived resolving enzyme converted a supercoiled plasmid DNA containing a cruciform into linear product, consistent with bilateral cleavage (Giraud-Panis & Lilley, 1997). However, when such reactions were followed as a function of time of incubation it was found that nicked DNA was formed as a transient intermediate. This was no longer observed at longer times, as the singly cleaved intermediate was subsequently converted into linear product by a second cleavage (Fogg & Lilley, 2001; Fogg et al., 2000). These data can be accommodated by a kinetic model of sequential cleavage (Fig. 3).

The rates of conversion of supercoiled DNA (concentration  $[S]_t$  at time  $t$ ) and nicked circular DNA ( $[N]_t$  at time  $t$ ) will be given by:

$$d[S]/dt = -k_1[S]_t \quad (1)$$

$$d[N]/dt = k_1[S]_t - k_2[N]_t \quad (2)$$

Integration of these first-order differential equations by standard analytical methods leads to the rate equations expressing the instantaneous fractional concentrations of the three species as:

$$[S]_t/[S]_0 = \exp(-k_1t) \quad (3)$$

$$[N]_t/[S]_0 = k_1/(k_2 - k_1) \cdot (\exp(-k_1t) - \exp(-k_2t)) \quad (4)$$

and by conservation, the fractional concentration of linear species  $[L]_t$  at time  $t$  will be:

$$[L]_t/[S]_0 = 1 - \exp(-k_1t) - k_1/(k_2 - k_1) \cdot (\exp(-k_1t) - \exp(-k_2t)) \quad (5)$$

The cruciform-containing plasmid is therefore incubated with the enzyme being studied and samples removed at different times and the

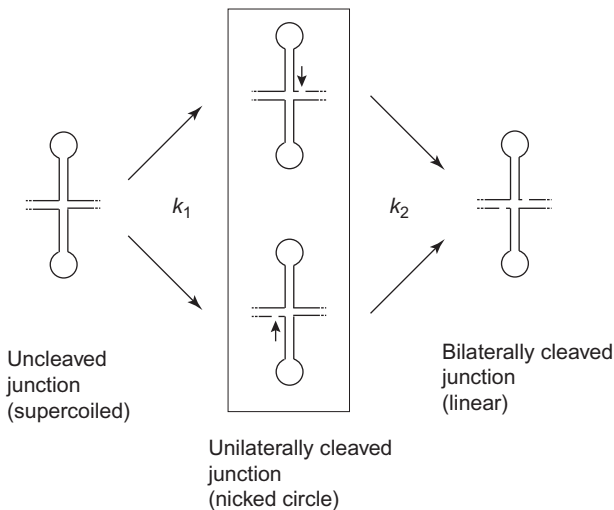
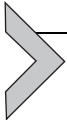


**Fig. 3** A simple kinetic scheme for cruciform cleavage by a junction-resolving enzyme. The rate of the initial cleavage is  $k_1$ , and that of the second is  $k_2$ . This leads to the rate Eqs. (1) and (2), used to analyze the data for CtGEN1. In principle the first cleavage could occur on either the top or bottom strand, followed in the second step by cleavage of the uncleaved strand. Since the sequences of the top and bottom sites are not identical in a cruciform,  $k_1$  and  $k_2$  could each have two values, and the corresponding equations have been solved in Fogg et al. (2000). For CtGEN1 this added complexity was not necessary (Freeman et al., 2014).

reaction terminated. This can be performed manually down to about 10 s, or using quench flow apparatus for faster rates. After deproteinization the DNA is separated by agarose gel electrophoresis, and the relative concentrations of supercoiled, nicked, and linear DNA quantified using a fluorimager. The data can then be fitted by nonlinear regression (e.g., in Kaleidagraph) to Eqs. (3)–(5), from which rates  $k_1$  (the first cleavage of the cruciform) and  $k_2$  (the second cleavage of the cruciform) are obtained. In principle one might expect that the rates of first and second cleavage would be similar, i.e.,  $k_1 = k_2$ , yet this is not the case in general. The general result is that  $k_1 < k_2$ , i.e., that cleavage of the second strand is accelerated relative to the first. In the case of the *E. coli* resolving enzyme RuvC we found that this factor was  $\sim 100$  (Fogg & Lilley, 2001). The net effect of this is that the second cleavage follows hard on the heels of the first, as if they were simultaneous. Importantly, the acceleration of the second cleavage ensures a productive resolution within the lifetime of the enzyme-junction complex.



## 4. PROCESSING OF HOLLIDAY JUNCTIONS IN EUKARYOTES

In eukaryotes Holliday junctions are processed by two quite dissimilar mechanisms, the key difference being whether or not they involve hydrolytic cleavage. These are:

*Dissolution.* This mechanism involves the combined action of a helicase and a topoisomerase. The helicase (the BLM helicase in human cells) translocates two adjacent junctions toward each other, where upon they are unlinked by topoisomerase III $\alpha$  (Cejka, Plank, Bachrati, Hickson, & Kowalczykowski, 2010; Ellis et al., 1995; Wu & Hickson, 2003). Dissolution seems to be the primary way of processing DNA junctions in mitotically dividing cells. In humans defects in the dissolution pathway lead to Bloom syndrome (Bloom, 1954) resulting in genomic instability (Chaganti, Schonberg, & German, 1974). We will not discuss dissolution further here.

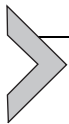
*Resolution.* This is the action of nucleases that are selective for the structure of a four-way DNA junction, as discussed earlier (Lilley, 2016; Matos & West, 2014; Svendsen & Harper, 2010). Junctions that fail to be processed by dissolution are probably subject to resolution.

There are two main resolution systems in eukaryotes. The first to be identified was GEN1 (Bailly et al., 2010; Ip et al., 2008; Rass et al., 2010), and its ortholog in yeast Yen1 (Ip et al., 2008). GEN1 is a member of the FEN1/XPG1 superfamily of 5' nucleases that are selective for various structural distortions of DNA including flaps, overhangs, and loops. The family includes EXO1, FEN1, and XPG (Lee & Wilson, 1999; Orans et al., 2011; Tsutakawa et al., 2011). GEN1 comprises a single polypeptide, and in most respects is very similar in properties and characteristics to the phage, bacterial, archaeal, and mitochondrial junction-resolving enzymes.

The second resolution system is rather more complex, comprising several different polypeptides that are all connected by the SLX4 protein (also called variously BTBD12 and FANCP), a large protein that forms a complex with a number of different nucleases involved in DNA repair (Agostinho et al., 2013; Andersen et al., 2009; Fekairi et al., 2009; Munoz et al., 2009; Svendsen et al., 2009). These are SLX1, MUS81, and EME1. The first cleavage is introduced into the junction by SLX1, a member of the UvrC family of endonucleases that contains a GIY-YIG element that creates a metal ion-binding active center in several

nucleases (Aravind, Walker, & Koonin, 1999; Mak, Lambert, & Stoddard, 2010). The second cleavage is made by the MUS81–EME1 nuclease (Boddy et al., 2001; Chen et al., 2001; Gaillard, Noguchi, Shanahan, & Russell, 2003). The combined action of these nucleases generates a productive resolution of the Holliday junction. This model is also supported by genetic and cytological experiments in *Caenorhabditis elegans* where SLX1 and MUS81 appear to act in conjunction to resolve Holliday junctions in meiosis (Agostinho et al., 2013; O’Neil et al., 2013; Saito, Lui, Kim, Meyer, & Colaiacovo, 2013). The resolving enzyme is the SLX4–SLX1–MUS81–EME1 tetramer, although it is part of the larger complex of repair enzymes coordinated by SLX4.

Neither GEN1 nor SLX4–SLX1–MUS81–EME1 are essential for cell viability, but the combined depletion of GEN1 and SLX4 leads to synthetic lethality in human cells, with defects resulting in unprocessed junctions and consequently dysfunctional mitosis (Garner, Kim, Lach, Kottemann, & Smogorzewska, 2013). The meiotic phenotype of *mus81*  $\Delta$  fission yeast was restored by expression of human GEN1 (Lorenz, West, & Whitby, 2010), and persistent DNA junctions in meiotic yeast were resolved by Yen1 (Matos, Blanco, Maslen, Skehel, & West, 2011). In what follows we shall focus on GEN1.



## 5. GENES FOR THE FEN1/XPG1 SUPERFAMILY IN THERMOPHILIC FUNGI

We reasoned that GEN1 enzymes derived from thermophilic organisms might be thermodynamically more stable and amenable to biochemical and structural analysis. GEN1 is not encoded in prokaryotes. We thus searched for GEN1-related enzymes in thermophilic fungi, that had previously been subject to genome sequencing (Morgenstern et al., 2012). Species analyzed included *Chaetomium thermophilum*, *Myceliophthora thermophila*, *Talaromyces marneffei*, *Talaromyces stipitatus*, and *Thielavia terrestris*. These species grow at temperatures up to 55°C. Given that FEN1, EXO1, XPG, and GEN1 nucleases all belong to the FEN1/XPG1 superfamily, we needed to establish orthologous relationships between those proteins from thermophilic fungi and known budding yeast and mammalian orthologs. This required the identification of all candidate FEN1/XPG1 family nucleases from those fungi via blast searching and their alignment with already known family members from budding yeast, *C. elegans*, *Drosophila melanogaster*,

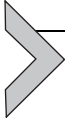
and various mammals using the JALVIEW sequence analysis suite and employing the MAFT algorithm (Clamp, Cuff, Searle, & Barton, 2004). An unrooted phylogenetic tree was then generated using the SplitsTree program (Huson, 1998) and application of the neighbor joining method. This analysis allowed the unambiguous identification of the GEN1 ortholog from *C. thermophilum* (Freeman et al., 2014).



## 6. EXPRESSION AND PURIFICATION OF GEN1 FROM *C. THERMOPHILUM*

Having identified the gene for GEN1 in *C. thermophilum*, we initially constructed a synthetic gene encoding amino acids 1–530 polypeptide with codon optimization for *E. coli*. This was systematically truncated at the C-terminus in stages as a result of which we chose to study the construct comprising amino acids 1–487 (hereafter called CtGEN1). This was found to be expressed best and has the greatest stability to loss of activity. CtGEN1 was expressed as a C-terminal fusion with green fluorescent protein (GFP) separated by a tobacco etch virus (TEV) protease site, and followed by a C-terminal octahistidine peptide (Freeman et al., 2014). The CtGEN1–GFP fusion protein was expressed from the plasmid pWaldo (a pET derivative) transformed into *E. coli* BL21 (DE3) RIL. Immediately after transformation the cells were grown at 37°C in LB supplemented with kanamycin and chloramphenicol until the culture reached an absorbance at 600 nm ( $A_{600}$ ) of 0.4 after which the cells were grown at 20°C. Once the culture reached  $A_{600} = 0.6$ , expression of CtGEN1–GFP was induced by addition of 0.1 mM IPTG and incubated for a further 20 h. After centrifugation the cells were lysed with 1 mg/mL lysozyme in 50 mM NaHPO<sub>4</sub> (pH 8), 1 M NaCl and protease inhibitors and the extract sonicated. After clarification by centrifugation the extract was applied to Ni<sup>2+</sup>-IDA metal chelate resin and eluted using a gradient of 0–0.5 M imidazole while monitoring the absorbance of GFP. The CtGEN1–GFP fusion was cleaved using TEV protease, and the protein extract applied to a heparin HP column and eluted using a gradient of 0.1–1 M NaCl. The protein was finally applied to a Superose 12 gel filtration column in 25 mM Hepes (pH 7.5), 1 M NaCl. The peak fraction of CtGEN1 was dialyzed against 25 mM Hepes (pH 7.5), 0.1 M NaCl, 50% glycerol and stored at –80°C.

The purified CtGEN1 was analyzed by electrophoresis in 10% polyacrylamide gels under denaturing conditions in the presence of SDS. The protein migrated as a single band even when heavily overloaded.



## 7. THE BIOCHEMICAL PROPERTIES OF CtGEN1

We have analyzed the biochemical properties of the N-terminal 1–487 fragment of *C. thermophilum* GEN1. The properties will be discussed in the sequence following the scheme of Fig. 1. Unless otherwise stated all the following experiments were carried out in 10 mM Hepes (pH 7.5), 50 mM NaCl, and 1 mM DTT (buffer A).

### 7.1 The State of Oligomerization of CtGEN-1 in the Absence of DNA

Following cleavage of CtGEN1–GFP protein with TEV protease the digest was applied to Superdex 75 10/300GL gel filtration column in buffer A. The released CtGEN1 eluted in between BSA (66 kDa) and carbonic anhydrase (29 kDa) (Freeman et al., 2014). This indicates that CtGEN1 (calculated mass 55.1 kDa) exists predominantly in monomeric form in free solution. However, at high concentration some dimer could be detected indicating that mass action will drive some dimerization.

### 7.2 Binding of CtGEN1 to a Four-Way DNA Junction

The binding of CtGEN1 to a four-way DNA junction is most readily studied using gel electrophoresis. For this we use our well-characterized junction 3 sequence (Duckett et al., 1988), which is incapable of branch migration. This is assembled from four synthetic oligonucleotides (e.g., each of 50 nt) and is radioactively [ $5'$ - $^{32}\text{P}$ ]-labeled. 100 pM junction was incubated with a range of concentrations of CtGEN1 in the presence of either 1 mM EDTA or 1 mM  $\text{Ca}^{2+}$  ions in buffer A, 0.1 mg/mL BSA, and electrophoresed in a 6% polyacrylamide gel under nondenaturing conditions in 90 mM Tris–borate (pH 8.5) with either 2 mM EDTA (TBE) or 1 mM  $\text{Ca}^{2+}$ . CtGEN1 is essentially inactive in the presence of  $\text{Ca}^{2+}$  ions, so no cleavage occurs during the analysis.

In contrast to analogous studies with human GEN1 (Rass et al., 2010), CtGEN1 forms complexes with DNA junctions that migrate as very discrete bands in gel electrophoresis under nondenaturing conditions without requiring the addition of competitor DNA (Freeman et al., 2014) (Fig. 4A). Incubation in the absence of metal ions leads to the formation of two complexes at intermediate protein concentrations, but a single species is present at higher concentration. Incubation in the presence of 1 mM  $\text{Ca}^{2+}$  ions results in a single discrete complex. These results suggest the formation

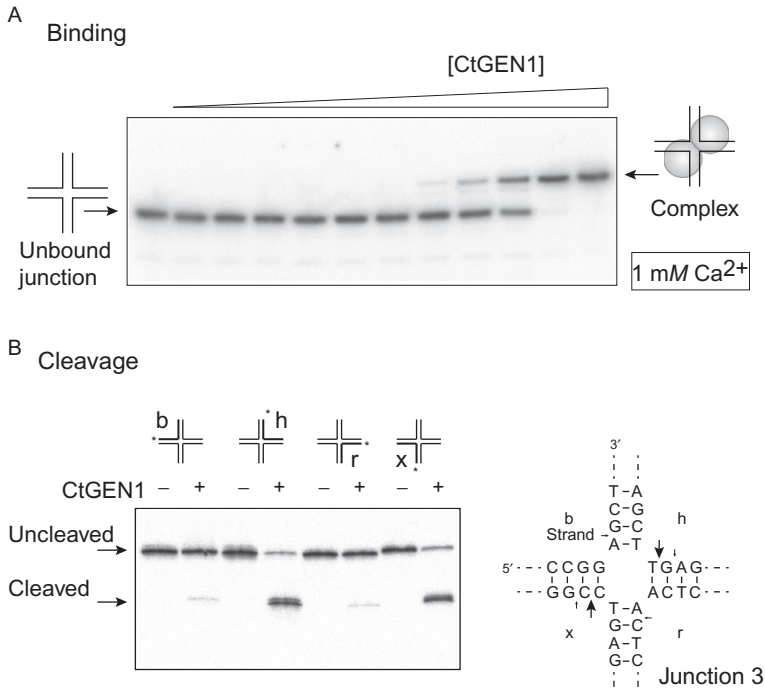


**Fig. 4** CtGEN1 binding to and cleaving a four-way DNA junction. (A) Analysis of binding by gel electrophoresis in polyacrylamide. 82 pM of four-way junction 3 was incubated with increasing concentrations of CtGEN1 in 10 mM Hepes (pH 7.5), 50 mM NaCl, 1 mM DTT, and 0.1 mg/mL BSA plus 1 mM  $\text{Ca}^{2+}$  ions to prevent cleavage. DNA–protein complexes (arrowed right) migrate more slowly than the free junction. Additional experiments discussed in the text show that the upper band comprises a dimer of CtGEN1 bound to the junction. (B) Cleavage of junction 3 by CtGEN1. Four junction substrates were used, each with the same sequence, but individually radioactively [ $5' \text{-}^{32}\text{P}$ ]-labeled on a single strand (named b, h, r, and x). Each species was incubated with (+) or without (–) CtGEN1 in 10 mM Hepes (pH 7.5), 50 mM NaCl, 1 mM DTT, 0.1 mg/mL BSA plus 1 mM  $\text{Mg}^{2+}$  ions, and the products separated by electrophoresis in a polyacrylamide gel. The junction is strongly cleaved on two diametrically opposite strands (h and x), and weakly on the other two (b and r), as shown by the larger arrows on the sequence (right). Both cleavages are 1 nt 3' to the point of strand exchange.

of complexes with one and two molecules of GEN1, and this is characterized in the following section.

The fraction of bound junction ( $f_b$ ) was determined by autoradiography, and the resulting isotherms fitted to two different binding models. One is a simple model lacking cooperativity:

$$f_b = \left\{ K_d + P_t + D_t - \left( (K_d + P_t + D_t)^2 - 4P_t \cdot D_t \right)^{1/2} \right\} / 2D_t \quad (6)$$

where  $K_d$  is the dissociation constant,  $P_t$  is the total protein dimer concentration, and  $D_t$  is the total DNA concentration. Nonlinear regression analysis gives a binding affinity of  $K_d = 10$  nM. However, the data deviate significantly from this model, suggesting cooperativity. The data were therefore fitted to the Hill equation for cooperative binding:

$$f_b = P_t^n / (P_t^n + K_d) \quad (7)$$

where  $n$  is the Hill coefficient. This gave a significantly better fit to the experimental binding data (Freeman et al., 2014) with a value of  $n = 2.2$ . Thus the binding is significantly cooperative.

### 7.3 CtGEN1 Binds to a Four-Way DNA Junction in Dimeric Form

The oligomerization state of CtGEN1 bound to a DNA junction was characterized using two forms of the enzyme of different size, i.e., the CtGEN1–GFP fusion and the nonfusion CtGEN1. In this experiment radioactively [ $5'$ - $^{32}$ P]-labeled four-way junction 3 was incubated with 40 nM CtGEN1 plus an additional concentration of CtGEN1–GFP between 0 and 125 nM. The inverse experiment was also performed, where the junction was incubated with CtGEN1–GFP plus a range of concentrations of CtGEN1. In both cases the samples are then electrophoresed in parallel in a 6% polyacrylamide gel in the presence of 1 mM  $\text{Ca}^{2+}$  ions under non-denaturing conditions. Binding of the single proteins resulted in the formation of a single retarded band corresponding to the complex. However, addition of the second protein led to the formation of three bands of complex (Freeman et al., 2014). This indicates that CtGEN1 binds to the junction in dimeric form. The mixture of long (CtGEN1–GFP) and short (CtGEN1) proteins statistically gives rise to three junction–protein complexes, corresponding to long–long, long–short, and short–short dimers of CtGEN1.

Thus, CtGEN1 is predominantly monomeric in free solution, but binds to the junction in dimeric form, explaining the cooperativity in binding. All the resolving enzymes function as dimers, consistent with the bilateral cleavage required for resolution.

### 7.4 CtGEN1 Introduces Symmetrically Paired Cleavages Into a Four-Way DNA Junction

Sites of cleavage by CtGEN1 into a four-way DNA junction were mapped on the four versions of junction 3 in which a different single strand is radioactively [ $5'$ - $^{32}$ P]-labeled. 1 nM DNA junction was incubated with 50 nM

CtGEN1 in the presence of 10 mM Hepes (pH 7.5), 50 mM NaCl, 10 mM MgCl<sub>2</sub>, 0.1 mg/mL BSA, and 1 mM DTT for 60 min. After termination of the reaction by addition of EDTA and proteinase K, the substrate and products were separated by electrophoresis in 15% polyacrylamide sequencing gels under denaturing conditions in the presence of 8 M urea (Fig. 4B). Comparison with a sequence marker generated by citrate-induced depurination revealed that CtGEN1 cleaved junction 3 1 nt 3' to the junction on two diametrically related strands (termed h and x) (Freeman et al., 2014). Cleavage 1 nt 3' to a structural discontinuity is the hallmark of the XPG1 superfamily of nucleases.

Cleavage reactions on junction 3 were also performed under single-turnover conditions as a function of time to determine the kinetics of cleavage (Freeman et al., 2014). 5 nM junction radioactively [5'-<sup>32</sup>P]-labeled on a given strand was incubated with 20 nM CtGEN1 in buffer A, 0.1 mg/mL BSA, and the reaction initiated by addition of MgCl<sub>2</sub> to a final concentration of 10 mM. Aliquots were removed at various times and the reaction terminated by addition of an excess of EDTA to chelate divalent metal ions. Following denaturing gel electrophoresis and quantification by phosphorimaging, reaction progress curves of cleaved fraction ( $F_t$ ) as a function of time ( $t$ ) were fitted to:

$$F_t = F_f \cdot (1 - \exp(-k_c t)) \quad (8)$$

where  $F_f$  is the fraction of DNA cleaved at the end of the reaction and  $k_c$  is the single-order rate constant for cleavage. Cleavage rates of  $k_c = 0.008$  and  $0.01 \text{ s}^{-1}$  were measured for cleavage of the h and x strands, respectively, of junction 3 under these conditions (Freeman et al., 2014).

## 7.5 CtGEN1 Exhibits Second Strand Cleavage Acceleration

The relative rates of first and second strand cleavage were analyzed using the cruciform cleavage assay described in Section 3. This was achieved using the supercoiled plasmid pHRX3 containing a 34 nt inverted repeat with a central (TA)<sub>12</sub> sequence that ensures facile extrusion of the cruciform (Greaves et al., 1985). The plasmid was transformed into *E. coli* DH5 $\alpha$ , grown to  $A_{600} = 0.6$  at 37°C and amplified by treatment with 150  $\mu\text{g/mL}$  chloramphenicol overnight. Plasmid DNA was subjected to two rounds of isopycnic CsCl/ethidium bromide ultracentrifugation, and the supercoiled fraction purified by extraction with *n*-butanol and extensive dialysis

against 20 mM Tris (pH 8.0), 1 mM EDTA (Murchie & Lilley, 1992). The resulting plasmid preparations are typically >95% supercoiled.

To analyze cleavage 10 nM supercoiled plasmid was preincubated with 200 nM CtGEN1 in 10 mM cacodylate (pH 5.75), 50 mM NaCl, 0.1 mg/mL BSA for 3 min at 37°C whereupon cleavage was initiated by addition of  $\text{MgCl}_2$  to a final concentration 1 mM. Aliquots were removed at specific times and 20 mM EDTA was added to terminate the reaction, followed by incubation with 1  $\mu\text{L}$  proteinase K at 1–2 mg/mL. The DNA was electrophoresed in 1% agarose gels in TBE buffer to separate supercoiled, linear, and nicked species, stained with Safeview nucleic acid stain (NBS Biological Ltd.). After washing with water the gel was imaged using a FLA-2000 fluorescent image analyzer (Fuji) using excitation at 473 nm with an emission filter at 580 nm.

Incubation with CtGEN1 converts pHRX3 into linear product, revealing bilateral cleavage occurring within the lifetime of the enzyme-junction complex (Fig. 5). However, at early times a small fraction of nicked-circular DNA is apparent. This species is a transient intermediate, consistent with an initial unilateral cleavage, that is then converted to a bilaterally cleaved junction by the action of the second CtGEN1 subunit. Fitting the data to Eqs. (3)–(5) gave rates of  $k_1 = 0.025$  and  $k_2 = 0.125 \text{ s}^{-1}$  for the first and second strand cleavage, respectively. This shows that after the cleavage of the first strand, the second strand is cleaved five times faster, thus promoting productive resolution within the lifetime of the enzyme-junction complex.

## 7.6 CtGEN1 Distorts the Structure of a Four-Way DNA Junction

All junction-resolving enzymes distort the shape of the four-way junction on binding. The global shape of a four-way DNA junction bound by CtGEN1 was determined using comparative gel electrophoresis (Liu et al., 2015). In this method we compare the electrophoretic mobility of the six possible forms of a junction with two long (e.g., 40 bp) and two short (e.g., 14 bp) arms. These can be generated in a variety of ways, but in general we simply synthesize all 16 component strands and hybridize the required 6 combinations of 4 strands, some of which are radioactively [ $5' \text{-}^{32}\text{P}$ ]-labeled. The six junctions with two long and two short arms are electrophoresed side by side in a polyacrylamide gel under non-denaturing conditions. This method was originally used to determine the structure of the four-way DNA junction in free solution (Duckett et al., 1988) and has been extended to study the shape of junctions bound to junction-resolving

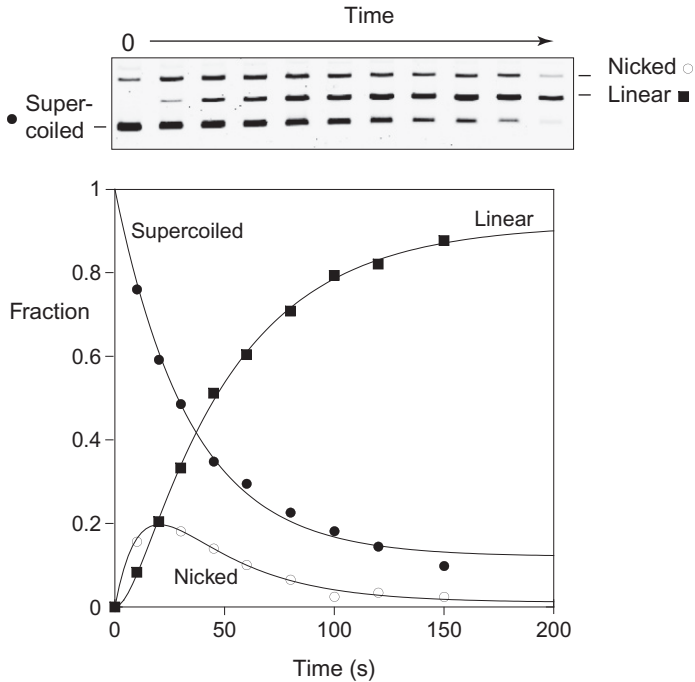


**Fig. 5** Analysis of the acceleration of second strand cleavage using a supercoil-stabilized cruciform structure. 10 nM of cruciform-containing plasmid pHRX3 was incubated with 200 nM CtGEN1 in 10 mM cacodylate (pH 5.75), 50 mM NaCl, 0.1 mg/mL BSA, and 1 mM MgCl<sub>2</sub> at 37°C. Aliquots were removed at various times and the reaction stopped by addition of 20 mM EDTA. The samples were treated with proteinase K and electrophoresed in a 1% agarose gel in TBE, followed by staining in SYBRsafe. The gel is shown at the top of the figure. The fractions of supercoiled (filled circles), nicked (open circles), and linear (filled squares) DNA were quantified and plotted as a function of time. These were fitted to the integrated rate Eqs. (3)–(5) with an adjustment to take account of a small uncleaved fraction. This gave rates of first and second strand cleavage of  $k_1 = 0.025 \text{ s}^{-1}$  and  $k_2 = 0.125 \text{ s}^{-1}$ , reflecting a fivefold rate acceleration for second strand cleavage.

enzymes (Duckett et al., 1995; Giraud-Panis & Lilley, 1998; Pöhler et al., 1996; White & Lilley, 1996, 1997b).

To study the complex we incubate the six long-short species with 100 nM CtGEN1 in the presence of 1 mM CaCl<sub>2</sub> (the enzymatic activity is completely inhibited by the Ca<sup>2+</sup> ions) and electrophorese in a 5% polyacrylamide gel in buffer containing 1 mM CaCl<sub>2</sub>. The resulting electrophoretic pattern can be described as slow-slow-slow-slow-fast-slow (Liu et al., 2015) (Fig. 6). This was interpreted in terms of structure where the uncleaved arms were coaxial, and all the remaining included angles were 90 degrees. The two cleaved arms extended perpendicular to the coaxial

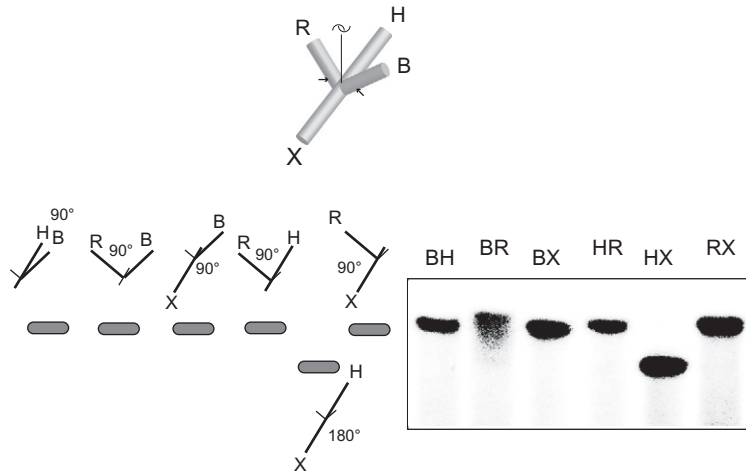


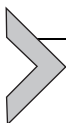
**Fig. 6** The global shape of a four-way DNA junction bound to CtGEN1 in solution determined by comparative gel electrophoresis. The six species of junction 3 with all combinations of two long and two short helical arms were bound to CtGEN1 in 10 mM Hepes (pH 7.5), 50 mM NaCl, 1 mM CaCl<sub>2</sub>, 1 mM DTT, 0.1 mg/mL BSA and electrophoresed in a polyacrylamide gel under nondenaturing conditions. The pattern of migration reflects the geometry of the DNA helical arms in the complex, interpreted in terms of the model shown at the top (with the position of the cleavage sites in the B and R arms indicated by arrows), and the six long-short arm species shown on the left.

arms, and to each other. This agreed well with the crystal structure determined for the complex—see later.

We also explored the central opening of the junction on binding CtGEN1 (Liu et al., 2015). This was done in two contrasting ways, by chemical probing and by a spectroscopic approach. We analyzed the environment of thymine bases close to the center of the junction using probing by permanganate ion (Sasse-Dwight & Gralla, 1989). Junctions radioactively [5'-<sup>32</sup>P]-labeled on a chosen strand with or without bound CtGEN1 were reacted with 1 mM KMnO<sub>4</sub> for 2 min at 25°C in the presence of 1 mM CaCl<sub>2</sub>. Modified thymine nucleotides were cleaved by piperidine, and the products separated by gel electrophoresis. This revealed that thymine bases close to the point of strand exchange were structurally distorted in the complex, but not in the free junction, consistent with an opening induced by CtGEN1 (Liu et al., 2015).

In the second approach we studied junctions in which a chosen adenine nucleotide was replaced by 2-aminopurine (2-AP) (Declais & Lilley, 2000; Jean & Hall, 2001; Ward, Reich, & Stryer, 1969). The fluorescence of 2-AP is strongly lowered by static quenching when stacked, so an opening that

unstacks the 2-AP leads to a marked enhancement of fluorescence. These experiments are performed as ensemble, steady-state fluorescence measurements by excitation of 2-AP at 315 nm and measuring emission between 330 and 460 nm. 2-AP substituted junctions were titrated with CtGEN1, in the presence of 1 mM  $\text{Ca}^{2+}$  ions to prevent cleavage. We found that two 2-AP base located immediately adjacent to the point of strand exchange exhibited marked increases in fluorescence intensity (in one case  $\sim 40$ -fold) on binding CtGEN1 (Liu et al., 2015), suggesting an opening of the junction center. This was repeated for the product of cleavage, finding an enhancement of 2-AP fluorescence about half that for the intact junction (Liu et al., 2015).



## 8. THE CRYSTAL STRUCTURE OF A CtGEN1-PRODUCT COMPLEX

For crystallization studies, the CtGEN1<sub>1-487</sub> construct was modified by addition of a C-terminal His<sub>6</sub> tag following amino acid 487 (called CtGEN1-His). The protein was expressed in *E. coli* using normal and selenomethionine-containing medium with the same strategy as described earlier. The cells were collected by centrifugation, lysed with 1 mg/mL lysozyme and the extract sonicated. After clarification by centrifugation, the extract was applied to Ni<sup>2+</sup>-IDA metal chelate resin and eluted using 1 × PBS, 0.2 M imidazole. The peak fraction of CtGEN1-His protein was applied to a heparin HP column and eluted using a gradient of 5 mM Hepes (pH 7.0), 0.1–1 M NaCl. The protein was finally applied to a Superose 12 gel filtration column in 5 mM Hepes (pH 7.0), 150 mM NaCl. The purified peak fraction was concentrated to 100 μM and kept on ice until usage. CtGEN1-His was crystallized with a four-way junction with the central sequence of the well-characterized junction 3 with 15 bp in each helical arm (Liu et al., 2015). 100 μM each of CtGEN1-His protein and junction 3 were mixed in a final concentration of 100 mM Hepes (pH 7.5), 2 mM MgCl<sub>2</sub>, 20% PEG10000, and 150 mM NaCl. Crystallization was performed using hanging drop vapor diffusion at 7°C in the same buffer. Initial phases were acquired using single-wavelength anomalous diffraction by locating the selenium atoms with Autosol (Adams et al., 2010). The initial model was generated automatically by PHENIX autobuild wizard, and then applied to the native data sets by molecular replacement using Phaser (McCoy et al., 2007). The model was adjusted manually, and subjected to several rounds of adjustment and optimization. The CtGEN1 complex in Mg<sup>2+</sup> was solved at a resolution of 2.5 Å.

The enzyme was of natural sequence (i.e., not an active site mutant) and was crystallized with  $Mg^{2+}$  ions in the buffer, so it was expected that the resulting complex would be the product of cleavage bound to CtGEN1. Moreover an extra molecule of CtGEN1 was bound in a crystallographically equivalent position so that contributions from both halves of the product DNA became averaged in the electron density map. Within the crystals the functional unit was one CtGEN1 monomer with one complete DNA product. Extracting the DNA from the crystals on return from the synchrotron and analysis by gel electrophoresis revealed that only one of the two possible products had crystallized with the enzyme.

For the full details of the structure of CtGEN1 and its bound product DNA the reader is referred to [Liu et al. \(2015\)](#). In brief, the structure of CtGEN1 is similar to that of FEN1 ([Tsutakawa et al., 2011](#)), based on a seven-strand  $\beta$ -sheet flanked by  $\alpha$  helices ([Fig. 7](#)). CtGEN1 lacks the helical arch of FEN1 that functions to select the single strand flap and has an

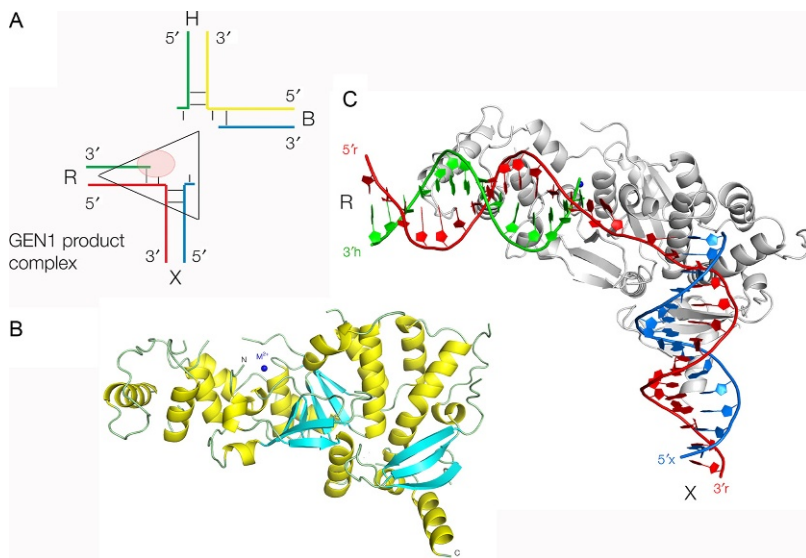
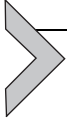


**Fig. 7** The crystal structure of a CtGEN1 monomer, and the complex with the product of resolution cleavage. (A) Scheme showing the cleavage of a four-way junction. Cleavage of the junction gives rise to the two products shown. Only that based on the R and X arms was present in the crystals. This is shown schematically by the triangular shape representing a CtGEN1 monomer; the pink oval shape represents the active site. (B) The structure of a CtGEN1 monomer. The protein structure is shown in cartoon form, with  $\alpha$  helices and coil regions colored yellow, and  $\beta$  sheet cyan. (C) The structure of the functional unit of the product complex in the crystal. The arms of the junction are perpendicular, and each is bound to the enzyme at multiple sites. The strand coloring is consistent with that used in part (A).

additional chromodomain at the C-terminal end allowing it to bind an extra turn of helix. The trajectory of the DNA is closely similar to that of DNA bound to human FEN1 (Tsutakawa et al., 2011), with the two arms of the product being mutually perpendicular. The DNA follows an electropositive path on the surface of the protein. The active site contains two bound metal ions coordinated by six acidic amino acid side chains.



## 9. THE INTERACTION OF CtGEN1 WITH FOUR-WAY DNA JUNCTIONS DEDUCED FROM THE CRYSTAL LATTICE

CtGEN1 crystallized as a trigonal lattice of space group  $P3_121$ . Chains of product complexes are oriented at 120 degrees to each other, related by the threefold symmetry. Within this lattice, protein–protein interaction between CtGEN1 monomers brings two bound DNA products into close proximity as though forming a four-way junction (Fig. 8).

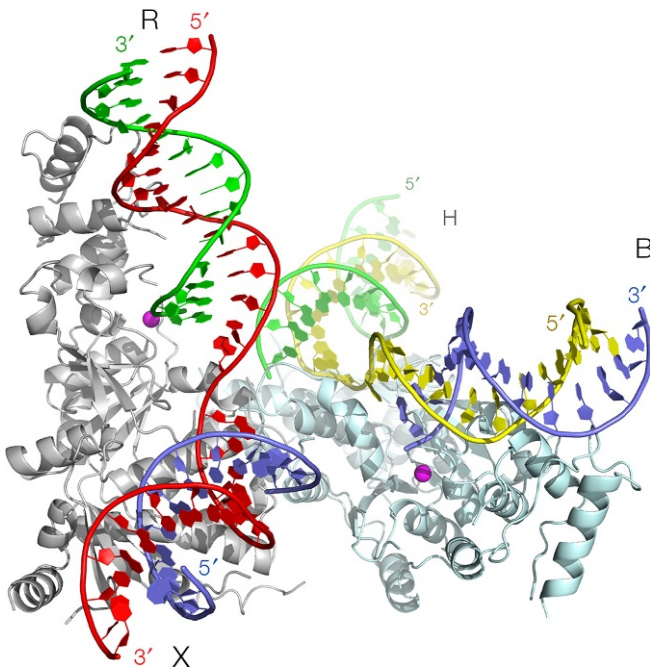
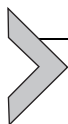


**Fig. 8** A dimeric form of the CtGEN1–DNA complex in the crystal lattice that is closely related to a four-way junction. Within the crystal lattice two product complexes are juxtaposed mediated by a protein–protein dimer interface. The uncleaved arms are coaxial and the two cleaved arms are perpendicular to the uncleaved arms and to each other. The two CtGEN1 monomers are distinguished by *color*, and the strands have been *colored* to correspond to those of a resolved four-way junction (as in Fig. 7A). The metal ions in the active sites are indicated by the *magenta spheres*.

The dimerization is mediated through contact between three  $\alpha$ -helices from each monomer, interacting with a relatively small interface burying  $530 \text{ \AA}^2$ . The interaction leads to a virtually coaxial alignment of the un-cleaved DNA helices, while the cleaved helical arms rotate toward each other on the major groove side such that they include an angle of close to 90 degrees. This structure is essentially identical to that deduced for the complex of CtGEN1 and the intact four-way junction by comparative gel electrophoresis discussed earlier. Using computer graphics it is straightforward to reconnect the 5' ends of the strands in the product complex to generate a covalently intact four-way junction. This requires some disruption of the basepairing at the center of the junction, consistent with the permanganate probing, and 2-aminopurine fluorescence discussed earlier. These data also indicate a smaller degree of central disruption in the product complex, and structural reorganization following the first cleavage may be responsible for the acceleration of second strand cleavage, and thus integral to the function of GEN1.



## 10. COMPARISON WITH OTHER JUNCTION-RESOLVING ENZYMES

The study of fungal GEN1 has opened the door to the analysis of the biochemistry and structure of this eukaryotic junction-resolving enzyme. The biochemical properties of CtGEN1 conform to the scheme shown in [Fig. 1](#). The enzyme binds in dimeric form to a four-way DNA junction and generates two cleavages, where the second cleavage is accelerated relative to the first to ensure productive resolution. These characteristics are typical of the great majority of junction-resolving enzymes isolated from phage, bacteria, archaea, and yeast mitochondria and are clearly required for enzymes of this class. The structure of CtGEN1 is closely similar to that of human GEN1 in a nonspecific complex with DNA ([Lee et al., 2015](#)), so it is probably representative to GEN1 structures in general. Furthermore, the core structure is closely similar to those of other members of the FEN1/EXO1 family, adapted for its specific requirements in the resolution of four-way junctions. This CtGEN1 lacks the helical arch of FEN1 that likely selects for the single-strand flap of the FEN1 substrate. In addition CtGEN1 has the additional chromodomain at the C-terminal end that allows it to bind an extra turn of DNA, and it is clearly required to dimerize on the junction. At present the dynamic properties of GEN1 are of considerable interest, and for this the fungal enzyme should prove highly informative.

## ACKNOWLEDGMENTS

We thank Cancer Research UK for funding research in the DMJL laboratory (program Grant A18604) and the Wellcome Trust for a Senior Research fellowship to A.G. (0909444/Z/09/Z).

## REFERENCES

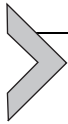
- Adams, P. D., Afonine, P. V., Bunkoczi, G., Chen, V. B., Davis, I. W., Echols, N., et al. (2010). PHENIX: A comprehensive python-based system for macromolecular structure solution. *Acta Crystallographica. Section D, Biological Crystallography*, *66*, 213–221.
- Agostinho, A., Meier, B., Sonnevile, R., Jagut, M., Woglar, A., Blow, J., et al. (2013). Combinatorial regulation of meiotic Holliday junction resolution in *C. elegans* by HIM-6 (BLM) helicase, SLX-4, and the SLX-1, MUS-81 and XPF-1 nucleases. *PLoS Genetics*, *9*, e1003591.
- Andersen, S. L., Bergstralh, D. T., Kohl, K. P., LaRocque, J. R., Moore, C. B., & Sekelsky, J. (2009). Drosophila MUS312 and the vertebrate ortholog BTBD12 interact with DNA structure-specific endonucleases in DNA repair and recombination. *Molecular Cell*, *35*, 128–135.
- Aravind, L., Walker, D. R., & Koonin, E. V. (1999). Conserved domains in DNA repair proteins and evolution of repair systems. *Nucleic Acids Research*, *27*, 1223–1242.
- Bailly, A. P., Freeman, A., Hall, J., Declais, A. C., Alpi, A., Lilley, D. M., et al. (2010). The *Caenorhabditis elegans* homolog of Gen1/Yen1 resolvases links DNA damage signaling to DNA double-strand break repair. *PLoS Genetics*, *6*, e1001025.
- Bennett, R. J., & West, S. C. (1995). Structural analysis of the RuvC–Holliday junction complex reveals an unfolded junction. *Journal of Molecular Biology*, *252*, 213–226.
- Bloom, D. (1954). Congenital telangiectatic erythema resembling lupus erythematosus in dwarfs; probably a syndrome entity. *A.M.A. American Journal of Diseases of Children*, *88*, 754–758.
- Boddy, M. N., Gaillard, P. H., McDonald, W. H., Shanahan, P., Yates, J. R., 3rd, & Russell, P. (2001). Mus81–Eme1 are essential components of a Holliday junction resolvase. *Cell*, *107*, 537–548.
- Cejka, P., Plank, J. L., Bachrati, C. Z., Hickson, I. D., & Kowalczykowski, S. C. (2010). Rmi1 stimulates decatenation of double Holliday junctions during dissolution by Sgs1–Top3. *Nature Structural & Molecular Biology*, *17*, 1377–1382.
- Chaganti, R. S., Schonberg, S., & German, J. (1974). A manyfold increase in sister chromatid exchanges in Bloom's syndrome lymphocytes. *Proceedings of the National Academy of Sciences of the United States of America*, *71*, 4508–4512.
- Chen, X. B., Melchionna, R., Denis, C. M., Gaillard, P. H., Blasina, A., Van de Weyer, I., et al. (2001). Human Mus81-associated endonuclease cleaves Holliday junctions in vitro. *Molecular Cell*, *8*, 1117–1127.
- Clamp, M., Cuff, J., Searle, S. M., & Barton, G. J. (2004). The Jalview java alignment editor. *Bioinformatics*, *20*, 426–427.
- Clegg, R. M., Murchie, A. I. H., Zechel, A., Carlberg, C., Diekmann, S., & Lilley, D. M. J. (1992). Fluorescence resonance energy transfer analysis of the structure of the four-way DNA junction. *Biochemistry*, *31*, 4846–4856.
- Courey, A. J., & Wang, J. C. (1983). Cruciform formation in negatively supercoiled DNA may be kinetically forbidden under physiological conditions. *Cell*, *33*, 817–829.
- Declais, A. C., & Lilley, D. M. (2000). Extensive central disruption of a four-way junction on binding CCE1 resolving enzyme. *Journal of Molecular Biology*, *296*, 421–433.

- Duckett, D. R., Giraud-Panis, M.-E., & Lilley, D. M. J. (1995). Binding of the junction-resolving enzyme bacteriophage T7 endonuclease I to DNA: Separation of binding and catalysis by mutation. *Journal of Molecular Biology*, *246*, 95–107.
- Duckett, D. R., Murchie, A. I. H., Diekmann, S., von Kitzing, E., Kemper, B., & Lilley, D. M. J. (1988). The structure of the Holliday junction and its resolution. *Cell*, *55*, 79–89.
- Eichman, B. F., Vargason, J. M., Mooers, B. H. M., & Ho, P. S. (2000). The Holliday junction in an inverted repeat DNA sequence: Sequence effects on the structure of four-way junctions. *Proceedings of the National Academy of Sciences of the United States of America*, *97*, 3971–3976.
- Ellis, N. A., Groden, J., Ye, T. Z., Straughen, J., Lennon, D. J., Ciocchi, S., et al. (1995). The Bloom's syndrome gene product is homologous to RecQ helicases. *Cell*, *83*, 655–666.
- Fekairi, S., Scaglione, S., Chahwan, C., Taylor, E. R., Tissier, A., Coulon, S., et al. (2009). Human SLX4 is a Holliday junction resolvase subunit that binds multiple DNA repair/recombination endonucleases. *Cell*, *138*, 78–89.
- Fogg, J. M., & Lilley, D. M. J. (2001). Ensuring productive resolution by the junction-resolving enzyme RuvC: Large enhancement of second-strand cleavage rate. *Biochemistry*, *39*, 16125–16134.
- Fogg, J. M., Schofield, M. J., Déclais, A.-C., & Lilley, D. M. J. (2000). The yeast resolving enzyme CCE1 makes sequential cleavages in DNA junctions within the lifetime of the complex. *Biochemistry*, *39*, 4082–4089.
- Freeman, A. D. J., Liu, Y., Déclais, A.-C., Gartner, A., & Lilley, D. M. J. (2014). GEN1 from a thermophilic fungus is functionally closely similar to non-eukaryotic junction-resolving enzymes. *Journal of Molecular Biology*, *426*, 3946–3959.
- Gaillard, P. H., Noguchi, E., Shanahan, P., & Russell, P. (2003). The endogenous Mus81-Eme1 complex resolves Holliday junctions by a nick and counternick mechanism. *Molecular Cell*, *12*, 747–759.
- Garner, E., Kim, Y., Lach, F. P., Kottemann, M. C., & Smogorzewska, A. (2013). Human GEN1 and the SLX4-associated nucleases MUS81 and SLX1 are essential for the resolution of replication-induced Holliday junctions. *Cell Reports*, *5*, 207–215.
- Gellert, M., O'Dea, M. H., & Mizuuchi, K. (1983). Slow cruciform transitions in palindromic DNA. *Proceedings of the National Academy of Sciences of the United States of America*, *80*, 5545–5549.
- Giraud-Panis, M.-J. E., & Lilley, D. M. J. (1997). Near-simultaneous DNA cleavage by the subunits of the junction-resolving enzyme T4 endonuclease VII. *The EMBO Journal*, *16*, 2528–2534.
- Giraud-Panis, M.-J. E., & Lilley, D. M. J. (1998). Structural recognition and distortion by the DNA junction-resolving enzyme RusA. *Journal of Molecular Biology*, *278*, 117–133.
- Grainger, R. J., Murchie, A. I. H., & Lilley, D. M. J. (1998). Exchange between stacking conformers in a four-way DNA junction. *Biochemistry*, *37*, 23–32.
- Greaves, D. R., Patient, R. K., & Lilley, D. M. J. (1985). Facile cruciform formation by an (A-T)<sub>34</sub> sequence from a *Xenopus* globin gene. *Journal of Molecular Biology*, *185*, 461–478.
- Holliday, R. (1964). A mechanism for gene conversion in fungi. *Genetical Research*, *5*, 282–304.
- Huson, D. H. (1998). SplitsTree: Analyzing and visualizing evolutionary data. *Bioinformatics*, *14*, 68–73.
- Ip, S. C., Rass, U., Blanco, M. G., Flynn, H. R., Skehel, J. M., & West, S. C. (2008). Identification of Holliday junction resolvases from humans and yeast. *Nature*, *456*, 357–361.
- Jean, J. M., & Hall, K. B. (2001). 2-Aminopurine fluorescence quenching and lifetimes: Role of base stacking. *Proceedings of the National Academy of Sciences of the United States of America*, *98*, 37–41.

- Lee, S. H., Princz, L. N., Klugel, M. F., Habermann, B., Pfander, B., & Biertumpfel, C. (2015). Human Holliday junction resolvase GEN1 uses a chromodomain for efficient DNA recognition and cleavage. *eLife*, 4. <https://doi.org/10.7554/eLife.12256>.
- Lee, B. I., & Wilson, D. M., 3rd. (1999). The RAD2 domain of human exonuclease 1 exhibits 5' to 3' exonuclease and flap structure-specific endonuclease activities. *The Journal of Biological Chemistry*, 274, 37763–37769.
- Lilley, D. M. J. (1980). The inverted repeat as a recognisable structural feature in supercoiled DNA molecules. *Proceedings of the National Academy of Sciences of the United States of America*, 77, 6468–6472.
- Lilley, D. M. J. (1985). The kinetic properties of cruciform extrusion are determined by DNA base-sequence. *Nucleic Acids Research*, 13, 1443–1465.
- Lilley, D. M. J. (2016). Holliday junction-resolving enzymes—structures and mechanisms. *FEBS Letters*, 591, 1073–1082.
- Lilley, D. M. J., & Hallam, L. R. (1984). Thermodynamics of the ColE1 cruciform. Comparisons between probing and topological experiments using single topoisomers. *Journal of Molecular Biology*, 180, 179–200.
- Lilley, D. M. J., & Kemper, B. (1984). Cruciform-resolvase interactions in supercoiled DNA. *Cell*, 36, 413–422.
- Lilley, D. M. J., & White, M. F. (2000). Resolving the relationships of resolving enzymes. *Proceedings of the National Academy of Sciences of the United States of America*, 97, 9351–9353.
- Lilley, D. M. J., & White, M. F. (2001). The junction-resolving enzymes. *Nature Reviews. Molecular Cell Biology*, 2, 433–443.
- Liu, Y., Freeman, A. D. J., Déclais, A.-C., Wilson, T. J., Gartner, A., & Lilley, D. M. J. (2015). Crystal structure of a eukaryotic GEN1 resolving enzyme bound to DNA. *Cell Reports*, 13, 2565–2575.
- Lorenz, A., West, S. C., & Whitby, M. C. (2010). The human Holliday junction resolvase GEN1 rescues the meiotic phenotype of a *Schizosaccharomyces pombe* mus81 mutant. *Nucleic Acids Research*, 38, 1866–1873.
- Mak, A. N., Lambert, A. R., & Stoddard, B. L. (2010). Folding, DNA recognition, and function of GIY-YIG endonucleases: Crystal structures of R.Eco29kl. *Structure*, 18, 1321–1331.
- Makarova, K. S., Aravind, L., & Koonin, E. V. (2000). Holliday junction resolvases and related nucleases: Identification of new families, phyletic distribution and evolutionary trajectories. *Nucleic Acids Research*, 28, 3417–3432.
- Matos, J., Blanco, M. G., Maslen, S., Skehel, J. M., & West, S. C. (2011). Regulatory control of the resolution of DNA recombination intermediates during meiosis and mitosis. *Cell*, 147, 158–172.
- Matos, J., & West, S. C. (2014). Holliday junction resolution: Regulation in space and time. *DNA Repair*, 19, 176–181.
- McClellan, J. A., Boublikova, P., Palecek, E., & Lilley, D. M. J. (1990). Superhelical torsion in cellular DNA responds directly to environmental and genetic factors. *Proceedings of the National Academy of Sciences of the United States of America*, 87, 8373–8377.
- McClellan, J. A., & Lilley, D. M. J. (1987). A two-state conformational equilibrium for alternating (A-T)<sub>n</sub> sequences in negatively supercoiled DNA. *Journal of Molecular Biology*, 197, 707–721.
- McCoy, A. J., Grosse-Kunstleve, R. W., Adams, P. D., Winn, M. D., Storoni, L. C., & Read, R. J. (2007). Phaser crystallographic software. *Journal of Applied Crystallography*, 40, 658–674.
- McKinney, S. A., Déclais, A. C., Lilley, D. M., & Ha, T. (2003). Structural dynamics of individual Holliday junctions. *Nature Structural Biology*, 10, 93–97.
- Mizuuchi, K., Kemper, B., Hays, J., & Weisberg, R. A. (1982). T4 endonuclease VII cleaves Holliday structures. *Cell*, 29, 357–365.

- Mizuuchi, K., Mizuuchi, M., & Gellert, M. (1982). Cruciform structures in palindromic DNA are favored by DNA supercoiling. *Journal of Molecular Biology*, *156*, 229–243.
- Morgenstern, I., Powlowski, J., Ishmael, N., Darmond, C., Marquetteau, S., Moisan, M. C., et al. (2012). A molecular phylogeny of thermophilic fungi. *Fungal Biology*, *116*, 489–502.
- Munoz, I. M., Hain, K., Déclais, A.-C., Gardiner, M., Toh, G. W., Sanchez-Pulido, L., et al. (2009). Coordination of structure-specific nucleases by human SLX4/BTBD12 is essential for DNA repair. *Molecular Cell*, *35*, 116–127.
- Murchie, A. I. H., Clegg, R. M., von Kitzing, E., Duckett, D. R., Diekmann, S., & Lilley, D. M. J. (1989). Fluorescence energy transfer shows that the four-way DNA junction is a right-handed cross of antiparallel molecules. *Nature*, *341*, 763–766.
- Murchie, A. I. H., & Lilley, D. M. J. (1987). The mechanism of cruciform extrusion in supercoiled DNA: Initial opening of central basepairs in salt-dependent extrusion. *Nucleic Acids Research*, *15*, 9641–9654.
- Murchie, A. I. H., & Lilley, D. M. J. (1992). Supercoiled DNA and cruciform structures. *Methods in Enzymology*, *211*, 158–180.
- O’Neil, N. J., Martin, J. S., Youds, J. L., Ward, J. D., Petalcorin, M. I., Rose, A. M., et al. (2013). Joint molecule resolution requires the redundant activities of MUS-81 and XPF-1 during *Caenorhabditis elegans* meiosis. *PLoS Genetics*, *9*, e1003582.
- Orans, J., McSweeney, E. A., Iyer, R. R., Hast, M. A., Hellinga, H. W., Modrich, P., et al. (2011). Structures of human exonuclease 1 DNA complexes suggest a unified mechanism for nuclease family. *Cell*, *145*, 212–223.
- Orr-Weaver, T. L., Szostak, J. W., & Rothstein, R. J. (1981). Yeast transformation: A model system for the study of recombination. *Proceedings of the National Academy of Sciences of the United States of America*, *78*, 6354–6358.
- Parkinson, M. J., & Lilley, D. M. J. (1997). The junction-resolving enzyme T7 endonuclease I: Quaternary structure and interaction with DNA. *Journal of Molecular Biology*, *270*, 169–178.
- Pöhler, J. R. G., Giraud-Panis, M.-J. E., & Lilley, D. M. J. (1996). T4 endonuclease VII selects and alters the structure of the four-way DNA junction; binding of a resolution-defective mutant enzyme. *Journal of Molecular Biology*, *260*, 678–696.
- Potter, H., & Dressler, D. (1976). On the mechanism of genetic recombination: Electron microscopic observation of recombination intermediates. *Proceedings of the National Academy of Sciences of the United States of America*, *73*, 3000–3004.
- Rass, U., Compton, S. A., Matos, J., Singleton, M. R., Ip, S. C., Blanco, M. G., et al. (2010). Mechanism of Holliday junction resolution by the human GEN1 protein. *Genes & Development*, *24*, 1559–1569.
- Saito, T. T., Lui, D. Y., Kim, H. M., Meyer, K., & Colaiacovo, M. P. (2013). Interplay between structure-specific endonucleases for crossover control during *Caenorhabditis elegans* meiosis. *PLoS Genetics*, *9*, e1003586.
- Sasse-Dwight, S., & Gralla, J. D. (1989).  $\text{KMnO}_4$  as a probe for *lac* promoter DNA melting and mechanism *in vivo*. *The Journal of Biological Chemistry*, *264*, 8074–8081.
- Schwacha, A., & Kleckner, N. (1995). Identification of double Holliday junctions as intermediates in meiotic recombination. *Cell*, *83*, 783–791.
- Svendsen, J. M., & Harper, J. W. (2010). GEN1/Yen1 and the SLX4 complex: Solutions to the problem of Holliday junction resolution. *Genes & Development*, *24*, 521–536.
- Svendsen, J. M., Smogorzewska, A., Sowa, M. E., O’Connell, B. C., Gygi, S. P., Elledge, S. J., et al. (2009). Mammalian BTBD12/SLX4 assembles a Holliday junction resolvase and is required for DNA repair. *Cell*, *138*, 63–77.
- Tsutakawa, S. E., Classen, S., Chapados, B. R., Arvai, A. S., Finger, L. D., Guenther, G., et al. (2011). Human flap endonuclease structures, DNA double-base flipping, and a unified understanding of the FEN1 superfamily. *Cell*, *145*, 198–211.

- Ward, D. C., Reich, E., & Stryer, L. (1969). Fluorescence studies of nucleotides and polynucleotides. I. Formycin, 2-aminopurine riboside, 2,6-diaminopurine riboside and their derivatives. *The Journal of Biological Chemistry*, *244*, 1228–1237.
- West, S. C. (2003). Molecular views of recombination proteins and their control. *Nature Reviews Molecular Cell Biology*, *4*, 435–445.
- White, M. F., & Lilley, D. M. J. (1996). The structure-selectivity and sequence-preference of the junction-resolving enzyme CCE1 of *Saccharomyces cerevisiae*. *Journal of Molecular Biology*, *257*, 330–341.
- White, M. F., & Lilley, D. M. J. (1997a). Characterization of a Holliday junction resolving enzyme from *Schizosaccharomyces pombe*. *Molecular and Cellular Biology*, *17*, 6465–6471.
- White, M. F., & Lilley, D. M. J. (1997b). The resolving enzyme CCE1 of yeast opens the structure of the four-way DNA junction. *Journal of Molecular Biology*, *266*, 122–134.
- White, M. F., & Lilley, D. M. J. (1998). Interaction of the resolving enzyme YDC2 with the four-way DNA junction. *Nucleic Acids Research*, *26*, 5609–5616.
- Wu, L., & Hickson, I. D. (2003). The Bloom's syndrome helicase suppresses crossing over during homologous recombination. *Nature*, *426*, 870–874.



# Preparation and Resolution of Holliday Junction DNA Recombination Intermediates

Rajvee Shah Punatar, Stephen C. West<sup>1</sup>

The Francis Crick Institute, London, United Kingdom

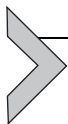
<sup>1</sup>Corresponding author: e-mail address: stephen.west@crick.ac.uk

## Contents

|  |     |
|--|-----|
| 1. Introduction  | 569 |
| 2. Preparation of DNA Substrates                       | 571 |
| 2.1 Preparation of gDNA                                | 571 |
| 2.2 Radioactive Labeling of the Linear Duplex DNA      | 580 |
| 3. Generation and Purification of $\alpha$ -Structures | 583 |
| 4. In Vitro Resolution Assays                          | 585 |
| 5. Notes   | 587 |
| Acknowledgments  | 588 |
| References   | 589 |

## Abstract

Holliday junctions provide a covalent link between recombining DNA molecules and need to be removed prior to chromosome segregation at mitosis. Defects in their resolution lead to mitotic catastrophe, characterized by the formation of DNA breaks and chromosome aberrations. Enzymes that resolve recombination intermediates have been identified in all forms of life, from bacteriophage, to bacteria, yeast, and humans. In higher eukaryotes, Holliday junctions are resolved by GEN1, a nuclease that is mechanistically similar to the prototypic resolvase *Escherichia coli* RuvC, and by the SMX trinuclease complex. Studies of these enzymes have been facilitated by the use of plasmid-sized DNA recombination intermediates made by RecA-mediated strand exchange. Here, we detail the preparation of these recombination intermediates, which resemble  $\alpha$ -structures, and their resolution by RuvC and GEN1.



## 1. INTRODUCTION

DNA recombination intermediates are useful tools for the study of enzymes that resolve Holliday junctions (HJs) (Wyatt & West, 2014). They also provide a model system for the analysis of branch migration, which may

occur spontaneously or be driven by cellular enzymes (Constantinou, Davies, & West, 2001; Constantinou et al., 2000; Karow, Constantinou, Li, West, & Hickson, 2000; Panyutin & Hsieh, 1994; Tsaneva, Müller, & West, 1992). In the cell, DNA recombination intermediates arise during double-strand break repair or in response to replication fork breakage and are regarded as part of a general housekeeping function that maintains the integrity of our genome (Cox, 2001).

In bacteria, recombination intermediates are produced by RecA-mediated homologous pairing and strand exchange (West, 2003). Electron microscopic imaging of the intermediates revealed that they contain four-way junctions, also known as HJs (Cunningham, DasGupta, Shibata, & Radding, 1980; West, Countryman, & Howard-Flanders, 1983). These junctions are resolved by the structure-specific endonuclease RuvC protein (Dunderdale et al., 1991; Iwasaki, Takahagi, Shiba, Nakata, & Shinagawa, 1991). In higher organisms, recombination intermediates are made by RAD51 protein (Baumann, Benson, & West, 1996; Sung, 1994) and are processed in one of two ways: First, double HJs may be “dissolved” by the actions of the BLM-Topoisomerase III-RMI1-RMI2 (BTR) complex which promotes branch migration and dissolution of the resultant hemicatenane (Raynard, Bussen, & Sung, 2006; Wu & Hickson, 2003). Second, persistent double HJs, and single HJs, may be resolved by structure-selective endonucleases such as GEN1 or the SLX1-SLX4-MUS81-EME1-XPF-ERCC1 (SMX) complex (Chan & West, 2015; Ip et al., 2008; Wyatt, Laister, Martin, Arrowsmith, & West, 2017). Dissolution/resolution is a prerequisite for proper chromosome segregation at mitosis (Garner, Kim, Lach, Kottmann, & Smogorzewska, 2013; Sarbajna, Davies, & West, 2014; Wechsler, Newman, & West, 2011).

Here, we describe the generation of recombination intermediates from gapped circular and linear duplex DNA (West, Cassuto, & Howard-Flanders, 1982). The gapped molecule contains a short (174 nt) region of single-stranded DNA (ssDNA) that serves as the site for the initiation of RAD51 binding and nucleoprotein filament formation. The terminus of the linear duplex is designed so that it is homologous to the gapped region and is the location where strand exchange begins and then proceeds in a progressive and polar manner until the two DNAs are fully heteroduplex. However, in the system used here, strand exchange proceeds through 1536 bp of homologous DNA and is then blocked by a region of heterology (643 bp) in the linear duplex, allowing the accumulation of recombination

intermediates (Shah, Bennett, & West, 1994b). The reaction products, which we term “ $\alpha$ -structures,” serve as excellent substrates for HJ-processing enzymes (Eggleston, Mitchell, & West, 1997; Shah et al., 1994b; Shah Punatar, Martin, Wyatt, Chan, & West, 2017).



## 2. PREPARATION OF DNA SUBSTRATES

The methods presented here are based on those previously described (Constantinou & West, 2004; Müller & West, 1994). However, there are several marked differences, which include the use of DNA containing the heterologous block (plasmid pDEA2) and the incorporation of novel or revised procedures. These include the preparation and purification of ssDNA (Sections 2.1.1 and 2.1.2), purification of the complementary strand (Section 2.1.3), and the 3'-<sup>32</sup>P labeling of linear duplex DNA (Section 2.2). This has led to simpler and more efficient schemes for producing high-quality gapped circular DNA (gDNA) and  $\alpha$ -structures.

### 2.1 Preparation of gDNA

To generate gDNA, supercoiled plasmid pDEA-7Z f(+) DNA is cut with *BsaI* and *PstI* to remove a 174-bp fragment. The 2826-bp linear DNA is then purified, denatured, and annealed with homologous single-stranded pDEA-7Z f(+) circular DNA (Fig. 1). The resulting gDNA molecules are then purified by preparative agarose gel electrophoresis followed by electroelution.

#### 2.1.1 Preparation of ssDNA

Single-stranded DNA (ssDNA) is produced from *Escherichia coli* BIOBlue cells transformed with plasmid pDEA-7Z f(+) using the helper phage VCSM13. The latter stages of this procedure use a revised version of the Qiagen supplementary method: Isolation of ssDNA from M13 phage using Qiagen plasmid kits (<https://www.qiagen.com>).

#### Materials

- Plasmid pDEA-7Z f(+). This 3.0 kb plasmid contains a unique *PstI* site and derives from the replacement of the *ScaI*–*BsaI* fragment of pGEM-7Z f(+) (Promega) with the *ScaI*–*BsaI* fragment of pBR322 (Promega) (Shah, Bennett, & West, 1994a). A stock of form I plasmid DNA is prepared using a Qiagen plasmid maxi kit.

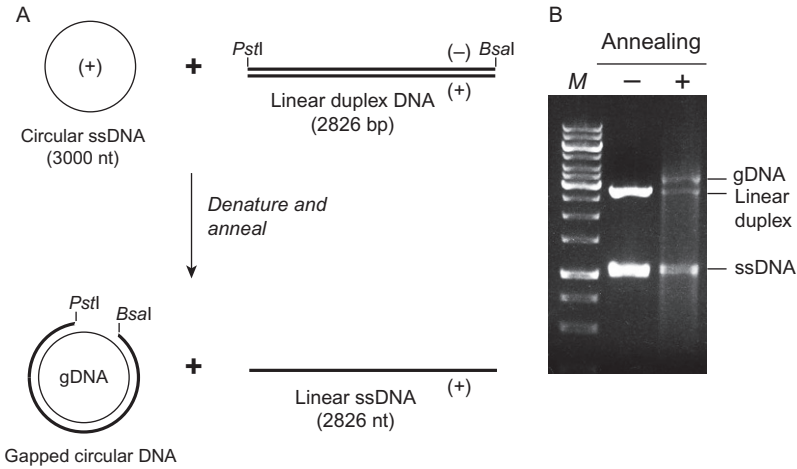


**Fig. 1** Formation and purification of gapped circular DNA. (A) Denaturation of the *BsaI*–*PstI* 2826 bp fragment of pDEA-7Z and subsequent annealing with closed circular single-stranded pDEA-7Z yields circular gapped duplex DNA (gDNA). (B) Samples before (–) and after (+) annealing were separated on a 0.8% agarose gel. The positions of ssDNA, linear duplex DNA, and gapped DNA are indicated. *M*, size markers.

- *E. coli* BIOBlue chemically competent cells (BioLine; cat BIO-85037).
- Antibiotic stocks: Ampicillin (50 mg/mL), tetracycline (10 mg/mL), kanamycin (70 mg/mL).
- 2 × Yeast Tryptone (YT) media.
- 20% (w/v) Glucose.
- Helper phage VCSM13 (Agilent; cat 200251).
- PEG 6000 (or PEG 8000), NaCl.
- M2 buffer: 1% (v/v) Triton-X100, 500 mM guanidine-HCL, 10 mM MOPS pH 6.5. Store at room temperature.
- Qiagen-tip 500, buffers QBT, QC, and QF (Qiagen Maxi Kit; cat 12162).
- 50 mL Polypropylene Falcon tubes.
- Ethanol.
- Isopropanol.
- TE buffer: 10 mM Tris-HCl pH 8.0, 1 mM EDTA.
- Agarose.
- Horizontal gel electrophoresis equipment (Bio-Rad wide mini-sub cell GT system or equivalent).
- TAE electrophoresis buffer: 40 mM Tris base, 1.1% (v/v) glacial acetic acid, 1 mM EDTA.

- Ethidium bromide stock solution (10 mg/mL).
- 10× Agarose gel loading buffer (50 mM Tris-HCl pH 8.0, 50% (v/v) glycerol, 0.2% (w/v) xylene cyanol, and 0.2% (w/v) bromophenol blue).

### Methods

1. Transform plasmid pDEA-7Z f(+) into *E. coli* strain BIOBlue using standard methods (this strain contains the F' episome that allows the M13 helper phage to infect). Plate transformed cells onto LB plates containing 50 µg/mL ampicillin and incubate overnight at 37°C.
2. Pick a freshly grown colony and inoculate into 5 mL 2× YT supplemented with 0.1% glucose, 50 µg/mL ampicillin, 10 µg/mL tetracycline and grow overnight at 37°C.
3. Seed 1 mL of the overnight culture into 50 mL of the same media and grow at 37°C with shaking to  $A_{600} = 0.4$  (should take approximately 1 h).
4. Remove 3 × 8 mL aliquots of exponentially growing culture and infect each aliquot with 80 µL helper phage VCSM13.
5. Grow for 60 min with shaking at 37°C.
6. Use each 8 mL aliquot to inoculate 800 mL 2× YT containing 0.1% glucose, 50 µg/mL ampicillin, 10 µg/mL tetracycline, and 70 µg/mL kanamycin.
7. Grow cultures overnight at 37°C with shaking (see Note 1).
8. Pellet cells from overnight cultures by centrifugation at 10,000 × g for 15 min at 4°C in a Sorvall SLC-6000 rotor using 1 L buckets.
9. Transfer supernatant to fresh buckets and respin. This is to avoid any carry over of bacterial cells to prevent contamination of the M13 ssDNA with chromosomal or bacteriophage RF DNA.
10. Decant supernatant and measure volume (typically 2.5 L).
11. Precipitate the phage by addition of 40 g of PEG 6000 and 40 g NaCl per liter of supernatant. Stir on ice in cold room for 2 h to precipitate phage. The supernatant will go cloudy.
12. The precipitate is collected by centrifugation for 20 min at 10,000 × g at room temperature in 1 L Sorvall SLC-6000 buckets.
13. A creamy white phage pellet should be clearly visible on the bottom and sides of the buckets.
14. Discard supernatant (see Note 2), scrape off the pellets, and resuspend well by pipetting in 30 mL M2 buffer per phage pellet.
15. Incubate the mixture in a water bath at 80°C for 40 min. This will lyse the phage and release ssDNA.
16. Mix by inversion and allow the solution to cool to room temperature.

17. Transfer the lysate to sterile 50 mL polypropylene Falcon tubes and centrifuge in an Eppendorf 5810R benchtop centrifuge at  $16,000 \times g$  for 30 min at room temperature. This will pellet the precipitated protein (see Note 3).
18. Meanwhile equilibrate two Qiagen-tip 500s with 10 mL QBT buffer.
19. Carefully decant the supernatants from step 17 and immediately apply 30 mL to each Qiagen-tip 500.
20. Wash with 30 mL QC buffer.
21. Apply 15 mL QF buffer to elute the DNA.
22. Transfer the eluate to 50 mL polypropylene tubes and add 0.7 volume (i.e., 10.5 mL) isopropanol to each eluate and mix. Strands of DNA may become visible.
23. Pellet the DNA by centrifugation in an Eppendorf 5810R benchtop centrifuge at  $12,000 \times g$  for 30 min at room temperature (see Note 4).
24. Discard the supernatant and wash the DNA pellets with 5 mL of 70% ethanol at room temperature, and centrifuge again for 10 min.
25. Remove the supernatant and allow the pellets to air-dry briefly.
26. Resuspend the DNA in a total of 0.5 mL TE buffer. Do not pipette up and down as this may shear the DNA.
27. Determine the yield of ssDNA, using  $1 A_{260} \text{ unit} = 33 \mu\text{g/mL}$  (see Note 5). A typical yield of 4–5 mg ssDNA is expected.
28. Analyze the quality of 1  $\mu\text{g}$  DNA by electrophoresis on a 1% agarose gel using TAE gel electrophoresis buffer containing 5  $\mu\text{g/mL}$  ethidium bromide. Visualize under UV to make sure it is not contaminated with other DNA species.

### 2.1.2 Gel Purification of ssDNA

Large-scale purification of the ssDNA is strongly recommended. The presence of even a small amount of double-stranded DNA (i.e., 2% of total DNA) adversely affects the production of high-quality gapped DNA. To avoid any damage or shearing of the labile ssDNA, purification by preparative agarose gel electrophoresis and electroelution is recommended.

#### Materials

- Agarose, horizontal gel electrophoresis equipment, and buffers (as in [Section 2.1.1](#)).
- Ethidium bromide stock solution (10 mg/mL).
- Snakeskin™ dialysis tubing (Thermo Scientific; cat 68100).
- Disposable sterile 50 mL polypropylene Falcon tubes.

- 3 M Sodium acetate pH 5.2.
- Ethanol.
- Glycogen (Ambion; cat AM9510).

### Methods

1. Pour a 100 mL 1% (w/v) agarose/TAE wide mini-sub gel using a single large sample well (see Note 6). Do not add any stains or dyes to the gel.
2. Mix 100  $\mu$ L of ssDNA (i.e., 400–500  $\mu$ g) with 10  $\mu$ L of agarose sample loading buffer and load onto gel.
3. Electrophoresis should be performed for 90 min at 80 V in TAE buffer at 4°C.
4. Cut 1 cm wide slices from the sides of each gel and stain these with 5  $\mu$ g/mL ethidium bromide (in TAE buffer).
5. View the band corresponding to ssDNA in these side slices using a UV transilluminator and excise. The cutouts then serve as a reference marker when the slices are realigned with the main part of the preparative gel. Remove a single long gel slice containing the ssDNA from the main body of the gel.
6. To prepare a dialysis bag for electroelution, cut a 20-cm length of Snakeskin tubing. Hydrate with distilled water, wash in TAE buffer, and tie a knot at one end (a plastic clamp can also be used).
7. Pipette 7 mL TAE electrophoresis buffer into the dialysis bag and insert the gel slice containing the ssDNA. Remove air bubbles, trim if necessary, and tie (or clamp) the other end of the bag.
8. Place dialysis bag in a wide mini-sub gel tank containing TAE buffer. Electroelute overnight at 25 V in the cold room. The ssDNA will transfer from the gel slice into the TAE solution.
9. Reverse the polarity of the current for 2 min to detach any DNA that might be adsorbed onto the dialysis membrane.
10. Remove buffer containing the ssDNA from dialysis bag with a pipette. Wash bag with 3 mL TAE buffer and pool to give a total of approximately 10 mL per bag.
11. Transfer the DNA solution into 50 mL polypropylene Falcon tubes (5 mL per tube). Precipitate DNA by adding 0.1 volume 3 M sodium acetate (pH 5.2) and 2.5 volumes ethanol. Incubate on dry ice for 30 min. As an optional step, 2.5  $\mu$ L glycogen can be added to aid precipitation.
12. Pellet the DNA by centrifugation in an Eppendorf 5810R benchtop centrifuge at 15,000  $\times g$  for 1 h at 4°C (see Note 7).
13. The DNA pellets should be clearly visible. Remove supernatant, wash with 5 mL ice-cold 70% ethanol, and centrifuge again for 10 min.

14. Remove supernatant and allow the pellets to air-dry briefly.
15. Gently resuspend the DNA in 500  $\mu\text{L}$  TE pH 8.0. Do not pipette up and down, as this may cause shearing of the delicate ssDNA.
16. Determine the yield of ssDNA, using 1  $A_{260}$  unit = 33  $\mu\text{g}/\text{mL}$  (see Note 5). It is normal to recover between 50% and 60% of input DNA.
17. Analyze an aliquot of purified ssDNA on a 0.8% agarose gel to confirm the removal of contaminating DNA.

### 2.1.3 Preparation of the Complementary DNA Strand

The linear strand that will be annealed to the ssDNA is prepared by excising a 174-bp *BsaI*–*PstI* fragment from plasmid pDEA-7Z DNA. The resulting 2826 bp linear DNA is purified by preparative gel electrophoresis and recovered by electroelution.

#### Materials

- Plasmid pDEA-7Z f(+) (Shah et al., 1994a). Form I DNA stock prepared using a Qiagen plasmid maxi kit.
- Restriction enzymes *BsaI*-HF and *PstI*-HF (New England Biolabs).
- 10 $\times$  CutSmart buffer (New England Biolabs).
- 0.5 M EDTA pH 8.0.
- 2 mL Eppendorf tubes.
- Phenol/chloroform/isoamyl alcohol (v/v/v, 25:24:1).
- Chloroform/isoamyl alcohol (v/v, 24:1).
- Agarose, horizontal gel electrophoresis equipment, and buffers (as in Section 2.1.1).
- Snakeskin<sup>TM</sup> dialysis tubing (as in Section 2.1.2).
- 50 mL Polypropylene Falcon tubes.
- Ethanol.
- 3 M Sodium acetate pH 5.2.
- Glycogen (as in Section 2.1.2).

#### Methods

1. Digest 250  $\mu\text{g}$  of Form I pDEA-7Z plasmid DNA in a 4.0-mL reaction using 200 units of *BsaI*-HF and 200 units of *PstI*-HF in 1 $\times$  NEB CutSmart buffer. Incubate for 90 min at 37°C.
2. Stop the reaction by addition of 80  $\mu\text{L}$  0.5 M EDTA (10 mM final) and transfer 1 mL aliquots to 4 $\times$  2 mL Eppendorf tubes.
3. Check an aliquot of the reaction on a 1% agarose gel to confirm digestion is complete. DNA fragments of 2826 and 174 bp, generated by the double digest, should be clearly visible.

4. Extract the DNA solution twice with phenol/chloroform/isoamyl alcohol and once with chloroform/isoamyl alcohol.
5. Precipitate DNA by addition of 0.1 volume of 3 *M* sodium acetate and 2.5 volumes of ethanol. Incubate on dry ice for 30 min.
6. Pellet DNA by centrifugation in an Eppendorf 5810R benchtop centrifuge at 15,000  $\times g$  for 45 min at 4°C (see Note 7).
7. Resuspend the DNA in a total of 200  $\mu\text{L}$  TE buffer.
8. Pour two 100 mL 1% agarose wide mini-sub gels, each with one large sample well and one small well for markers (see Note 6). Do not add any stains or dyes to the gel (see Note 8).
9. Load 100  $\mu\text{L}$  of the digested pDEA-7Z in each of the large sample wells. Load 5  $\mu\text{L}$  of a DNA marker ladder in the small well.
10. Electrophorese for 90 min at 80 V in 1  $\times$  TAE buffer.
11. Cut 1 cm wide slices from the sides of each gel and stain DNA with 5  $\mu\text{g}/\text{mL}$  ethidium bromide (in TAE buffer).
12. View DNA using a UV transilluminator and excise the section of gel corresponding to the 2.8-kb DNA fragment.
13. Realign the stained gel slices and use as a reference to excise the 2.8-kb DNA fragment from the preparative gels.
14. Prepare two Snakeskin dialysis bags as described in Section 2.1.2. Place each agarose gel slice (containing the 2.8-kb DNA fragment) into a Snakeskin dialysis bag containing 7 mL 1  $\times$  TAE buffer. Seal the bags and cover with 1  $\times$  TAE buffer in a wide mini-sub gel tank and electroelute overnight at 25 V in the cold room. The DNA will transfer from the gel slice into the TAE buffer.
15. Reverse the polarity of the current for 2 min to detach any DNA that might be adsorbed onto the dialysis membrane.
16. Collect the buffer from the bags and wash gel slices with a further 3 mL of 1  $\times$  TAE buffer. Pool wash with eluate and transfer DNA solution to 50 mL polypropylene Falcon tubes (approx. 10 mL per tube).
17. Precipitate DNA by adding 0.1 volume 3 *M* sodium acetate (pH 5.2), 2.5 volumes ethanol and incubating on dry ice for 30 min. As an optional step, 5  $\mu\text{L}$  glycogen can be added to aid precipitation.
18. Pellet DNA by centrifugation in an Eppendorf 5810R benchtop centrifuge at 15,000  $\times g$  for 45 min at 4°C (see Note 7). Discard supernatant.
19. Wash DNA pellet with 5 mL ice-cold 70% ethanol and centrifuge again for 15 min.

20. Discard wash buffer and allow DNA to air-dry before resuspending in a total of 0.3–0.5 mL TE.
21. Determine yield of DNA, using  $1 A_{260}$  unit = 50  $\mu\text{g}/\text{mL}$  (see Note 5). It is normal to recover between 50% and 60% of input DNA.

### 2.1.4 Annealing and Purification of gDNA

An annealing reaction is performed between circular single-stranded pDEA-7Z (ssDNA) and the linear 2.8-kb *BsaI*–*PstI* fragment of pDEA-7Z (Fig. 1A). The resulting gDNA is then purified from other species by preparative agarose gel electrophoresis followed by electroelution.

#### Materials

- Purified single-stranded pDEA-7Z (see Section 2.1.2).
- Purified 2.8 kb *BsaI*–*PstI* fragment of pDEA-7Z (see Section 2.1.3).
- 10 $\times$  Annealing buffer (0.1 M Tris–HCl pH 7.5, 0.1 M MgCl<sub>2</sub>, 0.5 M NaCl).
- Slide-A-Lyzer<sup>®</sup> Dialysis Cassette (Thermo Scientific; cat 66380).
- Screw cap 1.5-mL tubes.
- Mineral oil.
- Heated magnetic stirrer block.
- Polystyrene igloo.
- Agarose and gel buffers (as in Section 2.1.1).
- Horizon<sup>®</sup> Maxi 20–25 horizontal gel electrophoresis system (GIBCO-BRL) or equivalent.
- Snakeskin<sup>™</sup> dialysis tubing (as in Section 2.1.2).
- 50 mL Polypropylene Falcon tubes.
- Ethanol.
- 3 M Sodium acetate pH 5.2.
- Glycogen (as in Section 2.1.2).

#### Methods

1. Perform trial annealing reactions (40  $\mu\text{L}$ ) to determine the optimum ratio of ssDNA:linear duplex DNA for generating gapped DNA prior to carrying out the large-scale preparation, as described previously (Constantinou & West, 2004). During preparative gel electrophoresis, the linear duplex DNA runs quite near to the gDNA product, so it is important to utilize as much as possible of the dsDNA in the annealing reaction. A ratio of ssDNA:dsDNA of approximately 1.5:1 (w/w) is usually optimal (Fig. 1B).
2. Set up a large-scale annealing reaction by mixing 180  $\mu\text{g}$  of ssDNA with 120  $\mu\text{g}$  of the 2.8-kb linear DNA fragment. Bring volume to 1 mL with ddH<sub>2</sub>O.

3. Dialyze in a Slide-A-Lyzer<sup>®</sup> cassette against 2 L of TE buffer at 4°C, for a minimum of 2 h. This step is required to remove any impurities still present in the DNA and aids efficient annealing.
4. Split dialyzed sample into 4 × 250 μL aliquots in screw cap tubes. Add 50 μL 10 × annealing buffer and 200 μL ddH<sub>2</sub>O to each tube (total volume = 500 μL). Cover with 200 μL of mineral oil and tighten lids securely.
5. Denature the dsDNA by placing the tubes in a beaker of boiling water for 5 min using a floating tube rack. Remove the beaker from heat, cover with foil, and place in a polystyrene igloo. Reanneal the DNA by allowing the tubes to cool slowly to room temperature overnight.
6. The next day, pierce bottom of tubes with a hot needle and collect the annealed reaction dropwise into fresh tubes, taking care to leave behind any mineral oil. Place tubes on ice.
7. Pour two 300 mL 1% (w/v) agarose maxi gels, each containing two large sample wells (see Note 6). Do not add any stains or dyes to the gel (see Note 8).
8. Add 50 μL of 10 × agarose gel loading buffer to each annealing mix and load onto the gels. Separate the DNA products by electrophoresis at 200 V for 3–4 h at 4°C in TAE buffer.
9. To localize the band corresponding to gapped DNA, remove a 2-cm wide slice from the sides of the gels and stain with ethidium bromide (5 μg/mL). The newly formed gDNA will migrate below the xylene cyanol dye and just above the 2.8-kb *Pst*I–*Bsa*I linear fragment.
10. View the DNA using a UV transilluminator and excise a section of the gel corresponding to the position of the gapped DNA.
11. Realign the stained gel slices and use as a reference to excise a single long gel slice containing the gapped DNA from each of the preparative gels. Care should be taken to avoid excising any of the linear fragment which runs just below the gDNA (see Note 9).
12. Prepare four Snakeskin dialysis bags as described in Section 2.1.2. Place the agarose gel slices into Snakeskin<sup>™</sup> dialysis bags using as small a volume of TAE buffer as possible (approximately 10 mL per bag, being careful to avoid trapping any air).
13. Seal dialysis bags and cover with 1 × TAE buffer in the maxi gel tank and electroelute DNA overnight at 40 V at 4°C.
14. Before collecting the samples, reverse the polarity of the current for 2 min to detach any DNA that might be adsorbed onto the dialysis tubing.

15. Collect buffer from the bags and wash gel slices with a further 3 mL of  $1 \times$  TAE buffer. Pool wash with eluate and transfer DNA solution to 50 mL polypropylene Falcon tubes.
16. Precipitate DNA by adding 0.1 volume 3 M sodium acetate pH 5.2, 2.5 volumes ethanol, and 5  $\mu$ L glycogen. Incubate on dry ice for 30 min. The addition of glycogen is required to aid precipitation as the volumes are large and the concentration of DNA will be low (see Note 10).
17. Pellet the gDNA by centrifugation in an Eppendorf 5810R benchtop centrifuge at  $15,000 \times g$  for 45 min at  $4^\circ\text{C}$  (see Note 7). Discard supernatant.
18. Wash the DNA pellet with 5 mL ice-cold 70% (v/v) ethanol and centrifuge again for 15 min.
19. Discard wash buffer and allow the DNA to air-dry before resuspending it in a total of 0.3–0.5 mL TE buffer.
20. Dialyze overnight against 2 L of TE buffer at  $4^\circ\text{C}$ . This is a key step and should not be omitted, as any impurities will adversely affect subsequent strand exchange reactions.
21. Determine the DNA yield using  $1 A_{260}$  unit = 50  $\mu\text{g}/\text{mL}$  and calculate the concentration. For reactions with RecA, the DNA concentrations are usually expressed as moles of nucleotides (see Note 5).
22. Dilute the gDNA to give a final working concentration of between 150 and 300  $\mu\text{M}$  (nucleotides).
23. The final gDNA preparation should be aliquoted and stored at  $-20^\circ\text{C}$ . Once thawed, store at  $4^\circ\text{C}$  and do not refreeze as repeated freeze/thaw cycle will destabilize the gDNA.

## 2.2 Radioactive Labeling of the Linear Duplex DNA

Plasmid pDEA2 is homologous to pDEA-7Z, except for the presence of a 643-bp region of heterology (Fig. 2A). It is linearized by digestion with *Pst*I and then 3'- $^{32}\text{P}$ -end labeled using [ $\alpha$ - $^{32}\text{P}$ ] cordycepin 5'-triphosphate and terminal transferase.

### Materials

- Plasmid pDEA2 f(+) (Shah et al., 1994a). Form I DNA stock prepared using a Qiagen plasmid maxi kit.
- Restriction enzyme *Pst*I-HF (New England Biolabs).
- $10 \times$  CutSmart buffer (New England Biolabs).
- 0.5 M EDTA pH 8.0.
- Phenol/chloroform/isoamyl alcohol (v/v/v, 25:24:1).

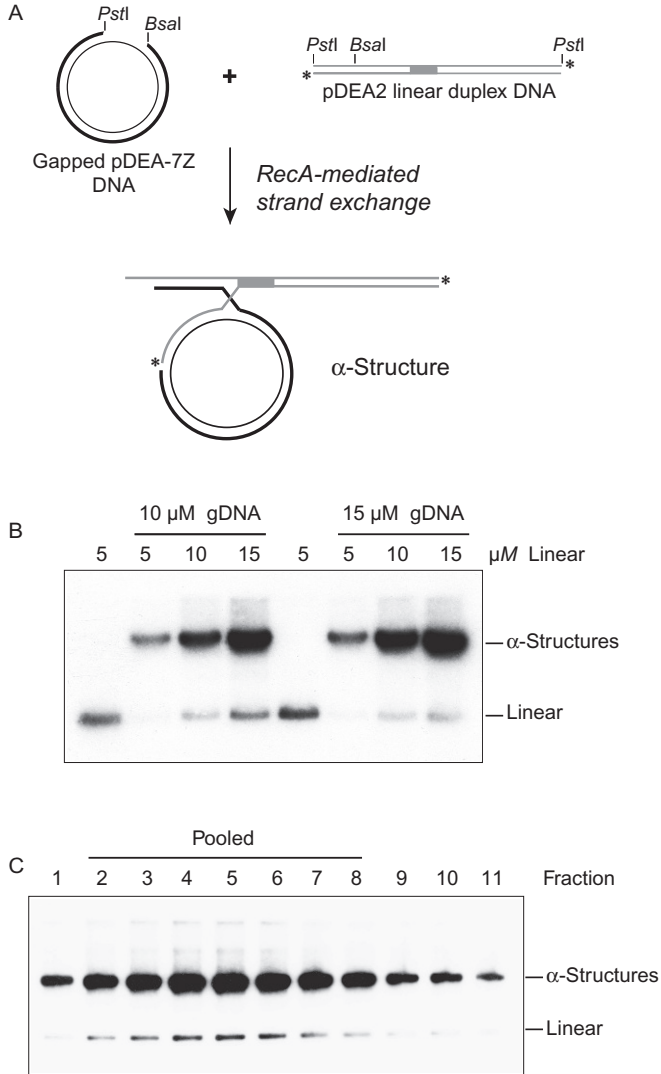


**Fig. 2** Generation and purification of recombination intermediates. (A) Schematic diagram showing RecA-mediated strand exchange between gapped circular pDEA-7Z DNA and 3'-<sup>32</sup>P-labeled linear duplex pDEA2 DNA, leading to the production of recombination intermediates ( $\alpha$ -structures) containing a single Holliday junction. Strand exchange proceeds through 1536 bp of homology up to a heterologous block (*gray box*; 643 bp in length) such that recombination intermediates accumulate throughout the course of the reaction. 3'-<sup>32</sup>P-end labels are indicated with *asterisks*. (B) Small-scale trial strand exchange reactions between gapped circular DNA (gDNA) and 3'-<sup>32</sup>P-end-labeled linear duplex DNA, to establish optimal conditions. Reaction products were separated by (Continued)

- Chloroform/isoamyl alcohol (v/v, 24:1).
- Ethanol.
- 3 M Sodium acetate pH 5.2.
- TE buffer: 10 mM Tris-HCl pH 8.0, 1 mM EDTA.
- Agarose, horizontal gel electrophoresis equipment, and buffers (as in Section 2.1.1).
- Terminal transferase (TdT), 10× TdT reaction buffer and 10× cacodylate buffer (New England Biolabs; cat M0315S).
- 3'-[ $\alpha$ -<sup>32</sup>P] Deoxyadenosine 5'-triphosphate (cordycepin 5'-triphosphate), 10 mCi/mmol (Perkin Elmer; cat NEG026250UC).
- Illustra MicroSpin™ S-400 HR columns (GE Healthcare; cat 27-5140-01).

## Methods

1. Digest 250  $\mu$ g of Form I pDEA2 plasmid DNA in a 4-mL reaction using 200 units *Pst*I-Hf in 1 × NEB CutSmart buffer for 2 h at 37°C. Check an aliquot for complete digestion on a 0.8% agarose gel.
2. Stop the reaction by addition of 80  $\mu$ L 0.5 M EDTA (10 mM final) and extract twice with phenol/chloroform/isoamyl alcohol and once with chloroform/isoamyl alcohol.
3. Precipitate the DNA with 0.1 volume of 3 M sodium acetate pH 5.2 and 2.5 volumes ethanol. Incubate on dry ice for 30 min.
4. Pellet the DNA by centrifugation in an Eppendorf benchtop centrifuge at 15,000 × *g* for 45 min at 4°C (see Note 7). Discard the supernatant.
5. Wash the pellet with 5 mL ice-cold 70% ethanol and centrifuge again for 15 min. Allow DNA pellet to air-dry and resuspend in a total of 0.3–0.5 mL TE. Determine the DNA concentration using 1 *A*<sub>260</sub> unit = 50  $\mu$ g/mL.
6. Label 8  $\mu$ g of the linearized pDEA2 in a 50- $\mu$ L reaction containing 50  $\mu$ Ci [ $\alpha$ -<sup>32</sup>P] cordycepin 5'-triphosphate, 10 units of terminal transferase, 1 × terminal transferase buffer, and 1 × cacodylate buffer. Incubate for 90 min at 37°C.

---

**Fig. 2—Cont'd** electrophoresis through a 1.2% agarose gel in the presence of ethidium bromide and analyzed by autoradiography. (C) Purification of 3'-<sup>32</sup>P-labeled recombination intermediates. The products of a large-scale RecA-mediated strand exchange reaction were applied to a Sepharose CL-2B column. Fractions were collected and 10  $\mu$ L aliquots were analyzed on a 1% agarose gel followed by autoradiography. Peak fractions containing the highest concentration of recombination intermediates are pooled for use in resolution assays.

7. Stop the reaction by addition of 0.8% (w/v) SDS (2  $\mu$ L of a 20% (w/v) stock) and 25 mM EDTA (2.5  $\mu$ L 0.5 M stock).
8. Extract once with 1 volume of phenol/chloroform/isoamyl alcohol and back extract the organic phase with 50  $\mu$ L TE buffer.
9. Pool aqueous phases and pass through a Illustra MicroSpin™ S-400 HR column as described by the manufacturer, to remove any unincorporated counts (see Note 11).
10. Add 0.5 volume ethanol and store labeled DNA at  $-20^{\circ}\text{C}$  until required. The addition of ethanol reduces damage caused by radioactive decay.
11. Determine the yield of DNA using 1  $A_{260}$  unit = 50  $\mu\text{g}/\text{mL}$  and calculate the concentration expressed as moles of nucleotides (see Note 5).
12. Dilute DNA to give a final working concentration of between 150 and 300  $\mu\text{M}$  (nucleotides).



### 3. GENERATION AND PURIFICATION OF $\alpha$ -STRUCTURES

RecA-mediated strand exchange is carried out between gapped circular pDEAZ DNA and 3'- $^{32}\text{P}$ -labeled linear duplex pDEA2 DNA (Fig. 2A). The products of the reaction are  $^{32}\text{P}$ -labeled recombination intermediates, or  $\alpha$ -structures, which can then be purified by column chromatography.

#### Materials

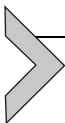
- Circular gapped DNA (gDNA, prepared as described in Section 2.1).
- 3'- $^{32}\text{P}$ -labeled linear duplex DNA (prepared as described in Section 2.2).
- RecA protein (New England Biolabs; cat M0355S), 2 mg/mL stock (52  $\mu\text{M}$ ).
- Phosphocreatine (Sigma; cat P1937).
- Creatine phosphokinase (Sigma; cat C3755).
- Proteinase K (Promega; cat V3021).
- 5  $\times$  Strand exchange buffer (250 mM triethanolamine-HCl pH 8.0, 75 mM  $\text{MgCl}_2$ , 10 mM ATP, 5 mM DTT, 500  $\mu\text{g}/\text{mL}$  bovine serum albumin), with an ATP regeneration system consisting of 100 mM phosphocreatine and 10 U/mL creatine phosphokinase.
- 5  $\times$  Stop buffer (100 mM Tris-HCl pH 7.4, 10 mg/mL proteinase K, 4% (v/v) SDS).
- Sepharose® CL-2B (Sigma; cat CL-2B-300).
- 10 mL Poly-Prep® chromatography columns (Bio-Rad; cat 7311550).
- Sepharose column buffer: 20 mM Tris-HCl pH 8.0, 1 mM dithiothreitol, 100  $\mu\text{g}/\text{mL}$  bovine serum albumin, 5 mM  $\text{MgCl}_2$ .

- Agarose, horizontal gel electrophoresis equipment, and buffers (as in Section 2.1.1).
- DE81 Anion Exchange paper (GE Healthcare; cat 3658-915).
- 3MM Chromatography paper (GE Healthcare; cat 3030-917).

## Methods

1. Optimal conditions for strand exchange need to be established for each new batch of gapped circular and 3'-<sup>32</sup>P-labeled linear duplex DNA by performing small-scale reactions (10  $\mu$ L) in which the concentrations of each DNA substrate are varied (Fig. 2B).
2. Add gDNA (10 or 15  $\mu$ M) to 1  $\times$  strand exchange buffer, prechilled on ice. Supplement with 6  $\mu$ M RecA, leave for 5 min on ice and then move to 37°C for 5 min.
3. Add varying concentrations of 3'-<sup>32</sup>P-labeled linear duplex pDEA2 DNA and incubate for a further 45 min at 37°C.
4. Stop reactions by the addition of 2.5  $\mu$ L 5  $\times$  stop buffer. Continue incubation at 37°C for 15 min to deproteinize the DNA.
5. Add 3  $\mu$ L gel loading dye and analyze reactions on a 1.2% agarose wide mini-sub gel for 3 h at 70 V in TAE buffer. Both the gel and running buffer should contain 0.5  $\mu$ g/mL ethidium bromide to block spontaneous branch migration and help stabilize the  $\alpha$ -structures during electrophoresis.
6. Transfer gels onto DE81 chromatography paper (or 3MM chromatography paper), dry down, and detect <sup>32</sup>P-labeled products by autoradiography.
7. Typically, reactions containing 15  $\mu$ M gapped DNA and 15  $\mu$ M 3'-<sup>32</sup>P-end-labeled linear DNA give the best yield of  $\alpha$ -structures.
8. Using the optimal amounts of the two substrates, scale-up the strand exchange reaction to a final volume of 400  $\mu$ L.
9. During incubation, prepare a 3.5-mL Sepharose™ CL-2B column in a 10-mL Poly-Prep chromatography column. Equilibrate with 5 volumes of column buffer at room temperature.
10. Stop the strand exchange reaction by addition of 0.2 volume of 5  $\times$  stop buffer (100  $\mu$ L) and incubate at 37°C for a further 15 min.
11. To purify the 3'-<sup>32</sup>P-labeled recombination intermediates, pipette the strand exchange reaction dropwise onto the equilibrated Sepharose CL-2B column. Top up with more column buffer and allow the DNA products to pass through the column by gravity. Collect two-drop fractions and monitor for Cerenkov counts using a hand-held monitor. Store fractions at 4°C.

12. To determine which fractions should be pooled, analyze 10  $\mu\text{L}$  aliquots on a 100-mL 1% (w/v) agarose wide mini-sub gel for 3 h at 70 V in TAE buffer. Both the gel and running buffer should contain 0.5  $\mu\text{g}/\text{mL}$  ethidium bromide to block spontaneous branch migration and stabilize the  $\alpha$ -structures during electrophoresis.
13. Transfer the gels onto DE81 chromatography paper (or 3MM chromatography paper), dry down, and detect  $^{32}\text{P}$ -labeled products by autoradiography.
14. Usually the  $^{32}\text{P}$ -labeled recombination intermediates elute in a broad peak (Fig. 2C), which also contains some unreacted 3'- $^{32}\text{P}$ -labeled linear duplex DNA. This is normal and does not interfere with subsequent reactions.
15. Pool the peak fractions to give a total volume of approximately 400  $\mu\text{L}$  and determine the yield of DNA, using 1  $A_{260}$  unit = 50  $\mu\text{g}/\text{mL}$ . Calculate the concentration, expressed as moles of nucleotides (see Note 5).
16. Store the  $^{32}\text{P}$ -labeled  $\alpha$ -structures at 4°C in aliquots and for best results use within 2–5 days. Do not freeze/thaw, as this will destabilize them.



## 4. IN VITRO RESOLUTION ASSAYS

1. Recombination intermediates, such as the  $\alpha$ -structures prepared above, contain a single HJ within significant lengths of duplex DNA and are excellent substrates for the analysis of HJ resolution activities. Indeed, they are more physiological substrates than the commonly used small synthetic HJs which are produced by annealing partially complementary oligonucleotides. When treated with HJ resolvases such as *E. coli* RuvC or human GEN protein, the  $\alpha$ -structures are resolved in one of two possible orientations to produce: (i)  $^{32}\text{P}$ -labeled linear dimers or (ii)  $^{32}\text{P}$ -labeled gapped linear and  $^{32}\text{P}$ -labeled nicked circular molecules, as illustrated (Fig. 3A). These products can be analyzed by agarose gel electrophoresis followed by autoradiography (Fig. 3B).

### Materials

- 3'- $^{32}\text{P}$ -labeled  $\alpha$ -structures (prepared as described in Section 3).
- *E. coli* RuvC protein, purified as described (Dunderdale, Sharples, Lloyd, & West, 1994).
- Human GEN1 protein, purified as described (Chan & West, 2015, 2018).

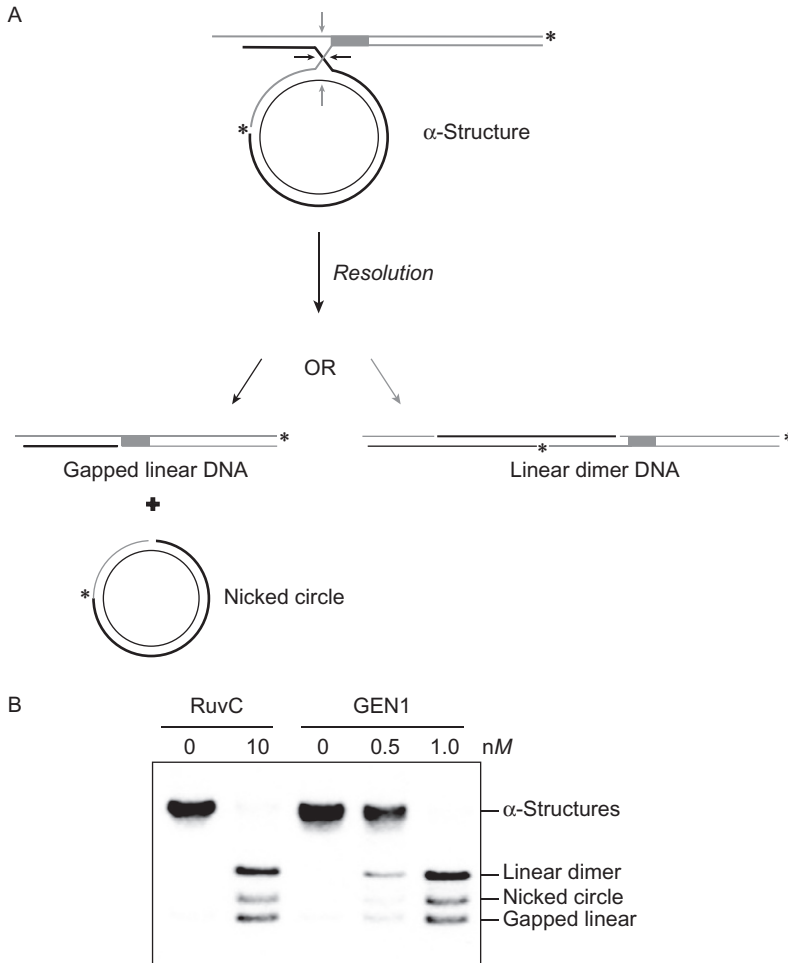


**Fig. 3** Resolution of recombination intermediates by GEN1. (A) Schematic diagram showing resolution of  $\alpha$ -structures leading to the production of either nicked circles and gapped linear DNA products or linear dimer molecules. The products correlate with cleavage in the orientation indicated by either *black* or *gray* arrows.  $3'$ - $^{32}\text{P}$ -end labels are indicated with *asterisks*. (B) The products of resolution by RuvC or GEN1 were separated on a 1.2% agarose gel and visualized by autoradiography.

- RuvC dilution buffer: 20 mM Tris-HCl pH 8.0, 50 mM NaCl, 20% (v/v) glycerol, 1 mM dithiothreitol, and 1 mM EDTA.
- GEN1 dilution buffer: 50 mM Tris-HCl pH 7.5, 250 mM NaCl, 10% (v/v) glycerol, 1 mM dithiothreitol, and 0.05% (w/v) Nonidet-P40.
- 10 $\times$  Resolution reaction buffer: 500 mM Tris-HCl pH 8.0, 10 mM dithiothreitol, and 1 mg/mL bovine serum albumin.

- Agarose, horizontal gel electrophoresis equipment, and buffers (see [Section 2.1.1](#)).
- 6× Purple gel loading dye (New England Biolabs; B7024).
- Ethidium bromide (10 mg/mL).
- DE81 Anion Exchange paper and 3MM chromatography paper (see [Section 3](#)).

### Methods

1. Resolution reactions (10  $\mu$ L volume) contain 1.5 nM 3'-<sup>32</sup>P-labeled  $\alpha$ -structures with purified enzymes (0–10 nM) in 1× resolution buffer. Reactions with RuvC are supplemented with 10 mM MgCl<sub>2</sub>. Although GEN1 requires 0.5–1 mM MgCl<sub>2</sub>, this requirement is satisfied by the carryover of MgCl<sub>2</sub> from the  $\alpha$ -structure storage buffer (see Note 12). Prior to use, RuvC and GEN1 should be diluted in their respective dilution buffers.
2. Incubate reactions at 37°C for 15 min and stop by the addition of 2  $\mu$ L 6× purple gel loading dye (contains SDS and EDTA).
3. Analyze the reaction products on a 100-mL 1.2% agarose/TAE gel run for 3 h at 70 V. Both the gel and running buffer should contain 0.5  $\mu$ g/mL ethidium bromide to block spontaneous branch migration and stabilize the  $\alpha$ -structures during electrophoresis.
4. Transfer gels onto DE81 chromatography paper (or 3MM chromatography paper), dry down, and detect <sup>32</sup>P-labeled products by autoradiography. Alternatively, the DNA can be directly visualized by exposing the gel to UV. This is a good option when the reactions are scaled up two- to threefold as it eliminates the need for radioactive labeling.
5. Resolution can occur in one of two possible orientations to produce either <sup>32</sup>P-labeled linear dimers or gapped linear and nicked circles ([Fig. 3](#)).



## 5. NOTES

1. The Qiagen protocol recommends that cultures be grown for 4–5 h. However, we find that greater M13 phage yields are obtained after overnight growth. Cultures should be seeded as late as possible in the day, and total incubation should not exceed 12 h. Cultures may appear to be less turbid than expected, as cells will lyse when releasing M13 phage into the medium.
2. It is essential that the PEG is completely removed. After decanting the supernatant, spin again briefly and remove any accumulated supernatant with a pipette. Alternatively drain by inverting bucket for 1 min.

3. Alternatively, transfer to autoclaved 30 mL COREX tubes and centrifuge in a SS34 rotor at  $20,000 \times g$  for 20 min at room temperature.
4. Alternatively, use 30 mL COREX tubes (or equivalent) and precipitate DNA by centrifugation in a SS34 rotor at  $12,000 \times g$  for 30 min at room temperature.
5. For ssDNA,  $1.0 A_{260}$  unit =  $33 \mu\text{g}/\text{mL} = 0.1 \text{ mM}$  (total nucleotides). For double-stranded DNA,  $1.0 A_{260}$  unit =  $50 \mu\text{g}/\text{mL} = 0.15 \text{ mM}$  (total nucleotides).
6. The wells of the comb can be taped over to create one large well. The first well can be left alone for markers, if desired.
7. Alternatively use autoclaved 30 mL COREX tubes (or equivalent) and centrifuge in a SS34 rotor at  $20,000 \times g$  for 30 min at  $4^\circ\text{C}$ .
8. No ethidium bromide (or any other dye) should be present in the agarose gel or TAE buffer since any residual dye may carry over to the gapped DNA stock and will hinder subsequent strand exchange reactions.
9. The gel should be stained with  $5 \mu\text{g}/\text{mL}$  ethidium bromide after excision of the gDNA to confirm that no linear DNA has been excised at the same time.
10. As an optional step, before ethanol precipitation, the samples can be concentrated to a workable volume by two extractions with an equal volume of butan-2-ol (discard the upper phase). This is followed by one extraction with diethyl ether. Tubes should then be left open in a fume hood to evaporate any residual ether.
11. As an alternative or additional step, the radiolabeled DNA can be ethanol precipitated and resuspended in TE buffer.
12. GEN1 requires  $0.5\text{--}1 \text{ mM}$   $\text{MgCl}_2$  for efficient resolution. However, as the required amount of  $\text{MgCl}_2$  is carried over from the Sepharose column buffer that the  $3'$ - $^{32}\text{P}$ -labeled  $\alpha$ -structures are stored in, there is no need to supplement the resolution reaction.

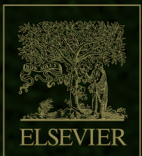
## ACKNOWLEDGMENTS

We thank our colleagues, past and present, who have developed substrates and methods for the analysis of Holliday junction processing enzymes. Work in the author's laboratory is supported by the Francis Crick Institute (FC10212), the European Research Council (ERC-ADG-66640), and the Louis-Jeantet Foundation. The Francis Crick Institute receives core funding from Cancer Research UK, the Medical Research Council, and the Wellcome Trust.

## REFERENCES

- Baumann, P., Benson, F. E., & West, S. C. (1996). Human RAD51 protein promotes ATP-dependent homologous pairing and strand transfer reactions *in vitro*. *Cell*, *87*, 757–766.
- Chan, Y. W., & West, S. C. (2015). GEN1 promotes Holliday junction resolution by a coordinated nick and counter-nick mechanism. *Nucleic Acids Research*, *43*, 10882–10892.
- Chan, Y. W., & West, S. C. (2018). GEN1 endonuclease: Purification and nuclease assays. In M. Spies & A. Malkova (Eds.), *Methods in enzymology. Mechanisms of DNA recombination and genome rearrangements: Methods to study homologous recombination* (pp. 527–542). Burlington, New York: Academic Press.
- Constantinou, A., Davies, A. A., & West, S. C. (2001). Branch migration and Holliday junction resolution catalyzed by activities from mammalian cells. *Cell*, *104*, 259–268.
- Constantinou, A., Tarsounas, M., Karow, J. K., Brosh, R. M., Bohr, V. A., Hickson, I. D., et al. (2000). Werner's syndrome protein (WRN) migrates Holliday junctions and co-localizes with RPA upon replication arrest. *EMBO Reports*, *1*, 80–84.
- Constantinou, A., & West, S. C. (2004). Holliday junction branch migration and resolution assays. In A. Waldman (Ed.), *Methods in molecular biology: Genetic recombination* (pp. 239–253). Totowa, NJ: Humana Press.
- Cox, M. M. (2001). Recombinational DNA repair of damaged replication forks in *Escherichia coli*: Questions. *Annual Review of Genetics*, *35*, 53–82.
- Cunningham, R. P., DasGupta, C., Shibata, T., & Radding, C. M. (1980). Homologous pairing in genetic recombination: RecA protein makes joint molecules of gapped circular DNA and closed circular DNA. *Cell*, *20*, 223–235.
- Dunderdale, H. J., Benson, F. E., Parsons, C. A., Sharples, G. J., Lloyd, R. G., & West, S. C. (1991). Formation and resolution of recombination intermediates by *E. coli* RecA and RuvC proteins. *Nature*, *354*, 506–510.
- Dunderdale, H. J., Sharples, G. J., Lloyd, R. G., & West, S. C. (1994). Cloning, overexpression, purification and characterization of the *Escherichia coli* RuvC Holliday junction resolvase. *The Journal of Biological Chemistry*, *269*, 5187–5194.
- Eggleston, A. K., Mitchell, A. H., & West, S. C. (1997). *In vitro* reconstitution of the late steps of genetic recombination in *E. coli*. *Cell*, *89*, 607–617.
- Garner, E., Kim, Y., Lach, F. P., Kottemann, M. C., & Smogorzewska, A. (2013). Human GEN1 and the SLX4-associated nucleases MUS81 and SLX1 are essential for the resolution of replication-induced Holliday junctions. *Cell Reports*, *5*, 207–215.
- Ip, S. C. Y., Rass, U., Blanco, M. G., Flynn, H. R., Skehel, J. M., & West, S. C. (2008). Identification of Holliday junction resolvases from humans and yeast. *Nature*, *456*, 357–361.
- Iwasaki, H., Takahagi, M., Shiba, T., Nakata, A., & Shinagawa, H. (1991). *Escherichia coli* RuvC protein is an endonuclease that resolves the Holliday structure. *The EMBO Journal*, *10*, 4381–4389.
- Karow, J. K., Constantinou, A., Li, J.-L., West, S. C., & Hickson, I. D. (2000). The Bloom's syndrome gene product promotes branch migration of Holliday junctions. *Proceedings of the National Academy of Sciences of the United States of America*, *97*, 6504–6508.
- Müller, B., & West, S. C. (1994). An assay for *in vitro* recombination between duplex DNA molecules. In G. G. Neale (Ed.), *Methods in molecular biology. DNA-protein interactions: Principles and protocols* (pp. 413–423). Totowa, NJ: Humana Press Inc.
- Panyutin, I. G., & Hsieh, P. (1994). The kinetics of spontaneous DNA branch migration. *Proceedings of the National Academy of Sciences of the United States of America*, *91*, 2021–2025.
- Raynard, S., Bussen, W., & Sung, P. (2006). A double Holliday junction dissolvasome comprising BLM, topoisomerase IIIa, and BLAP75. *The Journal of Biological Chemistry*, *281*, 13861–13864.
- Sarbajna, S., Davies, D., & West, S. C. (2014). Roles of SLX1-SLX4, MUS81-EME1 and GEN1 in avoiding genome instability and mitotic catastrophe. *Genes & Development*, *28*, 1124–1136.

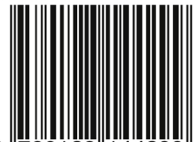
- Shah, R., Bennett, R. J., & West, S. C. (1994a). Activation of RuvC Holliday junction resolvase *in vitro*. *Nucleic Acids Research*, *22*, 2490–2497.
- Shah, R., Bennett, R. J., & West, S. C. (1994b). Genetic recombination in *E. coli*: RuvC protein cleaves Holliday junctions at resolution hotspots *in vitro*. *Cell*, *79*, 853–864.
- Shah Punatar, R., Martin, M. J., Wyatt, H. D., Chan, Y. W., & West, S. C. (2017). Resolution of single and double Holliday junction recombination intermediates by GEN1. *Proceedings of the National Academy of Sciences of the United States of America*, *114*, 443–450.
- Sung, P. (1994). Catalysis of ATP-dependent homologous DNA pairing and strand exchange by yeast Rad51 protein. *Science*, *265*, 1241–1243.
- Tsaneva, I. R., Müller, B., & West, S. C. (1992). ATP-dependent branch migration of Holliday junctions promoted by the RuvA and RuvB proteins of *E. coli*. *Cell*, *69*, 1171–1180.
- Wechsler, T., Newman, S., & West, S. C. (2011). Aberrant chromosome morphology in human cells defective for Holliday junction resolution. *Nature*, *471*, 642–646.
- West, S. C. (2003). Molecular views of recombination proteins and their control. *Nature Reviews. Molecular Cell Biology*, *4*, 435–445.
- West, S. C., Cassuto, E., & Howard-Flanders, P. (1982). Postreplication repair in *E. coli*: Strand exchange reactions of gapped DNA by RecA protein. *Molecular & General Genetics*, *187*, 209–217.
- West, S. C., Countryman, J. K., & Howard-Flanders, P. (1983). Enzymatic formation of biparental figure-8 molecules from plasmid DNA and their resolution in *Escherichia coli*. *Cell*, *32*, 817–829.
- Wu, L., & Hickson, I. D. (2003). The Bloom's syndrome helicase suppresses crossing over during homologous recombination. *Nature*, *426*, 870–874.
- Wyatt, H. D. M., Laister, R. C., Martin, S. R., Arrowsmith, C. H., & West, S. C. (2017). The SMX DNA repair tri-nuclease. *Molecular Cell*, *65*, 848–860.
- Wyatt, H. D. M., & West, S. C. (2014). Holliday junction resolvases. *Cold Spring Harbor Perspectives in Biology*, *6*, a023192.



**ACADEMIC PRESS**

An imprint of Elsevier  
[elsevier.com/books-and-journals](http://elsevier.com/books-and-journals)

ISBN 978-0-12-814429-9



9 780128 144299